ANKLE JOINT BIOMECHANICS

Thesis presented for the Degree of Doctor of Philosophy

by

Philip Procter B.Tech.Eng.

Bioengineering Unit
University of Strathclyde
Glasgow

September 1980

The Mechanisms - J.A. Procter 1980

"The purpose of this treatise is to place before inventors and designers concise, illustrated descriptions of many of the most ingenious mechanical movements ever devised. These mechanisms have been selected not only because they are regarded as particularly ingenious, but also because they have stood the test of actual practice."

from "Ingenious Mechanisms for Designers and Inventors".
Jones (1935)

ABSTRACT

The object of the present study was to investigate the three-dimensional kinematic and dynamic behaviour of the human ankle joint during walking and in particular to calculate joint and muscle forces. A review of the relevant literature is presented.

In the analysis, the ankle is treated as consisting of two joints: the talocrural (Tc.) and the Talocalcaneo-navicular (Tcn.).

Five cadaveric legs were dissected to ascertain the joint axes, the lines of action of the relevant tendons, and the positions of the ligaments.

Seven adult male subjects were studied during bare-foot level locomotion, and on planes sloping sideways at $^{+}$ 10 . Observations were made with a force plate, and with three orthogonally placed cine-cameras.

Stance phase forces were estimated as follows: inertia forces were neglected; anthropometric data from the cadavers were scaled to fit the walking subjects; the number of unknown forces was reduced to match the available equations by (a) combining muscles into four groups, and (b) assuming no antagonistic activity. Two free bodies were used: the hindfoot plus the talus alone. The Mark I solution excludes the Peroneal and Posterior Tibial groups; the Mark II solution includes them.

The Mark II model gave a peak resultant Tc. joint force of 3.9 Body Weight (B.W.) mean, for normal locomotion. The Tcn. joint anterior and posterior facet peak resultants are 2.4 and 2.8 B.W. respectively. The Anterior Tibial/Calf group peak forces are 1.0/2.5 B.W. mean. The Peroneal/Posterior Tibial group peak forces are 0.7/1.1 B.W.

mean.

Side slope walking is shown to require greater Peroneal/Posterior Tibial muscle group activity than in normal locomotion.

A Mark III model, including ligamentous constraint, is presented and recommendations made for its development.

The relationship between the results of the study and clinical problems such as joint replacement is considered.

ACKNOWLEDGEMENTS

The Author wishes to record his expression of gratitude to the following:

Judy Procter, whose ankles appear in the frontispiece

Professor J.P. Paul and Dr N. Berme for the opportunity to develop the work presented herein, and their critical eye

Maggie Jordan, for successfully reconciling her political work with typing this thesis

Dr. J. Shaw-Dunn, for his guidance and enthusiasm during the anatomical work

The Students of bioengineering for their ankles, time and conversation

The Staff of the Wolfson and National Centres for their contributions

The Science Research Council for their funding of this project and visits abroad during the work

NOTATION

In general all terms have been defined when they occur in the thesis. Repetition has occurred in some cases but it is hoped that it is always clear which term is referred to at any time.

Six orthogonal coordinate axes systems are used in the analysis, Talocrural, Talocalcaneonavicular, External hindfoot, External Shank, Laboratory ground and Anthropometric dissecting table systems. Using the Talocrural axis system as an example, the three orthogonal axes are referred to by subscript, thus $X_{Tc.}$, $Y_{Tc.}$ and $Z_{Tc.}$, and the origin by $O_{Tc.}$. The manipulation of vectors and reference points from one axis system to another is achieved by rotation matrices and translation vectors. For example, to refer a point P from the ground system to the Talocrural system requires coordinate translation by vector $\{T\}_{OG \rightarrow OTc.}$ and rotation by matrix $[R]_{G \rightarrow Tc.}$.

Note that throughout the thesis S.I. units have been used except where it is specifically stated to the contrary.

a	Anterior band of the deltoid ligament
a, al, ar	Apparent, left and right
a, ant	Anterior
(a) to (g)	Annotated peaks in force and moment records
aft	Anterior fibulotalar ligament
A	A marker outer bead coordinates
Ap	Muscle physiological cross-section
At	Tendon physiological cross-section
B	A marker inner bead coordinates
B.W.	Body Weight
c, C	Calf Muscle Group
cross	Vector cross-product
C	Skin thickness coefficients
C(x,y,z)	Tendon centroid coordinates
d16-2	Distance between marker beads 16 and 2
d17-2	Distance between marker beads 17 and 2
d_1, d_2	Cadaver joint distance parameters
dB	Decibel
det|....|	Determinant
D,Dist	Distal
D_1, D_2	Cadaver joint distance parameters
e, E	External
Eh	External hindfoot
Emg	Electromyograph
Es	External Shank
Ex	Extension
Ext dig long (edl)	Extensor digitorum longus muscle
Ext hall long(ehl)	Extensor hallucis longus muscle
Fc	Fibulocalcaneal ligament
F	Force
FD	Front camera distance

Fl	Flexion
Flex dig long (fdl)	Flexor digitorum longus muscle
Flex hall long (fhl)	Flexor hallucis longus muscle
g	Gravitational constant, or due to gravity
Gastroc	Gastrocnemius muscle
h	Height of camera optical axes above laboratory floor
h	Height of ramp insert above force platform origin
i	Inertia
i, I	Insertion
Ig	Rotary moment of inertia of foot about centre of gravity
Ih	Rotary moment of inertia of foot about heel
J	Joint
K	Arbitrary point
l	Direction cosine of a vector relative to an x axis
lat	Lateral
ligt, L	Ligament
LD	Left camera distance
m	Direction cosine of a vector relative to a y axis
m	Midband of the deltoid ligament
m	Mass of the foot
med	Medial
mid	Middle
M	Moment
M	Mid malleolar
n	Direction cosine of a vector relative to a z axis

n	Nth frame of data
N	Number of frames of cine data
O	Origin
p	Posterior band of the deltoid ligament
pft	Posterior fibulotalar ligament
post	Posterior
P	*Participation factor*
P	Peroneal group
P	Bony prominence or point in space
P, prox	Proximal
PT	Posterior tibial group
P(x)n	Centre of pressure x coordinate for Nth frame
P(y)n	Centre of pressure y coordinate for Nth frame
P(z)n	Centre of pressure z coordinate for Nth frame
Peron brev, pb	Peroneus brevis muscle
Peron long, pl	Peroneus longus muscle
r	Radius of foot centre of gravity with relation to heel
r, R	Radius
[R]	Rotation matrix (3x3)
R, Ra, Rp	Cadaver joint distance parameters
RD	Right camera distance
Ret, Retinac	Retinaculum
Ri	Inferior band of Inferior extensor retinaculum
Rs	Superior band of Inferior extersor retinaculum
s	Static film data
S	An arbitrary point

$S(x,y,z)$	Anthropometric scale factors
Sol	Soleus muscle
t	Time
t	Skin thickness
t	Tendon thickness
$\{T\}$	Translation vector (3x1)
Tc	Talocrural
Tcn	Talocalcaneonavicular
Tib ant, ta	Tibialis anterior muscle
Tib post, tp	Tibialis posterior muscle
Tt	Transverse tarsal
w	Tendon width
x,y,z	Directions
X,Y,Z	Directions, axes
$(X,Y,Z)_{scale}$	Cine film scale factors

Additional symbols

α,β,γ	Bony marker dimensions
$(\ldots\ldots)_{\alpha}$	α = x,y,z component
θ	Side slope ramp angle
θ	Angular rotation error due to projection mechanism errors
θ_1, θ_2	Talar wedging angle parameters
$\dot{\theta}$	Angular velocity
$\ddot{\theta}$	Angular acceleration
θ_1, θ_2, θ_3, θ_4	Cadaver joint angle parameters
$\lambda,(\eta/\mu)$	Centre of pressure parameters
$\lvert\ldots\ldots\rvert$	Modulus
2 to 17	Marker bead numbers
$\rightarrow$	Translation or rotation from one axis system to another
$\{\ \}$	Vector (3x1)

[.....]	Matrix (3x3)
Σ	Sum
.	Product
$\sim(0)$	Of the order of
$\propto$	Approximately
$\equiv$	Equivalent to
$<$	Less than
$\wedge$	Peak

CONTENTS

CHAPTER 1

INTRODUCTION AND REVIEW OF NORMAL ANKLE ANATOMY

1.1 Introduction

The work of Paul (1967) and of Morrison (1968), on the hip and knee respectively, established the basis for rigid body modelling of the dynamic behaviour of these joints in 'normal' human locomotion activities. The ankle has already been widely studied from anatomical and clinical viewpoints but remains the last major joint system in the leg for which a comprehensive three-dimensional force analysis has yet to be performed. Force analysis would provide data essential to the complete description of normal joint behaviour and is an important prerequisite for endoprosthesis mechanical design.

In the present study the biomechanics of 'normal' locomotion ankle joint behaviour was investigated, the particular objectives of the study are presented in 1.2. It should be noted that whilst biomechanical techniques of force analysis often permit quantitative description of locomotion activity, the 'Art' is insufficiently advanced for such description to be considered exact.

1.2 Objectives of the Ankle Biomechanics Study

The following objectives were formulated for the study

To establish the basis for a mathematical model of the ankle complex of joints, which would allow investigation of the three-dimensional kinematic and dynamic behaviour of the ankle during normal locomotion activities.

To investigate the anatomy of the normal ankle,

identifying the structures thought to influence mechanical function and to collect anthropometric data relating to these structures.

To estimate the magnitudes of muscle, ligamentous and joint forces for normal locomotion activities of human subjects.

To identify in the results any criteria that may be of use in the design and evaluation of ankle endo-prostheses.

1.3 Anatomy of the Ankle

1.3.1 Introduction

The anatomy of the normal ankle will be briefly presented. It is hoped that this will make the later discussions more easy to understand for the lay reader. Where greater detail is required the reader is referred to the anatomical texts of Warwick and Williams (1973), Calliet (1974) and Shoji (1977). In general the anatomical terminology presented in Warwick and Williams will be used.

1.3.2 Definition of Motions at the Upper and Lower Ankle Joints

The terminology used in the literature when referring to motion at the upper or Talocrural joint (hereafter Tc. joint) and the lower or Talocalcaneonavicular joint (hereafter Tcn. joint) is often confusing. The main reason for this is that the foot components and articulations are oblique to all the standard anatomical reference planes. The terms used in this study to refer to the major motions occurring at the Tc. and Tcn. joints are here defined to avoid ambiguity.

In figure 1.1(a) the tibia and fibula are regarded as fixed and Tc. axis is defined by a vector. Looking along the positive direction of the vector, motion of the talus about the Tc. axis in an anticlockwise direction (arrow A) is defined as Extension or Dorsi-flexion; motion in the opposite sense (arrow B) as Flexion or Plantarflexion.

In figure 1.1(b) the talus is considered as fixed and the Tcn. axis is defined by a vector. Looking along the positive direction of the vector, rotation of the hindfoot about the Tcn. axis in an anticlockwise direction (arrow A) is defined as Eversion, whilst the opposite motion (arrow B) as Inversion. The question of axes and their definition will be discussed in 2.2.

In addition the term Pronation is used to describe the simultaneous motions of dorsiflexion plus eversion and Supination to describe plantarflexion plus inversion. It is common practice in the literature to use these terms for describing gross movements of the whole foot relative to the shank.

The terms medial and lateral are illustrated in figure 1.1(a), medial being the side of the leg nearer to the midline of the body and lateral referring to the side further from the midline. Anterior and posterior mean front and back respectively.

1.3.3 Surface Anatomy

Many internal structures of the shank and foot can be seen as surface features or may be palpated through the skin and fascial layers. Such features are of particular use to the bioengineer when siting surface markers in order to define the approximate

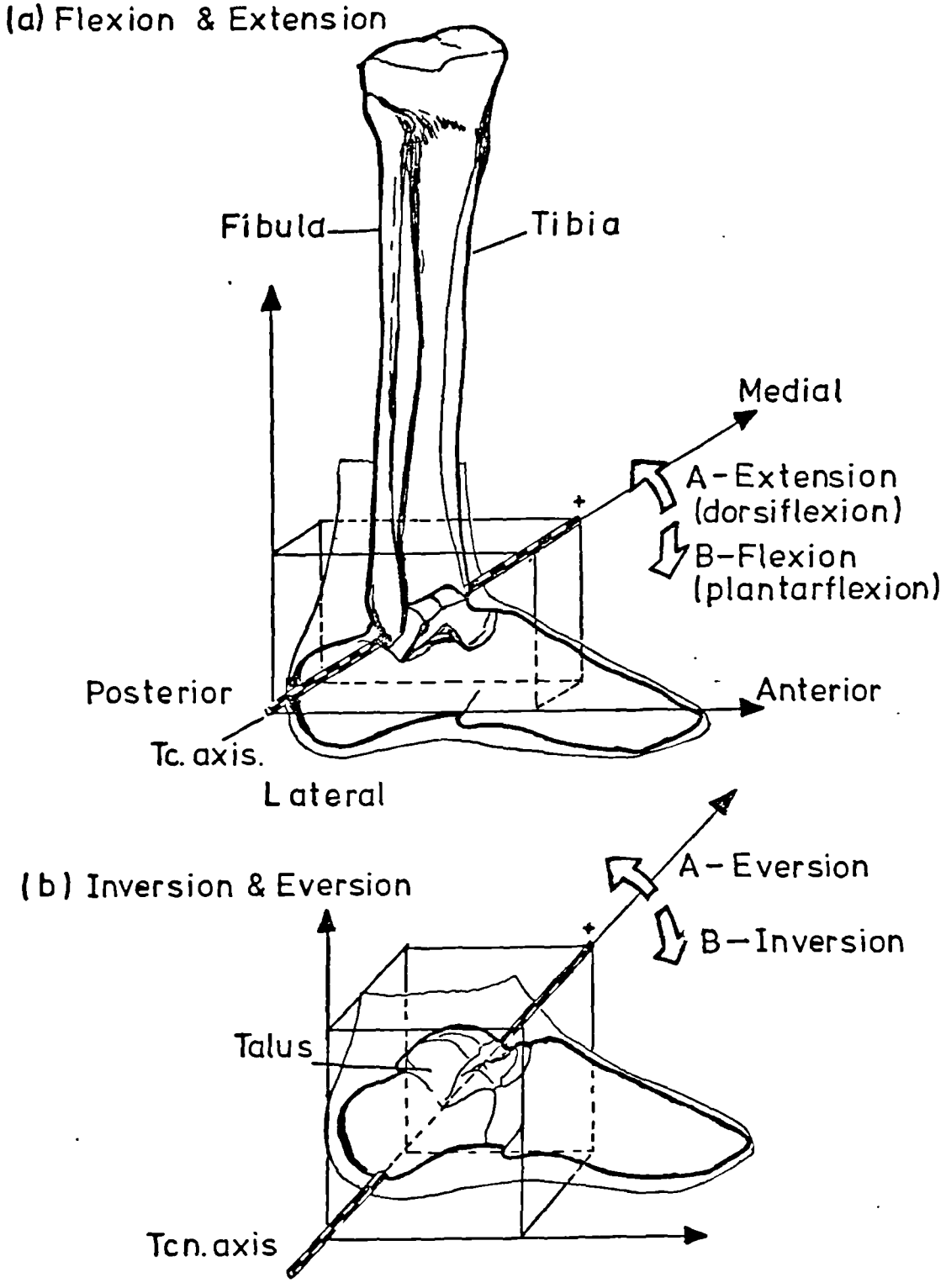

Figure 1.1 Motions at the Upper (Tc.) and Lower (Tcn.) Ankle Joints shown in the Right Foot

location of internal structures. The landmarks of special interest in the present study are annotated in figure 1.2. The surface anatomy is treated in greater depth by Shoji (1977) and Royce (1965).

1.3.4 Bones of the Shank and Foot

The bones of the foot divide into three segments, tarsal, metatarsal and phalangeal, as shown in figure 1.3. The tarsus is composed of seven bones; talus, calcaneus, cuboid, navicular and three cuneforms. The talus and calcaneus form the hindfoot and the remainder of the foot is referred to as the forefoot, although other divisions are possible (Calliet, 1974).

The Talus: This rests on the calcaneus and navicular bones. The talar trochlea (the superior aspect of the body) articulates with the tibia and fibula, see figure 1.4. The medial talar surface articulates with the medial malleolus of the tibia, the superior surface with the distal end of the tibia and the lateral surface with the lateral malleolus of the fibula. The trochlea is generally wider anteriorly than posteriorly, the functional interpretations of this feature are discussed in 2.4.2.

Posteriorly the talus has two tubercles separated by a shallow groove. The tubercles are insertion areas for ligaments whilst the groove acts as a pulley surface for the flexor hallucis longus muscle; the talus has no direct muscular attachments.

The talar neck projects anteriorly and the head forms a shallow spherical joint with the navicular whilst underneath it forms a shallow joint with the anterior superior calcaneal facet. These two articulations

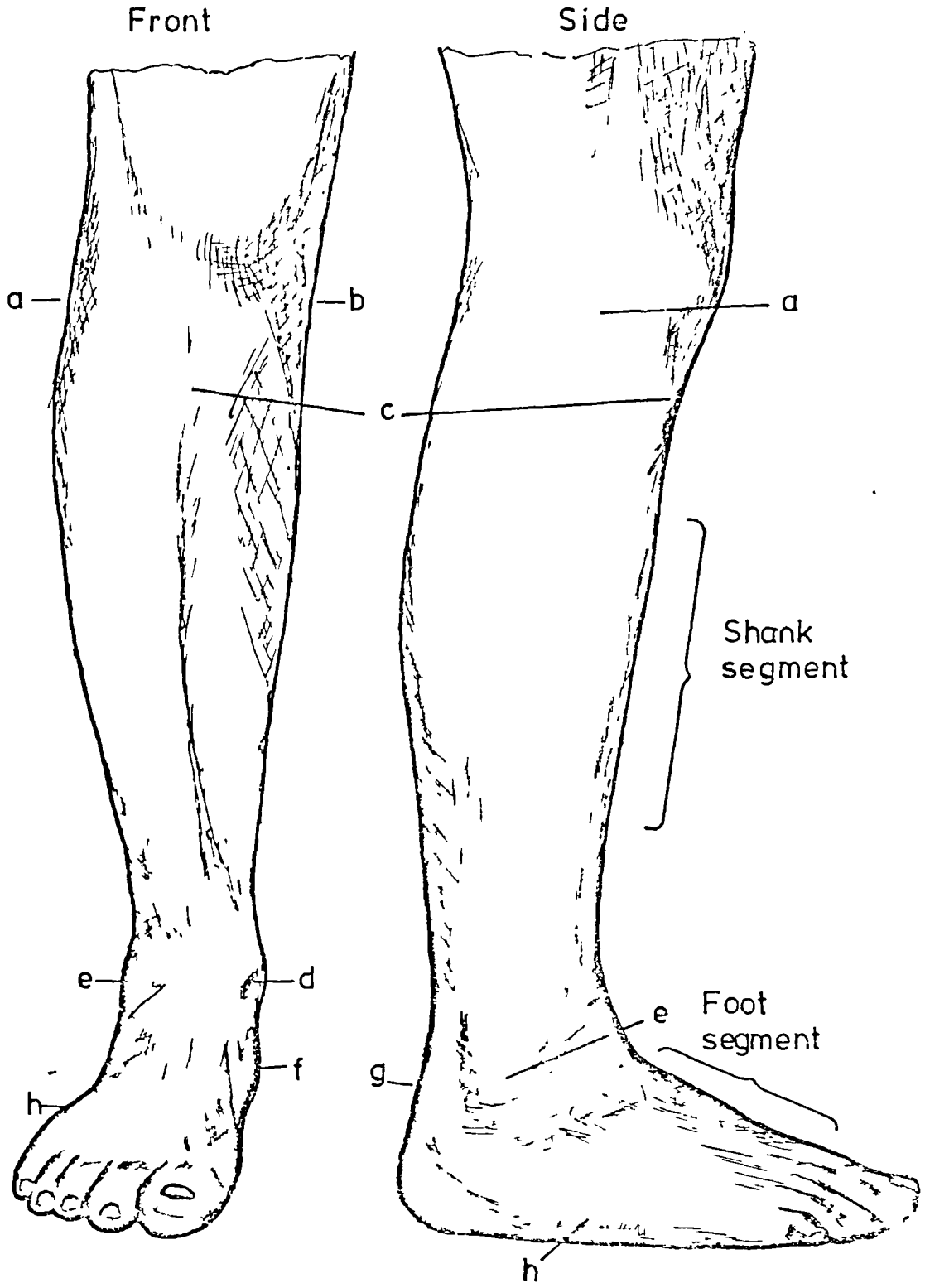

Key: a - Lateral condyle, b - Medial condyle, c - Tibial tubercle, d - Medial malleolus, e - Lateral malleolus, f - Navicular tuberosity, g - Insertion of achilles tendon, & h - base of metatarsal five.

Figure 1.2 Front and Side Views of the Right Shank and Foot

(a) Medial view

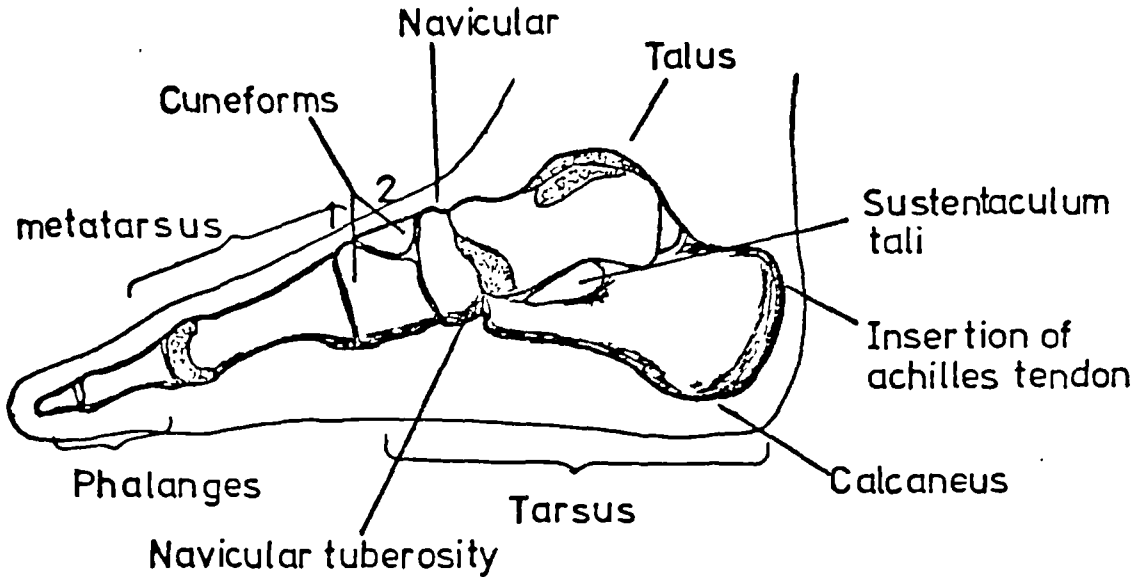

(b) Lateral view

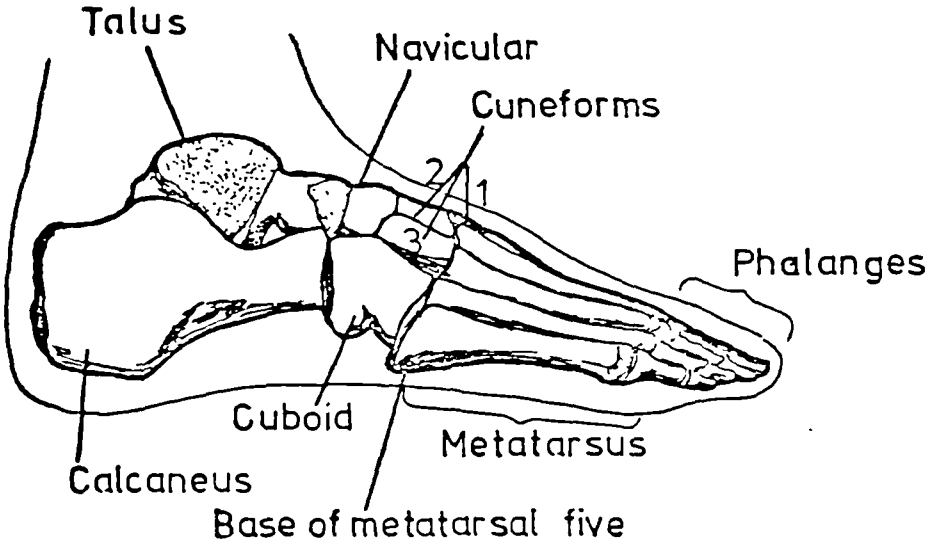

(c) Superior view

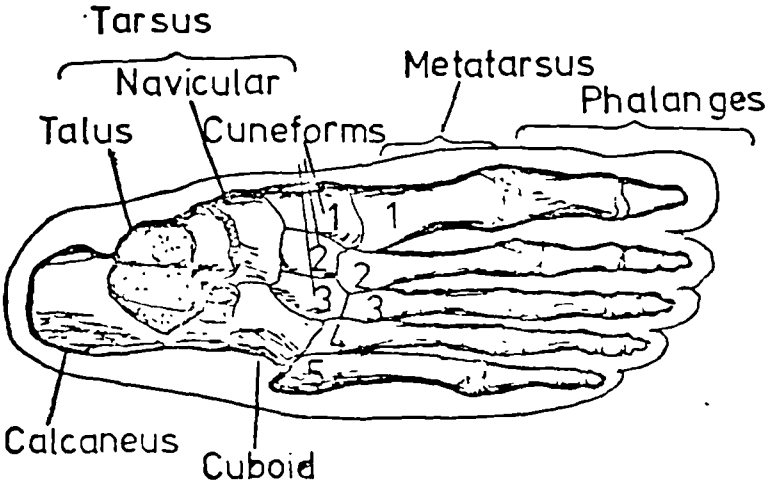

Figure 1.3 Bones of the Foot

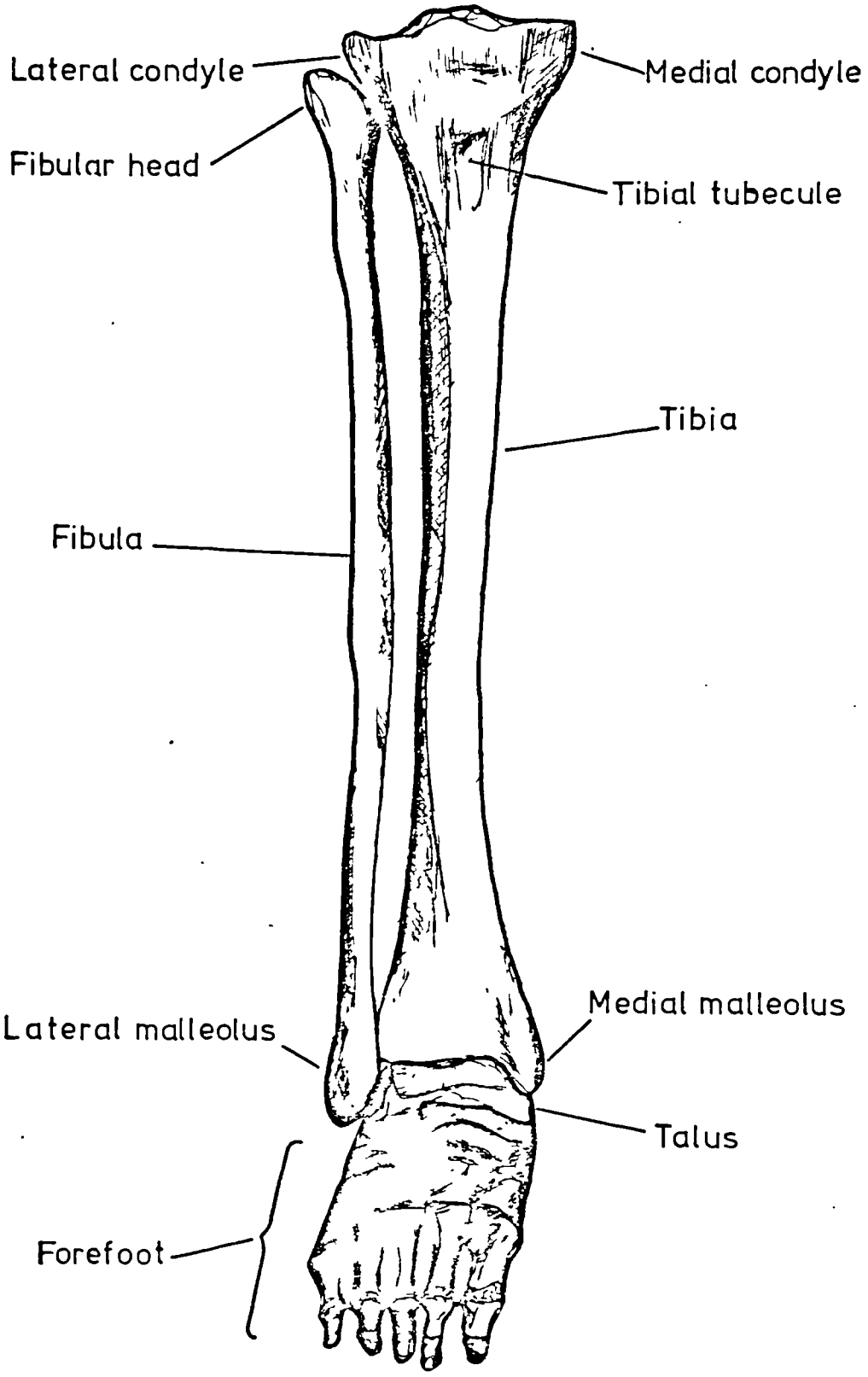

Figure 1.4 Fibula and Tibia - Anterior View of Right Leg

share the same joint capsule. The remaining talar articulation, the posterior talocalcaneal joint is also underneath. On the talus the posterior talocalcaneal joint is concave, whilst the anterior talocalcaneal and talonavicular joints are convex, see figures 1.5(a), (c) and (d).

The talocalcaneal facets are separated by a channel - the sinus tarsi - of which the talar portion forms the roof and the calcaneal portion the floor. This canal carries nervous and vascular trunks as well as ligamentous structures, see figure 1.5(a).

The Calcaneus: This is the heel bone; in addition to the articulations that it shares with the talus, it projects anteriorly to articulate with the cuboid bone. Medially it has a bony projection, the sustentaculum tali (see figure 1.3), which forms an anchor point for the medial ligaments and inferiorly forms a pulley surface for flexor hallucis and flexor digitorum longus muscles. Underneath, the calcaneus is the origin for many of the deep structures of the sole of the foot. The posterior surface is the insertion point for the largest group of shank muscles, the Calf group, which insert via the achilles tendon, see figure 1.8.

The Cuboid: The posterior surface articulates with the calcaneus, anteriorly it articulates with the fourth and fifth metatarsal bones and medially with the third cuneform, see figure 1.3. The medial surface is very close to the navicular bone but usually has no common articulation, the gap between the two being made up by strong interosseous ligaments. The tendon of the peroneus longus tendon passes over a groove on the lower surface of the cuboid, see figure 1.7(c).

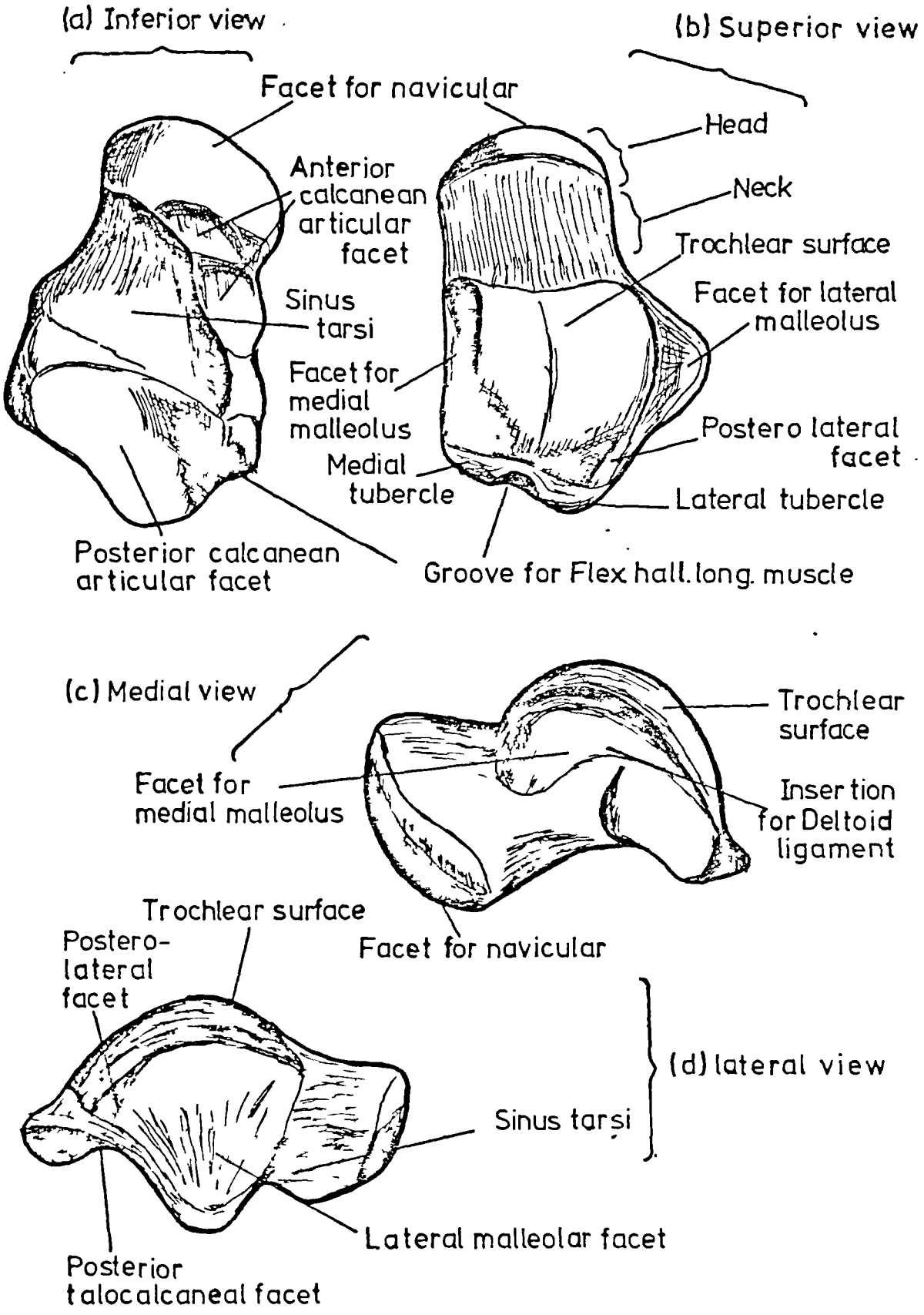

Figure 1.5 Detail of the Right Talus and its Articular Surfaces

The Navicular: This articulates posteriorly with the head of the talus and anteriorly with the three cuneforms. The medial surface has a palpably large prominence, the navicular tuberosity, which is the main part of the insertion of the posterior tibial muscle, see figure 1.3(a) and (c).

The Cuneforms: These are three squat bones, their articulations with the talus and cuboid have already been mentioned. There are two intercuneform articulations, one between cuneforms one and two and another between cuneforms two and three. The cuneforms articulate anteriorly with the first three metatarsals, see figure 1.3(c).

The Metatarsus: This segment consists of five bones. They are all similar in shape, and each has an articulation proximally with the tarsus and distally with the phalangeal segment. Metatarsal five has a prominent tuberosity at the base, which is the insertion of the peroneus brevis muscle, see figure 1.3(b).

The Phalanges: There are fourteen phalangeal bones, making up the five toes. The great toe has two phalanges, the remaining toes having three phalanges each.

1.3.5 Functional Joints of the Tarsus

The Tc. and Tcn. joints have already been briefly mentioned (1.3.2). The Tc. joint is made up of all the articulations common to the fibula, tibia and the talus; it is usually described as a hinge joint, the axis of the hinge being approximately defined in figure 1.1(a).

The Tcn. joint comprises all the articulations common to the talus, navicular and calcaneus; this is also usually described as a simple hinge joint, the approximate axis being illustrated in figure 1.1(b).

In the literature different names have sometimes been associated with the Tcn. joints, for example Subtalar and Peritalar. Subtalar has sometimes been used to describe the talocalcaneal articulations only, but since there is general agreement that talocalcaneal and talonavicular articulations function together, the more embracing name Talocalcaneonavicular will be used.

The talonavicular and calcaneocuboid joints are considered to have closely linked functions, and are referred to together as the Transverse tarsal joint (hereafter Tt); the movements at the Tt joint are too complex to be considered as the action of a simple hinge. These movements are examined in 2.2.4.

It is generally thought that the main movements of the tarsal bones are confined to the Tc., Tcn. and Tt. joints, the remaining tarsal bones are bound closely together by ligaments and have little independent freedom.

1.3.6 Ligaments of the Ankle Complex

The ankle complex of joints is reinforced medially and laterally by collateral ligament groups. The medial group, the Deltoid (shown in figure 1.6(b)), originates from the medial malleolus and has five bands inserting on the calcaneus, talus and navicular. The bands divide into a deep layer - the deep anterior and posterior talotibial ligaments - and a superficial layer - the superficial posterior talotibial, tibiocalcaneal and tibionavicular ligaments. The functional behaviour of these bands is discussed in 2.6.2. Some of the superficial fibres insert on the calcaneonavicular ligament, (also called 'spring' ligament), which bridges the gap

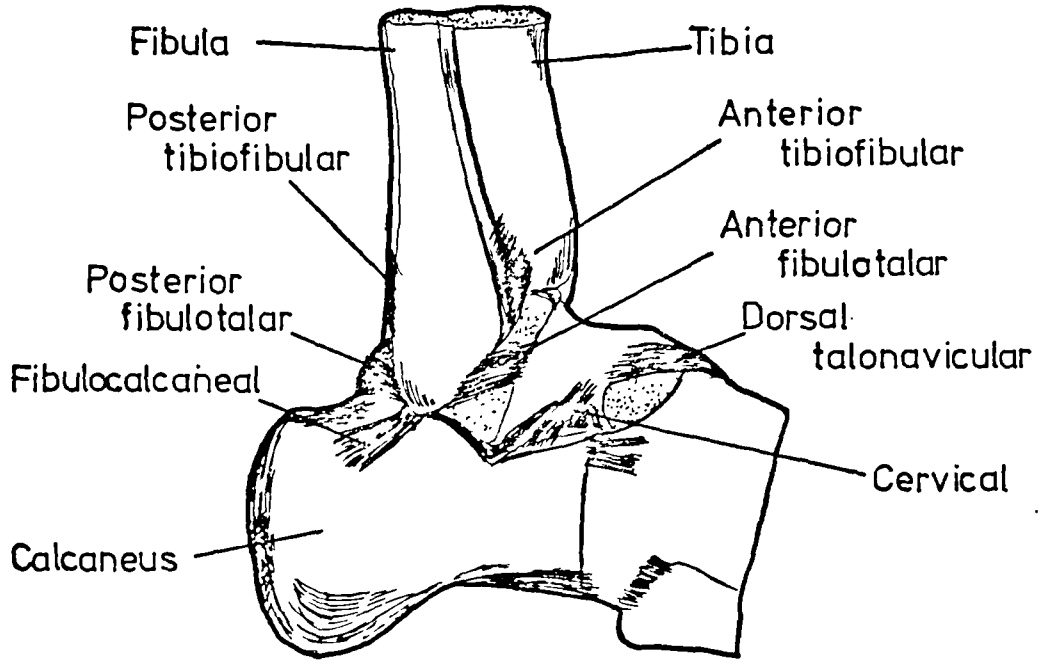

(a) Lateral ligaments

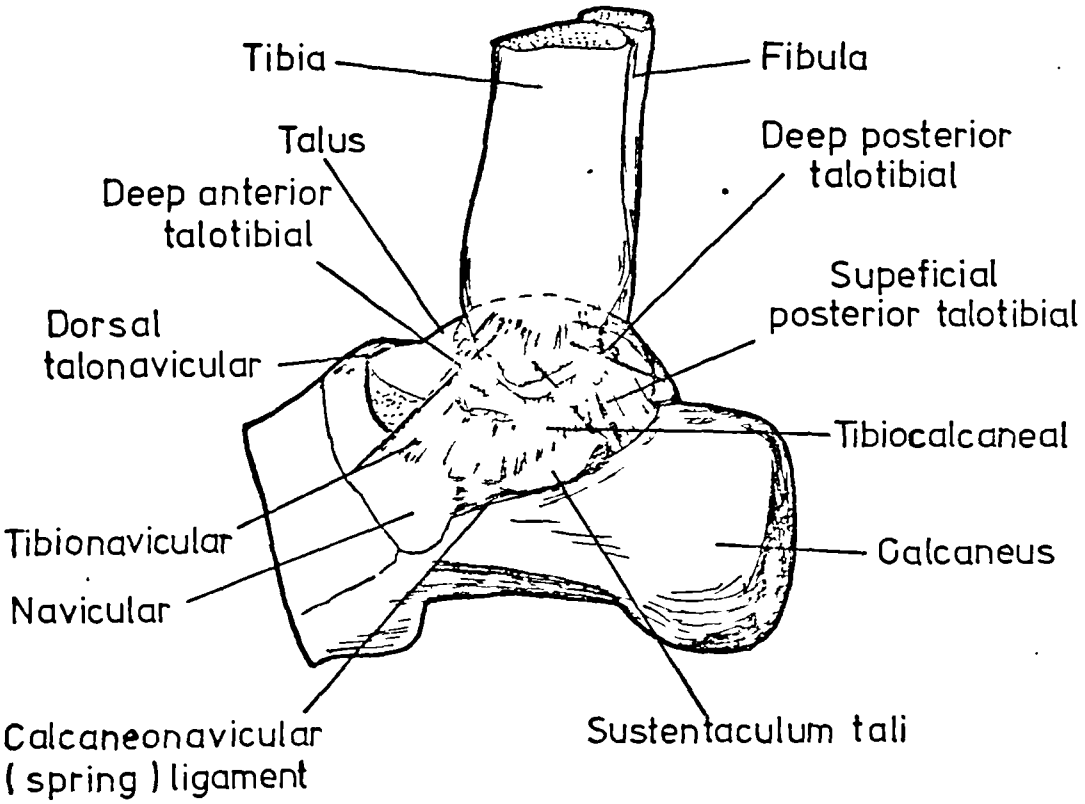

(b) Medial ligament components

Figure 1.6 Ligaments of the Right Ankle

between the calcaneus and navicular. This ligament also forms part of the Tcn. joint as it articulates with the underside of the talar head, and is lined with articular cartilage.

The lateral collateral group of ligaments is far more discrete than the deltoid and consists of three main bands, the anterior and posterior fibulotalar and the fibulocalcaneal as shown in figure 1.6(a).

Two ligaments which are also situated laterally are the anterior and posterior fibulotibial, these are very strong ligaments which unite the tibia and fibula closely whilst still allowing small relative movements.

Between the talus and calcaneus are the cervical ligament - a flattened band between the neck of the talus and the calcaneus - and the interosseous talo-calcaneal ligament. The cervical ligament (see figure 1.6(a)) is situated in the mouth of the sinus tarsi canal while the interosseous ligament is deep within the canal itself. These ligaments will be discussed in 2.6.4.

The talus has one further ligament the dorsal talonavicular, this is thin and sheetlike and blends in with the joint capsule.

1.3.7 Muscles of the Shank

The muscles of the shank and foot are divided geographically into those having both origin and insertion in the foot, the intrinsic musculature, and those having their origin in the shank but inserting in the foot, the extrinsic musculature. Interest in the present study is confined to the extrinsic muscles only.

The shank muscles divide into four groups anatomically,

on the grounds of innervation and the deep fascial compartments, and for another reason discussed in 2.7.3. There are twelve muscles altogether but two, plantaris and peroneus tertius, are small and sometimes entirely absent and so are neglected in the later work.

The four groups are: Calf and Peroneal, with two muscles each, and Posterior and Anterior tibial, with three muscles each. The individual muscles are illustrated in figures 1.7 and 1.8 and are tabulated together with their groupings in table 1.1. The Calf group is by far the largest and is exceptional for a shank muscle in having a common insertion, the achilles tendon, for its members, soleus and gastrocnemius.

In biomechanics muscles are frequently modelled by joining their origin and insertion and considering this to be the line of action. Amongst the shank muscles, soleus is the only muscle for which this is possible, all the other muscles (gastrocnemius included) pass over pulley surfaces deflecting so that origin and insertion are no longer in direct view of each other. For this reason discussion of the precise origin and insertion of each muscle is omitted.

The action of each muscle at the Tc. and Tcn. joints as it is most commonly reported in the literature is tabulated in table 1.1(a). Attention is drawn to the action of the anterior tibial muscle, tabulated as extensor-invertor, the inversion capability of this muscle is still in contention and it should be considered to be more or less neutrally placed with respect to the Tcn. axis, see 2.7.4. Accepting this the action of the groups on the free foot is as follows; Calf and Posterior tibial are flexor-invertors, the Peroneal is flexor-

Muscle / (a) Action	Calf group		Post. tibial group			Peroneal group		Ant. tibial group		
	Gastroc.	Sol.	Post. Tib.	Flex. Hall. Long.	Flex. Dig. Long.	Peron. Brev.	Peron. Long.	Ant. Tib.	Ext. Hall. Long.	Ext. Dig. Long.
Tc. Plantar-flexor	*	*	*	*	*	*	*			
Tc. Dorsi-flexor								*	*	*
Tcn. Invertor	*	*	*	*	*			*		
Tcn. Evertor						*	*		*	*
(b) Joint										
Knee	*									
Talocrural	*	*	*	*	*	*	*	*	*	*
Talocalcaneo-navicular	*	*	*	*	*	*	*	*	*	*
Transverse Tarsal			*	*	*	*	*	*	*	*
Metatarso-phalangeal				*	*				*	*

Table 1.1 Muscles of the Shank grouped by a) their action at the Talocrural and Talocalcaneo-navicular joints in the Free Foot
b) the principal joint systems crossed

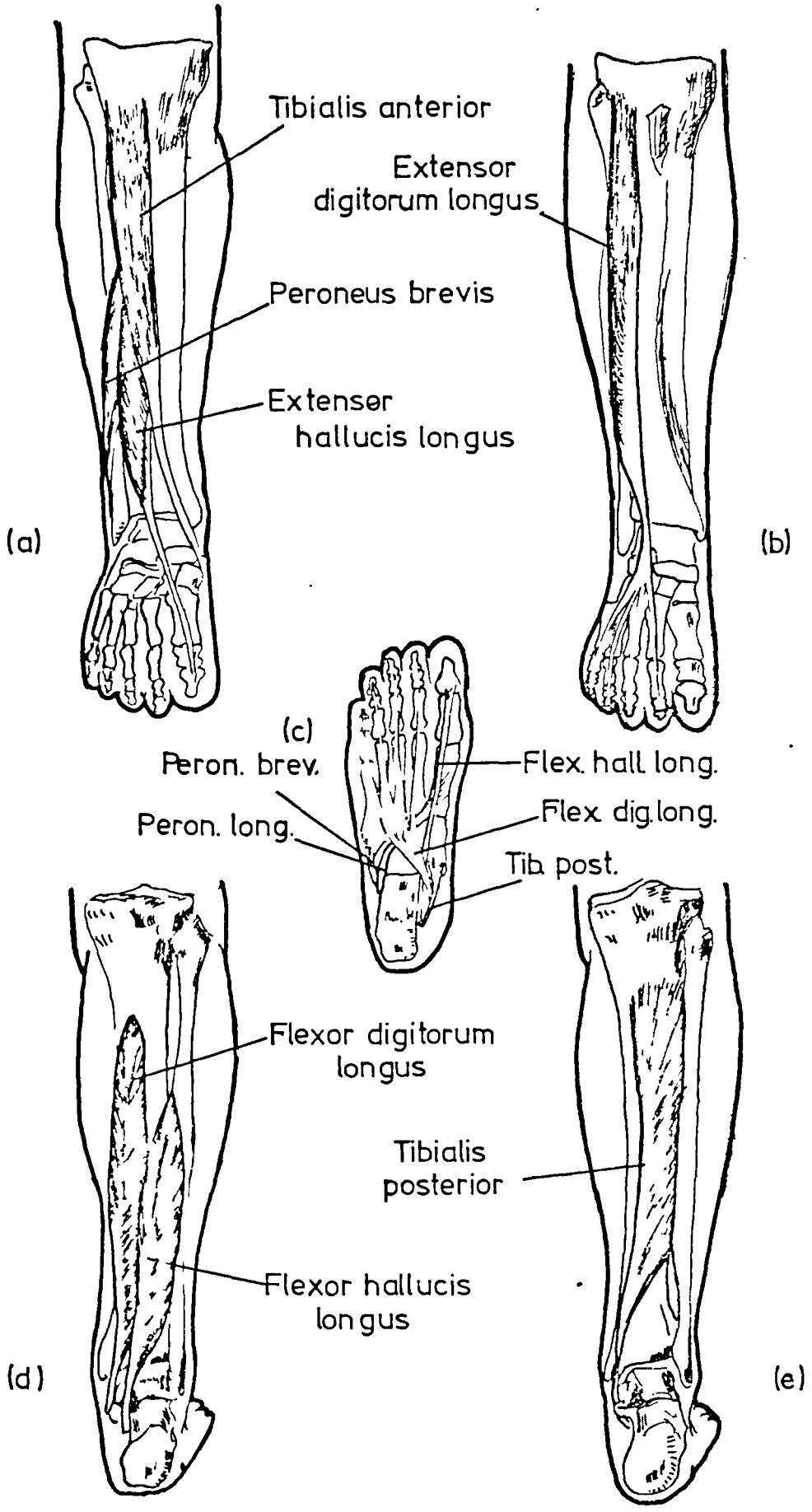

Figure 1.7 Muscles of the Shank - Right Leg

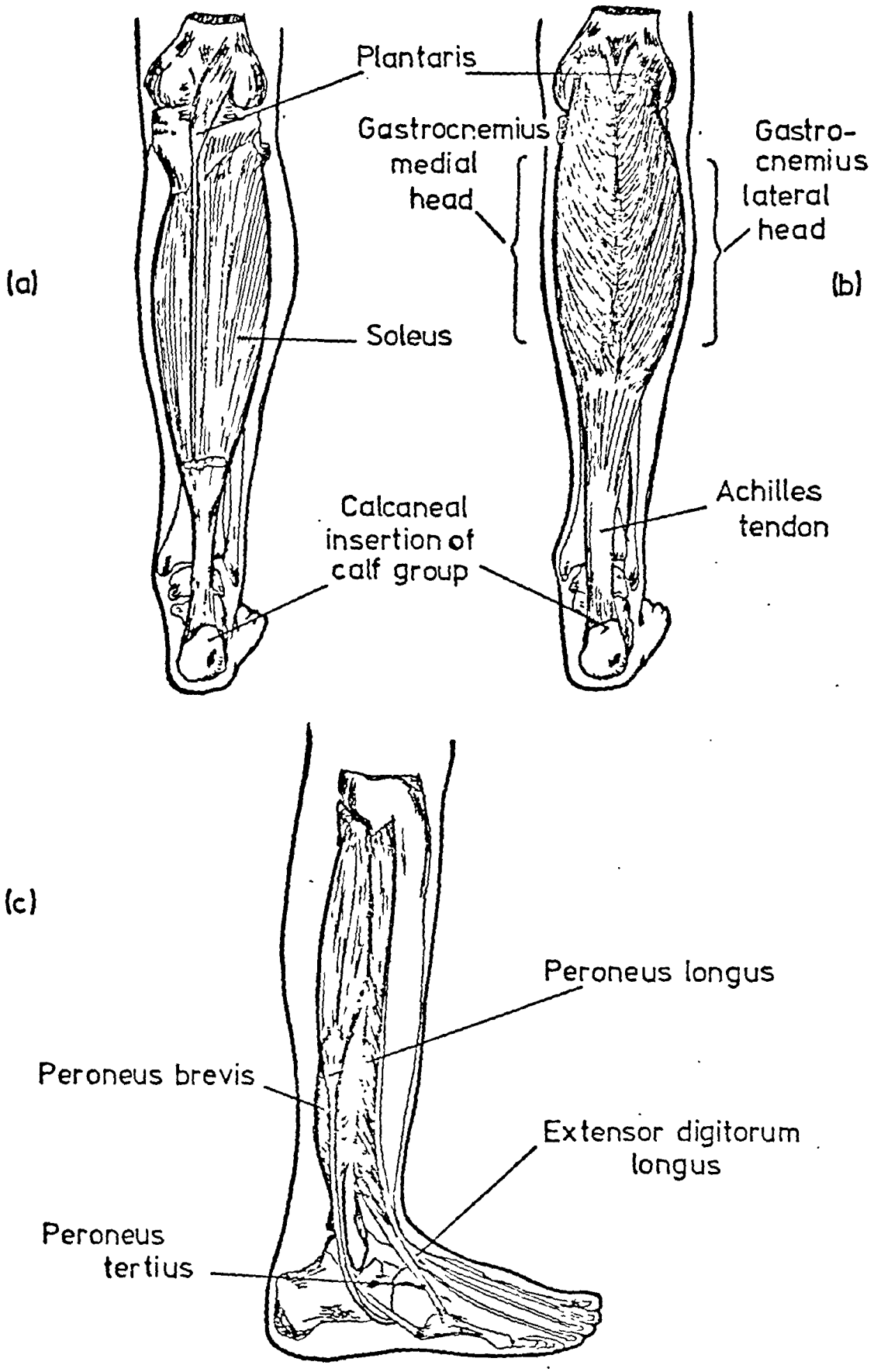

Figure 1.8 Muscles of the Shank - Right Leg

evertor and the Anterior tibial is basically extensor-evertor. The action of extensor-invertor is absent (excepting for the possible contribution of the anterior tibial muscle).

In table 1.1(b) the muscles are tabulated to show the number of principal joint systems crossed. The term 'Principal joint system' excludes such joints as the naviculo-cuneiform joints where very little motion occurs. Only one shank muscle, the gastrocnemius crosses the knee. The soleus is the only two joint muscle the rest crossing three to four joints using either bony or retinacular pulleys.

1.3.8 Retinacular and Bony Pulleys of the Shank and Foot

The shank retinacula are specialised thickenings of the deep fascia which have an important role in controlling the line of action of certain shank muscles. The most important anterior divisions are the superior extensor retinaculum, and the inferior extensor retinaculum which bifurcates into superior and inferior bands, see figures 1.9 and 1.10. The inferior extensor retinaculum has an important attachment to the calcaneus as shown in figure 1.11. The extensor retinacula control the line of action of the anterior tibial group of muscles.

The remaining retinacula are associated with the bony pulleys formed by the posterior inferior aspects of the medial and lateral malleoli. The Posterior tibial group use the medial pulley, tibialis posterior using the malleolor bony surface, flexor hallucis longus the posterior groove of the talus and the undersurface of the sustentaculum tali and flexor digitorum longus running between these two, see figure 1.9(b).

(a) Lateral view.

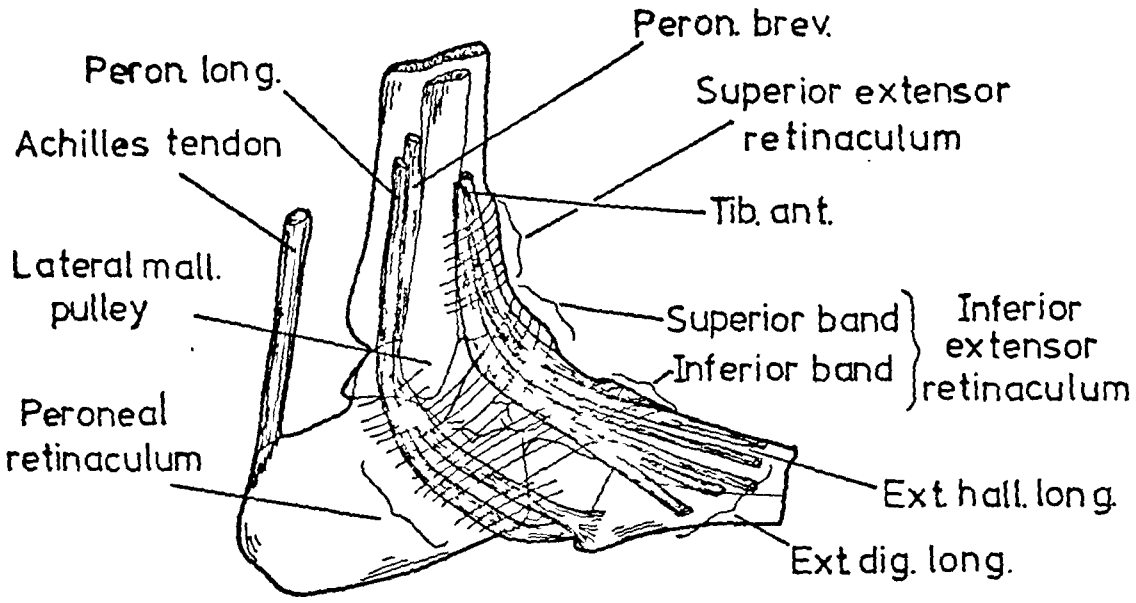

(b) Medial view.

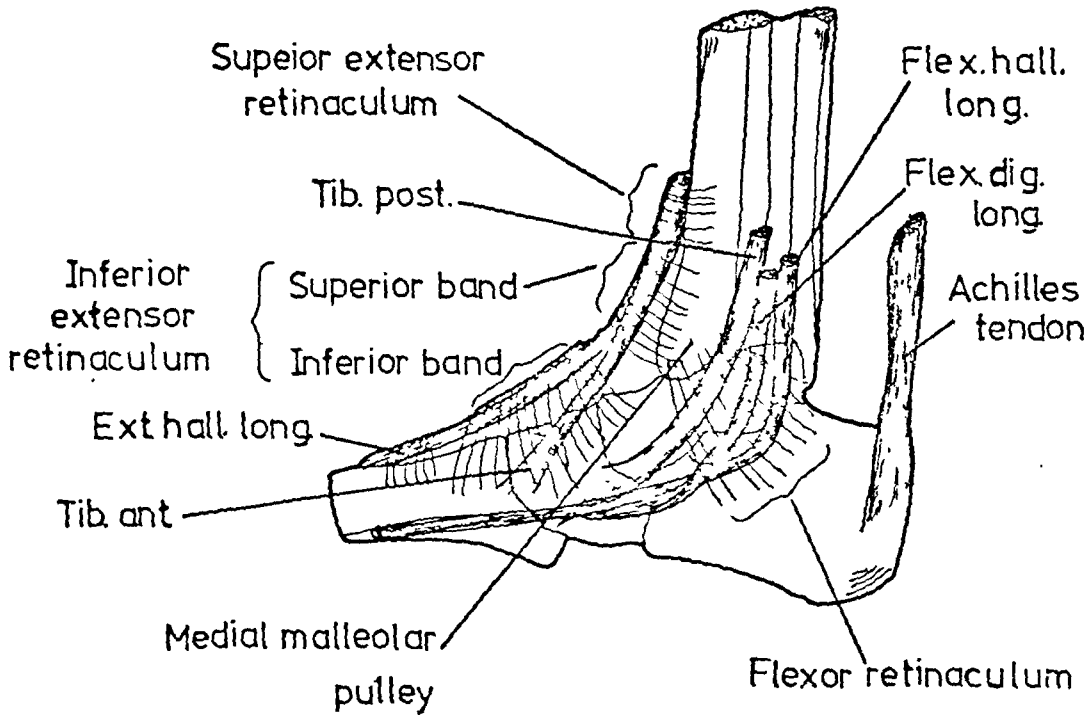

Figure 1.9 The Bony Pulleys and Retinacula of the Right Foot

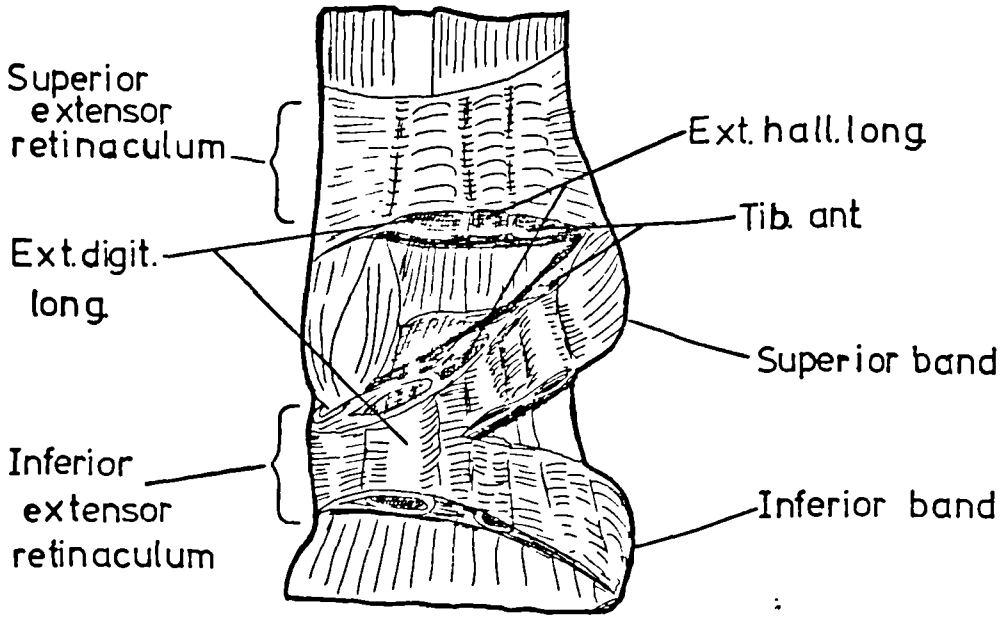

Figure 1.10 The Extensor Retinacula of the Right Ankle after removal of the Deep Fascia and the Extensor Tendons (After Wood-Jones, 1943)

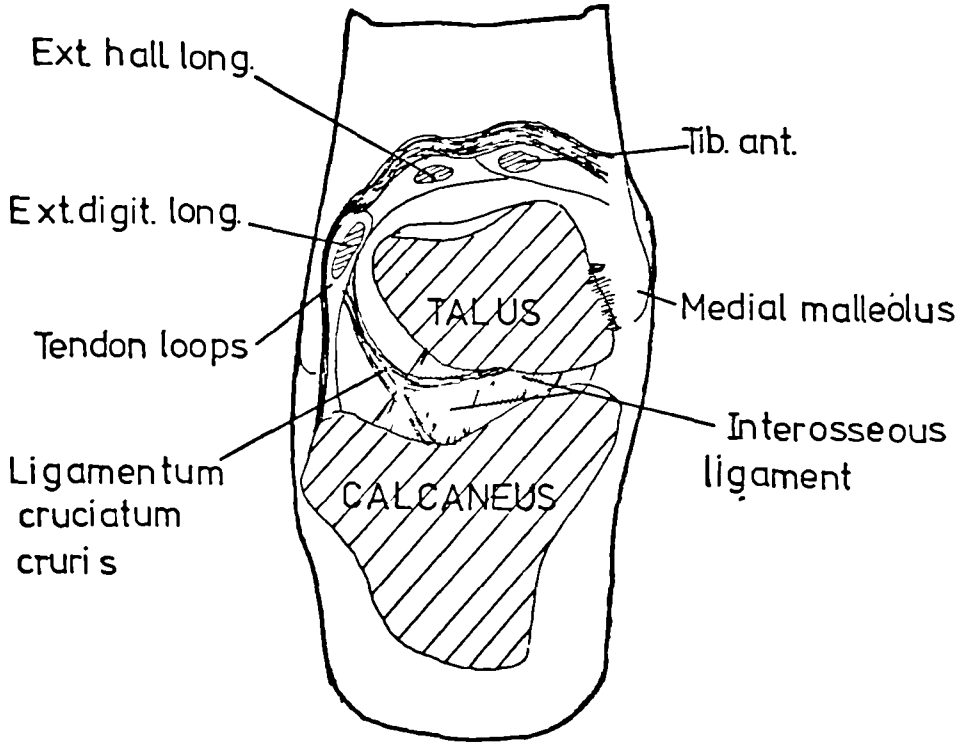

Figure 1.11 Oblique Coronal Section through the Posterior Part of the Right Foot to Illustrate the Ligamentum Cruciatum Cruris (After Stamm, 1931)

The Peroneal group use the lateral malleolor pulley, peroneus brevis is in close contact, whilst peroneus longus rides on top of brevis and uses it as a pulley surface, see figure 1.9(a).

Both the Peroneal and Posterior tibial groups are bound closely to the bony pulleys by retinacular bands which roof over the pulley paths.

The pulleys are all lubricated by synovial fluid produced by the lining of the pulley tunnels, and are virtually frictionless.

CHAPTER 2

REVIEW OF BIOMECHANICAL AND OTHER LITERATURE RELATING TO THE ANKLE

2.1 Introduction

It is the purpose of this chapter to review literature relevant to the study of biomechanics with particular reference to the Ankle joint.

2.2 Axes of the Ankle Complex of Joints

The literature relating to the ankle axes is extensive and virtually every source discussing the ankle joint refers to the axes. Inman (1976) comprehensively reviewed the literature concerned with determination and location of the ankle axes. The main studies contributing to debate in this area are reviewed below.

2.2.1 The Talocrural Axis

The view that the Talocrural joint functions as a single axis hinge joint has been questioned by Hicks (1953) and Barnett and Napier (1952).

Barnett and Napier studied 152 cadaver tali and measured the curvature of the talar trochlea medially and laterally. They found that the lateral profile was part of a circular arc but that the medial side consisted of two differing curvatures, see figure 2.1. They defined two axes by joining the lateral centre of curvature with the medial centres, the larger and smaller medial arcs corresponding to Plantarflexion and Dorsiflexion respectively. Hicks used a trial and error method, with pointers and bent wires, to establish axes positions in cadaver ankles and arrived at the same conclusion as Barnett and Napier. He defined both axes as passing through a circle 1 centimetre in diameter near the centre of the body of the talus, see figure 2.2.

Isman and Inman (1969) determined the position of

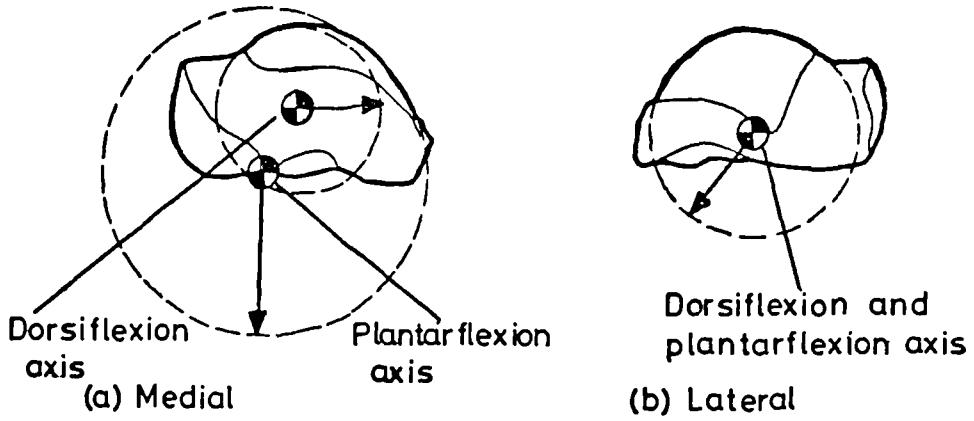

Figure 2.1 Illustration of the Medial and Lateral Profiles of the Right Talar Dome (After Barnett and Napier, 1952)

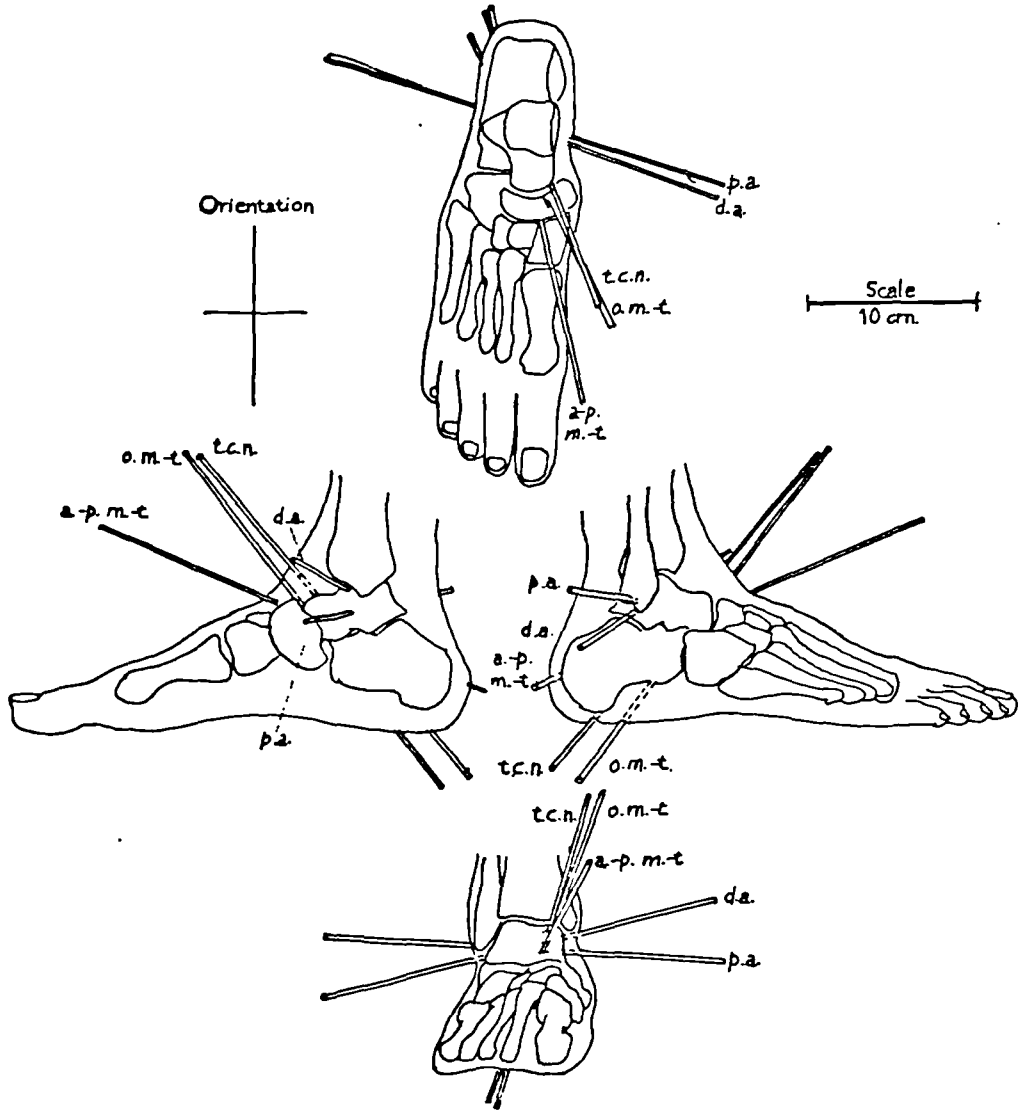

The ankle axes; *d.a.* dorsiflexion ankle axis; *p.a.* plantarflexion ankle axis; *t.c.n.* talo-calcaneo-navicular axis; *o.m.-t.* oblique mid-tarsal axis; *a.-p. m.-t.* antero-posterior mid-tarsal axis.

Figure 2.2 The Ankle Axes (After Hicks, 1953)

the Tc. and Tcn. axes on forty-six cadaver ankles using a simple optical technique. They concluded that both the Tc. and Tcn. joints could be considered as single axis joints, for the purposes of orthopaedic bracing, but that the variation in the positions of the different axes is such that they require individual determination. They further concluded that the use of certain skeletal landmarks, for example the malleoli, to determine the axis of the Tc. joint appeared to be feasible. The results that they obtained for the relations between the Tc. axis and the most medial point and the most lateral point of the medial and lateral malleoli, respectively, are reproduced in figure 2.3.

Elftman (1969) reviewed dynamic behaviour of the human foot and suggested that the concept of an invariant Tc. axis needed revision. He drew attention to the results of Barnett and Napier (vide supra), and Close and Inman (1952) who showed that the talus may be able to rotate about an axis corresponding to the long axis of the tibia. Elftman proposed that the Tc. and Tcn. axes should be combined as an instantaneous axis capable of changing in position rather than as independent axes.

Sammarco et al (1973) used instant centre of rotation analysis to determine the Tc. axis position from sequential two-dimensional X-ray views of the ankle. They contend, from their experimental results, that "there does not exist a single or even a double axis of rotation". However they only used five views between full-flexion and extension and, as Inman (1976) comments, this makes their findings somewhat questionable.

Inman (1976) reappraised the question of a single axis, using similar techniques to his 1969 study, together

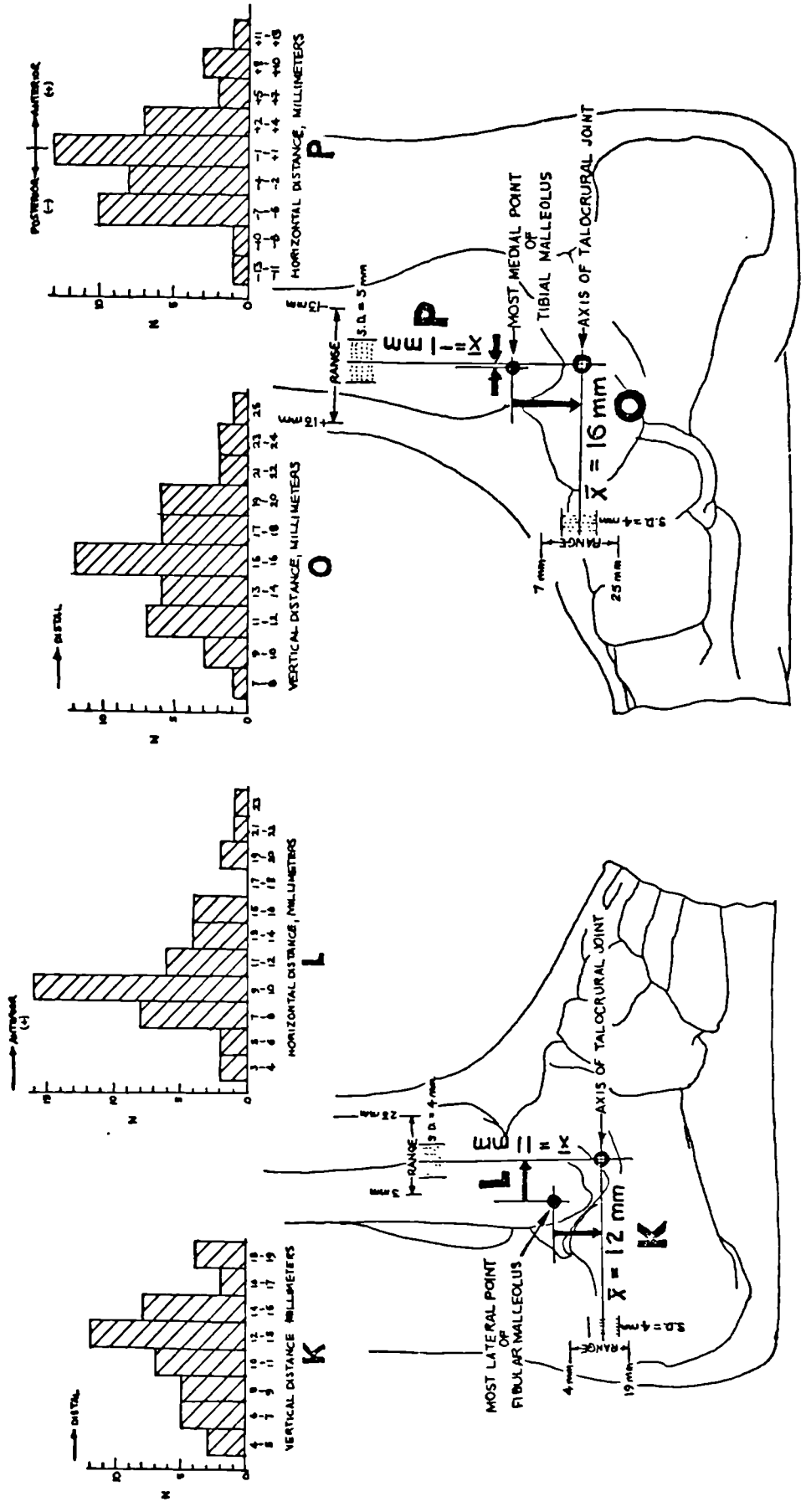

Figure 2.3 The Location of the Talocrural Joint Axis with Respect to, (a) the Most Lateral Point of the Lateral Malleolus and (b) the Most Medial Point of the Medial Malleolus

with a review of reported literature and concluded that, "for all practical purposes, motion at the ankle joint can be considered to be about a single axis". He stated that the Tc. axis is inclined by 10° to the horizontal sloping downward from medial to lateral, and 96° to the midline of the foot sloping backwards from medial to lateral as shown in figure 2.4.

2.2.2 The Talocalcaneonavicular Axis

The Tcn. joint is considered to act as a single hinge, Manter (1941), Hicks (1953), Lapidus (1955), Isman and Inman (1969) and Inman (1976). The reported Tcn. axis is oblique to the anatomical reference planes and the absence of defined reference points in the foot makes comparison of the reported Tcn. orientations difficult - results due to Manter, and Isman and Inman are illustrated in figure 2.4.

Isman and Inman concluded that there appeared to be no accurate method of determining the axis of the Tcn. joint from skeletal landmarks in the living subject. The position of the axis is most frequently given as a line joining the posterolateral tubercle of the calcaneus and the medial aspect of the talar neck (Hicks, 1953; Close and Inman, 1953), see figures 2.2 and 2.4.

2.2.3 The Transverse Tarsal Axes

In contrast to the Tc. and Tcn. joints the Tt., also referred to as midtarsal, is considered to be biaxial, Manter (1941), Shephard (1951), Hicks (1953), Lapidus (1955) and Bojsen-Møller (1979). The first axis is located longitudinally in the foot passing slightly upwards from posterior lateral to anterior medial,

(a) Superior view

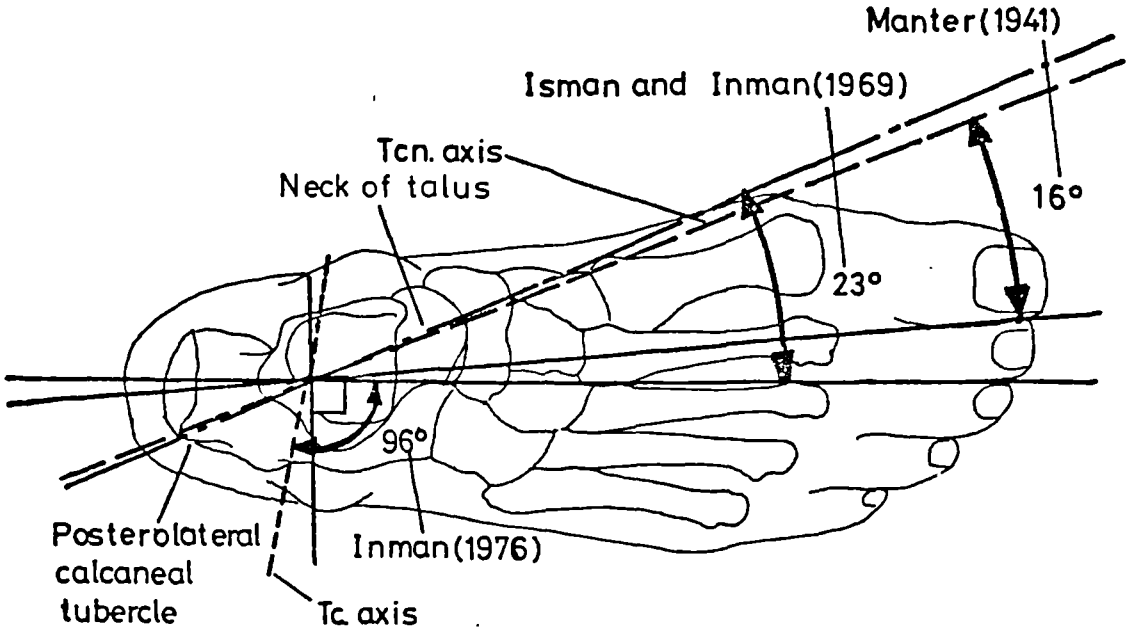

(b) Lateral view

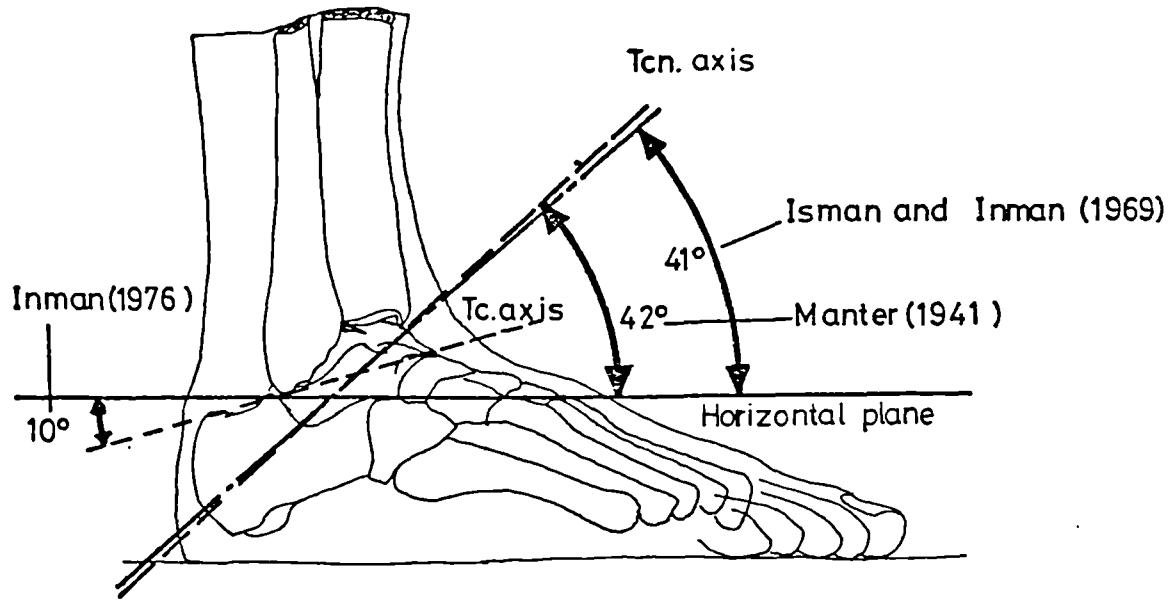

Figure 2.4 The Tc. and Tcn. Axes Projected on the Right Foot

inclined at ≃15° to the horizontal (Manter). The second axis, the transverse also called oblique, passes downward posterolaterally through the head of the talus and the anterior calcaneus. These axes are illustrated in figure 2.5, adapted from Manter. There are slight differences between this illustration and others reported in the literature but since these sources do not quote quantitative data no direct comparison is possible.

2.2.4 Motions Occurring About the Axes and Reported Ranges

The motions occurring about the axes will be discussed concurrently since it is thought that the ankle axes are closely linked in their function.

The principal action at the Tc. joint is flexion and extension. The largest range of motion reported for the free foot is 48° plantarflexion and 51° dorsiflexion (Glanville and Kreezer, 1937). The range reported for normal locomotion is much less, about 30°, 20° in flexion and 10° in extension (Root et al, 1971; Murray et al, 1964; Wright et al, 1964; Close and Inman, 1952). Some secondary motions are attributed to the Tc. joint, the most significant of which is rotation of the talus in the tibiofibular mortise about the long axis of the tibia.

Barnett and Napier (1952) indicated that the talus rotated medially in the mortise at full plantarflexion; Close (1956) also observed this tendency and estimated its magnitude to be about 5-6°, the trend reversing during dorsiflexion. Close and Inman (1952) evaluated this in locomotion from the relative movements of pins implanted in the shank and talus. Their results showed about 6° movement of the talus relative to the mortise occurred between full internal and external rotation of

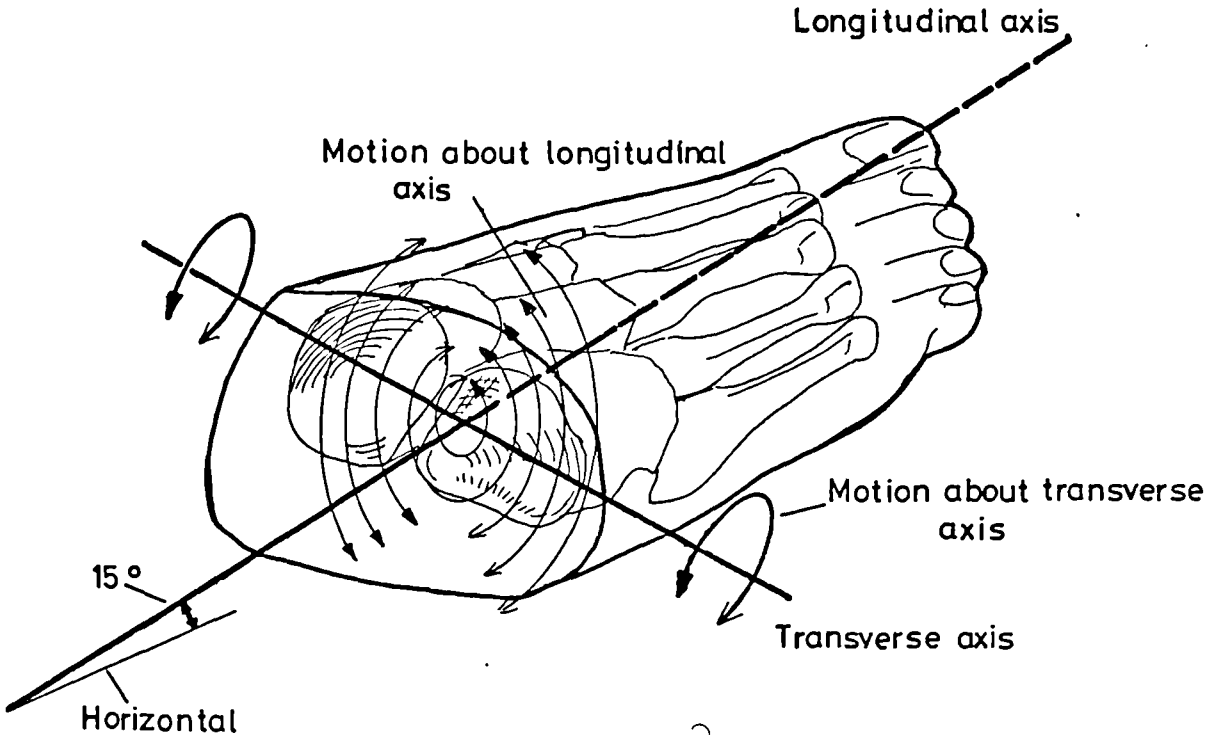

Figure 2.5 View of the Forefoot Illustrating the Transverse Tarsal Joint Axes and the Motions of the Forefoot Relative to the Hindfoot (Adapted from Manter, 1941)

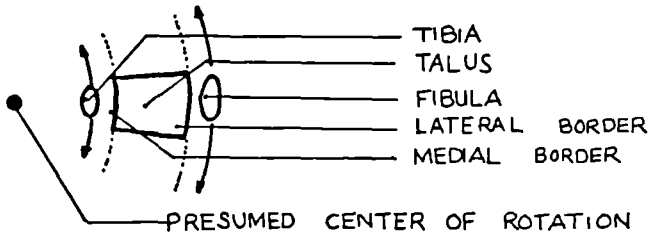

TALUS AS VIEWED FROM ABOVE

Figure 2.6 Illustration of the Mechanism Allowing the Tibia and Fibula to Rotate Axially Relative to the Talus

the shank relative to the foot. They found that little or no separation of the malleoli occurred during this motion and concluded that it must be due to the tibia and fibula rotating on the talus. They suggested that the motion took place mainly at the lateral malleolus, the medial malleolus being less mobile, see figure 2.6 illustrating their model for this effect; Laurin and Mathieu (1975) also subscribed to this view.

The principal action at the Tcn. joint is inversion and eversion. Inman (1976) examined free motion about this axis in 100 subjects and reported a range of 20°-65° with 40° mean. The locomotion studies of Wright et al (1964) and Close and Inman (1953) indicate a range of 10° in walking - divided almost equally between inversion and eversion. Close and Inman concluded that motion at the Tcn. joint is virtually absent during the 'propulsion' phase of locomotion.

The actions at the Tt. and Tcn. joints are thought to be very closely linked. Manter and Elftman (1935) state that motion occurs simultaneously at the Tt. and Tcn. joints and that this is only possible because their common articulation, the talonavicular joint, is spherical with the Tcn. and transverse Tt. axes intersecting at its centre of curvature.

The motion about the Tt. transverse axis, illustrated in figure 2.5, is thought to add to the range of plantar-flexion and dorsiflexion obtaining at the Tc. joint (Manter, 1941). Hicks (1953) measured a mean range of 22° in cadaver specimens, however the range of transverse axis motion occurring in locomotion is thought to be very small (Close and Inman, 1953).

Motion about the Tt. longitudinal axis, see figure 2.5,

is thought to contribute to the range of inversion and eversion at the Tcn. joint. Lapidus (1955) attributed this inversion eversion freedom to 'limited' gliding mobility at the Calcaneocuboid joint, and Manter (1941) suggested that this freedom was effectively restricted by ligaments. Hicks (1953) recorded a range of 8° for cadaver feet and put forward the view that the longitudinal axis allowed rotation to occur between the hind and fore foot. The working range during normal locomotion is reported to be about 6° (Root et al, 1971).

2.3 Fibular Load Bearing and Motion

Two areas of contention surround the fibula. Firstly there is the question of whether or not the fibula is involved in axial load bearing and secondly, the nature of fibular movements resulting from flexion-extension activity at the Tc. joint.

Lambert (1971) argued that the shape of the proximal and distal fibular articulations indicated that the fibula must be involved in axial load bearing. He measured surface strains, using strain gauges, on cadaver tibias and fibulas that were subjected to a static axial load approximating to body weight. He concluded from the measurement of five subjects that up to 1/6 Body Weight was transmitted through the fibula. This result must be treated with some reserve since the application of strain gauge methods under such circumstances is suspect. In addition the fibula would be considered a 'slender' column, from the engineering viewpoint, and as such liable to buckle under axial load; the normal curvature of the fibula would predispose to this. The interosseous membrane between the fibula and tibia may help to resist

buckling.

The contention that significant fibular movement resulted from flexion-extension activity at the Tc. joint arose through observation that the talar trochlea is wider anteriorly than posteriorly (comprehensively discussed by Inman, 1976). This observation implies that the talus is a tighter fit in the mortise during dorsiflexion than plantarflexion, or that the talus be a loose fit during plantarflexion, alternatively that there is some other accomodating mechanism - for example axial rotation of the fibula. The view that the fibula deflects laterally as the wider anterior portion of the talus enters the mortise was supported by Warwick and Williams (1973), Cedell (1975) and Scranton et al (1976). Widening of the mortise by up to 1.8 millimetres (1mm. mean) during locomotion was reported by Close and Inman (1952); Close (1956) repeated the measurement in vitro with essentially similar results.

Grath (1960) maintained that there was little or no physiological requirement for separation of the malleoli. After thorough experimental study of the ankle mortise he reported that no separation greater than 2 millimetres had been demonstrated for the dorsiflexion and plantar-flexion ranges of either the cadaver or living ankle. In addition clinical study of patients in whom the fibula and tibia had been united proximally by osseous union or screw had shown that such constraint of relative motion did not, in general, lead to joint symptoms.

The fibula is thought to rise a few millimetres, during dorsiflexion, due to the varying inclination of the lateral malleolar facet (Cedell, 1975; Calliet, 1974). An opposing view was advanced by Scranton et al (1975)

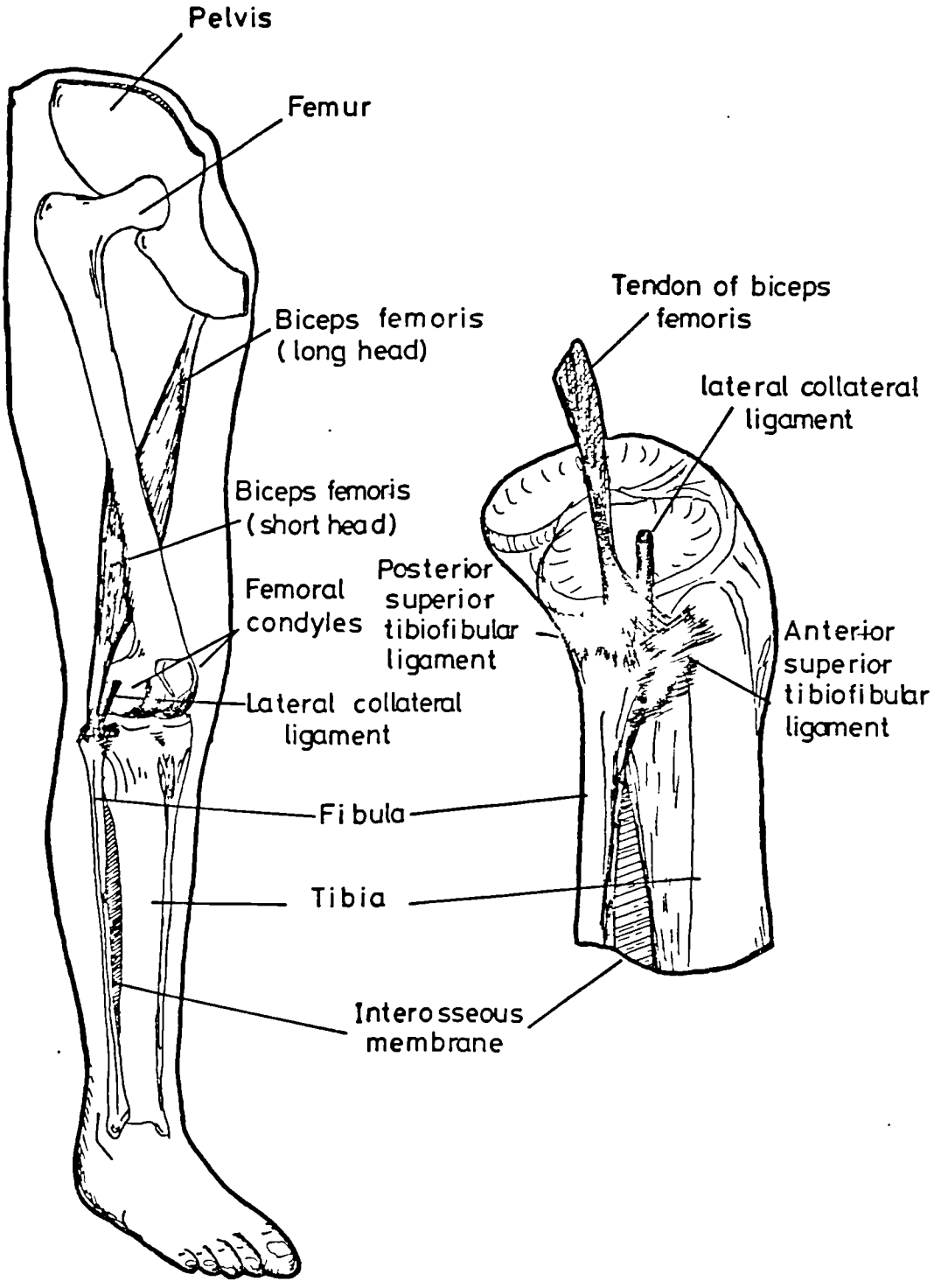

Figure 2.7 Illustrations of the Proximal Fibular Attachments

who contended that the fibula descends - dynamically through the action of shank muscles pulling distally on the fibula, and statically about 2.5 millimetres due to weight bearing compression of soft tissues. A few degrees lateral rotation of the fibula during dorsiflexion was suggested by Laurin and Mathieu (1975) as an alternative mechanism for accomodating the wider anterior talar portion in the mortise.

One factor frequently neglected in consideration of fibular motion is the proximal tibiofibular articulation and its relations, illustrated in figure 2.7. The lateral collateral ligament of the knee connects the lateral femoral condyle and the head of the fibula. In addition the hip muscle biceps femoris has two heads - longus and brevis - which have a common insertion into the fibular head. Thus fibular motion may be influenced actively by contraction of the biceps group and passively through tension in the lateral collateral ligament.

The author concludes that there is sufficient basis for assuming that the relative motion between the fibula and tibia is small enough to neglect in the present study.

2.4 Study of the Ankle Articulations

2.4.1 Introduction

The literature relating to the ankle articulations will be presented. The reader is referred also to Inman (1976) for a comprehensive review. Further description of the Tt. joint is omitted, because it is thought to be less important to the function of the ankle than the Tc. and Tcn. joints and was considered outwith the brief for the present study.

2.4.2 Talocrural Joint

The congruency of the Talocrural articulations was investigated by Inman (1976). The investigation included direct measurement of talar geometry and consideration of X-ray opaque dye arthograms of the Tc. joint cavity. His conclusions supported the view that the Talar trochlea fits closely in the Tibiofibular mortise for most of the mid range of motion of the talus, but is slightly incongruent at the extremes of dorsiflexion and plantar-flexion. Sewell (1904) implied that the Tc. joint was incongruent at the region of the triangular postero-lateral facet of the Talar dome, see figure 1.5 (b) and (d); Barnett and Napier (1952) and Lane (1887-1888) observed that this facet is actually opposed by a triangular pad of soft tissue, the distal part of the tibiofibular ligament, see figure 2.8.

The contact areas in the Tc. joint were investigated by Greenwald et al (1977). They adapted the results of Isman and Inman (1969) and Brewster et al (1976), who had established geometric and normal locomotion load bearing criteria, respectively, for the Tc. joint. In their experiments cadaver legs were subjected to a sequence of five axial loads corresponding to five instants between heel strike and toe off. A reversible staining technique was employed to indicate the contact areas of the Tc. joint. They contended that their study established the Tc. joint as an incongruent articulation, particularly so in early stance. The maximum contact area recorded, at a position equivalent to locomotion mid-stance, was $13.3 \pm 1.7 cm^2$ for a corresponding pressure of 232 ± 14 N/cm^2 (axial load $\simeq$ 3100N). They did not comment upon how their results would be influenced by the shearing forces

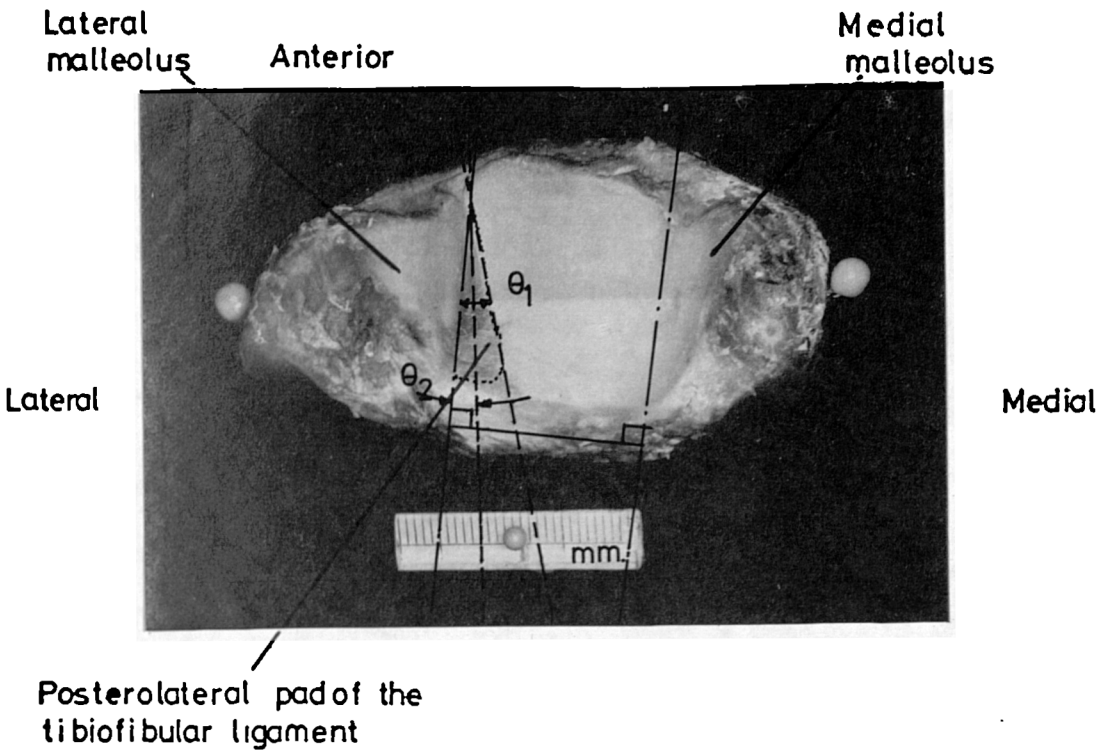

Figure 2.8 Inferior View of the Tibiofibular Mortise

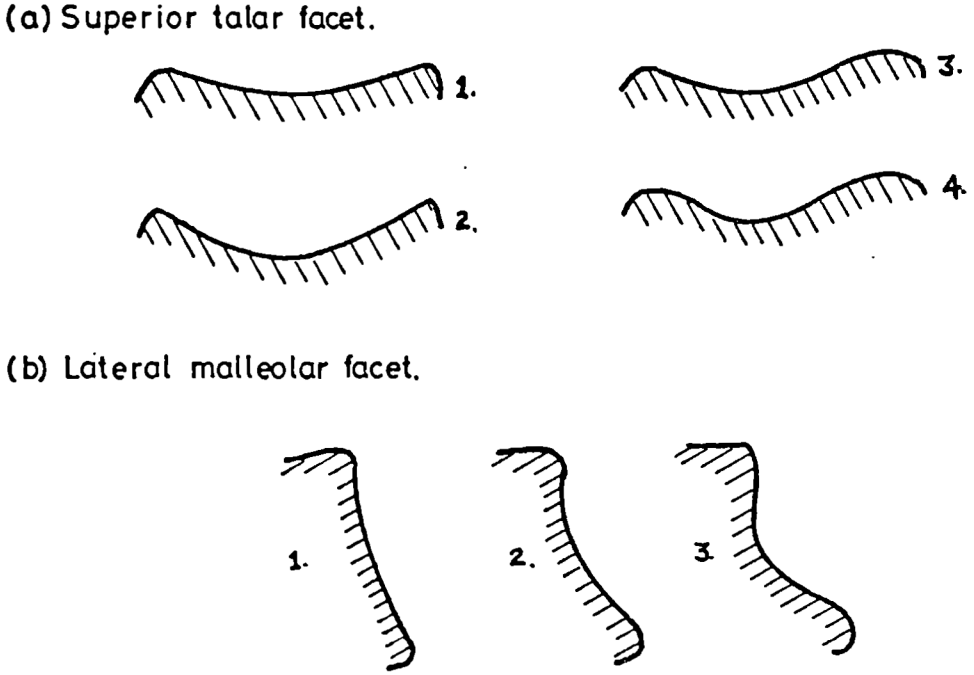

Figure 2.9 Mediolateral Talar Profiles (After Sewell, 1904)

and moments transmitted by the Tc. joint. In an essentially similar study, Ramsey and Hamilton (1976) considered the effect of laterally displacing the talus relative to the tibiofibular mortise on the contact areas of the superior talar facets. In their tests the shank and foot were in positions corresponding to erect stance and bearing an axial load approximating to body weight. The reported maximum contact area, 4-6cm^2, was considerably less and is probably due to the difference in axial loads used. Their results indicated that the contact area was reduced by 42% when the talus displaced the fibula laterally by one millimetre, but in view of the simple loading used, these figures should be accepted with caution.

The profiles of the talar trochlea were described in considerable detail by Sewell (1904). In a series of 1000 tali he identified two classes of mediolateral curvature of the talar dome. The first class was concave, see figure 2.9 (a) profiles 1 and 2, and occurred with a frequency of 80%, the remainder of the specimens made up the second class, concavo convex, figure 2.9 (a) profiles 3 and 4. The range of mediolateral profiles of the lateral malleolar facet is illustrated in figure 2.9 (b). The anteroposterior curvature of the talar dome was markedly convex in all the specimens. The anteroposterior curvature of the lateral malleolar facet was reported to be, almost without exception, convex; this feature was used by Close and Inman (1952) as part of a model, see figure 2.6, to explain axial rotation of the talus in the mortise.

Close and Inman (1952), also Inman (1976), proposed a model for the superior talar articular facets, which was

conical, with the apex medially, the axis of which coincided with the Tc. axis. Inman (1976) illustrated how the conic model was formed with a sequence of sketches, see figure 2.10. He drew particular attention to the medial facet, which in the conic model was developed from an elliptical cross-section. An ellipse has varying curvature thus neatly explaining the double curvature observed by Barnett and Napier (1952). Inman contoured the medial and lateral facets in planes normal to the Tc. axis and found in a series of 107 tali, that 86 had perfect circular arcs for both facets.

The wedging or tapering of the talar trochlea, referred to in 2.3, was investigated by Barnett and Napier (1952) who found evidence of variation between specimens. They expressed that variation as 100(X/Y), where X was the difference between the talar anterior and posterior mediolateral widths and Y the anteroposterior length. The variation, 100(X/Y), was found to lie in the range 0-14: Inman (1976) repeated their work and reported 0-19 range. The ratio X/Y is in fact the tangent of the wedging angle, (angle θ_1, figure 2.8), thus arctan (19/100) $\simeq 11^\circ$, which puts the wedging range in perspective as a smaller effect than the figures 0-19 appear to convey. Lane (1887-1888) observed that if the oblique facet for the distal tibio fibular ligament was included in the measurement of the wedging effect, the lateral and medial borders of the trochlea run quite parallel and never differ more than 2.5mm, see angle θ_2 in figure 2.8.

Inman (1976) commented that the tibio fibular mortise was required to accomodate about half of the talar trochlea at any point throughout the full range of flexion and

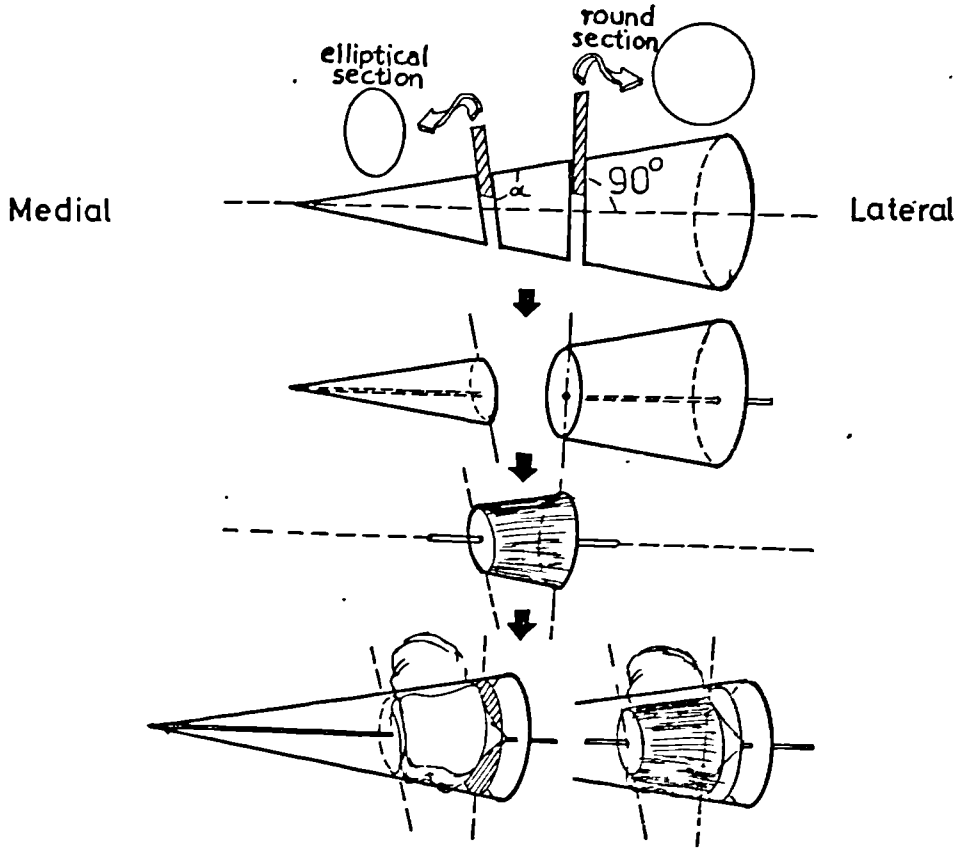

Figure 2.10 Inman's Conical Model of Talar Trochlea (After Inman, 1976)

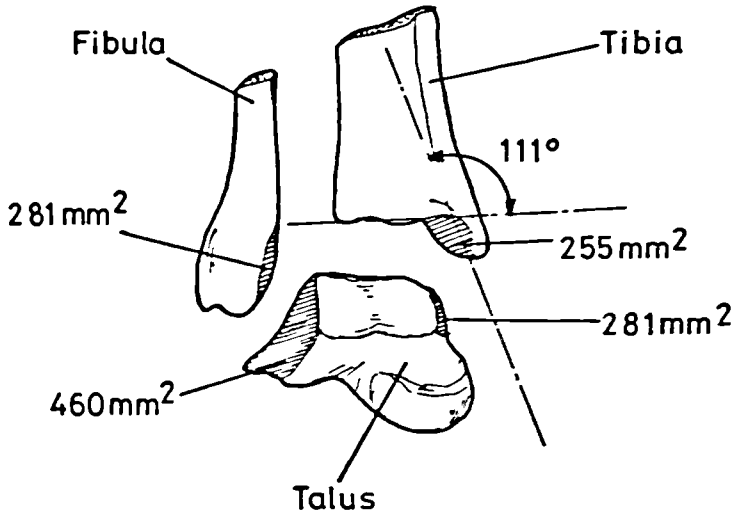

Figure 2.11 Tc. Joint Malleolar Surface Areas (After Sosa and Pasini, 1975)

extension of the ankle and so only a very small amount of motion of the lateral malleolus was necessary to accomodate the wedging (see the earlier discussion of fibular motions in 2.3).

The surfaces of the Tc. articulation were studied by Sosa and Pasini (1975). In a series of 93 cadaver joints they estimated the average area of the medial and lateral malleolar facets, for both the trochlea and the mortise; these are annotated in figure 2.11; note how much smaller (40%) the lateral malleolar facet is than the corresponding talar facet. They estimated the ratio of the facet heights, medially as 1.2:1 (tibial: talar) and laterally as 1.1:1 (fibula:talar). The large difference observed in the areas laterally was attributed to the fibula "following a larger radius of horizontal curvature than the tibial malleolus", a view consistent with the model of Close and Inman (1952) see figure 2.6. The included angle between the tibial malleolus and the inferior tibial articular surface was 111° mean corresponding well to the opposing angle of the talus.

Mariani and Patella (1977) performed an extensive survey of the dimensions of cadaver tali and the corresponding mortises for the purpose of identifying critical dimensions for ankle endoprostheses. The most variable dimensions were found to be those relating to anteroposterior and mediolateral widths of the talar dome.

An interesting but rarely occurring deformity of the Tc. articulation is the ball and socket ankle joint, where the talar dome takes a hemispherical form and the tibio fibular mortise is shaped like a cup. The clinical aspects of this deformity were reviewed by Channon and Brotherton (1979), who observed that it was usually the

case that patients presented for reasons other than the deformity itself, and in only one subject out of fifteen was there evidence of instability of the affected ankle. The aetiology of the ball and socket ankle was examined and amongst the possible causes suggested were loss of hindfoot mobility or an embryological defect of the foetus. That such a deformity occurs without by itself being particularly disabling leads the author to wonder what are essential facets in normal Talocrural joint geometry?

2.4.3 Talocalcaneonavicular Joint

The talocalcaneal facets of the Tcn. joint are variable and may occur in one, two or three faceted form, Bunning and Barnett (1965). These facets are illustrated in figure 2.12, note that there are three distinct facets in this particular example, the most frequently reported number for Europeans. The variations reported to exist by Bunning and Barnett are, type (1), which has facets 1 and 2 merged, and type (2), where all three facets are joined to make a single continuous surface. In type (2) variation a substantial portion of the deep interosseous ligament must be absent, suggesting that this may not be a structure essential to normal function of the Tcn. joint, see figure 2.12 and section 2.6.4.

The question of incongruity between the Tcn. articulations has been considered by Huson (1961), who suggested that true congruence only occurred at the mid position of the Tcn. joint and that any movement from this position reduced the contact areas. Inman (1976) also observed the incongruence described by Huson and noted that some degree of incongruence was apparent at the extremes of

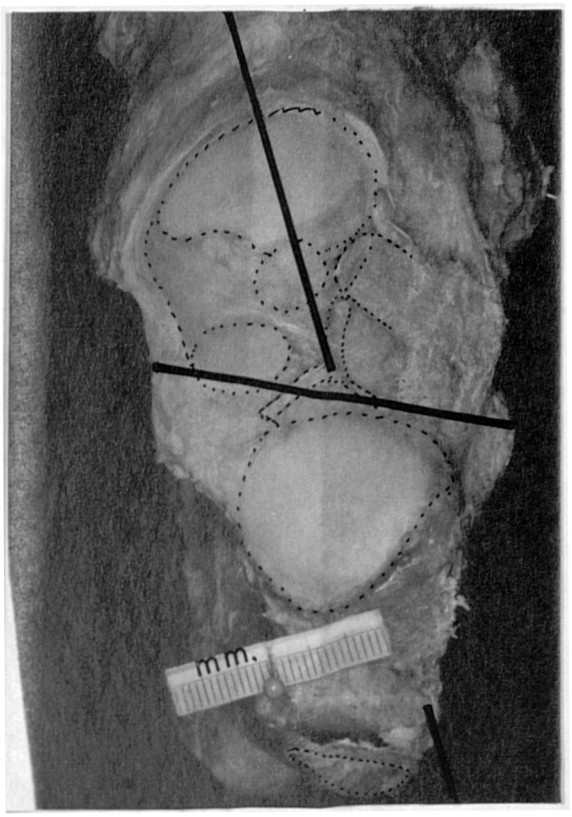

Superior view - right Tcn. joint

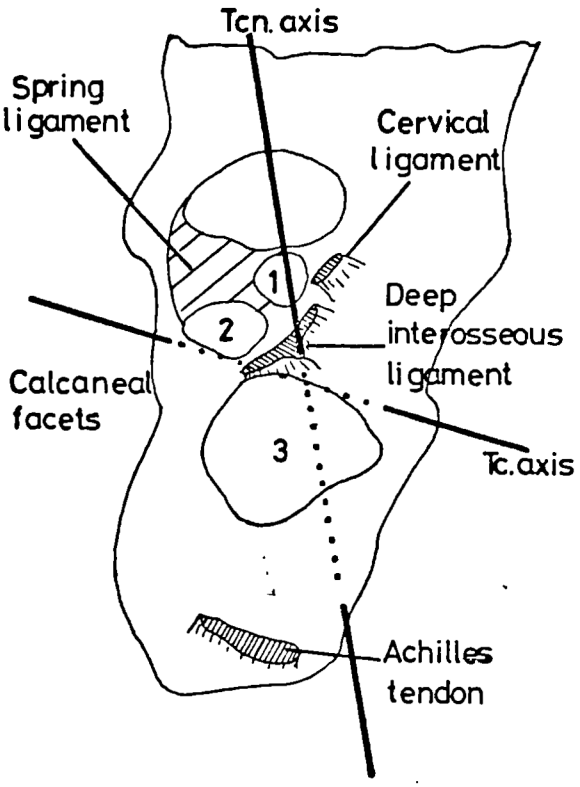

Key to photograph

Figure 2.12 The Tcn. Joint Articular Facets

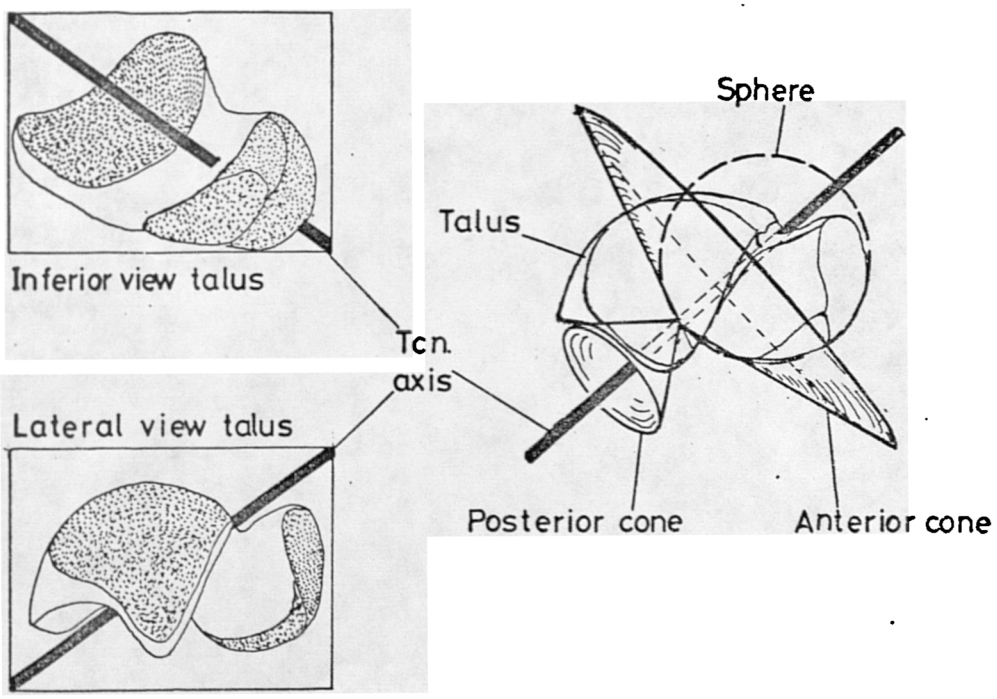

Figure 2.13 Model of the Tcn. Articulations (After Von Lanz and Watchsmuth, 1939)

Tcn. joint motion. Shephard (1951) inserted a wire through cadaver ankle bones to correspond with the Tcn. axis and found that the talus could be rotated on the calcaneus with their common articulations in good apposition throughout the range of Tcn. joint motion. Huson (1976) expressed the view that the Tcn. articulations were incongruent and described their surfaces as "curved irregularly and assymetrically".

The complex appearance of the Tcn. facets has lead to different interpretations of how this joint system should be modelled. Von Lanz and Watchsmuth (1939) modelled the posterior talocalcaneal facet as part of a convex conic surface, and the anterior talocalcaneal facet and part of the spring ligament as a broader concave conic surface; the talonavicular articulation was represented as a shallow spherical socket, see figure 2.13. The axes of the two conical surfaces and the sphere were represented as a single line coincident with the Tcn. axis, shown in figure 2.13.

Manter (1941) compared the talocalcaneal facets, in particular the posterior articulation, with a screw-like or helical surface, see figure 2.14. For the posterior facet to function effectively as a screw surface required that the facets be congruent throughout the range of Tcn. motion. From the dimensions of sixteen cadaver specimens, Manter calculated an average helix angle of 12°, treating the helix as a right handed screw (considering the right foot). The displacement of the talus relative to the calcaneus, along the Tcn. axis, for a point on the talus 2cm from the axis, was estimated to be 1.5mm for every 10° rotation about the axis.

Hicks (1953) did not detect the screw-like motion

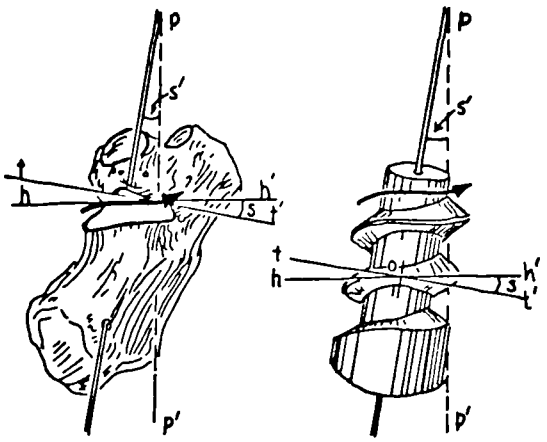

Comparison of the posterior calcaneal facet of the right subtalar joint with a right-handed screw. Arrow represents the path of a body following the screw. hh' is the horizontal plane in which motion is occurring. tt' is a plane perpendicular to the axis of the screw. s is the helix angle of the screw, equal to the angle s' which is obtained by dropping a perpendicular pp' from the axis.

Figure 2.14 Manter's Screw Model of the Talocalcaneal Facets

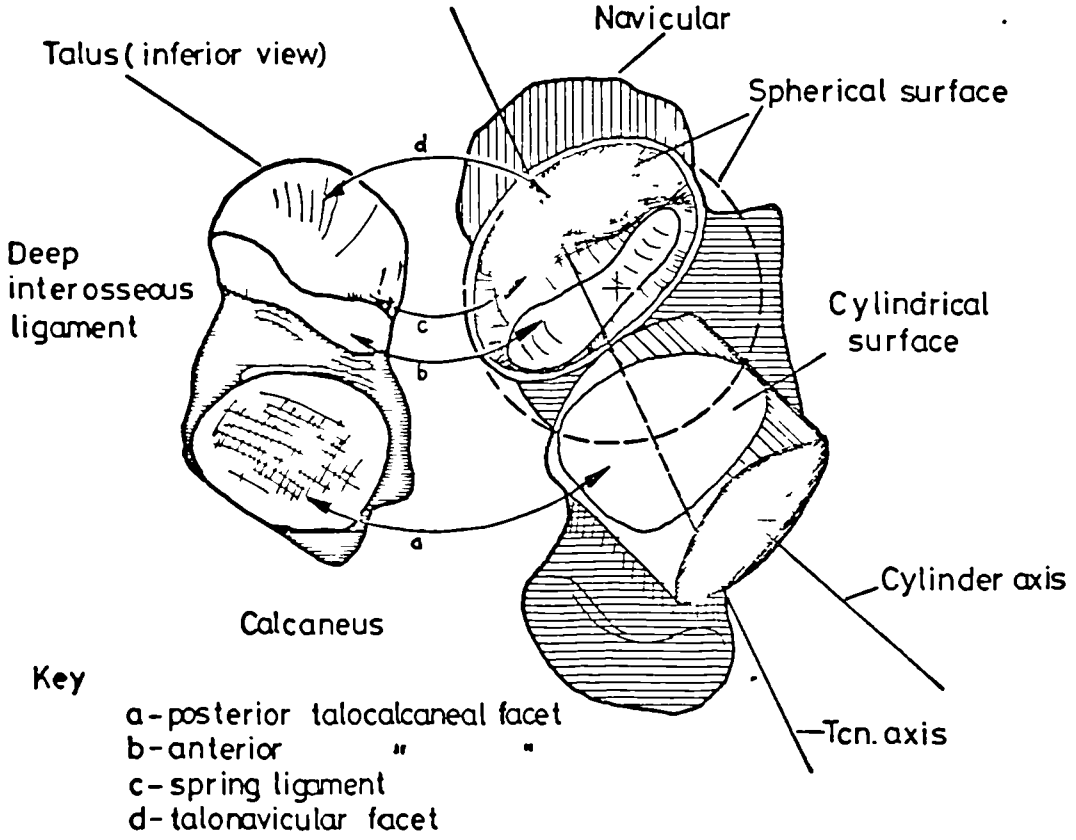

Figure 2.15 Kapanji's Representation of the Tcn. Joint

and commented that if such motion had occurred in his experiments it was less than 2-3mm.

Inman (1976) raised the question of screw behaviour of the Tcn. joints again and conducted an X-ray study of fifty dry bones and a motion study of one hundred cadaver ankles. Manter had indicated that the posterior talo-calcaneal facet was the key factor dictating whether or not the talus migrated backward or forward on the calcaneus; from this Inman argued that contouring of this facet should therefore reveal axial displacement on rotation at the Tcn. joint. He found that 58% of the cadaver subjects followed a linear relationship between rotation and axial displacement, indicating a screw-like motion. The remainder of the specimens "behaved in a variety of unscrew-like ways"; some showing reversal in axial direction during the motion and a few indicating pure rotation. From the X-ray study a mean helix angle of 25° was estimated (range 0°-40°); Inman's calculation of helix angle was based on single plane X-ray views of the ankle which may have introduced projection errors.

Kapandji (1970) drew an analogy between the posterior talocalcaneal facet and a cylindrical surface. The remaining Tcn. articulations were compared to part of a spherical surface, see figure 2.15. The axis of the cylinder and the centre of the sphere do not appear to coincide with the approximate Tcn. axis superimposed in figure 2.15 by the present author. Kapandji did not relate his model to the Tcn. axis and gave no indication of how the model geometry was consistent with the observed uniaxial rotation about the Tcn. axis.

2.5 Functional Interpretations of the Obliquity of the Ankle Axes

The most frequent explanation for the oblique orientation of the Tc. and Tcn. axes is that together they form a mechanism allowing axial rotation of the leg to be transmitted to the foot. The way that this mechanism works is effectively illustrated by simple models of the foot and shank linked by two hinges representing the Tc. and Tcn. joints (Jones, 1945; Rubin, 1971; Inman, 1976). Jones, using such a model, see figure 2.16, demonstrated that lateral (outward) rotation of the shank element whilst the foot element was in contact with the floor resulted in inversion of the foot element, medial rotation of the shank causing eversion. He was able to compare the model with the living ankle through a simple experiment; a seated subject bearing a load on the knee to simulate weight bearing was asked to relax his leg muscles, whilst a lateral moment was applied about the long axis of the shank, and then a medial moment. The results showed that the laterally app ied moment reduced the pressure beneath metatarsal one, and the medial moment reduced the pressure under metatarsal five. Unfortunately when a similar experiment was tried with standing subjects the results were inconclusive. Jones attributed this inconsistency to the influence in standing of the long leg muscles on the distribution of load under the ball of the foot.

Wright et al (1964) drew an analogy between the Tc. and Tcn. axes behaviour and that of a universal joint, since a universal joint enables rotation to be transmitted from one segment to another even when the segments do not have their rotational axes coincident. Inman (1976) pointed out that such an analogy was invalid

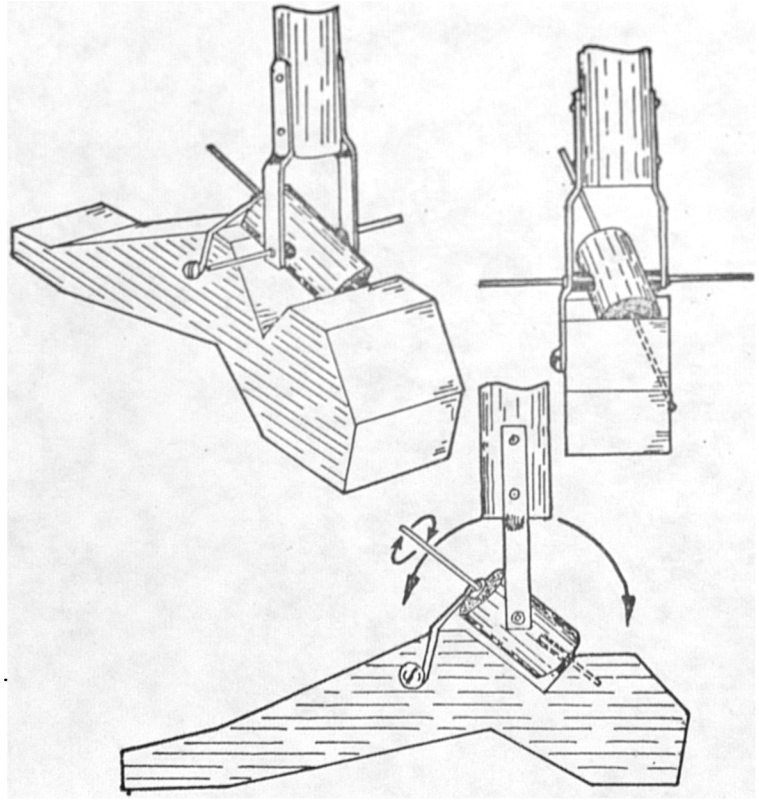

Figure 2.16 Jones' Model Demonstrating the Ankle Axes

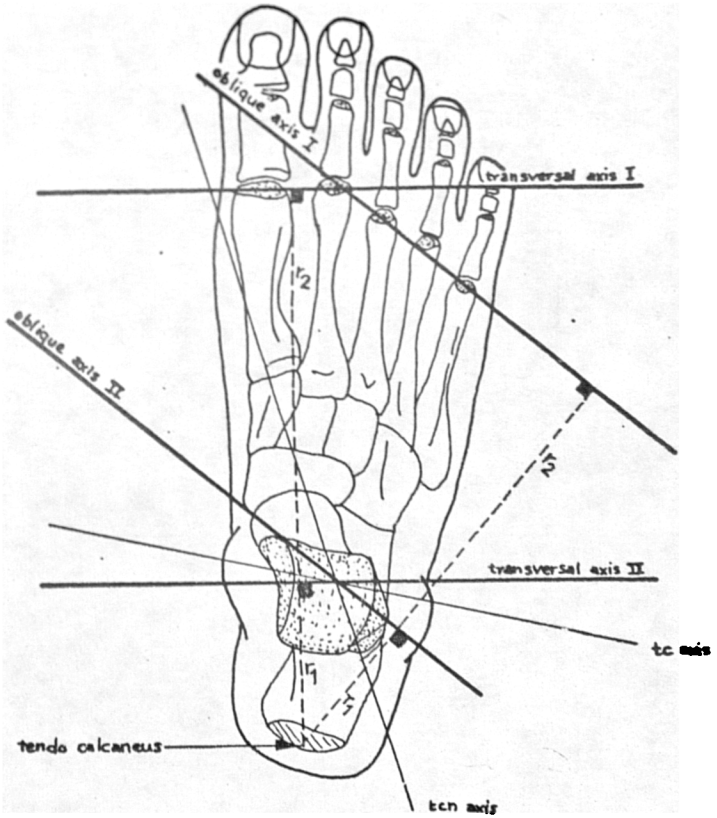

Figure 2.17 Bojsen-Møller's Model of the Two Speed Ankle

for in a true universal joint the axes are oriented at 90° and intersect, conditions that the Tc. and Tcn. axes clearly did not fulfil.

The obliquity of the Tcn. joint is thought to be essential for the foot to be able to adapt to locomotion activity on uneven or sloping terrain; the locomotion studies of Wright et al demonstrated this in side slope walking. It has also been observed clinically that patients with damage to the Tcn. joint, for example arthritis, are likely to experience problems in walking over rough ground.

Lapidus (1955) suggested that the 'toe in' or 'toe out' orientation of the foot in walking was adjusted to maintain the Tcn. axis approximately parallel to the line of progression; it was argued that this reduced the tendency of the weight-bearing line to force the heel into inversion or eversion (that is to say, external force vector passes closer to the Tcn. axis).

Bojsen-Møller (1978) introduced a novel interpretation of the function of the oblique axes at the ankle. Two axes were identified at the metatarsus, transverse I and oblique I and corresponding axes were established at the ankle, transverse II and oblique II respectively. These axes are illustrated in figure 2.17. Transverse II was approximately normal to the long axis of the foot whilst oblique II was about halfway between the Tc. and Tcn. axes. The mean ratio of the lever arms for both pairs of axes was estimated as 5:6 mean (oblique: transverse), and was verified in vivo using a dynamometer. Bojsen-Møller inferred from this and film studies of the foot during activity that the foot functions as a two speed device in push off, having a low gear for going

uphill or starting walking, using the oblique axes, and a high gear using the transverse axes for sprinting.

2.6 Studies of the Ankle Ligaments

2.6.1 Introduction

Ligaments are essentially passive structures constraining the type and range of movement between two or more bones. They are also thought to prevent the disruption of articulations under the influence of tensile and/or shearing forces (Root et al, 1971; Warwick and Williams, 1973; Bock, 1974). An additional function attributed to ligaments by Bock is the storage of elastic energy; Warwick and Williams state that the ligaments are protected by reflex contraction of appropriate muscles when subject to excessive tension. This suggests that there is a limit to the potential for elastic energy storage. Huson (1961) expressed the general view that ligaments are an essential constraint of motion between incongruent articulations.

2.6.2 The Medial Collateral Ligaments

The medial ligament of the ankle, the deltoid, appears to be particularly variable; Pankovich and Shivram (1979) identified five different reported forms. Barclay Smith (1896) made the cautionary remark referring in particular to the ankle ligaments, "the human frame is to a large extent but clay in the dissector's hands - the ligaments are the most plastic in this respect". He regarded the term deltoid, meaning delta shaped, as misleading and identified the main portion of this ligament as "a quadrilateral mass of coarsly fasiculated fibres".

The origin of the deltoid is consistently reported as the medial malleolus, the ligament usually dividing into five bands, two deep and three superficial, see figure 1.6. The deep fibres form the most substantial part of the deltoid; Pankovich and Shivram stated that only rupture of the deep portion allowed significant displacement of the talus relative to the tibia. They also described the superficial fibres as relatively thin, in particular the tibionavicular fibres. Close (1956) examined the mediolateral orientation of the deltoid bands and noted that the principal orientation of the deep fibres was almost horizontal whilst the superficial bands were vertical.

All of the deltoid fibres cross the Tc. joint and it is frequently suggested that, because medially the Tc. axis passes beneath the origin of the deltoid, see figure 2.3(b), the anterior fibres tense on plantarflexion and the posterior fibres on dorsiflexion (Lapidus, 1955; Calliet, 1974); it has not been established whether this occurs only at the extremes of motion at the Tc. joint or for lesser degrees of flexion and extension. The deltoid bands crossing the Tcn. joint, the tibionavicular and tibiocalcaneal, are thought to be tensed by eversion and relaxed by inversion (Lapidus); again there is doubt as to whether this occurs only at the extremes of motion or for the much smaller ranges of motion obtaining in normal locomotion.

Inman (1976) compared the compact form of the deltoid bands with the discrete well separated appearance of the lateral collateral ligaments, with reference to his conical model of the ankle shown in figure 2.10. He suggested that the medial malleolar being closer to

the apex of the cone, of which the talar trochlea was the frustrum, exhibited less anteroposterior excursion than the lateral malleolus, as a result of which the fibres constituting the deltoid could be concentrated into a single structure.

2.6.3 The Lateral Collateral Ligaments

The three lateral collateral ligaments, anterior fibulotalar, posterior fibulotalar and fibulocalcaneal (see figure 1.6(a)), are well defined discrete bands. Lapidus (1955) compared the bands with radial spokes of a wheel, diverging from a common origin which was stated to coincide with the lateral exit of the Tc. axis, see figure 2.18(a). It was suggested that the radial pattern allowed the ligaments to remain taut for the range of dorsiflexion and plantarflexion. Calliet (1974) supported this view extending its application to all movements of the foot relative to the shank. Warwick and Williams (1973) stated that the anterior fibulotalar ligament limited plantarflexion and the posterior fibulotalar and fibulocalcaneal ligaments limited dorsiflexion.

Inman (1976) contended that the radial pattern leads to little or no change in ligament tension during normal dorsiflexion and plantarflexion; he investigated the lateral ankle ligaments in primates and other species to see if evolutionary changes were responsible for the present pattern in man. Inman concluded that the anterior fibulotalar ligament played a significant role in stabilisation of the ankle, and speculated that, since, this ligament was usually the first to be damaged in inversion sprains of the ankle, it must in some

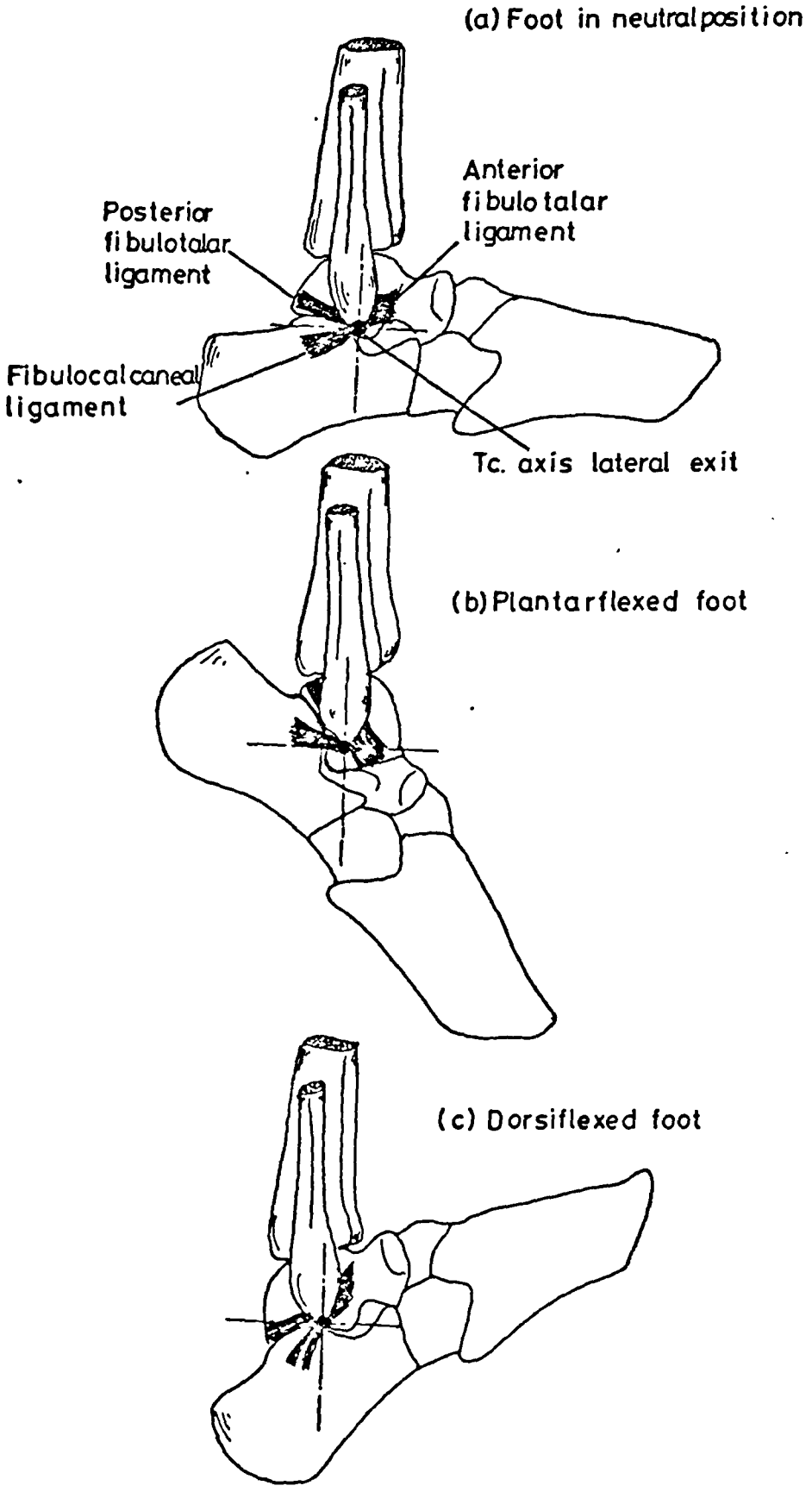

Figure 2.18 Orientation of the Lateral Collateral Ligaments for Different Foot Positions

manner restrict medial tilting of the talus in its mortise.

Rubin and Witten (1960) regarded excessive medial tilting of the talus in the mortise as a positive clinical sign - the talar tilt sign (see figure 2.19(a)) - of injury or rupture of the anterior fibulotalar ligament. Laurin and Mathieu (1975) and Cedell (1975) however showed that the range of talar tilt for normal subjects overlapped that obtained in cases where the anterior fibulotalar ligament was damaged.

The anterior fibulotalar ligament is frequently stated to be important for anteroposterior stability (Laurin and Mathieu, 1975; Staples, 1975; Cedell, 1975; Warwick and Williams, 1973). Laurin and Mathieu showed that it was possible to displace the talus anteriorly relative to the fibula and tibia in normal ankles, but in cases where the anterior fibulotalar ligament was ruptured the displacement was sufficiently large to be considered a positive clinical indication of damage - the anterior drawer sign, see figure 2.19(b). Sosna and Sosna (1977) found with cadaver ankles that only after section of the anterior fibulo talar ligament was the talus free to dislocate anteriorly, "usually more than 1cm". Broström (1965) reviewed ankle injuries and observed that partial or complete rupture of the lateral collateral ligaments always lead to ankle instability.

Inman (1976) argued that the anterior fibulotalar and fibulocalcaneal ligaments must share the role of the lateral collateral ligament. He considered that the line of action of the fibulocalcaneal ligament passed very close to the Tcn. axis (see figure 2.20, note that

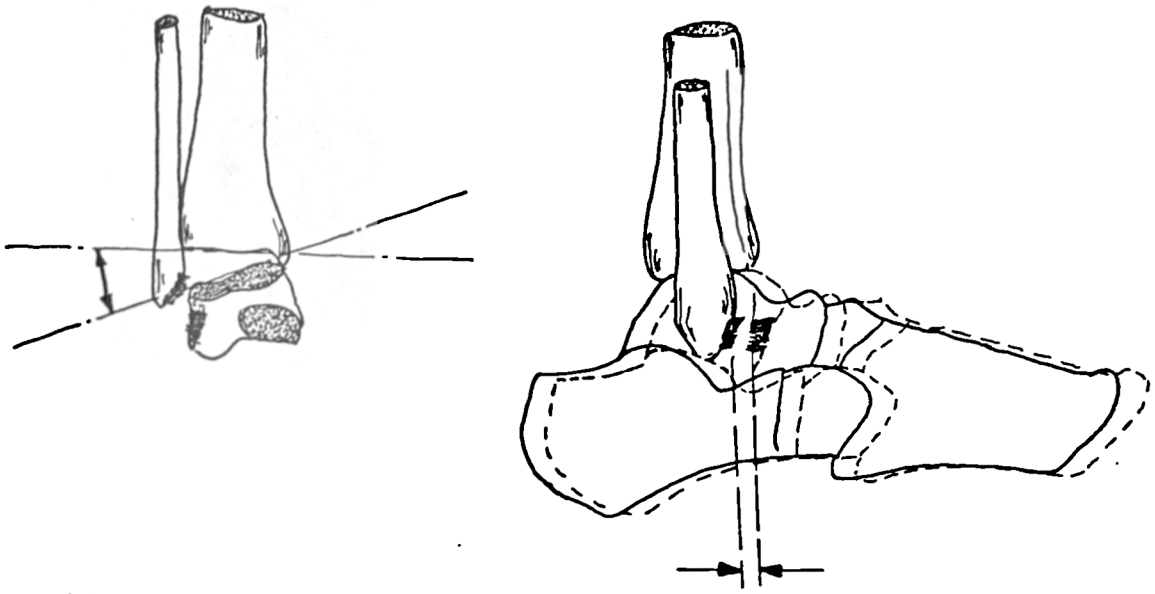

Figure 2.19 Clinical Signs Used to Indicate Rupture of the Anterior Fibulotalar Ligament

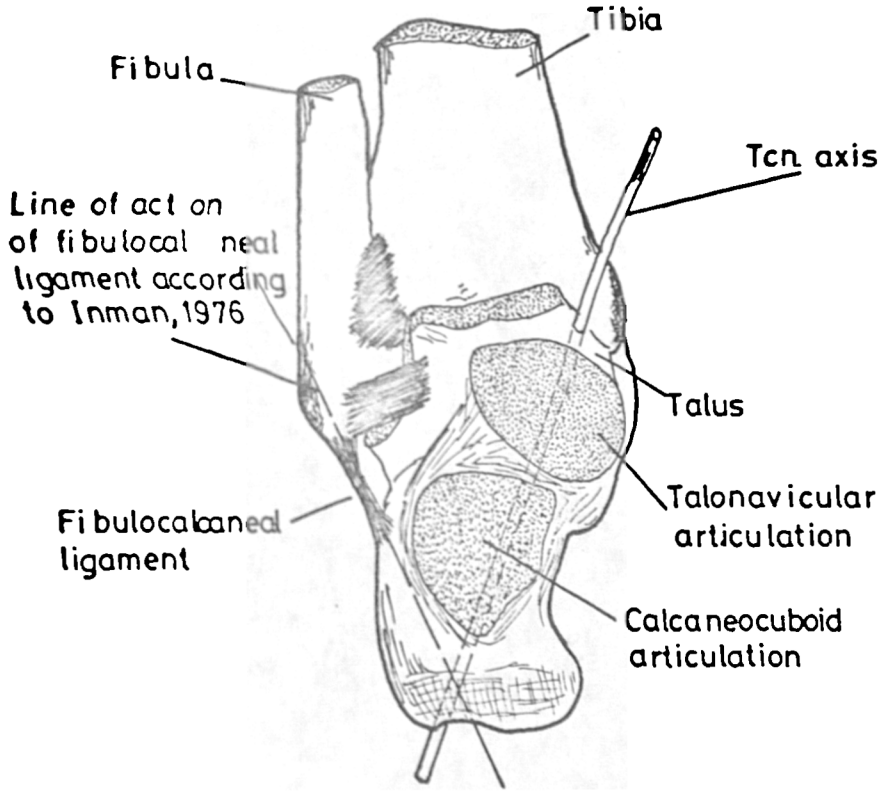

Figure 2.20 Anterior View of the Line of Action of the Fibulocalcaneal Ligament According to Inman (1976)

only one view is reproduced) and since it also passed through the Tc. axis that it did not limit rotational motion about either axis. It was suggested that in dorsiflexion the fibulocalcaneal ligament was ideally situated to act as a collateral ligament, demonstrated in figure 2.18(c), whereas in plantarflexion the anterior fibulotalar ligament assumed this function, see figure 2.18(b). Lapidus (1955) stated that the fibulocalcaneal ligament was tensed by inversion of the foot. Rubin and Witten (1960) contended that the fibulocalcaneal ligament was always lax in the normal foot for the normal range of use.

It is the author's opinion that, because the study of the fibulocalcaneal ligament is usually confined to dissected cadaver preparations, another functional interpretation has been neglected. Inman (1976), for example, illustrated the fibulocalcaneal ligament passing in a str ight line between its origin and insertion, see figure 2.20, but as is frequently the case in such illustrati ns all the overlying structures were removed to de n tra e the form of the ligament. Kaye and Bohne (1977) pres nted a comprehensive X-ray study of the a kle liga ents, in which the ligaments of a fresh cadaver were coated with an X-ray opaque medium. One of heir X-ray plates, an oblique posterolateral view of he left ankle, sketched in figure 2.21(a), clearly de nstrated that the ligament was deflected by overlying structures. It was observed that the fibulocalcaneal ligament was intimately related to these structures - the peroneal tendons and retinacular sheathing - see figure 2.21(b).

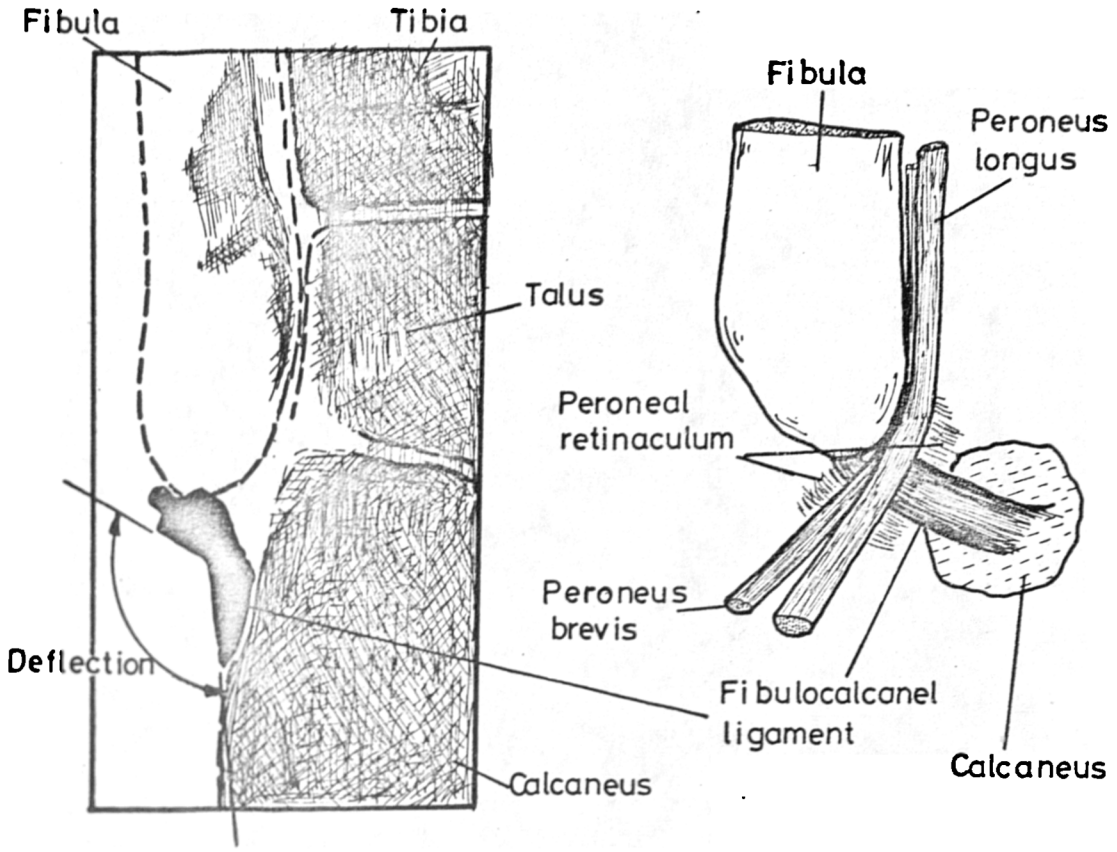

(a) Sketch of posterolateral X-ray view of left ankle.

(b) Relation of peroneal tendons to the fibulocalcaneal ligament lateral view

Figure 2.21 Deflection of the Fibulocalcaneal Ligament on the Left Foot

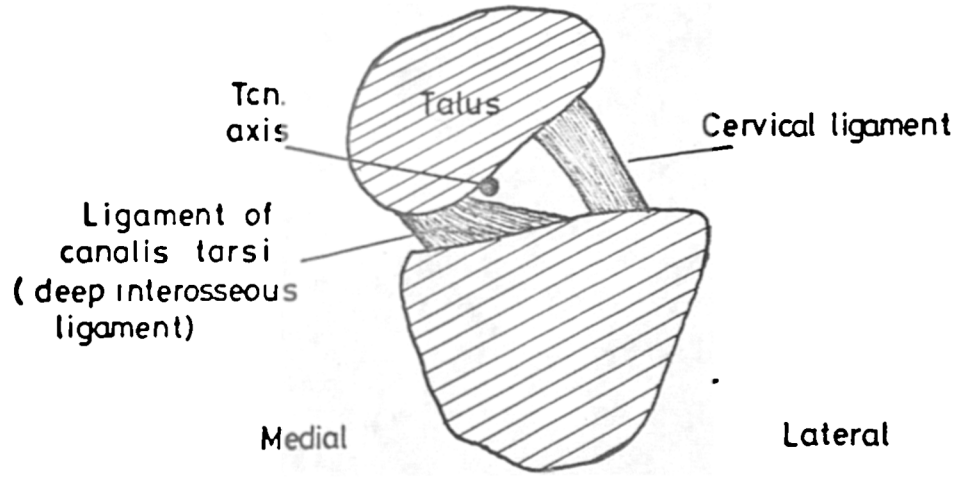

Figure 2.22 Diagrammatic Representation of the Relationship of the Tcn. Axis to the Cervical and Deep Interosseus Ligaments (After Smith, 1958)

2.6.4 The Cervical and Deep Interosseous Ligaments

The ligaments associated with the sinus tarsi are the cervical and deep interosseous ligaments, illustrated in figures 1.6(a), 1.11 and 2.12.

Barclay Smith (1896) regarded the cervical ligament as the more important of the two, the deep ligament being relatively weak; he found that the talus and calcaneus were inseparable until these ligaments were severed. There is some evidence to suggest that the deep interosseous ligament may not be essential for normal function of the Tcn. joint, see 2.4.3.

Smith (1958) defined the position of the Tcn. axis on cadaver preparations, by a wire passed through the ankle bones, and dissected down to the sinus tarsi. He found that the ligaments were situated on either side of the Tcn. axis, see figure 2.22, and inferred from this that the cervical ligament was concerned with limiting inversion and the deep interosseous ligament with limiting eversion. Calliet (1974) also considered that the cervical ligament limited inversion.

The most frequently reported functions associated with the ankle ligaments together with the joints each ligament crosses are tabulated in table 2.1.

2.6.5 The Retinacula

The ankle retinacula, in particular the anterior bands, are attributed with the function of pulleys. Root et al (1971) observed that the pulleys had no mechanical advantage, but rather, directed the tendons through different lines of action, depending upon the orientation of the foot relative to the leg.

The anatomical relations of the retinacula and

Ligament	Joints crossed		The most frequently reported functions in the literature
	Tc.	Tcn.	
Deltoid	*	*	limiting of eversion, plantarflexion and dorsiflexion
Anterior fibulotalar	*		limiting of inversion, plantarflexion and anterior displacement of the talus
Posterior fibulotalar	*		limiting of inversion, dorsiflexion and posterior displacement of the talus
Fibulocalcaneal	*	*	limiting of inversion, dorsiflexion and posterior displacement of the talus
Cervical		*	limiting of inversion and resisting separation of talus and calcaneus
Deep interosseous talocalcaneal		*	limiting of eversion and resisting separation of talus and calcaneus

Table 2.1 Ligaments of the Ankle; the joints crossed and the most frequently reported functions

their tendon sheaths were demonstrated by Barclay Smith (1896), Stamm (1931) and Wood-Jones (1943). Stamm dissected in detail the inferior extensor retinaculum and demonstrated the existence of a loop - he named it the 'ligamentum cruciatum cruris' - linking talus, calcaneus and the retinaculum. He also observed that the anterior tibial muscle was not always provided with a retaining band from the inferior branch of the inferior extensor retinaculum, which was attributed to a more proximal insertion of this tendon, see figure 1.10.

2.7 Muscle Studies

2.7.1 Introduction

The general properties of skeletal muscles have been comprehensively reviewed elsewhere, Needham (1971), Bourne (1972), Warwick and Williams (1973), Huxley (1974) and Komi (1979). It is sufficient for the purposes of the present study to give a brief synopsis of the most relevant properties.

Force generation may be achieved by muscles during either lengthening or shortening or whilst maintaining constant length (isometric contraction). Active force generation is preceded by electrical potential signals, from individual contracting muscle cells, collectively termed electromyographic - Emg. - activity. The electro-mechanical delay between the first electrical activity and the onset of force generation is termed the latency period and was reported by Komi (1979) to be about 45-55 milliseconds (range 20-100 milliseconds). Inman et al (1951) reported that 80±20 milliseconds elapsed between the observed maximum in an Emg. signal and the corresponding maximum force. Electromechanical delay

is also apparent at the end of muscular activity where the Emg. signal ceases before the end of force generation.

The level of force generated by a muscle is known to depend upon a large number of parameters, principally; the muscle fibre - type, number, orientation, cross-section and length (at any instant between full contraction and full extension); the mode of contraction - isometric, lengthening or shortening; and the physical condition of the subject - whether fatigued or at rest.

Special terms are used when referring to the action of a muscle at a joint. A muscle causing the desired action at a joint is said to be an agonist or prime mover; usually a muscle having the opposite effect at a joint must relax to permit the action to occur. This second muscle is termed the antagonist. Where the joint is either multiaxial or the muscle crosses more than one joint the agonist may produce unwanted movements as well as the prime movement; control of these unwanted motions is usually effected by additional muscles referred to as synergists.

2.7.2 Physiological Cross-section and Strength of the Shank Muscles

It is, in general, considered that the cross-sectional area of all the fibres in a muscle - the physiological cross-section, is a reliable index of the maximum force which that muscle can produce. Ultrasound techniques have been used to estimate physiological cross-section in living subjects (Komi, 1979) although this is presumably only possible where the muscle structure is simple and well defined. More commonly, cadaver material is used to provide muscle physiological cross-section

data.

Haxton (1944) used the physiological cross-section data from cadavers, corrected for the partial contraction of the muscles occurring at death and for the differences in build between the cadavers and living subjects, in the calculation of the maximum uniformly distributed stress acting in the Calf group. In a simple test subjects exerted the maximum voluntary plantarflexing moment they could against a resistance under isometric conditions; the maximum force in the achilles tendon was estimated from the force under the ball of the foot and the ratio of the distance of the ball of the foot from the ankle, to the distance of the achilles tendon to the ankle. For a mean physiological cross-section of $0.0113 m^2$ the maximum mean stress in the Calf group muscles was estimated to be about 380 kN/m^2, corresponding to a maximum force of 4300 N. in the achilles tendon.

Alexander and Vernon (1975) calculated the physiological cross-section for shank muscles using the following formula.

$$\frac{P}{\sigma} = \frac{m}{2\rho t} \sin(2\alpha) \qquad \ldots 2.1$$

where P = the component of force along the muscle tendon (N)

σ = the uniform stress acting on the muscle physiological cross-section (N/m^2)

t = muscle layer thickness (m)

α = pennation angle (°)

ρ = density of muscle fibres (kg/m^3).

m = total mass of the muscle fibres (Kg)

Their results for the shank muscles from a single cadaver are tabulated in table 2.2. The formula was developed for application to a wide range of muscle forms, see figure 2.23. They then performed a series of experiments in which the forces acting on major leg muscles were estimated from force platform and two-dimensional cine film data together with cadaver anthropometric data. The inertial contribution of the foot to the moments acting about the ankle Tc. axis was not taken into account, being less than 2Nm. maximum (at heel strike). The peak stresses calculated in the Calf group were 200 kN/m^2 for walking and 400 kN/m^2 for running, corresponding to ankle dorsiflexion moments of about 100Nm. and 200Nm. respectively. Note that the stress in running was greater than Haxton's 380 kN/m^2 reported maximum for voluntary effort of the Calf group, probably reflecting differences in experimental technique and cadaver measurements. Komi (1975) commented on the wide range of reported maximum muscle stress, 240-1000 kN/m^2, and pointed out that the determination of absolute muscle force is subject to many variables, some of which are difficult to control. Komi cited an experiment where a subject under isometric resistance training increased his muscle strength by nearly 40% whilst the corresponding muscle cross-section only increased by 23%. This result casts some doubt over the validity of using muscle physiological cross-section as an index of maximum muscle force.

Physiological cross-section data has been utilised in two main ways for the assessment of muscles cooperating in activity at joints. Firstly Fick (1911) in a comprehensive study of the action of shank muscles used

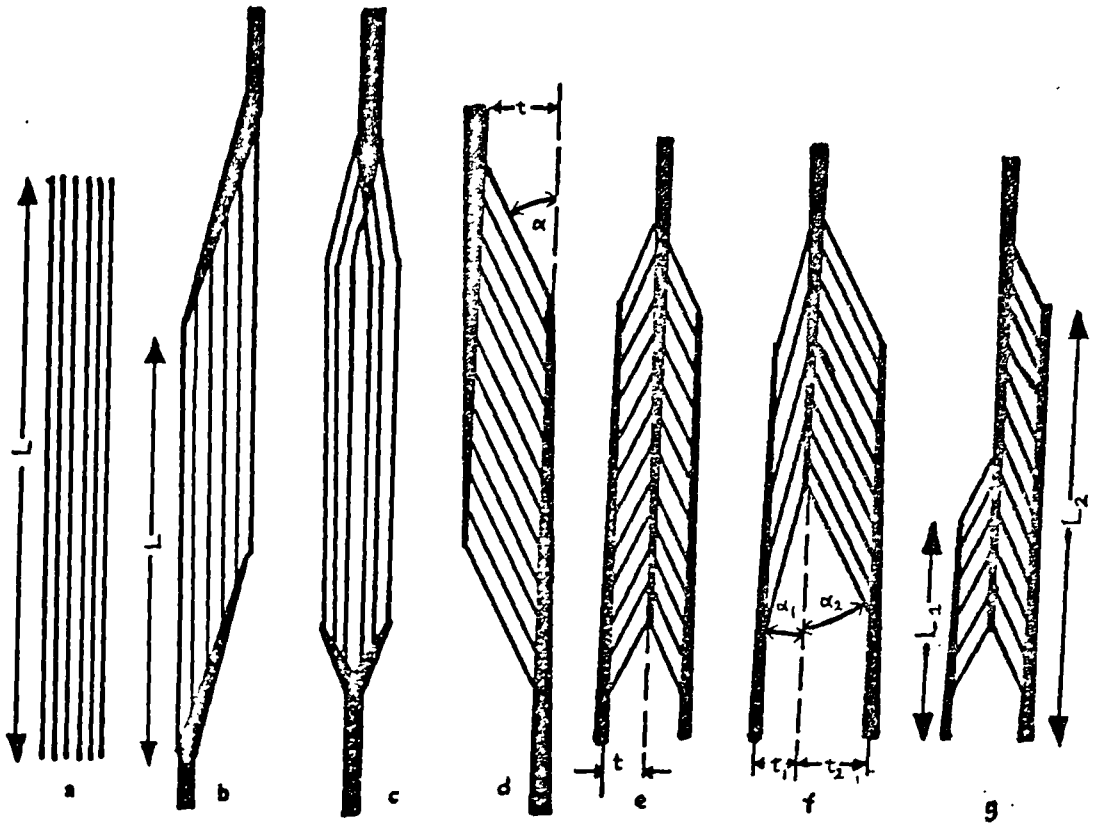

Figure 2.23 Diagrams of Parallel Fibred (a to c) and Pennate (d to g) Muscles, Adapted from Alexander and Vernon (1975)

Muscle	Mass (kg.)	Pennation Angle (°)	Layer Thickness (m.)	Force Stress ($m.^2$)
Gastroc. lat.	0.091	8	0.009	0.0013
Gastroc. med.	0.142	16	0.016	0.0022
Sol.	0.264	20	0.012	0.0067
Post. tib.	0.062	20	0.011	0.0017
Ant. tib.	0.110	8	0.010	0.0014
Ext. dig. long.	0.049	14.5	0.014	0.0008
Peron. long.	0.046	11	0.007	0.0011

Table 2.2 Shank Muscle Physiological Cross-Section Data Adapted from Alexander and Vernon (1975)

physiological cross-section in the calculation of the maximum moments acting about the Tc. and Tcn. axes. After review of the literature it was concluded that the maximum reported muscle stress was 10 kg/cm^2 (about 1000 kN/m^2). Fick multiplied the physiological cross-section by this figure to obtain the maximum force generated by each muscle. The product of the muscle force and its perpendicular distance from each axis, see figure 2.24, was calculated thus giving the maximum moments due to each muscle, tabulated in table 2.3; note that Fick considered the anterior tibial muscle to be neutrally placed with respect to the Tcn. axis and divided its moment almost equally between eversion and inversion. Alexander and Vernon (1975) asserted that Fick had neglected pennation angles in his calculation of muscle physiological cross-section; it appears however from Ficks' text and included calculations that the effect of pennation angle was taken into account.

A second use of muscle physiological cross-sections is as a participation factor to weight the contribution of muscles cooperating in a particular activity. Alexander and Vernon (1975) suggested that knowledge of muscle dimensions might be helpful in assessing the contribution each muscle was likely to make at a particular instant. They asserted that similar stresses would act in similar muscles and added the rider that this was particularly likely in strenuous activities in which all appropriate muscles presumably made contributions near the limits of their capability. Amis (1978) used this approach in the estimation of muscle forces acting at the elbow joint. Ripperger et al (1980) used a similar technique to calculate

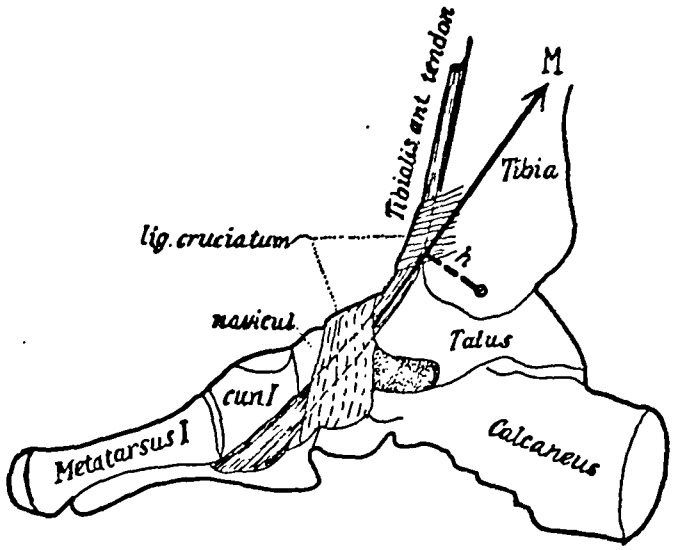

Figure 2.24 Fick's Illustration of the Method of Calculating Ankle Moments with Reference to the Anterior Tibial Muscle

Moment (kgm.) / Muscle	Plantar-flexion	Dorsi-flexion	Inversion	Eversion
Gastroc.	8.97		2.53	
Sol.	7.40		2.32	
Tib. post.	0.41		1.45	
Flex. hall. long.	0.85		0.67	
Flex. dig. long.	0.36		0.57	
Peron. long.	0.44			1.05
Peron. brev.	0.25			0.86
Tib ant.		2.54	0.32	0.33
Ext. hall. long.		0.82		0.48
Ext. dig. long.		0.42		0.12

Table 2.3 Fick's Calculated Maximal Moments for the Shank Muscles

the relative contribution of shank muscles at the ankle. They calculated the 'potential' moment due to each muscle as the vector cross-product of the radius vector of each muscle and its line of action, multiplied by its proportion of the total shank musculature cross-section; a polar diagram of their results is illustrated in figure 2.24_2. The ratio of plantarflexion to dorsiflexion strength was reported to be 9:1, and the dorsiflexion strength was divided 4:2:1 between anterior tibial, extensor digitorum longus and extensor hallucis longus muscles respectively. However it appears that their calculation of physiological cross-section may be in error, since they divided muscle volume by muscle length which would only give the correct physiological cross-section for parallel fibred muscles, see figure 2.23(a-c); for pennate muscles, figure 2.23(d-g), muscle fibre length should be used rather than overall muscle length.

An alternative strategy to using muscle physiological cross-section as an index of maximum muscle force was suggested by Haughton (1867) who proposed the principle "that the force of a muscle is proportional to the cross-section of the tendon that conveys its influence to a distant point". Elliot (1965) investigated the thickness and collagen content of tendon relative to the strength and cross-sectional area of muscle in rabbits. The results suggested that, although the longer and stronger muscles tended to have longer tendons, muscle and tendon size were not strictly correlated. It was speculated that the differing internal muscle structure might be responsible for some of the observed differences and that the thickness of tendon ought to

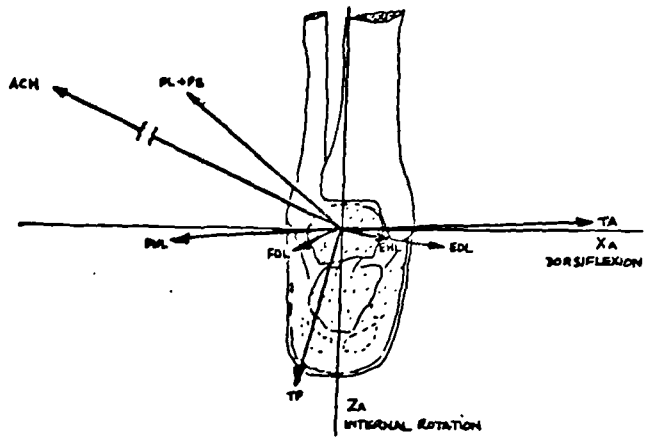

Polar moment diagram of the entire leg musculature with respect to ankle joint.

Figure 2.24$_2$ Ankle Moment Vector Diagram (After Ripperger, 1980)

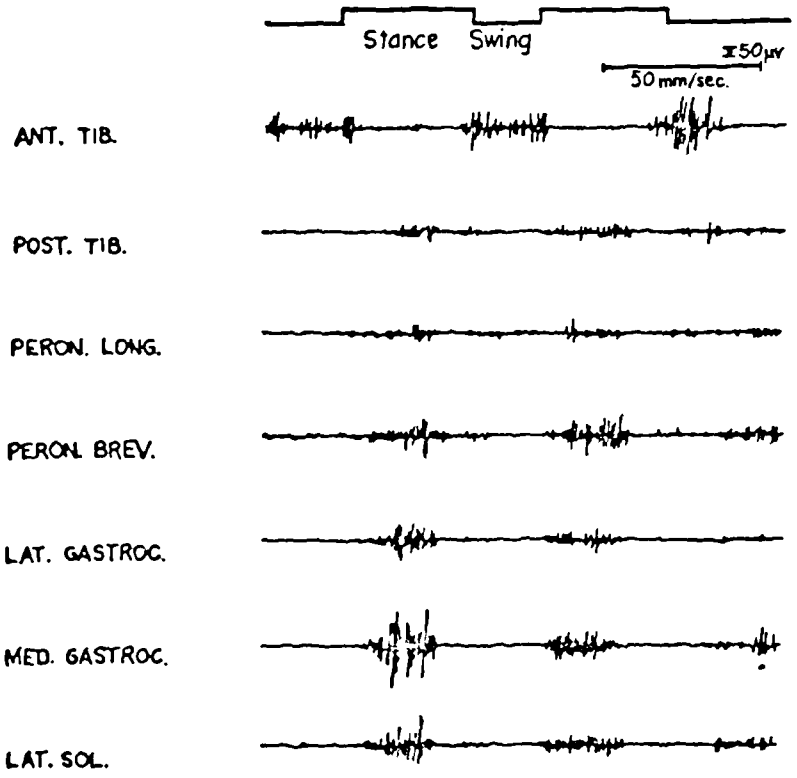

Pattern of electrical activity during barefoot walking.

Figure 2.25 Examples of Raw Emg. Signals for Muscles of the Shank (After Houtz and Walsh, 1959)

be determined, in part at least, by the characteristics of the stress to which the tendon is subject, such as the average tension and its duration.

2.7.3 Electromyographic Study of Shank Muscles

It was noted in 2.7.1 that electrical potential signals were associated with the activity of skeletal muscles. These potentials may be detected between two or more conducting surfaces placed either on the skin or within the muscle itself. The potential levels are reported to be typically in the range 0.01 to 5 millivolts (Grieve, 1975) and require specialised amplification and recording techniques in order to obtain reliable signal records. The raw Emg. signal, see figure 2.25, may be visually assessed but more usually it is processed in some way that gives quantitative information about the activity monitored; Grieve discusses the consequences of signal processing on the information content of the raw signal. The Emg. signal is known to depend upon a large number of parameters and unfortunately workers investigating Emg. do not, in general, give sufficient description of their experimental technique to permit direct comparison of their experimental results.

The use of Emg. as a quantitative measure of the force generated by muscles has been extensively investigated but, to date, the conclusion reached by Ralston (1961) still obtains - that the direct relationship of force to Emg. was only possible under very restricted conditions of muscular excursion, load and speed of contraction.

It is, however, generally considered that Emg. is

a reliable indicator of the temporal activity of muscles (Sutherland, 1966; Paul, 1971) and it is frequently used to characterise the phasic activity of the leg musculature during locomotion. The latency period discussed in 2.7.1 should be taken into account when relating muscle force and temporal Emg. data for locomotion activities. Paul (1971) reviewed literature on leg muscle Emg. and related walkpath measurements and made the recommendation that Emg. signals should not be interpreted in isolation or only in relation to measured kinematics since they depended much more on the relevant dynamics.

One of the first comprehensive studies of leg muscle Emg. during locomotion was undertaken by the University of California (1953). They asserted that a rectified and filtered electromyogram trace (providing an envelope picture of Emg. activity) was an acceptable semi-quantitative indication of muscle activity. They used wire electrodes (electrodes which are implanted directly in the muscle) but were only able to study one muscle at a time. Their summary Emg. curves for the shank muscles, for normal locomotion of six subjects, (five male, one female) are presented in figure 2.26. These curves were normalised in time to one complete stance and swing phase of locomotion. The temporal features of the curves are typical for normal locomotion and subsequent investigators confirm the general features of the patterns shown. The shank muscles divided approximately into two groupings, the Anterior tibial group and the remaining shank muscles. The Anterior tibial group was active at the end of stance phase, throughout swing and at the beginning of the next stance

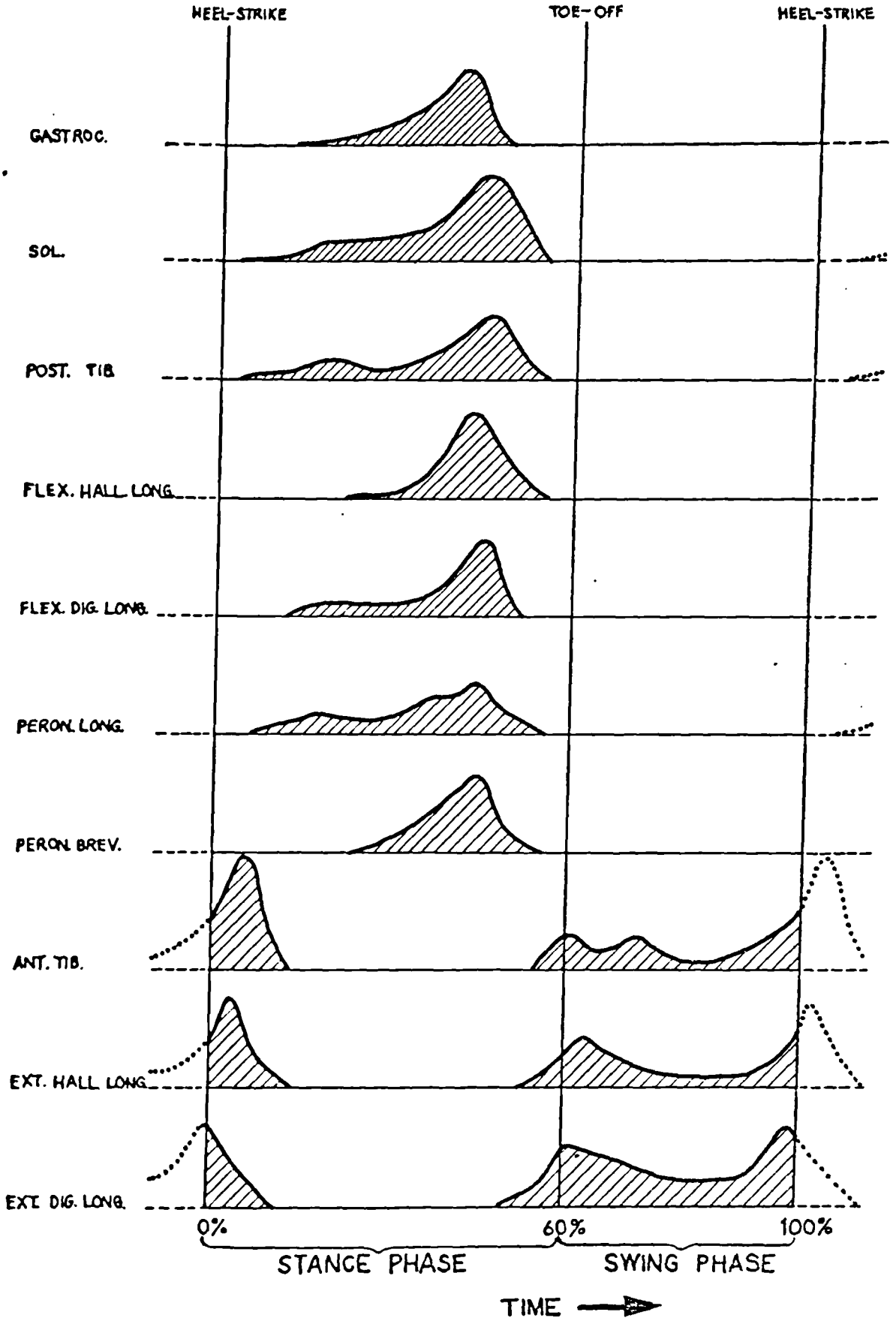

Figure 2.26 Emg. Curves for the Shank Muscles (After University of Califormia, 1953)

phase. Each member of the group showed a characteristic peak just after heel strike and immediately after toe off. The remaining shank muscles - the Calf, Posterior tibial and Peroneal groups, indicated activity from just after heel strike until just prior to toe off, with a pronounced peak occurring at about 45% of the walking cycle. The temporal division of the shank muscle groups will be used in formulating the analytical model in 4.2.

A survey of the literature relating to temporal Emg. characteristics of the shank muscles was undertaken; unfortunately for reasons indicated above, direct comparison was found to be difficult. In addition, in a few studies a number of subjects were studied but only a summary curve or a single representative trace was presented, and in some instances only a few of the shank muscles were investigated. The summary curves presented in figure 2.27 must therefore be treated with some reserve. The sources consulted - University of California (1953), Sheffield et al (1956), Close and Todd (1959), Houtz and Walsh (1959), Mann and Inman (1964), Sutherland (1966), Battye and Joseph (1966), Townsend et al (1978) and Ambagtsheer (1978) - encompass a total of eighty test subjects but for the reasons stated above it should be understood that the summary curves do not necessarily represent summary of eighty individual records. Attention is also drawn to the variation in toe off in figure 2.27 which is attributed to differences in measuring techniques (heel switch, visual inspection of cine records) and natural variation in gait.

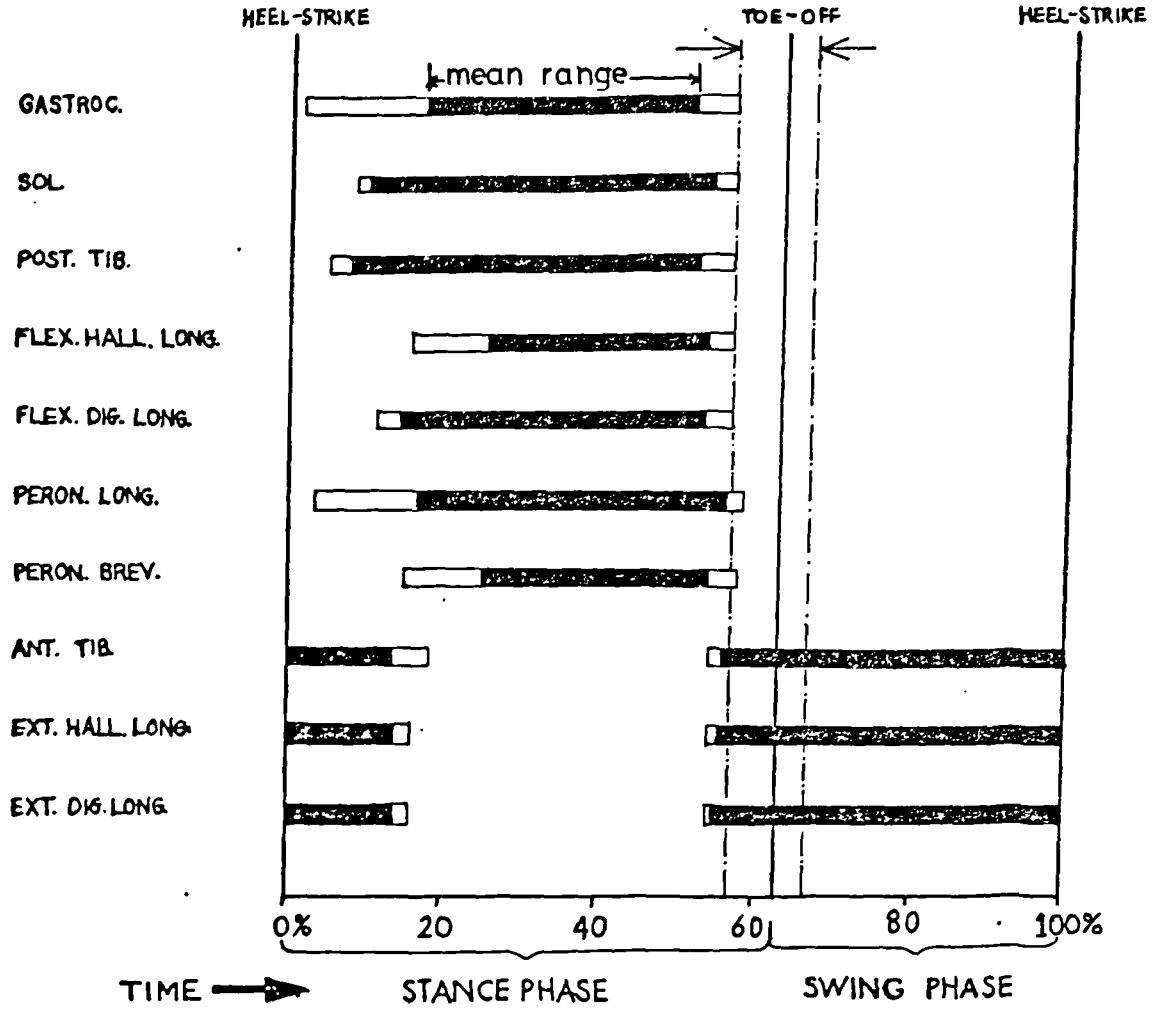

Figure 2.27 Summary Curves of Reported Temporal Emg. Activity in the Shank Muscles

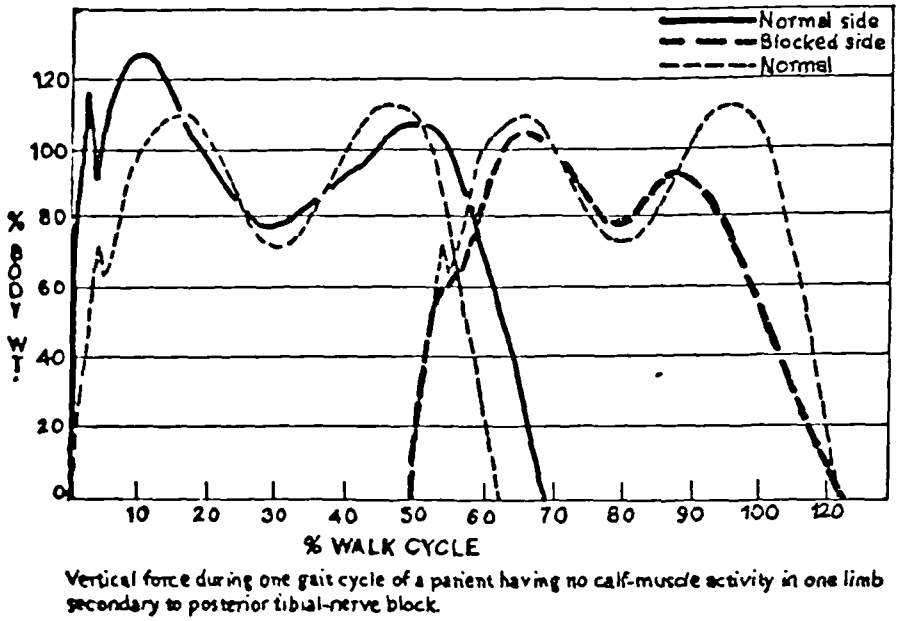

Figure 2.28 Effect of Posterior Tibial Nerve Paralysis on Gait (After Simon et al, 1978)

2.7.4 Notes on the Function of the Shank Muscles

Chhibber and Singh (1970) investigated the question of muscular dominance in cadaver lower limbs. They concluded, on the basis of muscle weight, that the left leg was dominant over the right. Weight by itself is however a questionable basis for inferring that the muscles of one leg are functionally dominant over the other.

Simon et al (1978) conducted normal locomotion experiments in which nerve block of the posterior tibial nerve was used to eliminate the Calf group of muscles for one leg. In their study force platform and cine film evidence was considered. It was reported that, in the affected limb, the centre of pressure was observed to remain under the region of the ankle joint until late stance when it progressed rapidly towards the toes. They concluded from their studies that the demands of locomotion do not require the Calf group and contended that the function of the Calf group is to restrain the forward momentum of the body rather than to propel it further. This begs the question - what muscles do act in propelling the body? Certainly figure 2.28 reproduced from their report indicates that the gait pattern was disrupted considerably. They did not report at which level the posterior tibial nerve block was effective and so it is possible that the Posterior tibial muscles were paralysed as well, leaving only the Peroneal muscles.

One interesting feature of figure 2.28 is the unusual spike in the force record just after heel strike. This spike has been investigated by Cavenagh et al (1980) who associated its amplitude particularly with the type of footwear, bare feet giving the greatest amplitude.

Nigg et al (1979) considered that the spike was part of the purely passive mechanical response (with little muscular activity) of the effective mass of the leg to the impact on the ground at heel strike.

Lapidus (1955), after survey of the literature, pointed out that the function of the Calf muscles was frequently wrongly stated. The Calf muscles were either credited with the role of evertors at the Tcn. joint; or another muscle altogether, for example the Posterior tibial muscle, was attributed with the role of most powerful invertor, whereas in fact they are the most powerful invertors of the ankle. It should be noted that some of the confusion may have arisen through the frequent and sometimes misleading tendency to describe muscle function with respect to the 'free' foot. Lapidus further commented that the Anterior tibial muscle is almost neutrally placed with respect to the Tcn. axis, acting only as a pure dorsiflexor at the upper ankle joint. This view was also subscribed to by Fick (1911) and Elftman (1960). In a study of shank muscle Emg., O'Connell (1958) reported that the Emg. activity of the Anterior tibial muscle was very variable during inversion of the free foot and was sometimes apparent during eversion. It was suggested that the switching to eversion activity might be due to the Anterior tibial muscle changing its line of action with respect to the Tcn. axis during inversion eversion movements of the foot.

Paul (1971), whilst reviewing reported leg Emg. activity, noted that there was little evidence of antagonistic muscle activity between the ankle dorsi-flexors and plantarflexors. He observed that positive

ankle moments up to 10% of the walking cycle corresponded to dorsiflexor Emg. activity whilst subsequent negative moments corresponded to plantarflexor Emg. activity. The reported Emg., see figures 2.25 to 2.28, indicates that there is antagonistic action in respect of the invertor-evertor muscles during locomotion. Calliet (1974) attributed the role of Tcn. joint stabilisers to the muscles with inversion and eversion action. Jones (1941) considered that the Posterior tibial and Peroneal muscle groups act weakly in controlling flexion-extension, their main role being in inversion-eversion actions. He also stated that these groups act to preserve the relative constancy of the ratio of weight distribution among the metatarsal heads of the ball of the foot.

2.8 Locomotion Studies

2.8.1 Introduction

The literature relating to locomotion studies is so extensive that it is far beyond the scope of the present study to give a complete review. Historical aspects of biomechanics and studies of particular relevance to the hip and knee joint are reviewed by Paul (1967) and Morrison (1968). More recently Jarrett (1976) has comprehensively reviewed systems for the kinematic analysis of gait. The present discussion will be confined to those studies having relevance to the ankle joint.

2.8.2 Gait Temporal Characteristics and Ankle Kinematics

The temporal nature of shank muscle Emg. has already been discussed in 2.7.3. Other temporal characteristics have been widely studied to establish normal patterns.

Murray et al (1964) investigated in a group of sixty subjects aged 20-65 the fundamental characteristics of gait in relation to age and height. It was found that the walking cycle duration in time was not related to age or height and did not, for a single subject, vary significantly from step to step. Stance and swing phase duration were not correlated with age and height but were closely related to total cycle time. Double limb support periods occurred twice in a single walking cycle for approximately equal time periods. The stride dimensions, step and stride length, were significantly shorter for the 60-65 age group than for the younger age groups. The step and stride lengths were correlated systematically and significantly with height; the shortest subjects took the shortest steps and stride, the taller subjects the longer steps and strides. The foot toe out angle was found to be greater in the older subjects. Stride width showed no significant differences with age and height. The mean values reported for stride dimensions and cycle temporal factors are shown in figure 2.29.

Murray et al also investigated leg rotations in two dimensions using reflective targets and cine film. Their results for the ankle rotation, about the Tc. axis, are illustrated in figure 2.30. The ankle rotation typically showed two waves of dorsiflexion (annotated Fl1 and F12) and two waves of plantarflexion (annotated Ex1 and Ex2) during each complete walking cycle.

Wright et al (1964) used electrogoniometers to measure the rotations occurring about the Tc. and Tcn. axes during normal locomotion. They used the axes defined by Hicks (1953). They investigated the effect

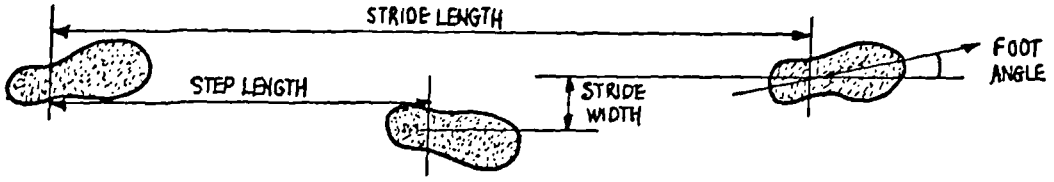

(a) Schematic representation of stride dimensions.

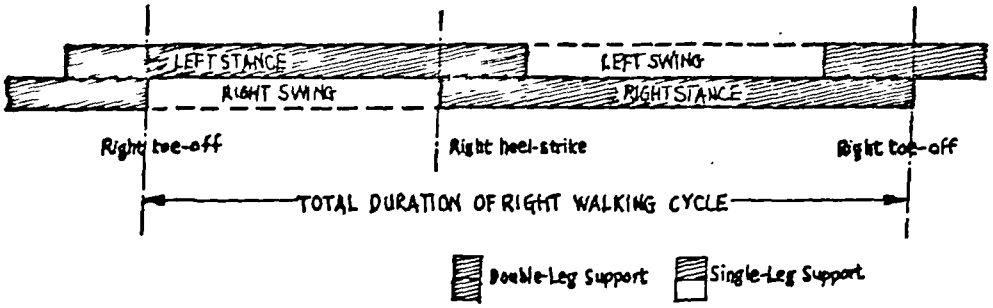

(b) Schematic representation of a right walking cycle showing temporal relationships.

(c) Tabulated Mean Values

Characteristic	Mean Value	(Std. Dev.)
Stride length	158.8 cm.	(12.4)
Step length	79.3 cm.	(6.0)
Stride width	7.2 cm.	(2.9)
Foot angle	6.8 toe out	(5.8)
Swing phase	0.42 s.	(0.04)
Stance phase	0.63 s.	(0.07)
Cycle duration*	1.04 s.	(0.10)
Double leg support	0.10 s.	(0.03)

* equivalent to a cadence of 115 steps per minute

Figure 2.29 Gait Dimensions and Temporal Characteristics (After Murray et al, 1964)

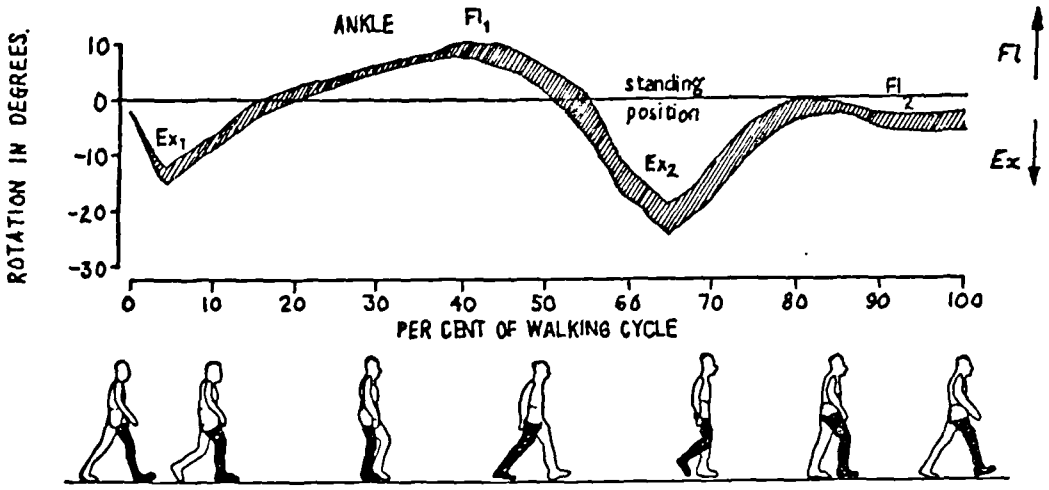

Mean patterns of sagittal rotation for five age groups, twelve men in each group, two trials for each man. Plantarflexion = Ex ; Dorsiflexion = Fl .

Figure 2.30 Normal Range of Ankle Rotation (Adapted from Murray et al, 1964)

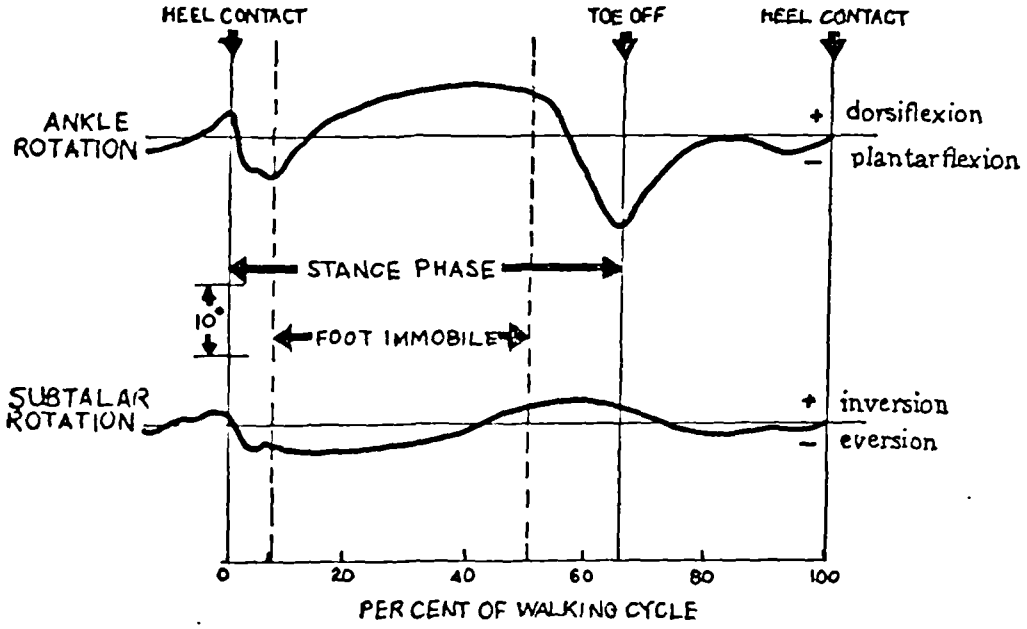

Ankle and subtalar rotations during normal walking (subject DGW).

Figure 2.31 Normal Tc. and Tcn. Joint Rotations Measured by Goniometer (After Wright et al, 1964)

of toe in/out angle, side slope walking and hill slope walking upon the ankle angles. The results of particular interest to the present study, normal and side slope walking, are reproduced in figures 2.31 and 2.32. They drew an analogy between the Tc. and Tcn. axes and a universal joint to illustrate how rotations can be transmitted between the shank and foot. Referring to figure 2.31, for normal locomotion, a sharp negative rotation occurred about both axes during the first 5% of the cycle immediately after heel strike. In both joints a progressive rotation occurred from 20 to 50% of the cycle as the body moved forwards over the foot. Then the Tc. joint abruptly became plantarflexed whilst the rotation at the Tcn. joint more or less ceased. In side slope walking, figure 2.32(b) with the test foot uphill in an everted position, the test curve patterns were similar in form to the normal locomotion patterns. The main differences were that the range of Tc. motion increased and the Tcn. motion indicated a shift towards eversion. With test foot downhill, figure 2.32(a), in an inverted position, the patterns were again similar to the normal locomotion curves, the main change being a shift at the Tcn. joint towards inversion. They concluded that the Tc. and Tcn. joints were interdependent and acted as a single mechanism during walking. The average locomotion range of Tc. and Tcn. joint rotation was reported to be 14° and 6° respectively for one subject.

Close and Inman (1952) studied the rotational freedom of the foot with respect to the shank, during locomotion, by cine filming implanted pins. They measured the rotation about the Tc. axis in two dimensions

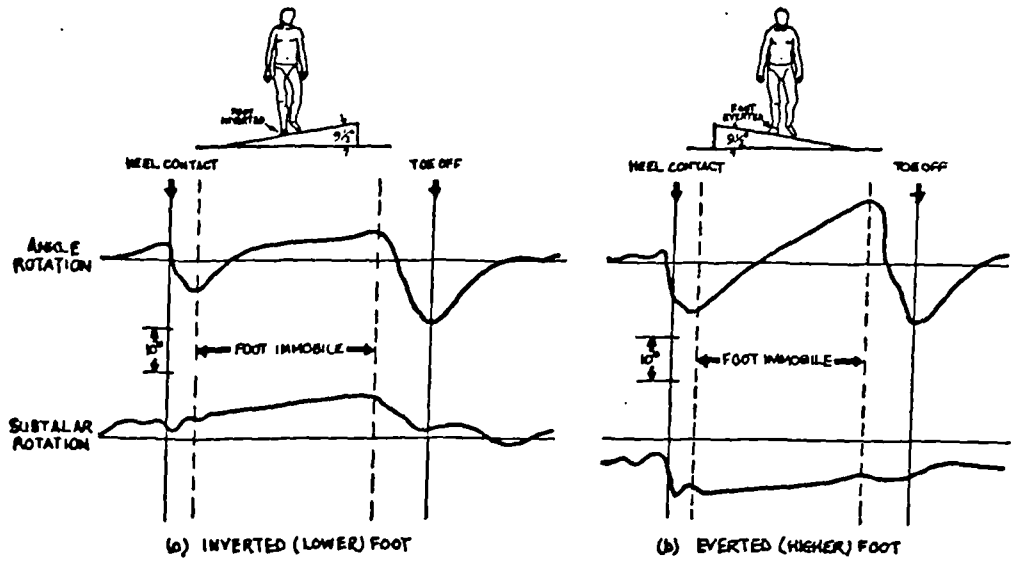

Ankle and subtalar rotations during sidehill walking (subject DGW).

Figure 2.32 Patterns of Tc. and Tcn. Joint Rotation due to Side Slope Walking (After Wright et al, 1964)

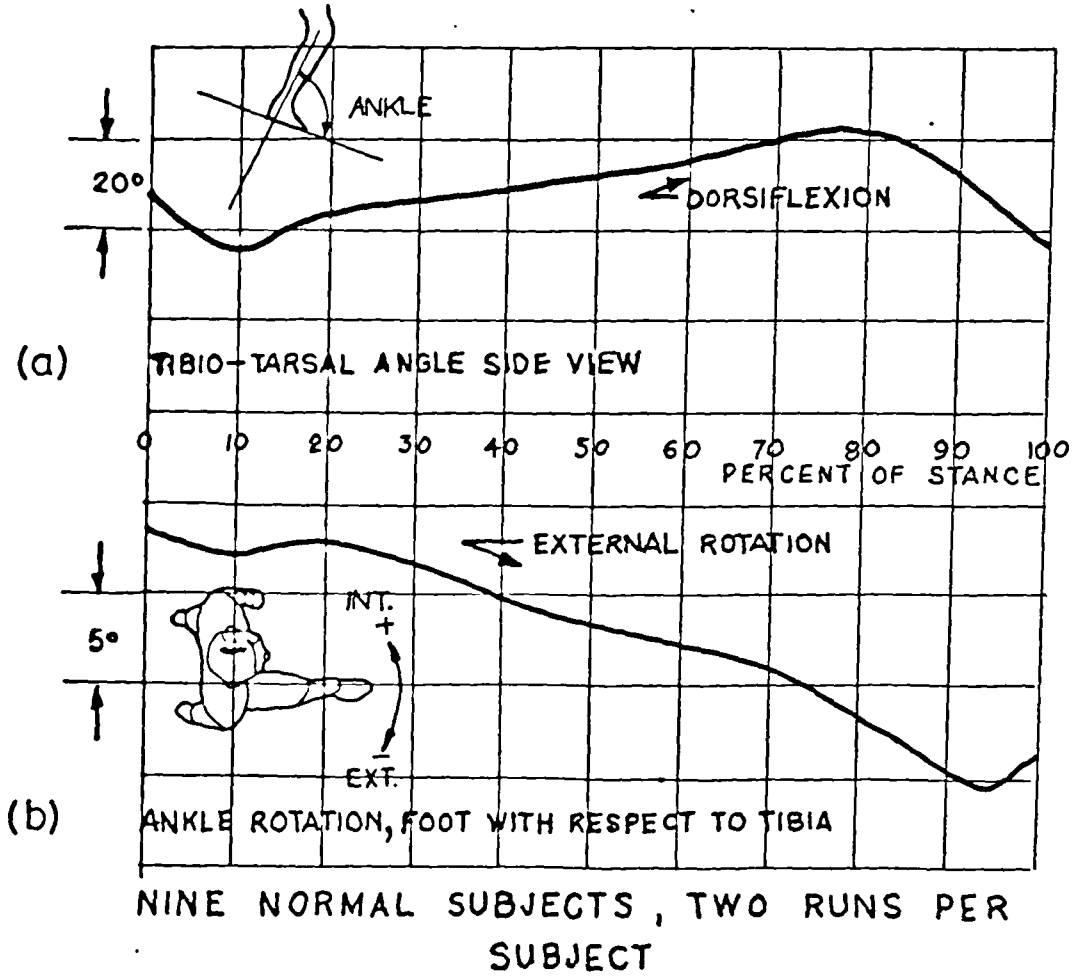

Figure 2.33 Ankle Rotation Studies (Adapted from Close and Inman, 1952)

only and, for nine normal subjects, a range of approximately 25° was reported, see figure 2.33(a). They also measured the horizontal rotation of the foot with respect to the tibia and found that, after slight internal rotation of the tibia, for the greater part of stance phase the tibia rotates externally relative to the foot. The total range of internal/external rotation was shown to be about 15°, see figure 2.33(b). In 1953 the same authors used similar methods to establish the locomotion range of motion about the Tcn. axis. Typical results for one subject, shown in figure 2.34, indicate an overall range of 11°.

Lamoreaux (1971) studied gait determinants using a goniometer exoskeleton, with which lower limb joint angles were measured in three dimensions. He presented summary curves of Tc. joint angular displacement with time and the derivatives - angular velocity and angular acceleration - for normal walking as shown in figure 2.35. Note that the peak angular velocity and acceleration are associated with heel strike having their peaks at the very beginning of stance phase.

2.8.3 Ankle Joint Forces and Moments in Gait

The magnitudes of the external forces, acting on the foot in locomotion, referred to the ankle were first calculated by Bresler and Frankel (1950). They performed free body analysis of the whole leg. Ground reaction forces measured by force platform together with cine film in three dimensions were used to calculate the external forces and moments acting at the hip, knee and ankle. They included the inertial and gravitational effects of leg segment mass and typical results curves

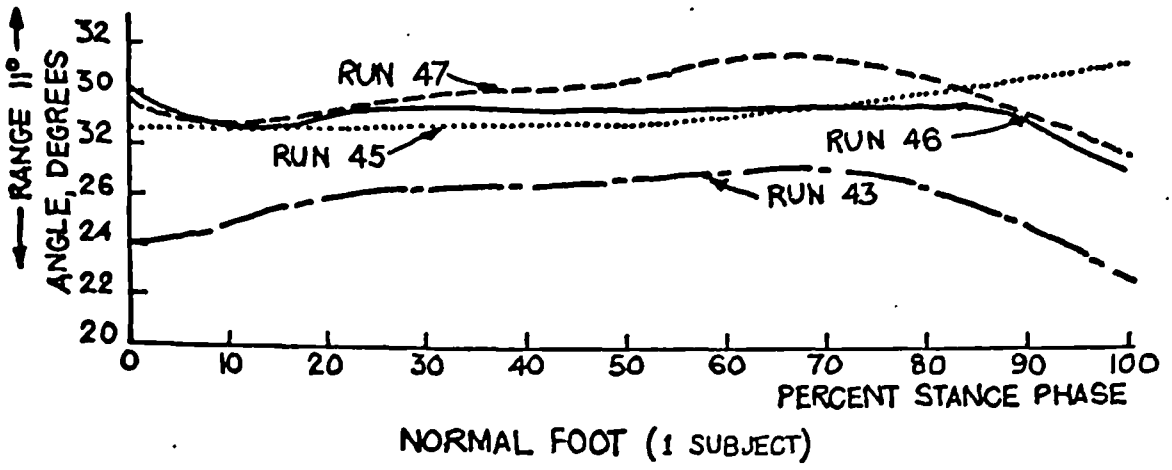

Figure 2.34 Rotation at the Tcn. Axis during Locomotion (After Close and Inman, 1953)

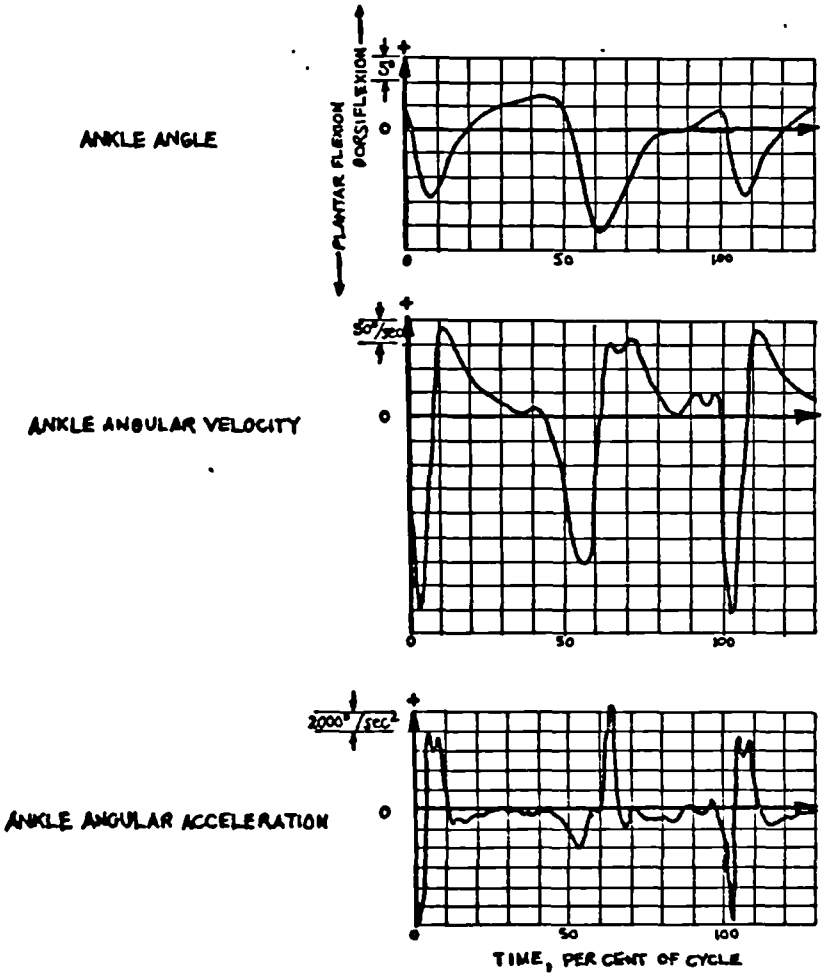

Figure 2.35 Rotation at the Tc. Axis during Locomotion and Higher Derivatives (Adapted from Lamoreaux, 1971)

are shown in figure 2.36. Their analysis indicated that the contribution of the gravity and inertial components were negligible at the level of the ankle. They did not proceed further to estimate the muscle tensions and the internal joint forces.

Peizer and Wright (1971) reviewed biomechanics of gait and presented curves for ankle rotations and moments during gait as shown in figure 2.37. They do not quote their source for the curves; the Tc. moments, figure 2.37(a), typically show two peaks, one negative -18 to 20 ft-lbf (-24 to 27Nm.) corresponding to a peak plantarflexion at 10% cycle and the second peak - 60 to 80 ft-lbf (81 to 108Nm.) corresponding to peak dorsiflexion at about 45% of the cycle. The internal/ external rotation moment, figure 2.37(b), shows three peaks, 2 ft-lbf (2.7Nm.) at about 5% cycle, -0.2 ft-lbf (-0.27Nm.) at 15% of the cycle and 5 ft-lbf (6.8Nm.) at 42% cycle. The negative peak at 15% of the cycle corresponded to a change in tibial rotation from internal to external. The Tcn. moment curve shown in figure 2.37(c) represents the only known source of published data regarding moments for this joint. The moment curve indicates a peak inverting moment of 15 ft-lbf (20Nm.) at 12% of the cycle corresponding with maximum eversion angle at the Tcn. joint.

2.8.4 Lower Limb Joint Force Analyses

Paul (1967) analysed the hip joint for locomotion activity in three dimensions. In his analysis the twenty-two muscles crossing the hip were reduced to six groups, through similarity of lines of action and phasic Emg. evidence. The use of the equilibrium

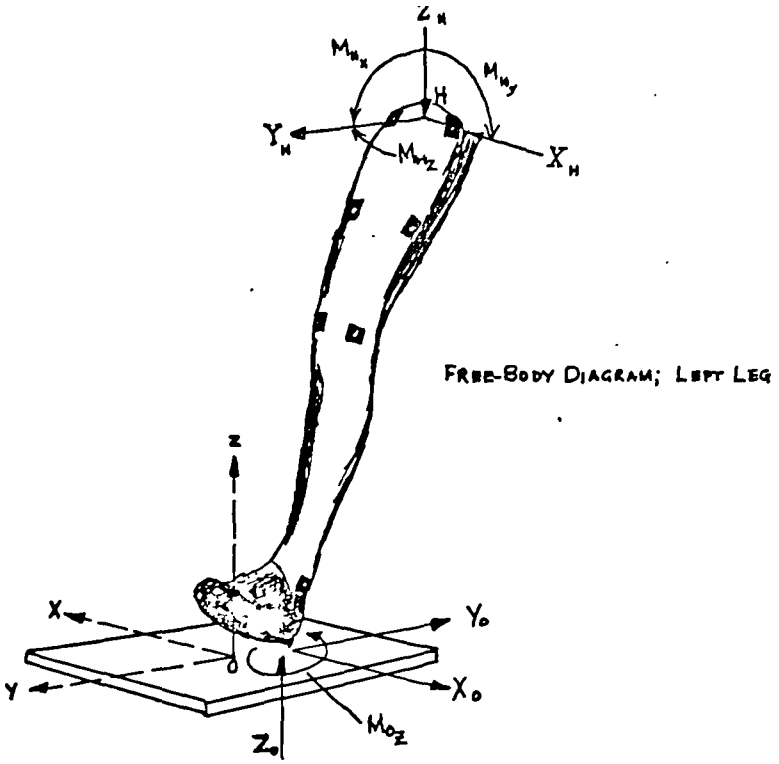

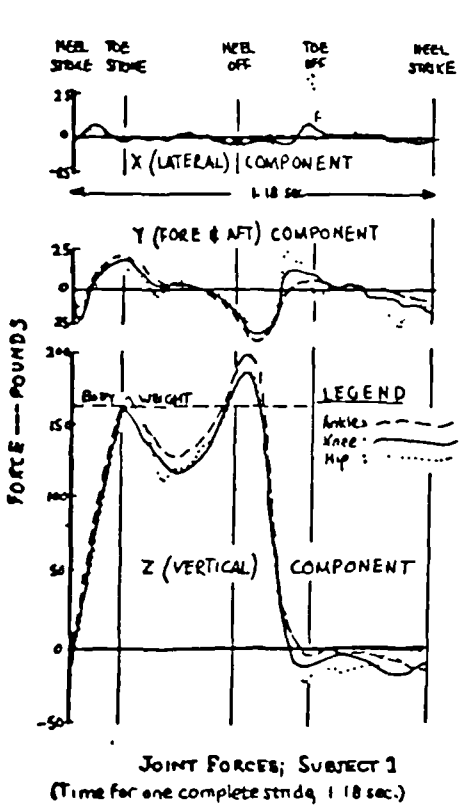

JOINT FORCES; SUBJECT 1
(Time for one complete stride, 1.18 sec.)

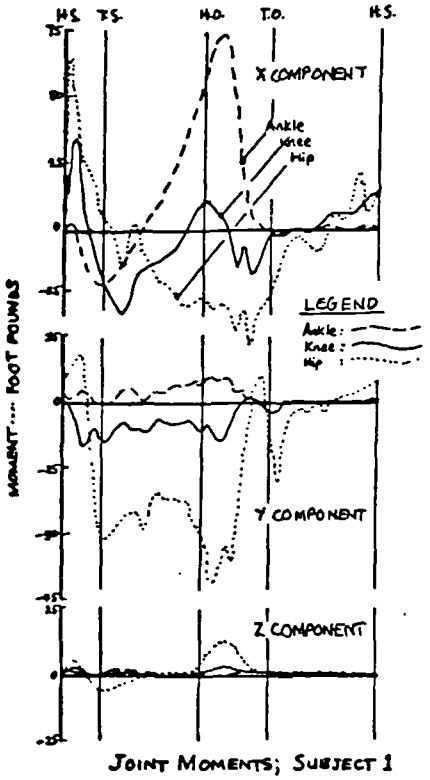

JOINT MOMENTS; SUBJECT 1

Figure 2.36 External Forces and Moments at the Leg Joints due to Normal Locomotion (After Bresler and Frankel, 1950)

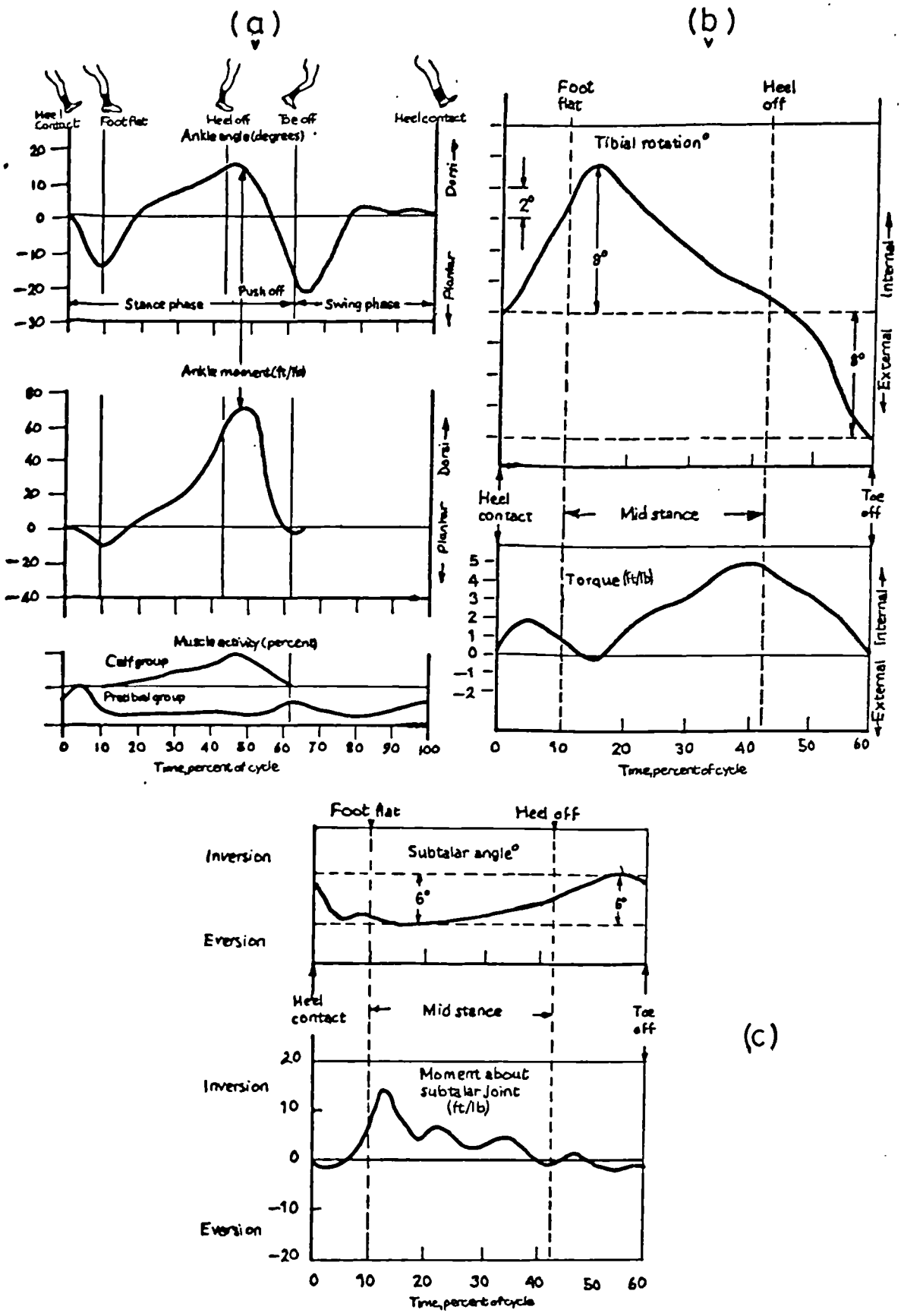

Figure 2.37 Rotations and External Moments Acting at the Ankle in Locomotion (Adapted from Peizer and Wright, 1971)

equation referring to moments acting about the long axis of the femur was rejected and the remaining five equations, (three force and two moment), were used to solve joint and muscle forces at the hip. This, however, left six unknowns to be determined by five equations. The procedure adopted was, therefore, to obtain a solution corresponding to (a) the action of one flexor or extensor group, and (b) the action of the other flexor/extensor group. The values of joint force determined from these two possibilities were taken to be extremes between which the true values would lie. This established upper and lower bound solutions for hip joint force, the lower values being accepted. The peak joint force reported for the hip in normal locomotion was in the range 2.3 to 5.8 times Body Weight.

In 1968 Morrison presented a similar three-dimensional approach to modelling of the knee joint in locomotion. He analysed a knee model which included the three main muscle groups namely the Hamstrings, Gastrocnemius, and Quadriceps femoris, and the Collateral and Cruciate ligaments. Minimum joint force was used as a criterion for selecting solutions to the equilibrium equations. The knee joint force peak was estimated as two to four times Body Weight during stance phase. In addition one phase of activity was reported for the gastrocnemius muscle from 25/30% to 50/60% of the walking cycle, and from ten subjects a mean muscle force of 1020N at 45/50% of the cycle was estimated, see figures 2.38(a) and (b).

Poulson (1974) analysed the hip and knee simultaneously, for locomotion, using the techniques developed

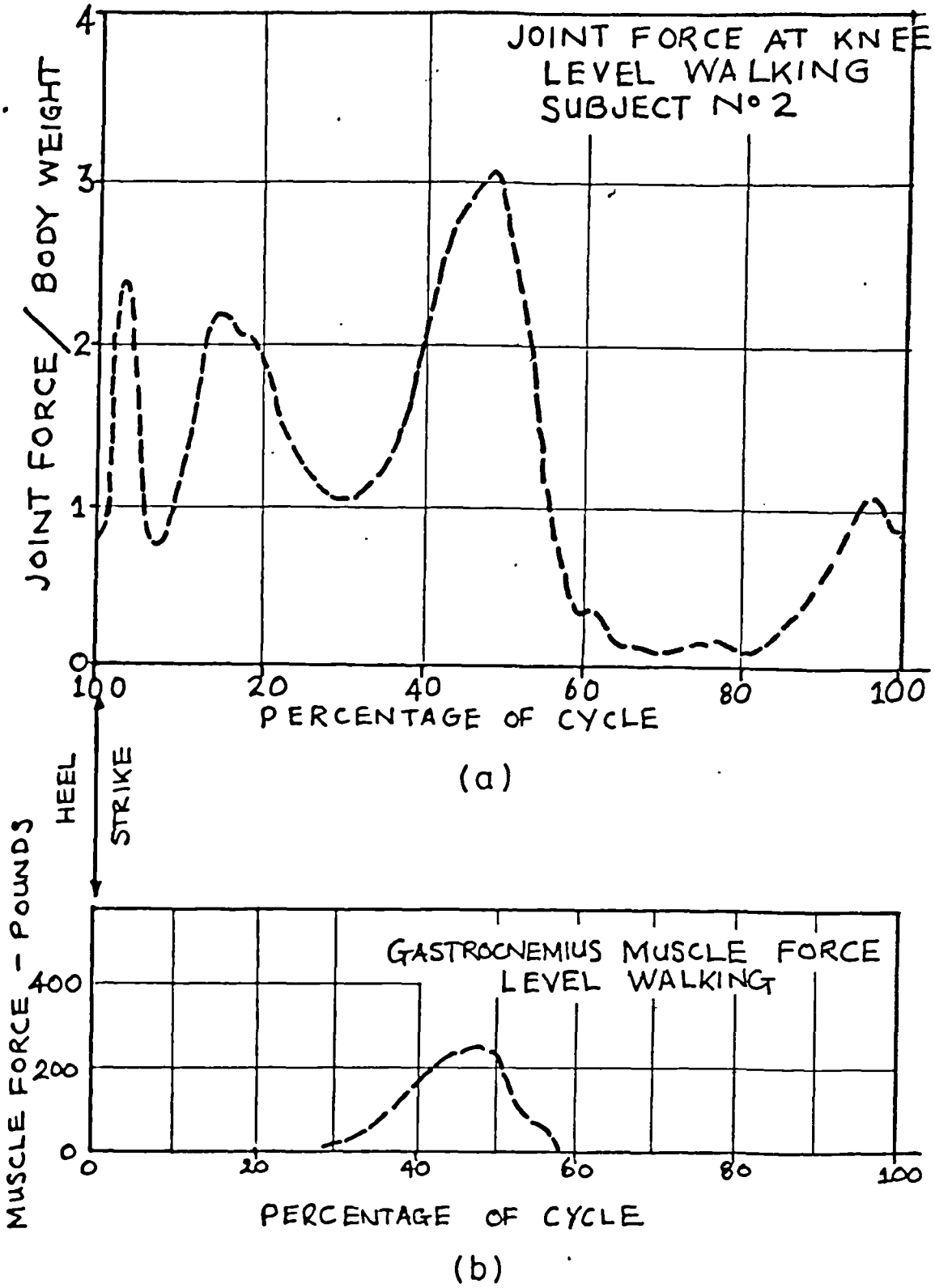

Figure 2.38 Knee Joint and Gastrocnemius Muscle Forces during Normal Locomotion (Adapted from Morrison, 1968)

by Paul and Morrison. The muscles of the thigh and shank were grouped and recruited to minimise hip and knee joint reaction. The results obtained were essentially similar to the earlier studies, however it is notable that two phases of gastrocnemius activity were reported. The first in stance phase, as reported by Morrison, and an additional one in swing phase. Poulson's results showed that the gravitational and inertial components of the moments acting at the ankle are small enough to be considered insignificant in comparison with the external force components.

One of the first locomotion analyses of the ankle to include joint forces was reported by Brewster et al (1974). They recorded two-dimensional cine and force platform data for five normal males and one male with degenerative joint disease. A simple uniaxial hinge model of the ankle was used with just two muscle groups, the Calf and the Anterior tibial groups. Foot switches were used to divide stance phase into three periods; heel strike to heel off, heel off to metatarsal off and metatarsal off to toe off. Different local coordinate systems were used for each period of stance. A typical ankle joint force pattern is shown in figure 2.39. These curves have one curious feature in that they indicate that the Calf group is active throughout stance phase. The Emg. evidence presented in figures 2.25 to 2.27 shows that the Calf group is usually inactive at early stance phase. In addition, if the sign of the external moment about the ankle Tc. axis were to be used as the basis for including the Calf muscle (positive ≡ active, negative ≡ inactive), then as figure 2.37(a) shows, there would only be Calf activity from about 15% cycle

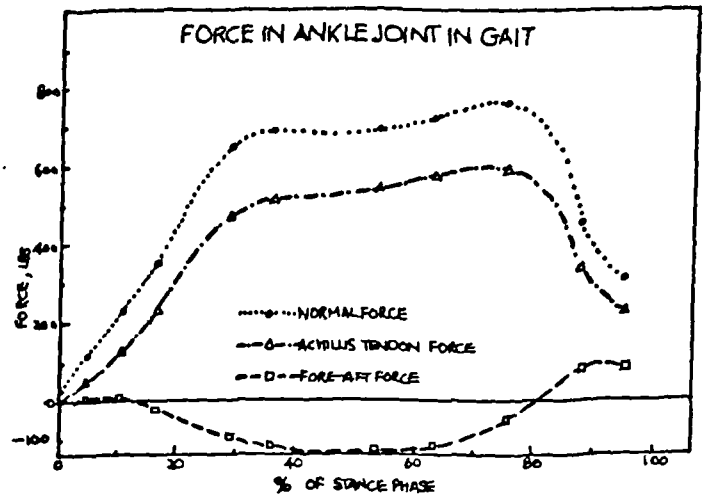

Figure 2.39 Forces at the Ankle in Locomotion, a Two-Dimensional Analysis (Brewster et al, 1974)

Part (a): $F_N = F_A\cos\alpha - F_H\sin\theta + F_V\cos\theta$

$F_T = F_A\sin\alpha - F_H\cos\theta - F_V\sin\theta$

$$F_A = \frac{-F_H(A\sin\theta + B\cos\theta) + F_V(A\cos\theta - B\sin\theta - C)}{D\cos\alpha - E\sin\alpha}$$

Part (b): $F_N = F_K\cos\sigma - F_H\sin\sigma + F_V\cos\theta$

$F_T = F_K\sin\sigma - F_H\cos\theta - F_V\sin\theta$

$$F_K = \frac{-F_H(A\sin\theta + B\cos\theta) + F_V(A\cos\theta - B\sin\theta - C)}{G\sin\sigma - A\cos\sigma}$$

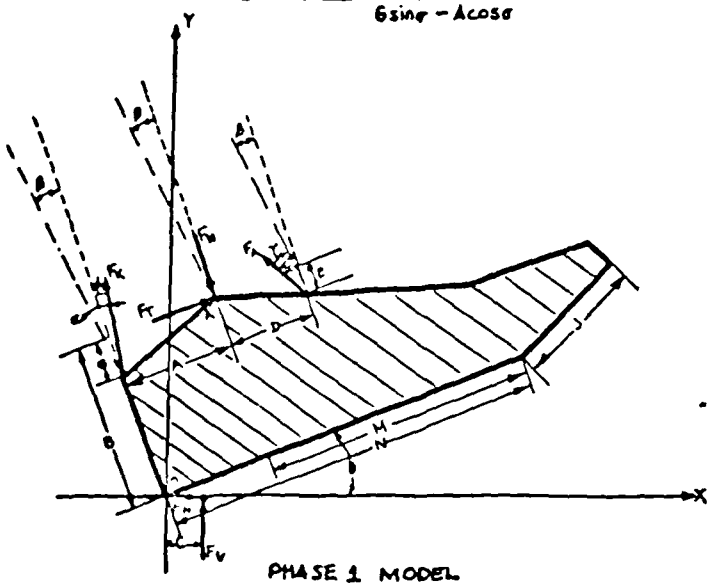

FIG. 1. Free-body diagram of the foot during Phase 1 of the stance cycle (heel strike to heel off) and equations derived to solve for compressive force (F_N), tangential force (F_T), Achilles tendon force (F_K) and anterior tibial tendon force (F_A).

Figure 2.40 Two-Dimensional Rigid Body Model of the Foot Segment (After Stauffer et al, 1977)

onwards. A possible explanation for this apparently abnormal behaviour of the Calf group in the model of Brewster et al is that a two-dimensional model does not allow correct orientation of the Tc. axis and thus there is the possibility for error in calculating the moment due to the external force. Their results showed that the normal force (in line with the tibia) was a maximum during push off and varied between 4.5 to 5 times Body Weight. The achilles tendon force, (Calf group force), peaked at 3.5 times Body Weight coinciding with the peak normal force. The one subject with joint disease showed a peak normal force of 3.5 times Body Weight.

This model was developed further by Stauffer et al (1977) who subdivided period one (vide supra) into two parts, the first where the Calf group tension equalled zero and the Anterior tibial group was greater than equal to zero force. In the second the Anterior tibial group was absent, only the Calf group was capable of generating tension. A rigid rocker type of free body was used to model the foot, as shown for period one in figure 2.40. They neglected the inertial effects of the foot, but stated that they had included the much more significant effect of the remainder of the body mass. They did not elaborate on where or how this latter source of inertial force was included. The tip of the medial malleolus was used to locate the axis of the ankle. The foot was filmed in two dimensions at 100Hz., which was later sampled at 15 to 30Hz., and forces measured with the use of a force platform. The muscle and joint forces were estimated from the two-dimensional force and moment equilibrium equations

shown in figure 2.40. The mean range of motion about the Tc. axis was 24.4° for normal locomotion. They reported that the Anterior tibial group was active for less than the first 10% of stance phase and the greatest magnitude observed was less than 0.2 times Body Weight. It was observed that the pattern of achilles tendon force always paralleled the normal compressive force but at about 100% lesser magnitude. The levels of ankle fore-aft shear and compressive force were greater in normals (five) than in pre-operative patients (nine) and post ankle joint replacement subjects (six), as shown in figure 2.41. Compressive force levels of up to and exceeding five times Body Weight were recorded in normal subjects.

Finally the most recent force analysis of one of the leg joints was undertaken by Stokes et al (1979), who analysed the Metatarsophalangeal joint in the foot for locomotion. Unfortunately the model used was a very greatly simplified representation of the joint in two dimensions, which neglected the shearing forces transmitted from the sole. (Bojsen-Møller and Lamoreaux (1979) have demonstrated mechanisms amongst the plantar structures of the foot expressly designed to transmit shearing forces between the sole and the Metatarsophalangeal joints.) They estimated, using force equilibrium methods, forces of up to 600N. and 100N. acting in the first and fifth Metatarsophalangeal joints respectively. These peak forces occurring just prior to toe off in stance phase.

The basis of the analysis presented in this thesis was reported at the Warsaw meeting of the International Society of Biomechanics and is shortly to be published (Procter et al, 1980).

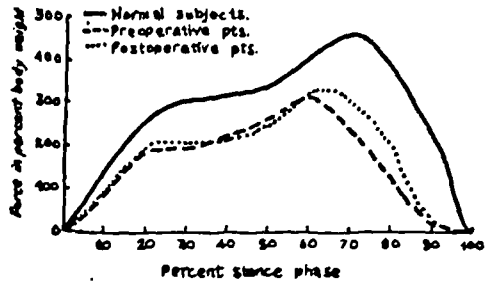

Mean patterns of compressive ankle force (F_N).

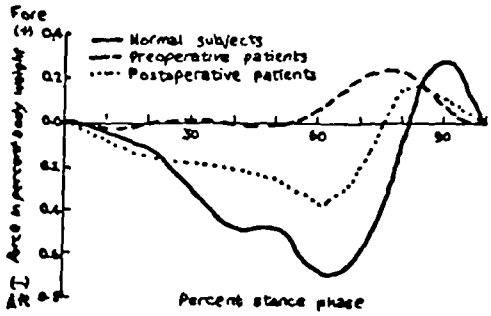

Mean patterns of tangential ankle force (F_T).

TABLE : Mean (and Standard Deviation) Values for Forces about Ankle Joint

Subjects	Achilles Tendon Force F_K	Forward Tangential Force (Shear) F_T (Fore)	Backward Tangential Force (Shear) F_T (Aft)	Compressive Force F_N
Normal Subjects	* 387 (± 57)	68 (± 17)	30 (± 7)	473 (± 63)
Preoperative Patients	243 (± 103)	3 (± 1)	24 (± 9)	323 (± 121)
Postoperative Patients	243 (± 97)	36 (± 15)	16 (± 12)	332 (± 102)

* Note Stauffer et al did not state units—lbf. assumed

Figure 2.41 Graphical and Tabulated Results from Analysis of the Two-Dimensional Ankle Model due to Stauffer et al (1977)

CHAPTER 3

ANTHROPOMETRIC STUDIES

3.1 Introduction

The review of published literature did not reveal any comprehensive source of anthropometric data sufficient to undertake three-dimensional force analysis at the ankle. An anthropometric study was therefore undertaken.

Various techniques for the measurement and collection of anthropometric data were considered. The recovery of coordinates from stereo pairs of photographs was found by experiment to be impractical. The ankle has several reentrant surfaces, and many photographic views would be required for adequate data recovery from cadaver material.

In several anatomical studies sectioning methods have been used. Cadaver material, either embedded in a suspending medium (Jensen and Metcalf, 1975) or frozen, is serially sectioned at equal intervals from head to toe. Then photographs of each cross-section are analysed using a digitiser to provide coordinate data for the internal structures. The complexity of the ankle structures together with the fact that many of the ankle structures turn through a right angle precludes the use of sectioning methods.

Recent advances in X-ray tomography have enabled the muscles and internal structures of living subjects to be defined. This is however an expensive technique and will require considerable refinement before it can be considered a practical solution for general anthropometric measurement.

In joint biomechanics studies such as those of Paul (1967) and Morrison (1968) direct measurement of anatomical structures in embalmed cadavers was used. The method is tedious, costly in time and can only,

in general, be used with embalmed cadaver material. There are however advantages in that structures may be defined in whatever detail is necessary, with good precision and accuracy, and time is not as pressing as with fresh cadavers. For these reasons a direct measurement method was adopted in the present study.

The range of measurements required was determined after experience had been gained from two preliminary dissections. The first dissection showed that the embalmed ankle was fixed in about 30° plantarflexion and due to the set of the muscles at death or subsequently could not be manipulated. It was observed that the lines of action of the ankle tendons relative to the shank are firmly controlled by the retinacula. It was found that if the entire leg musculature was removed the ankle could be manipulated in a free and lifelike fashion; the proximal part of the tendon was maintained under light tension by a spring and fishook arrangement which pulled each tendon approximately along the line its muscle would have done in life, see figure 3.1.

It was found that the retinacula were very complicated structures. Their action as the foot was moved relative to the shank showed that they act as variable radius pulley surfaces. In addition their sheet-like form suggests that simple, single line of action modelling would be an oversimplification.

Measurements of the second dissection subject showed that, excepting the achilles tendon and the tendon of flexor hallucis longus, the line of action of the tendons was virtually constant with respect to the foot segment (for definition of tendon line of action see 3.4.4). This was found to be valid for the distal part of each

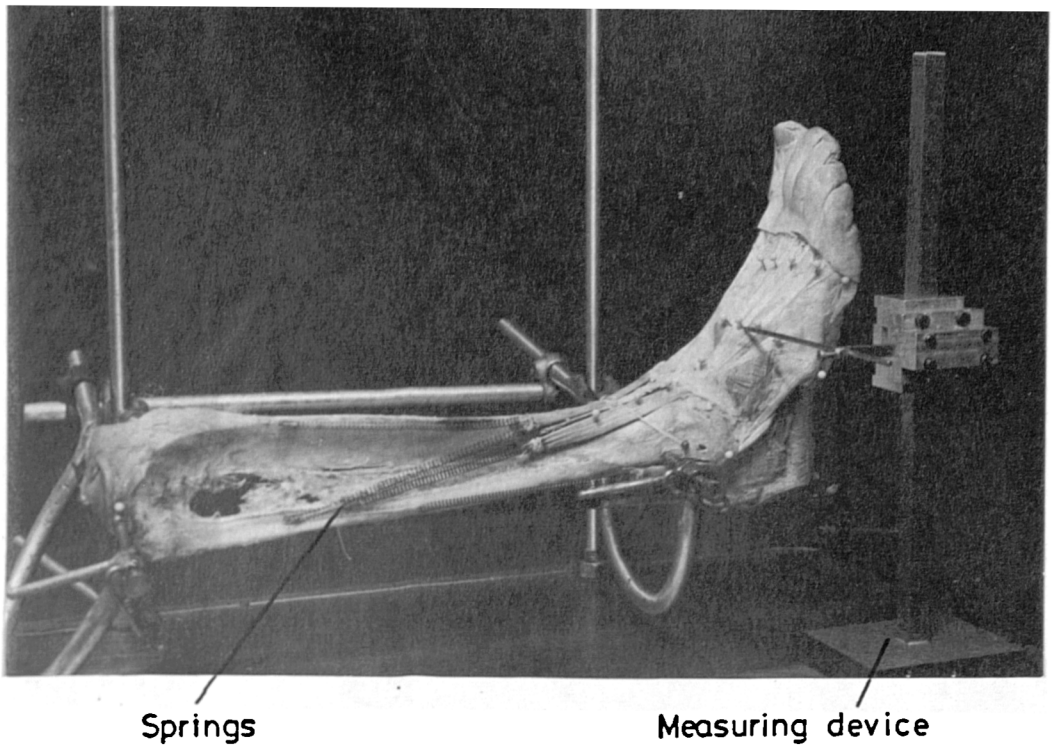

Figure 3.1 Photograph of a Typical Cadaver Preparation

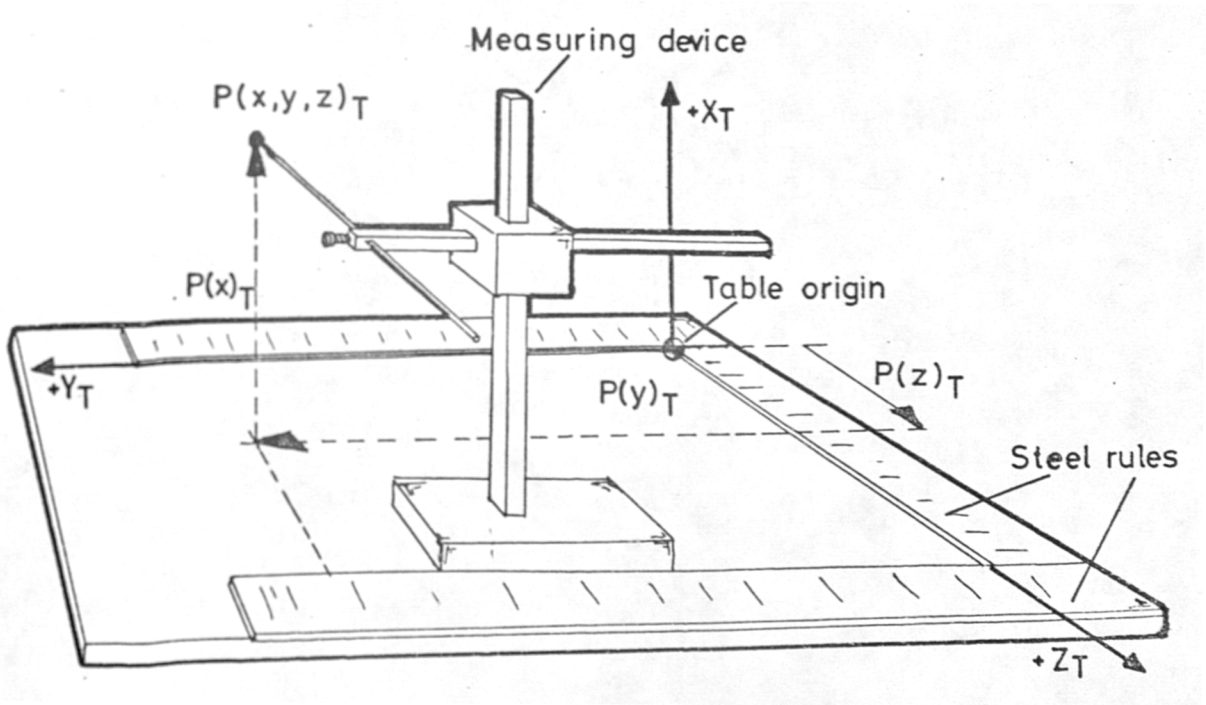

Figure 3.2 Definition of a Point P Relative to the Anthropometric Measuring Table

tendon as it joined the foot, and for the range of movement met in normal locomotion. Two fixed reference points on the foot were used to construct a line against which tendon lines of action were compared. In figure 3.3 it can be seen that the line of action of the achilles tendon changes from 78° to 98°, relative to the reference line, over the range 20° dorsiflexion to 25° plantar-flexion respectively. Over the same range the peroneus brevis changes from 28° to 33° and the anterior tibial tendon from 34° to 38°, both relatively small changes compared to that of the achilles tendon. This feature was used to advantage in the analytical model, discussed in chapter 4.

Finally, it took about six weeks on average to perform complete measurement and evaluation for each cadaver. Thus the study was restricted by time to collection of five complete sets of data. Such a small sample size precludes the use of statistical measures of variation. All data are therefore presented in the form of mean values and the range observed either side of the mean.

3.2 Measurement Equipment

A special steel table was constructed for the anthropometric measurement exercise, see figure 3.2. The cadaver material could be fixed in any chosen orientation relative to the table base plate. The base plate was machined flat to within ±0.2mm. A measuring device, designed and manufactured by J. Szulc*, was used together with vernier calipers, a height gauge, depth gauge and steel rulers to make measurements of points

* Ph.D. student, Bioengineering Unit, Strathclyde University.

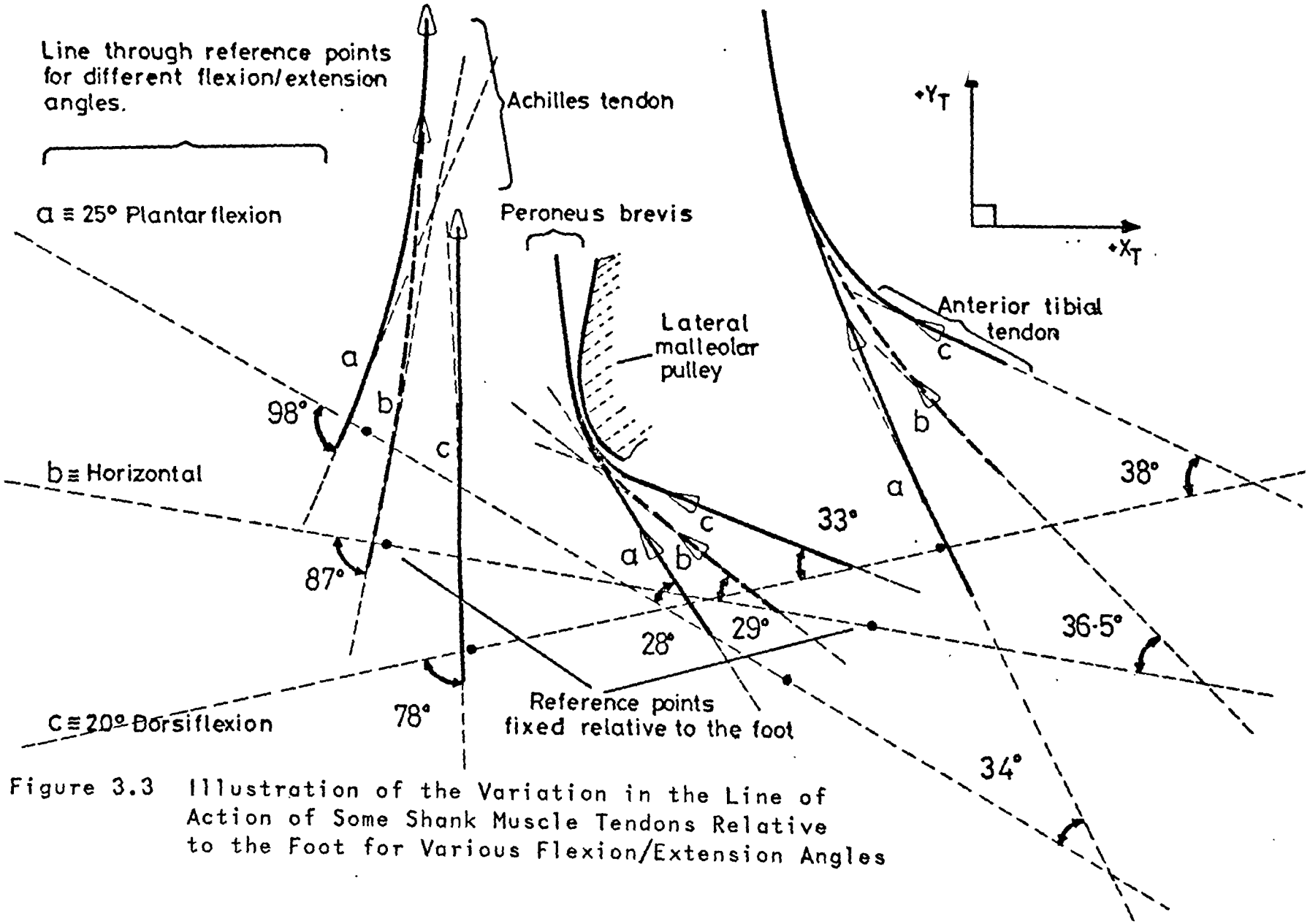

Figure 3.3 Illustration of the Variation in the Line of Action of Some Shank Muscle Tendons Relative to the Foot for Various Flexion/Extension Angles

in space. It was possible to define repeatably a point in space relative to the table origin to within ±0.4mm. using this equipment.

3.3 Dissection Material

The embalmed cadaver material was Glaswegian in origin. Each subject was male and was selected for relatively normal condition and cause of death. None of the subjects showed any signs of degenerative joint disease and appeared to be free of any foot or ankle deformity. In each case the right leg was used. Unfortunately the material came from quite elderly subjects and may have been affected by muscle wasting and other forms of physical deterioration apparent with increasing age. The age, approximate height, weight and cause of death are recorded for each subject in Appendix 1.1.

Embalmed material is subject to moisture loss by evaporation if left uncovered and care was taken to ensure that the specimens were kept moist at all times.

3.4 The Measurements

The measurement techniques and anthropometric measurements will be presented.

3.4.1 Tissue Cover of the Bony Landmarks

The bony landmarks, see figure 1.2, were palpated on each cadaver leg prior to dissection and marked with steel pins. This enabled some assessment of how well an internal point could be located by external palpation. In general it was found that an internal point could be defined to within ±5mm. of the corresponding externally

defined point.

Additionally the thickness of skin and fat overlying each point was measured with calipers. The measured thicknesses are tabulated in Appendix 1.2. (Note that the bony landmarks have been assigned numbers from one to eight; these will be used where space is limited.) It is accepted that these measurements may not be truly representative due to embalming effects upon soft tissue, and the age and condition of the subjects.

3.4.2 Preparation of the Cadaver Leg

After the bony landmarks had been defined the leg was disarticulated through the knee, taking care to preserve the femoral origin of the two heads of gastrocnemius. The skin and superficial fascial layers were then stripped from the shank and foot with the exception of the sole and the toes. The leg muscles were systematically stripped out and weighed before being sealed in plastic bags for later study. Care was taken to avoid disturbing the line of action of the tendons. Each was placed under light tension by springs, connected to the tendon by fishhooks and to the corresponding muscle origin by pins, see figure 3.1.

The shank and foot were then mounted over the anthropometric table in the following way, as shown in figure 3.4: firstly a long axis was defined on the shank as the line passing through points midway between the malleolar and tibial condylar bony landmarks. This axis was oriented to be parallel to the table Y_T axis (note the subscript T is used to indicate the dissecting table axis system), and the shank rotated until the tibial tubercle was uppermost. A line was then drawn

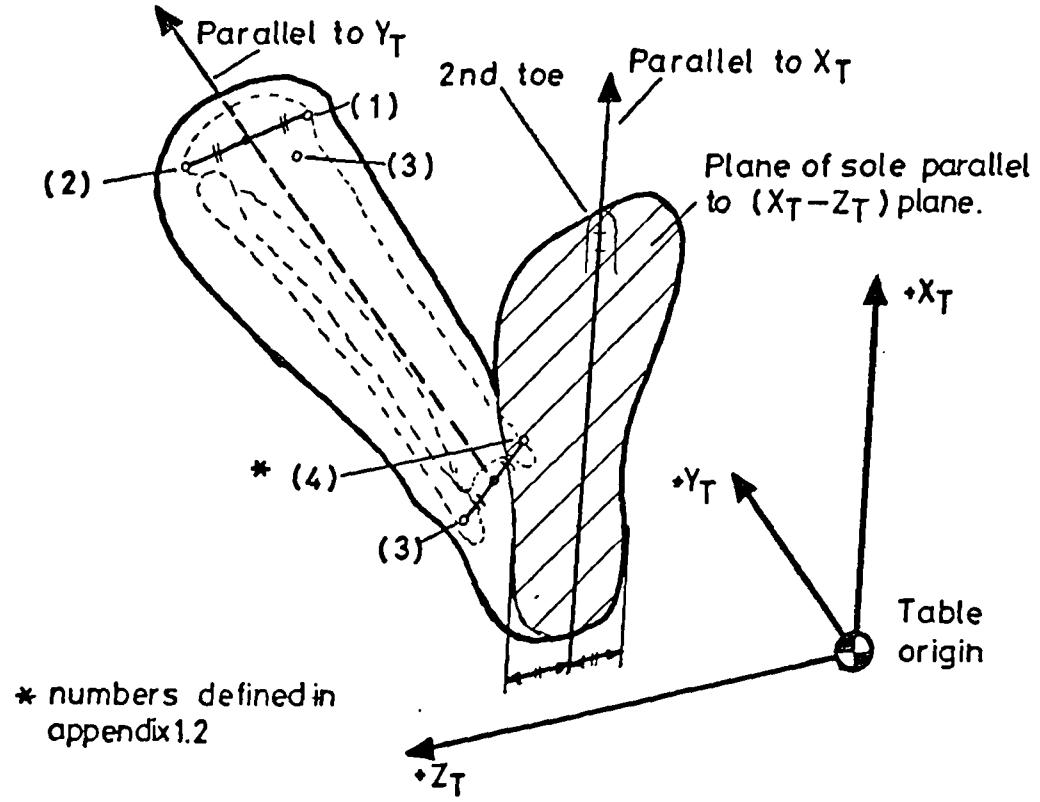

Figure 3.4 Orientation of the Cadaver Limb Relative to the Dissecting Table

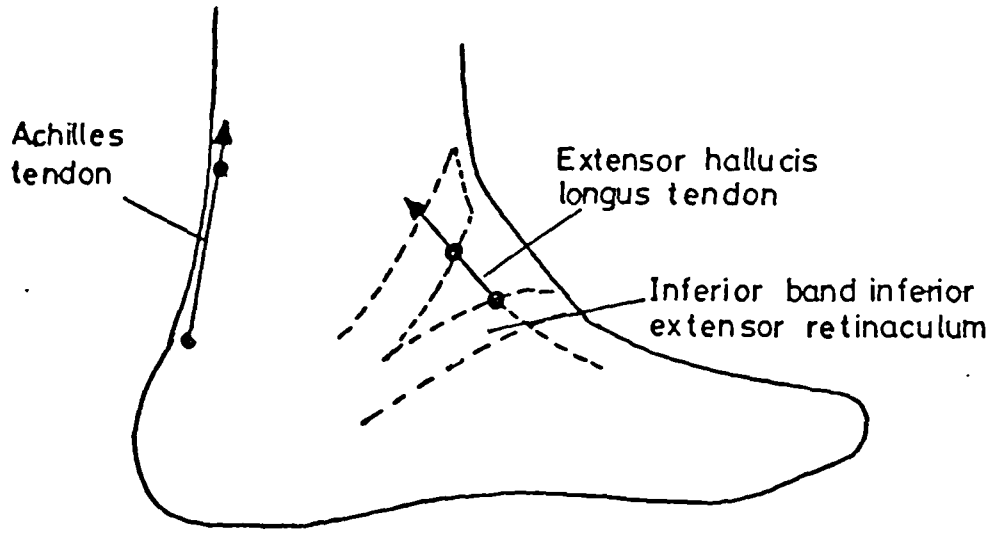

Figure 3.5(a) Definition of Tendon Line of Action

on the sole of the foot, passing midway between the medial and lateral edges of the heel pad and through the middle of the second toe; this was oriented to be parallel to the X_T axis. The sole of the foot was then aligned to be parallel with the X_T-Z_T plane. This procedure was followed for each subject.

3.4.3 The Bony Landmarks and the Mid Malleolar Origin

Once the defined limb orientation had been achieved the coordinates of each bony landmark were measured. These are presented in summary form, for the five cadavers, in Appendix 1.3. For the purpose of comparison all the cadaver dimensions reported are referred to an arbitrary origin on the leg. This was chosen to be the point midway between the medial and lateral malleolar bony markers, referred to as the mid malleolar origin; this point was thought to be appropriate since the malleoli are closely associated with the major joint of the ankle system - the talocrural joint.

3.4.4 The Tendons

Definition of Tendon line of action: The definition of the line of action of the Calf, Peroneal and Posterior tibial groups was relatively straightforward. The line of action of each tendon in these groups was taken as the tangent to the point at which the tendon left the foot segment, defined by marker pins at this point and another point more proximal on the tendon as it passed to the shank segment. This is illustrated for the achilles tendon in figure 3.5(a).

The case of the Anterior tibial group tendons is complicated by their interaction with the inferior

extensor retinaculum bands. Consideration of figure 1.10 suggests that tension in the Anterior tibial tendons can be transmitted to these bands. Now Stamm (2.6.5) observed that the anterior tibial muscle tendon is not always provided with a loop from the inferior band, the present author noted that where such a loop was present it consisted of only a few thin fibres. The line of action of the anterior tibial tendon was therefore defined in the same way as illustrated for the achilles tendon in figure 3.5(a).

Careful definition of the foot segment as a free body simplified the interpretation of extensor retinacular constraint. The foot segment was defined to include the inferior band of the Inferior extensor retinaculum. The lines of action for the tendons of extensors hallucis longus and digitorum longus were taken as the tangent to the point at which each tendon left the inferior band as illustrated in figure 3.5(a).

The superior band of the Inferior extensor retinaculum only acts directly on the lateral aspect of the hindfoot segment, its origin being on the shank segment. A large number of fibres from this band insert, together with fibres from the inferior band, on the superior surface of the calcaneus near to the insertion of the cervical ligament. As a simplification the retinacular insertion was taken to be the only point through which tension in the superior band is transmitted to the hindfoot. The line of action of the superior band was taken to be a tangent passing through the insertion point. The effect on the hindfoot of tension in the band will be discussed in 4.2.2.

One further point is that the line of action of the

Anterior tibial group may change relative to the foot for acute dorsiflexion angles where the tendons pass around a much smaller retinacular radius of curvature. The results of Wright et al (reviewed in 2.8.2) show that the foot at heel strike is slightly dorsiflexed ($\simeq 5°$) and subsequently, in early stance, plantarflexes ($\simeq 8°$). These angular movements probably have little effect on the Anterior group tendons. The Emg. evidence (reviewed in 2.7.3) suggests that stance phase activity of the Anterior tibial group is mainly confined to the first 15% of the walking cycle, so the assumptions regarding the line of action of these tendons only apply to a small part of the walking cycle.

The measurements: Each tendon was marked by five or six steel pins locating surface points on the broadest surface; the most distal pair defining the tendon line of action with respect to the foot. The tangent angle to the tendon at each marker point, in the (X_T-Z_T) plane, was estimated using a protractor. The angle was used together with the measured thickness to calculate the correction factors ΔX and ΔZ, illustrated in figures 3.5(b) and (c). These factors enabled the true centroid coordinates to be estimated. The factors were generally small, the largest being 5mm.

Once the centroid path had been determined for each tendon, the tendons were sectioned in the (X_T-Z_T) plane at the level of each marker pin and the cross-sectional profile assessed. The thickness and width were measured with calipers and the approximate cross-section calculated according to the type of profile. The tendons had mainly three types of cross-section, rectangular, ellipsoid and circular, see figure 3.5(d), although there were

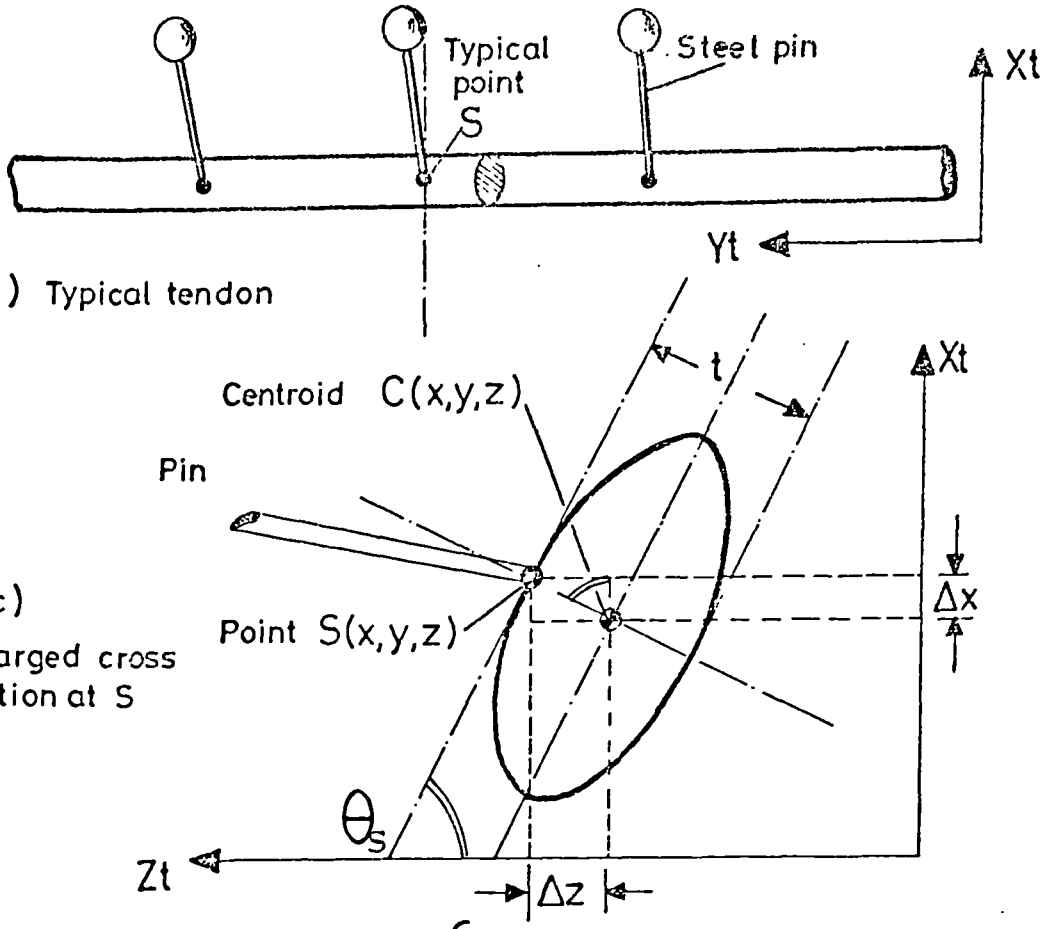

(b) Typical tendon

(c) Enlarged cross section at S

Coordinates of centroid

$$\begin{cases} Cx = Sx - \Delta x \quad (\Delta x = \frac{t}{2}\cos.\theta s) \\ Cy = Sy \\ Cz = Sz - \Delta z \quad (\Delta z = \frac{t}{2}\sin.\theta s) \end{cases}$$

(d) Models for tendon cross section-A_t

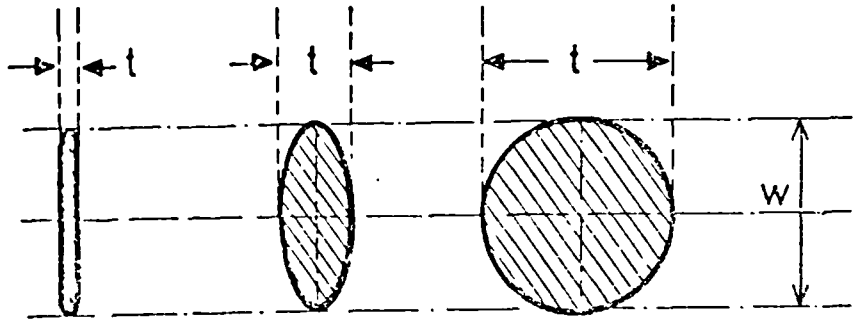

Rectangular	Ellipsoid	Circular
$A_t \simeq t.w$	$A_t = \frac{\pi t.w}{4}$	$A_t = \frac{\pi . t.w}{4}$

Figure 3.5(b), (c) and (d) Calculation of Tendon Centroid and Cross-Sectional Area

occasional thickenings where bony surfaces deflected tendons. The cross-sectional area was averaged for five points along each tendon. The cross-sections were not exactly constant along a particular tendon; the limitations of the method of measurement and calculation, together with local thickenings at bony points and the material changes due to embalming, made exact assessment impossible.

The tendon line of action data are tabulated for the most distal pair of markers in Appendix 1.4 and graphically presented in figures 3.6 and 3.7. The tendon cross-section data are presented in Appendices 1.5 and 1.6 and figure 3.8.

3.4.5 Muscle Physiological Cross-sections

The physiological cross-section of each cadaver muscle was determined using the methods and formula of Alexander and Vernon (1975), see section 2.7.2. The fibre length was measured with a steel rule and the pennation angle estimated with a protractor. The muscle weight was recorded and then the physiological cross-section together with the effective component acting along the tendon was calculated. A complete set of results for one cadaver and summary results for all five are presented in Appendices 1.5 and 1.6.

For visual comparison of the muscle and tendon data the distribution of both quantities is graphed in figure 3.8 together with the ratio of (muscle/tendon) cross-section; note that for convenience muscle physiological cross-section was expressed in m^2 whilst tendon cross-section in cm^2.

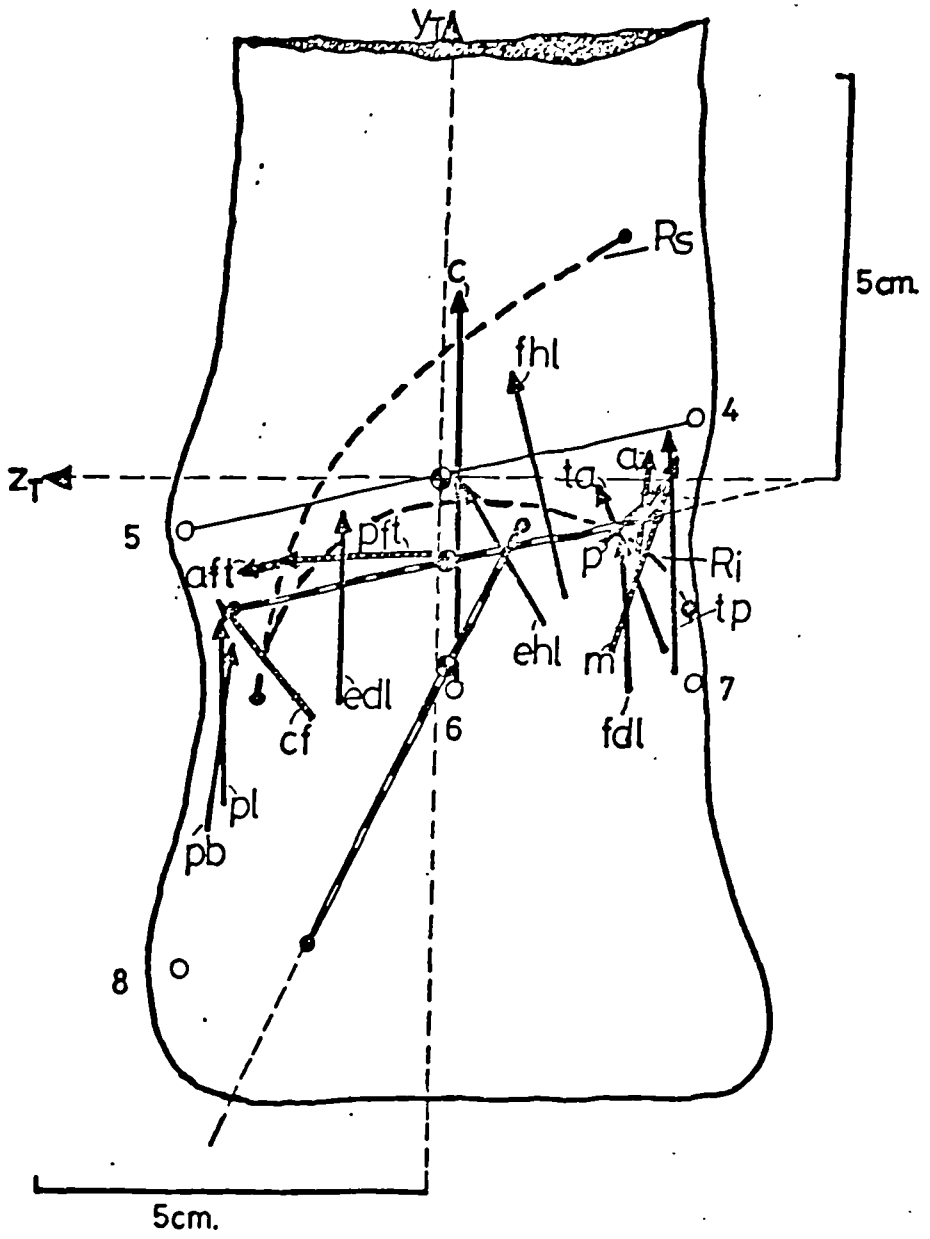

KEY

- Rs (superior band) Ri (inferior band) Inferior Extensor retinaculum
- Ligaments
- Muscles
- o Bony Prominences
- ◉ Origins

4 to 8 Bony prominences, see Appendix 1.2

a, m, p, aft, pft, and cf are ligaments defined under Figure 4.3

continued under Figure 3.7

Figure 3.6 Anterior View of Summary Anthropometric Data Plot

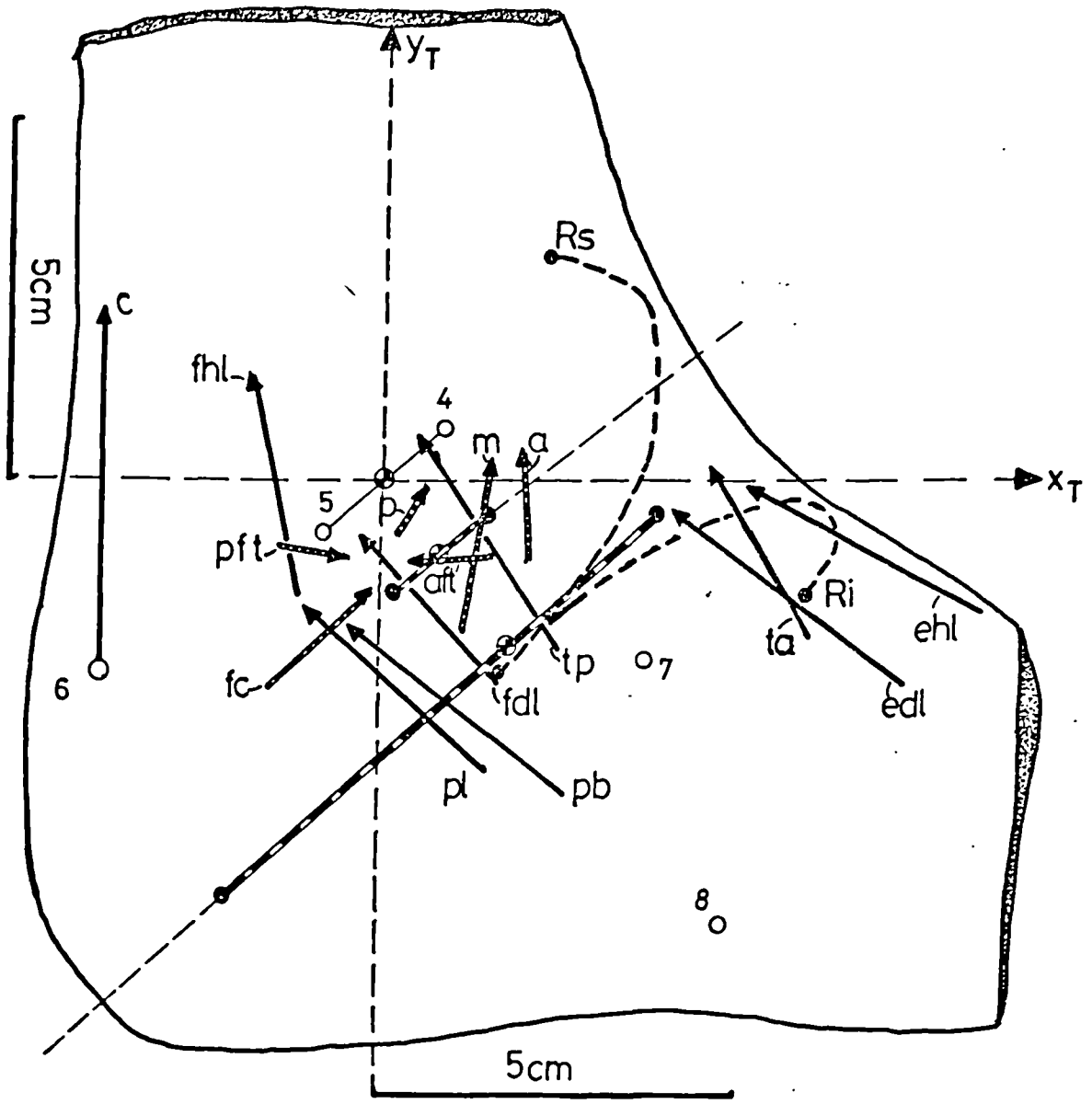

Key - continued from Figure 3.6

muscles: c = gastrocnemius plus soleus, ta = anterior tibial, edl = extensor digitorum longus, ehl = extensor hallucis longus, tp = posterior tibial, fdl = flexor digitorum longus, fhl= flexor hallucis longus, pl = peroneus longus, pb = peroneus brevis

Figure 3.7 Lateral View of Summary Anthropometric Data Plot

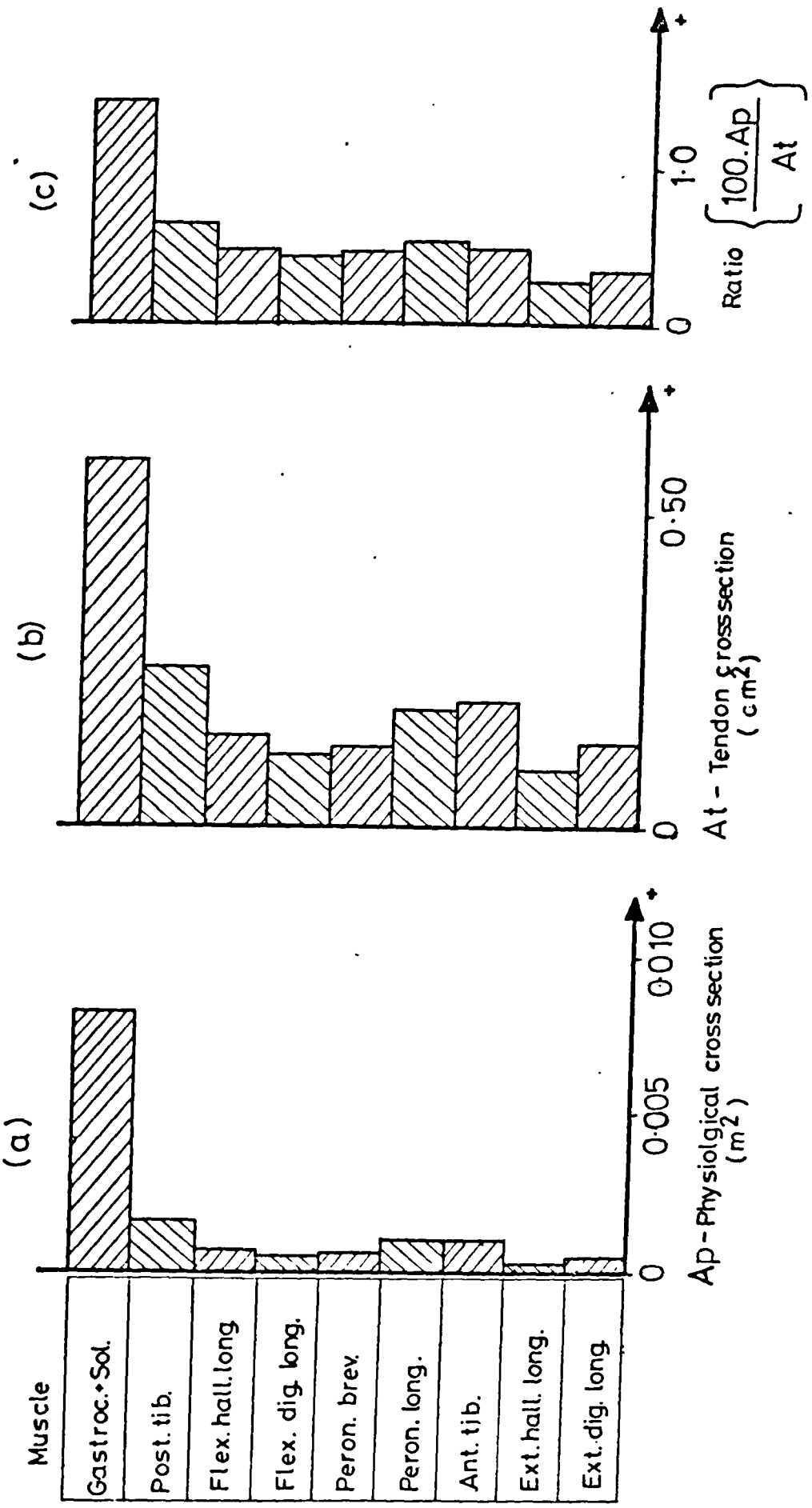

Figure 3.8 Comparison of Shank Muscle Physiological Cross-Section and Tendon Cross-Section

3.4.6 Ligaments and Retinacula

After the tendon measurements were completed, the specimen was dissected down to the ligaments. The lateral collateral ligaments were defined by a pair of pins, one for the origin and one for the insertion (judging by eye the points of attachment). The deltoid was defined as three bands, anteriorly - tibiotalar, midline - tibiocalcaneal and posteriorly - tibiotalar; again each band was defined by points of origin and insertion. The origin and insertion coordinates were then recorded relative to the mid malleolar origin.

In addition, the calcaneal insertion of the Inferior extensor retinaculum and its line of action were defined and measured.

The ligament and retinaculum measurements are tabulated in Appendix 1.7 and graphically presented in figures 3.7 and 3.8.

3.4.7 Determination of the Tc. and Tcn. Axes

The positions of the Tc. and Tcn. axes were determined by the approximate optical techniques of Hicks (1953) and Inman (1976). The shank of the subject was kept stationary whilst the foot segment was rotated firstly in flexion-extension, and then in inversion-eversion. With the aid of soft leadwires attached to the forefoot, the points of minimal movement, corresponding to the approximate position of each axis, were located as illustrated in figure 3.9. The range of movement used at each joint, corresponded to the ranges reported for normal locomotion, see 2.2.4. It is accepted that this is not a method of great precision and accuracy but a more exact method would probably not be justified where

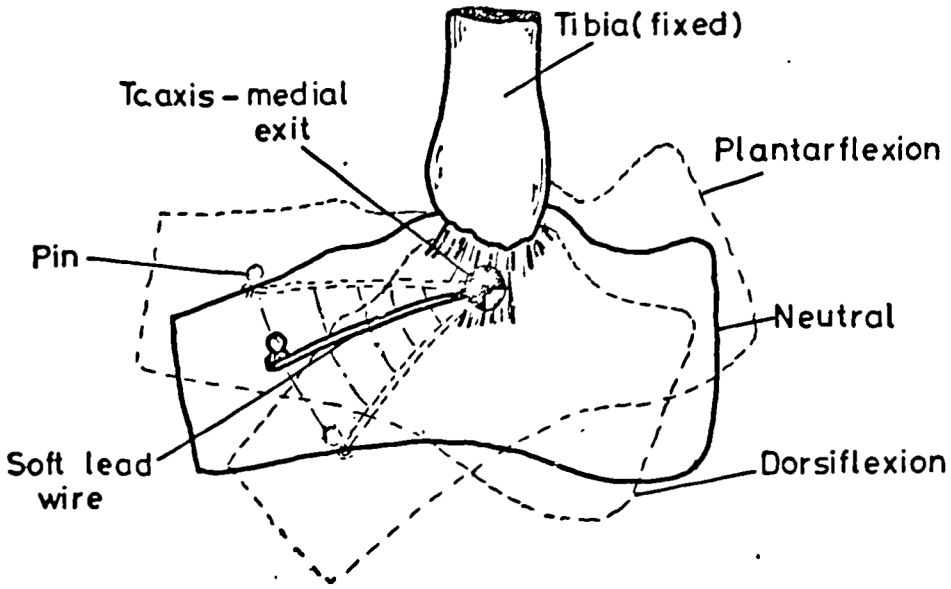

Figure 3.9 Method of Locating the Axes, Example with the Medial Exit of the Tc. Axis

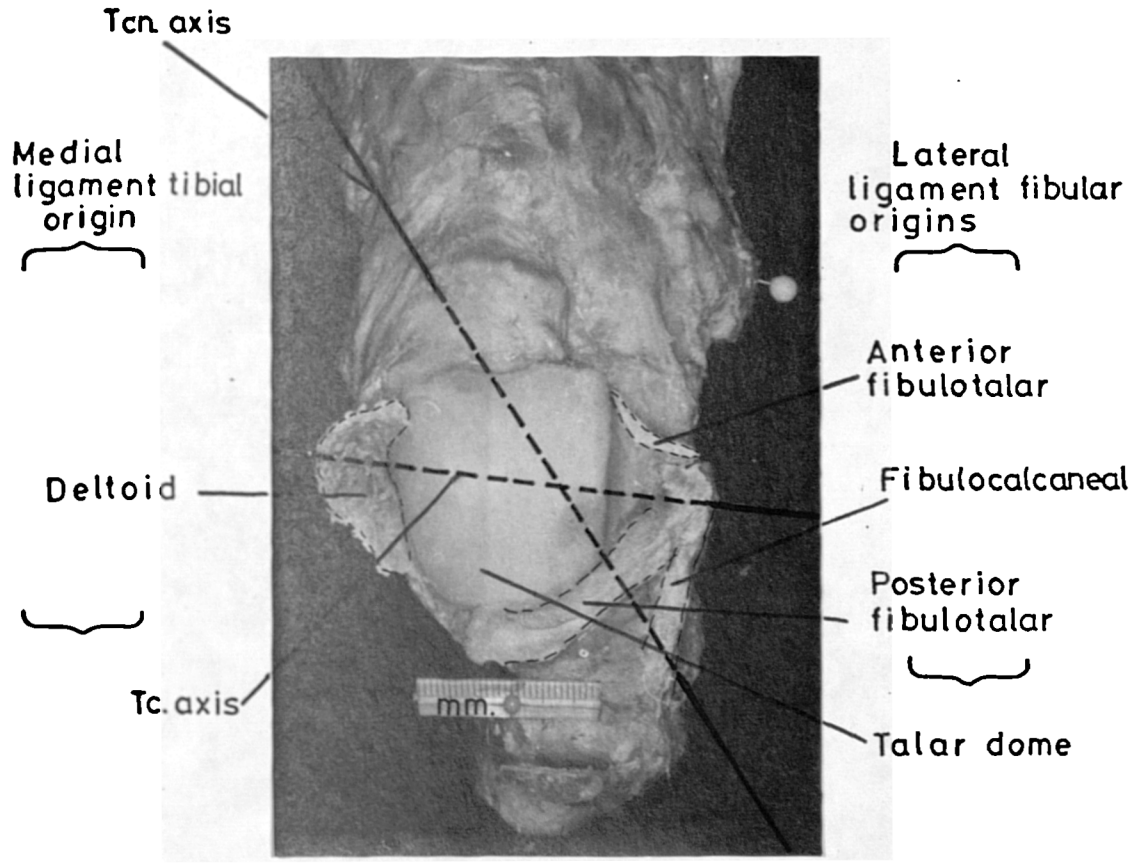

Figure 3.10 Illustration of the Tc. and Tcn. Axes

embalmed cadaver material is used.

The medial and lateral exit point of each axis were measured, see Appendix 1.8. A wire was inserted through each of these pairs of points to mark the axes, see figure 3.11.

3.4.8 The Mathematical Definition of the Tc. and Tcn. Axes Systems

Before the measurement of the joint profiles was undertaken an origin and a reference axis system was defined for each axis. The vector method used in defining the axes is common to every axis system used throughout this study and so will be presented in some detail for the Tc. system. Readers unfamiliar with vector algebra are referred to Kreyszig (1962).

Referring to figure 3.11(a), the Tc. joint origin, $O_{Tc.}$, was arbitrarily defined as the point midway between the medial and lateral Tc. axis exit points. The Tc. axis, already determined, was defined as the $Z_{Tc.}$ axis, positive from medial to lateral. A line, $(O_{Tc.}-P_{Tc.})$, was then constructed perpendicular to the measurement table (Z_T-X_T) plane. The $(Y_{Tc.}-Z_{Tc.})$ plane was then defined as the plane common to $(O_{Tc.}-P_{Tc.})$ and the $Z_{Tc.}$ axis. The vector cross-product $(\{O_{Tc.}-P_{Tc.}\}$ cross $\{Z_{Tc.}\})$ was then computed, which gives a vector orthogonal to the $(Y_{Tc.}-Z_{Tc.})$ plane - the $\{X_{Tc.}\}$ axis. The further vector cross-product of $(\{Z_{Tc.}\}$ cross $\{X_{Tc.}\})$ was then calculated, giving a vector orthogonal to both vectors and in the $(Z_{Tc.}-Y_{Tc.})$ plane - the $\{Y_{Tc.}\}$ axis. Thus an orthogonal (X,Y,Z) axis system was set up for the Tc. joint. Using identical procedures an orthogonal axis system was also established for the Tcn. joint: the $Z_{Tcn.}$ axis was defined

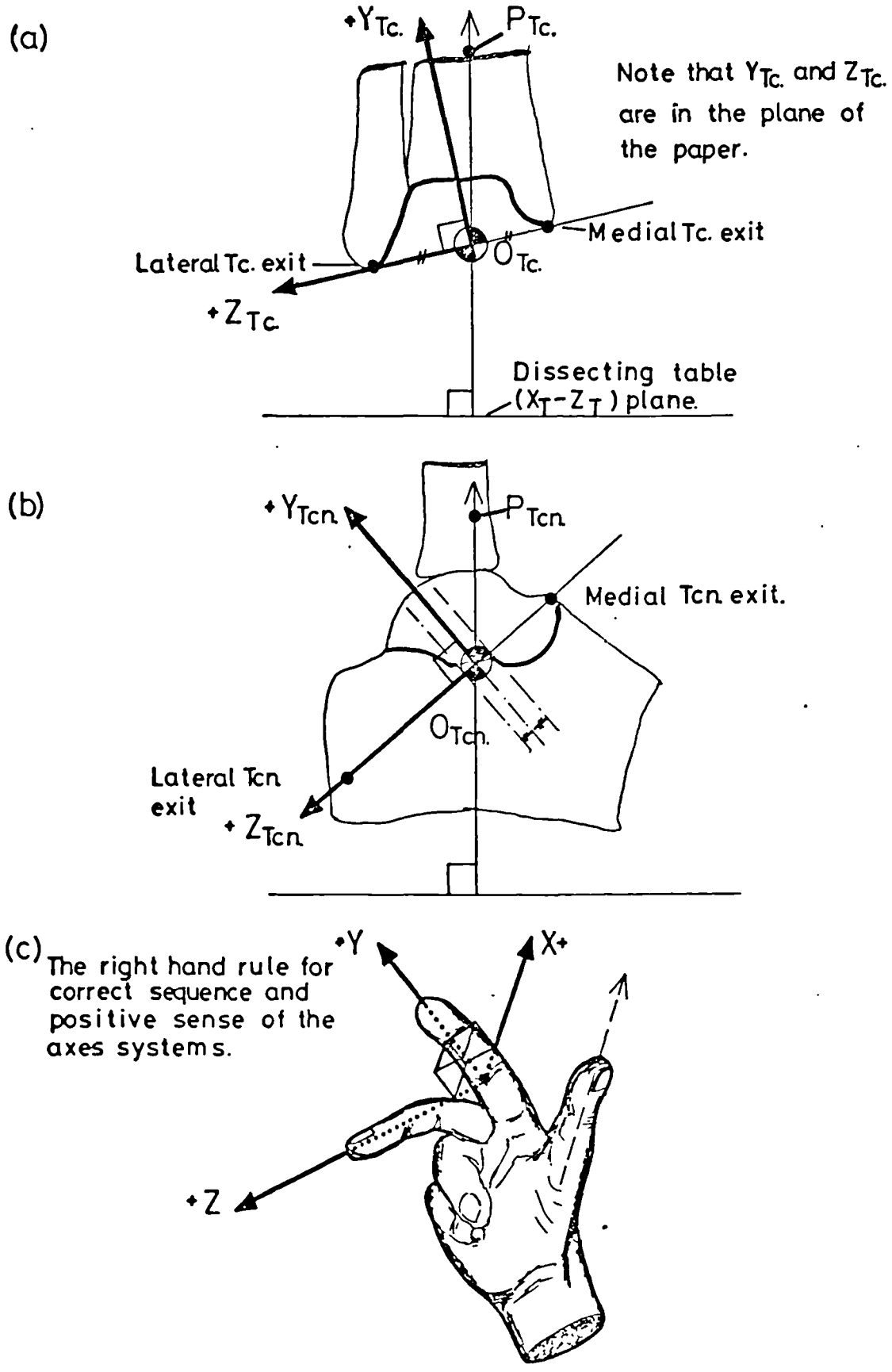

Figure 3.11 The Tc. and Tcn. Axes Systems for the Right Ankle

as positive going medial to lateral. The only difference in the method was that the origin was defined as being a point on the $Z_{Tcn.}$ axis, midway between the posterior and anterior talocalcaneal facets, see figure 3.11(b). Note also that both axes systems obey the 'right hand rule', illustrated in figure 3.11(c).

3.4.9 Profiles of the Tc. and Tcn. Joint Facets

The profiles of each joint were mapped out in two planes related to the joint axes systems; firstly at intervals of 5mm. along the Z axis in the (X-Y) plane, and then at the same intervals along the X axis in the (Y-Z) plane. The profiles were contoured using a 'VITREX' profile gauge, in a fashion similar to that used by Inman (1976): figure 3.12 illustrates its use on the talar dome.

For the Tc. joint the tibio fibular facets were profiled: being smaller than the corresponding talar facets the joint force must pass within their bands. Figure 3.13 illustrates the sections taken in the Tc. system. A representative set of profiles for cadaver three are shown in figure 3.14. For comparison of the five subjects, three specific profiles were taken. The first, in the $(Y\text{-}Z)_{Tc.}$ plane passing through $O_{Tc.}$; two parameters, d_1 and d_2, defined the lateral and medial widths respectively of the superior tibio talar facet, see Appendix 1.9(a). The second two profiles were taken from $(X\text{-}Y)_{Tc.}$ planes, one at +1.0cm. and the other at -1.0cm. along the $Z_{Tc.}$ axis; three parameters, θ_1, θ_2 and R, were defined: for comparison of these profiles see Appendix 1.9(a) and (b).

The Tcn. joint calcaneonavicular facets were found

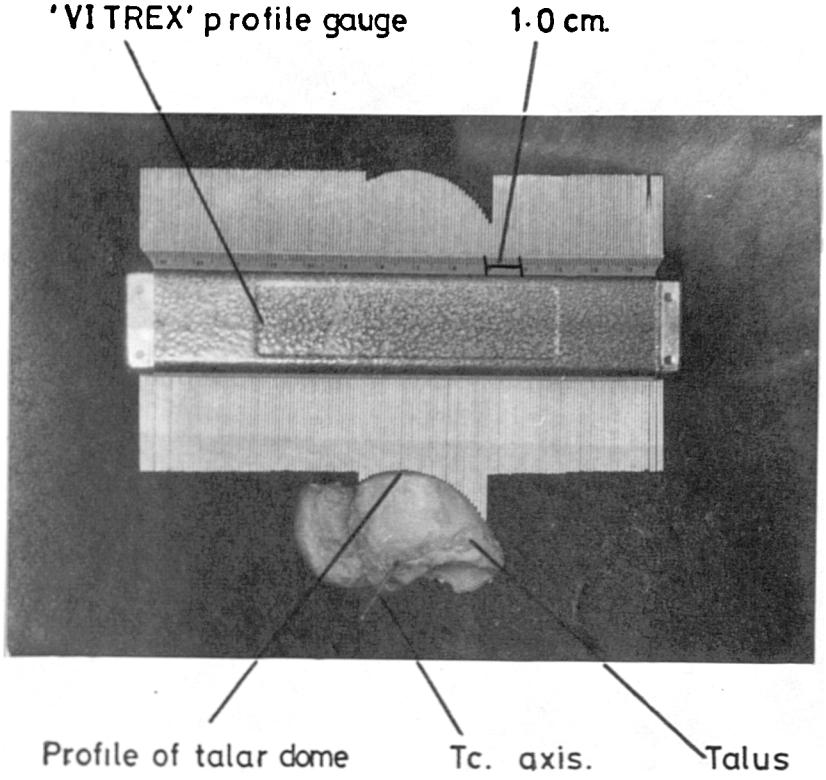

Figure 3.12 Illustration of the Profile Gauge Method used to Obtain Joint Facet Contours

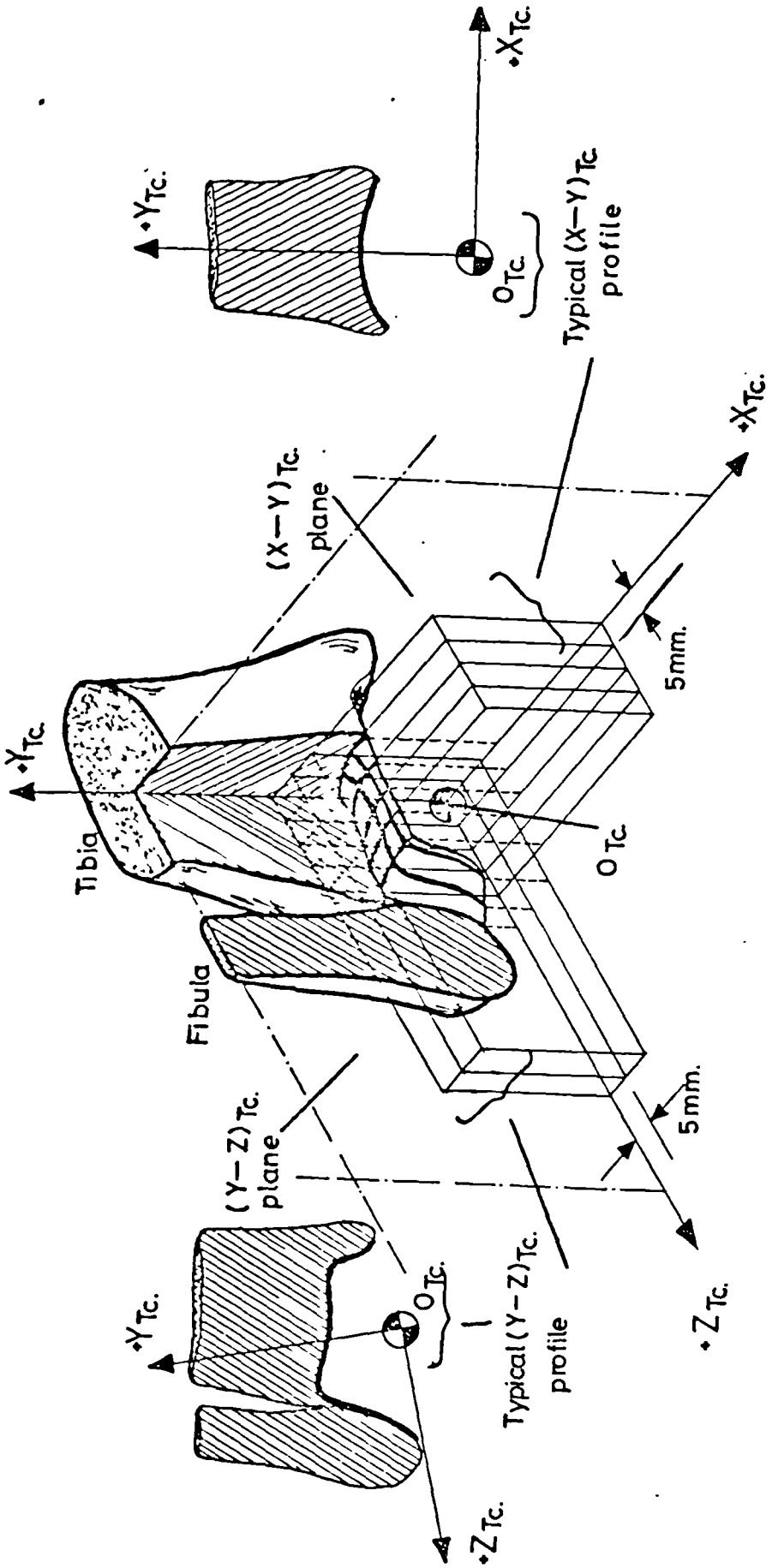

Figure 3.13 Sectional View of the Fibula and Tibia to Illustrate the Orientation of the Tc. Joint Profiles

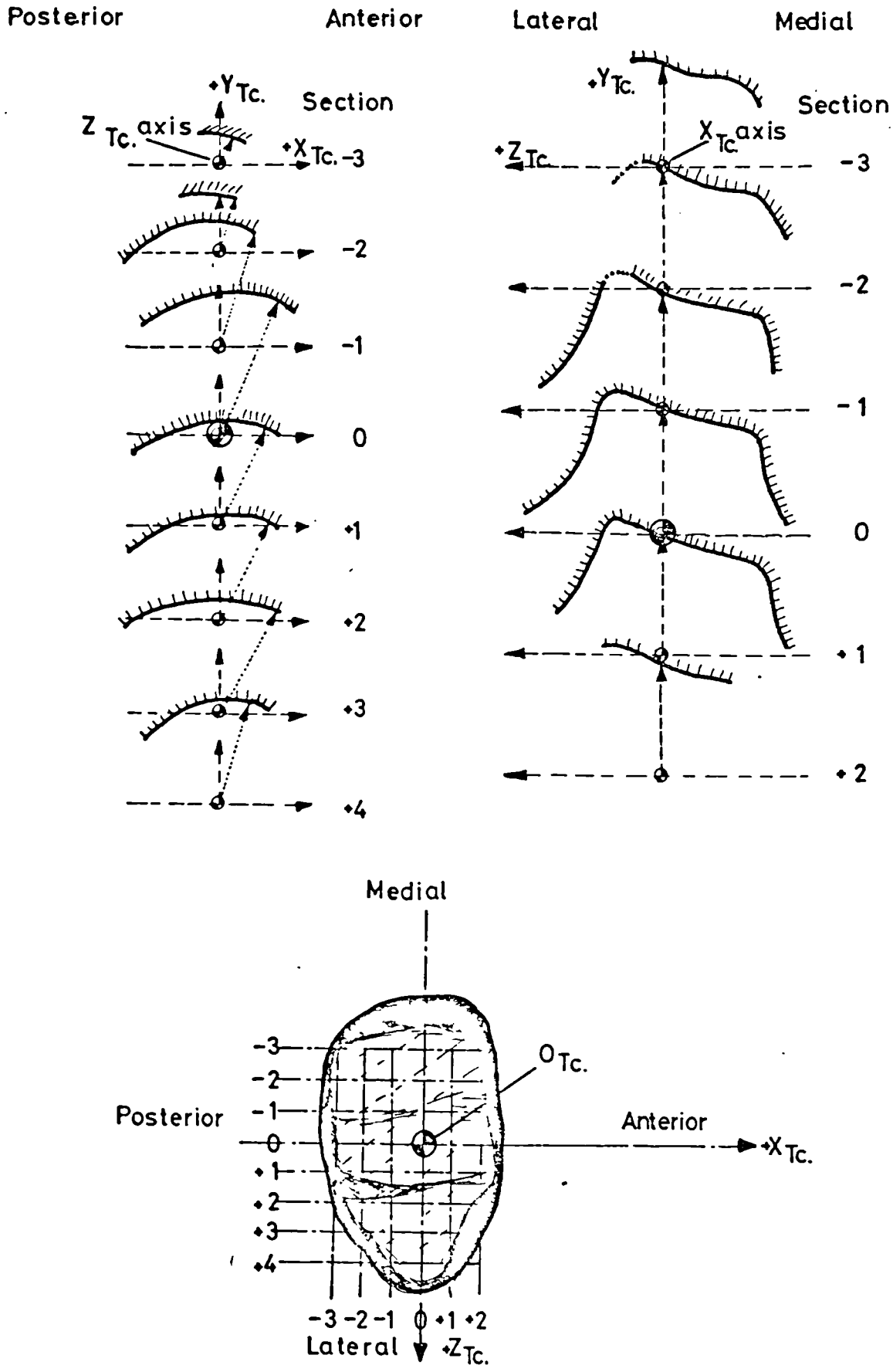

Figure 3.14 Typical Tc. Joint Facet Profiles (Cadaver Subject Three)

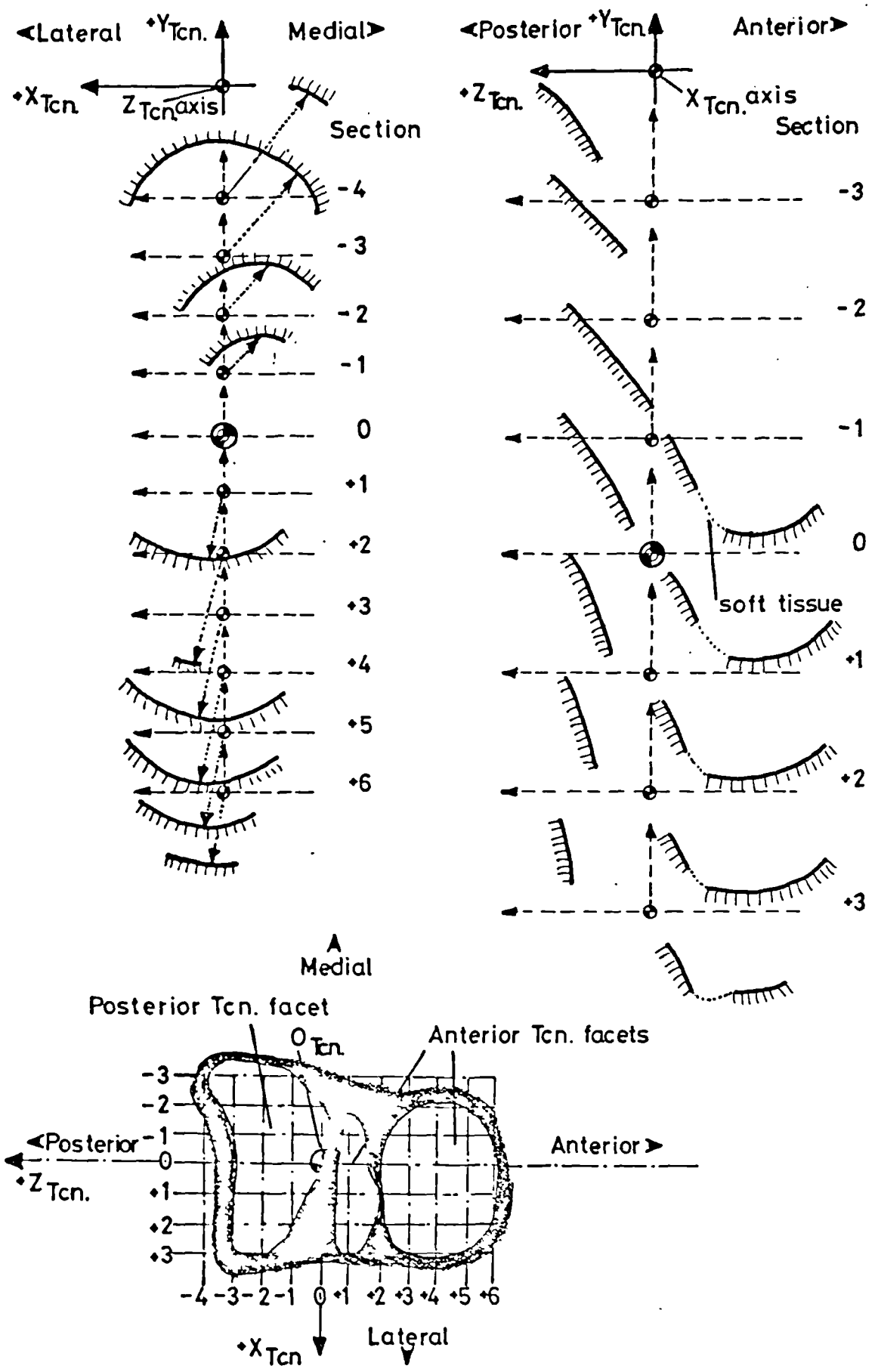

Figure 3.15 Typical Tcn. Joint Facet Profiles (Cadaver Subject Three)

to be slightly smaller than their talar counterparts and were therefore profiled. The method used was identical to that reported above for the Tc. joint. A complete set of Tcn. profiles for subject three is presented in figure 3.15. Again, three specific sections were selected for comparing the five subjects. The first section was the $(Y\text{-}Z)_{Tcn.}$ plane passing through $O_{Tcn.}$. On this section two distance parameters, D_1 and D_2, were defined to indicate the extent of the facets either side of the $O_{Tcn.}$ origin, see Appendix 1.10(b). The second two sections were taken from $(X\text{-}Y)_{Tcn.}$ planes at +1.5cm. and -1.5cm. along the $Z_{Tcn.}$ axis: for comparison of these sections four parameters, θ_3, θ_4, R_a, R_p, were defined, see Appendix 1.10(a) and (b).

3.4.10 Anthropometric Scaling Factors

The cadaver data collected in the present study were related to an arbitrary origin - the mid malleolar origin - and then simply averaged to obtain mean values. The application of such data in biomechanics for predicting in vivo musculoskeletal geometry has been studied in depth by Lewis and Lew (1977). They reviewed existing methods and proposed an alternative, rather complex method, suited to matrix algebra techniques of computation. However, by their own admission, this was no better than the simple uniform dilation method used by Morrison (1970). Morrison formulated a set of local coordinate axes at the knee centre and then used three linear deformation scaling factors, one for each axis, to relate cadaver geometry to the living test subject. This relatively straightforward approach was adopted for the present study.

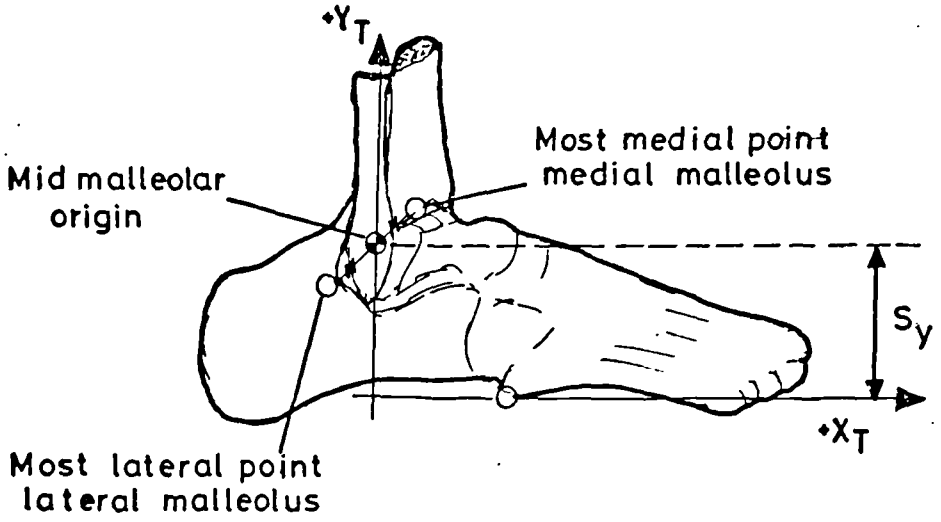

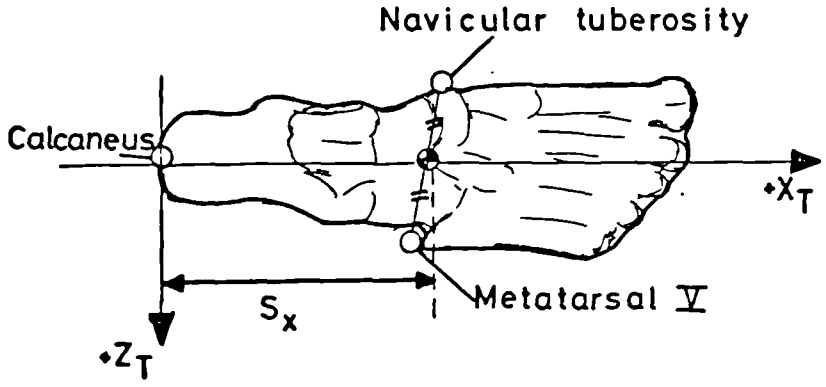

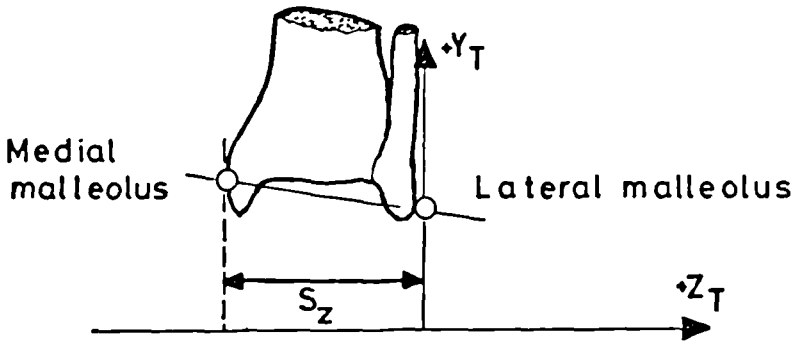

Scale factor	Mean value – five cadavers (m)	Range either side of the mean +	−
S_x	0·0842	0·0120	0·0101
S_y	0·0616	0·0019	0·0025
S_z	0·0656	0·0062	0·0101

Figure 3.16 The Anthropometric Scale Factors

Three scale factors were selected, relating to the dissecting table axis system, so that they could be easily computed for the living subject. The scale factors chosen are illustrated in figure 3.16, together with tabulated summary values.

3.5 Concluding Comments

The joint profiling exercise indicated that the centre of curvature approximately coincided with the axis of rotation in the Tc. and Tcn. joints. The joint profile comparison undertaken, in Appendices 1.9 and 1.10, showed that close geometric similarity existed between the different subjects surveyed. It was noted in each dissection that the anterior portion of the posterior talocalcaneal facet of the Tcn. joint was slightly incongruent: this explains the mediolateral profiles (-1) and (-2) (figure 3.15), where the centre of curvature and the Tcn. axis of rotation were not coincident.

The preliminary study demonstrated that the line of action of each tendon could be considered more or less constant with respect to the foot, during normal locomotion range of movements, with the exception of the calf and flexor hallucis longus tendons. There appeared to be overall geometric similarity between the five subjects - noting of course that this is a small sample. Figures 3.6 and 3.7 illustrate the mean values obtained in respect of tendon, ligament and bony point data. It is considered that sufficient data have been presented in this chapter to undertake force analysis of the ankle joints.

CHAPTER 4

MODELLING OF THE ANKLE COMPLEX

4.1 Selection of the Analytical Method

4.1.1 Introduction to the Problem of Force Analysis in Biomechanics

In normal locomotion forces are generated at the ankle joints. These forces are due in part to the muscles functionally associated with the joint and their response to the external loading environment of the foot. In addition there are components due to gravitational and inertial forces, but as estimated in Appendix 2.3, in the case of the ankle these are probably negligibly small when compared to the muscle force components.

Using anthropometric data relating to the ankle internal structures, it is possible, for certain constraint conditions, to calculate the joint and muscle forces using the equations of force and moment equilibrium. The constraint conditions most frequently used are that muscle and ligament forces are tensile (greater than or equal to zero) and that the joint forces are compressive and normal to the to the joint surfaces through which they pass. Even introducing these constraints, there are still more unknown ankle muscle forces than there are equilibrium equations which means that a unique solution is not possible. This problem is known in engineering as indeterminacy - where the number of unknowns exceeds the number of relevant equilibrium equations. There are three principal strategies that the bioengineer can adopt to overcome this problem.

4.1.2 Invasive Methods

The direct measurement of tendon and joint forces is a possible, if somewhat unattractive, method. It would only be considered acceptable to use an invasive

technique where surgery is contemplated for joint replacement purposes, and only when it in no way increases the risks for the patient. An example of an implanted force measurement device was reported by Rydell (1966). He used a modified Austin Moore hip endoprosthesis with a force transducer built into the femoral component. This relied upon hard wire connections which were terminated subcutaneously at operation and were post-operatively connected to amplification and recording devices. This provided some in vivo hip loading data for standing and walking. The main disadvantages of this study were that only two patients were reported and that the joint force data only provided the joint force components; it still left a large number of muscle unknowns.

4.1.3 Reduction of Variables Method

Solutions may be obtained by grouping the muscles on functional grounds and so reducing the number of unknowns until it equals the number of equilibrium equations. This method was employed by Paul (1967) to assess the forces at the hip joint; the muscles were grouped on anatomical and functional grounds. The same technique was also used successfully by Morrison (1968) - knee, and Nicol (1977) - elbow.

4.1.4 Optimisation Techniques

An alternative to the two approaches outlined above is to keep all the variables and to select a unique solution corresponding to a specified constraint. This constraint is usually chosen to optimise some quantity. There appears to be a widespread belief expressed in the relevant literature that normal locomotion

is in some way optimal. There is little agreement however on what quantity should be optimised.

It has been suggested that either total muscle energy or power is minimised. Nubar and Contini (1961) proposed a minimum 'effort' criterion intended to be analogous to energy but this 'effort' was defined by the product of the joint moments squared and the interval with respect to time of application - corresponding to neither energy nor power. There is some evidence to suggest that energy expenditure in locomotion is minimal for walking at preferred speed (Margaria, 1976), as measured by oxygen consumption/distance travelled. Pedotti et al (1978) suggested that a minimum energy criterion applied in normal locomotion. They used an objective function in which the sums of squares of the muscle forces weighted relative to their cross-sectional area was minimised: this does not correspond either to energy or power. Hardt (1978) considered it "a small logical step" to postulate a minimum energy criterion for muscle activation in walking. He developed an optimisation model in which the energy consumption of the muscles was related to their mechanical output. His results indicate weaknesses which appear to be a frequent failing in linear optimisation criteria: namely that the model shows some muscles carrying all the load and zero force was predicted for others where temporal Emg. has already demonstrated activity; for example, the model predicted that soleus, tibialis posterior and peroneus longus were inactive for the whole of stance phase which is quite contrary to Emg. evidence. In addition to this, amongst the muscles predicted to be active, some muscles generated abnormally high levels

of force for walking; for example, flexor digitorum longus - twelve times Body Weight, and the medial and lateral heads of gastrocnemius - twelve times Body Weight between them. Chow and Jacobsen (1971) investigated leg movements and joint angle and suggested a model in which muscular energy was minimised.

MacConnail (1967) postulated that the sum of the muscle forces is a minimum - no more force being generated than is necessary for the task to be performed. Seirig and Arvikar (1975) suggested minimising the weighted sum of muscle forces and developed criteria minimising "the sum of all the muscle forces plus four times the sum of the moments at all the joints". They went on to modify these functions by adding in K times the joint reactions. It was not at all clear what the physiological grounds for formulating such expressions were and it was evident from their results that their linear models suffered from the same shortcomings as that of Hardt (vide supra). Chao and An (1977) discussed possible solution strategies for indeterminate systems. They favoured a permutation-combination method, including all the variables, to establish the ranges of possible solution. Then the use of minimisation criteria (they suggested seven alternatives including minimising the sum of muscle and joint forces, also constraint moments), together with muscle tension constraints, to obtain the 'best' optimal criterion in modelling the hand. Crowninshield (1978) proposed minimising the sum of muscle stresses, which was stated to favour force prediction in the muscles having the greatest product of physiological cross-section and lever arm.

To confuse the picture of optimisation even further,

Hatze (1976) studied a leg movement exercise and fitted data to a time optimal function.

There are two principal requirements for an optimisation condition. The first is that it is physiologically justifiable and the second that there must be some independent validation method. The optimisation studies reviewed above all include some contentious element in their physiological justification. The most frequently used source of validation is the comparison with temporal Emg. measurements, but frequently the optimisation models predict activity in conflict with the reported Emg. data (vide supra): an additional problem is that the Emg. data from different sources is inconsistent. There have been two convincing challenges to one of the minimal criteria - the principle of Minimal muscular force proposed by MacConnaill (1967) - by Barbenel (1972) and Yeo (1976). The former, investigating the biomechanics of the temperomandibular joint by linear programming, concluded that for this joint the principle did not apply. The latter considered that for elbow flexion, again studied by linear programming, the principle was unlikely to be true.

4.1.5 Approach Adopted in the Present Study

In the present study the forces in at least ten important muscles must be considered as well as the forces at joint surfaces. One of the above methods has to be used in order to make the force analysis tractable.

The uncertainty attached to optimisation methods makes them unattractive at the present time. The use of invasive methods is precluded for ethical reasons.

The method of choice is the second option, 4.1.3, using simplification of the system together with equilibrium equations. It has the advantage that the governing equilibrium equations are well understood. The following sections are therefore slanted towards developing a model suitable for such a solution method. It should be understood however that, although it has been the method of choice in many previous joint force analyses, it has not up to the present time been proved correct by any independent validation method.

There are other possible approaches to force analysis in the human body; for example, finite element methods which are currently being developed. The author does not feel that these are well enough established in biomechanics to be considered as a viable alternative to the methods already discussed.

4.2 Formulation of the Analytical Model

4.2.1 The Muscles - Grouping and Participation Factors

The ten muscles of the shank were grouped on anatomical, 1.3.7, and functional, 2.7.3, grounds into four groups - Calf, Posterior tibial, Anterior tibial and Peroneal. Thus the total number of variables is reduced by six. When combining the muscles into groups muscle physiological cross-section is frequently used as a weighting or participation factor. In the earlier study of muscle and tendon cross-sections, shown in figure 3.8, it appeared that the distribution for muscle and tendon were very similar. On closer inspection it can be seen that either the achilles tendon is relatively small compared to the other tendons, figure 3.8(b) or the calf muscle is relatively large compared to the

other muscles, figure 3.8(a). This becomes more obvious when the ratio (100 Ap/At), figure 3.8(c), is examined where the ratio for the calf muscles is seen to be more than twice that of any of the other shank muscles. It might be that experimental error, normal anthropometric variation or perhaps the method of calculating tendon cross-section in embalmed cadaver material accounts for this discrepancy. It is the author's opinion however that there may be more to estimating the relative strength of a muscle than is indicated by the method for calculating physiological cross-section outlined in 2.7.2. Komi (1979) discussed the influence of muscle fibre type on maximum force generation in muscles and noted that there was some evidence to suggest that maximal isometric force generation may depend upon muscle fibre composition. The formula quoted in 2.7.2. does not take fibre type into account. Because of the doubt surrounding calculation of physiological cross-section it was decided to use the tendon cross-section as a participation factor.

The participation factors were calculated for a group by summing the component tendon cross-sections and dividing the value for each tendon by the sum. An example of the calculation is shown in table 4.1, taking the Peroneal group tendon cross-section data from Appendix 1.6. The participation factors for the Anterior and Posterior tibial groups are tabulated in Appendix 2.1. Since the Calf group has one common tendon, its participation factor is equal to one.

Muscle	Tendon Cross-section At $(cm.)^2$	Participation Factor $(At/\Sigma At)$
Peron. brev.	0.130	0.42
Peron. long.	0.189	0.58
ΣAt	0.319	Σ 1.00

Table 4.1 Calculation of the Peroneal Group Participation Factors

4.2.2 The Ligaments - A Static Study

The ankle ligaments are complicated in form and present some difficulty from the modelling point of view. There is uncertainty attached to their functional role in locomotion activity. Insight into the possible role of the ligaments was gained by calculating the 'potential moment' due to each ligament and the Inferior extensor retinacular band, from the cadaver anthropometric data.

The summary cadaver data was used to set up axes systems in the manner defined in 3.4.8. These axes systems are shown in figure 4.1 together with a typical ligament defined by origin - oL - and insertion - iL. The steps in calculating 'potential moments' are formulated here and given as a numerical example in Appendix 2.2.

The direction cosines of the ligament in the table system are given by

$$L(l)_T = \left(\frac{(RoL)_x - (RiL)_x}{\left|\{RoL\}_T - \{RiL\}_T\right|}\right) \quad \ldots 4.1$$

$$L(m)_T = \left(\frac{(RoL)_y - (RiL)_y}{\left|\{RoL\}_T - \{RiL\}_T\right|}\right) \quad \ldots 4.2$$

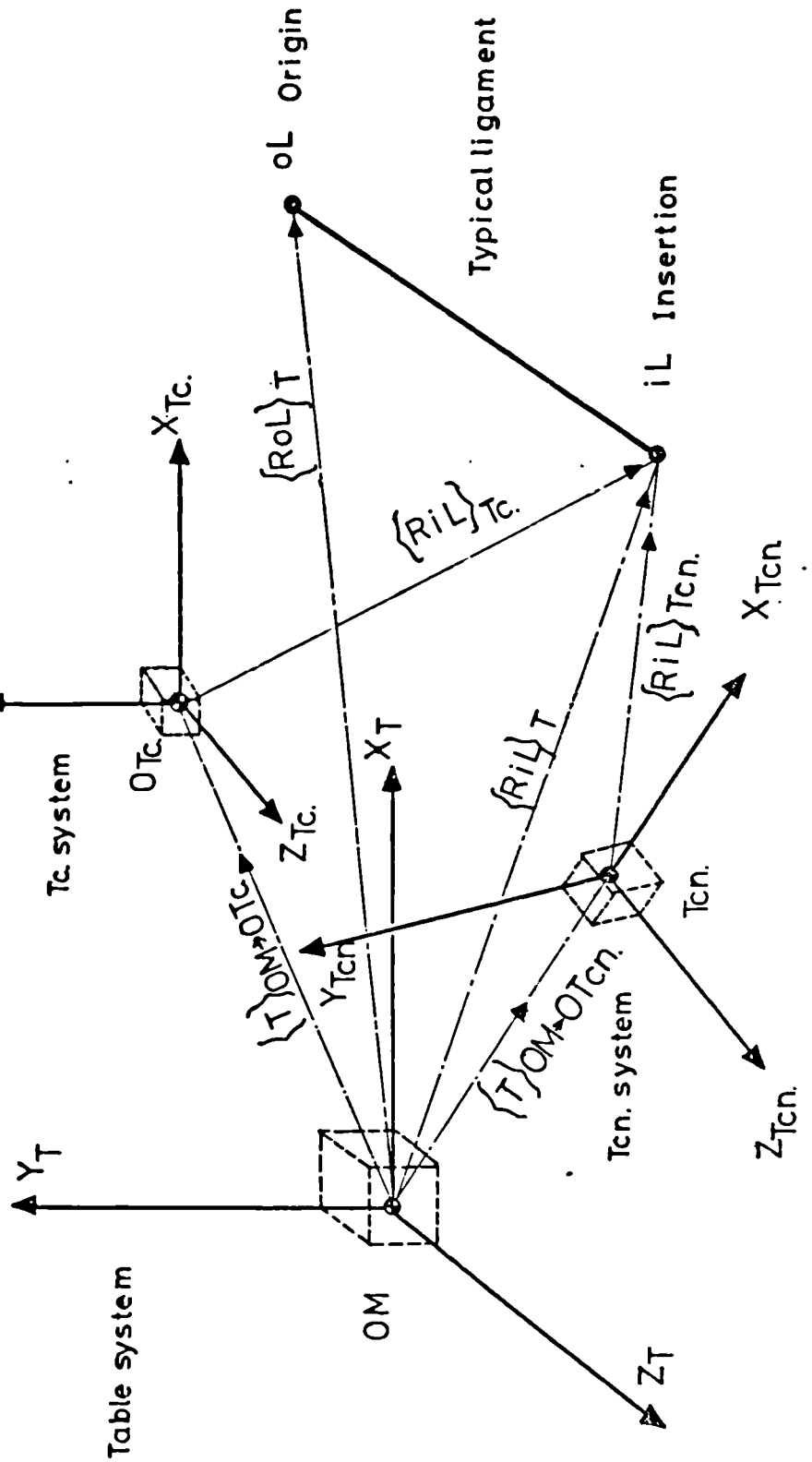

Figure 4.1 Illustration of a Typical Ligament in Relation to the Axes Systems

$$L(n)_T = \left(\frac{(RoL)_z - (RiL)_z}{\left|\{RoL\}_T - \{RiL\}_T\right|}\right) \quad \ldots 4.3$$

where

subscript T refers to the table system

$L(l, m, n)_T$ are the ligament direction cosines

$\{RoL\}_T$ is the radius vector of the ligament origin

$\{RiL\}_T$ is the radius vector of the ligament insertion

$(RoL)_\alpha$ are components of the RoL_T vector (α=x,y and z)

$(RiL)_\alpha$ are components of the RiL_T vector (α=x,y and z)

referring the direction cosines to the Tc. system,

$$L\{l, m, n\}_{Tc.} = [R]_{T\rightarrow Tc.} . L\{l, m, n\}_T \quad \ldots 4.4$$

where

$[R]_{T\rightarrow Tc.}$ is the rotation matrix linking the table and Tc. systems.

referring the direction cosines to the Tcn. system,

$$L\{l, m, n\}_{Tcn.} = [R]_{T\rightarrow Tcn.} . L\{l, m, n\}_T \quad \ldots 4.5$$

where

$[R]_{T\rightarrow Tcn.}$ is the rotation matrix linking the table and Tcn. systems.

referring the ligament insertion to the Tc. system,

$$\{RiL\}_{Tc.} = [R]_{T\rightarrow Tc.} \cdot \{\{T\}_{OM\rightarrow OTc.} - \{RiL\}_T\} \quad \ldots 4.6$$

and to the Tcn. system,

$$\{RiL\}_{Tcn.} = [R]_{T \rightarrow Tcn.} \cdot \{\{T\}_{OM\ OTcn.} - \{RiL\}_{T}\} \quad \ldots 4.7$$

The 'potential' moment of the ligament is here defined by the vector cross-product of the insertion vector and the direction cosine vector for the line of the ligament. Thus in the Tc. system the 'potential' moment $\{ML\}_{Tc.}$ is,

$$\{ML\}_{Tc.} = \{RiL\}_{Tc.} \text{ cross } L\{l, m, n\}_{Tc.} \quad \ldots 4.8$$

and in the Tcn. system the 'potential' moment $\{ML\}_{Tcn.}$ is,

$$\{ML\}_{Tcn.} = \{RiL\}_{Tcn.} \text{ cross } L\{l, m, n\}_{Tcn.} \quad \ldots 4.9$$

The potential moments tabulated in Appendix 2.2 are plotted on vector diagrams - figures 4.2 and 4.3. The moments calculated correspond to zero degrees, flexion/extension, and inversion/eversion at the Tc. and Tcn. axis respectively. The retinaculum, fibulocalcaneal and mid deltoid bands act directly across the Tcn. joint whilst the remaining ligaments, by their attachment to the talus, are able to act indirectly. A simple criterion was adopted, that the largest potential moment component indicates the major action due to a particular ligament in either the Tc. (annotated * in table A2.2.1, Appendix 2.2) or Tcn. (annotated **) systems.

Five of the ligaments have their largest component about the $Y_{Tc.}$ axis, the deltoid posterior band and anterior fibulotalar acting in a negative sense in opposition to the posterior fibulotalar, fibulocalcaneal

and retinacular bands. The remaining two ligaments, the deltoid mid and anterior bands, have their largest components about the $X_{Tc.}$ axis acting in a positive sense, see figure 4.2.

In the Tcn. system five of the ligaments have their principal components about the $Y_{Tcn.}$ axis, the retinacular and fibulocalcaneal bands acting in a positive sense in opposition to the deltoid posterior, deltoid mid and anterior fibulotalar bands. The deltoid anterior and posterior fibulotalar bands act about the $Z_{Tcn.}$ axis in a negative sense, see figure 4.3.

With this simple analysis it can be seen that the medial and lateral collateral ligaments are in the most advantageous position to transmit $Y_{Tc.}$ moments. This is consistent with the view that the ankle plays an important role in transmission of rotation between the shank and foot. The potential resistance to $Z_{Tc.}$ and $X_{Tc.}$ moments is relatively small excepting for the deltoid resistance to negative $X_{Tc.}$ moments. The right hand convention adopted for the consistent sign and sense of moments is shown in figure 4.4.

The analysis of ligament was left at this stage until the preliminary analysis had been completed. The models developed in the later sections of this chapter will enable feasible solutions to be obtained without including the action of ligaments. The solutions will be assessed to see whether or not criteria for the inclusion of ligaments can be found. The further development of the models to include ligamentous activity is discussed in chapter seven.

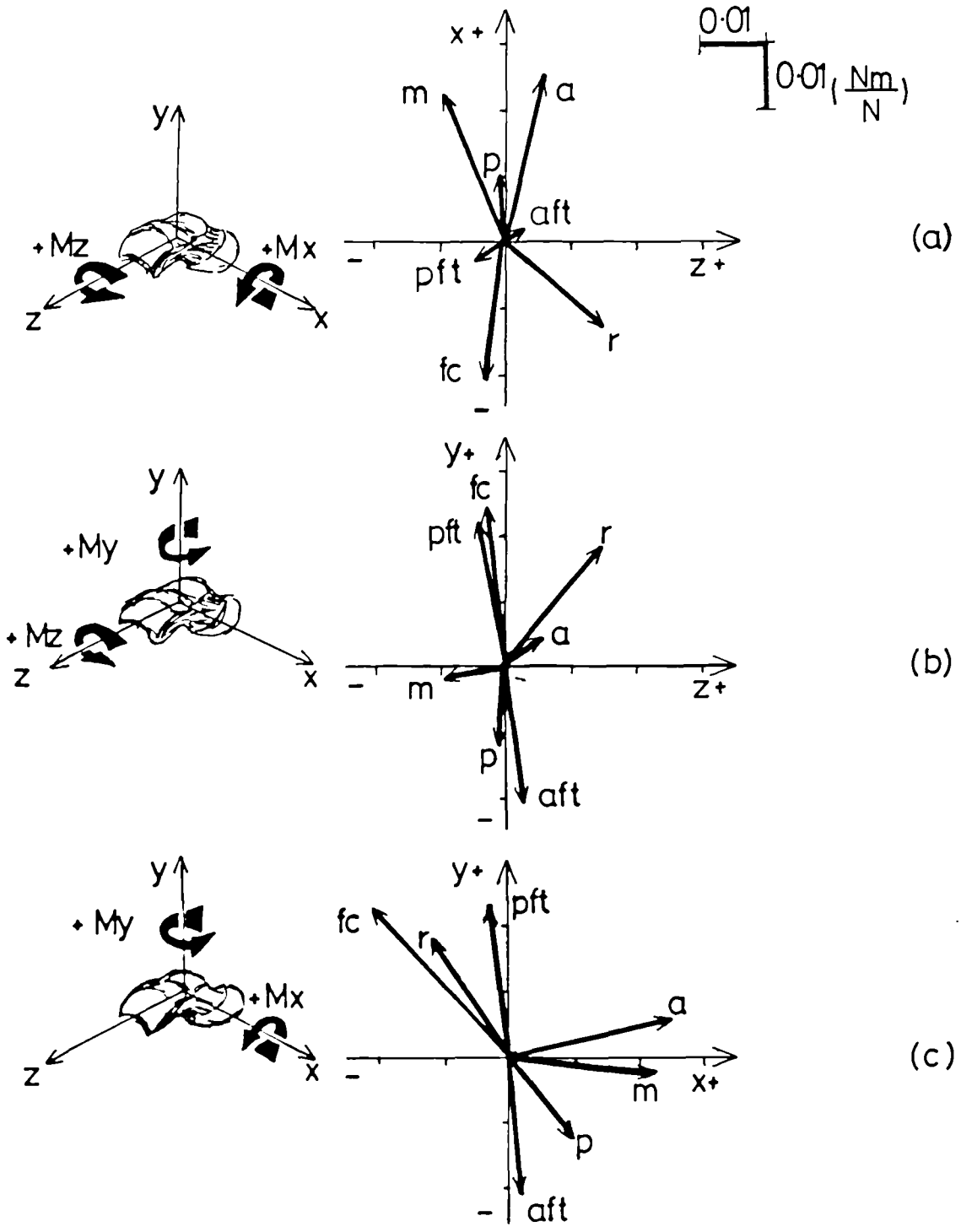

key: see figure 4.3

Figure 4.2 Ankle Ligaments 'Potential' Moments in the Tc. System

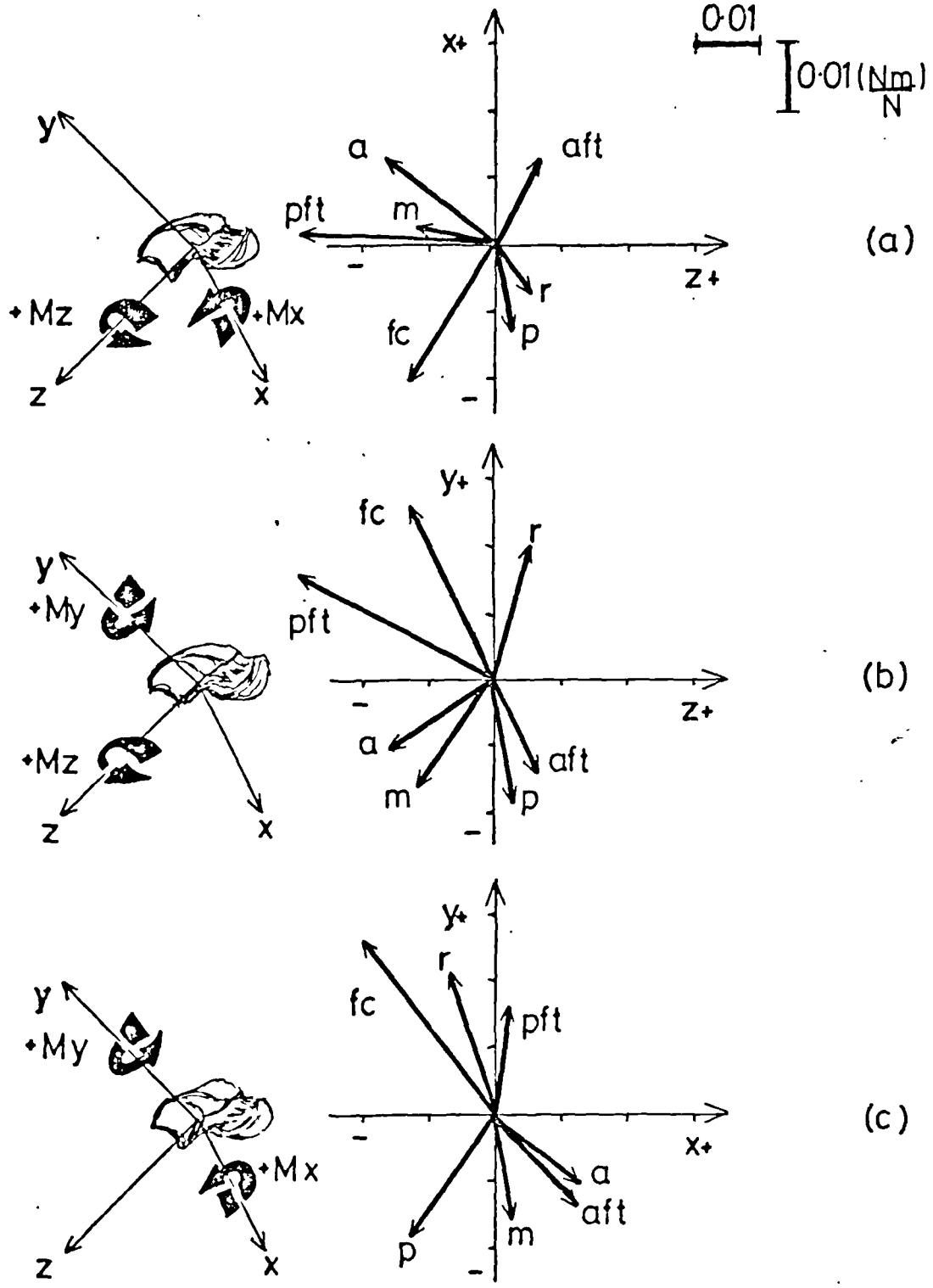

key: Deltoid bands: p_posterior, m_middle & a_anterior, aft_anterior fibulotalar, pft_posterior fibulotalar, fc_ fibulocalcaneal & r_ retinacular band.

Figure 4.3 Ankle Ligament 'Potential' Moments in the Tcn. System

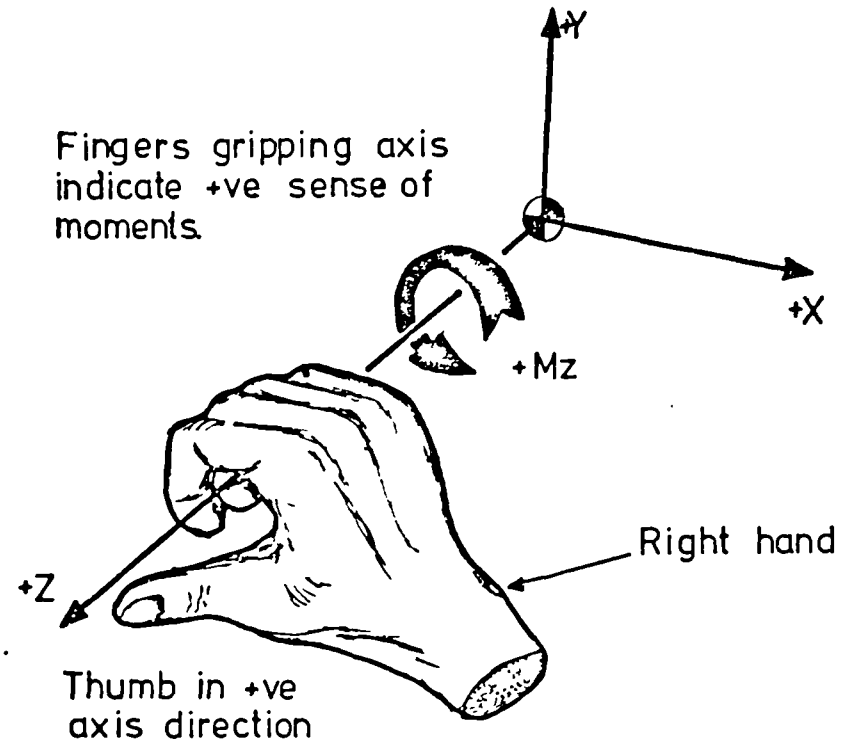

Figure 4.4 The Sign Convention Used for Defining the Positive Sense of a Moment acting about an Axis

4.2.3 Modelling the Tc. Joint

The Tc. and Tcn. joint facets were considered from the point of view of what force actions they could transmit. It is necessary to ensure that the models contain sufficient constraints, otherwise unphysiological solutions may be forced to appear. For example, if no F_z force component was included in the Tc. system model, the tendons would be forced to balance any F_z component due to the external force system (there being no ligaments in the preliminary model). If the tendons had only a small component acting in the z direction balancing the F_z external force component would result in abnormally high muscle forces.

Considering the (Y-Z) profiles of the Tc. joint, figure 3.14, the joint is clearly capable of resisting (F_y) vertical force and medio lateral shear (F_z). In addition the profiles show that the joint is slightly bicondylar and thus the vertical force may be divided into parallel medial (F_{Ym}) and lateral (F_{Yl}) components. This division would allow the vertical forces to contribute to the balancing of axial (M_x) moments acting about the $X_{Tc.}$ axis. Note that concentrated forces components are referred to here, there being no method at present for predicting the distribution of forces over the joint surfaces.

The Tc. (X-Y) profiles in figure 3.14 indicate that the Tc. joint may offer some resistance to antero-posterior shear (F_x). By splitting the F_x shear into medial (F_{xm}) and lateral (F_{xl}) components, each component corresponding to its respective talar condyle, the Tc. joint is able to resist axial moments (M_y) about the $Y_{Tc.}$ axis. In the anthropometric studies it was found

that the centre of curvature of the Tc. joint approximately coincided with the axis of rotation. It was assumed that the resultant Tc. joint force passes through the $Z_{Tc.}$ axis, leaving the equilibrium of $Z_{Tc.}$ moments to the muscles.

The medial and lateral components (F_x and F_y) were set to pass, as a first approximation, through points -0.01(m.) and +0.01(m.) respectively on the $Z_{Tc.}$ axis; the F_z component was assumed to act along the $Z_{Tc.}$ axis. This model is illustrated in figure 4.5 with the components as they would act on the talus. The choice of ±0.01m. was not altogether arbitrary: the mediolateral profile of the Tc. joint facets was found, from the joint profiling exercise, to extend about ±0.02m. either side of the Tc. origin.

There is a second option for transmitting M_y moments by using joint forces. The F_z component could be split into components directed medially and laterally acting on the lateral and medial facets of the talus respectively. The medial facet is however small and so this option was not included in the preliminary analysis.

The extent of the Tc. profiles was used to judge whether or not solutions were physiologically acceptable. For a solution to be acceptable the joint force resultant had to pass through the area defined by the tibial part of the Tc. profiles and be normal to the articular surfaces.

4.2.4 Modelling the Tcn. Joint

Considering the profiles of the Tcn. joint in the (Y-Z) place, figure 3.15, the posterior and anterior facets are both capable of transmitting vertical force

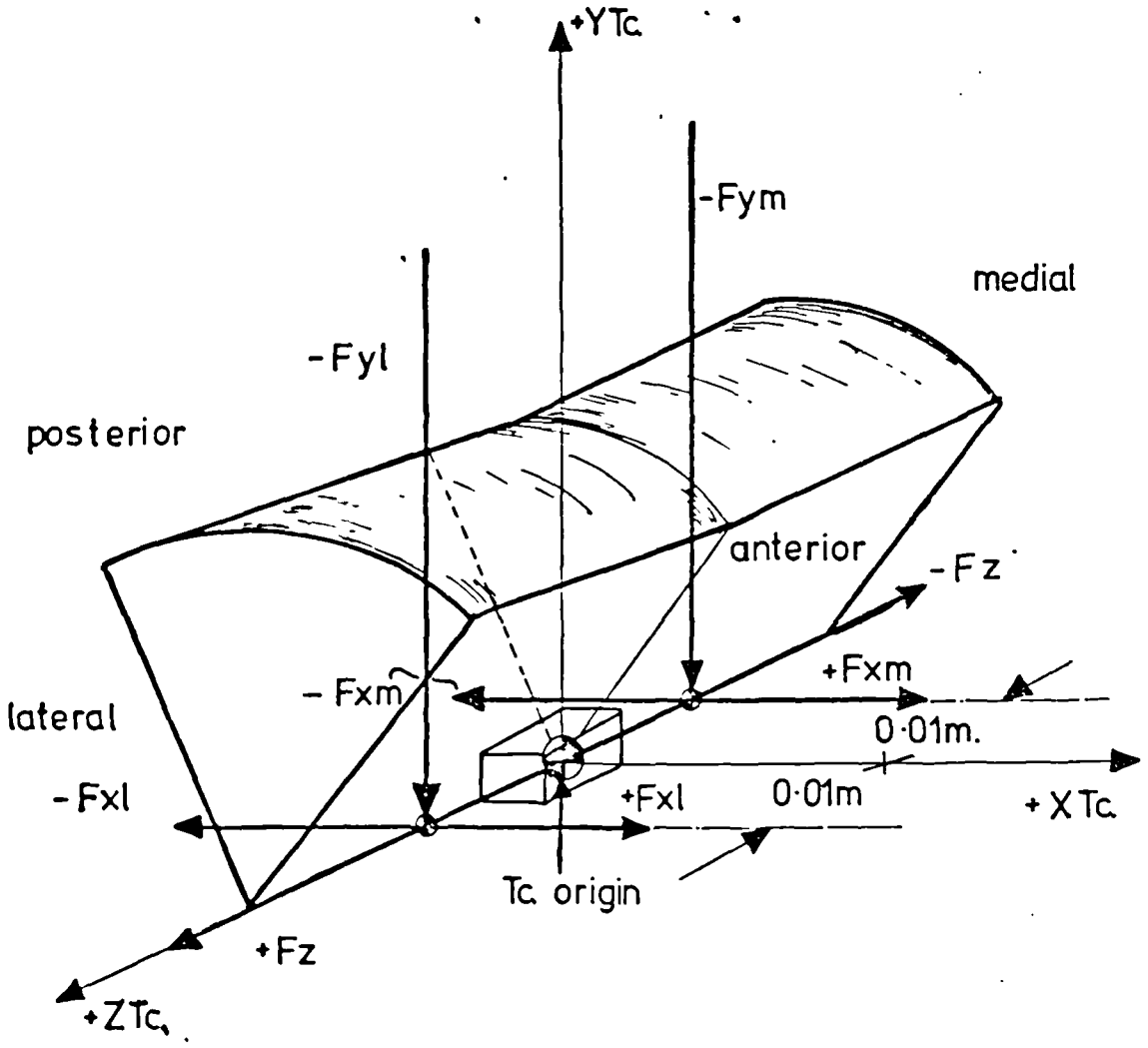

Figure 4.5 Sketch of the Tc. System Joint Force Model (Talar Facets shown in Sketch)

(F_{yp} and F_{ya} respectively), and incidently can control axial moments (M_x) about the $X_{Tcn.}$ axis. The facets are also able to transmit anteroposterior shearing force (F_z). The anterior facet is able to balance positive anteroposterior shearing force (F_{za}) but the posterior facet is not. The anterior and posterior facets both have surfaces capable of resisting negative anteroposterior shearing force, the anterior facet is however relatively small and partially composed of soft tissue so this role was assumed to be taken wholly by the posterior facet (F_{zp}). It was further assumed that either F_{za} or F_{zp} acted alone since they are exactly opposite in sense and thus only one z force can act on the Tcn. facets.

The Tcn. (X-Z) plane profiles, figure 3.15, indicate that the anterior and posterior facets are able to transmit mediolateral shear (F_{xa} and F_{xp} respectively), either as pure shear or as a combination of shear plus an axial moment (M_y) about the $Y_{Tcn.}$ axis.

The anthropometric studies indicated some incongruency between the Tcn. facets, but after careful consideration of their profiles it was thought a fair assumption that they would not.contribute moment components about the $Z_{Tcn.}$ axis.

The anterior and posterior components (F_x and F_y) were assumed (after consideration of the Tcn. joint profiles) to pass through points -0.02(m.) and +0.02(m.) respectively on the $Z_{Tcn.}$ axis; the F_{za}/F_{zp} components were assumed to act along the $Z_{Tc.}$ axis. This model is illustrated in figure 4.6, the components acting on the talar Tcn. facets.

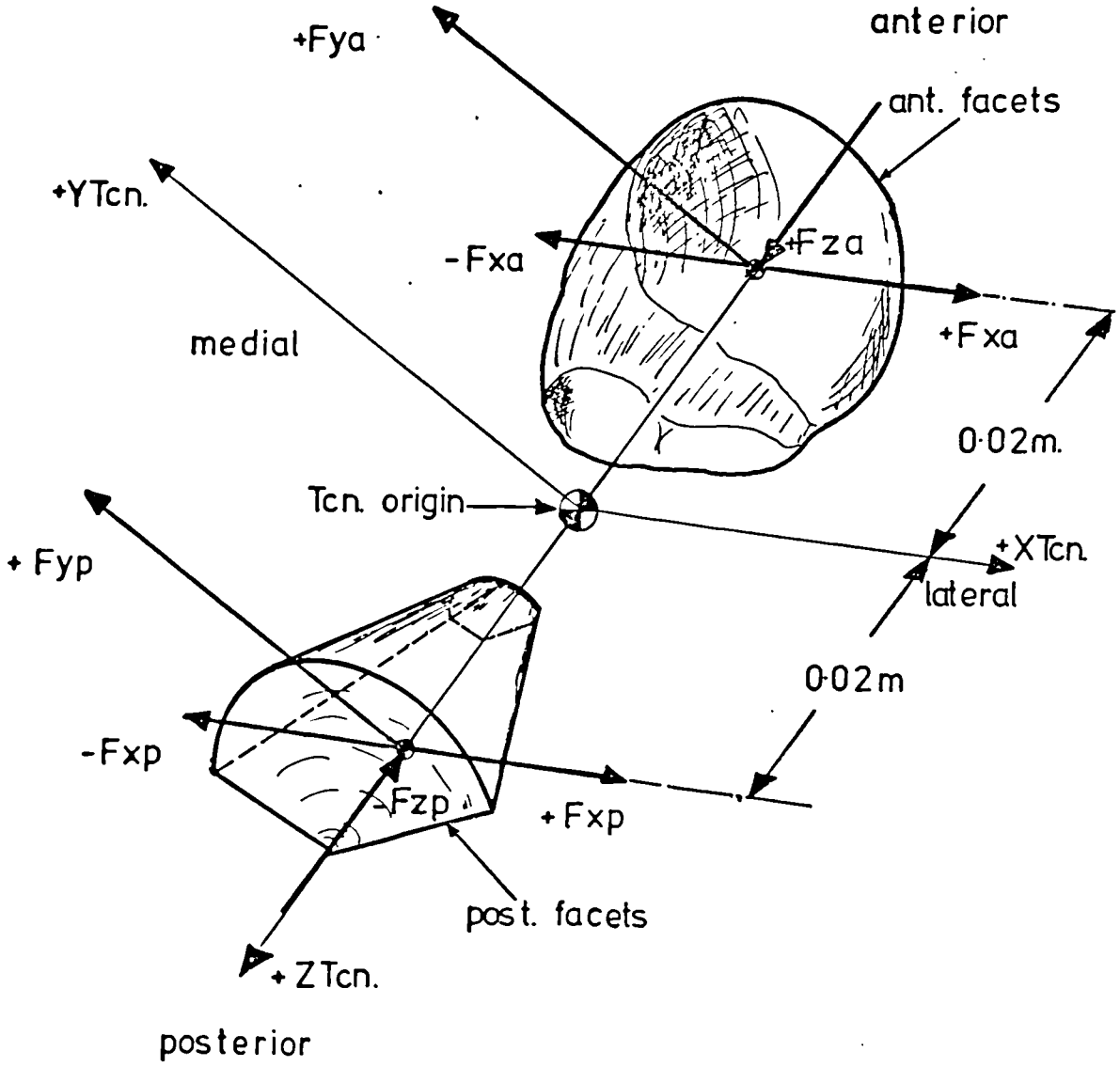

Figure 4.6 Sketch of the Tcn. System Joint Force Model
(The Talar Facets are shown)

4.2.5 The Free Body Diagrams

The Tc. and Tcn. joint systems were assumed to be uniaxial and so allow two degrees of rotational freedom between the shank and hindfoot segments. The foot was divided into two free bodies for the purposes of force analysis. The first free body was the talus plus the hindfoot, and the second the talus by itself, see figures 4.7(a) and (b).

One major advantage of choosing the foot as the segment for analysis, rather than the tibial segment, is that the effects of gravity and inertia are small enough to be neglected during stance phase. The peak inertial component was estimated to be of the order 0.5Nm. (for a peak angular acceleration at heelstrike of 40 rad/s^2, and the inertia of foot considered as rotation of foot segment about the heel point of contact was 0.013 kgm^2 - for a typical subject). See Appendix 2.3 for the calculation of this estimate. The corresponding gravitational component (at 0.1s after heelstrike) was estimated as -0.8Nm. giving a net moment acting on the foot of (0.5-0.8) = -0.3Nm. The inertial component was estimated by Alexander and Vernon (1975) to be about 2Nm. peak; the difference may be due to the assumptions made over subject anthropometric data, however this is still small compared to order of the moments due to the external forces.

The advantage of having two free bodies, as well as giving more accurate model, is that six equilibrium equations may be formulated for each. This gives twelve component equations altogether, so that up to twelve unknown variables may be solved for simultaneously.

Of the four muscle groups, three - Posterior tibial,

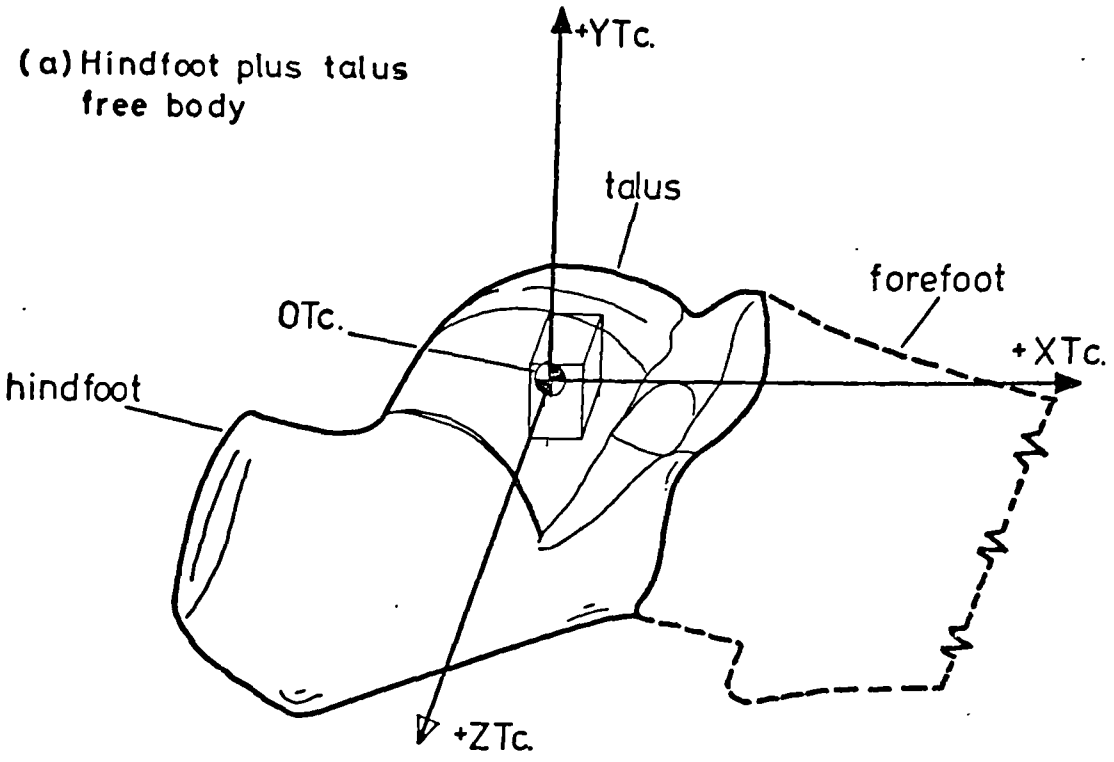

(b) Talus free body

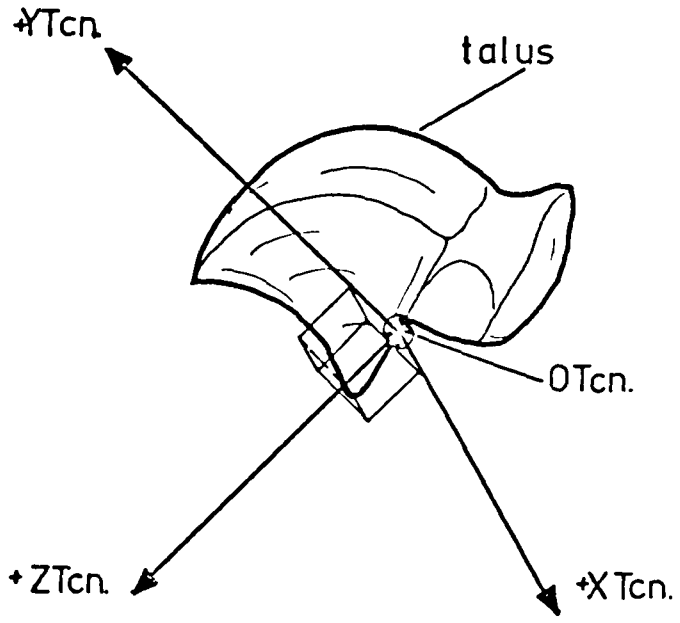

Figure 4.7 Free Body Diagrams for the Ankle

Anterior tibial and Peroneal - were assumed to have a constant line of action with respect to the hindfoot plus talus free body. The Calf line of action was represented by an origin point attached to the shank segment, and an insertion point that was attached to the hindfoot plus talus free body, see figure 4.8.

The Tc. axis system, defined in 3.4.8, was defined as fixed relative to the shank segment and to move with it. The Tc. system was used as the reference axis system when solving the hindfoot plus talus free body equations.

The Tcn. axis system, defined in 3.4.8, was defined as fixed relative to the hindfoot segment, and was used as the reference axis system when solving the talus free body equations.

There is now sufficient information to be able to formulate the analytical models and their governing equations.

4.2.5 Summary of the Important Assumptions So Far

Before formulating the equations it was thought appropriate to reiterate the most important assumptions made so far.

i) The action of ligaments is not included in the preliminary analysis since it is thought that a feasible solution may be obtained without them.

ii) The joint centre of curvature coincides with the axis of rotation for the Tc. and Tcn. systems.

iii) The muscles are assumed to act as four independent groups - Calf, Posterior tibial, Anterior tibial and Peroneal.

iv) The effects of gravity on the foot and inertia of

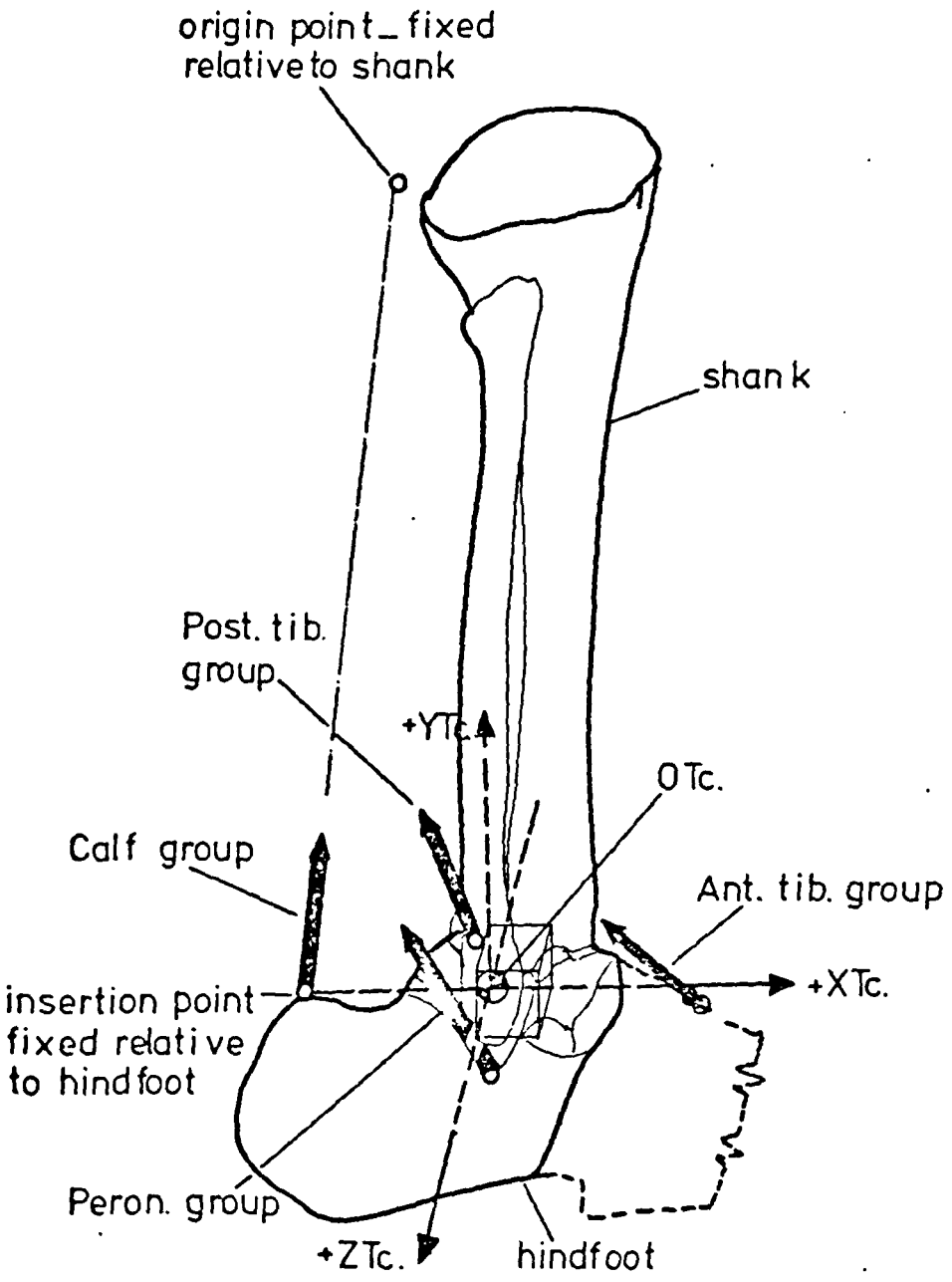

Figure 4.8 The Muscle Groups

the foot are neglected.

v) The lines of action of all the muscle groups, except the Calf, are assumed to be constant with respect to the hindfoot plus talus free body.

4.2.6 The Equations - Mark I Solution

As pointed out in 4.2.4 there are twelve equilibrium equations - six each for the Tc. and Tcn. systems. These equations are all that is available to solve for five Tc. joint force components (4.2.3), five Tcn. joint force components (4.2.4) and four muscle groups - making fourteen unknowns altogether. This gives two more unknowns than equilibrium equations and the problem is therefore indeterminate at first sight. Two further simplifications may be made to render the equations determinate, and form the basis for the Mark I solution.

Referring now to the Tc. system, the major action at the Talocrural joint is plantar/dorsiflexion. This is controlled principally by the Calf and Anterior tibial muscle groups, the Peroneal and Posterior tibial groups having relatively small lever arms about the $Z_{Tc.}$ axis. The elimination of the Peroneal and Posterior tibial groups reduces the unknowns by two. Further, it may be assumed that there is no antagonistic action between the Calf and Anterior tibial groups (Paul, 1971, reported Emg. evidence which supports this assumption). The Tc. system now becomes determinate having either the Calf or the Anterior tibial group plus five Tc. joint force components, making six unknowns and six equilibrium equations.

The equilibrium equations for the Tc. system, using the hindfoot plus talus free body, and using the Anterior

tibial group are (referred to hereafter as Case I)

Summing Force components,

$$(F_{At})_x + F_{xl} + F_{xm} + \ldots\ldots\ldots + (Fe)_x = 0 \quad \ldots 4.10$$

$$(F_{At})_y + \ldots\ldots + F_{yl} + F_{ym} + \ldots + (Fe)_y = 0 \quad \ldots 4.11$$

$$(F_{At})_z + \ldots\ldots\ldots\ldots + F_{zTc.} + (Fe)_z = 0 \quad \ldots 4.12$$

and Summing moment components, moments about the Tc. origin,

$$(M_{At})_x + \ldots\ldots\ldots + 0.01F_{yl} - 0.01F_{ym} + (Me)_x = 0 \quad \ldots 4.13$$

$$(M_{At})_y - 0.01F_{xl} + 0.01F_{xm} + \ldots\ldots\ldots + (Me)_y = 0 \quad \ldots 4.14$$

$$(M_{At})_z + \ldots\ldots\ldots\ldots\ldots\ldots + (Me)_z = 0 \quad \ldots 4.15$$

where

$(F_{At})_\alpha$ = Anterior tibial group force component α (α=x,y,z)

$(M_{At})_\alpha$ = Anterior tibial group moment component α

F_{xl} = lateral compartment $X_{Tc.}$ joint force component

F_{xm} = medial compartment $X_{Tc.}$ joint force component

F_{yl} = lateral compartment $Y_{Tc.}$ joint force component

F_{ym} = medial compartment $Y_{Tc.}$ joint force component

F_{zTc} = $Z_{Tc.}$ joint force component

$(F_e)_\alpha$ = external force component α

$(M_e)_\alpha$ = moment due to external force, component α

In Case II, where the Calf group is active, the Tc. system equations are identical to equations 4.10 to 4.15 excepting that the Calf group variables, F_C and M_C, are substituted for the Anterior tibial group variables, F_{At} and M_{At} respectively. Cases I and II are determinate and once solved attention may be turned to the Tcn. system and the talus free body. The selection of muscle group is based upon the sign of the $Z_{Tc.}$ moment due to the external force. Thus if $(Me)_z$ is positive, the Calf group is recruited - generating negative $Z_{Tc.}$ moments; negative $(Me)_z$ corresponding to the Anterior tibial group.

Considering the talus free body, the talus has no muscular attachments and the effect of ligaments is neglected. The only forces acting on the talus free body are the Tc. joint force components (corresponding to either Case I or Case II, vide supra) together with the five Tcn. joint force components. The equilibrium equations for the Tcn. system, using the talus free body are,

summing the force components,

$$(F)_x + F_{xp} + F_{xa} + \ldots\ldots\ldots = 0 \qquad \ldots 4.16$$

$$(F)_y + \ldots\ldots + F_{yp} + F_{ya} + \ldots = 0 \qquad \ldots 4.17$$

$$(F)_z + \ldots\ldots\ldots\ldots + F_{ZTcn.} = 0 \qquad \ldots 4.18$$

and summing moment components, taking moments about the Tcn. origin,

$$(M)_x + \ldots\ldots\ldots\ldots + 0.02\,F_{yp} - 0.02\,F_{ya} = 0 \quad \ldots\ 4.19$$

$$(M)_y - 0.02\,F_{xp} + 0.02\,F_{xa} + \ldots\ldots\ldots\ldots = 0 \quad \ldots\ 4.20$$

$$(M)_z + \ldots\ldots\ldots\ldots\ldots\ldots\ldots\ldots = 0 \quad \ldots\ 4.21$$

where

$(F)_\alpha$ = the Tc. joint force (in the Tcn. system) component α

$(M)_\alpha$ = the Tc. joint moment (in the Tcn. system) component α

F_{xa} = anterior facet $X_{Tcn.}$ joint force component

F_{xp} = posterior facet $X_{Tcn.}$ joint force component

F_{ya} = anterior facet $Y_{Tcn.}$ joint force component

F_{yp} = posterior facet $Y_{Tcn.}$ joint force component

Notice that there is no equilibrant for the $(M)_z$ component in equation 4.21, there being only five unknowns for six equations. There are two possibilities to consider for this situation, the first being that the $(M)_z$ component is equal to zero throughout stance phase. The second, and more likely answer, is that the $(M)_z$ - hereafter referred to as the residual $Z_{Tcn.}$ moment - is finite and is an indication that some additional equilibrating factor should be added to the equilibrium equations. The inclusion of an equilibrant for the residual leads to the Mark II solution.

4.2.7 The Equations - Mark II Solution

There are two main options for balancing the residual

$Z_{Tcn.}$ moment, considering the joint forces to be adequately described already. Firstly the ligaments acting across the Tcn. joints, the tibiocalcaneal portion of the deltoid and the fibulocalcaneal ligaments, may be recruited. It is suggested in the literature that these ligaments are only recruited towards the extremes of ankle joint movement - rather than the mid range experienced in normal locomotion.

This leaves the possibility of including the Posterior tibial and Peroneal muscle groups for whose inclusion there are strong arguments. It is a widely held opinion in the literature that both muscle groups play a significant role in stabilising the Tcn. joint in inversion/eversion, reported in 2.7.4. The temporal Emg. data suggests that both groups, along with the Calf group, are active for most of stance phase, see 2.7.3. The geometry of the Posterior tibial and Peroneal groups suggests that they are positioned to much greater mechanical advantage with respect to the Tcn. system than with respect to the Tc. system. From these considerations a Mark II solution including both of these groups was formulated.

With regard to the number of unknowns, including the Calf/Anterior tibial groups as one unknown, the Tc. and Tcn. joint force components as ten unknowns, the addition of the Posterior tibial and Peroneal groups brings the total to thirteen. This is one more than the number of equilibrium equations. The temporal Emg. evidence reported in 2.7.3 indicates that there is antagonistic activity between the Peroneal and Posterior tibial groups. In order to render the equations solvable it was decided to incorporate only one of these groups at a time and to use the sign of the residual $Z_{Tcn.}$

moment to decide which group was active.

The approach used for solving the Mark II version of the equations is as follows. To begin with, the Mark I Tc. and Tcn. system solutions are obtained and the residual $Z_{Tcn.}$ moment calculated. If the residual is positive in sense the Posterior tibial group is recruited - generating negative $Z_{Tcn.}$ moments; a negative residual corresponding to the Peroneal group. Then the Mark II Tc. equations are reformulated. For an example, take Case I - where the Anterior tibial group has already been selected - and where the residual $Z_{Tcn.}$ moment was negative - corresponding to Peroneal group activity. The Tc. equations, 4.10 to 4.15 become,

$$(F_{At})_x + (F_P)_x + F_{xl} + F_{ym} + \ldots + (F_e)_x = 0 \quad \ldots 4.22$$

$$(F_{At})_y + (F_P)_y + F_{yl} + F_{ym} + \ldots + (F_e)_y = 0 \quad \ldots 4.23$$

$$(F_{At})_z + (F_P)_z + F_{zTc.} + \ldots + (F_e)_z = 0 \quad \ldots 4.24$$

$$(M_{At})_x + (M_P)_x + 0.01\,F_{yl} + 0.01\,F_{ym} + (M_e)_x = 0 \quad \ldots 4.25$$

$$(M_{At})_y + (M_P)_y - 0.01\,F_{xl} + 0.01\,F_{xm} + (M_e)_y = 0 \quad \ldots 4.26$$

$$(M_{At})_z + (M_P)_z + \ldots + (M_e)_z = 0 \quad \ldots 4.27$$

where

$(F_P)_\alpha$ = Peroneal group force component α (α=x,y,z)

$(M_P)_\alpha$ = Peroneal group moment component α (α=x,y,z)

the remaining terms being defined after equation 4.15.

These six equations now contain seven unknowns and are indeterminate by themselves but the Tcn. equations are now used to bring the balance up to twelve equations in twelve unknowns. The joint forces in these equations

are still the only terms to be carried forward to the Tcn. system solution and for the purposes of the present argument their equivalent - in terms of the muscle and external force components in equations 4.22 to 4.27 - may be written

$$(F_J)_x = -(F_e)_x - (F_{At})_x - (F_P)_x \quad \ldots 4.28$$

$$(F_J)_y = -(F_e)_y - (F_{At})_y - (F_P)_y \quad \ldots 4.29$$

$$(F_J)_z = -(F_e)_z - (F_{At})_z - (F_P)_z \quad \ldots 4.30$$

$$(M_J)_x = -(M_e)_x - (M_{At})_x - (M_P)_x \quad \ldots 4.31$$

$$(M_J)_y = -(M_e)_y - (M_{At})_y - (M_P)_y \quad \ldots 4.32$$

$$(M_J)_z = -(M_e)_z - (M_{At})_z - (M_P)_z \quad \ldots 4.33$$

where

$$(F_J)_x = (F_{x1} + F_{xm})$$
$$(F_J)_y = (F_{y1} + F_{ym})$$
$$(F_J)_z = (F_{zTc.})$$
$$(M_J)_x = (0.01F_{y1} - 0.01F_{ym})$$
$$(M_J)_y = (-0.01F_{x1} + 0.01F_{xm})$$
$$(M_J)_z = (0)$$

equations 4.28 written more conveniently in vector notation give

$$\{F_J\} = -\{\{F_e\} + \{F_{At}\} + \{F_P\}\} \quad \ldots 4.34$$

$$\{M_J\} = -\{\{M_e\} + \{M_{At}\} + \{M_P\}\} \quad \ldots 4.35$$

where the curly brackets indicate vectors .

Now taking the radius vector of the Tc. origin relative

to the Tcn. origin as $\{R\}_{OTc. \rightarrow OTcn.}$, with components (r_x, r_y, r_z), the moment about the Tcn. origin due to $\{F_J\}$, $\{M_J\}_{OTcn.}$, is given by

$$\{M_J\}_{OTcn.} = \{R\}_{OTc. \rightarrow Tcn.} \text{ cross } \{F_J\} \qquad \ldots 4.36$$

which is evaluated as

$$\det. \begin{vmatrix} r_x & r_y & r_z \\ (F_J)_x & (F_J)_y & (F_J)_z \end{vmatrix} = \begin{Bmatrix} r_y.(F_J)_z - r_z.(F_J)_y \\ r_z.(F_J)_x - r_x.(F_J)_z \\ r_x.(F_J)_y - r_y.(F_J)_x \end{Bmatrix} \qquad \ldots 4.37$$

The total moment about the Tcn. origin - $\{M\}_{Tot}$ - is obtained by adding $\{M_J\}$ and $\{M_J\}_{OTcn.}$, and from 4.35 and 4.37

$$\{M\}_{Tot} = \begin{Bmatrix} r_y.(F_J)_z - r_z.(F_J)_y + (M_J)_x \\ r_z.(F_J)_x - r_x.(F_J)_z + (M_J)_y \\ r_x.(F_J)_y - r_y.(F_J)_x + (M_J)_z \end{Bmatrix} \qquad \ldots 4.38$$

This is still oriented to the Tc. system and must be multiplied by the rotation matrix linking the Tc. and Tcn. systems - $[R]_{Tc. \rightarrow Tcn.}$. Since only the $Z_{Tcn.}$ moment equation is required in the present argument the $[R]_{Tc. \rightarrow Tcn.}$ matrix may be written with only the z row terms as,

$$[R]_{Tc. \rightarrow Tcn.} = \begin{bmatrix} - & - & - \\ - & - & - \\ R_{z1} & R_{z2} & R_{z3} \end{bmatrix} \qquad \ldots 4.39$$

where square brackets [ ] denote a 3x3 matrix

and the product $[R]_{Tc.\rightarrow Tcn.}.\{M\}_{Tot}$ (calculated from equations 4.38 and 4.39) is equated to the residual $Z_{Tcn.}$ moment which is set to zero,

$$\text{Residual } Z_{Tcn.} \text{ moment} = 0 = R_{z1}((r_y.(F_J)_z - r_z.(F_J)_y)+(M_J)_x + R_{z2}(r_z.(F_J)_x - r_x.(F_J)_z)+(M_J)_y + R_{z3}(r_x.(F_J)_y - r_y.(F_J)_x)+(M_J)_z) \quad \ldots 4.40$$

By substituting the muscle forces for the joint force components using equations 4.28 to 4.30, equation 4.40 may be written in terms of two unknowns only - the Peroneal and Anterior tibial group forces. (Note that although the muscle group components in equations 4.22 to 4.27 number six, because the line of action and the point of application of each muscle group is known, there are now actually only two unknowns - the magnitude of each muscle group force.) In addition equation 4.27 contains the same two unknowns and so the Anterior tibial and Peroneal group forces are given by solving the equations 4.27 and 4.40 simultaneously. The remaining Tc. equations 4.22 to 4.26 may now be solved. The Tcn. equations are now formulated in exactly the same way as in the Mark I solution, equations 4.16 to 4.21, but - the residual $Z_{Tcn.}$ moment being now zero - there are now five equations in five unknowns.

The Mark II solution outlined above may be used equally well substituting the Calf for the Anterior tibial group, or where the Posterior tibial group is active instead of the Peroneal group.

4.3 Concluding Remarks

The models presented are intended to be as realistic as the method of solution would permit.

In addition to the assumptions already stated, it should be understood that the models described refer to rigid bodies and deformation of the foot is not taken into account.

The Mark I and II models form the basis for the experimental studies. The performance of the models and their further development to include the action of ligamentous forces will be considered in chapter seven.

CHAPTER 5

DETAIL OF THE EXPERIMENTAL METHOD

5.1 Introduction

In this chapter the experimental set up, measurement systems and the experiments will be presented and discussed.

5.2 Experimental Data Collection and Measurement

5.2.1 Kinematic System

There are currently many options to be considered when selecting a system for the collection and recovery of three-dimensional kinematic data from locomotion studies. Briefly the main options are; light-emitting diode marker systems for example SELSPOT - manufactured by Selcom AB (Sweden), television systems using some form of reflective marker such as that developed by Jarrett (1976), and cine filming of surface markers as used by Paul (1967) and Morrison (1968). The first two options have a particular advantage in that they allow rapid recovery of kinematic data coordinates when used together with an on-line computer. It should be noted that both SELSPOT and TV systems in general, provide only coordinates for points that have been specifically marked, which may make data recovery difficult where markers are totally or partially obscured by limb movement. In the case of television systems markers may give rise to ambiguous signals where they become physically close to each other, and become indistinguishable; this problem is understood to be overcome in the SELSPOT system where light-emitting diodes are flashed in sequence and only one diode is emitting light at any instant. SELSPOT is known to have reflection problems when markers close to the floor are used. One of the drawbacks of automatic data collection systems such as those used in SELSPOT or TV systems is that they usually require human operator

intervention where marker trajectories are incomplete or confused.

Cine film provides a complete visual image and, even where a marker is completely obscured for a short interval, the human operator can interpolate its position without too much difficulty. The particular disadvantage of cine film is that data recovery is both tedious and time consuming. Data recovery from cine film can only, at the present time, be achieved by indirect methods using a trace analyse or digitiser device.

For the detailed study of ankle kinematics it was felt that a complete visual image was desirable to permit subjective assessment of gait. In addition, considering that the markers defining the ankle and foot would be physically close to each other, notwithstanding the disadvantages noted above, cine film was the method of choice for the present study.

The laboratory environment for the study of ankle biomechanics is illustrated in figure 5.1 and is shown in plan view in Appendix 3.1. Three Bolex Paillard cine cameras were sited orthogonally to each other, giving left, right and front views of a subject on the locomotion walkpath area. The cameras were aligned so that their optical axes coincided at a point 0.495 metres vertically above the surface of a Kistler force platform (described in 5.2.2). Each camera was driven by an independent synchronous motor at mains frequency of 50Hz. (normal fluctuation less than 0.1Hz.) - the question of sampling frequency will be discussed in 6.4.1. The motors were wired to a single on/off switch enabling all three cameras to be powered simultaneously and, because of electromechanical inertia, a period of about two seconds

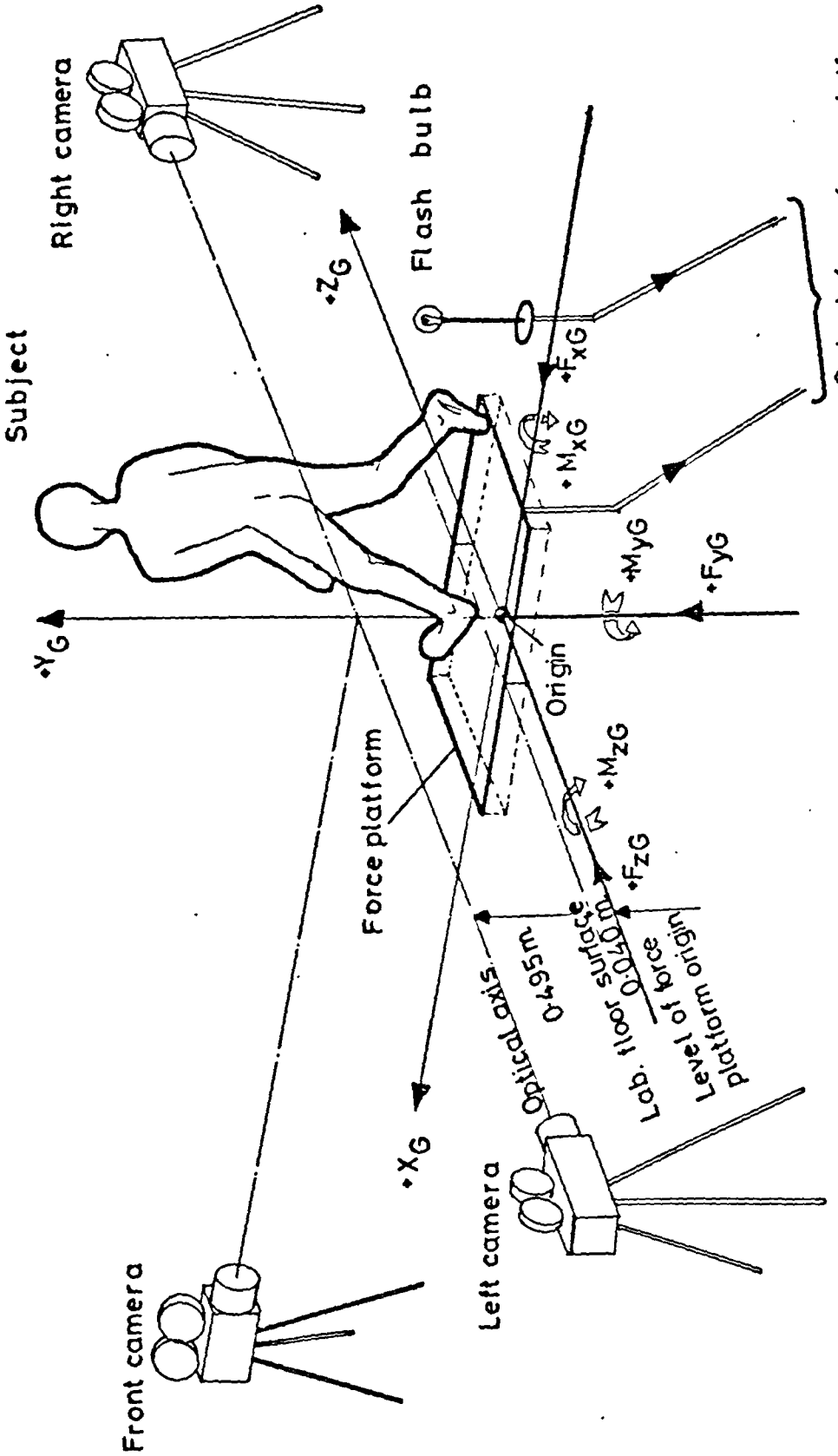

Figure 5.1 Sketch of a Subject on the Locomotion Walkpath

was allowed for the cameras to reach running speed.

The film used for all of the tests was Kodak Kodachrome (19DIN) colour film in either 50 or 100 metre lengths. Illumination adequate for colour cine filming was provided by flood lighting mounted in the laboratory ceiling.

5.2.2 Force Measurement System

The measurements of external forces and moments acting between the body and ground were made using a Kistler type 9261A piezoelectric force platform. The measurement of forces is made with respect to an origin 0.04 metres below the upper surface of the platform, and the moments are calculated with respect to an orthogonal axis system defined relative to this origin. For the purposes of the present study an orthogonal laboratory ground axis system was defined to coincide in directions and origin with the force platform axis system. The ground system is illustrated in figure 5.1, showing forces and moments acting in a positive sense on the body. The positive axes directions are X_G - directly towards the front camera, Y_G - vertically out of the floor towards the ceiling and Z_G - normal to the X_G-Y_G plane in the direction of the right camera. Note that the point at which the camera optical axes coincide (see 5.2.1) is on the Y_G axis and (0.495+0.04) metres above the ground system origin.

The forces and moments are output from summing and buffer amplifiers associated with the Kistler platform in the form of six channels of electrical analogue signals. Three channels give force components in X_G, Y_G and Z_G directions, and the remaining channels the

moments associated with these forces, acting about each of the ground reference axes. The magnitude of each analogue signal was directly related to either force in Newtons, or moment in Newton metres, by calibration constants. The calibration constants include factors to allow for the summing and buffer amplifier settings and were experimentally verified (discussed in 5.5.2).

Each analogue channel was routed directly to the analogue to digital convertor of a PDP12 digital computer, where it was sampled at a rate of 50Hz., corresponding to the cine film sampling frequency. The signals at this stage were in digital form and were output directly onto punched paper tape, as numbers in the range ±512 units. The calibration constants, noted above, were then used to convert these numbers into actual forces and moments in the computer programs.

5.2.3 Temporal Synchronisation of the Kinematic and Force Data

The cine film data and force platform data were synchronised temporally by means of a flash bulb, fired during each test run. The flash bulb was in clear view of each camera, illustrated in figure 5.1, and was fired by completing a simple electrical circuit. The switch completing the circuit was also connected in series to a sense line of the PDP12 computer so that when the circuit was made by closing the switch a pulse was sent to the computer at the same instant as the flash bulb fired. The sense line channel was sampled concurrently with the six force platform channels and so the electrical pulse due to the flash circuit could be related in time to the force data. The visual event of the flash bulb

firing was simultaneously recorded by the three cine cameras and so the force data could now be related directly to the kinematic data. There is however a small error introduced by the camera shutter mechanisms: because the camera shutter drives were not mechanically or electrically linked, and thus the shutter opening events not exactly synchronised, each camera would capture the flash event at slightly different times. In other words, one camera misses the first instant of flash, simultaneously a second camera captures it, then the next frame of the former camera captures the developing flash. This at worst may introduce one frame synchronisation error between the three cameras, corresponding to 1/50th of a second.

5.2.4 Spatial Relation of the Kinematic and Force Measurements

The relation of the kinematic and force data in spatial terms was achieved through the use of a calibration board together with field markers, fixed to the ground, in view of each camera. (Before describing the methods used the result of a preliminary experiment will be described.) For calibration a board, shown in figure 5.2, was filmed with a single field marker placed in front, using the front camera. The board was aligned so that its origin was directly above the ground system origin and its surface was in the Y_G-Z_G plane. (The cine film, once processed was closely examined.) The digitising process used required that any stationary markers in the field of view of the cine camera should, on projection on to the digitising table, remain stationary from one frame to the next. Three forms of displacement

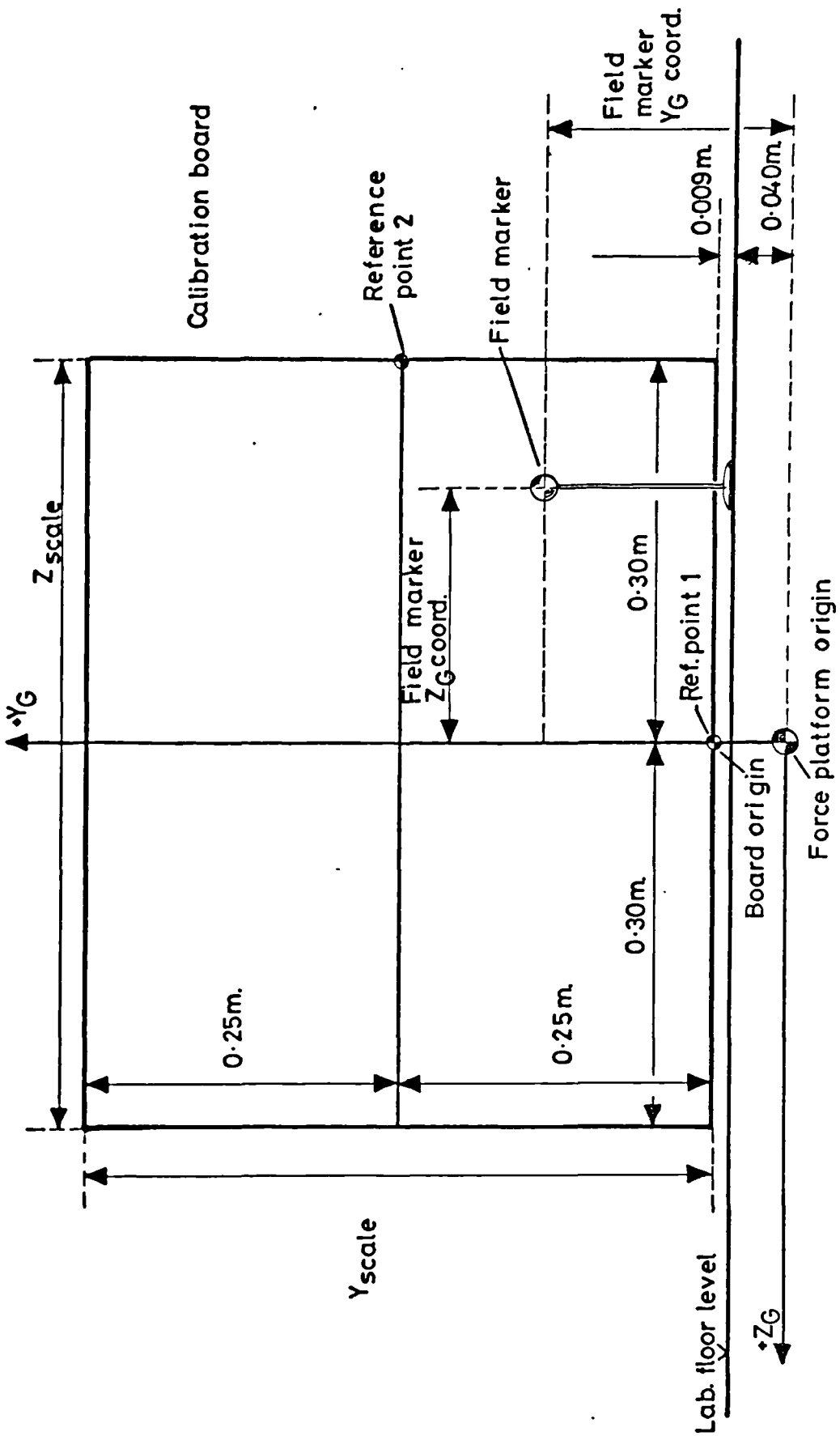

Figure 5.2 Calibration Board and Field Marker for the Front Camera

error were identified from the cine film projection: one was rotational and two were linear DC shifts, and are illustrated as errors between consecutive projected frames in figure 5.3. These errors are caused by mechanical imperfections in the film advance mechanisms of both the camera and the cine film projector. It was found over a sequence of one hundred consecutive frames that the range of rotation error was less than 0.2 degrees. This is small enough to reject as a source of significant error. However, the linear displacement errors annotated ΔY_G, ΔZ_G in figure 5.3 were found to be significant, particularly so ΔY_G, which if not corrected could introduce errors of up to $\pm$5mm. These DC shifts were eliminated by adopting the field marker as a reference origin.

To relate the cine film data to the force platform origin a calibration test was performed, for each cine camera, once before and once after a subject test. Field markers, attached firmly to the ground, were placed so that one was visible to each camera. These field markers were placed in position before the testing began and were left undisturbed throughout all of the tests for one subject. For the calibration test the calibration board was centred over the ground system origin and turned to face the left camera and a few frames of film exposed: this exercise was then repeated for the front camera and finally the right camera. This entire procedure was repeated at the end of the experimental tests for each subject to ensure that no significant changes had occurred, for example a field marker being moved. This gave on each film a record of the calibration board plus field marker before and after the subject test runs. The distance between the calibration board origin and

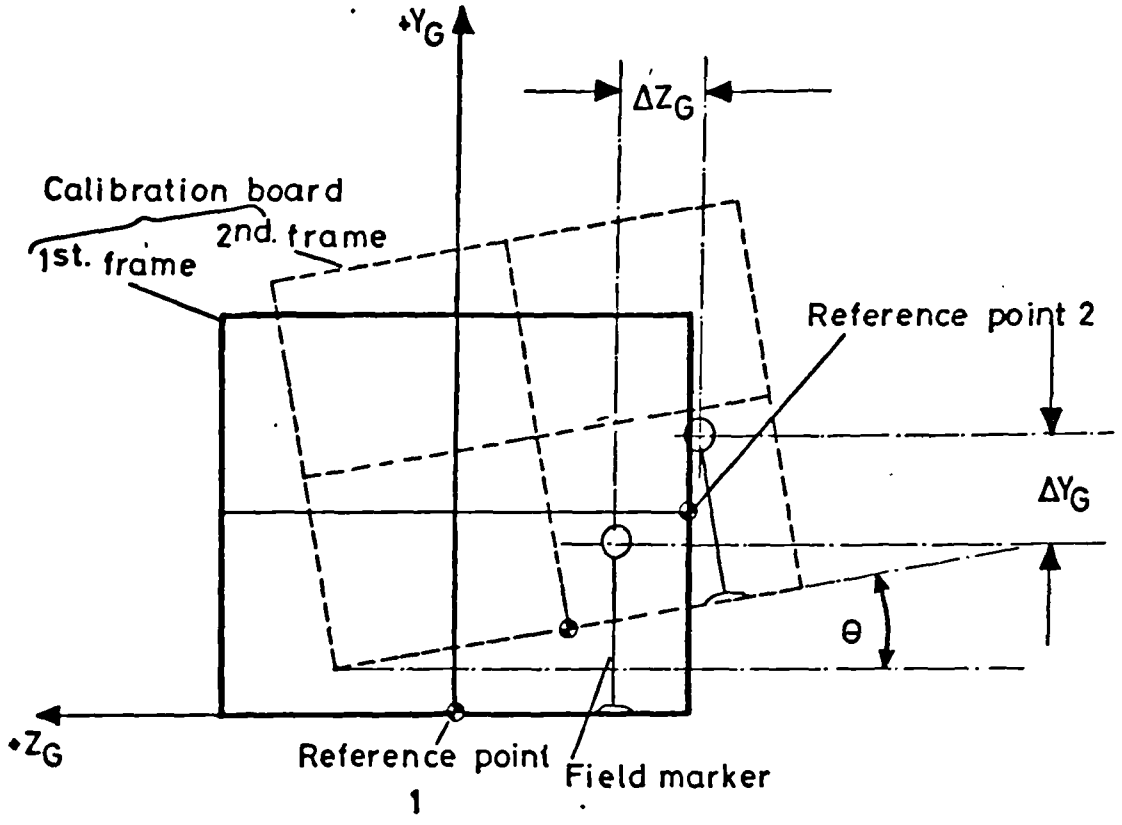

Figure 5.3 Illustration of Errors due to Cine Camera and Projector Shutter Mechanism Misalignment, Front Camera View

of the ground system was 0.049m. in the Y_G axis direction (the board being centred over the force platform origin). From the picture of the calibration board and field marker together therefore, the DC shifts relating the latter to the ground system origin could be calculated. Further, in the tests (where the calibration board was removed), the kinematic data in view of each camera could be related to the ground system origin through the measurement of the appropriate field marker coordinates. Three further sources of error are parallax, lens distortion and dimensional changes in the cine film due to processing. The parallax errors, due to perspective effects, were corrected for in the data analysis programs. The equations of parallax used together with a diagram illustrating this effect are included in Appendix 3.1 The parallax corrections to space coordinates were never greater than five millimetres.

The dimensional changes due to film processing were thought to be small. Any stretch or shrinkage occurring in the length or width of the cine film was taken into account by the calculation of scale factors. The scale factors were taken from the calibration board, for example in the front camera calibration board views the scale factors Y_{scale} and Z_{scale} were calculated. Y_{scale} and Z_{scale} correspond to 0.5 and 0.6 metres respectively, illustrated in figure 5.2. These scale factors effectively solve two problems at the same time, in providing a correction for distortion and also giving calibrated distances against which to measure the marker data.

The effects of lens distortion are greatest towards the edges of the camera field of view. To minimise this

problem it was ensured, where possible, that test subject was centrally placed with respect to the field of view.

5.2.5 Recovery of the Kinematic Data

The marker data on each cine film was recovered using a D-MAC trace analyser. The film was projected on to the trace analyser table and run through frame by frame until the calibration board sequence appeared. The D-MAC table was then rotated until the calibration board axes coincided with the table digitising reference axes. This oriented subsequent test frames to the digitising table axes and then data points were digitised in the sequences detailed in Appendix 3.4. Coordinates of any required point were taken by placing a cursor over the point and the table then output the coordinates directly on to punched paper tape. The coordinates were in the form of table units, one unit being equivalent to 0.1mm. The calibration board dimensions, for example using the front camera view, Y_{scale} and Z_{scale} were then digitised to give known lengths in terms of table units which were later used to convert the unit equivalent of marker coordinates into real coordinates.

5.3 The Experiments

5.3.1 The Experimental Tests

One of the prime objectives in the present study was to study the ankle during normal locomotion activity. The results of Wright et al (1964), reviewed in 2.8.1, indicate that ankle joint kinematics are influenced by walking on a side slope of $9\frac{1}{2}^{\circ}$. It was considered likely that the dynamics of the ankle joint would also be affected in some way so two tests were planned in

addition to the normal locomotion test. Both additional tests involved walking on 10° side slope but in one case the test foot (the right foot) was uphill (+10°) and in the other downhill (-10°). Stance phase only was considered for each test.

5.3.2 The Side Slope Ramp and Force Platform Natural Frequency

For the side slope walking tests a ramp was constructed from wood with its upper surface covered with thin rubber sheet to prevent slipping. The ramp had 10° side slope and was about eight metres long by 1.5 wide, see figure 5.4. The ramp included a cut out section about halfway along its length into which fitted an insert positioned directly over the force platform. The insert base was the same size as the force platform surface, and its top surface was flush with the ramp. The union between the force platform and the insert was made by double sided adhesive tape. A gap of about 1-2mm. prevented the insert from contacting the ramp.

It was thought that the insert might affect the dynamic behaviour of the force platform and so the natural frequency of the force platform plus insert was compared with that due to the platform alone. The natural frequency was determined from harmonic analysis of the force platform signal, in the Y_G direction, in response to impact of a 0.5kg. mass on the platform surface. The force platform signal was sampled at 1kHz. by the PDP12 computer and analysed by an in-house fourier analysis package. The analysis showed that the free force platform natural frequency decreased by 5% from 112 to 107Hz. with the addition of the insert section;

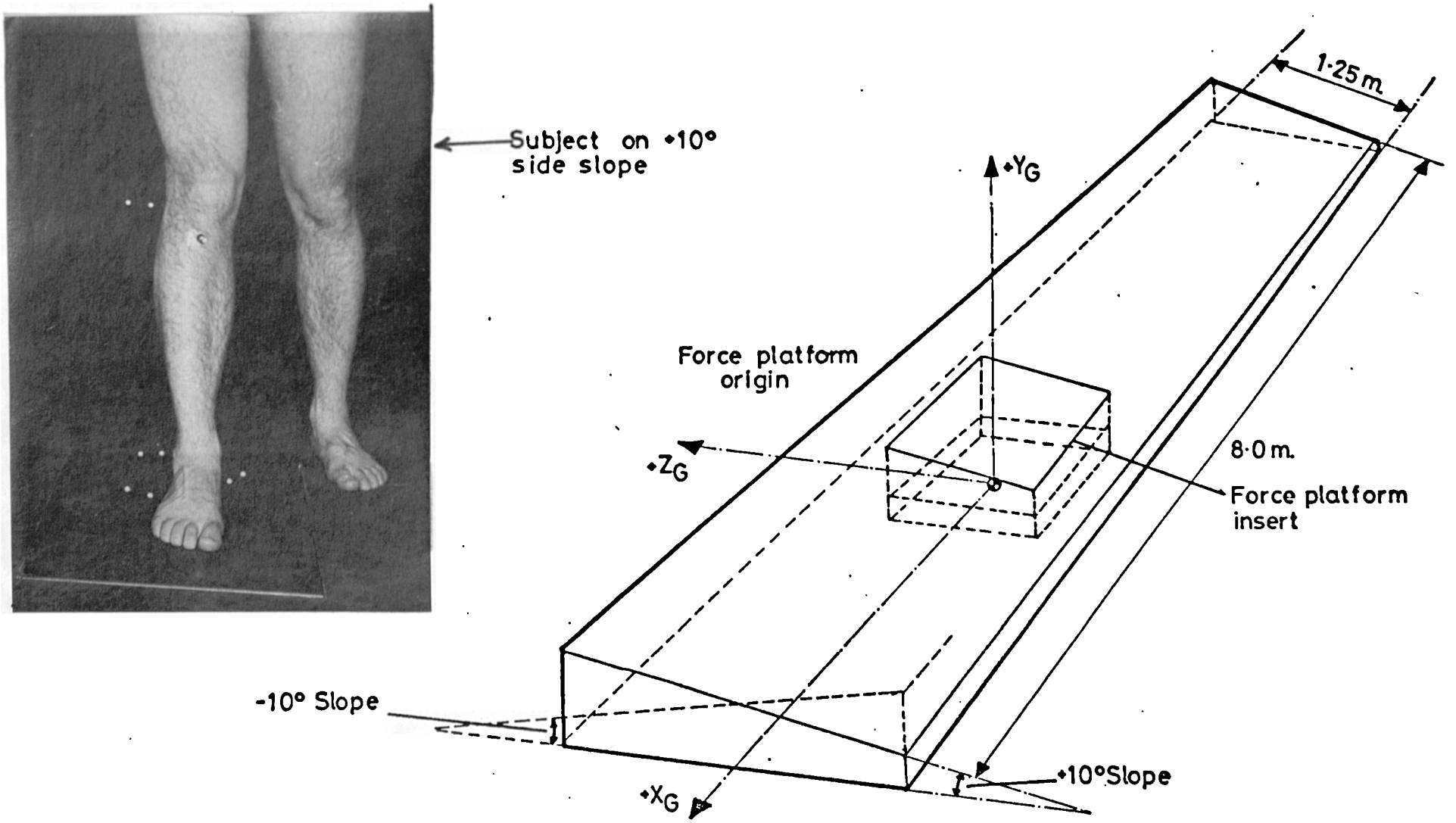

Figure 5.4 Illustration of the Side Slope Ramp and Force Platform Insert

the frequency spectrum was otherwise virtually unchanged. The decrease in natural frequency was not considered significant.

5.3.3 Protocol Observed for the Tests

The test subjects, all male, were volunteers drawn from the student population of the bioengineering unit. The subjects were assumed to be 'normal' and were only rejected if there was any history of joint disease, abnormality or injury, particularly in respect of the ankle joint. In each instance the right leg and ankle only was studied notwithstanding the contention by Chhibber and Singh (1970) that the left leg is functionally dominant, see 2.7.4.

For each subject, at the time of testing, a record was made of height, weight and age. Then just prior to the tests the bony prominences were palpated, the overlying skin shaved, and markers defining the prominences were affixed according to the scheme laid down in figure 5.6. The subject was then encouraged to walk barefoot freely on the locomotion walkpath in order to be quite at ease in the test situation. The subject was then asked to perform the test phases three and four, detailed in 5.3.4. It was frequently observed during the familiarisation period that the subject's locomotion pattern was disrupted by conscious attempts to hit the force platform surface when he had wandered slightly off course. To avoid this problem the subject was asked to concentrate upon a distant target - for example the front camera - and walk towards this. By trial and error it was possible to set a starting point

from which the subject would successfully contact the force platform more or less centrally without having to make any conscious effort.

The minimum number of runs necessary to ensure adequate description of the natural gait variation occurring during locomotion was determined by experiment. The first subject tested was asked to perform five normal locomotion runs. The kinematic and force data for each run were compared and found to be similar in form and magnitude (discussed further in chapter seven). The variation occurring was considered to be described just as adequately by three runs as by five and so in all later tests only three runs were required.

5.3.4 Experimental Sequence

The experiments concerning each subject were conducted in four phases the first and last of which did not require the subject to be present. The phases were:

Phase one: Kinematic Calibration

The field markers were set in place and the calibration board filmed facing each camera in turn, explained in greater detail in 5.2.4.

Phase two: Static Tests

The subject with markers in place was filmed whilst standing on the force platform. The position of the leg relative to the foot approximated as well as possible to that adopted when setting the cadaver feet up for anthropometric measurement, shown in 3.4.2. Two views were taken one with the subject facing the front camera and the other facing directly away from the front camera. The reasons behind this are elaborated in chapter six.

Phase three: Dynamic Tests

In these the subject was asked to walk at preferred speed performing three runs each for the normal locomotion, side slope+10° and side slope-10° locomotion tests. For the latter two tests the side slope ramp was assembled on the walkpath area, as shown in figure 5.4. During each test run the subject was filmed by the three cine cameras, the synchronising flash was fired and, simultaneously the flash circuit pulse and force platform data were sampled by the PDP12 computer.

Phase four: Kinematic Calibration

Phase one was repeated to ensure that the field markers had not been disturbed during the static and dynamic tests.

5.4 Bony Point Markers

The markers used to define bony prominences were made from two plastic beads, threaded on to a wooden dowel, with half of a third bead forming the base, sketched in figure 5.5. The dowel and base were painted matt black whilst the marker beads were painted fluorescent yellow - a colour found to contrast well with most background colours. The marker beads were seven millimetres in diameter and a bead twelve millimetres in diameter was used for the base. Two different lengths of marker were made - short (4cm.) and long (5.5cm.) having 2.5cm. and 3.5cm. between the marker beads, respectively. The construction materials used were lightweight to ensure that inertial influences on the markers would be minimised. The skin was prepared by shaving and the markers were affixed using double sided adhesive tape. Eight markers altogether were sited over bony prominences

(a) Long marker

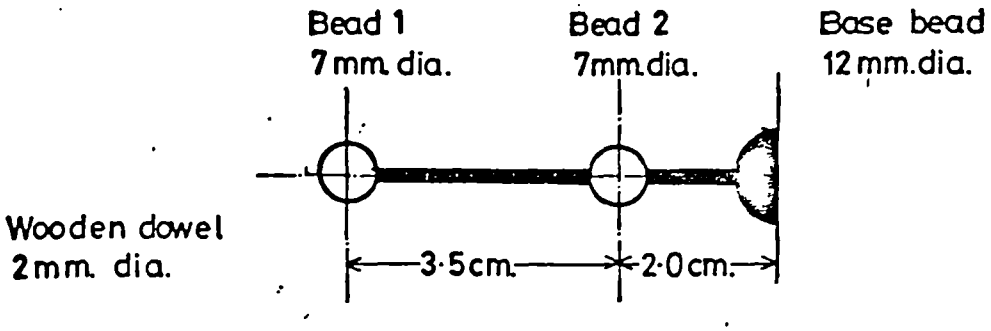

(b) Short marker

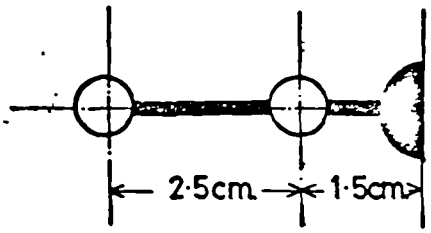

Figure 5.5 Bony Prominence Markers

and the marker beads were allocated reference numbers according to the scheme in figure 5.6. In the second experimental phase (5.3.4) all eight bony points were used whilst for the third phase, dynamic tests, the markers on the medial condyle and medial malleolus were removed; the reasons for this will be explained in chapter six.

The bony points were given two bead markers rather than one bead or just a surface point because from two points it is possible to make an estimate of the co-ordinates of the bony point itself. Once the coordinates of each bead (on one marker) are known in space, relative to the laboratory ground system, the marker geometry together with the bony point skin and fat cover (estimated from the cadaver studies) can be used to estimate the coordinates of the bony point. The bony prominence calculations are detailed in Appendix 3.2.

5.5 Accuracy of the Data Collection Systems

5.5.1 Kinematic Measurement System

In the recovery of kinematic data one point was always related to another; the measurements of the field markers were made relative to the calibration board origin, and the body markers were always measured relative to the field markers. After all the kinematic manipulations - digitising, DC shift, scaling and parallax correction - it was found that the distance between the beads on a long marker (nominally 35mm.) was repeatably estimated to within $\pm$0.5mm. for static tests. In the dynamic tests this tolerance increased to $\pm$1.0mm. (excepting at the very beginning and end of stance phase, where the shank markers moved fast enough to blur the

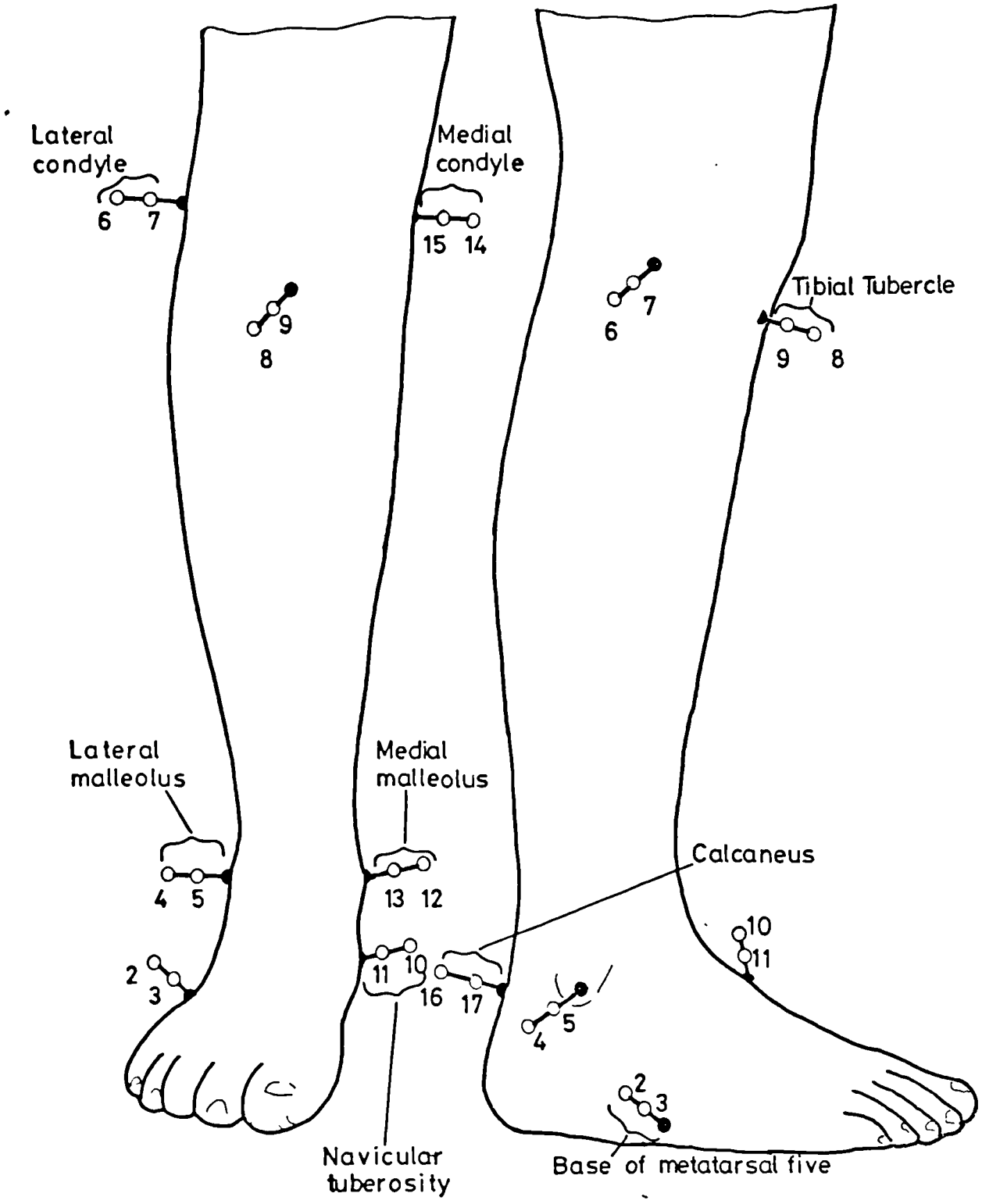

Figure 5.6 Bony Prominence Markers and Numbering Scheme

marker bead image). These results were consistent for each subject.

5.5.2 Force Platform System

The performance of the Kistler force platform-PDP12 computer system was assessed by comparing digitised paper tape output with known applied static force actions at the force platform. Static forces were applied by deadweight loading of the force platform in the X_G, Y_G Z_G directions in increments up to the magnitudes normally observed during locomotion. The curves of applied force versus digitised output (converted to force using Kistler calibration constants) were found to be linear over the ranges examined, and demonstrated an accuracy of $\pm$2.7% for each of the three force channels comparing favourably with the $\pm$2.5% claimed by Kistler. Each of the three moments output from the force platform-amplifier system is calculated from two of the measured forces and hence would have an accuracy of $\pm$5.4% (Kistler state $\pm$5%). Cross sensitivity between the channels was about $\pm$1%.

CHAPTER 6

THE THEORETICAL ANALYSIS AND ASSOCIATED COMPUTER PROGRAMS

6.1 Introduction

In chapter five the experimental systems and methods were described together with the adopted marker system. In the present chapter the methods used to relate the force platform and kinematic data to the models described in chapter four will be discussed. The associated numerical computations were performed by an ICL 1904B digital computer. Every calculation performed by computer was arithmetically checked against a master set of calculations.

The relation of the experimental kinematic data to the internal Tc. and Tcn. joint models will be discussed first and then the equations developed in three stages up to the point where solution of the Mark I and Mark II models is possible. The three stages developed correspond to three computer programs; the overall scheme of the calculations in relation to the programs is illustrated in figure 6.1 Discussion of the programs in the text will be made with reference to flow diagrams which describe each program. The computer file management scheme will also be referred to and is included in Appendix 3.4.

6.2 The External Shank and External Hindfoot Axes Systems

6.2.1 Introduction

Two further orthogonal reference axes systems were defined, the external shank and external hindfoot systems, which were related for each cine film frame to the internal Tc. and Tcn. systems respectively. The Tc. and Tcn. systems have already been described in 3.4.8 in relation to cadaver anthropometry: these systems are set up in an identical manner for the living subject with the exception that scale factors relating the cadaver anthropometry to the subject are included. The question of scale factors,

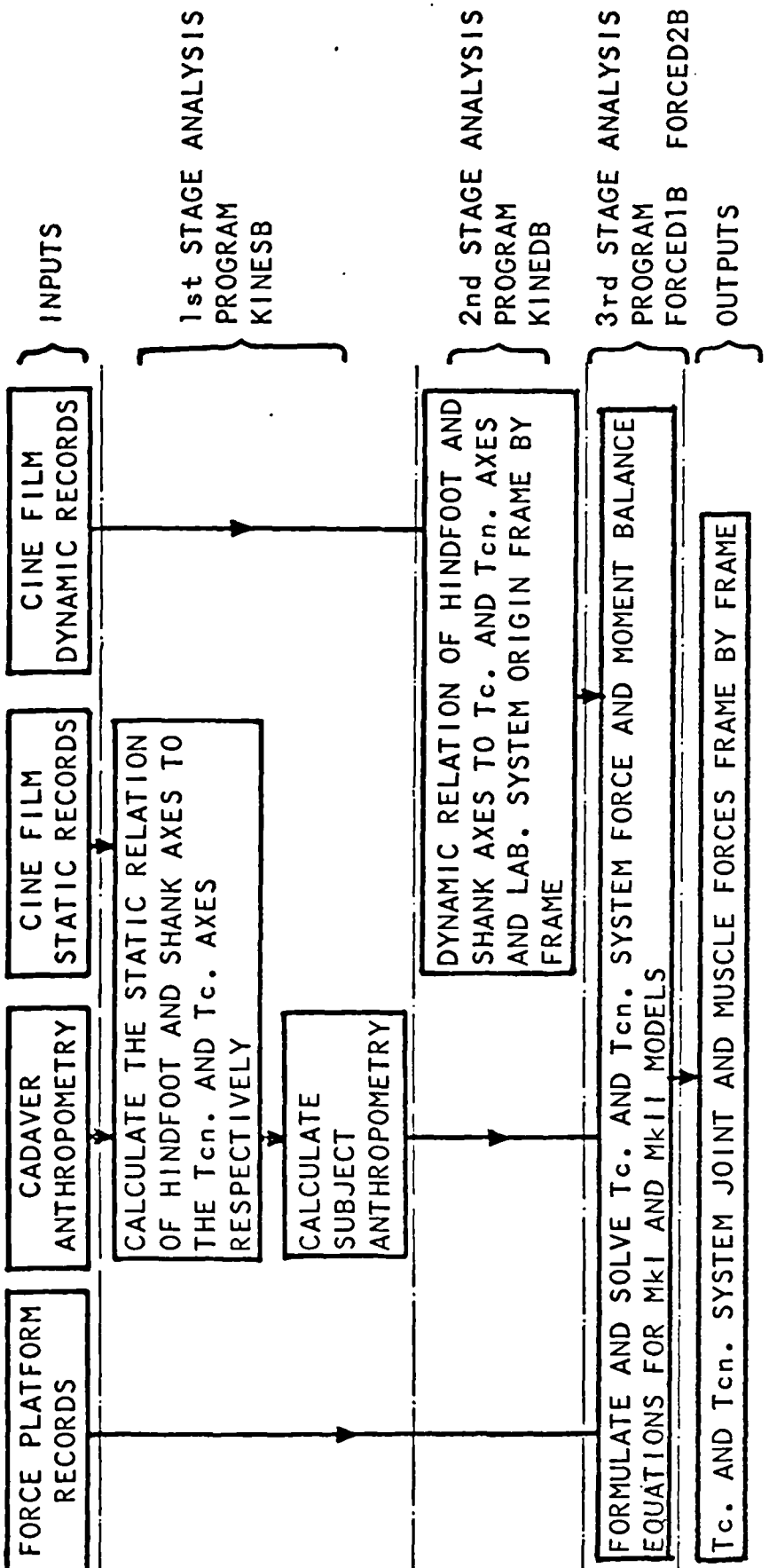

Figure 6.1 Block Diagram Showing the Main Calculation Stages and their Relation to the Program Sequence

already mentioned in 3.4.10, will be discussed further in 6.3.3; for the present it is assumed that the Tc. and Tcn. axes systems are defined as fixed with respect to the shank and hindfoot segments respectively. The reason for choosing to define segment external reference axes is that they form convenient intermediate reference systems between the subject internal geometry and the laboratory ground system.

(Note that it is implicitly assumed in the following axes definitions that the segments are rigid bodies. It has already been concluded in the literature review (2.3) that fibular motion relative to the tibia is small enough to neglect. Motions are known to occur between the bones comprising the hindfoot (2.2.4) but are neglected as a first approximation.)

6.2.2 Definition of the External Shank System

The External shank axis system is based upon marker points 5, 7 and 9, according to the number scheme adopted for marker beads in figure 5.6. It is assumed that the three space coordinates of each point are known relative to the laboratory ground system. With reference to figure 6.2(a) to set up the axis system, point 5 serves as the origin - $O_{Es.}$ (subscript Es. referring to External shank) and the vector $\{7\text{-}5\}$ as the $Y_{Es.}$ axis. The $Z_{Es.}$ axis is defined as normal to the plane in which points 5, 7 and 9 lie and therefore $X_{Es.}$ lies in this plane. The $Z_{Es.}$ axis is given by the vector cross-product of vectors $\{9\text{-}5\}$ and $\{7\text{-}5\}$ and from the condition of orthogonality the $X_{Es.}$ axis is defined by

$$X_{Es.} = Y_{Es.} \text{ cross } Z_{Es.} \qquad \ldots 6.1$$

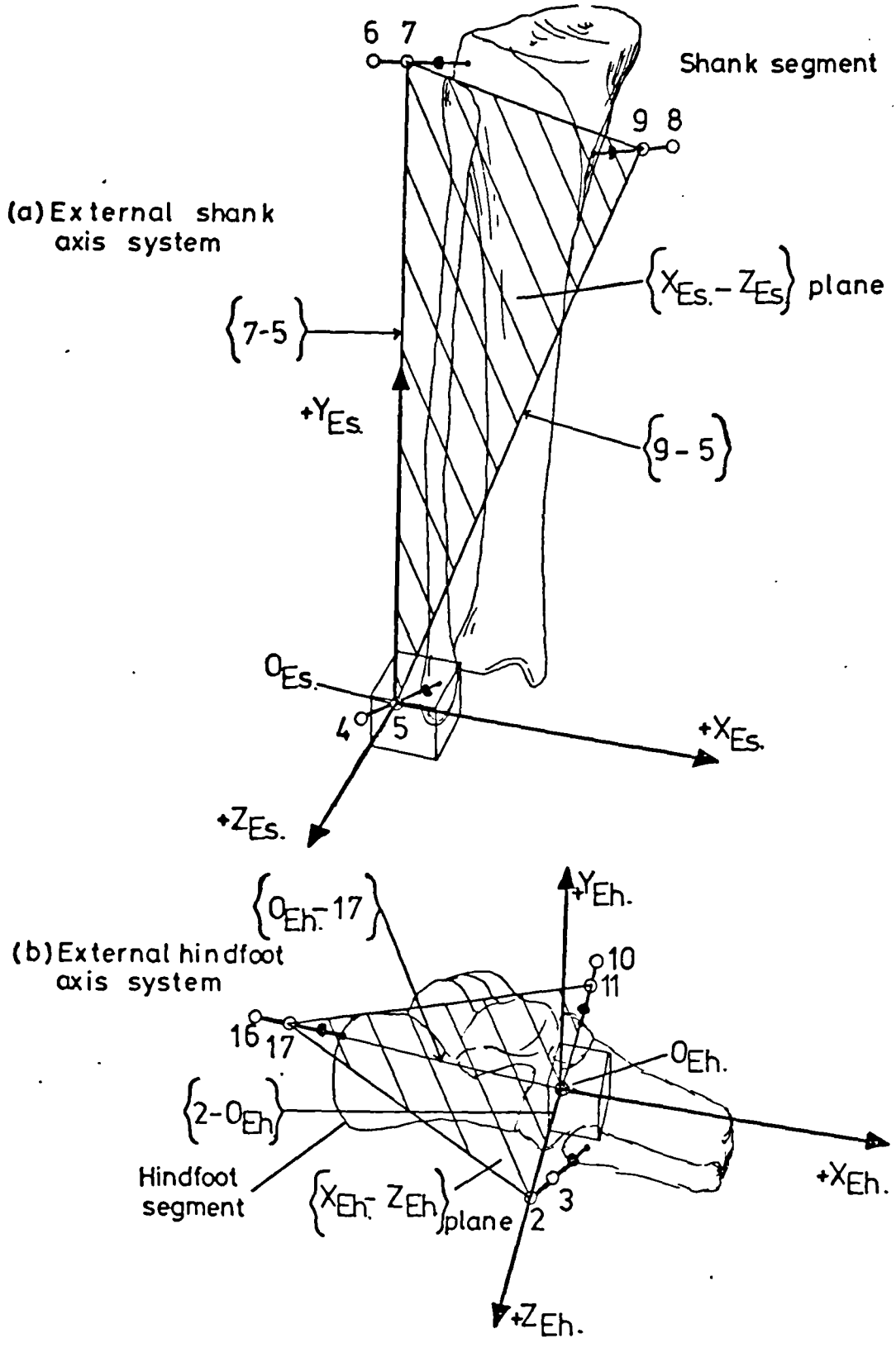

Figure 6.2 Definition of the External Shank and External Heel Axes Systems

6.2.3 Definition of the External Hindfoot System

The External hindfoot system is based upon marker points 2, 11 and 17. Note that 2 is the only outer marker bead used in defining axes, the remainder being inner beads, closer to the body. The reason for this is that it was found that the inner marker bead 3 (corresponding to 2 outer bead) was obscured from front camera view by the forefoot for the first part of stance phase, whilst 2 remained visible throughout stance phase. With reference to figure 6.2(b) the origin $O_{Eh.}$ (Eh. subscript refers to External hindfoot) was defined as midway between points 2 and 11. The $Z_{Eh.}$ axis was defined by the vector $\{2\text{-}O_{Eh.}\}$ and the plane containing 2, $O_{Eh.}$, 11 and 17 defined the $X_{Eh.}$-$Z_{Eh.}$ plane. The vector cross-product of $\{O_{Eh.}\text{-}17\}$ and $\{2\text{-}O_{Eh.}\}$ gives the $Y_{Eh.}$ axis normal to the $X_{Eh.}$-$Z_{Eh.}$ plane, and the $X_{Eh.}$ axis is given by orthogonality as

$$X_{Eh.} = Y_{Eh.} \text{ cross } Z_{Eh.} \qquad \ldots 6.2$$

6.3 The Analysis - Stage One

At this stage the static kinematic data collected under phases one and two in the experimental sequence, described in 5.3.4, are used. The program performing this stages analysis was called KINESB, see 6.6, figures 6.1 and 6.9 and KINESB flow chart in figure 6.10.

6.3.1 Preliminary Kinematic Data Conditioning

In the first part of KINESB the DC shifts relating the field markers to the force platform origin (detailed in 5.2.4), via the calibration board origin, were used

to calculate the apparent coordinates of all of the markers, for each camera view.

The apparent marker coordinates were then scaled, by scaling factors calculated from the calibration board dimensions (detailed in 5.2.4); the front camera data being scaled by factors calculated from the front view of the calibration board; the other camera views by their respective factors.

Then the three true coordinates of points 2 to 15, relative to the ground system, were calculated using the parallax equations, derived in Appendix 3.1.

Points 16 and 17, it will be recalled, belong to the heel marker and are not visible from the front of the leg. It was for this reason that in the second phase of the experiments, 5.3.4, a reverse static view of the subject was filmed with each camera. From the reverse view camera data, after performing the manipulations noted above, the true coordinates of points 2, 3, 16 and 17 were calculated. Then using Pythagorean algebra the distances between point 2 and points 16 and 17, d_{16-2} and d_{17-2} respectively, were calculated. Then, using point 16 as an example, a quadratic equation was formulated from the parallax equations and Pythagoras' equation, into which were substituted the true coordinates of point 2 and the apparent coordinates of point 16 (obtained from the right camera view). The quadratic was written in terms of the true Z coordinate of point 16 and then solved to give two roots, the smaller of which was accepted and used to calculate the true X and Z coordinates of point 16 using the parallax equations. The relevant equations are derived and solved in Appendix 3.3, and a numerical example is presented to illustrate the validity of

choosing the smaller root. The true coordinates of point 17 were calculated in the same manner. Morrison (1968) used a similar technique to calculate the coordinates of a marker hidden from one camera.

The true coordinates are now known for all of the marker points 2 to 17.

6.3.2 Estimation of Bony Point Coordinates

The coordinates of the bony point defined by each marker were estimated by projecting a line along the marker stem, through both known points, in the direction of the body. From the marker stem geometry and the estimated skin thickness (from the cadaver study) the bony point may now be located on this projected line.

The equations relating the known coordinates of marker points to the marker geometry and skin thickness data are described and illustrated in Appendix 3.2. These equations were used in KINESB to calculate the coordinates of the bony points.

The mid malleolar origin was now calculated, defined in 3.4.3, as the point midway between the most medial point of the medial malleolus and the most lateral point of the lateral malleolus. The coordinates of the bony points were then related to this origin.

6.3.3 Subject Anthropometric Scale Factors and Anthropometry

The anthropometric scale factors were calculated as defined under 3.4.10. The summary cadaver data relating to the muscle origins and insertions, Tc. and Tcn. axes and origins were then scaled by the subject scale factors. The following equations illustrate this calculation,

$$\{K\}_s = \begin{bmatrix} S_x & 0 & 0 \\ 0 & S_y & 0 \\ 0 & 0 & S_z \end{bmatrix} . \{K\}_c \qquad \ldots 6.3$$

where

$\{K\}_c$ is the coordinates of a typical cadaver point

$\{K\}_s$ is the coordinates of the same point for the test subject

S_α are the scale factors (α = x, y, z directions)

The summary cadaver anthropometric data, being referred to the cadaver mid malleolar origin, now effectively become the subject anthropometric data, referred to the subject mid malleolar origin.

6.3.4 Relation of the Tc. and External Shank Axes Systems

The Tc. axis system was calculated for the subject in exactly the same way as described for the cadaver in 3.4.8 but in this instance the Tc. system is related to the laboratory ground axes system. This gave the rotation matrix, $[R]_{G.\rightarrow Tc.}$ & translation vector, $\{T\}_{OG.\rightarrow OTc.}$, relating the ground and Tc. systems. The External shank system was then set up as detailed in 6.2.2 and then the rotation matrix, $[R]_{Es.\rightarrow Tc.}$, and translation vector, $\{T\}_{OEs.\rightarrow OTc.}$, relating the Tc. and External shank systems were calculated.

6.3.5 Relation of the Tcn. and External Hindfoot Axes Systems

The subject Tcn. axis system was calculated as for the cadaver, 3.4.8, to give the rotation matrix, $[R]_{G.\rightarrow Tcn.}$ and translation vector, $\{T\}_{OG.\rightarrow OTcn.}$ relating the ground

and Tcn. systems. The External hindfoot system was then defined in accordance with 6.2.3 and the rotation matrix $[R]_{Eh.\rightarrow Tcn.}$ and translation vector $\{T\}_{OEh.\rightarrow OTcn.}$ were calculated.

6.3.6 Relation of the Tc. and Tcn. Axes Systems

The Tc. and Tcn. axes systems have been defined in relation to the External shank and External hindfoot systems, respectively. The Tc. and Tcn. systems were now directly related by the rotation matrix $[R]_{Tc.\rightarrow Tcn.}$ and translation vector $\{T\}_{OTc.\rightarrow O\,Tcn.}$

Having defined the relations in 6.3.4, 6.3.5 and above, an illustration will be given to demonstrate the manipulations required to relate a point $\{K\}$, known in three space coordinate form relative to the Tcn. axis system, to the Tc. axis system. Referring to figure 6.3, $\{K\}$ related to the External hindfoot system, is given by,

$$\{K\}_{Eh.} = ([R]_{Tcn.\rightarrow Eh.} \cdot \{K\}_{Tcn.} - \{T\}_{OTcn.\rightarrow OEh.}) \quad \ldots 6.4$$

(it should be noted here that,

$$[R]^{-1}_{Tcn.\rightarrow Eh.} = [R]^{T}_{Eh.\rightarrow Tcn.}$$

where

superscript -1 indicates matrix inversion

superscript T denotes transpose of the matrix)

relating $\{K\}$ to the ground system,

$$\{K\}_{G.} = ([R]_{Eh.\rightarrow G.} \cdot \{K\}_{Eh.} - \{T\}_{OEh.\rightarrow OG}) \quad \ldots 6.5$$

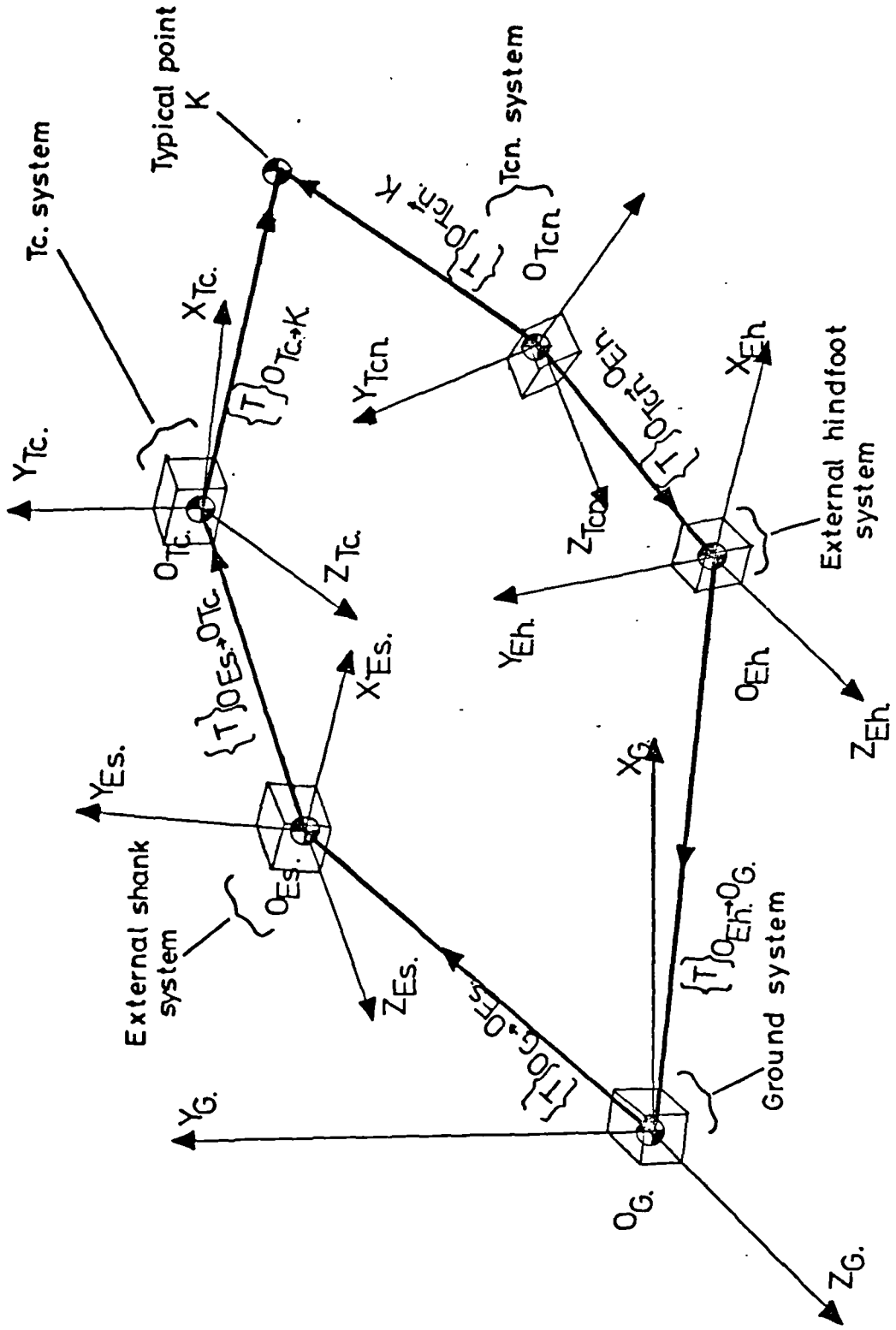

Figure 6.3 Relation of the Tc. and Tcn. Axes to the Ground System (Note that the Spatial Relationship between the Systems has been Exaggerated for Clarity)

relating $\{K\}$ to the External shank system,

$$\{K\}_{Es.} = ([R]_{G.\rightarrow Es.} \cdot \{K\}_{G.} - \{T\}_{OG.\rightarrow OEs.}) \quad \ldots 6.6$$

and finally relating $\{K\}$ to the Tc. system,

$$\{K\}_{Tc.} = ([R]_{Es.\rightarrow Tc.} \cdot \{K\}_{Es.} - \{T\}_{OEs.\rightarrow Otc.}) \quad \ldots 6.7$$

In practice Steps 6.4 to 6.7 can be performed in one step where Tc. and Tcn. systems are directly related by,

$$\{K\}_{Tc.} = ([R]_{Tcn.\rightarrow Tc.} \cdot \{K\}_{Tc.} - \{T\}_{OTcn.\rightarrow OTc.}) \quad \ldots 6.8$$

and this procedure can be simply reversed to refer a point known in the Tc. system to the Tcn. system.

The above relations allow any point known in relation to Tc. and Tcn. systems to be related via the external segment systems to the force platform system origin. This meant that moments and forces measured at the force platform could be related directly to the Tc. and Tcn. systems once the external segment system positions and orientations were known.

6.3.7 Subject Anthropometry in Relation to the Axes Systems

The muscle groups, Peroneal, Posterior tibial and Anterior tibial, were shown to have (see 3.1) a more or less constant line of action with respect to the hindfoot segment. The points defining each muscle in these groups were assumed therefore to be fixed in relation to the Tcn. axis system, and thus in relation to the External hindfoot system. The insertion of the Calf group was also assumed to be of constant position with respect to the Tcn. axis

system. The only muscle point that was defined as fixed with respect to the Tc. axis system, and therefore to the External shank system, was the origin of the Calf group. The precise location of the Calf group origin is difficult to define since it requires interpolation between both heads of gastrocnemius and soleus. An alternative definition was chosen. The line of action of the achilles tendon, as calculated for the standing subject, was extrapolated until it intersected with a plane, parallel to the ground system (X_G-Z_G) plane, that passed through the point midway between the medial and lateral tibial condyles. The point of intersection, illustrated in figure 6.4, was then regarded as fixed relative to the Tc. system. The line of action of the Calf group was later calculated in the force analysis programs, once the orientation of the Tc. system relative to the Tcn. system was known frame by frame.

The remaining muscles were expressed as 'potential force and moment' components relative to the Tcn. system. potential force refers to the direction cosines of a muscle line of action which may be converted to actual force components by calculating the product of muscle force magnitude and its direction cosine vector. Potential moment was defined in 4.2.2 when calculating the potential moment for ligaments, and is the vector cross-product of the radius vector of the distal point defining a muscle line of action and the direction cosine vector; the actual moment due to a muscle obtains from the product of muscle force magnitude and its potential moment. These 'potential' quantities are illustrated, by example, in their calculation for the peroneus brevis muscle. It is assumed that the distal and proximal points defining the peroneus brevis

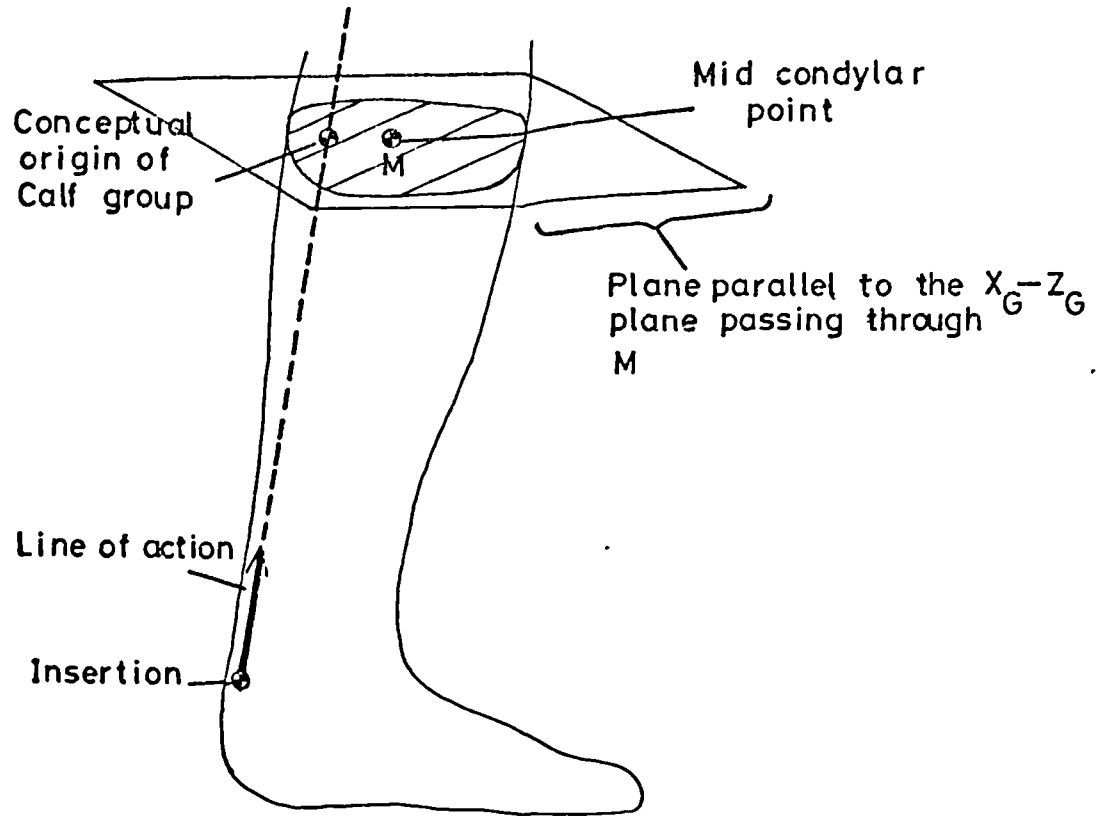

Figure 6.4 Definition of the Calf Group Origin

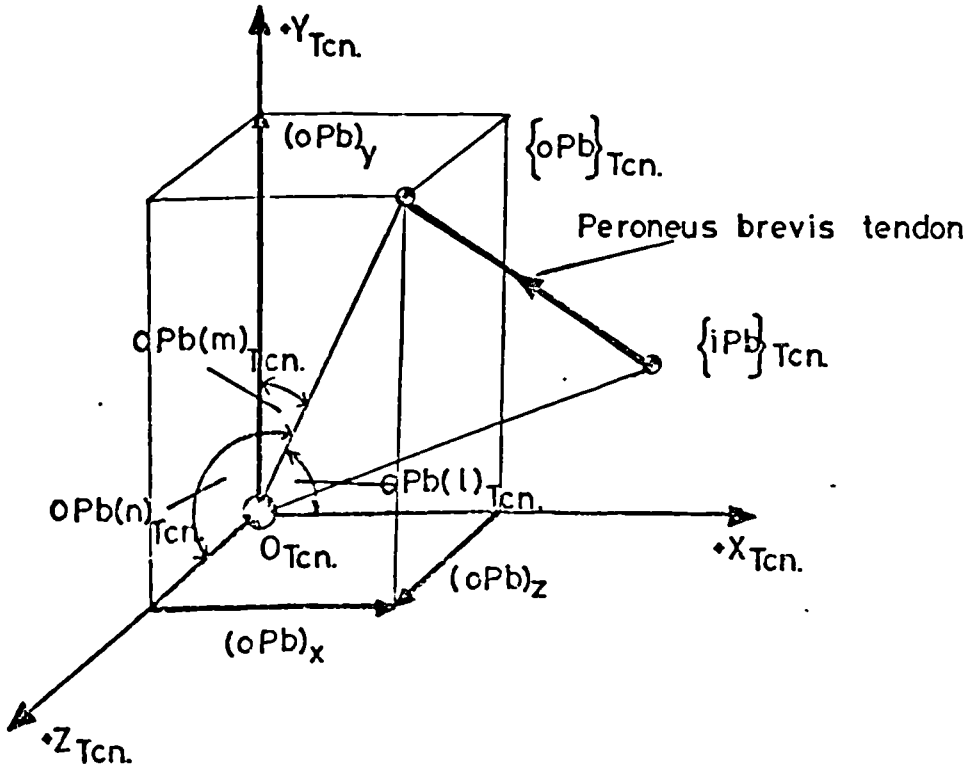

Figure 6.5 Example of Muscle Line of Action using Peroneus Brevis

line of action are known in coordinate form relative to the Tcn. system. Considering the distal point as the effective insertion - $\{iPb\}_{Tcn.}$, and the proximal point as the effective origin - $\{oPb\}_{Tcn.}$ (illustrated in figure 6.5), the direction cosines of the muscle are,

$$Pb(l)_{Tcn.} = \left(\frac{(oPb)x}{\left| \{iPb\}_{Tcn.} - \{oPb\}_{Tcn.} \right|} \right) \quad \ldots 6.9$$

$$Pb(m)_{Tcn.} = \left(\frac{(oPb)y}{\left| \{iPb\}_{Tcn.} - \{oPb\}_{Tcn.} \right|} \right) \quad \ldots 6.10$$

$$Pb(n)_{Tcn.} = \left(\frac{(oPb)z}{\left| \{iPb\}_{Tcn.} - \{oPb\}_{Tcn.} \right|} \right) \quad \ldots 6.11$$

where

$Pb\{l, m, n\}_{Tcn.}$ are the peroneus brevis muscle direction cosines in the Tcn. system

$(oPb)x, y, z$ are the coordinates of the peroneus brevis muscle origin

$|\ |$ denotes modulus

and the potential force vector $Pb\{l, m, n\}_{Tcn.}$ is related to actual force components thus,

$$\{FPb\}_{Tcn.} = \left| \{FPb\}_{Tcn.} \right| . Pb\{l, m, n\}_{Tcn.} \quad \ldots 6.12$$

where

$\{FPb\}_{Tcn.}$ is the peroneus brevis force vector in the Tcn. system

the potential moment is equal to

$$\{\{oPb\} \text{ cross } Pb\{l,m,n\}_{Tcn.}\} \quad \ldots 6.13$$

which becomes actual moment as

$$\{MPb_{Tcn.}\} = \left|\{FPb\}_{Tcn.}\right| . \{\{oPb\} \text{ cross } Pb\{l,m,n\}_{Tcn.}\} \quad \ldots 6.14$$

These calculations were performed for each member muscle of the Anterior tibial, Peroneal and Posterior tibial groups.

The subject muscle anthropometry was now known in relation to the Tc. and Tcn. systems.

This concludes the description of the Stage one analysis. The relation of the subject Tc. to External shank and Tcn. to External hindfoot systems was used in the Stage two analysis. The subject muscle anthropometry was used in the Stage three analysis.

6.4 The Analysis - Stage Two

At this stage the dynamic kinematic data collected under phase three in the experimental sequence, 5.3.4, was used. This stages computation was performed by the second program KINEDB, see 6.6, figure 6.1 and 6.9 and flow chart in figure 6.11

As previously noted, 5.4, only six bony point markers were used in the phase three tests. Figure 6.2 illustrates why this is so; only six marker points are required to define the External shank and External hindfoot systems, three markers for each system. As Stage one analysis showed, this is all that is required for the relation of the Tc. and Tcn. systems to the ground system.

6.4.1 Dynamic Kinematic Data - Preliminary Conditioning

The methods described in 6.3.1 were used to obtain the true coordinates of marker points 2, 5, 7, 9, 11 and 17 for each frame of the subject stance phase period.

It was decided that the marker trajectories should be filtered to reduce their random noise content, added to the original trajectory data by the kinematic data and data reduction systems. The specification of a suitable filter was discussed by Andrews (1975) and Tooth (1976). Both suggest a fourth order Butterworth digital filter; the reader is referred to these sources as well as Lanczos (1957) for precise details of the Butterworth filter characteristic gain and phase frequency response. The gain and phase response for a fourth order Butterworth filter is included in Appendix 3.9. For the present analysis it is sufficient to understand that the filter introduces no phase shift, phase shifts associated with the filter being compensated for by reversing the filtered data sequence and passing it again through the filter. The output sequence is then a filtered, in phase, version of the original data sequence. The filter subroutine written by Andrews requires specification of the 3dB cut off frequency in Hz., the sample interval in seconds, and the length of the input sequence of data points to be sampled. The sample interval is 0.02 seconds and the length of input corresponds to the number of cine frames occurring during the stance phase. The necessary cut off frequency is a matter still in contention.

Andrews' report indicated that the power spectrum of ankle displacement data was virtually all contained within the 0 to 10 Hz. range. Tooth cited Winter et al

(1974) as stating that 99.7% of marker trajectory signal power lay below the eighth harmonic. Tooth himself inspected power spectra associated with positional, velocity and acceleration data for the limbs of normal subjects and concluded 'intuitively' that signal fidelity should be maintained over a bandwidth of 10 Hz. Zarrugh and Radcliffe (1979) considered the frequency content of human gait kinematics and concluded that 7-12 harmonics represented a good compromise between information retained and noise rejected for most gait variables. They drew attention however to one exception, ankle flexion-extension angle where they considered twenty harmonics necessary for adequate signal reconstruction - some slight detail being lost where only seven harmonics were included. The author superimposed their seventh and twentieth harmonic curves for ankle angle and is of the opinion that - for stance phase - the agreement is sufficiently good to accept the seventh harmonic data, see figure 6.6.

In the present case, since only displacements were required, the cut off frequency was set at 10 Hz. The cine film sampling frequency of 50 Hz. is quite adequate for recovery of displacement harmonics up to 10 Hz.

6.4.2 Dynamic Relation of the Tc. and Tcn. Systems to the Ground System

Once the marker trajectories were filtered, they were used to set up the External shank and External hindfoot systems, frame by frame, as defined in 6.2.2 and 6.2.3. The relationship between the Tc. and the External shank systems, calculated in Stage one analysis, was used to relate the Tc. system to the ground system frame by frame; for the nth frame the rotation between

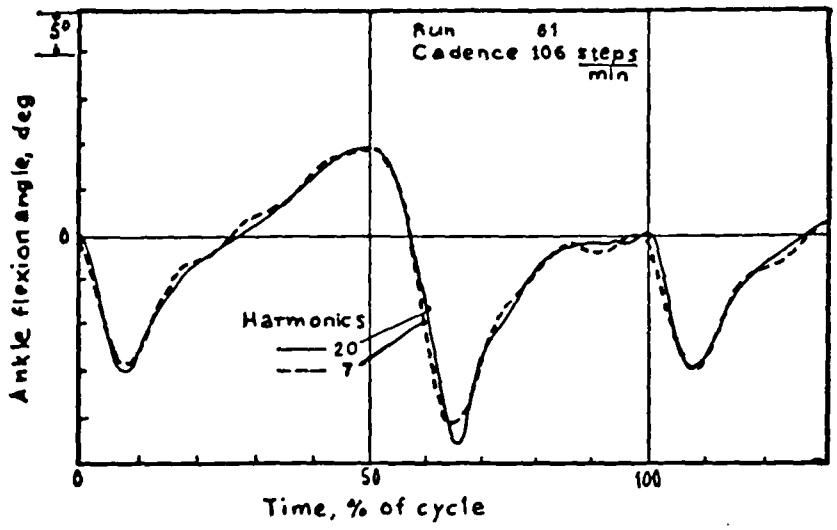

Effects of harmonic content on the reconstitution of ankle flexion as a time function.

Figure 6.6 Superimposition of Harmonic Curves for Ankle Flexion (Adapted from Zarrugh and Radcliffe, 1979)

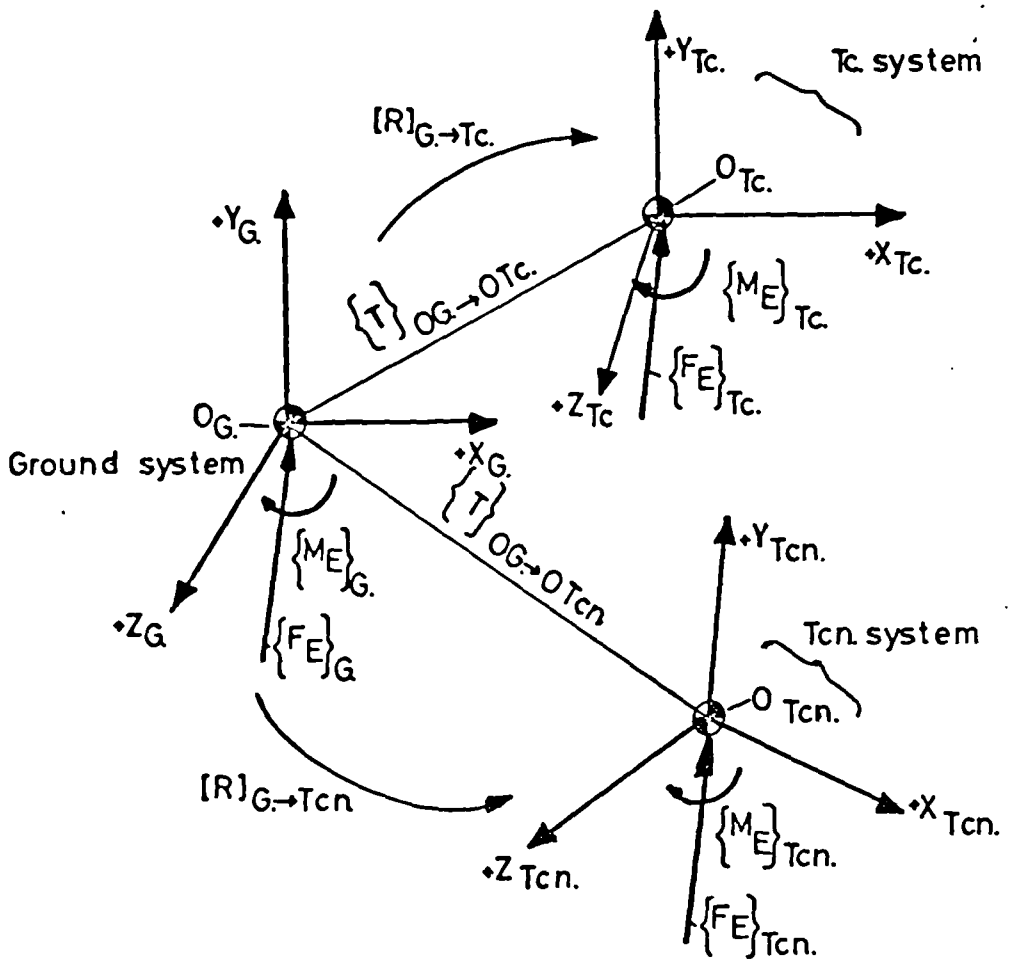

Figure 6.7 Illustration of the External Forces Referred to the Tc. and Tcn. Systems

ground and Tc. systems is,

$$\left[[R]_{G.\rightarrow Tc.}\right]_n = \left[[R]_{G.\rightarrow Es.}\right]_n \cdot \left[[R]_{Es.\rightarrow Tc.}\right]_s \qquad \ldots 6.15$$

and the translation,

$$\left\{\{T\}_{G.\rightarrow Tc.}\right\}_n = \left\{\{T\}_{OG.\rightarrow OEs.}\right\}_n + \left[[R]^T_{G.\rightarrow Es.}\right]_n \cdot \left\{\{T\}_{OEs\rightarrow OTc.}\right\}_s \qquad \ldots 6.16$$

where

subscript n = nth frame data

s = static data

by a similar calculation the frame by frame relation of the Tcn. and ground systems is obtained thus; the nth frame rotation between ground and Tcn. systems is,

$$\left[[R]_{G\rightarrow Tcn.}\right]_n = \left[[R]_{G.\rightarrow Eh.}\right]_n \cdot \left[[R]_{Eh.\rightarrow Tcn.}\right]_s \qquad \ldots 6.17$$

and the corresponding translation is

$$\left\{\{T\}\right\}_{G.\rightarrow Tcn.\ n} = \left\{\{T\}_{OG\rightarrow OEh.}\right\}_n + \left[[R]^T_{G.\rightarrow Eh.}\right]_n \cdot \left\{\{T\}_{OEh.\rightarrow OTcn.}\right\}_s \qquad \ldots 6.18$$

Thus for each frame throughout stance phase the location and orientation of the Tc. and Tcn. systems was known in relation to the laboratory ground system. This data was used in the final computer programs when relating the external force system to the internal axes.

6.4.3 Graphic Visualisation of the Segments

When calculating centre of pressure path over the sole of the foot, see 6.5.3, it is desirable to have an image of the sole to superimpose over the path trajectory. This makes the interpretation of deviations much easier, but in the present case there was no suitable device available to achieve this end. But the location of three fixed points on the foot is known, and defines a triangular image, see figure 6.2(b), equivalent to the frame by frame position of the foot. This was used as a substitute for a complete visual image of the foot and was used as a reference frame against which centre of pressure paths were compared. The six dynamic test marker points, defining the shank and hindfoot segments, were output for three frames, 1, n/3 and n where n is the number of frames corresponding to stance phase. Frame n/3 was chosen because at one third of the way through stance phase the foot is normally flat on the ground.

This concludes the Stage two analysis.

6.5 The Analysis - Stage Three

In the third stage of the analysis the equations are presented that lead up to the point where the Mark I and Mark II models presented in chapter four may be solved.

6.5.1 Force Data Conditioning

The force data as they are output on punched paper from the PDP12 computer required scaling by calibration constants, experimentally verified in 5.2.2, to obtain forces (in Newtons) and moments (in Newton-moments) with respect to the ground system. The data were left

unfiltered.

6.5.2 Calculation of the External Forces and Moments in the Tc. and Tcn. Systems

The translation and rotation data relating the Tc. and Tcn. systems to the ground system, calculated in the Stage two analysis, were used to calculate the external force and moment components in the Tc. and Tcn. systems. With reference to figure 6.7 the external forces referred to the Tc. system for frame n are given by,

$$\left\{\left\{F_E\right\}_{Tc.}\right\}_n = \left[[R]_{G\rightarrow Tc.}\right]_n \cdot \left\{\left\{F_E\right\}_G\right\}_n \qquad \ldots 6.19$$

where

subscript E refers to External force quantities

and the moments,

$$\left\{\left\{M_E\right\}_{Tc.}\right\}_n = \left[[R]_{G\rightarrow Tc.}\right]_n \cdot \left\{\left\{M_E\right\}_G - \{T\}_{OG\rightarrow OTc.} \text{ cross } \left\{F_E\right\}_G\right\}_n \qquad \ldots 6.20$$

similarly the external forces and moments referred to the Tcn. system for frame n are given by

$$\left\{\left\{F_E\right\}_{Tcn.}\right\}_n = \left[[R]_{G\rightarrow Tcn.}\right]_n \cdot \left\{\left\{F_E\right\}_G\right\}_n \qquad \ldots 6.21$$

$$\left\{\left\{M_E\right\}_{Tcn.}\right\}_n = \left[[R]_{G\rightarrow Tcn.}\right]_n \cdot \left\{\left\{M_E\right\}_G - \{T\}_{OG\rightarrow OTcn.} \text{ cross } \left\{F_E\right\}_G\right\}_n \qquad \ldots 6.22$$

Equations 6.19 and 6.20 provide the external force and moment components of equations 4.10 to 4.15, and equations 4.22 to 4.27.

6.5.3 Centre of Pressure

The centre of pressure is the point at which the external forces may be considered to act on the foot segment. The centre of pressure for frame n was defined by two coordinates, $P(x)_n$ and $P(z)_n$, which were calculated from the external force and moment frame n components (relative to the ground system origin).

The radius vector of any point P on the surface of the force platform is, $P\{x, y, z\}_G$ and the external force acting at this point is $\{F_E\}(x, y, z)_G$, for frame n, the moments due to this force about the force platform origin are,

$$\left\{\{M_E\}(x,y,z)\right\}_n = \left\{P\{x,y,z\} \text{ cross } \{F_E\}(x,y,z)\right\}_n \quad \ldots 6.23$$

where $\{M_E\}$ denotes moments due to $\{F_E\}$

expanding and evaluating 6.23 gives

$$M_E(x)_n = (P(y).F_E(z)-P(z).F_E(y))_n \quad \ldots 6.24$$

$$M_E(y)_n = (P(z).F_E(x)-P(x).F_E(z))_n \quad \ldots 6.25$$

$$M_E(z)_n = (P(x).F_E(y)-P(y).F_E(x))_n \quad \ldots 6.26$$

from 6.26,

$$P(x)_n = \left(\frac{M_E(z)+P(y).F_E(x)}{F_E(y)}\right)_n \quad \ldots 6.27$$

from 6.24,

$$P(z)_n = \left(\frac{P(y).F_E(z) - M_E(x)}{F_E(y)} \right)_n \quad \ldots 6.28$$

$P(y)$ was known to be 0.04m., thus the coordinates were obtained.

The calculation for the side slope ramp is a little more complicated because the $P(y)$ coordinate is no longer constant but varies with Z_G. Referring to figure 6.8,

$$P(y)_n = \tan(\theta).P(z)_n + h \quad \ldots 6.29$$

where

θ is the ramp slope, either +10° or -10°

h is the Y_G height of the mid point of the insert

In the side slope ramp cases, the value of $P(y)_n$ is calculated for the appropriate slope (+10° or -10°) and then substituted into equations 6.27 and 6.28 to give $P(x)_n$, $P(z)_n$.

The centre of pressure calculation becomes unreliable at the very beginning and end of stance phase, because $F_E(y)$ is close to zero and of the order of system resolution. The first and last few frames were frequently rejected.

6.5.4 Calf Group Calculations

The Calf group origin was defined (6.3.7) relative to the Tc. system whilst its insertion was defined relative to the Tcn. system. In the Stage two analysis, the direct relationship between the Tc. and Tcn. systems

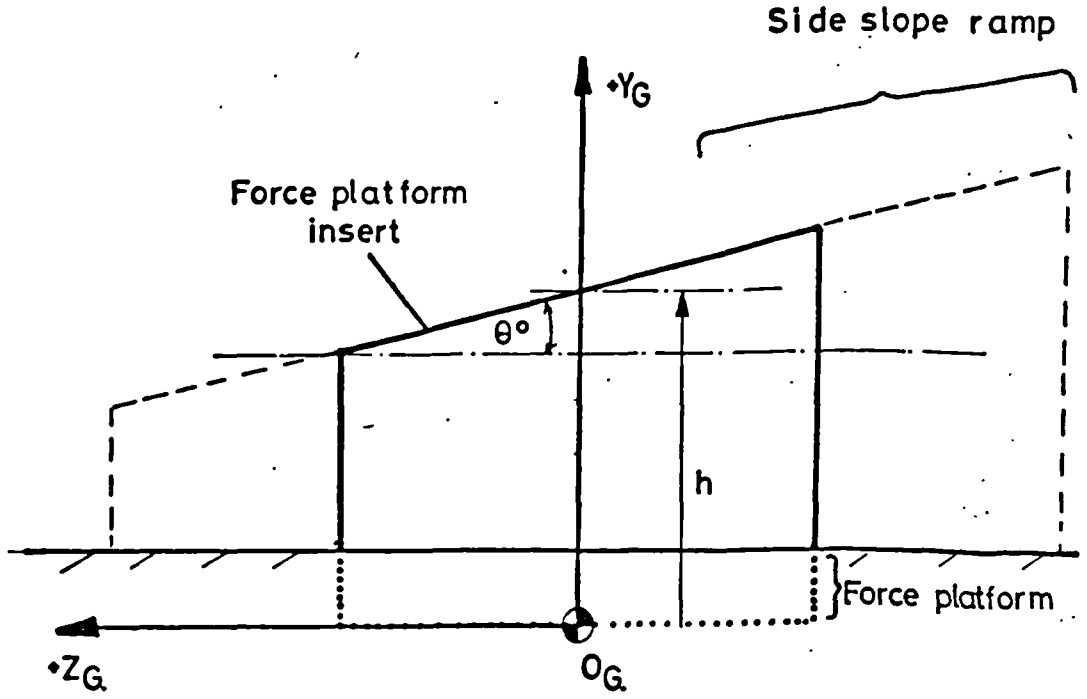

Figure 6.8 The Relation of the Side Slope Surface and the Ground System for Calculation of the Centre of Pressure

was established. Defining the Calf insertion in the Tcn. system as $\{iC\}_{Tcn.}$, the same point in the Tc. system is, for frame n,

$$\left\{\{iC\}_{Tc.}\right\}_n = \left\{[R]_{Tcn.\rightarrow Tc.} \cdot \{iC\}_{Tcn.} - \{T\}_{OTcn.\rightarrow OTc.}\right\}_n \quad \ldots 6.30$$

Given the origin and insertion in the Tc. system the 'potential moment and force' vectors in the Tc. system were calculated for the Calf group using the method described in 6.3.7.

6.5.5 Anterior Tibial, Posterior Tibial and Peroneal Group Calculations

The calculation to combine the components of a muscle group will be explained using the Peroneal group as an example. The total force in the Tcn. system due to the Peroneal group is given by,

$$\{F_P\}_{Tcn.} = \{F_{Pb}\}_{Tcn.} + \{F_{Pl}\}_{Tcn.} \quad \ldots 6.31$$

where

$\{F_P\}$ = total Peroneal group force vector
$\{F_{Pl}\}$ = peroneus longus force vector
$\{F_{Pb}\}$ = peroneus brevis force vector

The components of 6.31 expressed in direction cosines are, (see equation 6.12)

$$\left|\{F_P\}_{Tcn.}\right| . P\{l,m,n\}_{Tcn.} = \left|\{F_{Pb}\}_{Tcn.}\right| . Pb\{l,m,n\}_{Tcn.} + \left|\{F_{Pl}\}_{Tcn.}\right| . Pl\{l,m,n\}_{Tcn.} \quad \ldots 6.32$$

The muscle participation factor, introduced in 4.2.1, relates the force developed by the component muscle to the force developed by the group in the following expression, for peroneus brevis,

$$P_{Pb} = \frac{\left|\{F_{Pb}\}_{Tcn.}\right|}{\left|\{F_{P}\}_{Tcn.}\right|} \qquad \ldots 6.33$$

where

P_{Pb} is the peroneus brevis participation factor

and for peroneus longus

$$P_{Pl} = \frac{\left|\{F_{Pl}\}_{Tcn.}\right|}{\left|\{F_{P}\}_{Tcn.}\right|} \qquad \ldots 6.34$$

thus dividing equation 6.32 by $\left|\{F_P\}_{Tcn.}\right|$ and substituting the participation factors in equations 6.33 and 6.34 gives the potential force for the Peroneal group,

$$P\{l,m,n\}_{Tcn.} = P_{Pb}.Pb\{l,m,n\}_{Tcn.} + P_{Pl}.Pl\{l,m,n\}_{Tcn.} \qquad \ldots 6.35$$

The participation factors are calculated as shown in table 4.1 and the potential force vector for each muscle group component is calculated as shown in 6.3.7. The Peroneal group is now represented by a single vector in the Tcn. system and the remaining groups are calculated in the same manner.

The potential moment for the Peroneal group is derived in precisely the same way as the potential force and gives the result,

$$\{M_P\}_{Tcn.} = P_{Pb} \cdot \{M_{Pb}\}_{Tcn.} + P_{PI} \cdot \{M_{PI}\}_{Tcn.} \quad \ldots 6.36$$

where

$\{M_P\}$ is the Peroneal group total moment vector

The components of equation 6.36 are simply derived from equations like 6.14 and by following the same logic as outlined above to derive the potential force vector for the Peroneal group.

These equations were used to reduce each group of muscles to a single equivalent muscle whose direction cosines and potential moments are of the form of equations 6.35 and 6.36 respectively.

Each of the three groups, Peroneal, Posterior tibial and Anterior tibial were reduced to single equivalent muscle form, relative to the Tcn. system. For each frame, from the known orientation of the Tcn. system, relative to the Tc. system, these muscle groups were related to the Tc. system.

6.5.6 Conclusion of the Calculations

All the components of the equations forming the Mark I and Mark II model solutions, equations 4.10 to 4.15 and 4.22 to 4.27, are now known. The calculations for solution of the Mark I and II models follow the methods outlined in sections 4.2.7 and 4.2.8.

6.6 Computer Programs

Computer programs were written in FORTRAN for the calculations required to estimate the muscular and joint forces. The programs were divided into three since, as smaller packages, they require less storage space and

running time and a quick turn round was possible. This also gave the opportunity to check on the results at each intermediate stage. In biomechanical analysis where cine film and force platform data are obtained for a large number of tests an enormous amount of numbers are generated. This is an ideal task for the computer but requires careful management of data acquisition methods and filestore space. The three programs are illustrated in block diagram form in figure 6.9, together with their input and output files.

Each program refers to a particular stage in the analysis. Stage one analysis (see 6.3) was performed by KINESB, Stage two (see 6.4) by KINEDB and Stage three (see 6.5) by FORCED1B and FORCED2B. These programs are illustrated by flow diagrams in figures 6.10, 6.11 and 6.12. FORCED1B corresponded to the Mark I model solution and FORCED2B to the Mark II model solution. Program listings and details of the input data file formats are included in Appendices 3.4 to 3.8. The B after each program refers to the compiled form held in filestore in binary code.

For diagnostic and debugging purposes DUMP files, see figure 6.9, were used to hold intermediate variable values. These became redundant once each program had run successfully and are only included in the diagrams for completeness. To ensure that each program was arithmetically correct a complete set of experimental calculations, using actual test data, was used to check all intermediate and overall results.

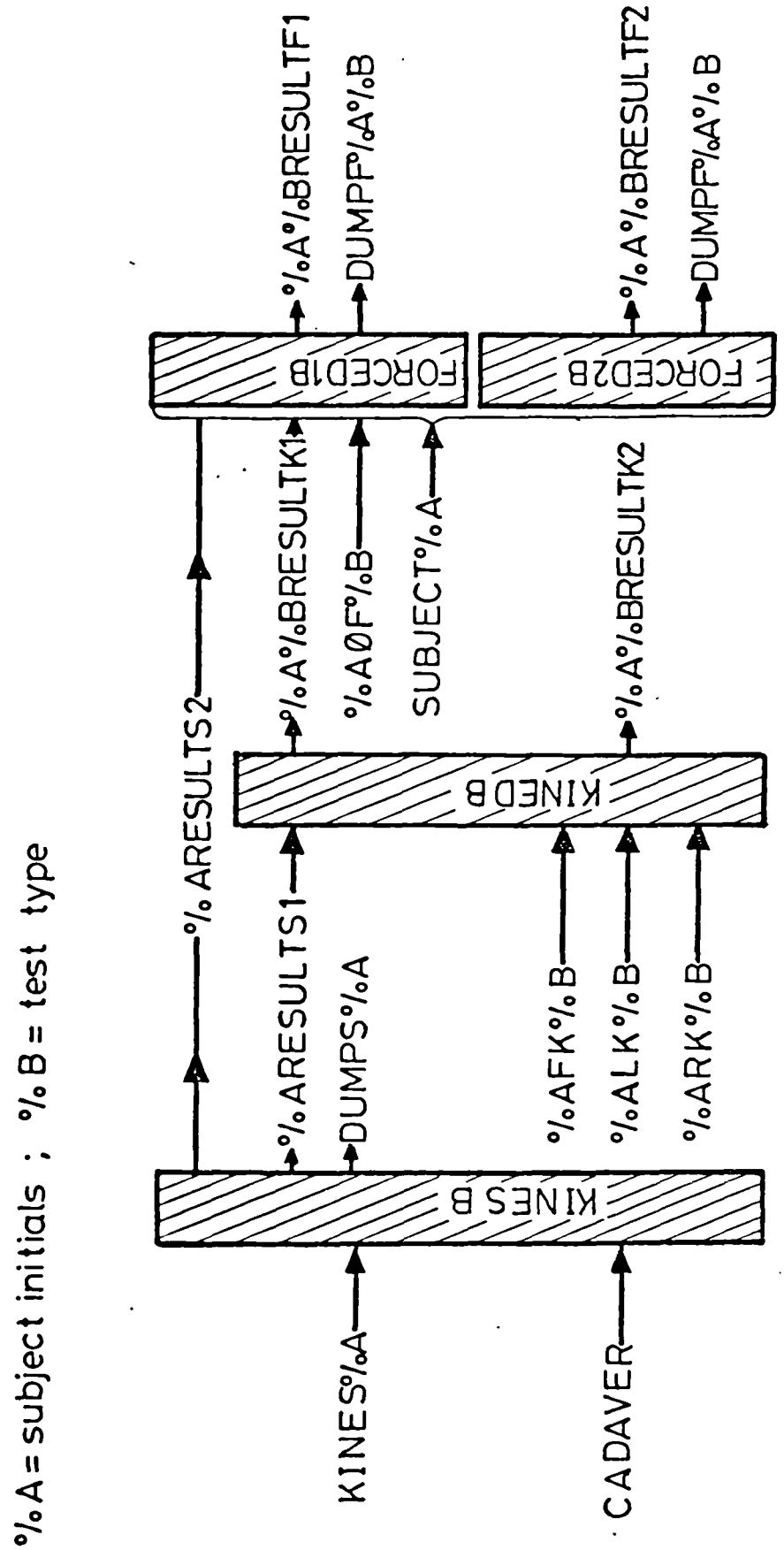

Figure 6.9 Flow Diagram of the Computer Programs and their Associated Data Files

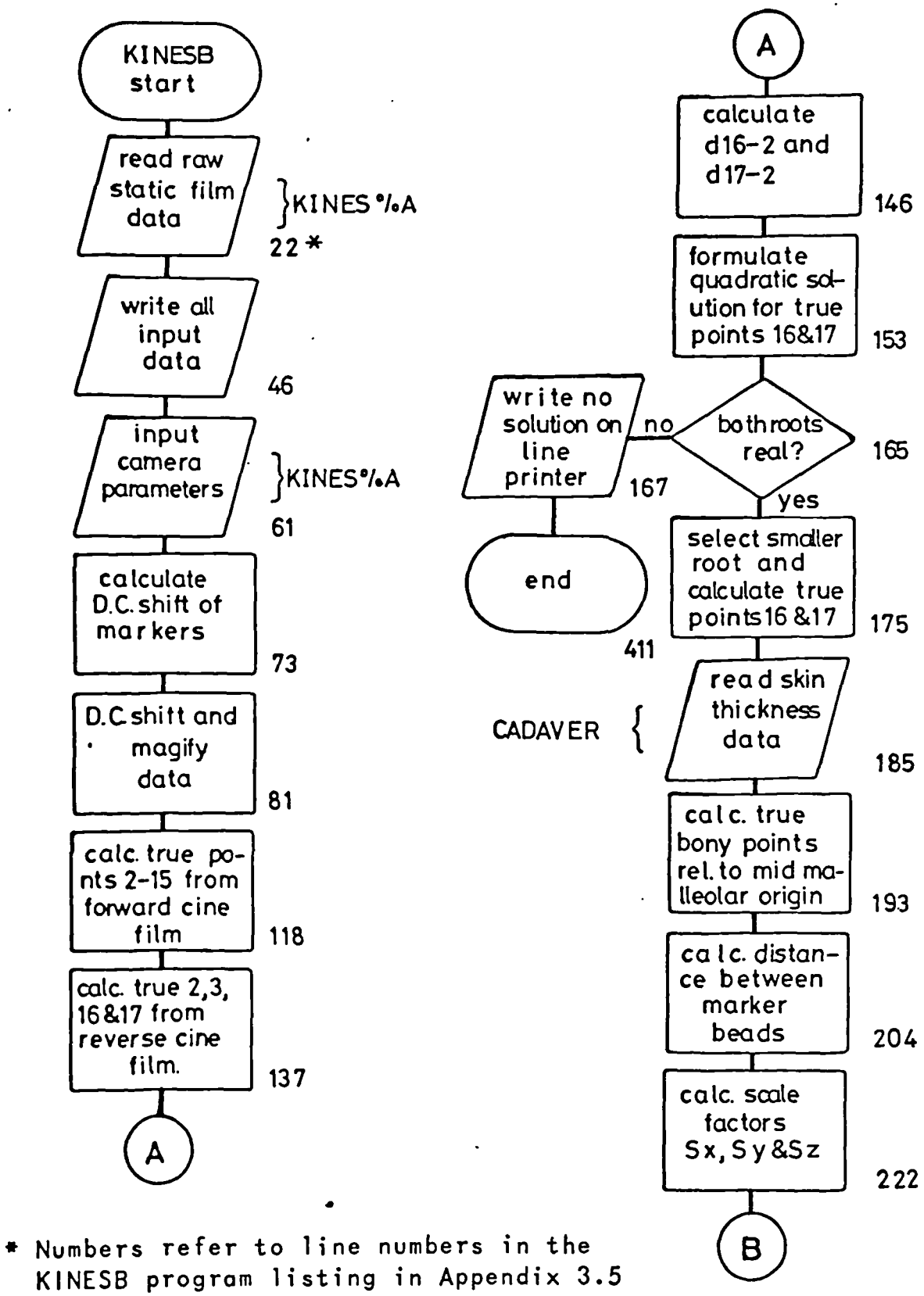

* Numbers refer to line numbers in the KINESB program listing in Appendix 3.5

Figure 6.10 KINESB Program Flow Chart

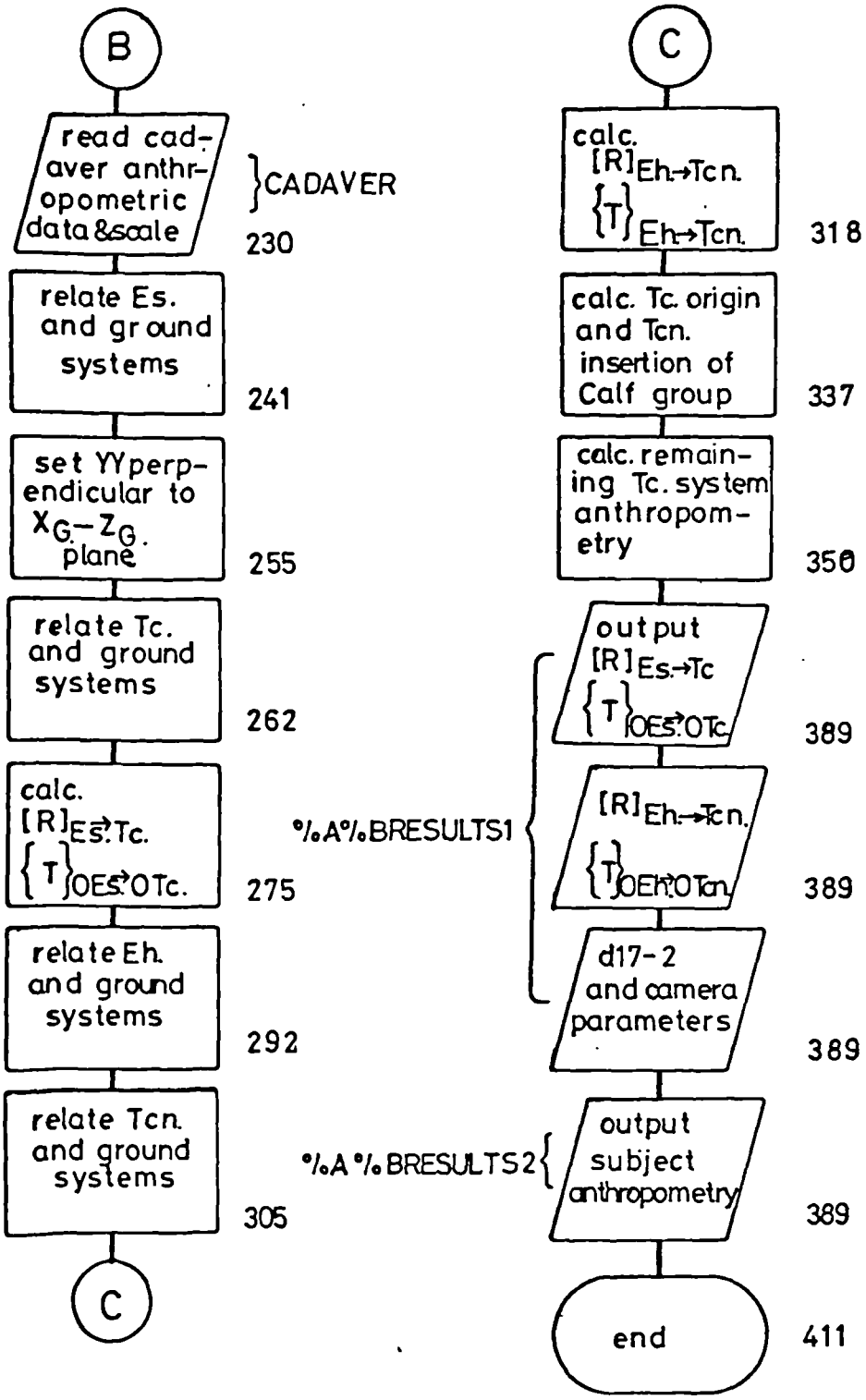

Figure 6.10 continued KINESB Program Flow Chart

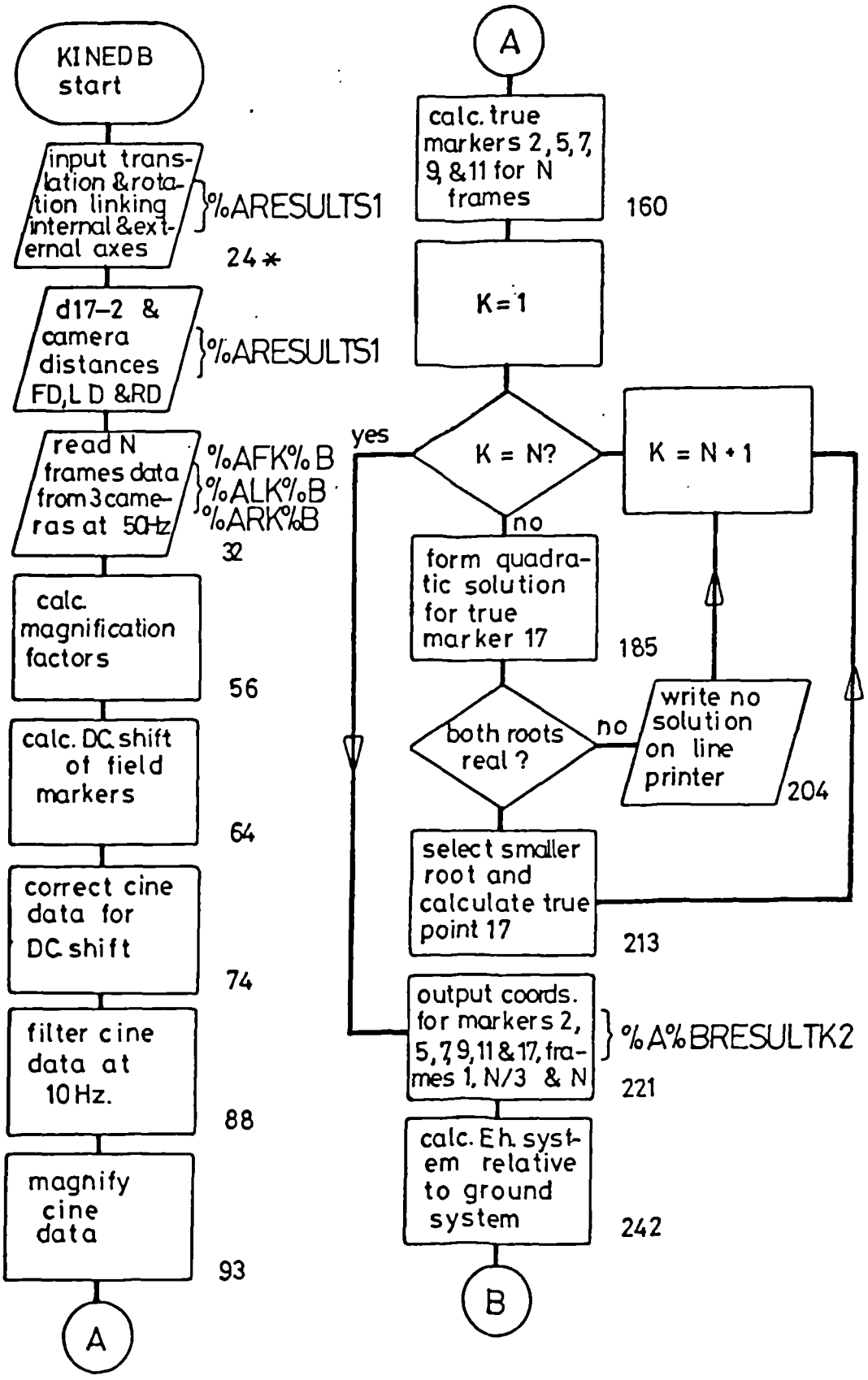

* Numbers refer to line numbers in the KINEDB program listing in Appendix 3.6

Figure 6.11 KINEDB Program Flow Chart

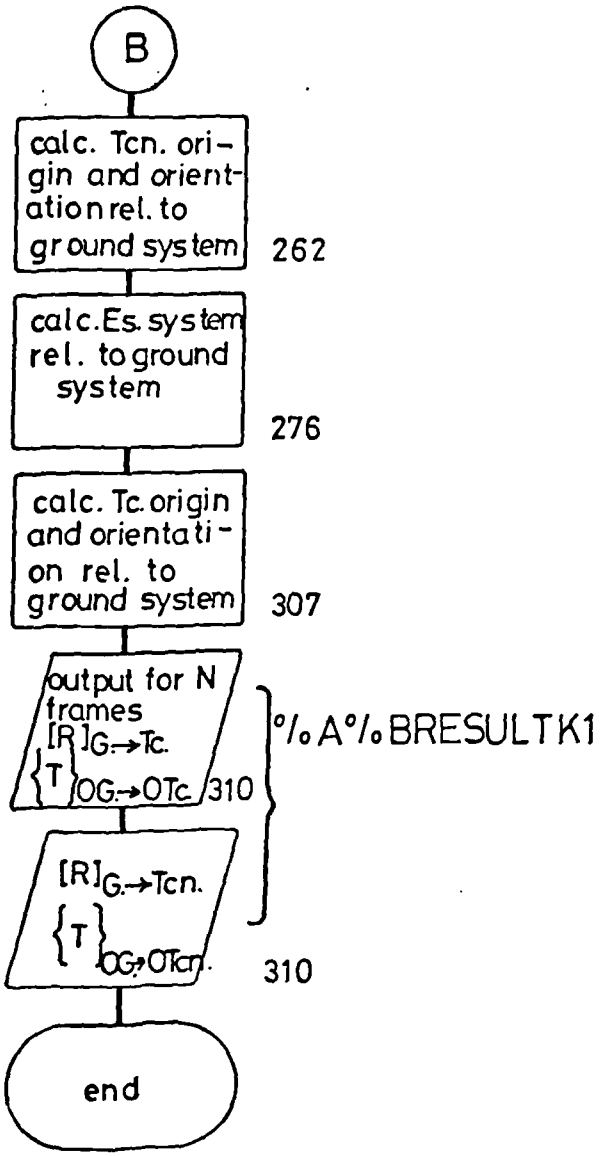

Figure 6.11 continued KINEDB Program Flow Chart

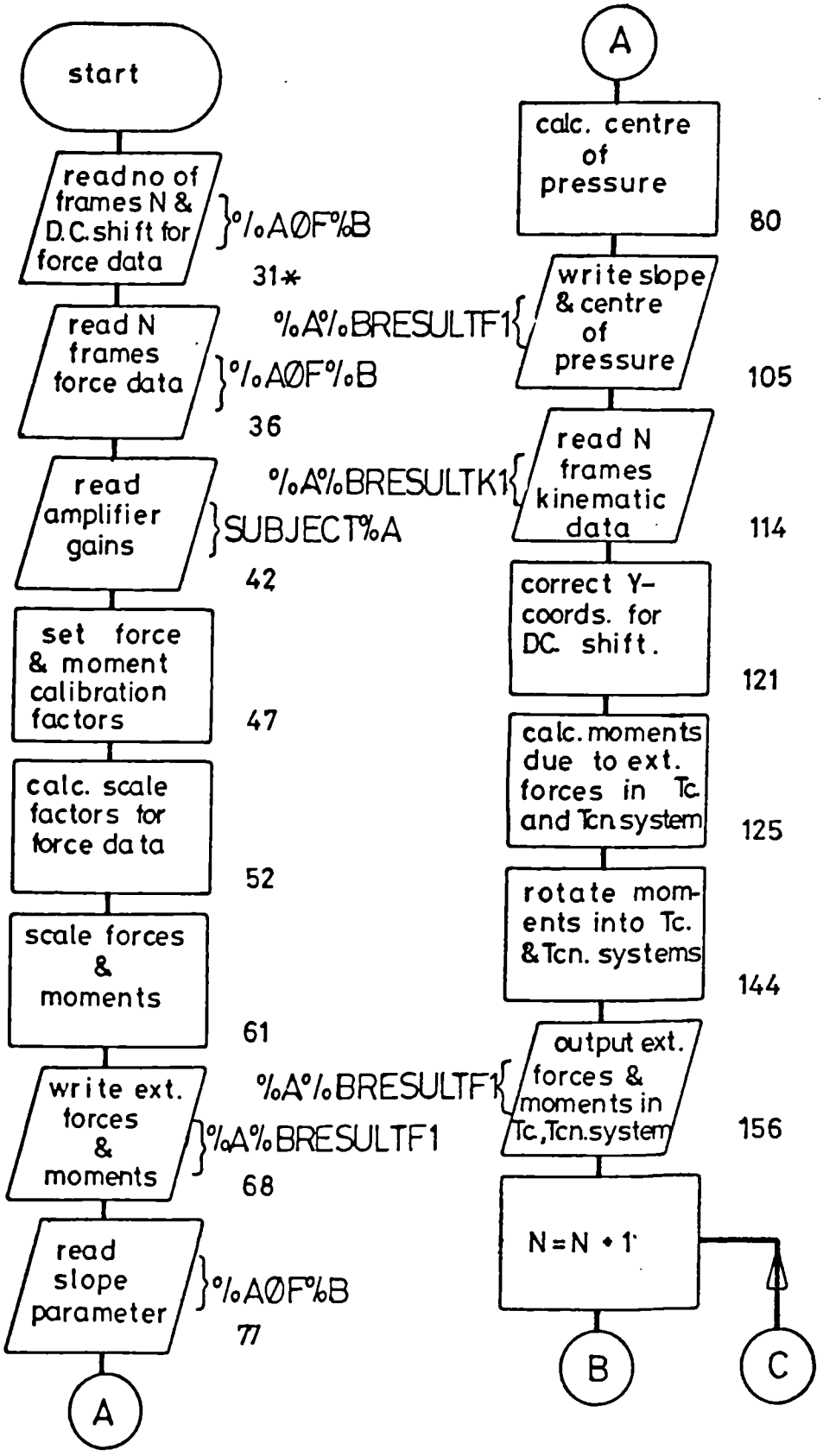

* Numbers refer to line numbers in the FORCED1B program listing in Appendix 3.7

Figure 6.12 FORCED1B Program Flow Chart

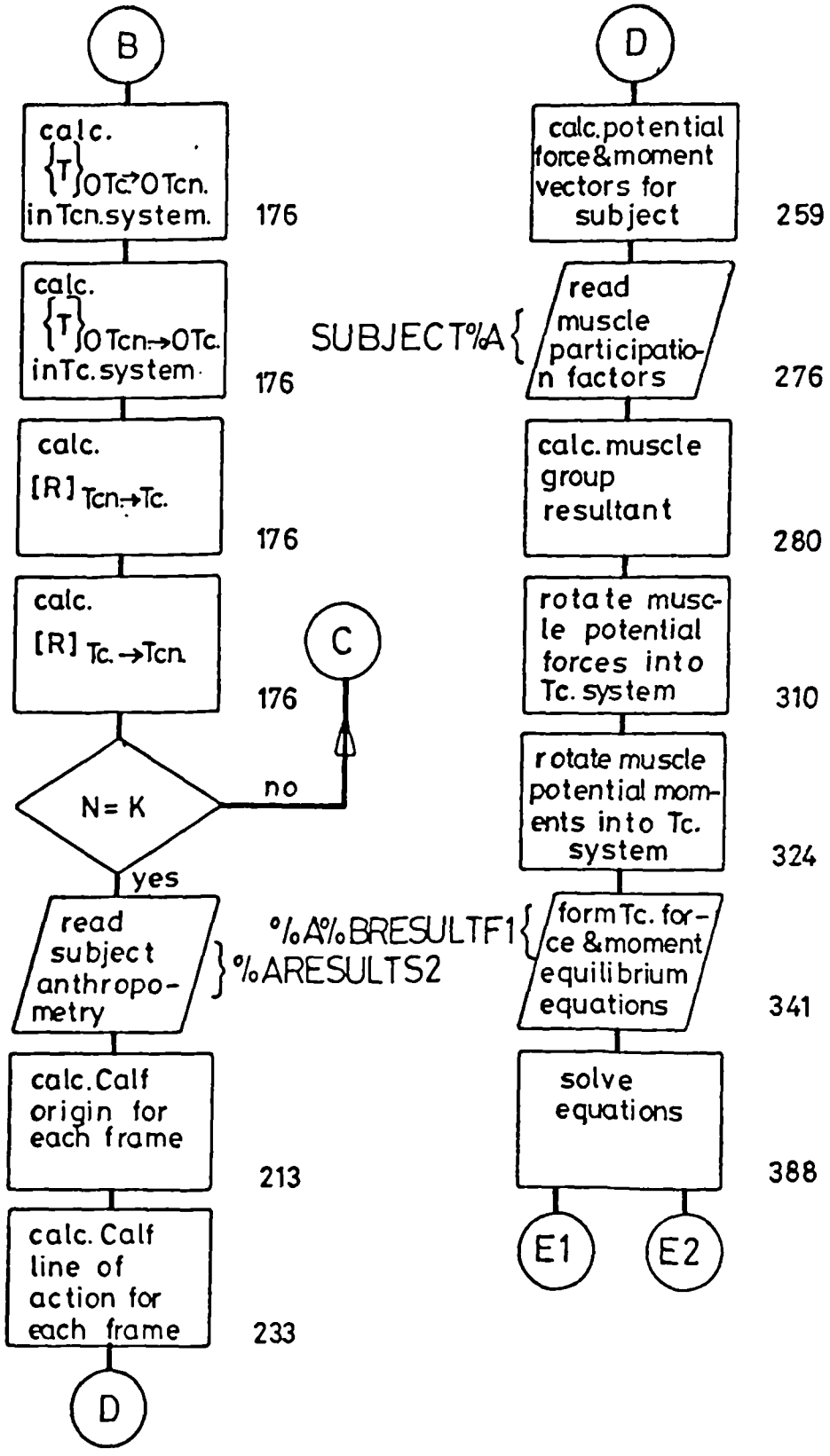

Figure 6.12 continued FORCED1B Program Flow Chart

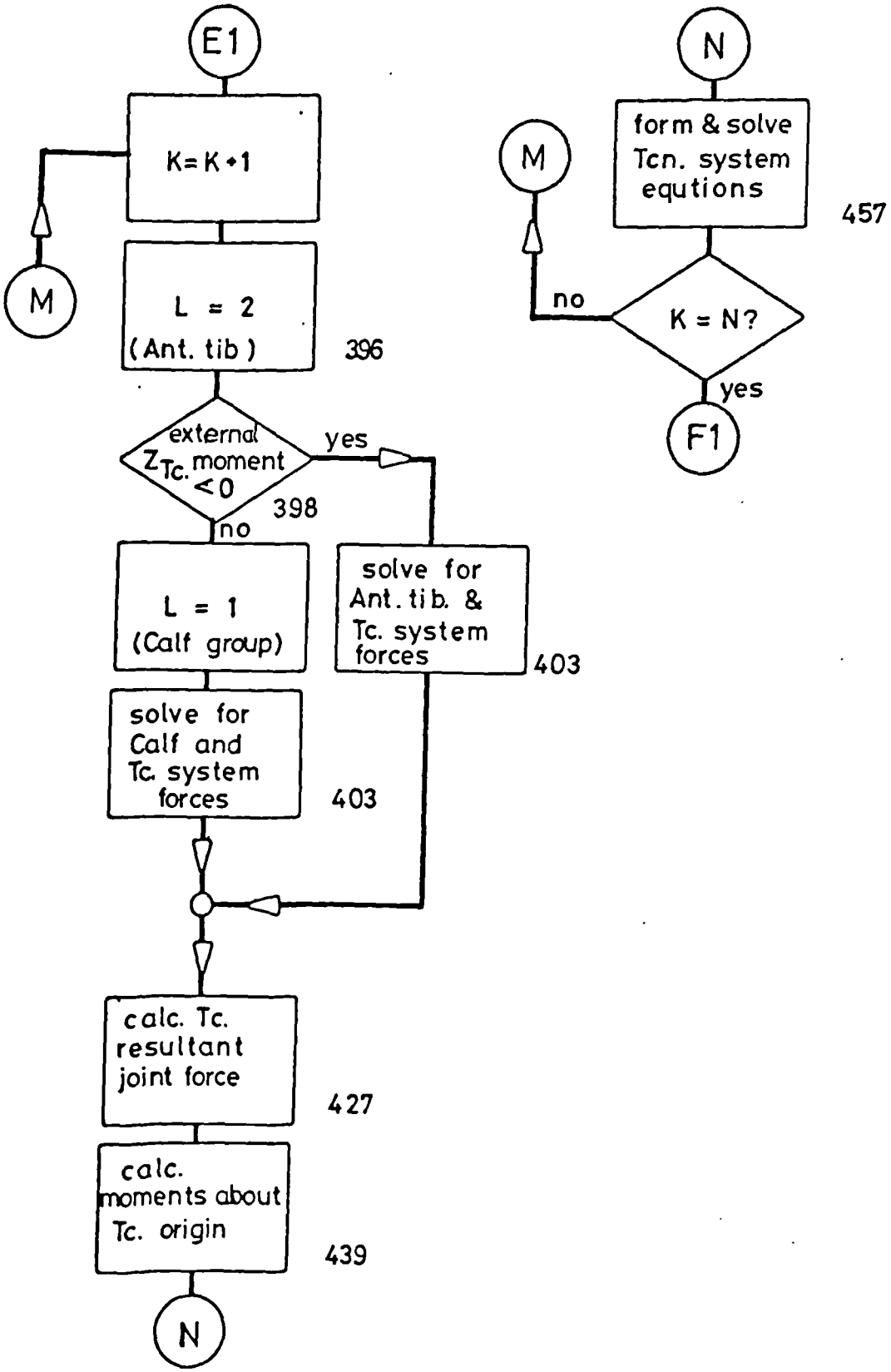

Figure 6.12 continued Mark I Model Solution Segment in FORCED1B Program

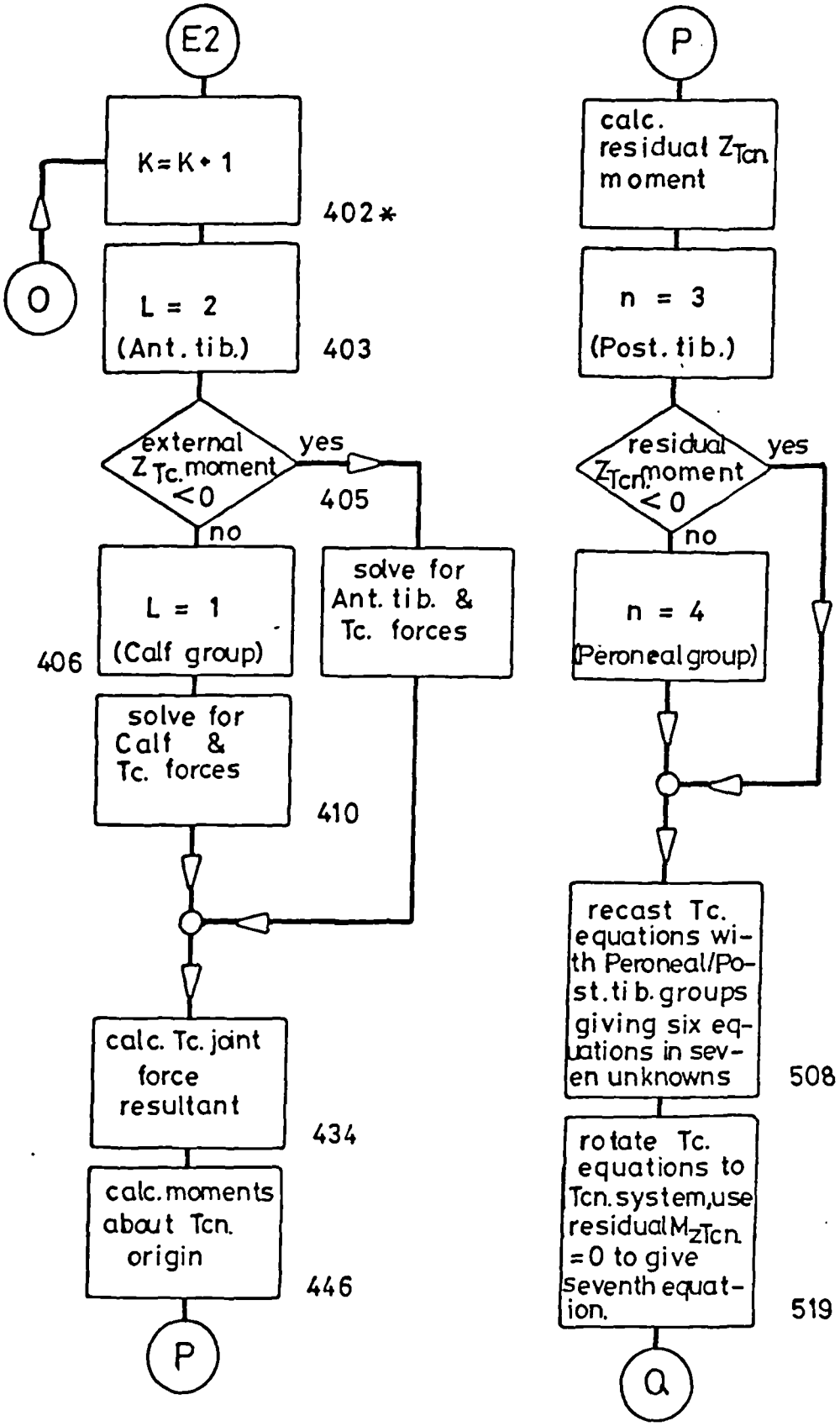

* Numbers refer to lines in FORCED2B program listing in Appendix 3.8

Figure 6.12 continued Mark II Model Solution Segment in FORCED2B Program

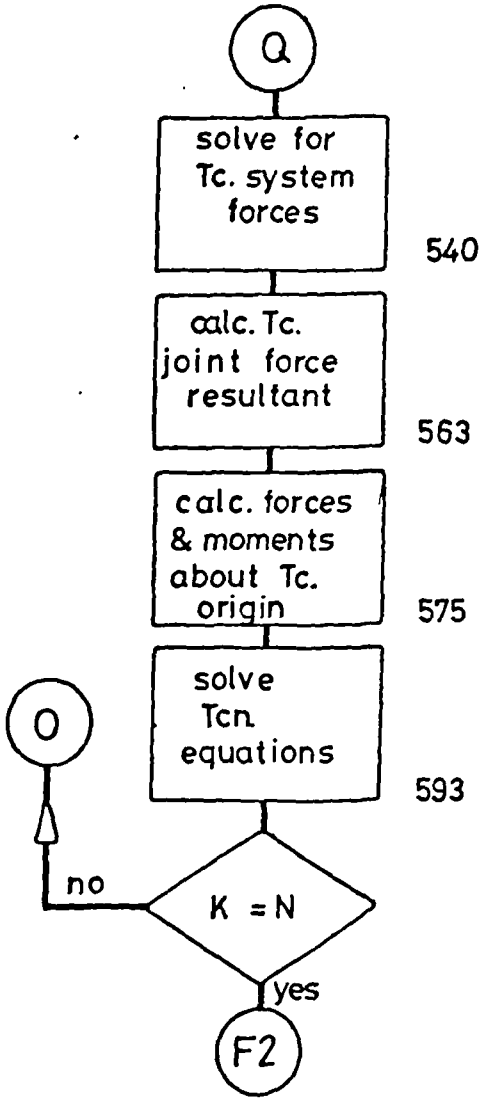

Figure 6.12 continued Mark II Model Solution Segment in FORCED2B Program

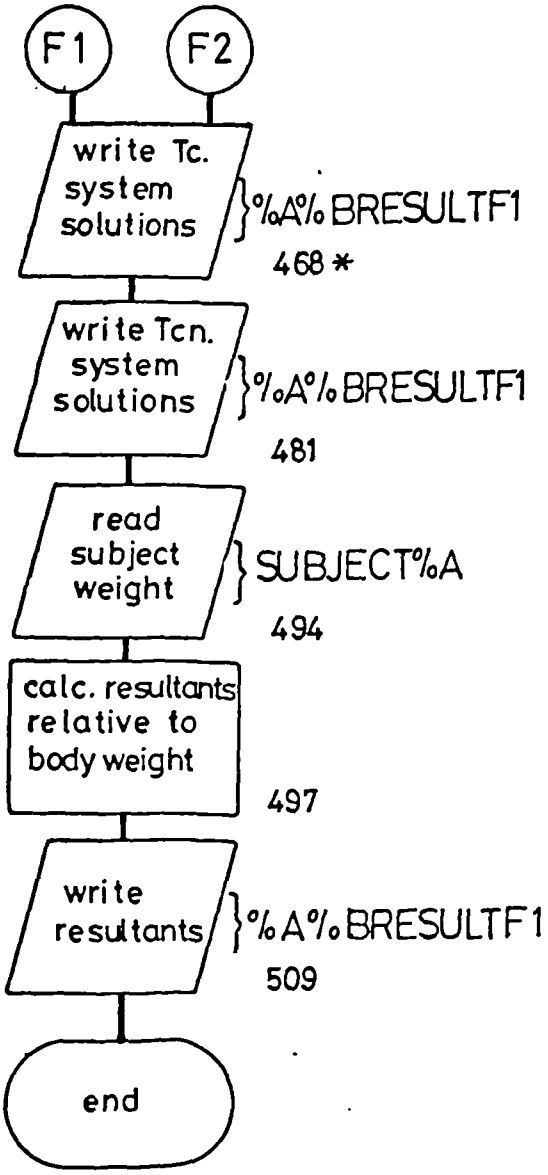

* Numbers refer to line numbers in the FORCED1B Program listing in Appendix 3.7

Figure 6.12 continued FORCED1B Program Flow Chart

CHAPTER 7

RESULTS, DISCUSSION AND CONCLUSIONS

7.1 Introduction

The results obtained for the analysis of seven test subjects will be presented. It is accepted that this is a small group but the consistent results obtained for normal locomotion were felt to justify the size of test group. The side slope tests were less consistent in some respects and for reasons discussed later this is attributed to causes other than sample size. The centre of pressure results will be considered first, followed by the solutions to the Mark I and II models. Then summary of the results for all of the subjects will be presented and followed by comments upon and the further development of the models.

7.2 Test Subject Gait Characteristics

The cine film data was analysed to obtain the basic temporal characteristics of the test group. The mean values obtained are tabulated in table 7.1. The test group compares well with test data presented by Murray et al (reviewed in 2.8.2) but represents a narrower age spectrum (22-27 years). There was no indication from these characteristics that side slope walking was in any way different to normal locomotion.

7.3 Centre of Pressure Characteristics

Eight subjects were available for comparison of the centre of pressure paths; the eighth dataset presented problems in kinematics, but was quite acceptable in respect of forces. These paths were compared by superimposing the hindfoot segment markers, 2, 11 and 17, for side slope and normal locomotion tests, see figures 7.1 and 7.2. The centre of pressure path (Cp-path) usually starts from the heel at the mid to lateral edge and then progresses

Characteristic / Test	Double stance % walking cycle	Foot flat % walking cycle	Heel off % walking cycle	Toe off % walking cycle	Cycle time (s.)	Stride length (m.)	Mean Cadence steps/min	Mean Speed (m./s.)
Normal Locomotion (7 subjects)	0.12 (0.02)*	0.12 (0.04)	0.37 (0.04)	0.60 (0.03)	1.15 (0.13)	1.66 (0.12)	105	1.47 (0.20)
+10° ** Side slope (7 subjects)	0.15 (0.02)	0.11 (0.04)	0.34 (0.07)	0.61 (0.02)	1.17 (0.11)	1.61 (0.17)	102	1.44 (0.24)
-10° *** Side slope (7 subjects)	0.13 (0.03)	0.14 (0.04)	0.37 (0.07)	0.57 (0.05)	1.10 (0.18)	1.61 (0.20)	109	1.50 (0.30)

* Numbers in brackets are one std. deviation

** Right (test) foot uphill

*** Right (test) foot downhill

Table 7.1 Gait Characteristics for the Test Group

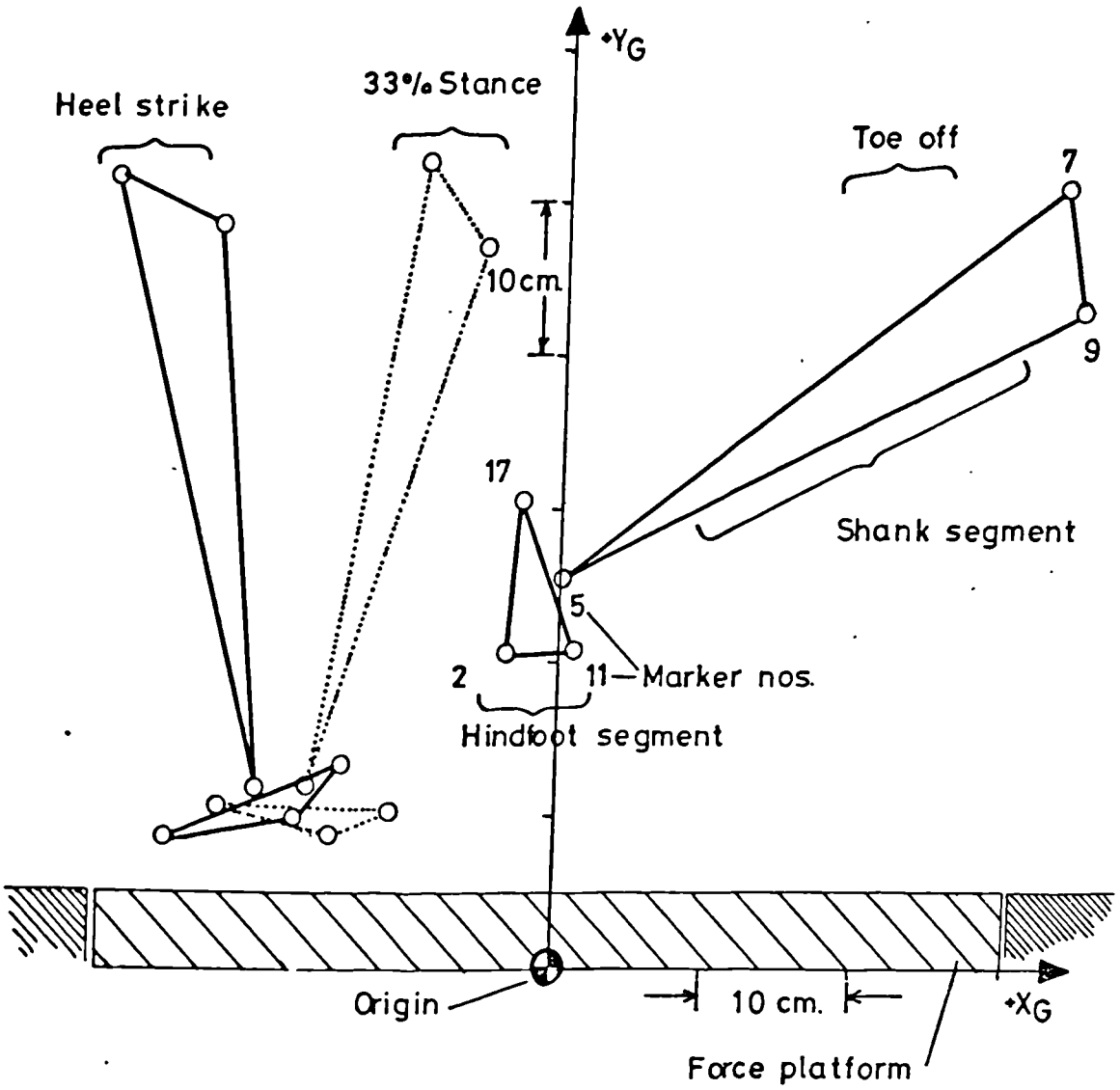

Figure 7.1 Normal Locomotion Kinematic Data for Subject Seven

towards the toes with some slight lateral deviation, finally deviating medially towards the great toe. Figures 7.2, 7.3 and 7.4 indicate that +10° side slope (right foot uphill) resulted in lateral deviation of the Cp-path whilst -10° side slope (right foot downhill) resulted in medial deviation of the Cp-path. The features of each path were similar overall, the deviation being the only obvious difference. Two measurement parameters were defined for comparing the Cp-path. The first, λ degrees, was a measure of the foot toe in/toe out angle with respect to the X_G axis. It was defined by the (X_G-Z_G) plane projection of the angle between the X_G axis and the line passing through marker beads 2 and 11. The second parameter (η/μ) defined the medial or lateral deviation of the Cp-path as it crosses the line joining marker beads 2 and 11. Both parameters are illustrated in figure 7.2 and tabulated for each test type in table 7.2. (Note that +10° side slope results for Subjects 1, 3 and 7 were not available due to markers being obscured by the side slope ramp). The results are quite consistent in their indications. Firstly that the toe in/toe out attitude ($\lambda°$) of the hindfoot is remarkably similar for both normal locomotion and side slope walking and indeed between subjects. This is contrary to the view that the orientation of the foot relative to the line of progression is quite variable. Secondly that $(\eta/\mu)_{-10°}<(\eta/\mu)_{0°}<(\eta/\mu)_{+10°}$, consistently showing lateral Cp deviation with +10° side slope and medial deviation with -10° side slope locomotion. This second result may be explained by the subject attempting to maintain the foot in the attitude for normal locomotion when on side slope, illustrated by a simple model in figure 7.5.

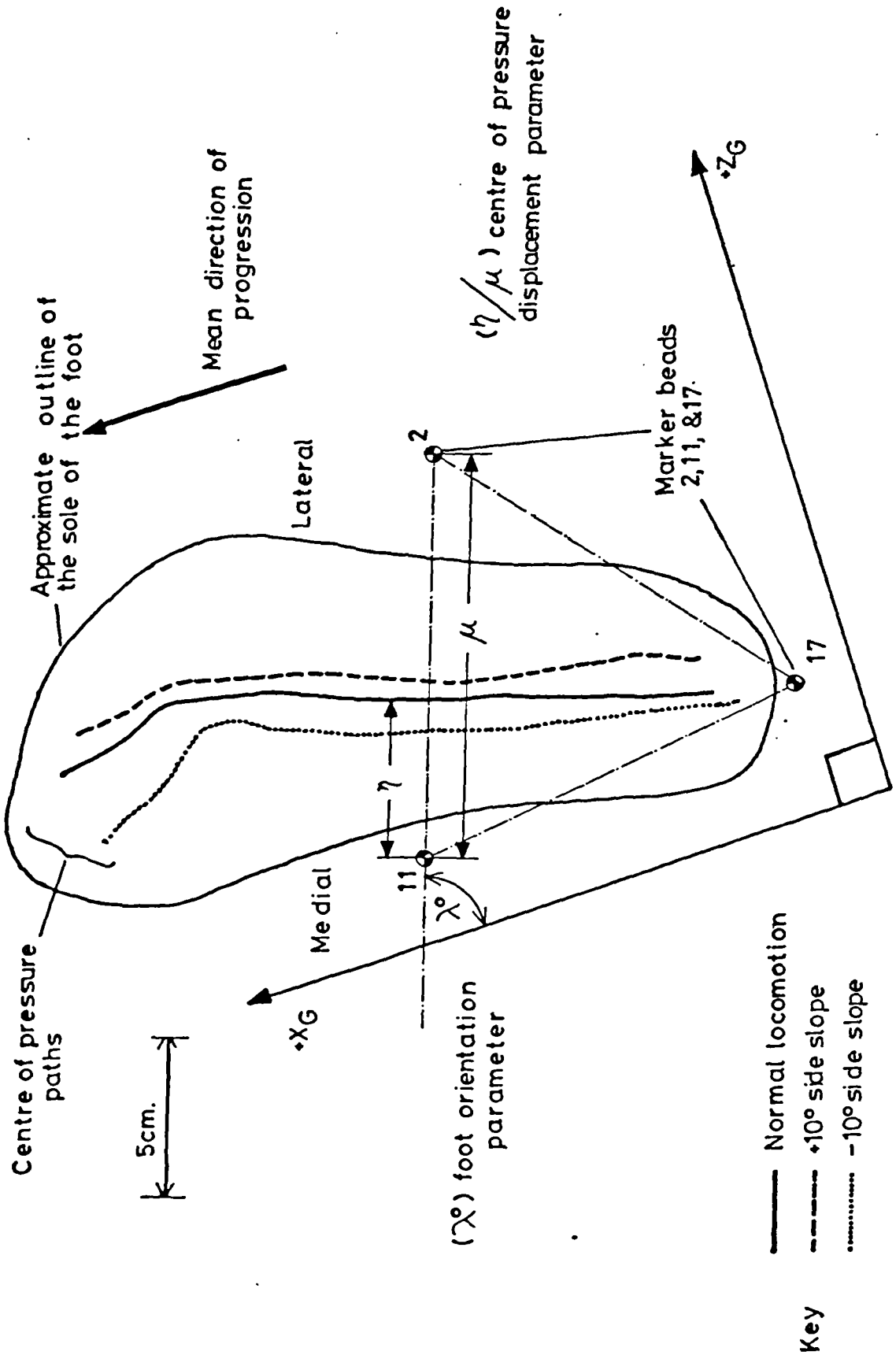

Figure 7.2 Centre of Pressure Parameters Illustrated for the Right Foot of Subject Two

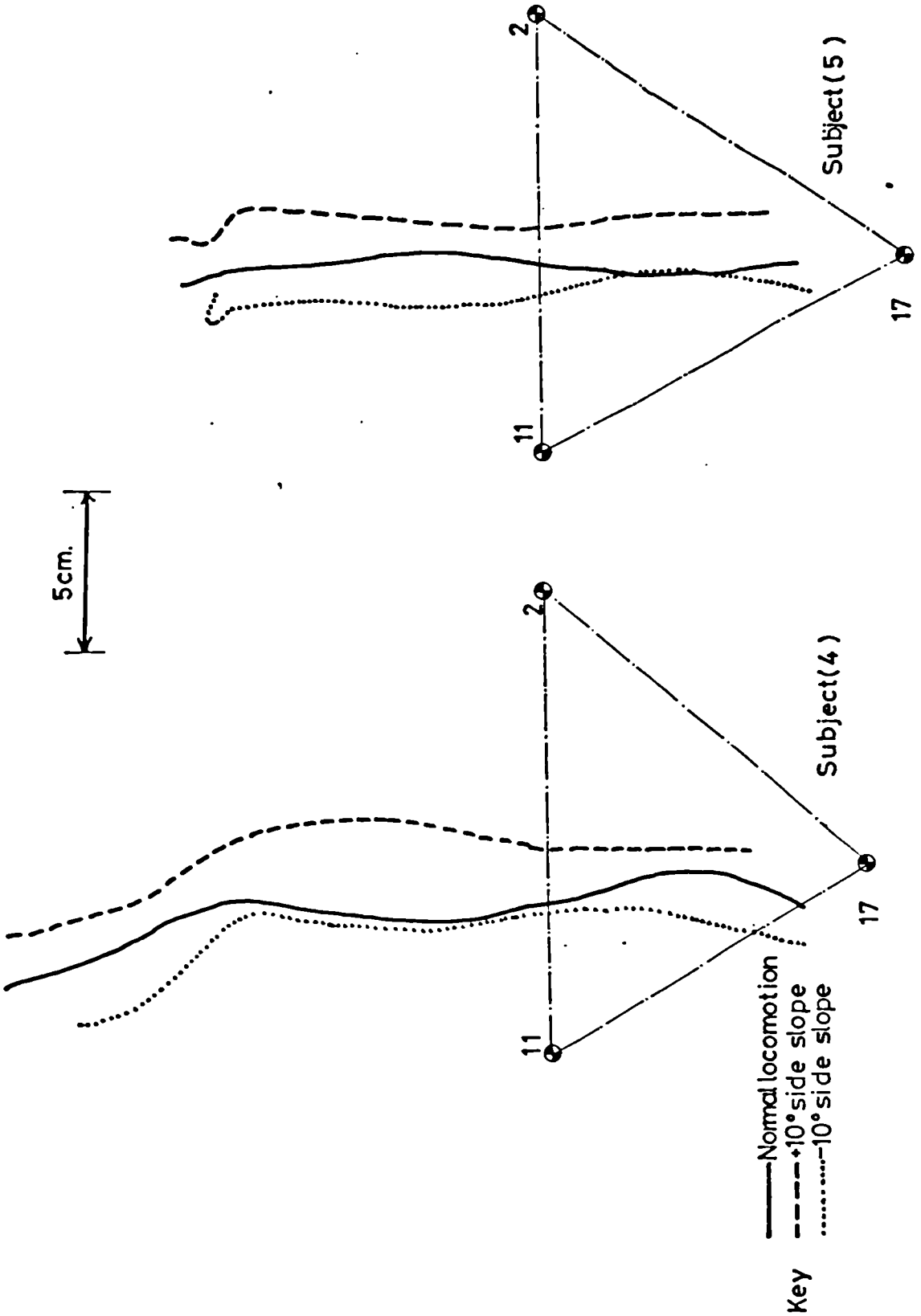

Figure 7.3 Centre of Pressure Diagrams for Subjects Four and Five (Right Foot)

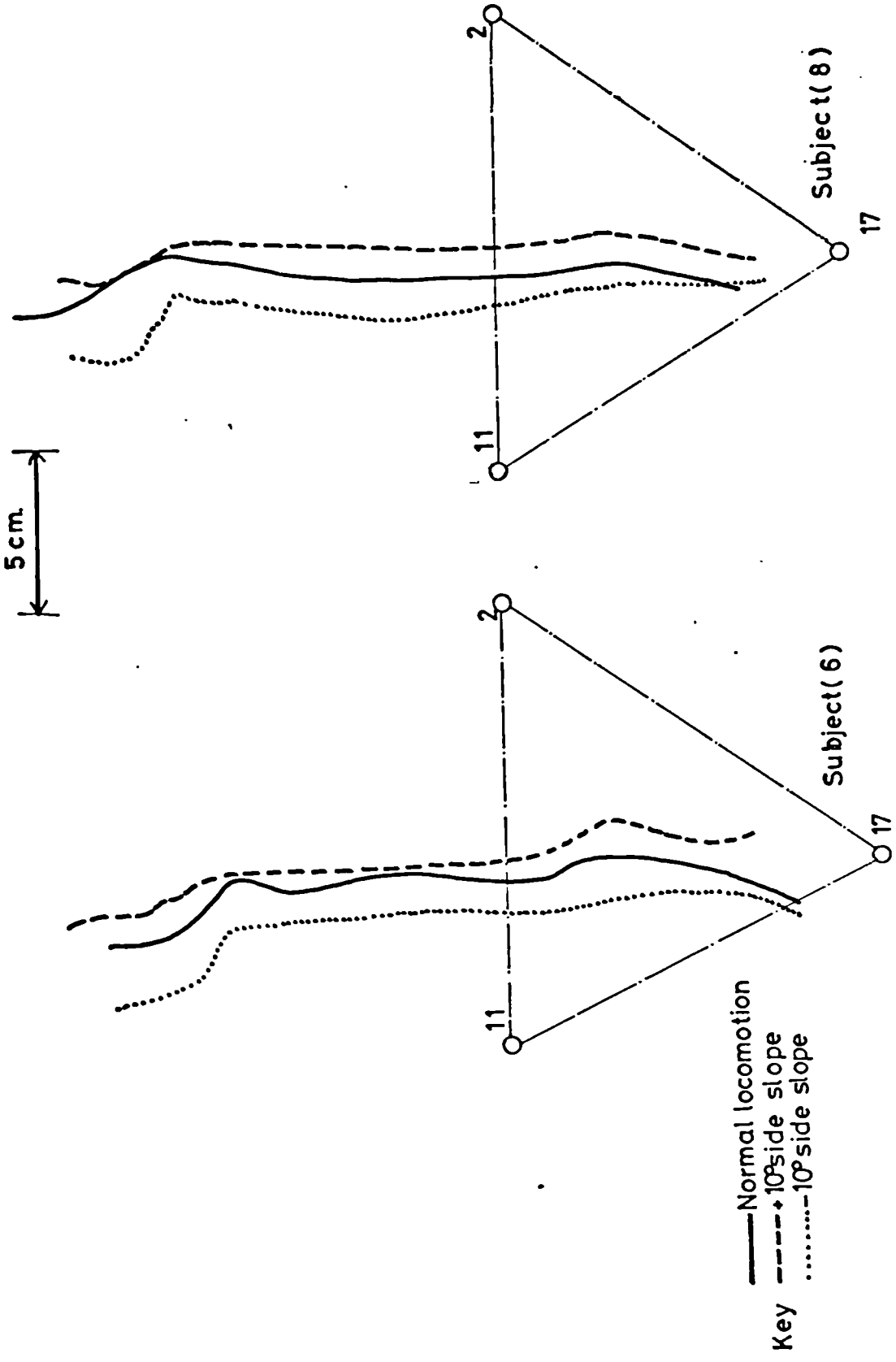

Figure 7.4 Centre of Pressure Diagrams for Subjects Six and Eight (Right Foot)

Table 7.2 Centre of Pressure Parameters

Parameter	λ°			(η/μ)		
Slope	-10°	0°	+10°	-10°	0°	+10°
Subject						
1	78.0	74.0	*	0.27	0.44	*
2	70.0	74.0	77.5	0.32	0.40	0.44
3	73.0	78.0	*	0.35	0.41	*
4	80.0	78.0	78.0	0.32	0.33	0.45
5	78.0	75.0	74.5	0.36	0.43	0.52
6	73.5	73.5	74.5	0.29	0.36	0.40
7	77.0	74.0	*	0.34	0.38	*
8	79.0	81.0	80.0	0.34	0.42	0.47

* Missing values

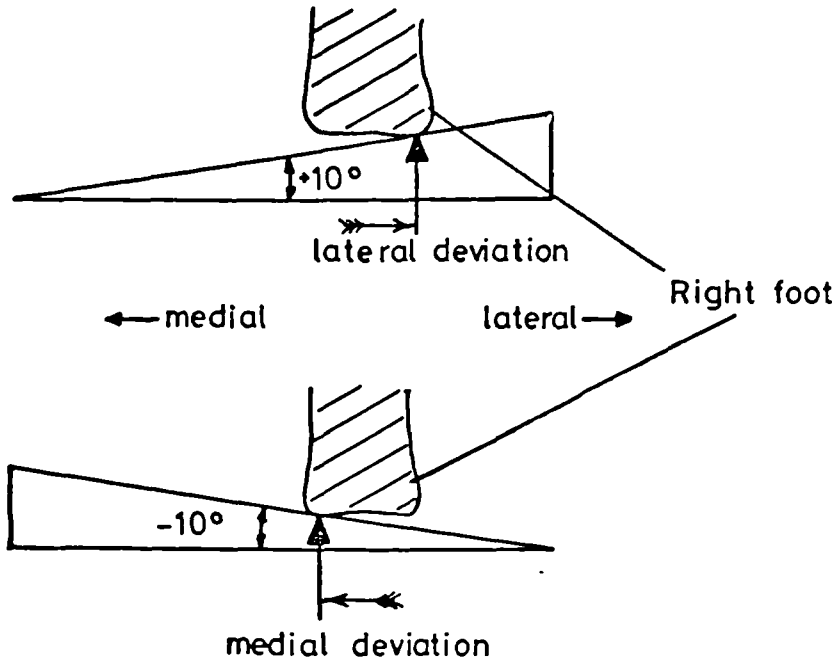

Figure 7.5 Model of the Foot Illustrating the Deviation of the Centre of Pressure with Side Slpoe

7.4 Solution to the Mark I and Mark II Models

7.4.1 External Forces and Moments in the Tc. and Tcn. Systems

Before presenting the solutions to the models the external forces and moments will be discussed. Figure 7.6 shows the x, y and z components of force acting on the foot in the ground, Tc. and Tcn. systems for subject seven. The F_y curves (axis system vertical force) show in general three peaks, one immediately after heel strike at ≃ 5% stance phase annotated (a) and two much larger peaks at ≃ 20% and ≃ 75% annotated (d) and (e) respectively. The (a) peak frequently appears in work reported elsewhere (reviewed in 2.7.4) and is particularly associated with heel strike. It was found by increasing the force data sampling frequency to 100 Hz. that some attenuation of this peak may have been introduced by sampling at 50 Hz. (but only where the peak actually existed - in some subjects it was absent). The two larger peaks have a much lower frequency spectrum and are consequently reproduced quite acceptably by sampling at 50 Hz. and compare well with other sources, for example Bresler and Frankel (1950). Both peaks are typically just over Body Weight in magnitude. The (d) peak corresponds to the foot becoming flat on the ground and toe off on the contralateral foot. The (e) peak is between heel off and toe off and is due to the posterior shank muscles balancing the external force, due to Body Weight on the forefoot, and the vertical movement as body mass is decelerated for the approaching contralateral heel strike.

The F_x shearing force curves show two peaks, one in early stance at 10%, the other late in stance at ≃ 85%, referred to as (b) and (f) respectively. The (b) peak

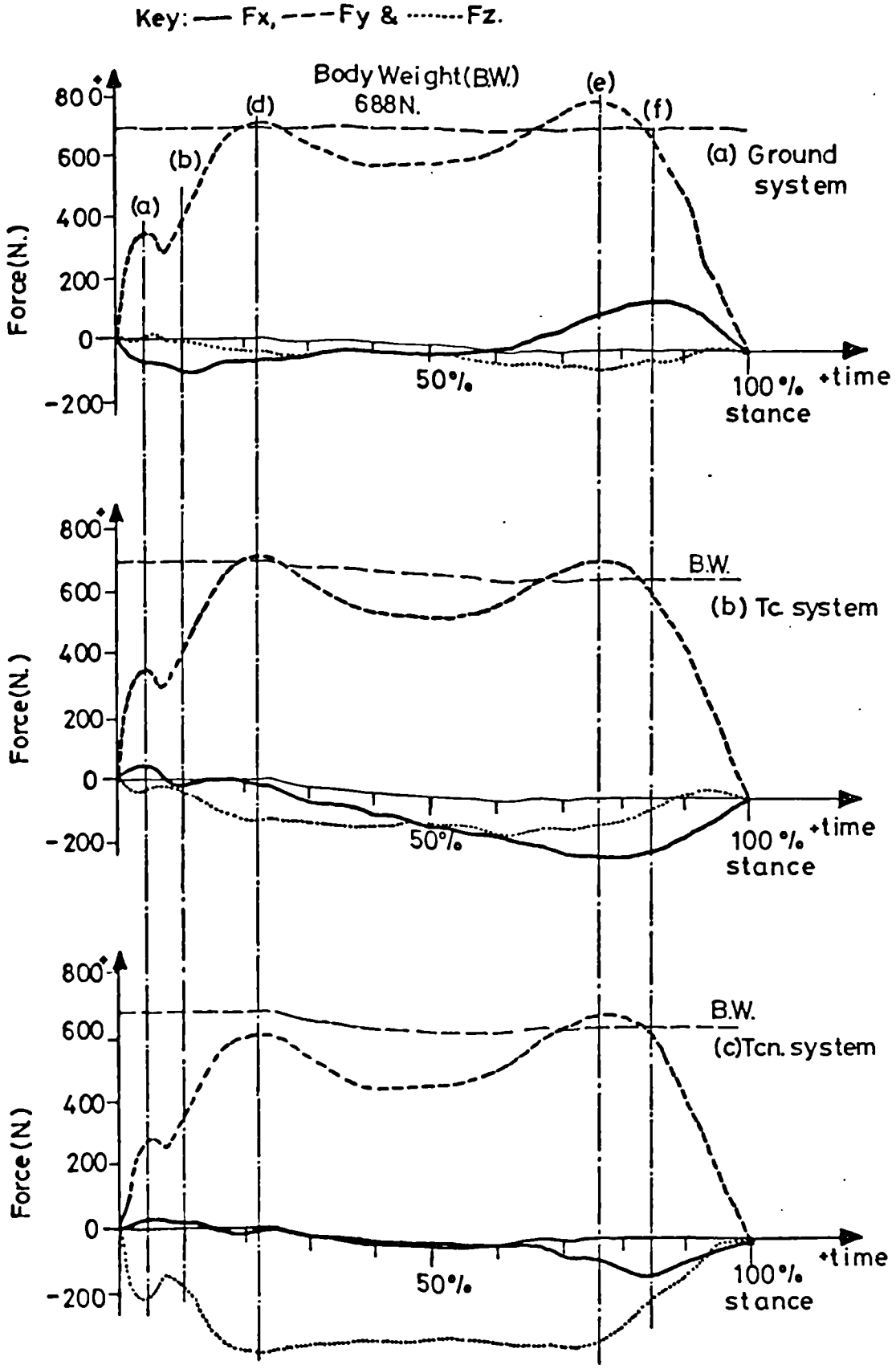

Figure 7.6 External Forces for Subject Seven (Normal Locomotion)

is negative and may be due to deceleration of the body after heel strike as stance begins, the second peak is positive and is a result of the body being propelled forwards to take the next step. The F_x curves in Tc. and Tcn. systems, figures 7.6(b) and (c), show similar temporal characteristics but the signs are reversed compared to the ground system curves, the first peak being slightly positive and the second negative. This is probably due to the different orientation of these axes systems with respect to the ground system. (The F_x peaks themselves are almost equal and opposite to the F_x peaks acting on the other foot.)

The F_z curves in particular show the influence of reorienting the axes. The ground system F_z curve is slightly negative, acting in a medial direction on the foot throughout stance phase. F_z in the Tc. system evidently has gained substantially from the first major F_y peak (d) and a little from the (e) peak. The Tcn. system F_z curve has completely taken on the character of the F_y curve, showing quite pronounced (a), (d) and (e) peaks, and is of comparable magnitude.

Turning now to consideration of the moments due to the external forces, refer to figures 7.7(a) and (b). (Note that the moments in the ground system are not illustrated since they were only referred to the ground system origin.) Both sets of curves are similar in their overall appearance. On closer inspection it can be seen that the difference in relative orientations of the Tc. and Tcn. axes has resulted in similarity between $(M_x)_{Tc.}$ and $(M_z)_{Tcn.}$ and also between $(M_z)_{Tc.}$ and $(M_x)_{Tcn.}$ The M_y characteristic for both systems is virtually identical. Because of these observed similarities the

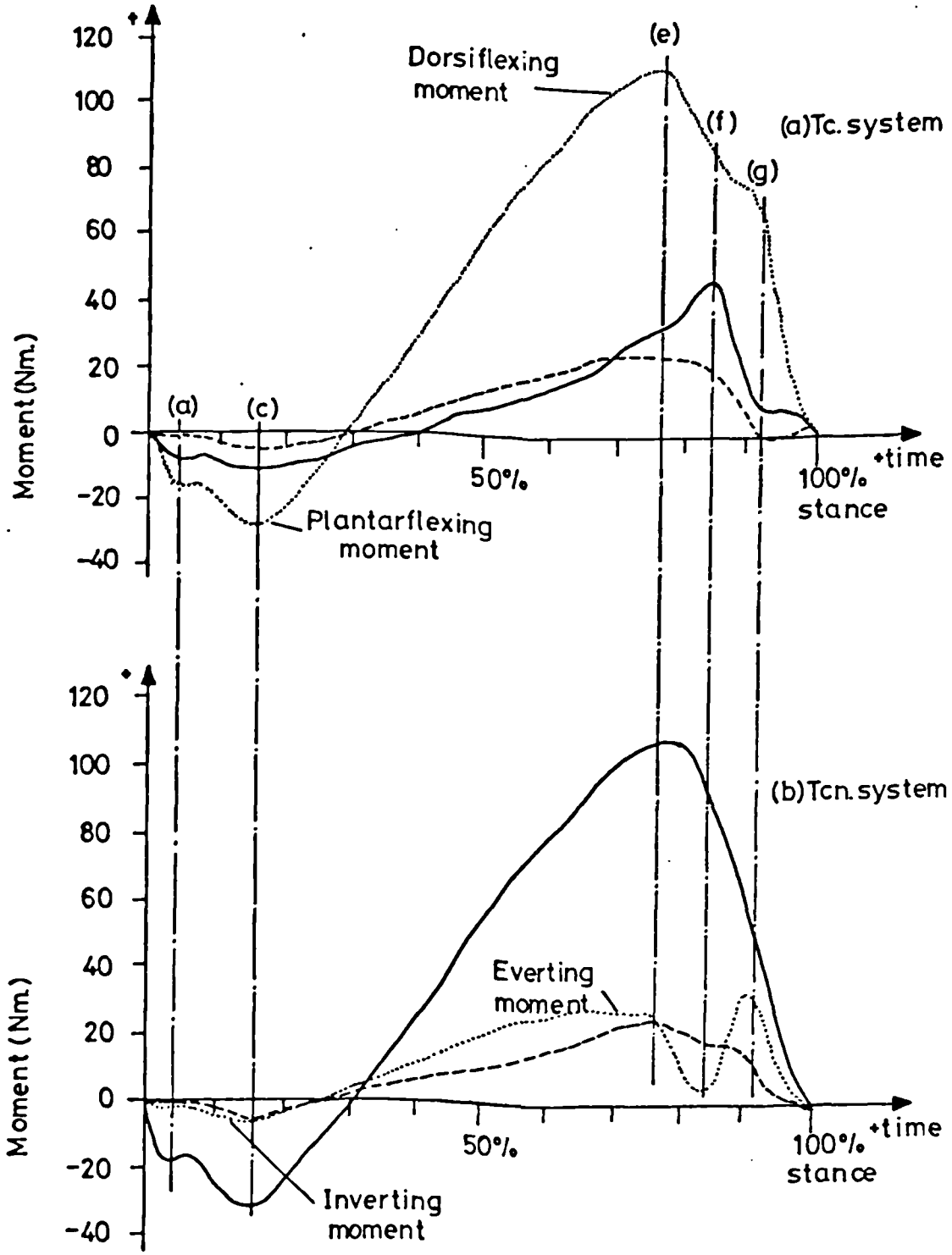

Figure 7.7 External Moments for Subject Seven (Normal Locomotion)

curves will be discussed in pairs.

$(M_z)_{Tc.}$ and $(M_x)_{Tcn.}$, both curves show three peaks, two negative and one positive. The first negative peak corresponds to the (a) peak noted in the F_y curves at 5% stance, the second at 17% stance ((c) peak) appears to have no counterpart in the force curves and is the largest negative moment at -30Nm. The positive peak occurs at ≃ 75% stance, corresponding to the (e) peak observed in the F_y curves and is ≃ 110Nm.

The $(M_x)_{Tc.}$ and $(M_z)_{Tcn.}$ curves are quite similar in their magnitudes. They both have a small negative (c) peak, -10Nm. and -5Nm. for $(M_x)_{Tc.}$ and $(M_z)_{Tcn.}$ respectively. The positive part of both curves is interesting in that where $(M_x)_{Tc.}$ peaks at +45Nm. (≃ 85%) stance - (f) peak - $(M_z)_{Tcn.}$ dips to +5Nm. with a peak either side, the (e) peak +30Nm. (≃ 75% stance) and (g) peak +35Nm. (90% stance).

The M_y curves for both Tc. and Tcn. systems are virtually identical having one negative peak at (c) (-5Nm.) and a positive peak at (e) (+25Nm.).

It is notable that both M_y and M_z in the Tcn. system are very small up to about 35% stance phase. The orientation of the Tcn. axis relative to the external force vector is evidently such that the inverting/everting effects are small which is consistent with Lapidus' argument reviewed in 2.5.

The major features of the external force and moment curves reported above for subject seven are quite typical for the other subjects. The variation due to natural fluctuations in subject gait was found to be ±10% for the peak forces and ±15% for the peak moments. This includes errors due to calculation and data processing as well as that due to natural variation.

The moment peaks (c) and (e) in figure 7.6(a) correspond exactly with peaks in plantarflexion and dorsiflexion reported in figure 2.31. The pattern of $(M_y)_{Tc.}$ follows the kinematic pattern for internal external rotation shown in figure 2.33(b), negative moment (internally rotating) peak corresponds to internal rotation peak (c) (15-20% stance phase) while positive moment (externally rotating) peak corresponds to external rotation peak (e) ($\simeq$ 75% stance). The inversion/eversion moment curve due to the external forces, $(M_z)_{Tcn.}$ curve figure 7.7(b) did not, in any of the test data considered, closely resemble that presented by Peizer and Wright (1971) figure 2.37(c), which had a very pronounced inverting moment peak at 25% stance and continued thereafter as inverting, but at a lower level for most of stance. This is considered to be partially incorrect for at heel strike the external force is medial to the $Z_{Tcn.}$ axis (looking along it) and is inverting - but only for a short period, for the external force quickly moves to the lateral of the $Z_{Tcn.}$ axis and becomes relatively large in magnitude as well as radius vector and therefore results in an everting peak moment.

The $Z_{Tc.}$ and $Z_{Tcn.}$ moment curves also indicate that up to $\simeq$ 27% stance the external force acts as on the foot invertor-plantarflexor, and beyond this point in an opposite sense as evertor-dorsiflexor for the remainder of stance. The results of Wright et al (1964), figure 2.31, indicate that kinematically the foot everts and plantarflexes simultaneously at early stance (10%) and thereafter gradually inverts and dorsiflexes up to about 80% stance, and for the remainder of stance everts and plantarflexes again.

7.4.2 Comparison of the Mark I and Mark II Model Force Curves

The results for subject seven are presented comparing the Mark I and Mark II solutions. The Mark I model, it will be recalled, includes only the Calf and Anterior tibial groups whilst the Mark II model includes in addition the Peroneal/Posterior tibial groups. Both models incorporate the Tc. and Tcn. system joint forces.

Figure 7.8 show the results obtained for muscle forces. The Calf/Anterior tibial activity shows the (a), (c) and (e) peaks, corresponding exactly to the $(M_z)_{Tc.}$ curve in figure 7.7(a). The Anterior tibial group is active for the first 30% of stance and thereafter the Calf is active. There are only slight differences between the Mark I and II models, confirming that the Peroneal/Posterior tibial muscles have a relatively small flexion/extension effect. The phasic relation contrasts strongly with the results of Stauffer et al (2.8.4) who stated that the Anterior tibial group was active for less than 10% of stance phase.

The residual $(Z)_{Tcn.}$ moment calculated for the Mark I model is illustrated in figure 7.14(b) and it will be seen that the result for the Posterior tibial/Peroneal group (figure 7.8) for the Mark II model follows these peaks exactly. The peak Peroneal group activity occurs at $\simeq$ 85% stance coinciding with peaks observed in the $(M_x)_{Tc.}$ and $(M_z)_{Tcn.}$ external moment curves described in 7.4.1. The profile of the $(M_z)_{Tcn.}$ residual curve is remarkably similar in form to that reported for the Peroneal muscles and Posterior tibial muscles in the University of California Emg. studies reviewed in 2.7.3, see figure 2.26, showing low level activity for most of

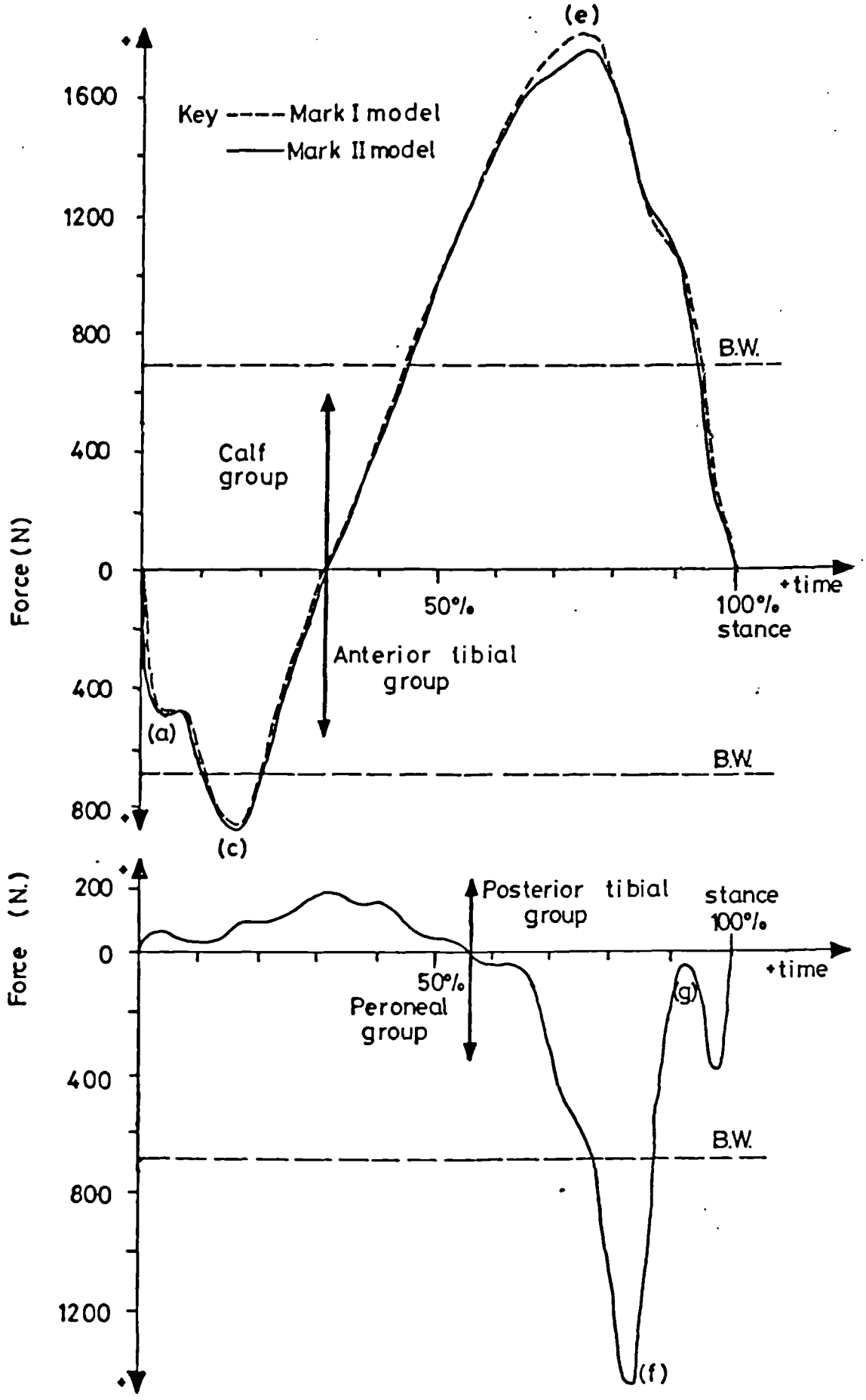

Figure 7.8 Muscle Forces for Mark I and II Model Solutions (Subject Seven, Normal Locomotion)

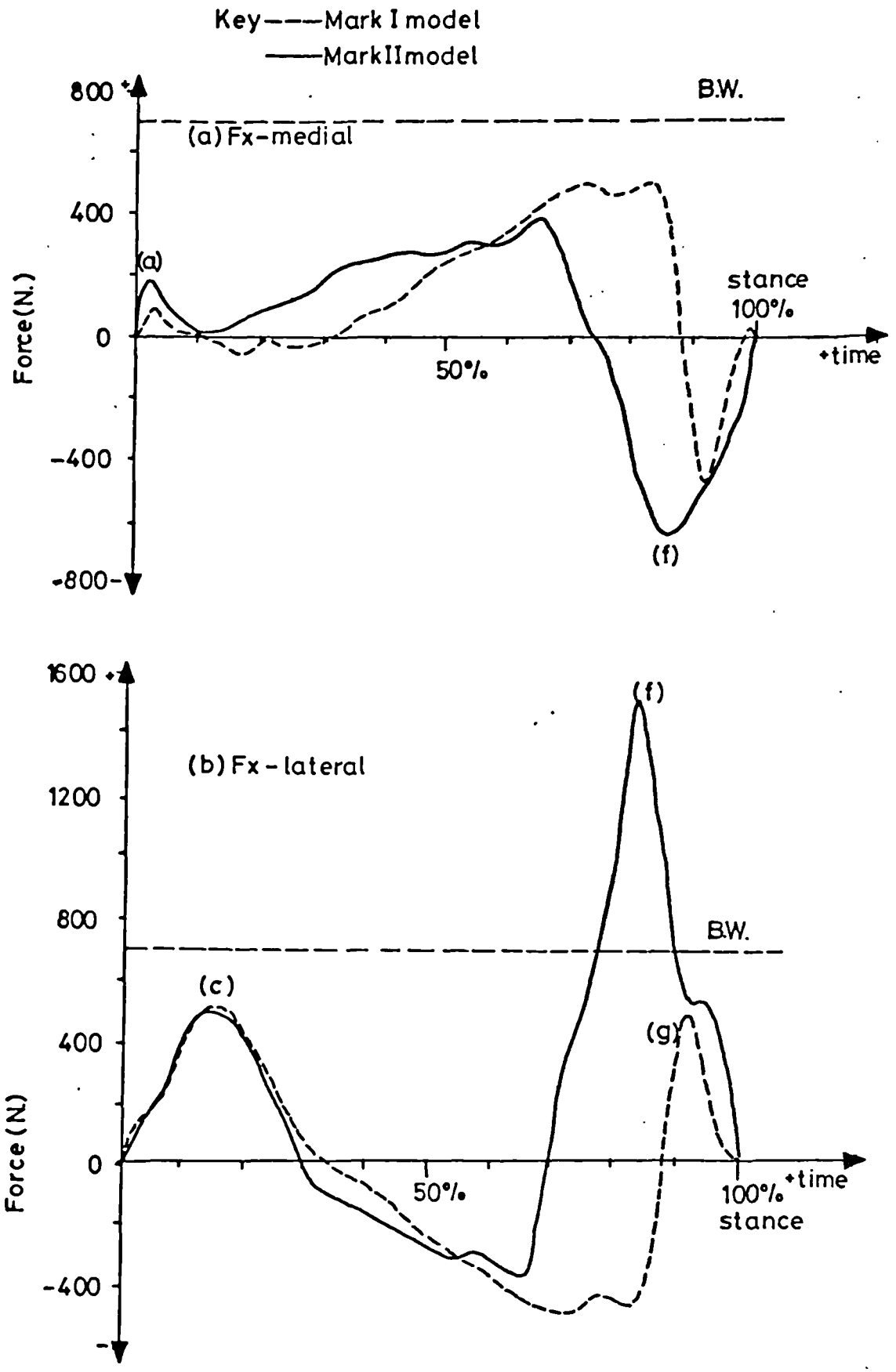

Figure 7.9 Tc. Joint F_x-Forces for Mark I and II Model Solutions (Subject Seven, Normal Locomotion)

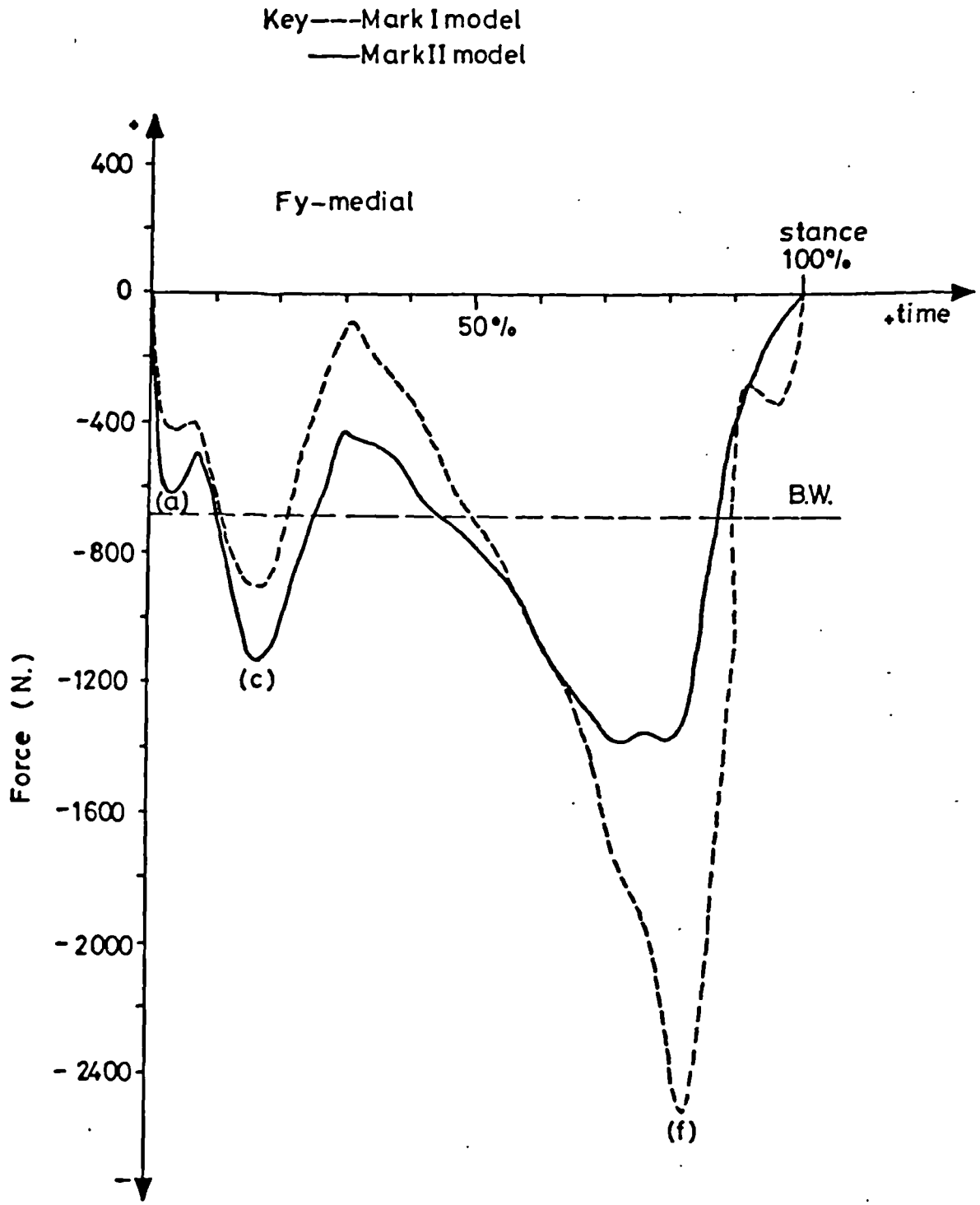

Figure 7.10 Tc. Joint F_y Medial Forces for Mark I and II Model Solutions (Subject Seven, Normal Locomotion)

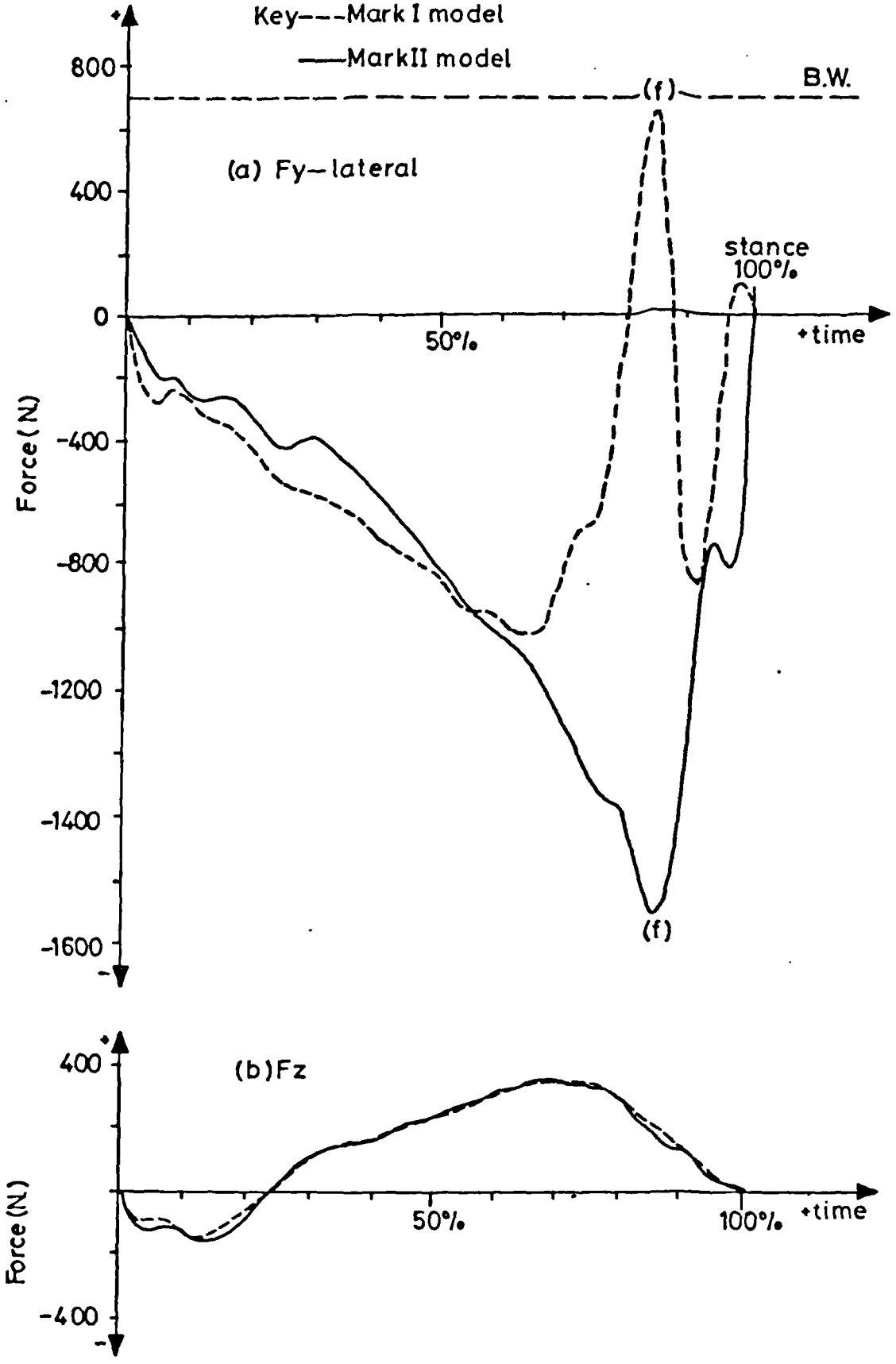

Figure 7.11 Tc. Joint F_y Lateral(a) and F_z(b) Forces for Mark I and II Model Solutions (Subject Seven, Normal Locomotion)

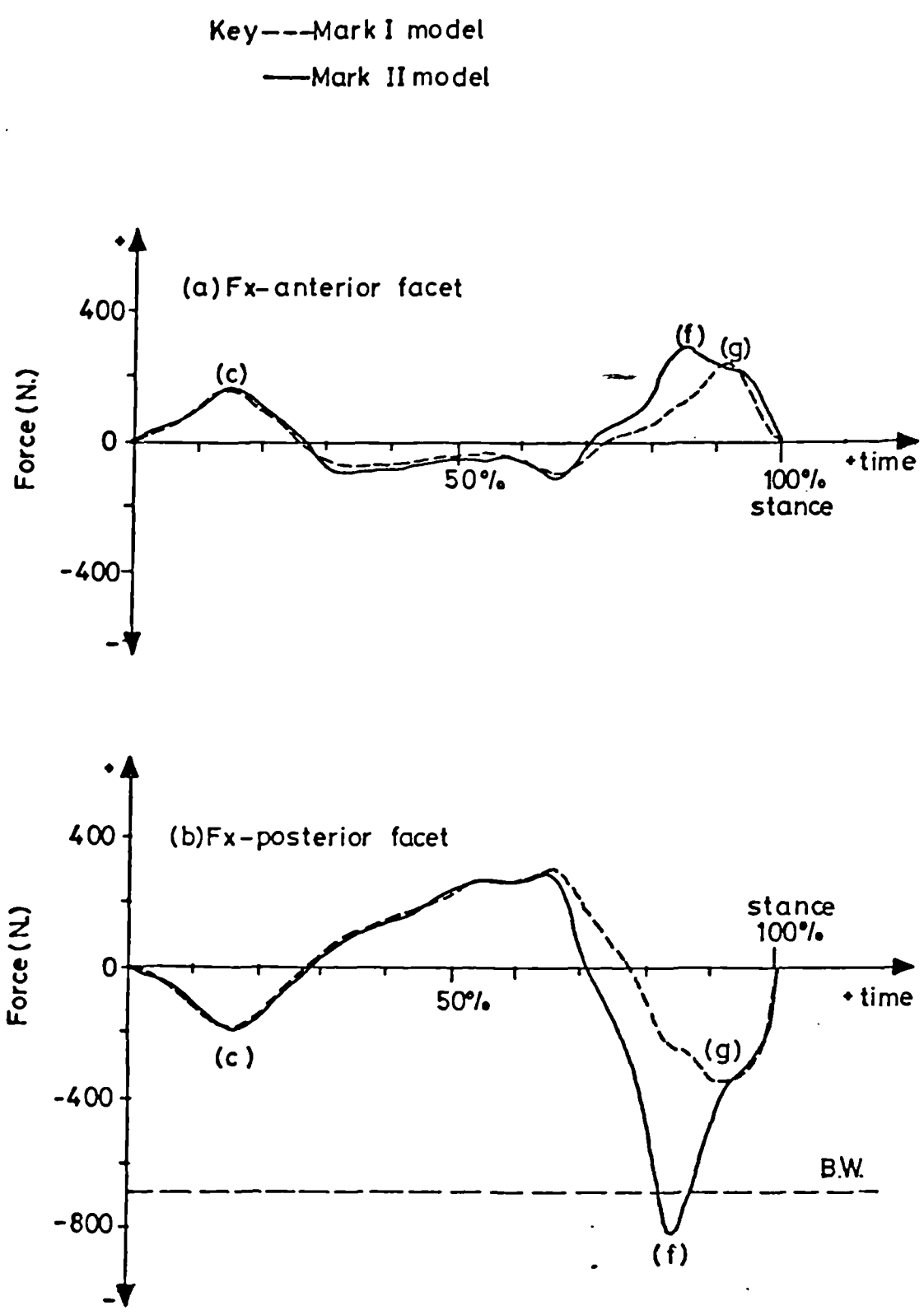

Figure 7.12 Tcn. Joint Anterior(a) and Posterior(b) Facet F_x Forces for Mark I and II Model Solutions (Subject Seven, Normal Locomotion)

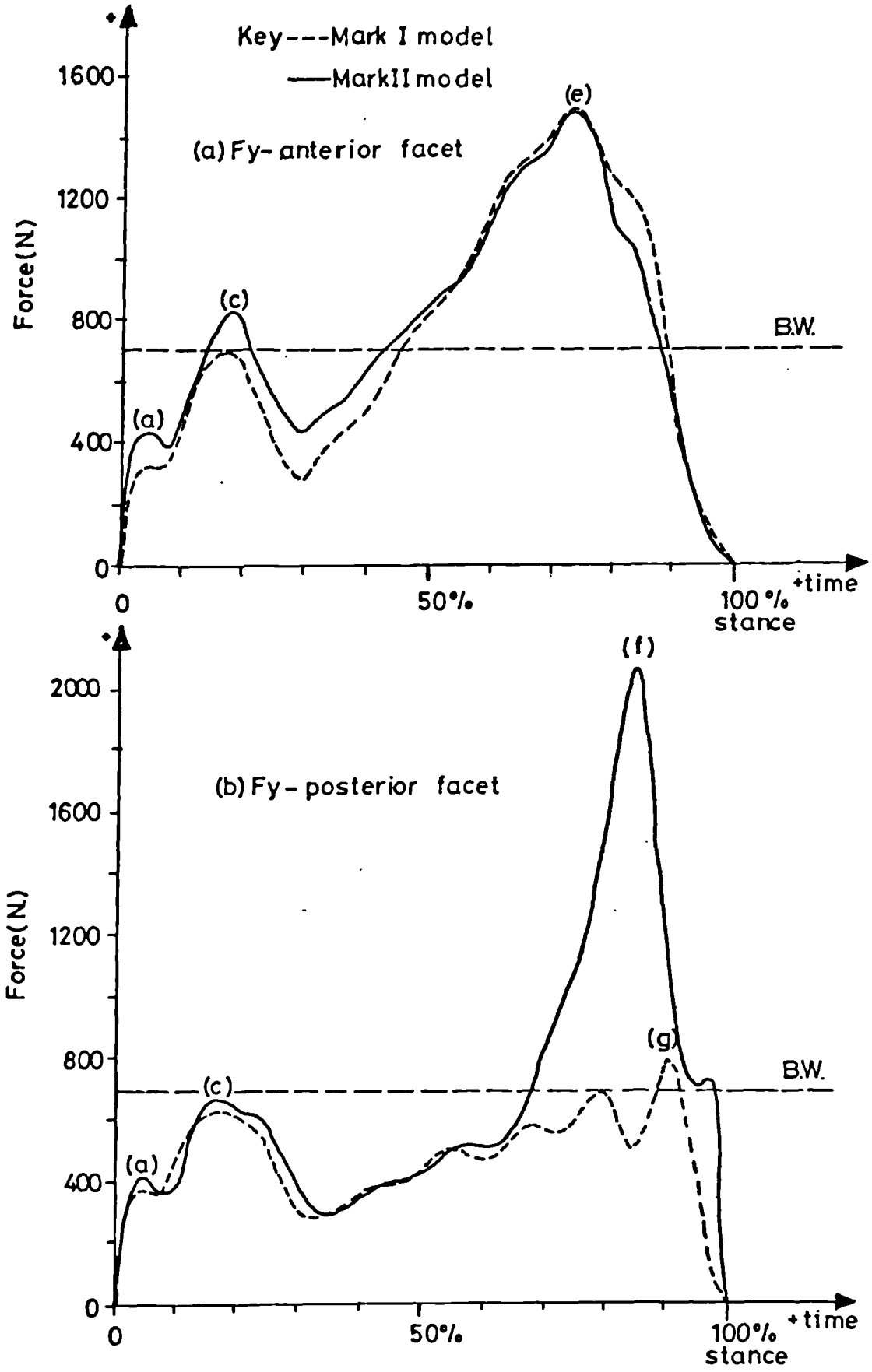

Figure 7.13 Tcn. Joint Anterior(a) and Posterior(b) Facet F_y Forces for Mark I and II Model Solutions (Subject Seven, Normal Locomotion)

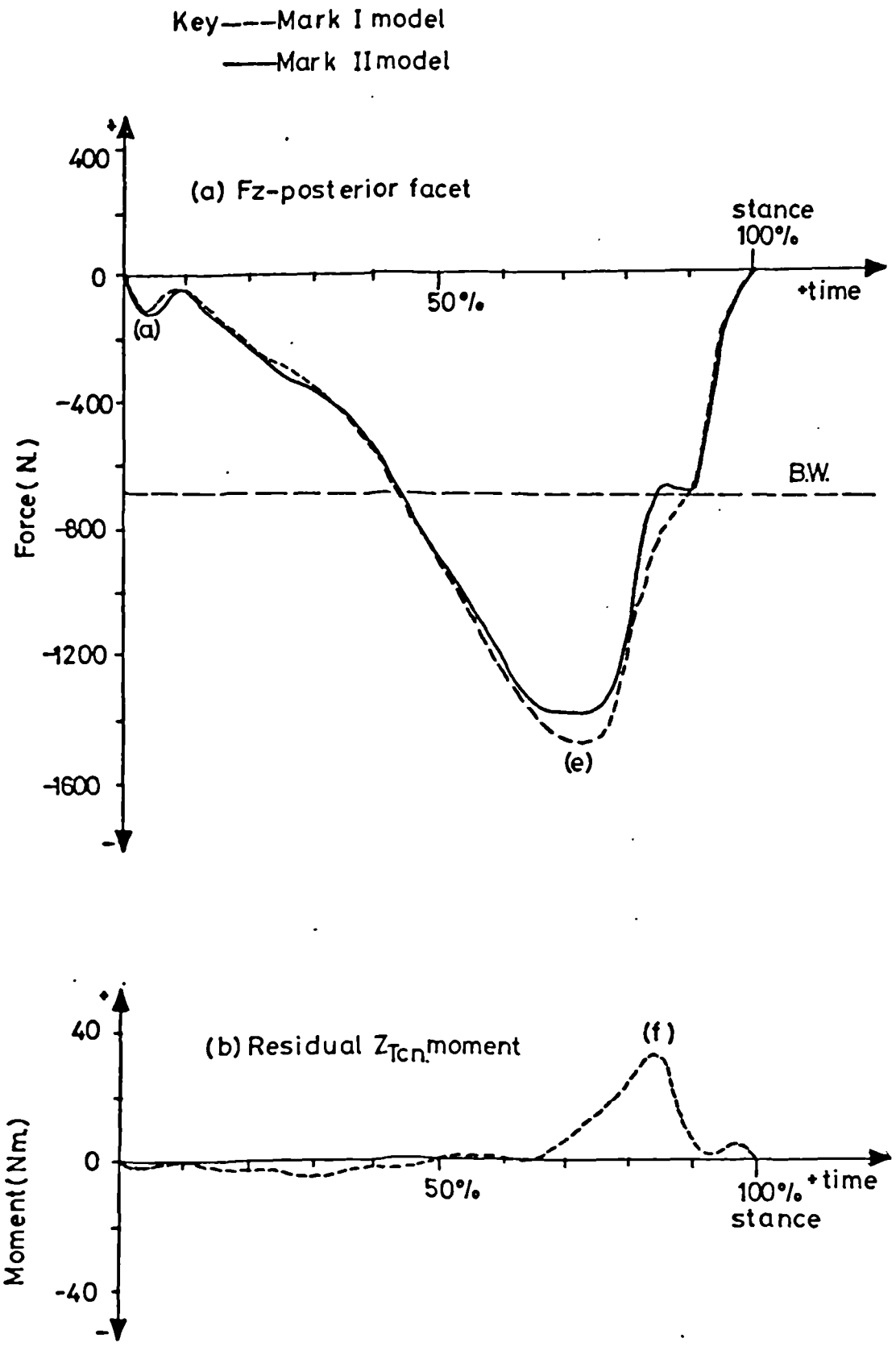

Figure 7.14 Tcn. Joint Posterior Facet F_z Force and Residual $Z_{Tcn.}$ Moment for Mark I and II Model Solutions (Subject Seven, Normal Locomotion)

stance with a higher peak at about 80% stance phase.

In figure 7.9 the lateral and medial $(F_x)_{Tc.}$ fore/aft shearing components are compared. The lateral F_x curve shows strong influence of the Anterior tibial group in early stance. After 30% stance the Mark I curves are almost mirror images of each other and show the (f) and (g) peaks. The Mark II solution curves are similar over the first half of stance but after this show the influence of the Peroneal group peak both F_x medial and lateral having pronounced (f) peaks.

The F_y curves for the Tc. joint are illustrated in figures 7.10 and 7.11(a). These are perhaps the most important graphs because they highlight the differences between the Mark I and Mark II models.

The medial F_y Mark I curve indicates the influence of the Anterior tibial group in early stance (a curious contrast to the F_x forces where the lateral F_x component showed strong Anterior tibial influence), followed by a large (f) peak of nearly-2500N. Negative sign throughout is physiologically acceptable since it means that F_y is compressive. The lateral F_y Mark I solution curve has one distinctive feature and that is an abrupt change in sign at the (f) peak giving +500N. tensile and therefore physiologically unacceptable value. The equations giving this solution were carefully examined for any evidence that a sign change in a sensitive parameter had caused the sudden swing in lateral F_y, but no such evidence was found. The Mark I solution was therefore rejected because of this failing. The Mark II solution reduced the medial component of $(F_y)_{Tc.}$ in the region of (f) peak and the lateral component was reversed completely at the (f) peak, now giving a negative peak of - 1600N. Thus the

Mark II solution becomes physiologically acceptable at the point where the Mark I solution failed.

Referring to the development of the models in chapter four the F_y components were required to meet $(F_y)_{Tc.}$ and $(M_x)_{Tc.}$ equilibrium requirements (equations 4.11 and 4.14). One interpretation of the above result is that these requirements must be in conflict with the condition that the $(F_y)_{Tc.}$ components must be greater than or equal to zero. The physical explanation for the action of the Mark II model is that, where the Mark I model allowed the Tc. joint force resultant to have a residual moment about the $Z_{Tcn.}$ axis, the Mark II model provided a balancing moment from the Peroneal/Posterior tibial group; at the same time this increased the loading on the lateral/medial (respectively) Tc. joint facet changing the joint force from tensile to compressive.

The $(F_z)_{Tc.}$ curves, figure 7.11(b), are virtually identical for both Mark I and II models and have two peaks. The first at 12% stance is medially directed whilst the second at 70% is laterally directed peaking at about 400N. The anterior and posterior Tcn. facet F_x curves, figure 7.12(a) and (b) respectively, show peaks (c) and (g) for the Mark I model solution. The Mark I curves are almost equal and opposite in sense but in the Mark II solution F_x posterior facet acquires a pronounced negative (f) peak of 600N. which has a much smaller (+300N.) counterpart on the F_x anterior facet curve.

The $(F_y)_{Tcn.}$ curves, anterior facet and posterior facet are shown in figures 7.13(a) and (b) respectively. The anterior facet shows the early stance influence of the Anterior tibial group and a later peak more or less corresponding to the (e) peak. Little difference is

apparent between the Mark I and II solutions; for the first half of stance there is slight increase in the Mark II solution values. The posterior facet F_y curve for the Mark I solution indicates early stance Anterior tibial group influence together with (g) peak Calf group influence in later stance. The Mark II solution was similar for early stance but in late stance showed a very large (f) peak of 1800N. corresponding to the peak in Peroneal group activity. It was observed in general that large Posterior tibial group forces (accompanied by relatively small Peroneal forces) were particularly reflected in the Tcn. joint anterior facet force curve, whilst relatively large Peroneal group forces were reflected mainly in the posterior facet forces. This is probably because the Peroneal group is closely physically related to the posterior facet and the Posterior tibial group with the anterior facet.

Finally consider the $(F_z)_{Tcn.}$ component in figure 7.14(a). This was directed consistently in the negative F_z direction showing only one peak (e); note that this is of considerable magnitude (1500N.) compared with the $(F_z)_{Tc.}$ component. The curve was little affected by the inclusion of the Peroneal or Posterior tibial groups.

7.4.3 Joint Force Resultants

The form chosen for comparison of the results was the joint force resultants rather than the components which would have resulted in too complex a picture for easy comparison of all the test subjects. In addition the forces will be referred to subject Body Weight (B.W.) since this is thought to be a fundamental element of the joint force characteristics. The joint forces for the

Tcn. joint were combined in the following way - the posterior Tcn. facet joint force resultant included the $(F_z)_{Tcn.}$ component since it was consistently directed in the negative Z direction; the anterior facet resultant only included the anterior facet $(F_x)_{Tcn.}$ and $(F_y)_{Tcn.}$ components. The resultant quantities for subject seven are graphically presented in figures 7.15 and 7.16 with the comparison between Mark I and II model solutions.

The Tc. joint force resultant (figure 7.15) indicates clearly the influence of the Anterior tibial group in both Mark I and II curves; peaks (a) and (c) are evident, (c) being about 2B.W. These are followed by a dip at 30% stance (down to about 1.2B.W.) which corresponds to the change over between Anterior tibial and Calf group activity. The (e) peak in late stance phase, for the Mark I solution (3.2B.W.), shows the influence of the Calf group. The peak in late stance for the Mark II solution (4.7B.W.) corresponds to the (f) peak, which indicates the shift due to the combined action of both the Calf and Peroneal groups.

The posterior Tcn. facet (figure 7.16(a)) resultant Mark I solution shows the three characteristic peaks (a), (c) and (e) and the Mark II solution has an (f) peak (3.4B.W.) corresponding to the influence of the Peroneal group.

The Tcn. anterior facet forces, figure 7.16(b) show (a), (c) and (e) peaks ,the (e) peak is largest at 2.1B.W. The Mark I and II model solutions are virtually coincident for this subject.

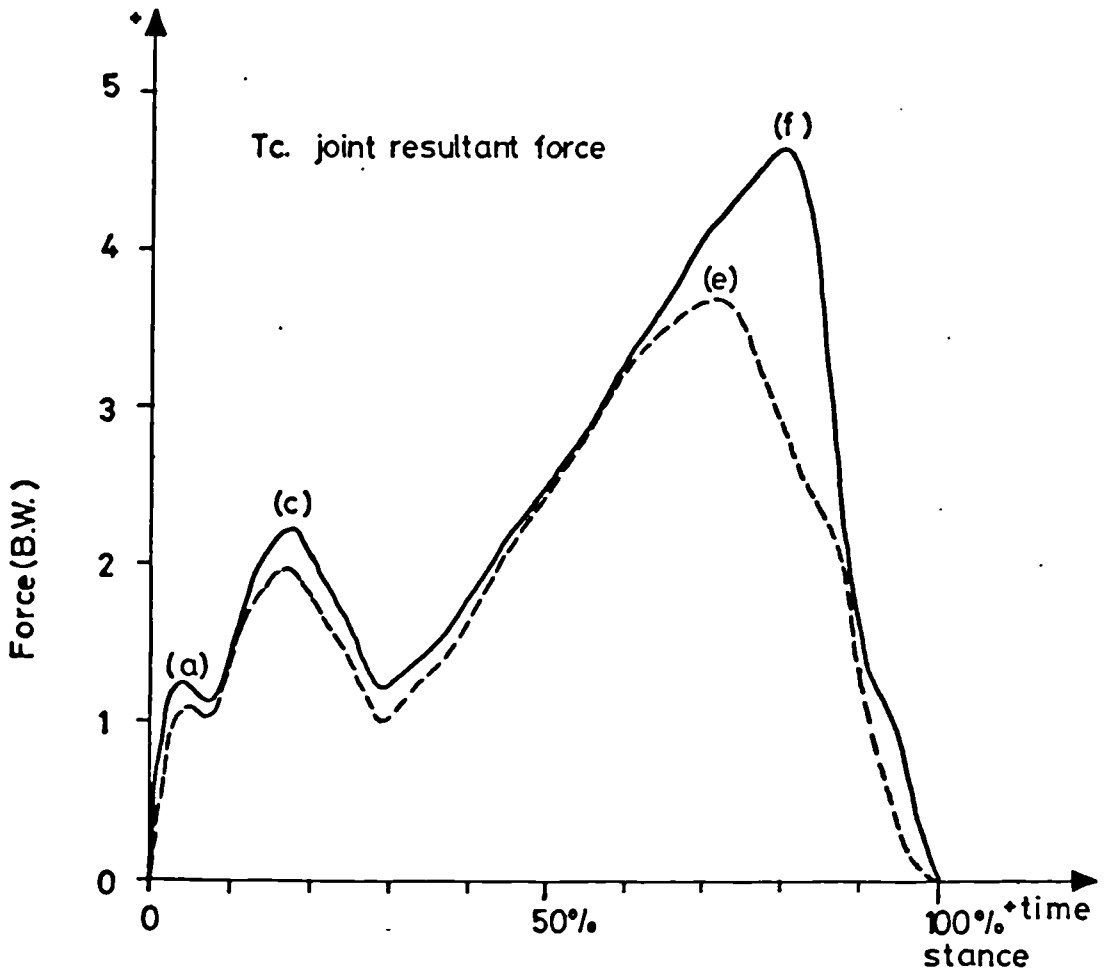

Figure 7.15 Tc. Joint Resultant Force for Mark I and II Model Solutions (Subject Seven, Normal Locomotion)

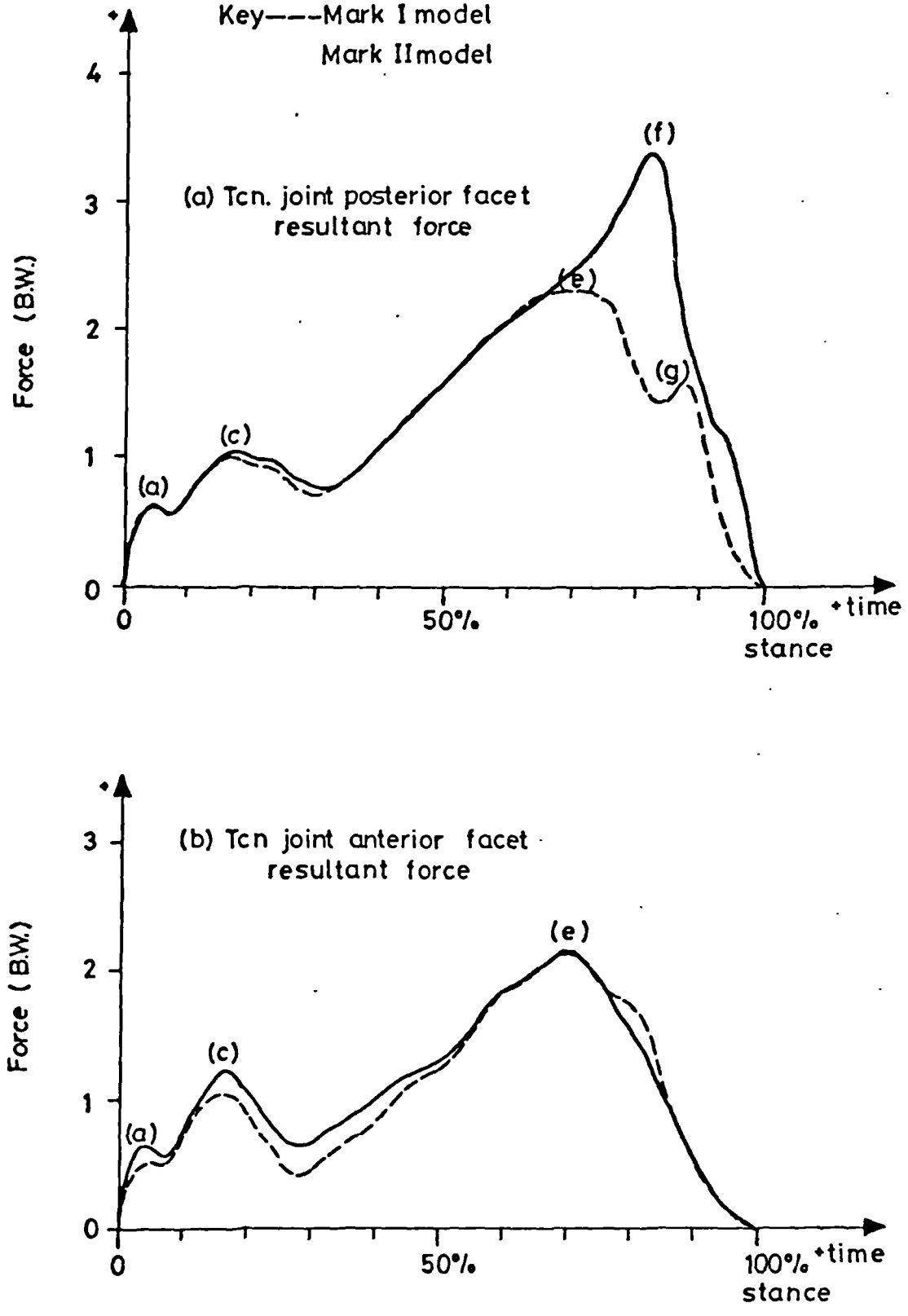

Figure 7.16 Tcn. Joint Resultant Forces for Mark I and II Model Solutions (Subject Seven, Normal Locomotion)

7.4.4 Perturbation of Muscle Group Components and Estimated Errors in the Analysis

Before presentation of the summary results it is appropriate to consider the effect of changing the participation factors for the muscles upon the solutions obtained. The participation factors assumed for the muscles are listed in Appendix 2.1. There is an infinite range to the relative participation values which can be assigned to individual muscles within a group so to confine the assessment to manageable proportions a simple perturbation exercise was undertaken, where extreme values were taken for muscle participation factors. For example, in Peroneal group the peroneus brevis component was assigned zero whilst the peroneus longus was assigned one as participation factors and solutions obtained with the remaining groups retaining their normal Mark II model relationship in respect of participation factors. Then the factors were reversed with peroneus brevis equal to one and peroneus longus equal to zero and solutions obtained again. Systematically solutions were obtained where each group was dominated by a single component, its remaining components being zero. The effect of this perturbation on muscle forces is shown for subject five in figures 7.17 and 7.18. It can be seen in both figures that with the exception of flexor digitorum longus (in figure 7.17) the effects in stance phase centre mainly around the early stance where the Anterior tibial group is active. The early stance Anterior tibial peak varied within the range 0.7-1.5B.W., with the participation factors assigned for the Mark II model giving 0.9B.W. The ranges shown in these figures are thought to be pessimistic.

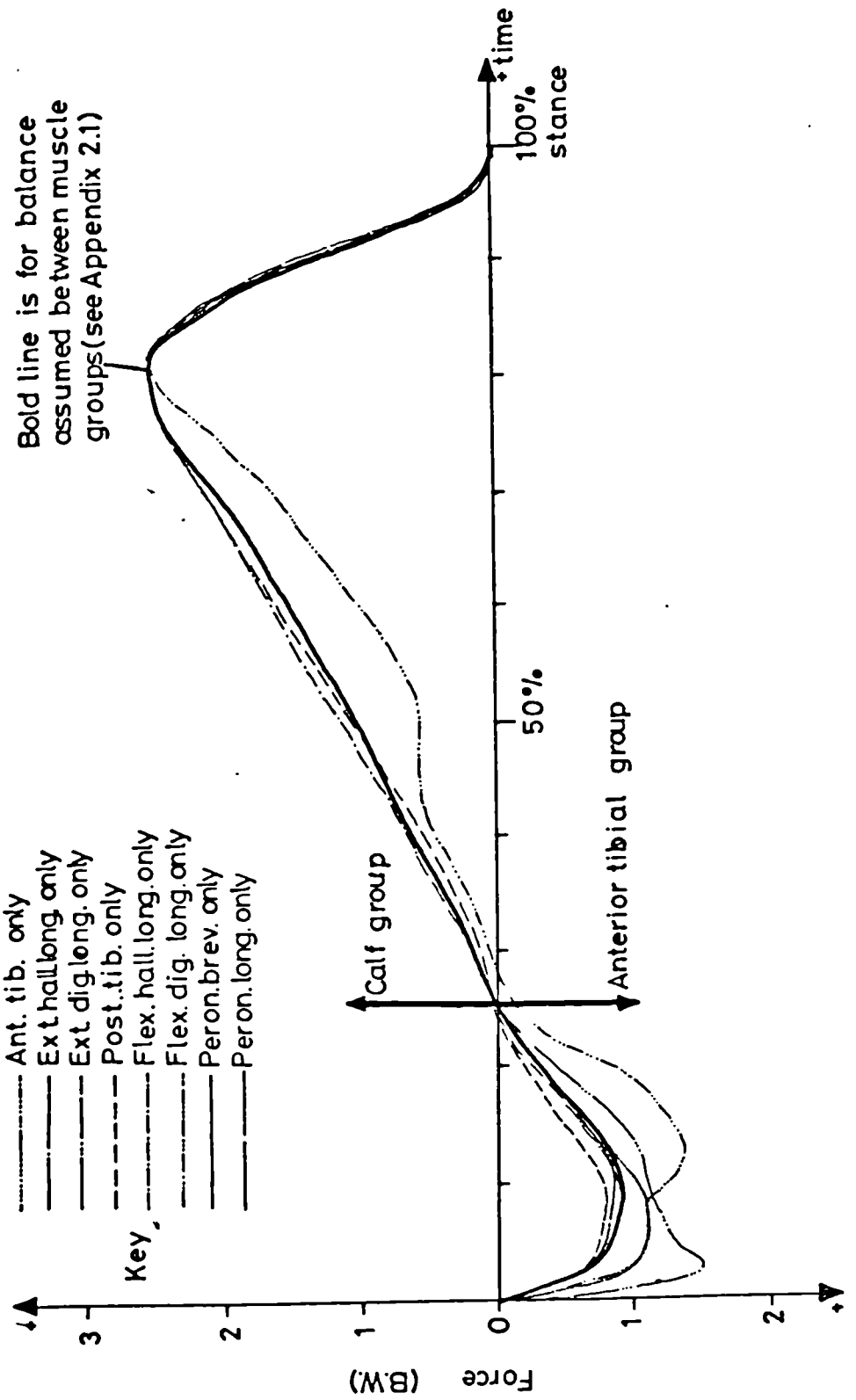

Figure 7.17 The Effect of Changing Muscle Group Participation Factors upon Muscle Forces Calculated for Subject Five (Normal Locomotion) Mark II Model Solution

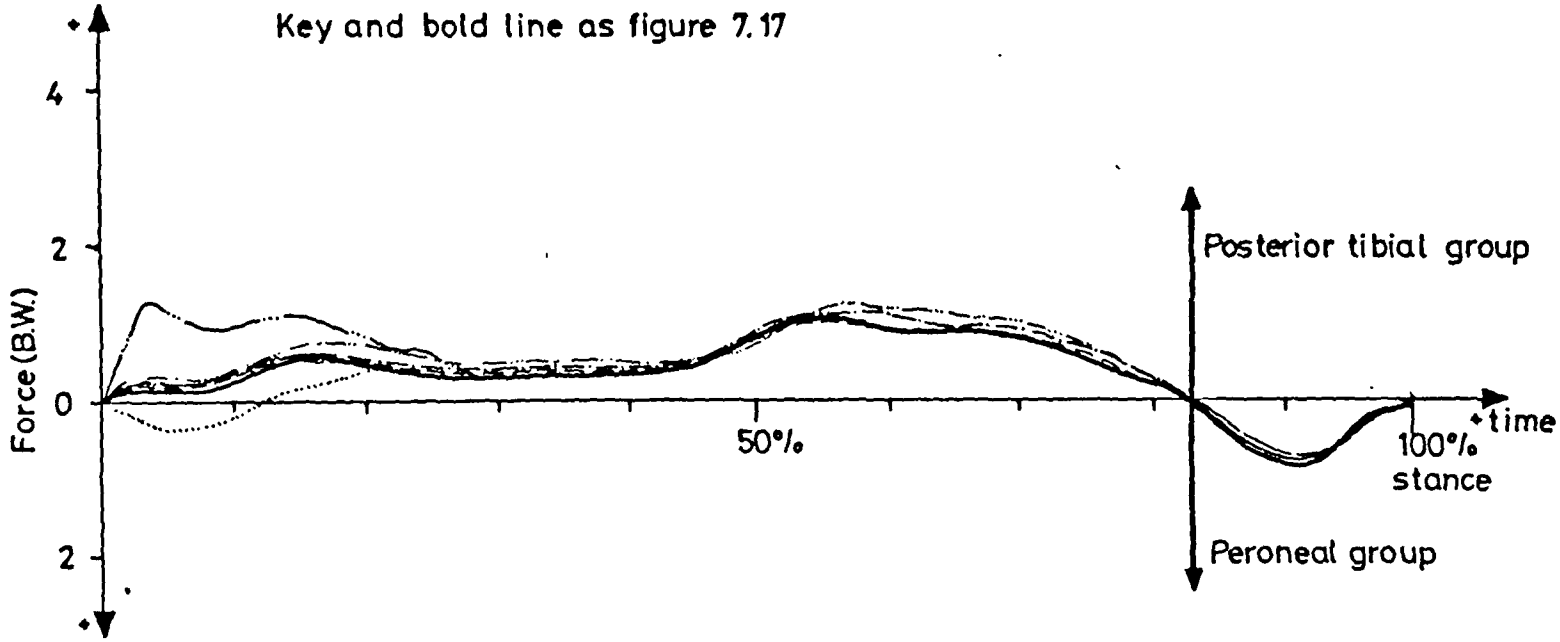

Figure 7.18 The Effect of Changing Muscle Group Participation Factors upon Muscle Forces Calculated for Subject Five (Normal Locomotion) Mark II Model Solution

One further consideration is the effect that anthropometric variation would have on these results. The Calf group is the most dominant muscle group and was used as an example of the effect of anthropometric errors. Consider the simple two-dimensional model illustrated in figure 7.19 with forces assumed to be acting as shown. Take for the sake of argument an external force of 1.25B.W. acting at 0.125m. from the Tc. joint. The values obtaining for Calf force and Tc. joint force corresponding to a Calf group $(X)_{Tc.}$ radius vector of 0.0485m. are tabulated under figure 7.19 (table row two). (The $(X)_{Tc.}$ radius vector is approximately 0.0485m. and is in the range 0.0583 to 0.0442m., estimated by relating the X_T coordinate of the Calf insertion, Appendix 1.4, to the Tc. origin given in Appendix 1.8)) Solutions for 0.0583 and 0.0442m. are shown in table rows one and three. This simple example shows that the effects of anthropometric variation may be less on the joint force than on the muscle force. Also that the worst error attributed to anthropometric variation is of the order of 20%, in practice it is thought that ±10-15% may obtain. To obtain an overall figure for accuracy the variation due to natural fluctuation in subject gait determinants must be included, $\sim (0) \pm 10\%$, thus overall ±20-25% is the expected peak variation due to experimental error, anthropometric data and individual subject variation.

7.4.5 Force Orientation with Respect to Joint Facets

The force components already presented in 7.3.2 for the Mark II model were plotted against the mean profiles of the joint facets estimated from the cadaver joint profiling exercise (see Appendices 1.9 and 1.10). Figure

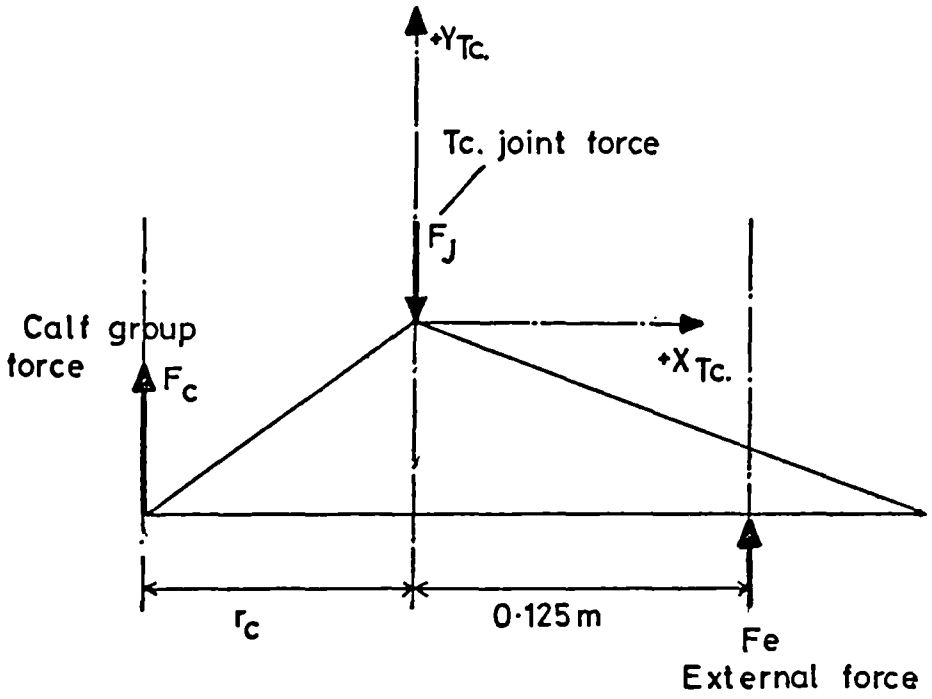

r_c (m.)	F_c^* (B.W.)	F_J^* (B.W.)
0.0583	2.1	3.35
0.0487	2.6	3.85
0.0442	2.8	4.05

* Corresponding to F_e = 1.25B.W.

Figure 7.19 Simple Model of the Foot used in Assessment of the Effect of Anthropometric Variation

7.20 shows the F_y medial and lateral Tc. forces plotted against $(F_z)_{Tc.}$. The question arises should the single F_z force component be subdivided into medial and lateral components, and if so how? The example illustrated has the F_z and lateral F_y components lumped together which leaves the medial F_y component as a single direction vector throughout stance. This looks a quite acceptable solution but clearly the medial component could just as well be combined with laterally directed F_z, and so give another possibility. The forces shown would in any case be distributed over a much wider area than the single point of contact suggests. The anteroposterior profiles, figure 7.21, indicate that the full extent of the tibial Tc. joint facet is used, and in the case of the medial facet the last few frames actually pass outwith the bounds of the cadaver joint surface (figure 7.21(b)). This is the only instance where this occurred and it was deliberately shown to emphasise that the Mark II model at early and late stance operates close to the limits of the Tc. joint capability in respect of transmitting shearing force between the shank and talus. This is an important clue towards the further development of the model discussed in 7.6.2. It also suggests that taking X-ray views of each experimental subject would have been desirable to establish with greater certainty the extent of the Tc. profiles. This would not be so useful in the case of the Tcn. profiles which are difficult to project on X-ray views. The Tcn. joint forces plotted in figures 7.22 and 7.23 show that the assumed points through which the joint forces pass, ± 0.02m. along the $Z_{Tcn.}$ axis, gave acceptable results; in no instance did the joint force pass beyond the bounds of the joint facets. The $(Y\text{-}Z)_{Tcn.}$

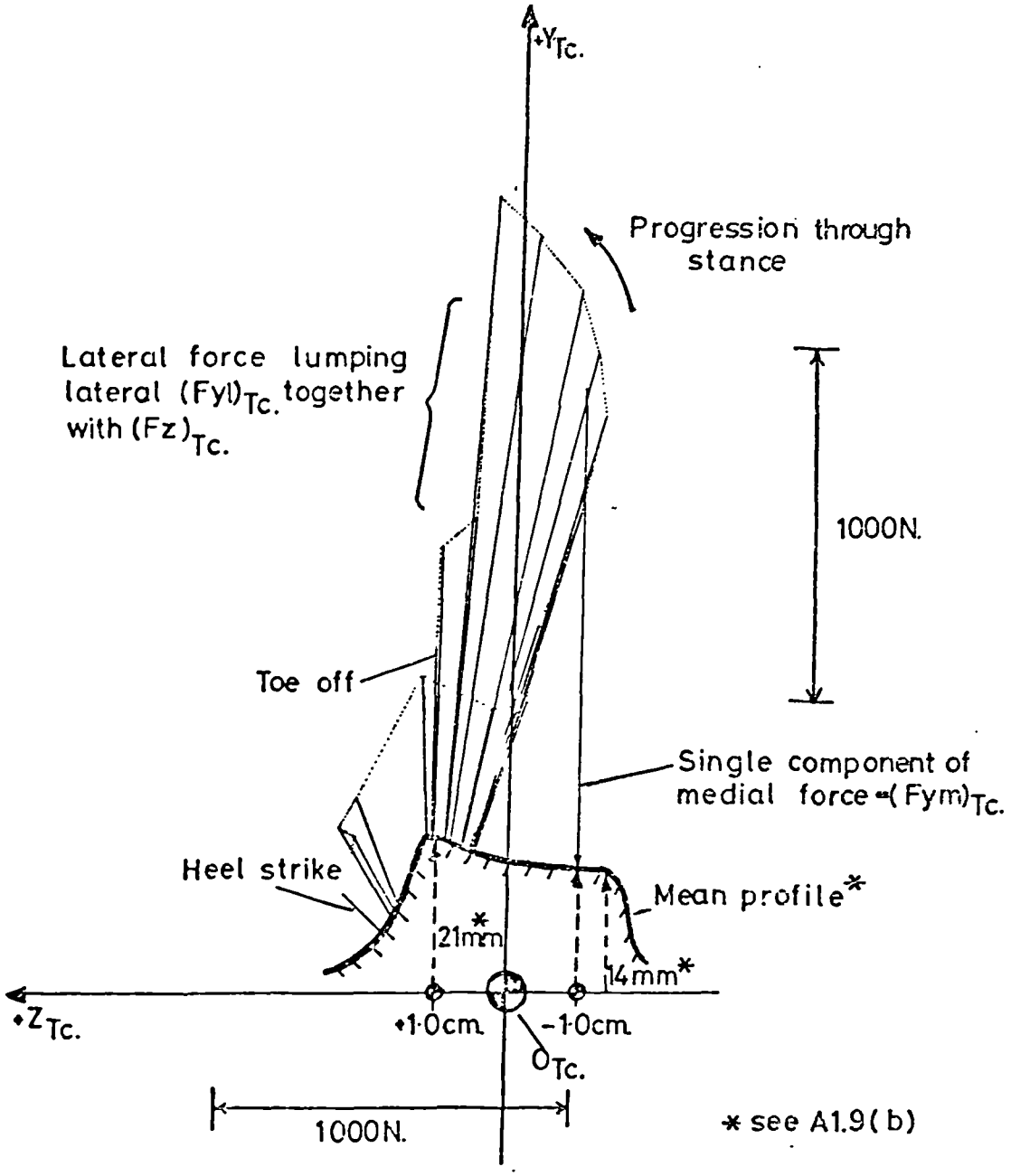

Note forces acting on the talus

Figure 7.20 Mark II Model Tc. Joint Forces for Normal Locomotion Stance Phase Superimposed upon the Mean $(Y-Z)_{Tc.}$ Profile (Subject Seven)

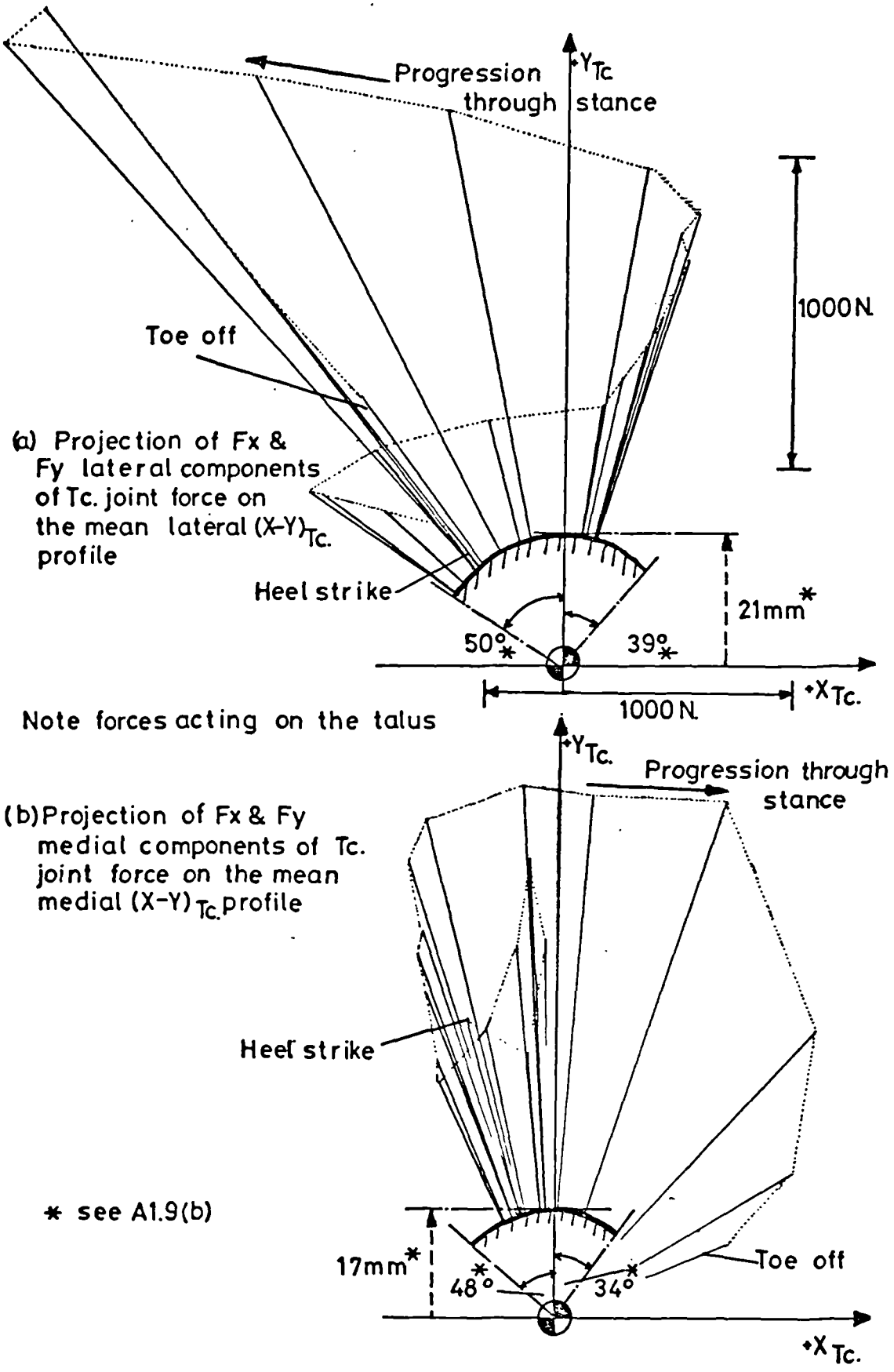

Figure 7.21 Mark II Model Tc. Joint Forces for Normal Locomotion Stance Phase Superimposed upon the Mean $(X-Y)_{Tc.}$ Profiles (Subject Seven)

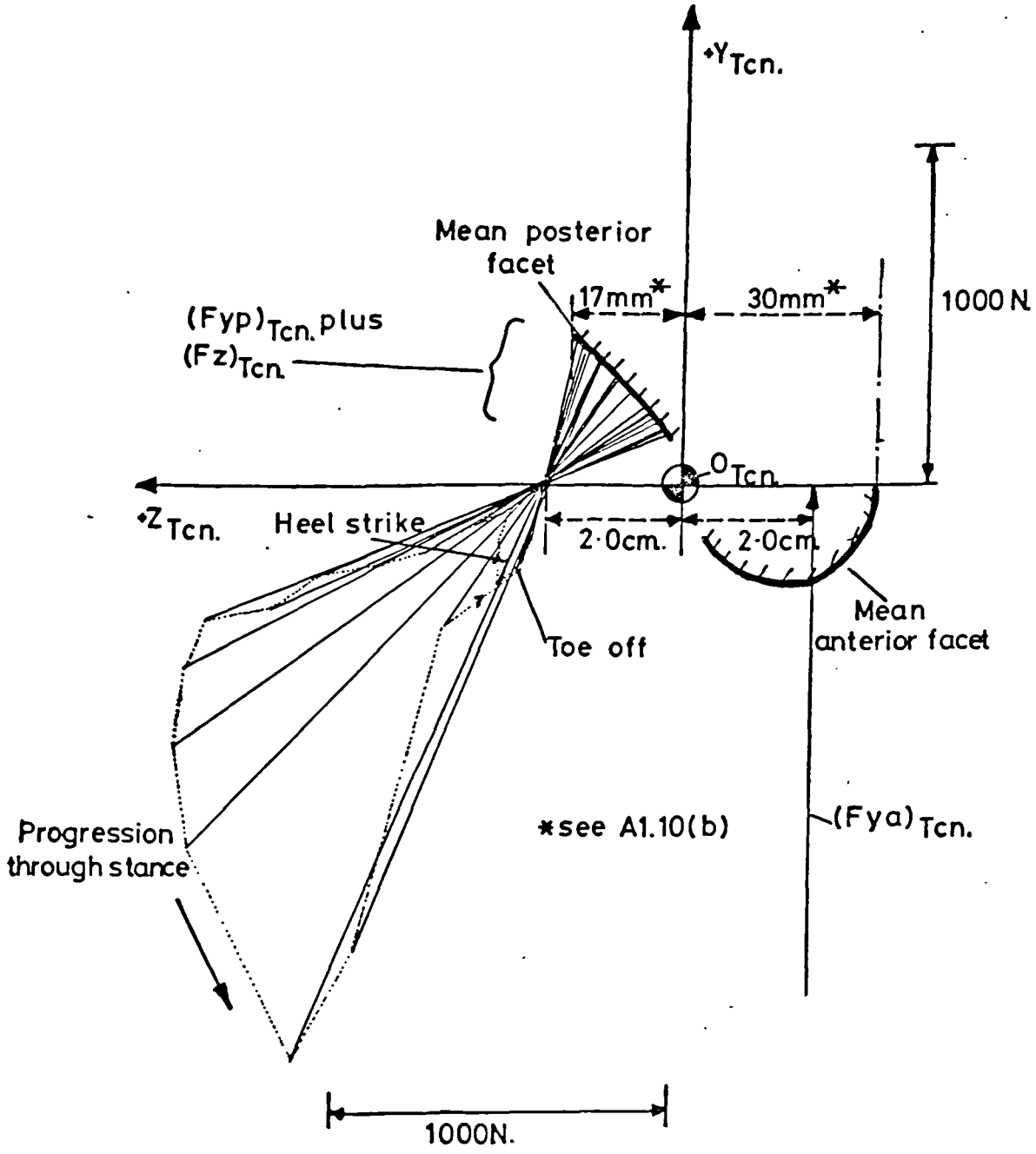

Note forces acting on the talus

Figure 7.22 Mark II Model Tcn. Joint Forces for Normal Locomotion Stance Phase Superimposed upon the Mean $(Y-Z)_{Tcn.}$ Profile (Subject Seven)

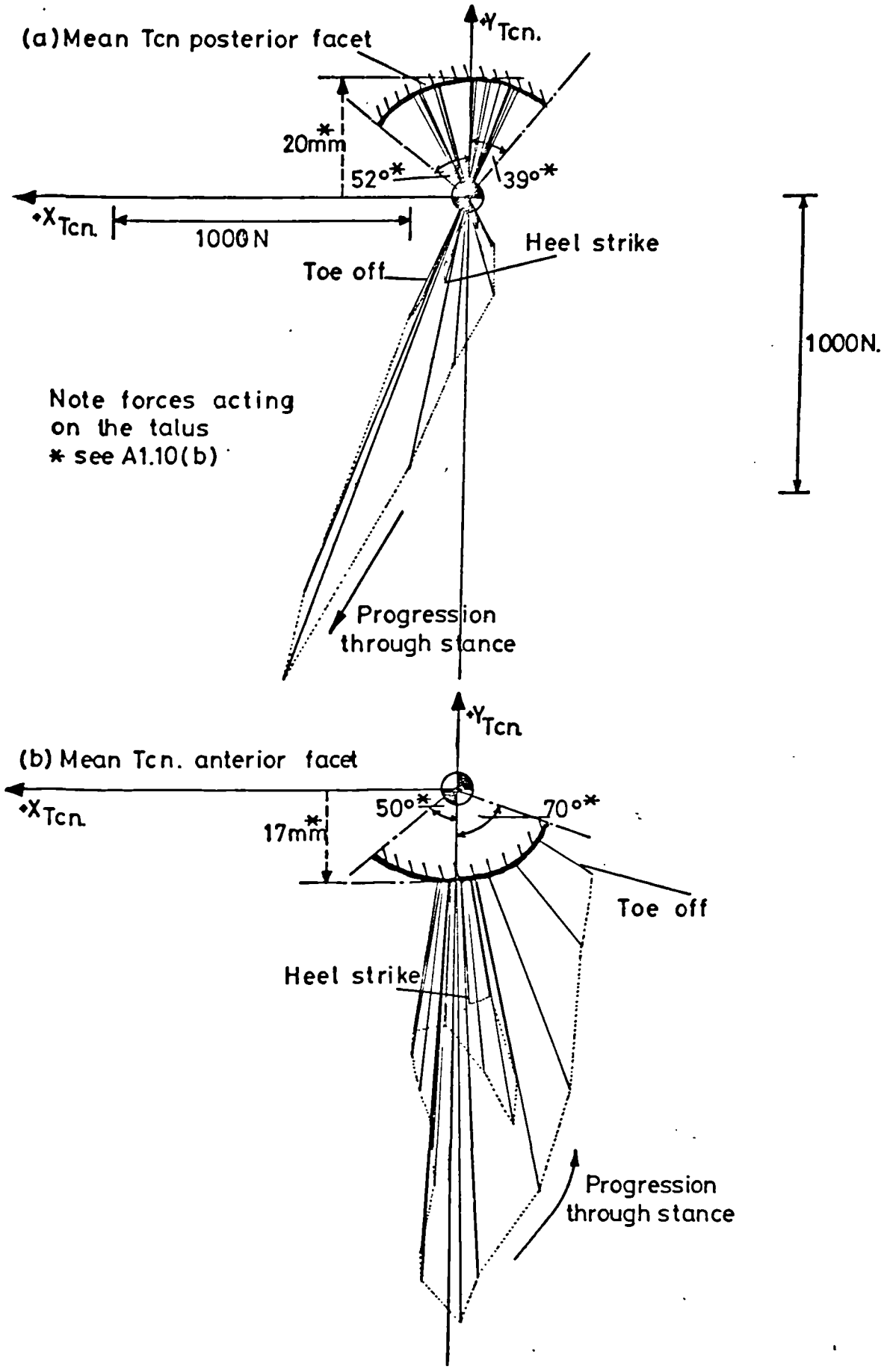

Figure 7.23 Mark II Model Tc. Joint Forces for Normal Locomotion Stance Phase Superimposed on Mean $(X\text{-}Y)_{Tcn.}$ Profiles (Subject Seven)

profile, figure 7.22, indicates that the force vectors do not pass quite normally through the posterior joint facet. It will be recalled from Elftman's screw model (illustrated in figure 2.14) for the posterior Tcn. facets that the posterior facet is helical in form. Thus the surface is more complex than the plane profile of figure 7.22 suggests. The orientation of this posterior facet changes substantially with movement along the $(X)_{Tcn.}$ axis, as the $(Y\text{-}Z)_{Tcn.}$ profiles in figure 3.15 show.

7.5 Summary of the Test Results

7.5.1 Graphic Presentation

The resultant Tc. and Tcn. joint forces and the muscle forces are plotted for all of the subjects in figures 7.25 to 7.33. The general features have already been discussed in 7.4.2.

The normal locomotion results, figures 7.25 to 7.27, show a small range of variation between subjects for Anterior tibial/Calf group resultant Tc. and posterior Tcn. joint forces, about ±0.5B.W. at the peak values. The curves are quite similar in form as well as magnitude. There is some greater variation apparent in the resultant anterior Tcn. joint force and the Posterior tibial and Peroneal group muscle forces.

The -10° side slope curves, figures 7.28 to 7.30, show two additional features, slight increases in the peak forces and much greater variation in the Posterior tibial/Peroneal group muscle forces - range of ≃ 5B.W. instead of 3B.W. for normal locomotion.

The +10° side slope (right, test, foot uphill) results were obtained for only four subjects; in three cases markers were obscured from one camera by the side

Subject	Symbol	Mean Velocity (m./s.)		
		Normal locomotion	-10° Side slope	+10° Side slope
1	———	1.50	1.56	-
2	—·—·—	1.46	1.32	1.18
3	— — —	1.24	1.23	-
4	——·—·——	1.23	1.38	1.23
5	—·—·—	1.64	1.63	1.63
6	——··——	1.84	2.14	1.73
7	—— ——	1.36	1.24	-

Figure 7.24 Key to figures 7.25 to 7.33

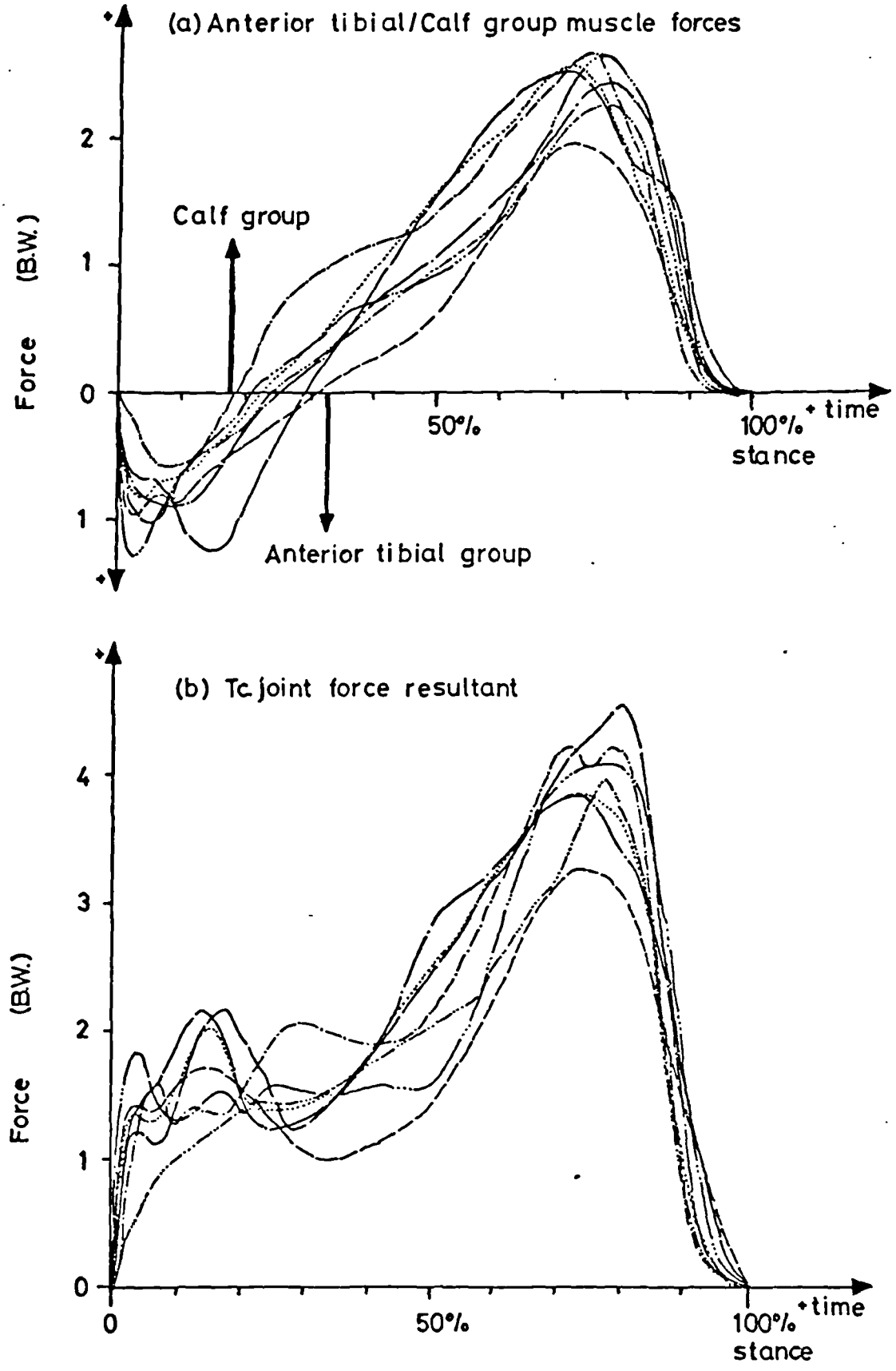

Figure 7.25 Normal Locomotion Test - Summary of Results

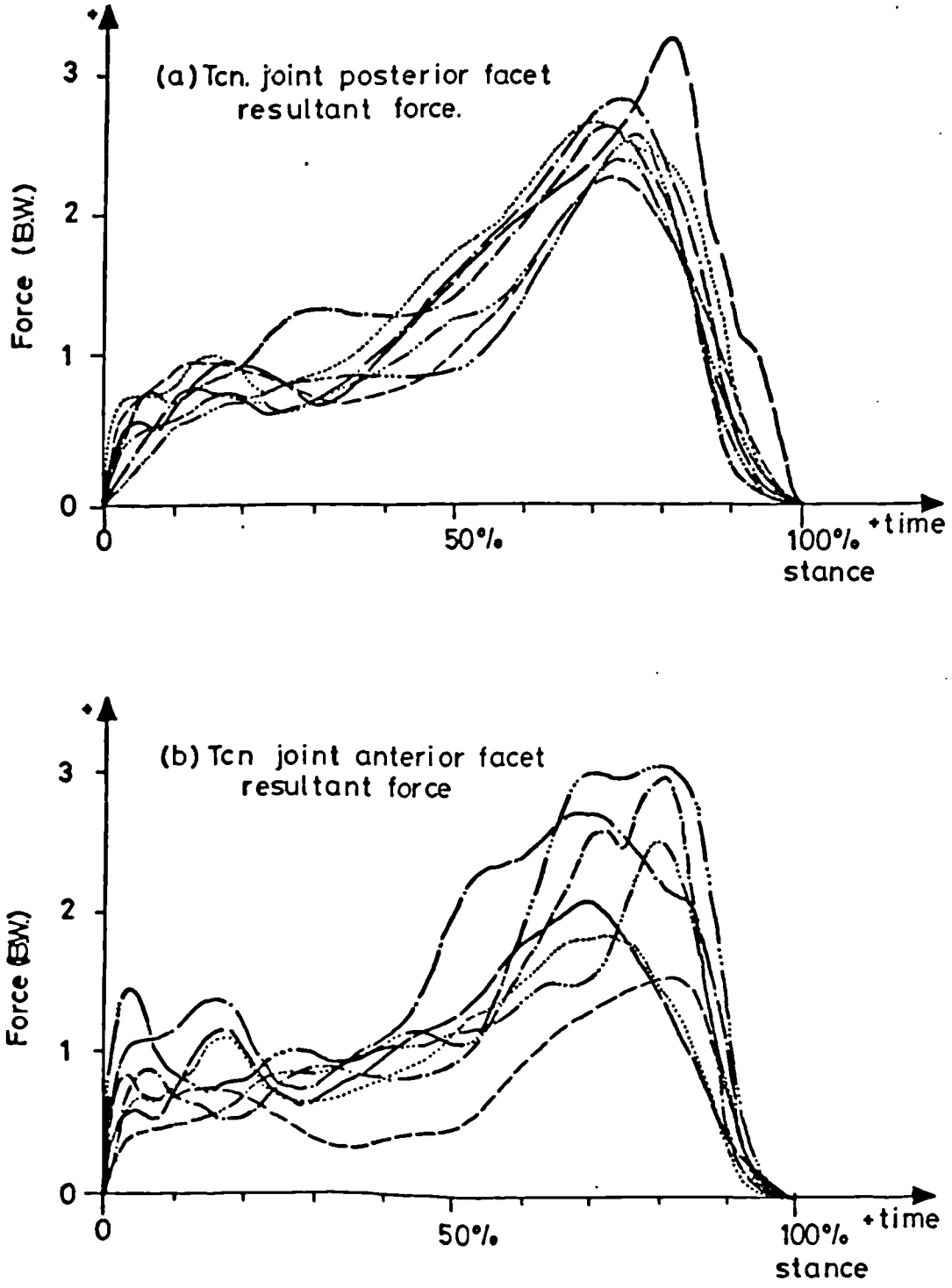

Figure 7.26 Normal Locomotion Test - Summary of Results

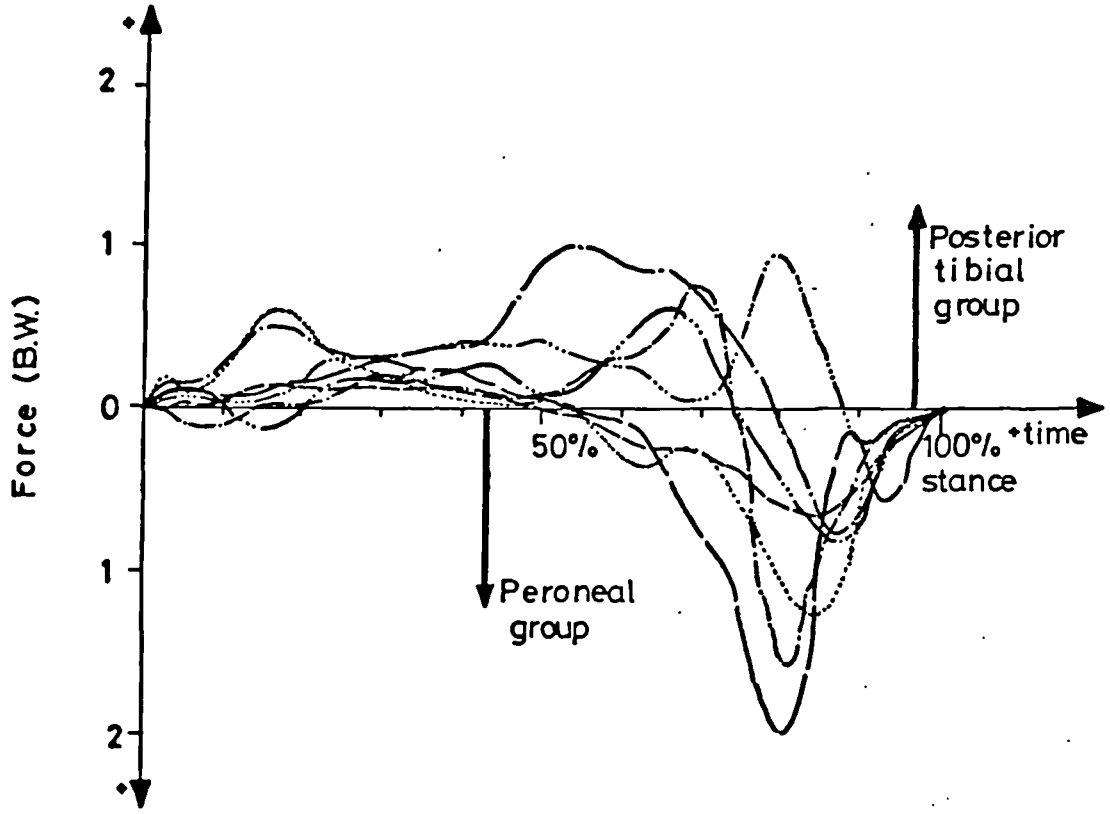

Figure 7.27 Normal Locomotion Test - Summary of Results

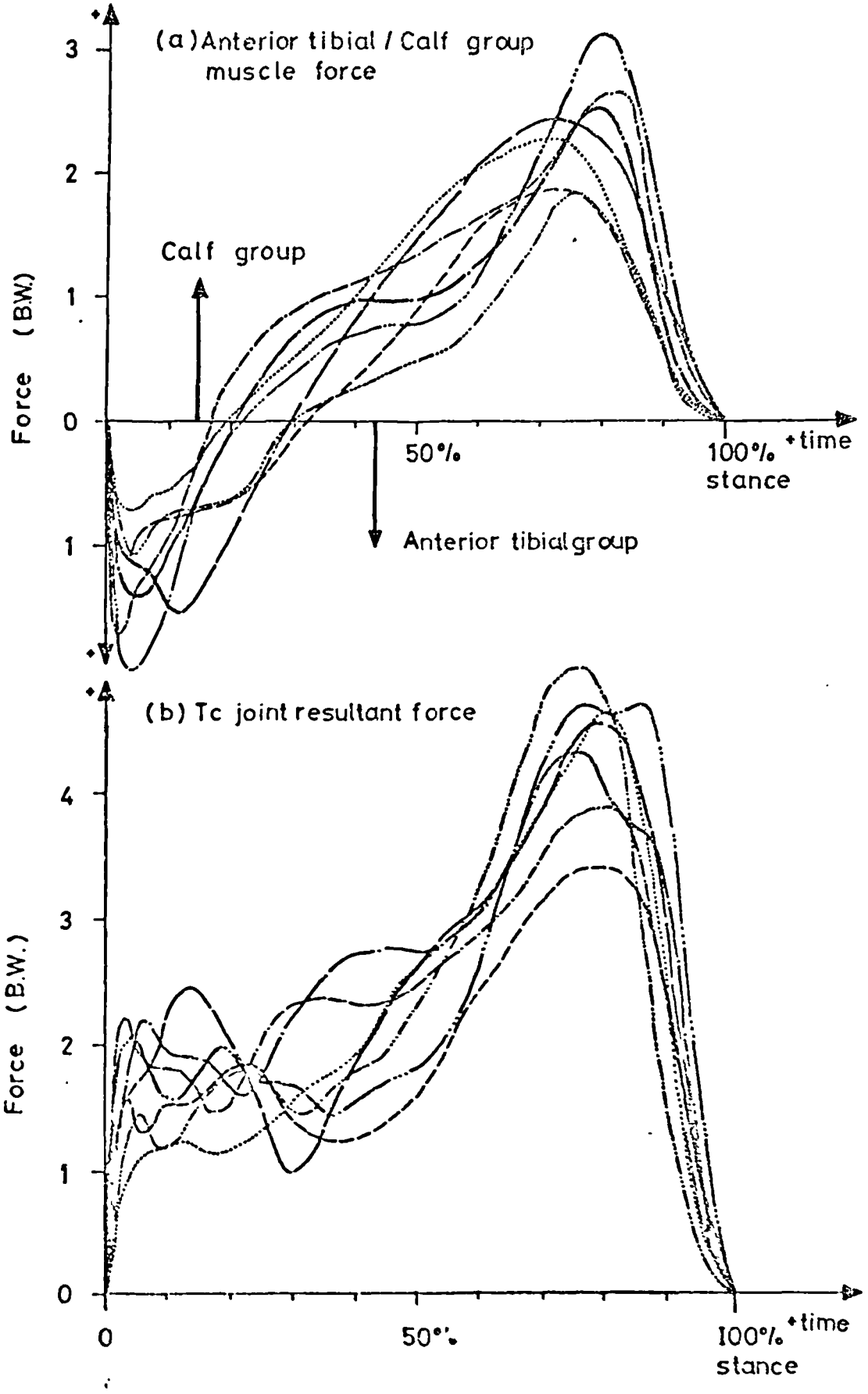

Figure 7.28 -10° Side Slope Locomotion Test (Test Foot Downhill) - Summary of Results

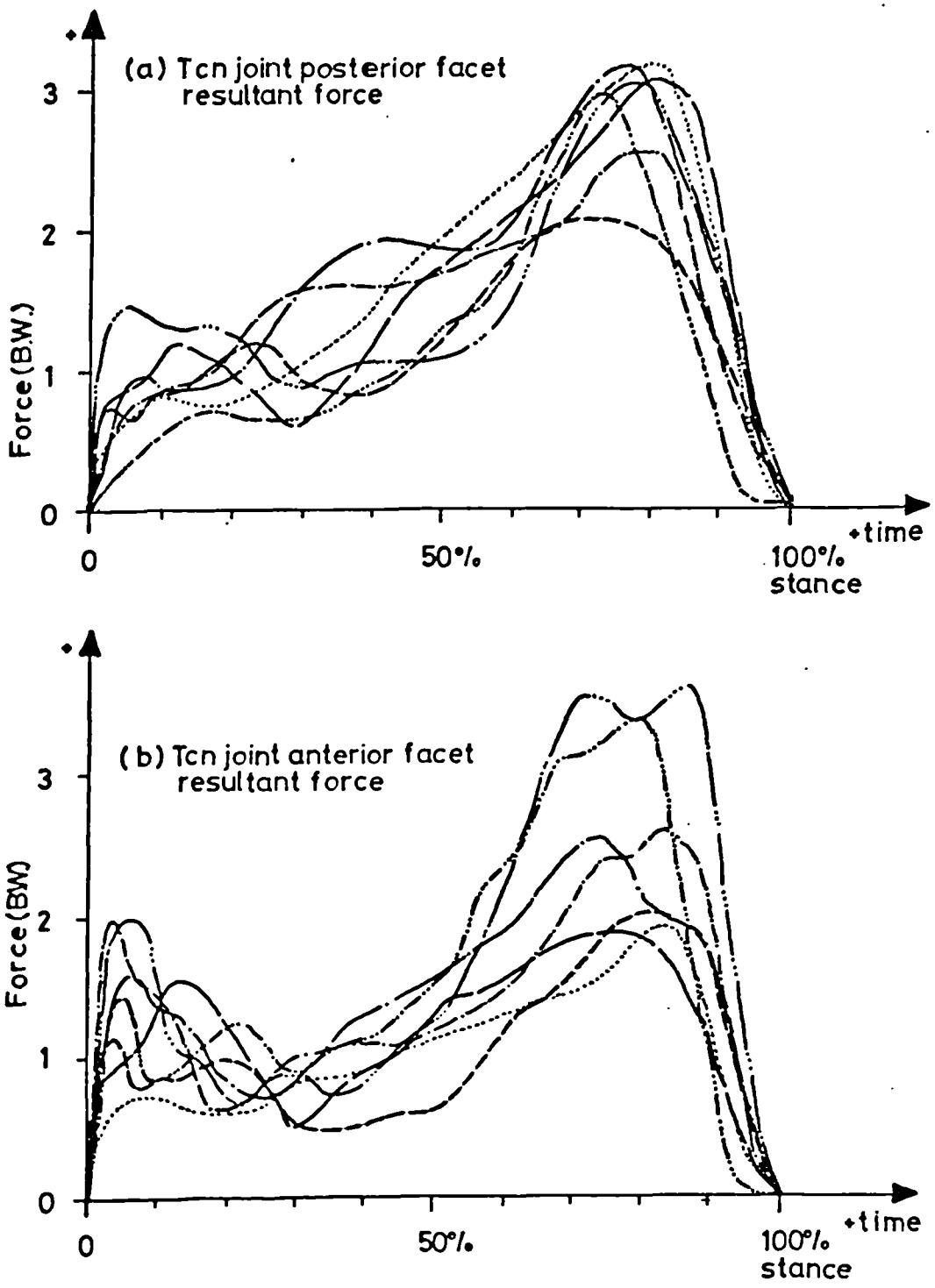

Figure 7.29 -10° Side Slope Locomotion Test (Test Foot Downhill) - Summary of Results

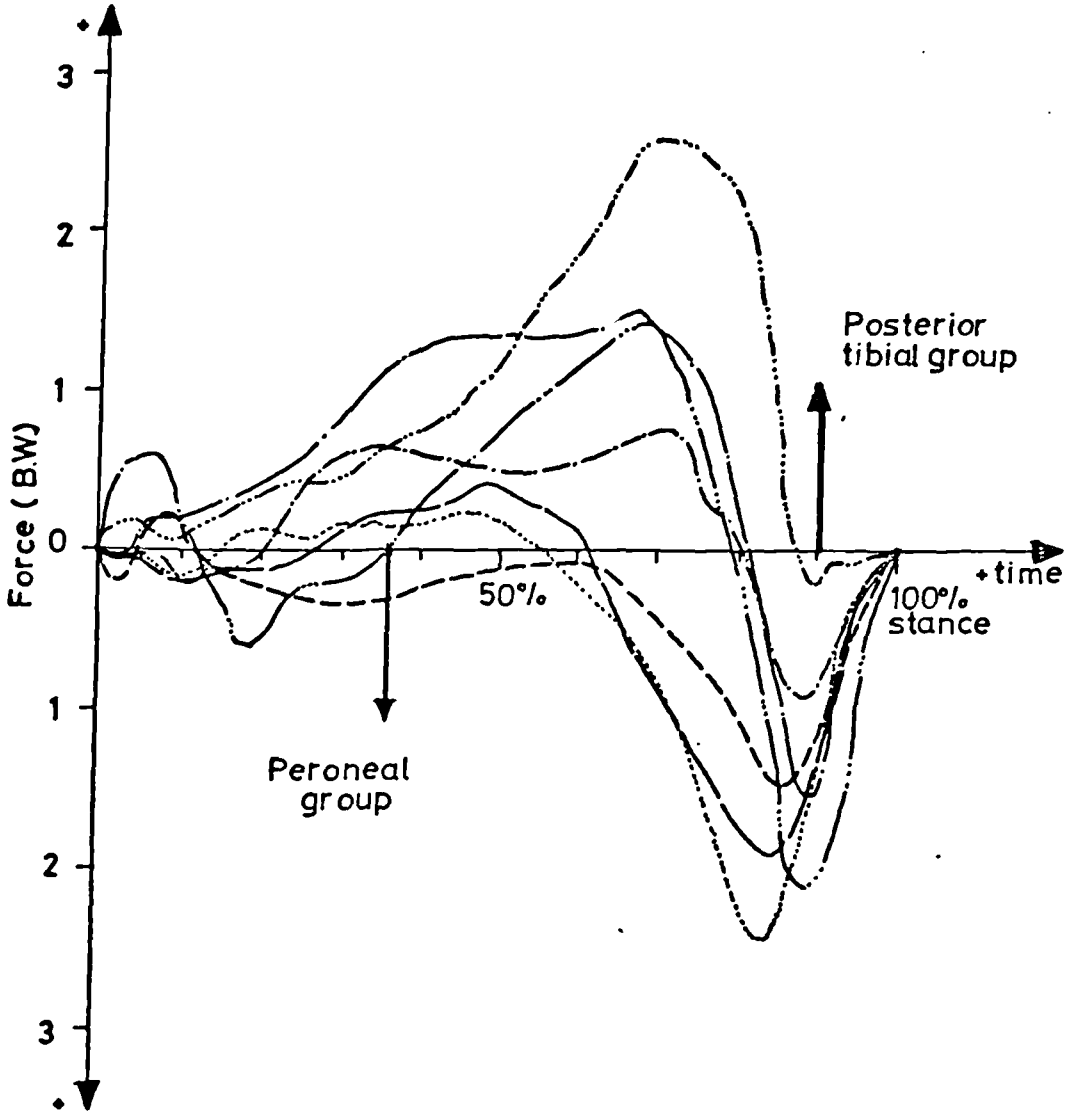

Posterior tibial / Peroneal group muscle force

Figure 7.30 -10° Side Slope Locomotion Test (Test Foot Downhill) - Summary of Results

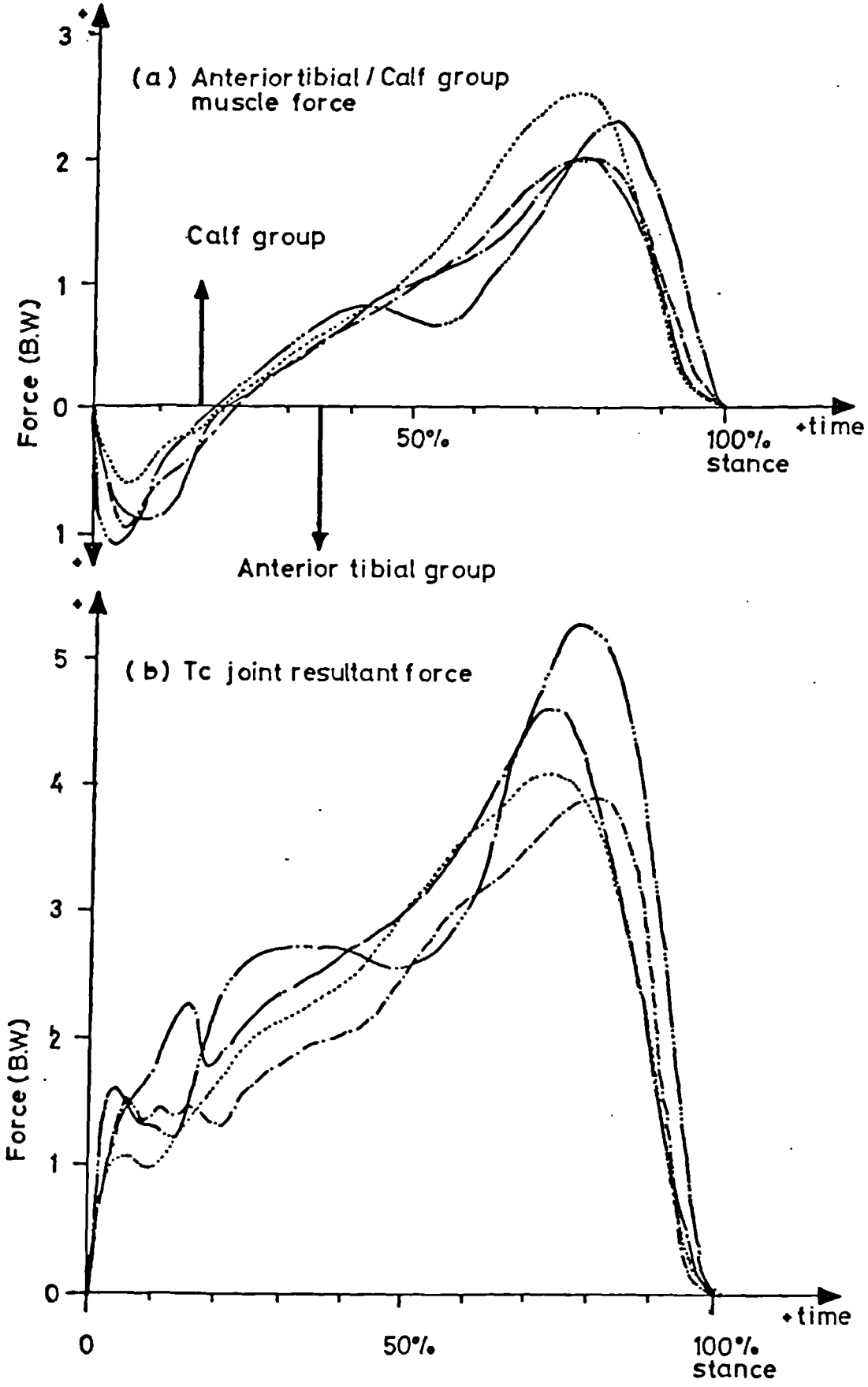

Figure 7.31 +10° Side Slope Locomotion Test (Test Foot Uphill) - Summary of Results

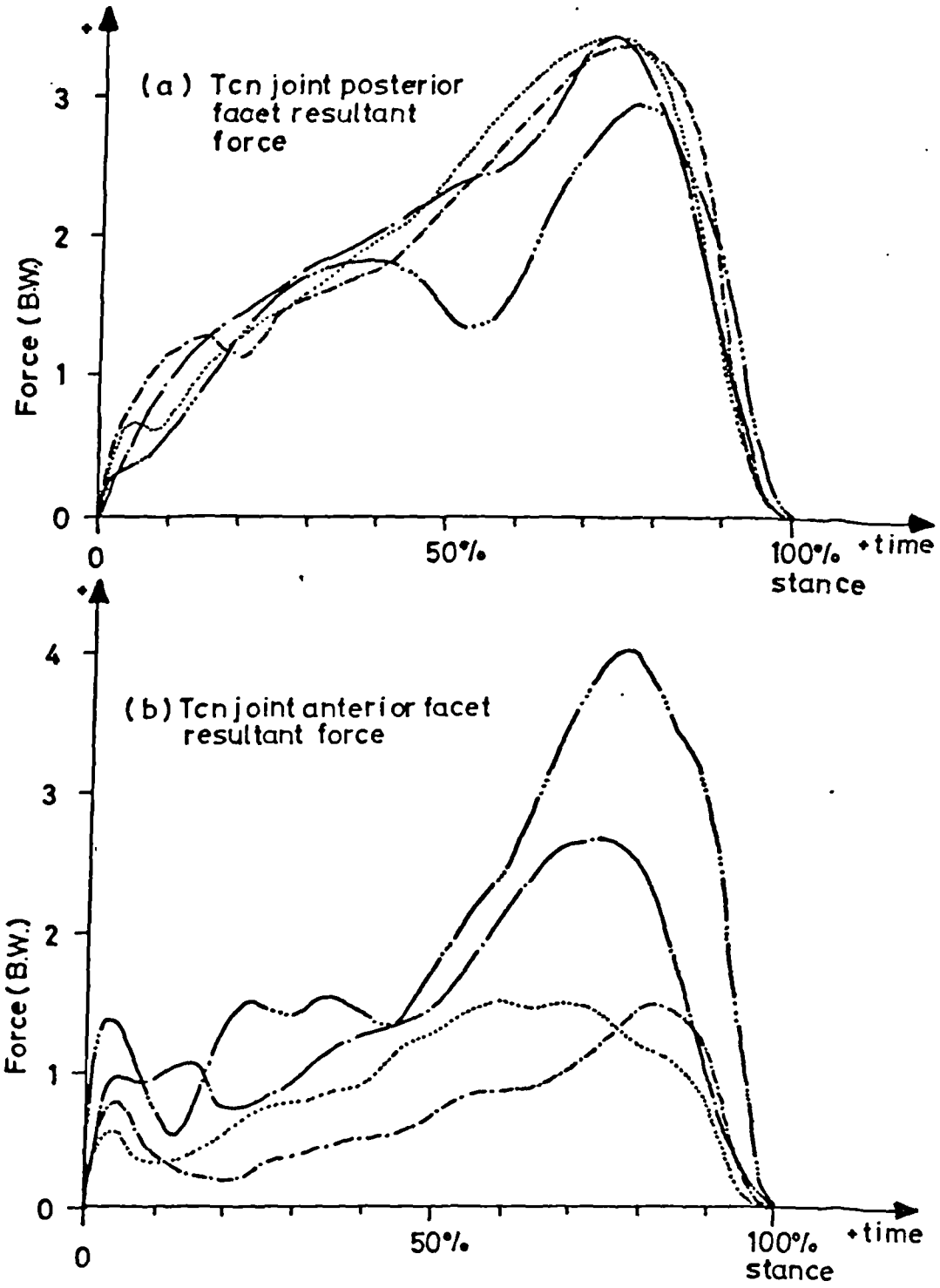

Figure 7.32 +10° Side Slope Locomotion Test (Test Foot Uphill) - Summary of Results

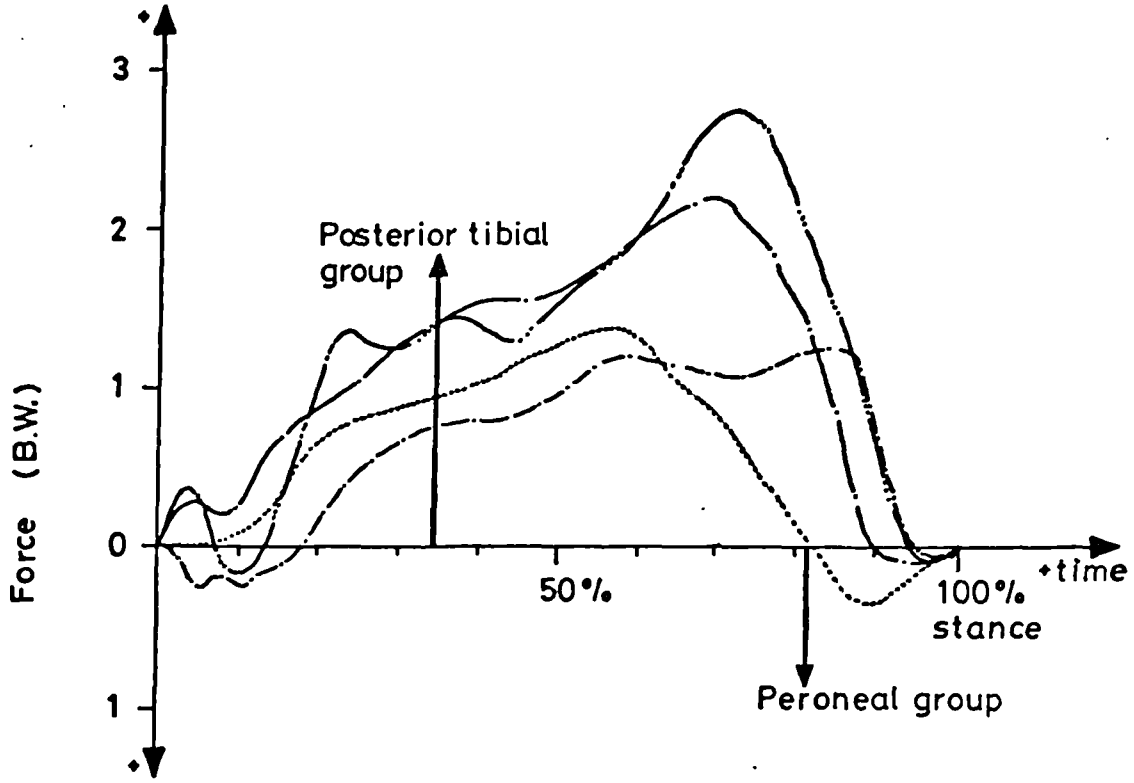

Posterior tibial/Peroneal group muscle force

Figure 7.33 +10° Side Slope Locomotion Test (Test Foot Uphill) - Summary of Results

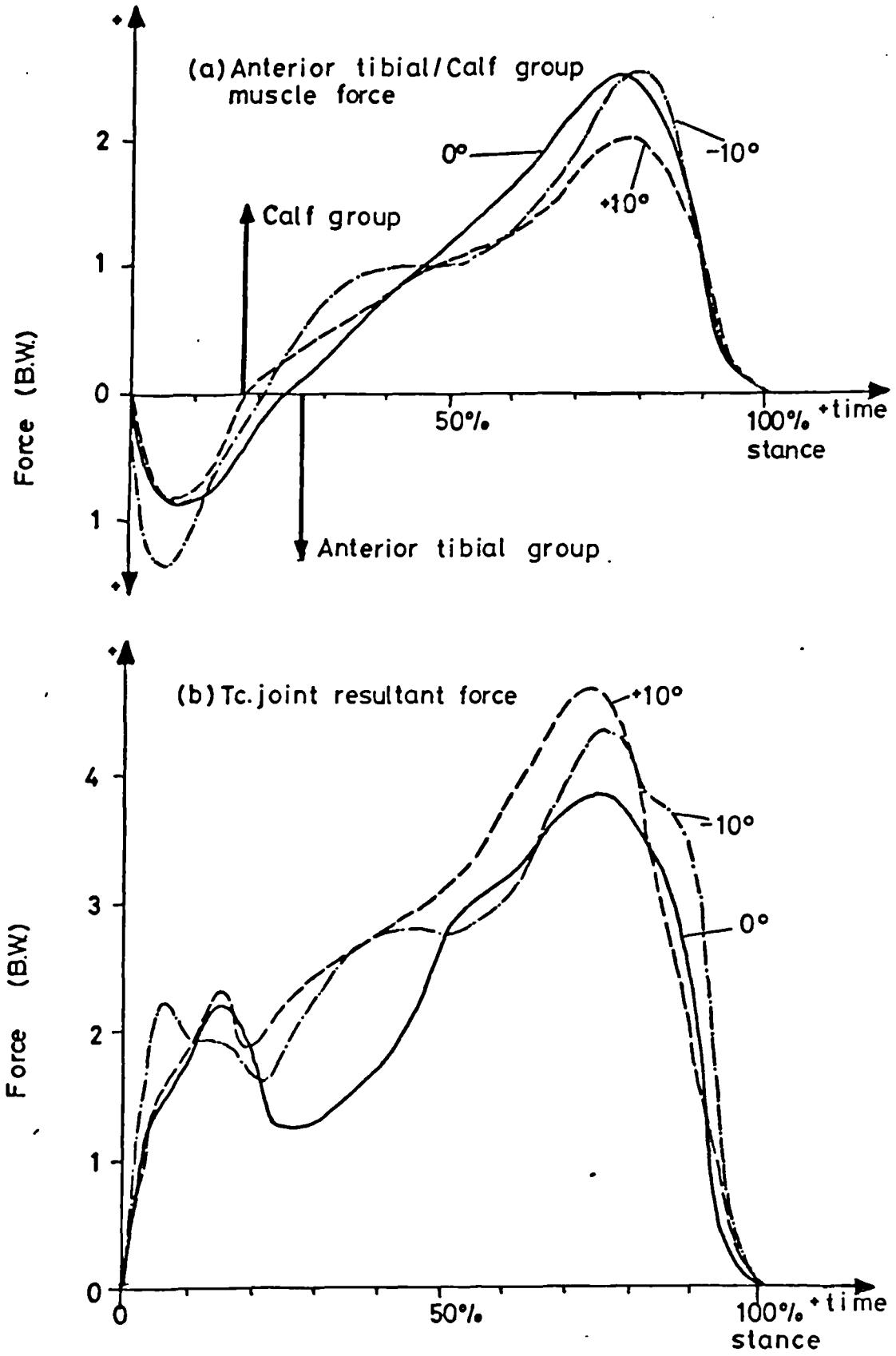

Figure 7.34 Comparison of Normal and Side Slope Locomotion Test Results for Subject Five

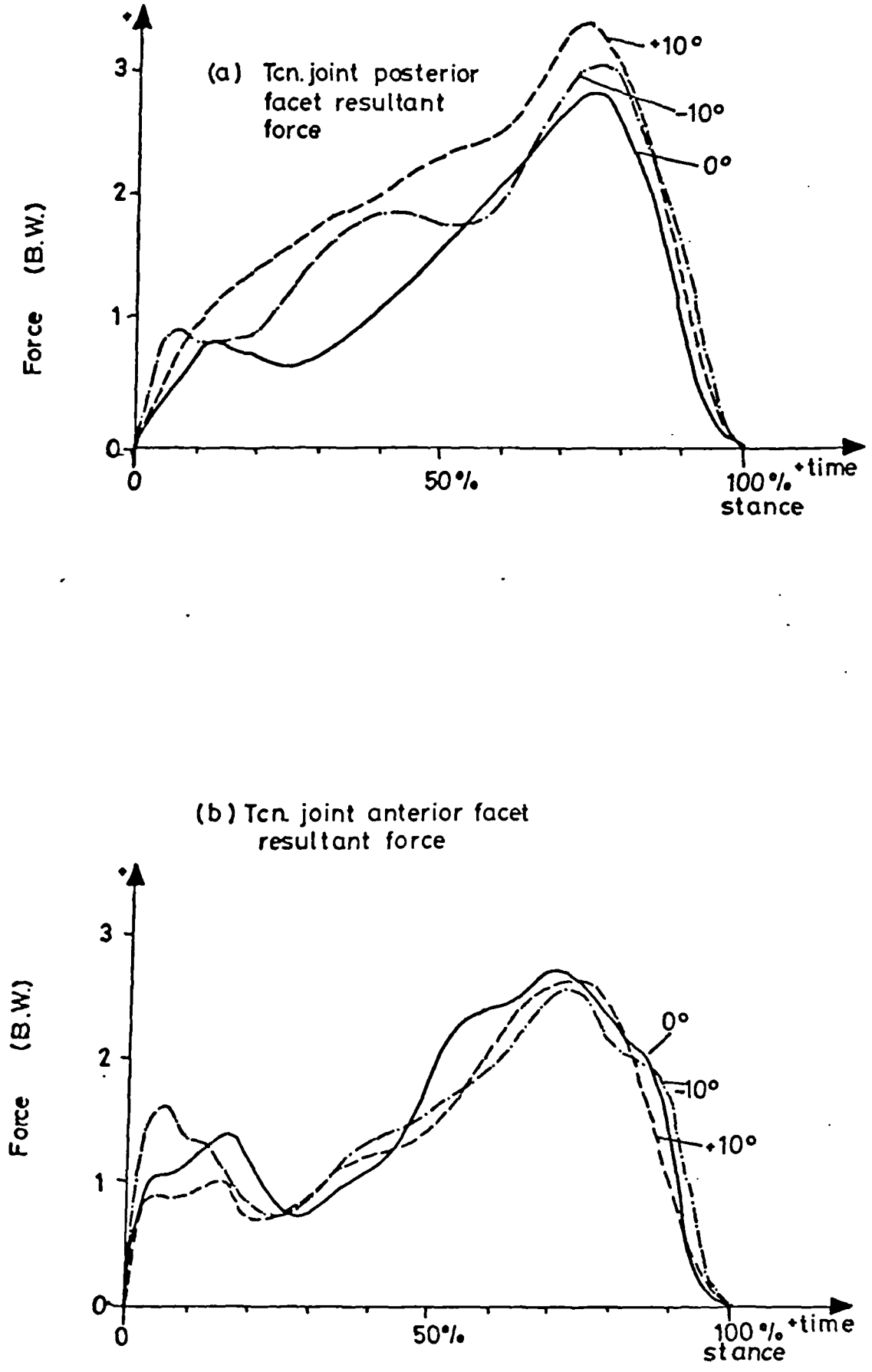

Figure 7.35 Comparison of Normal and Side Slope Locomotion Test Results for Subject Five

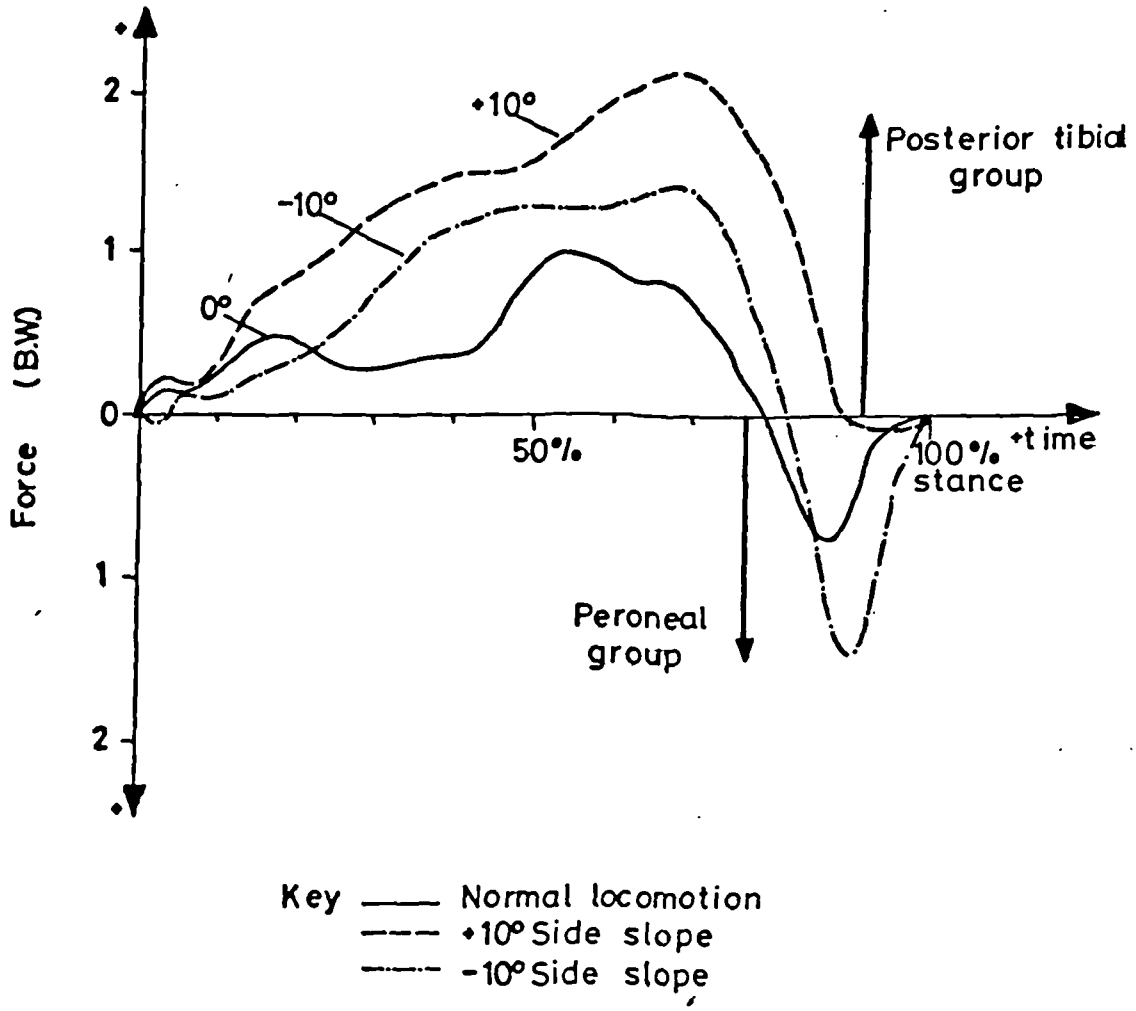

Posterior tibial/Peroneal group force

Figure 7.36 Comparison of Normal and Side Slope Locomotion Test Results for Subject Five

slope ramp. The general remarks made about normal locomotion are still considered to apply; additional features are slightly greater peak values, a wider range of resultant anterior Tcn. facet joint force at the peak late in stance and a shift towards Posterior tibial group activity for most of stance.

7.4.2 Tabulated Results

The peak values occurring through stance phase for normal locomotion, +10° and -10° side slope are tabulated in tables 7.3 to 7.11. The temporal data for the peak values is also presented. Mean values were calculated for overall comparison of side slope with normal locomotion.

The peak resultant Tc. joint force was 3.88B.W. for normal locomotion (range 2.9 to 4.67B.W.) which was less than the values obtaining for -10°—4.36B.W. (range 3.39-5.03) and +10°—4.50B.W. (range 3.89-5.32). The phasing of this peak was consistently about 80%, see table 7.3.

The anterior Tcn. facet joint force resultant peak value was very similar for -10°, +10° and normal locomotion, the latter value being 2.43B.W. (range 1.58-3.14) see table 7.4. The phasing of the peak was at 80%. So although the visual impression was of a wider range of peak values for -10° side slope, the mean values were much the same as normal locomotion.

The posterior Tcn. facet joint force resultant showed a similar result, the mean peak results for -10° and normal locomotion being quite close. The normal locomotion result, table 7.5, was 2.84B.W. (range 2.34-3.40B.W.), at about 80% stance phase.

The mean peak muscle forces were 2.46B.W. (range 1.96-2.73B.W.) and 0.99B.W. (range 0.84-1.33B.W.) for

Table 7.3 Peak Resultant Tc. Joint Force

	Peak Force (B.W.)			Phasing of Peak % Stance		
	-10°	0°	+10°	-10°	0°	+10°
Subject						
1	3.39	3.29	-	78	80	-
2	3.89	4.27	3.89	81	79	82
3	5.03	4.00	-	75	85	-
4	4.63	3.89	4.15	81	77	75
5	4.32	2.91	4.65	76	79	76
6	4.72	4.17	5.32	86	83	80
7	4.55	4.67	-	80	82	-
Mean	4.36	3.88	4.50	79	81	78

Table 7.4 Peak Resultant Tcn. Anterior Facet Force

	Peak Force (B.W.)			Phasing of Peak % Stance		
	-10°	0°	+10°	-10°	0°	+10°
Subject						
1	2.00	1.58	-	78	86	-
2	2.69	2.99	1.46	86	85	87
3	3.45	2.55	-	79	85	-
4	1.93	1.87	1.49	81	75	72
5	2.59	2.75	2.64	73	73	76
6	3.69	3.14	3.97	86	83	80
7	1.89	2.14	-	75	72	-
Mean	2.65	2.43	2.39	82	79	79

Table 7.5 Peak Resultant Tcn. Posterior Facet Force

	Peak Force (B.W.)			Phasing of Peak % Stance		
	-10°	0°	+10°	-10°	0°	+10°
Subject						
1	2.07	2.34	-	73	77	-
2	2.57	2.70	3.37	81	76	79
3	2.96	2.67	-	75	83	-
4	3.15	2.76	3.50	78	72	75
5	3.14	2.91	3.45	76	79	76
6	3.01	3.14	2.98	79	83	80
7	3.08	3.40	-	82	83	-
Mean	2.85	2.84	3.32	78	79	77

Table 7.6 Peak Anterior Tibial Group Force

	Peak Force (B.W.)			Phasing of Peak % Stance		
	-10°	0°	+10°	-10°	0°	+10°
Subject						
1	1.61	1.00	-	6	6	-
2	1.72	1.00	0.84	5	9	8
3	1.08	0.60	-	6	7	-
4	0.70	0.84	0.57	7	7	7
5	1.44	0.91	0.89	9	12	8
6	2.00	1.33	0.92	7	7	10
7	1.56	1.28	-	14	17	-
Mean	1.44	0.99	0.80	8	9	8

Table 7.7 Peak Calf Group Force

	Peak Force (B.W.)			Phasing of Peak % Stance		
	-10°	0°	+10°	-10°	0°	+10°
Subject						
1	1.84	1.96	-	76	77	-
2	2.65	2.73	1.93	84	79	82
3	1.81	2.26	-	77	83	-
4	2.24	2.57	2.55	71	71	80
5	2.49	2.45	1.91	82	78	82
6	3.04	2.71	2.26	92	79	86
7	2.40	2.55	-	73	75	-
Mean	2.35	2.46	2.16	79	77	82

Table 7.8 Peak Posterior Tibial Group Force

	Peak Force (B.W.)			Phasing of Peak % Stance		
	-10°	0°	+10°	-10°	0°	+10°
Subject						
1	0.25	0.16	-	12	23	-
2	0.70	0.80	1.23	70	73	87
3	2.63	0.97	-	71	83	-
4	0.22	0.61	1.42	46	20	60
5	1.47	1.05	2.17	70	59	71
6	1.47	0.68	2.66	69	31	73
7	0.40	0.32	-	50	32	-
Mean	1.01	0.66	1.87	55	45	73

Table 7.9 Peak Peroneal Group Force

	Peak Force (B.W.)			Phasing of Peak % Stance		
	-10°	0°	+10°	-10°	0°	+10°
Subject						
1	1.49	0.60	-	88	86	-
2	0.89	1.60	0.26	89	81	8
3	0.21	0.22	-	92	94	-
4	2.39	1.26	0.38	83	87	89
5	1.53	0.78	0.09	91	91	94
6	2.12	0.85	0.17	90	93	13
7	1.90	2.09	-	86	90	-
Mean	1.50	1.06	0.22	86	89	51

Table 7.10 Temporal Change from Anterior Tibial to Calf Group

	Phasing (% Stance Phase)		
	-10°	0°	+10°
Subject	%	%	%
1	35	35	-
2	18	22	24
3	28	22	-
4	20	24	19
5	23	25	19
6	26	22	18
7	31	31	-
Mean	26	26	20

Table 7.11 Phasing of the Peroneal/Posterior Tibial Groups

	Phasing (% Stance)		
	-10°	0°	+10°
Subject			
1	0 P 6 PT 12 P 100%	0 PT 53 P 100%	
2	0 P 23 PT 80 P 100%	0 PT 75 P 100%	0 P 19 PT 100%
3	0 PT 90 P 100%	0 PT 90 P 100%	
4	0 P 18 PT 46 P 100%	0 PT 56 P 100%	0 P 10 PT 82 P 100%
5	0 PT 80 P 100%	0 PT 84 P 100%	0 PT 91 P 100%
6	0 P 40 PT 77 P 100%	0 PT 14 P 22 PT 74 P 100%	0 PT 6 P 12 PT 100%
7	0 P 31 PT 60 P 100%	0 PT 55 P 100%	

Calf and Anterior tibial groups, respectively, in normal locomotion; the mean peak for Anterior tibial being at 10% and that for the Calf being at 80%. These results were not found to be substantially different for the side slope tests, see tables 7.7 and 7.8.

The main differences between the side slope and normal locomotion tests concern the magnitude and temporal phasing of the Peroneal and Posterior tibial groups. The mean peak value of the Posterior tibial group in normal locomotion was 0.66B.W. (range 0.16-1.05B.W.); it increased to 1.01B.W. (range 0.22-2.63B.W.) for -10° and 1.87B.W. (range 1.23-2.66B.W.) for +10° side slope locomotion. There was wide variation in the mean phasing of these peaks as table 7.8 shows.

The mean peak value of the Peroneal group was 1.06B.W. (range 0.22-2.09B.W.); it increased to 1.50B.W. (range 0.21-2.59B.W.) for -10° side slope but reduced to 0.22B.W. (range 0.09-0.38B.W.) for +10° side slope. The mean phasing of the peak was 85-90% stance for normal locomotion and -10° side slope but 51% for +10° side slope.

(The graphic comparison of normal locomotion and side slope locomotion has been plotted separately for subject five, graphs in figures 7.34 to 7.36.)

The phasic relations between the muscle groups were tabulated in tables 7.10 and 7.11. Those for the Anterior tibial/Calf group are straightforward, there being only one transition from the former to the latter at 20-25% stance phase.

The Posterior tibial and Peroneal groups deserve further discussion since as table 7.11 shows there is considerable variation in their activity. Figure 7.37 , illustrating temporal activity, should help to clarify

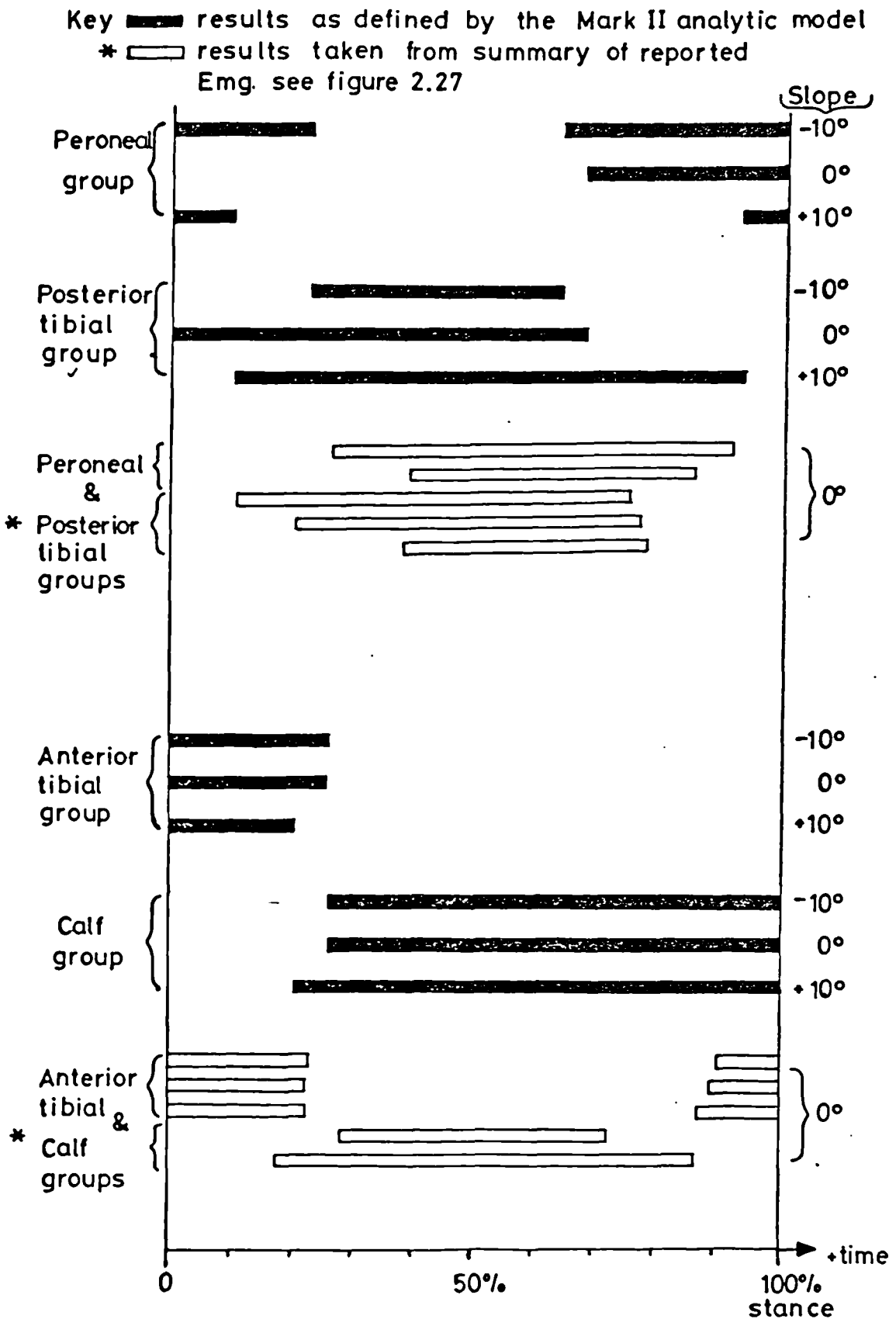

Figure 7.37 Comparison of Temporal Activity of the Shank Muscle Groups, as Defined by the Analytical Model with Temporal Emg. Reported in 2.7.3.

the results. For normal locomotion the Posterior tibial group has a long active period from 0-68% mean followed by Peroneal activity from 68-100% stance phase. In -10° side slope five subjects show an early Peroneal phase 0-23% mean stance, and all seven show a late Peroneal phase 64-100% mean stance, the interval between being Posterior tibial activity. The +10° side slope indicates a long Posterior tibial group period from 10-94% mean and some Peroneal activity either side. The Posterior tibial activity predicted by the model for normal locomotion compares favourably with the temporal Emg. results reported in figure 2.27. The late stance phase Peroneal group activity for normal locomotion also compares well with the temporal Emg. summarised for the Peroneal group in figure 2.27.

The Anterior tibial/Calf temporal activity indicated for normal locomotion by the model agrees very well with the temporal Emg. with the exception that the Calf extends up to 100% stance, and there was no evidence of late stance Anterior tibial group activity.

It should be remembered with this type of temporal comparison, that the reported Emg. results are often conflicting and inconsistent. In addition, the latency period of up to 0.1 seconds (reported in 2.7.1) indicates that exact comparison of Emg. and corresponding muscular force is not possible.

7.5.3 Some Interpretations of Side Slope Walking

There are four relevant results to consider; firstly the established result from Wright et al (1964) (figure 2.32) that walking on a negative slope - test foot downhill - shifts the Tcn. axis towards inversion and walking on a

positive slope - test foot uphill - shifts the Tcn. axis towards eversion.

The Centre of pressure results (7.3) indicated that negative slope resulted in a medial shift in the centre of pressure path, a positive slope reversing this trend.

Then the impression from the phasic activity of the Peroneal/Posterior tibial groups, figure 7.37, is that going from negative to positive slope (-10° +10°) the Peroneal group, in general, is less active, whilst the Posterior tibial group extends from occupying 40% to 85% of the mid portion of stance.

Finally, for +10° the mean peak Posterior tibial group force (1.87B.W.) was greater than the mean Peroneal group force (0.22B.W.), and for -10° the positions reversed (1.01B.W.) and (1.50B.W.) respectively. The dominant group mean peak in each instance was greater than the mean peak values tabulated for normal locomotion in tables 7.8 and 7.9.

The eversion angular shift and centre of pressure lateral displacement are geometric consequences of maintaining erect posture whilst the foot and ankle joints adapt to positive side slope. Eversion is a stable position for the ankle Tcn. joint; the stability requirement for Peroneal/Posterior tibial activity is therefore small, but the lateral shift in the point of application of the external force places an increased demand on the Posterior tibial group, hence the larger values for +10° side slope. These ideas are represented in figure 7.38(a).

The inversion angular shift and medialward shift of the centre of pressure path associated with negative slope locomotion bring the foot to a situation where the ankle Tcn. joint is less stable than in normal locomotion.

(a)Positive side slope ,+10°, test(right)foot uphill

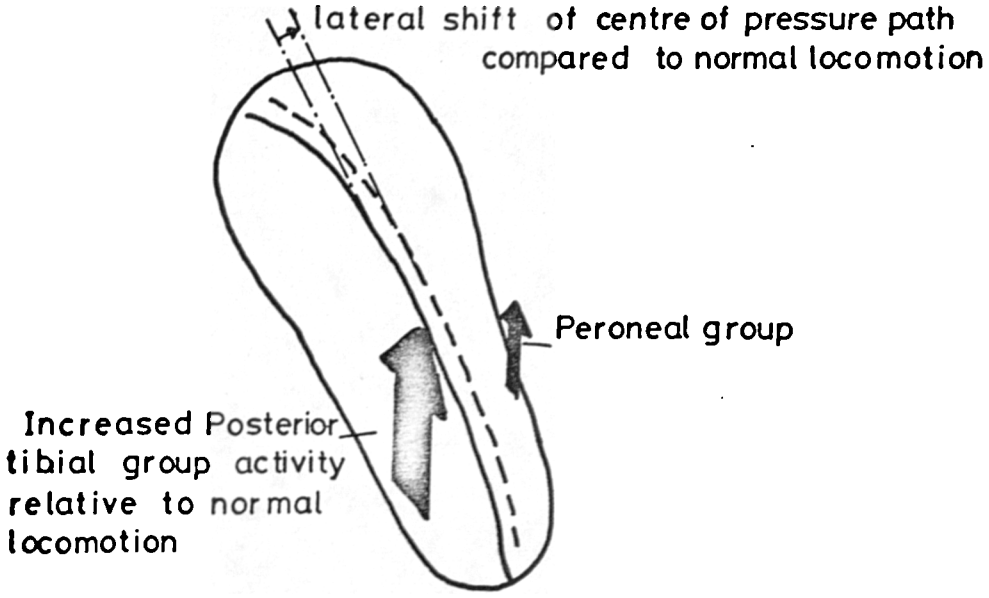

(b)Negative side slope,-10°, test(right) foot downhill

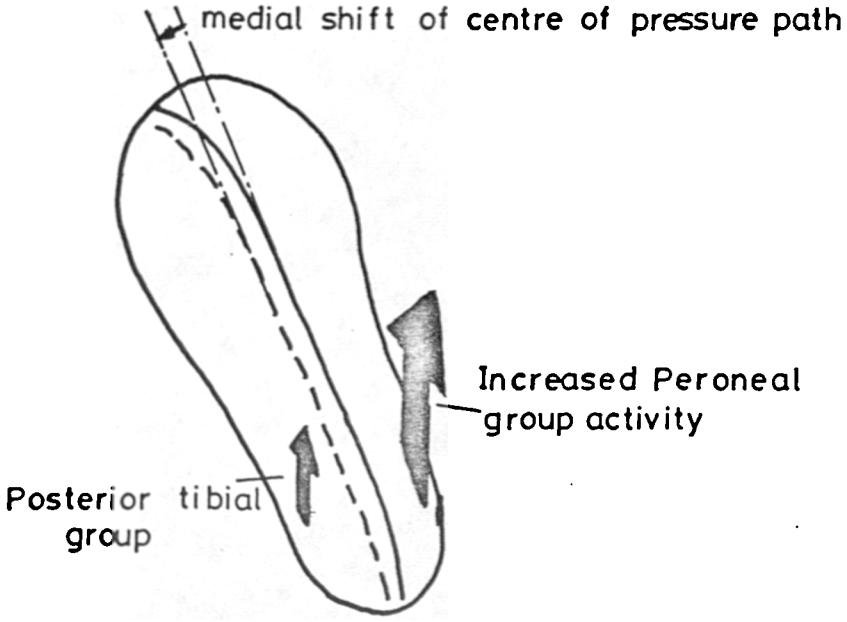

Figure 7.38 Graphic Interpretation of the Main Effects of Side Slope Locomotion on Peroneal/Posterior Tibial Group Activity and Centre of Pressure Path

There is therefore a greater requirement for stabilising actions on the part of the Peroneal and Posterior tibial groups. This occurs in particular towards the end of stance where the kinematics of the Tcn. joint normally indicate inversion in addition to that due to the side slope. The Peroneal group are particularly active at the end of stance for this reason, represented in figure 7.38(b).

There are of course other possible interpretations, and it is accepted that the test sample size is small, so these views are tentative suggestions. Notwithstanding these reservations, there is already considerable opinion in the literature that an essential role of the Posterior tibial and Peroneal groups is stabilisation of the Tcn. joint and the findings of the present study tend to support this view.

7.6 Consideration of the Mark II Model

7.6.1 Comparison with Existing Models

The only study of ankle joint for which an ankle model was formulated and then solved for muscular and joint forces was that due to Brewster et al (1974) - later developed by Stauffer et al (1977) (reviewed in 2.8.4). The relevant features of their model are, that it was two-dimensional and assumed rigid body for the foot and the Tc. joint was assumed uniaxial. The Anterior tibial group force was rejected in the solutions because its contribution was considered to be very small, whilst the Calf group was included. The remaining muscles were not included since it was argued that the Calf and Anterior tibial groups acted to greatest advantage in respect of ankle flexion/extension. No ligamentous constraint was considered.

There are two main areas to be considered when comparing the above model with that developed in the present study. Firstly, the predicted joint force characteristics: comparing figure 2.39 with figures 7.8 to 7.11, the muscle characteristics are very different. Brewster et al's model has no Anterior tibial muscle contribution, and although Stauffer et al quoted 0.2B.W. for tibialis anterior, between 0 and 10% stance phase, they did not include it either in their muscle force curves. The present study recorded a mean peak of 0.99B.W. for normal locomotion which is not considered insignificant. The Calf peak reported by Stauffer et al (at ≃ 80% stance) was reported as 3.5B.W., whereas in the present study the peak value recorded for normal locomotion was 2.8B.W. with a mean peak of 2.5B.W. In addition their estimate of normal joint force in line with the tibia — 4.5 to 5B.W. peak — is considerably above the resultant Tc. joint force peak mean value estimated for the present study at 3.9B.W. (range 2.9 to 4.7). This may reflect differences in the anthropometric data used and also the normal variation between subjects.

The second consideration is that the geometric form of their model is two-dimensional. The three-dimensional orientation of the Tc. and Tcn. joints clearly requires a three-dimensional analytical model. It has been shown in the present study that a three-dimensional model produces physiologically feasible solutions, whilst including the main shank muscles and Tc. and Tcn. joint forces. The further development to include ligaments will be discussed in 7.6.2.

There is one further comparison of interest to be made with respect to models and that is with the knee

analysis results of Morrison (1968). To begin with the knee joint resultant force, figure 2.38(a) compares quite well with the resultant Tc. joint force in form, having basically two peaks in early stance and a later peak at ≃ 80% stance (2 to 4B.W. peak) associated with Calf group activity. The gastrocnemius activity in Morrison's model, shown in figure 2.38(b) was from about 45 to 95% stance; the mean peak value for gastrocnemius (at ≃ 80% stance) estimated from Morrison's results was 1020N. In the present study the corresponding peak was ≃ 1780N. mean. This establishes that the knee and ankle models are not inconsistent in that the mean peak for soleus would be positive (1780-1020=760N.) and thus tensile. It is interesting to note that this simple calculation indicates that the force in soleus may, in normal locomotion, be substantially less than gastrocnemius, ratio 0.7:1. This is quite the reverse to the situation that would arise if muscle physiological cross-section were used as the participation factor for apportioning the relative contributions; from Appendix 1.6 muscle physiological cross-section data the ratio of soleus to gastrocnemius is 1.5:1.

7.6.2 Development of a Mark III Model to Include Ligaments

The question of validation has already been discussed in 4.1 and it was concluded that independent validation is at the present time not practical. One thing which can be done however is to improve the model making it more realistic in the hope that this will bring more accurate results. To this end the Mark II model was considered with a view to including ligaments. Three clues lead to one possible model using ligaments.

Firstly there is the clinical evidence that antero-posterior instability of the foot relative to the shank occurs with damage to or rupture of the anterior fibulo-talar ligament, as reported in 2.6.3, suggesting that this ligament contributes to stability in this direction. Next there is the evidence of the static ligament analysis (4.2.2) that one of the principal functions of the ankle collateral ligaments is in resisting axial rotation between the shank and foot, i.e. $(M_y)_{Tc.}$ moments. Finally, there is the indication from the experimental results that at early and late stance the Tc. joint facet operates close to its limits in respect of $(F_x)_{Tc.}$ shear (see 7.4.5).

These clues lead to the concept of $(F_x)_{Tc.}$ shearing stability and $(M_y)_{Tc.}$ control being in part attributable to the collateral ligaments.

There are however two problems from the analytical viewpoint over the inclusion of the ligaments in these roles. Consider figure 7.39; this illustrates the three ligaments in contention for transmitting shear and moment directly to the talus from the shank. There are two feasible combinations of ligament pairs, firstly deltoid plus anterior fibulotalar which resists basically $(+F_x)_{Tc.}$ shear and, depending upon which F_x component is larger, positive or negative $(M_y)_{Tc.}$ moments. The second combination of ligaments is deltoid plus posterior fibulo-talar which resists $(-F_x)_{Tc.}$ shear, with the possibility again of balancing $(M_y)_{Tc.}$ moments.

When the equations for solution of muscle, joint and ligamentous forces have been written, the first problem is how to solve for the ligament forces when the number of unknowns in equations 4.22 to 4.33 now numbers fourteen, with only twelve equilibrium equations. One method of

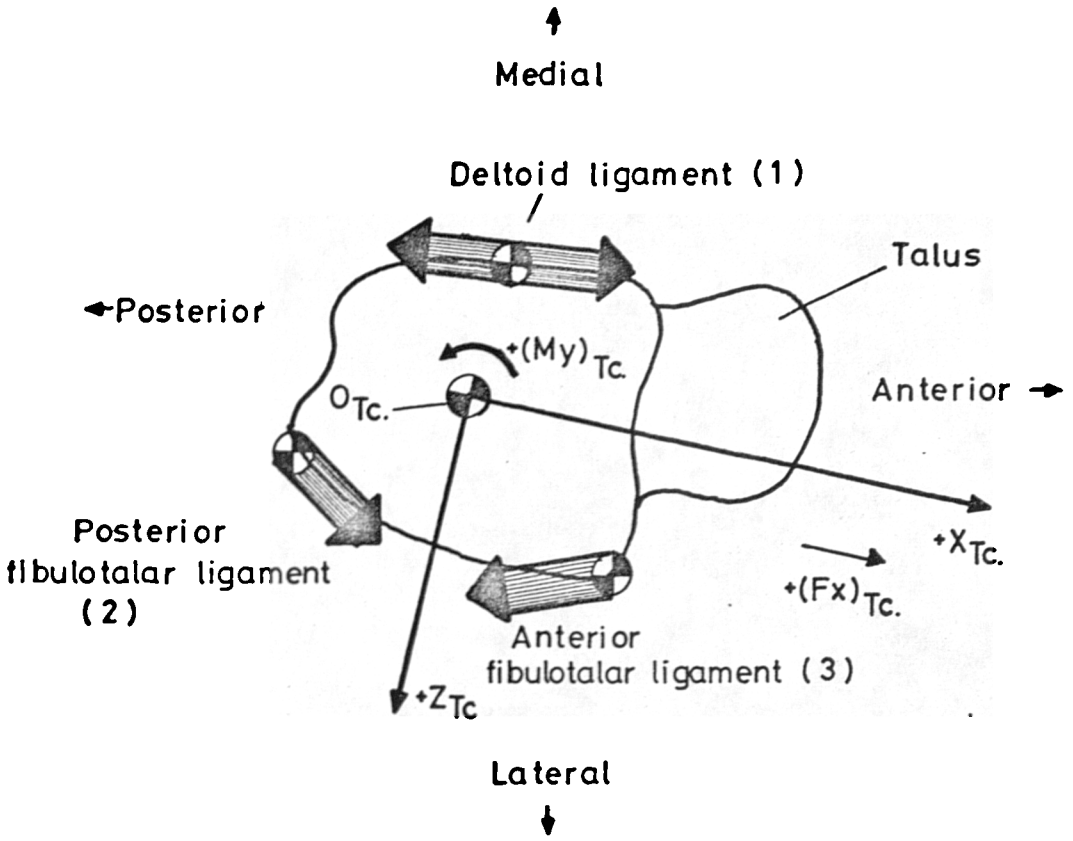

Ligament	Resisting force actions acting on the talus of	
	Force	Moment
(1)	$\pm(Fx)_{Tc.}$	$\pm(My)_{Tc.}$
(2)	$-(Fx)_{Tc.}$	$-(My)_{Tc.}$
(3)	$+(Fx)_{Tc.}$	$+(My)_{Tc.}$

Combinations considered feasible are (1)+(3) & (1)+(2)

Figure 7.39 Superior View of Right Talus Illustrating the Ligamentous Arrangements Proposed for the Mark III Analytical Model

solution would be to say that the medial and lateral $(F_x)_{Tc.}$ joint force components are zero and are replaced by a pair of medial and lateral ligaments. Whilst this results in analytically tractable equations it does not seem attractive on physiological grounds since the present study has shown that the Tc. joint facets have considerable potential for transmitting shear and moments. In addition there is considerable difficulty in deciding what criterion should be adopted for deciding which ligament pair should be chosen. An alternative strategy is to set a limit to the Tc. shearing/normal joint force resultant such that it will always pass within say x% of the bounds of the joint facet surface; once this is exceeded, excess shear is then progressively taken by the ligament pairs already defined (vide supra). This is an attractive concept since it makes the ligaments act as stabilisers, which is at least consistent with the clinical observation that damage to the anterior fibulotalar ligament results in instability.

If this latter solution to include the ligaments is adopted then it is necessary to define the factor x%, or to establish the anteroposterior bounds of the Tc. joint by X-ray. The Mark II model provided physiologically feasible results without requiring the inclusion of ligamentous constraint. In addition, there was no strong indication that F_x shear control was a problem for the Tc. joint for normal locomotion. However it is suggested that where more strenuous activities are studied, running for example, that the Mark III model developed above is used, since the constraining actions of ligaments will almost certainly be required.

7.6.3 Implications for Endoprosthesis Design

Swanson (1978) comprehensively reviewed general problems and trends in joint replacement. He discussed problems in mechanical design of endoprostheses with particular reference to the hip and knee. Evidently there is a wide range to the mechanical factors that should be considered. Briefly these are: basic mechanical strength and resistance to fatigue; obtaining an optimal compromise between minimal interference with the structures in the region of the affected joint whilst at the same time maintaining an acceptable minimum interface area between the prosthesis and bone, and achieving the best mechanical match between bone, cement and prosthesis properties. It is also essential to provide a prosthesis with the constraints necessary for normal joint function, for example, a plane tibial plateau knee endoprosthesis would withstand axial load, but would be totally inadequate in respect of shear and moment transmission.

In the case of the ankle there is a relatively low incidence of disabling disease of the ankle compared to the knee and hip joints according to Stauffer (1976). Stauffer evidently began investigating the pros and cons of total ankle joint replacement in 1971 as an alternative to arthrodesis (joint fusion). It was observed that the latter procedure resulted in good clinical results in only 60-65% of patients and it was for the remaining 35% that alternative surgical procedures such as joint replacement were considered. This lead to the development of a total ankle replacement. It was considered that the basic mechanical design requirements of an ankle endoprosthesis were that it should withstand periodic loading up to 5B.W. and permit a range of at least 25° flexion/

extension. A uniaxial cylindrical design was produced which had a concave polyethylene tibial component and a convex stainless steel talar component; both components being grouted to their respective bony surfaces by polymethylmethacrylate cement. The articulating surface area was stated to be 9cm.^{2} (but not whether this was tibial or talar). At the time of writing Stauffer reported favourable clinical results for the endoprosthesis, but had only two years clinical experience. In a follow up publication Stauffer (1977) commented that poor experience with total ankle replacement, as a sequel to attempted ankle fusion, had lead to reconsideration of the valid clinical indications for the use of ankle endoprostheses. The revised indications were rheumatoid arthritis and post traumatic degenerative ankle joint disease in older persons (60 years plus).

Kempson et al (1975) went through a comprehensive design exercise to produce an acceptable ankle prosthesis. Their prosthesis was in two parts each forming a segment of a cylinder, with a single axis of rotation. The tibial component was concave and manufactured from ultra high molecular weight polyethylene and the convex talar component was manufactured from medical grade stainless steel. At the time of writing, clinical trials had been conducted for two years and results of these together with laboratory wear test gave the authors considerable optimism regarding long term performance of the prosthesis.

The present author considers that ankle joint biomechanics studies like the present study, can contribute in two main ways to ankle endoprosthesis mechanical design: firstly by giving some insight into the likely mechanisms of load transfer which are essential to normal joint

function; secondly by assigning magnitudes to the various modes of loading identified.

Considering the mechanisms of loading, it is evident in some ankle endoprosthesis design exercises, excepting Kempson et al (vide supra), that the ability of the Tc. facets to transmit shearing forces and axial moments has been neglected. The anteroposterior length of the tibial component together with its curvature should be sufficient to allow the transmission of anteroposterior shear; here the normal anatomy of the ankle should serve as a guide to dimensions. In addition, the joint should be wide enough to transmit moments between the talus and shank, acting about the shank long axis. The fixation used must accordingly be capable of adequately transmitting these force actions to the talus and tibia without risking loosening of the respective components.

The loading magnitudes to be expected for the $(F_z)_{Tc.}$ shearing components and $(M_y)_{Tc.}$ axial moment are of the order of 1000N. and 30Nm. respectively for normal locomotion.

It is difficult to be certain which are the most useful mechanical criteria. If long term fatigue and loosening are the ultimate causes of endoprosthesis failure then fatigue damage loading criteria must be used together with peak values for wide ranges of subject activity including running, falling etc. One of the recommendations of this study is that the ankle be investigated under more stressful activities; for example walking up stairs, where the forefoot is mostly used and the ankle loading may be higher than in normal locomotion. The side slope walking studied in the present work might be extended to include much greater inclinations, which

would emphasise the effects apparent with walking on a slope. Uphill and downhill walking may also provide useful results.

7.7 Recommendations for Further Development Work

The present study has been concerned with establishing a feasible three-dimensional ankle model - the Mark II model - which can be studied during locomotion activities. It is recommended that the Mark III model developed in 7.6.2 be implemented and evaluated to gain insight into the possible action of ligaments. Two test situations would be of particular use in the evaluation. Firstly, fast walking - this would without doubt require the inclusion of ligaments in order to establish a physiologically acceptable model. This should be followed by a study of various ankle pathologies where the ligaments are injured, ankle sprain or complete ligament rupture. In this case the gait may be modified to reduce shearing forces across the ankle - preventing ligamentous loading. The results of Stauffer et al (1977) figure 2.40, indicate that shearing force may be a sensitive indicator of ankle mechanical defects due to pathology. The ankle should be further studied concurrently with the knee to establish the role of the soleus muscle in locomotion.

The author considers it essential that work is done towards developing a method by which biomechanical force analysis may be validated. It is inadequate for this purpose to use implanted joint force transducing devices since this only provides joint forces; muscle force prediction is a far more contentious issue. The attempts at using Emg. as a quantitative measure of muscle force generation are still at present an insufficient basis for

independent validation of muscle forces predictions. The only methods which appear to be likely, at present, to provide such validation are invasive methods. Whether or not these should be performed on humans or animals is likely to be as contentious an issue as the question of muscle force prediction itself.

7.8 Conclusions

The following conclusions are advanced:

An anthropometric data base relating to ankle structures has been established.

A physiologically acceptable three-dimensional model including the Talocrural and Talocalcaneonavicular joints has been developed. It has been evaluated for normal locomotion and side slope walking activities. In normal locomotion the peak resultant Tc. joint force was 3.9B.W. mean (range 2.9 to 4.7). The anterior facet of the Tcn. joint had a resultant force of 2.43B.W. mean (range 1.6 to 3.1B.W.) and 2.8B.W. mean (range 2.3 to 3.4B.W.) was reported for the posterior facet.

There was found to be some evidence that supported the view that an important role of the Peroneal and Posterior tibial muscles is to stabilise the Tcn. joint.

Finally, based upon the models presented, a model was proposed that would include ligamentous constraints.

BIBLIOGRAPHY

Alexander, R.McN. and Vernon, A. (1975) "The Dimensions of Knee and Ankle Muscles and the Forces they Exert" J. Human Movement Studies, 1, pp 115-123.

Ambagtsheer, J.B.T. (1978) "The Function of the Muscles of the Lower Leg in Relation to Movements of the Tarsus" Acta. Orthop. Scand. Suppl. No. 172.

Amis, A.A. (1978) "Biomechanics of the Upper Limb and Design of an Elbow Prosthesis" PhD. Thesis, University of Leeds.

Andrews, B.J. (1975) "Quantisation Effects in Digital Kinematic Measurement and Data Processing Systems" Internal Report, Bioengineering Unit, University of Strathclyde, Glasgow.

Barbenel, J.C. (1972) "The Biomechanics of the Temperomandibular Joint - A Theoretical Study" J. Biomechanics, 5, pp 251-256.

Barclay Smith, E. (1896) "The Astragalocalcaneonavicular Joint" J. Anat Physiol., 30, pp 390-412.

Barnett, C.H. and Napier, J.R. (1952) "The Axis of Rotation at the Ankle Joint in Man. Its Influence on the Form of the Talus and the Mobility of the Fibula" J. Anat., 86, pp 1-9.

Battye, C.K. and Joseph, J (1966) "An Investigation by Telemetering of the Activity of Some Muscles in Walking" Med. and Biol. Engng., 4, pp 125-135.

Bock, N.J. (1974) "The Avian Skeletomuscular System" In Avian Biology Vol. IV. Ed. Farmer, D.S. and King, J.R., Academic Press, New York and London.

Bojsen-Møller, F. (1978) "The Human Foot - a Two Speed Construction" In Biomechanics VI-A, Ed. Asmussen, E. and Jozgensen, K., University Park Press, Baltimore.

Bojsen-Møller, F. and Lamoreaux, L. (1979) "Significance of Free Dorsiflexion of the Toes in Walking" Acta. Orthop. Scand., 50, pp 471-479.

Bourne, G.H. (1972) "The Structure and Function of Muscle" Vol. 1 2nd Ed., Academic Press, New York and London.

Bresler, B. and Frankel, J.P. (1950) "The Forces and Moments in the Leg During Level Walking" Trans. A.S.M.E., 72, pp 27-36.

Brewster, R.C., Chao, E.Y. and Stauffer, R.N. (1974) "Force Analysis of the Ankle Joint During the Stance Phase of Gait" 27th A.C.E.M.B., Marriot Hotel, Philadelphia, Pub. Alliance for Engineers.

Broström, L (1965) "Sprained Ankles III: Clinical Observations in Recent Ligament Ruptures" Acta. Chir. Scand., 130, pp 560-569.

Bunning, P.S. and Barnett, C.H. (1965) "A Comparison of Adult and Foetal Articulations" J. Anat., 99, pp 71-76.

Calliet, R. (1974) "Foot and Ankle Pain" Pub. F.A. Davis Company, Philadelphia.

Cavenagh, P.R., Williams, K.R. and Clarke, T.E. (1980) "The Influence of Footwear on the Pattern of Ground Reaction Forces During Walking" In Biomechanics VII, Proc. VIIth Int. Congress of Biomechanics, Warsaw (1979).

Cedell, C-A. (1975) "Ankle Lesions" Acta. Orthop. Scand., 46, pp 425-445.

Chandler, R.F., Clauser, C.E., McConville-Reynolds, H.M. and Young, J.W. (1975) "Investigation of Inertial Properties of the Human Body" Wright Patterson Air Force Base, Aerospace Medical Research Laboratory.

Channon, G.M. and Brotherton, B.J. (1979) "The Ball and Socket Joint" J. Bone Joint Surg., 61-B, pp 85-89.

Chao, E.Y. and An, K.N. (1977) "Graphical Interpretation of the Solution to the Redundant Problem in Biomechanics", A.S.M.E. Paper 77-Bio. - 1.

Chhibber, S.R. and Singh, I (1970) "Assymetry in Muscle Weight and One Sided Dominance in the Human Lower Limbs" J. Anat., 106, pp 553-556.

Chow, C.K. and Jacobsen, D.H. (1971) "Studies of Human Motion Via Optimal Programming" Math. Bioscie., 10, pp 239-306.

Close, J.R. (1956) "Some Applications of the Functional Anatomy of the Ankle Joint" J. Bone Joint Surg., 38A, pp 761-781.

Close, J.R. and Inman, V.T. (1952) "The Action of the Ankle Joint" Prosth. Dev. Res. Project., University of California, Berkely, Ser. 11, Iss. 22.

Close, J.R. and Inman, V.T. (1953) "The Action of the Subtalar Joint" Prosth. Dev. Res. Project, University of California, Berkely, Ser. 11, Iss. 24.

Close, J.R. and Todd, F.N. (1959) "The Phasic Activity of the Muscles of the Lower Extremity and the Effect of Tendon Transfer" J. Bone Joint Surg., 41A, p 189.

Crowninshield, R.D. (1978) "Use of Optimisation Techniques to Predict Muscle Forces" Trans. A.S.M.E., 100, pp 88-92.

Elftman, H. (1960) "The Transverse Tarsal Joint and its Control" Clin. Orthop., 16, pp 41-45.

Elftman, H. (1969) "Dynamic Structure of the Human Foot" Artif. Limbs, 13, pp 49-58.

Elftman, H. and Manter, J. (1935) "The Evolution of the Human Foot, With Special Reference to the Joints" J. Anat., 70, pp 56-67.

Elliot, D.H. (1965) "The Growth of Tendon After Denervation or Excision of its Muscle" Proc. Roy. Soc. B., 162, pp 203-209.

Fick, R. (1911) "Handbuch der Anatomie und Mechanik der Gelenke unter Berucksicht der bewegenden Muskeln" Vols 2 and 3, Jena, Gustav Fischer.

Glanville, A.D. and Kreezer, G. (1937) "The Maximum Amplitude and Joint Velocity of Joint Movements in Normal Male Human Adults" Hum. Biol., 9, pp 197-211.

Grath, G.B. (1960) "Widening of the Ankle Mortise: A Clinical and Experimental Study" Acta. Chir. Scand. Suppl., 263.

Greenwald, A.S., Matejczyk, M-B., Keppler, B.S., Black, J.D., Moran, B.C.E., Porrit, R., Beck, D. and Wilde, M.D. (1976) "Preliminary Observations on the Weight-Bearing Surfaces of the Human Ankle Joint" Surg. Forum, 27, pp 505-506.

Grieve, D.W. (1975) "Electromyography" In Techniques for the Analysis of Human Movement. Pub. Lepus Books Ltd.

Hardt, D.E. (1978) "A Minimum Energy Solution for Muscle Force Control During Walking" PhD. Thesis, M.I.T.

Hatze, H. (1976) "The Complete Optimisation of Human Motion" Math. Bioscie., 28, pp 99-135.

Haughton, S. (1867) "On Some Elementary Principles in Animal Mechanics" Proc. Roy. Soc. Lond., 16, pp 19-24.

Haxton, H.A. (1944) "Absolute Muscle Force in the Ankle Flexors of Man" J. Physiol., 103, pp 267-273.

Hicks, J.H. (1953) "The Mechanics of the Foot. I the Joints" J. Anat., 87, pp 345-357.

Houtz, M.S. and Walsh, F.P. (1959) "Electromyographic Analysis of the Function of the Muscles acting on the Ankle During Weight Bearing with Special Reference to the Triceps Surae" J. Bone Joint Surg., 41-A, pp 1469-1481.

Huson, A. (1961) "Een Ontleedkundig Functioneel Onderzoek Van De Voetwortel" Thesis, Leiden.

Huson, A. (1976) "Quelques Consequences Fonctionelles du Croisement des Ligaments Articulaires" Bull. Assoc. Anat. Nancy, 60, pp 695-704.

Huxley, A.F. (1974) "Muscular Contraction - Review Lecture" J. Physiol., 243, pp 1-43.

Inman, V.T. (1976) "The Joints of the Ankle" Pub. Williams and Wilkins Co., Baltimore.

Isman, R.E. and Inman, V.T. (1969) "Anthropometric Studies of the Human Foot and Ankle" Bull. Prosth. Res., 10-11, pp 97-129.

Jarrett, M.O. (1976) "A Television/Computer System for Human Locomotion Analysis" PhD. Thesis, University of Strathclyde.

Jensen, R.H. and Metcalf, W.K. (1975) "A Systematic Approach to Quantitative Description of Musculo-skeletal Geometry" J. Anat., 119, pp 209-221.

Jones, D.J. (1935) "Ingenious Mechanisms for Designers and Inventors" 1st ed., Pub. The Machinery Publishing Co., Ltd.

Jones, R.L. (1941) "The Human Foot. An Experimental Study of its Mechanics and the Role of its Ligaments in Support of the Arch" Am. J. Anat., 68, pp 1-39.

Jones, R.L. (1945) "The Functional Significance of the Declination of the Axis of the Subtalar Joint" Anat. Rec., 93, pp 151-159.

Kapandji, I.A. (1970) "The Physiology of Joints. Vol. II. The Lower Limb" Pub. Churchill Livingstone.

Kaye, J.J. and Bohne, W.H.O (1977) "A Radiographic Study of the Ligamentous Anatomy of the Ankle" Diagnostic. Radiol., 125, pp 657-667.

Kempson, G.E., Freeman, M.A.R. and Tuke, M.A. (1975) "Engineering Considerations in the Design of an Ankle Joint" J. Biomed. Engng., 10, pp 166-171 and 180.

Komi, P.V. (1979) "Neuromuscular Performance: Factors Influencing Force and Speed Production" Scand. J. Sports Scie., 1, pp 2-15.

Kreyszig, E. (1962) "Advanced Engineering Mathematics" 3rd ed., Pub. Wiley International.

Lambert, K.L. (1971) "The Weight Bearing Function of the Fibula" J. Bone Joint Surg., 53-A, pp 507-513.

Lamoreaux, L.W. (1971) "Kinematic Measurements in the Study of Human Walking" Bull. Prosth. Res., 10-15, 3-84.

Lanczos, C. (1957) "Applied Analysis" Pub. Pitman.

Lane, W.A. (1887-1888) "The Movements of the Ankle Joint" J. Anat. Physiol. (Lond.), 22, p 408.

Lapidus, P.W. (1955) "Subtalar Joint, its Anatomy and Mechanics" Bull. Hosp. Joint Dis., 16, pp 179-195.

Laurin, C. and Mathieu, J. (1975) "Saggital Mobility of the Normal Ankle" Clin. Orthop. and Rel. Res., 108, pp 99-104.

Lew, W.D. and Lewis, J.L. (1977) "An Anthropometric Scaling Method with Application to the Knee Joint" J. Biomech., 10, pp 179-181.

Mann, R. and Inman, V.T. (1964) "The Phasic Activity of Intrinsic Muscles of the Foot" J. Bone Joint Surg., 46-A, pp 469-481.

Manter, J.T. (1941) "Movements of the Subtalar and Transverse Tarsal Joints" Anat. Rec., 80, pp 397-410.

MacConnaill, M.A. (1967) "The Ergonomic Aspects of Articular Mechanics" In Studies on the Anatomy and Functions of Bones and Joints, Ed. F.G. Evans, Pub. Springer-Verlag, Berlin.

Margaria, R. (1976) "Biomechanics and Energetics of Muscular Exercise" Pub. Clarendon Press, Oxford.

Mariani, G. and Patella, V. (1977) "Valuazione Statistica Del Parametri Articulari Della Tibio-Tarsica" Chir. Organi Mov., 63, pp 333-340.

Morrison, J.B. (1968) "Bioengineering Analysis of the Force Actions Transmitted by the Knee Joint" Biomed. Engng., 3, p 164.

Morrison, J.B. (1970) "The Mechanics of the Knee Joint in Relation to Normal Walking" J. Biomech., 3, pp 51-61.

Murray, M.P., Drought, A.B. and Kory, R.C. (1964) "Walking Patterns of Normal Men" J. Bone Joint Surg., 46-A, pp 335-360.

Needham, D.M. (1971) "Machina Carnis - The Biochemistry of Muscular Contraction in its Historical Development" Pub. Cambridge University Press.

Nicol, A.C. (1977) "Elbow Joint Prosthesis Design: Biomechanical Aspects" PhD. Thesis, University of Strathclyde, Glasgow.

Nigg, B.M., Denoth, J. and Neukomm, P.A. (1979) "The Load on the Lower Extremities in Selected Sports Activities" Int. Symp. Man Under Vibration, Udime Italy.

Nubar, Y. and Contini, R. (1961) "A Minimal Principle in Biomechanics" Bull. Math. Biophys., 23, pp 377-391.

O'Connell A.L. (1958) "Electromyographic Study of Certgin Leg Muscles During Movements of the Free Foot And During Standing" Am. J. Phys. Med., 37, pp 289-301.

Pankovich A.M. and Shivram, M.S. (1979) "Anatomical Basis if Variability in Injuries of the Medial Malleolus and the Deltoid Ligament, 1 - Anatomical Studies" Acta. Orthop. Scand., 50, pp 217-223

Paul, J.P. (1967) "Forces at the Human Hip Joint" PhD. Thesis, University of Glasgow, Glasgow.

Paul, J.P. (1971) "Comparison of Emg. Signals from Leg Muscles with Corresponding Force Actions Calculated from Walkpath Measurements" Conf. Hum. Locomotor Engng. University of Sussex, Pub. I. Mech. E.

Pedotti, A., Krishan, V.V. and Stark, L. (1978) "Optimisation of Muscle Force Sequencing in Human Locomotion" Math. Bioscie., 38, pp 57-76.

Peizer, E. and Wright, D.W. (1971) "Human Locomotion" Conf. Hum. Locomotor Engng. University of Sussex, Pub. I. Mech E.

Poulson, J. (1973) "Biomechanics of the Leg" PhD. Thesis, University of Strathclyde, Glasgow.

Procter, P., Berme, N. and Paul, J.P. (1980) "Ankle Joint Biomechanics" In Biomechanics VII, Proc. VIIth Int. Congress of Biomechanics, Warsaw (1979).

Ralston, H.J. (1961) "Uses and Limitations of Electromyography in the Quantitative Study of Skeletal Muscle Function" Am. J. Orthodontics, 47, pp 521-530.

Ramsey, P.L. and Hamilton, W. (1976) "Changes in Tibiotalar Area of Contact Caused by Lateral Talar Shift" J. Bone Joint Surg., 58-A, pp 356-357.

Ripperger, R.R., Chao, E.Y. and Stauffer, R.N. (1980) "A Quantitative Analysis of Leg Musculature" 26th Ann. ORS. Atlanta, Georgia.

Root, M.L., Orien, W.P. and Weed, J.H. (1971) "Normal and Abnormal Function of the Foot - Clinical Biomechanics" Vol. II, Pub. Clinical Biomechanics Corporation, Los Angeles.

Royce, J. (1965) "Surface Anatomy" Pub. F.A. Davis Co.

Rubin, G. (1971) "Tibial Rotation" Bull. Prosth. Res., 10-15, pp 95-101.

Rubin, G. and Witten, M. (1960) "The Talar-Tilt Angle and the Fibular Collateral Ligaments" J. Bone Joint Surg., 42, pp 311-326.

Rydell, N. (1966) "Forces Acting on the Femoral Head Prosthesis" Acta. Orthop. Scand. Suppl., 88.

Sammarco, G.J., Burstein, A.H. and Frankel, V.H. (1973) "Biomechanics of the Ankle: A Kinematic Study" Orthop. Clin. North. Am., 4, pp 75-96.

Scranton, P.E., McMaster, J.H. and Kelly, E. (1976) "Dynamic Fibular Function" Clin. Orthop. and Rel. Res., 118, pp 76-81.

Seirig, A. and Arvikar, R.J. (1975) "The Prediction of Muscular Load Sharing and Joint Forces in the Lower Extremities During Walking" J. Biomech., 8, pp 89-102.

Sewell, R.B.S. (1904) "A Study of the Astragalus" J. Anat., 85, pp 414-415.

Sheffield, J.F., Gersten, J.W. and Mastellone, A.F. (1956) "An Electromyographic Study of the Muscles of the Foot in Normal Walking" Am. J. Phys. Med., 35, pp 223-236.

Shephard, E. (1951) "Tarsal Movements" J. Bone Joint Surg., 33-B, pp 258-263.

Shoji, H. (1977) "The Foot and the Ankle" In Musculo-Skeletal Disorders: Regional Examination and Differential Diagnosis, Ed. R.D. D'Ambrosia, pp 487-523, Pub. J.B. Lippincott Co.

Simon, J.R., Mann, M.D., Hagy, J.L. and Larsen, L.J. (1978) "Role of the Posterior Calf Muscles in Normal Gait" J. Bone Joint Surg., 60-A, pp 465-472.

Smith, J.W. (1958) "Ligamentous Structure in the Canalis and Sinus Tarsi" J. Anat., 92, pp 616-620.

Sosa, T. and Pasini, J. (1975) "Biomechanically Important Articular Surfaces of the Talocrural Joint" Anat. Embryol., 147, pp 203-211.

Sosna, T. and Sosna, A. (1977) "Variability and Functional Significance of the External Ligament of the Ankle for Stability of the Talocrural Joint" Folia Morphol., XXV, pp 371-374.

Stamm, T.T. (1931) "The Constitution of the Ligamentum Cruciatum Cruris" J. Anat., 66, pp 80-83.

Staples, O.S. (1975) "Ruptures of the Fibular Collateral Ligaments of the Ankle" J. Bone Joint Surg., 57-A, pp 107.

Stauffer, R.N. (1976) "Total Ankle Joint Replacement as an Alternative to Arthrodesis" Geriatrics, 31, pp 79-82, 85.

Stauffer, R.N. (1977) "Total Ankle Joint Replacement" Arch. Surg., 112, pp 1105-1109.

Stauffer, R.N., Chao, E.Y. and Brewster, R.C. (1977) "Force and Motion Analysis of the Normal Diseased and Prosthetic Ankle Joint" Clin. Orthop., 127, pp 189-196.

Stokes, I.A.F., Hutton, W.C. and Stott, J.R.R. (1979) "Forces Acting on the Metatarsals During Normal Walking" J. Anat., 129, pp 579-590.

Sutherland, D.H. (1966) "An Electromyographic Study of the Plantarflexors of the Ankle in Normal Walking on the Level" J. Bone Joint Surg., 48-A, pp 66-71.

Swanson, S.A.V. (1978) "The State of the Art in Joint Replacement, Part III: Results, Problems and Trends" J. Med. Eng. and Tech., 2, pp 16-20.

Tooth, R. (1976) "The Biomechanics of Arthrodesis and Arthroplasty in the Human Leg" PhD. Thesis, University of Strathclyde, Glasgow.

Townsend, M.A., Shiavi, R., Lainhart, S.P. and Caylor, J. (1978) "Variability in Synergy Patterns of Leg Muscles During Climbing, Descending And Level Walking in Highly Trained Athletes and Normal Males" Electromyogr. Clin. Neurophysiol, 18, pp 69-80.

University of Califormia (1953) "The Pattern of Muscular Activity in the Lower Extremity During Walking" Prosth. Dev. Res. Proj. Inst. Engng. Res. U. Calif. Berkely, Ser. 11, Iss. 25.

Von Lanz, T. and Watchsmuth, W. (1939) "Pratische Anatomie, Band 1, Teil 4" Pub. J Springer, Berlin.

Warwick, R. and Williams, P.L. (1973) Editors 35th Ed. Gray's Anatomy. Pub. Longman.

Winter D.A., Sidwall, H.G. and Hobson, D.A. (1974) "Measurement and Reduction of Noise in Kinematics of Locomotion" J. Biomech., 7, 157.

Wood-Jones, F. (1943) "Structure and Function as Seen in the Foot" Pub. Bailliere, Tindall and Cox, London.

Wright, D.G., Desai, M.E. and Henderson, B.S. (1964) "Action of the Subtalar and Ankle Joint Complex During the Stance Phase of Walking" J. Bone Joint Surg., 46-A, pp 361-382.

Yeo, B.P. (1976) "Investigations Concerning the Principal of Minimal Total Muscular Force" J. Biomech., 9, pp 413-416.

Zarrugh, M.Y. and Radcliffe, C.W. (1979) "Computer Generation of Human Gait Kinematics" J. Biomech., 12, pp 99-111.

APPENDIX 1

SUMMARY CADAVER ANTHROPOMETRIC DATA

A1.1 Basic Cadaver Data

All subjects were Glaswegian and male.

Subject No	Age	Cause of Death	Height(m.) (at death)	Mass(kg.)
1	73	Cardiovascular accident	1.72	70.0
2	57	Myocardial infarction	1.75	76.4
3	88	Myocardial infarction	1.68	63.6
4	68	Congestive cardiac failure	1.62	64.1
5	81	Myocardial infarction	1.59	53.1

A1.2 Skin and Fat Cover of the Bony Landmarks

Bony Point		Mean Thickness (mm.)	Range either side of the mean (mm.) -	+
Medial Condyle	(1)	7.5	2.5	2.5
Lateral Condyle	(2)	7.4	3.6	1.6
Tibial Tubercle	(3)	3.0	1.5	1.2
Medial Malleolus	(4)	2.4	0.9	0.6
Lateral Malleolus	(5)	3.0	1.3	0.6
Calcaneus	(6)	5.6	1.6	2.4
Navicular Tuberosity	(7)	2.6	1.1	0.8
Metatarsal Five Base	(8)	4.5	0.5	0.8

Bony Points	Mean coordinates (m.)			Range of values either side of the mean (m.)					
	X_T	Y_T	Z_T	+ X_T -		+ Y_T -		+ Z_T -	
Medial Condyle	-0.0080	0.3314	-0.0432	0.0089	0.0122	0.0199	0.0135	0.0165	0.0187
Lateral Condyle	-0.0088	0.3397	0.0346	0.0060	0.0150	0.0211	0.0199	0.0051	0.0101
Tibial Tubercle	0.0278	0.3002	0.0075	0.0065	0.0059	0.0139	0.0126	0.0056	0.0034
Medial Malleolus	0.0085	0.0071	-0.0328	0.0008	0.0023	0.0008	0.0017	0.0051	0.0032
Lateral Malleolus	-0.0085	-0.0071	0.0328	0.0023	0.0008	0.0017	0.0008	0.0032	0.0051
Calcaneus	-0.0419	-0.0301	-0.0037	0.0112	0.0088	0.0032	0.0020	0.0012	0.0024
Navicular Tuberosity	0.0369	-0.0249	-0.0321	0.0054	0.0052	0.0055	0.0034	0.0052	0.0058
Metatarsal Five Base	0.0479	-0.0616	0.0323	0.0014	0.0013	0.0015	0.0019	0.0056	0.0060

A1.3 The Bony Reference Points: Data for Five Cadavers referred to the Mid Malleolar Origin

Muscle Tendon		Mean coordinates (m.) X_T	Y_T	Z_T	Range of values either side of the mean (m.) + X_T -		+ Y_T -		+ Z_T -	
Gastroc. plus Sol.	*P	-0.0401	0.0237	-0.0016	0.0037	0.0055	0.0188	0.0158	0.0020	0.0039
	*D	-0.0400	-0.0269	-0.0028	0.0093	0.0107	0.0052	0.0057	0.0003	0.0033
Post. tib.	P	0.0045	0.0062	-0.0286	0.0088	0.0071	0.0070	0.0103	0.0049	0.0022
	D	0.0245	-0.0237	-0.0302	0.0065	0.0095	0.0013	0.0035	0.0070	0.0074
Flex. hall. long.	P	-0.0182	0.0137	-0.0088	0.0038	0.0038	0.0068	0.0039	0.0036	0.0034
	D	-0.0121	-0.0160	-0.0150	0.0054	0.0047	0.0051	0.0042	0.0034	0.0039
Flex. dig. long.	P	-0.0030	-0.0079	-0.0232	0.0068	0.0128	0.0069	0.0162	0.0044	0.0043
	D	0.0136	-0.0264	-0.0239	0.0063	0.0136	0.0052	0.0111	0.0029	0.0029
Peron. brev.	P	-0.0045	-0.0208	0.0258	0.0094	0.0065	0.0073	0.0060	0.0042	0.0055
	D	0.0253	-0.0430	0.0288	0.0124	0.0125	0.0086	0.0096	0.0055	0.0058
Peron. long.	P	-0.0104	-0.0180	0.0275	0.0119	0.0082	0.0053	0.0108	0.0054	0.0059
	D	0.0049	-0.0402	0.0265	0.0097	0.0076	0.0015	0.0051	0.0025	0.0031
Ant. tib.	P	0.0453	0.0007	-0.0198	0.0079	0.0075	0.0046	0.0098	0.0086	0.0087
	D	0.0596	-0.0218	-0.0298	0.0052	0.0060	0.0054	0.0049	0.0068	0.0109
Ext. hall. long.	P	0.0509	-0.0008	-0.0031	0.0034	0.0030	0.0017	0.0012	0.0050	0.0019
	D	0.0829	-0.0181	-0.0134	0.0048	0.0123	0.0057	0.0057	0.0024	0.0025
Ext. dig. long.	P	0.0407	-0.0045	0.0127	0.0086	0.0072	0.0060	0.0050	0.0016	0.0022
	D	0.0724	-0.0281	0.0127	0.0110	0.0093	0.0068	0.0046	0.0053	0.0060

* Note P = Proximal point; D = Distal point

A1.4 The Muscle Tendon Line of Action Data: Data for Five Cadavers referred to the Mid Malleolar Origin

Muscle	Mass (kg.)	Pennation Angle (α°)	Fibre Length (m.)	Physiological Cross-section* ($m.^2$) A_p	$Ap.\cos(\alpha)$ ($m.^2$)	Tendon Cross-section $(cm.)^2$ At
Gastroc.	0.1644	13.5	0.046	0.00340	0.00328	0.690
Sol.	0.2613	35.0	0.025	0.00815	0.00668	
Post. tib.	0.0649	20.0	0.025	0.00232	0.00218	0.257
Flex. hall. long.	0.0447	30.0	0.040	0.00092	0.00079	0.174
Flex. dig. long.	0.0312	20.0	0.035	0.00080	0.00075	0.151
Peron. brev.	0.0185	10.0	0.040	0.00043	0.00042	0.117
Peron. long.	0.0495	15.0	0.040	0.00114	0.00109	0.202
Ant. tib.	0.0820	15.0	0.060	0.00126	0.00121	0.246
Ext. hall. long.	0.0251	7.0	0.070	0.00034	0.00034	0.107
Ext. dig. long.	0.0295	9.0	0.080	0.00035	0.00034	0.132

* Calculated using equation 2.1 taking ρ muscle fibre as 1050kg./m^2 (Alexander and Vernon, 1975)

A1.5 The Muscle Physiological and Tendon Cross-section Data (Cadaver 1)

Muscle	Mean Physiological Cross-section Ap ($m.^2$)	Range either side of the mean Ap +	Range either side of the mean Ap -	Mean Tendon Cross-section At ($cm.^2$)	Range either side of the mean At +	Range either side of the mean At -	Ratio $\frac{100Ap}{At}$
Gastroc.	0.00302	0.00055	0.00082	0.585	0.115	0.035	1.425
Sol.	0.00533	0.00138	0.00196				
Post. tib.	0.00161	0.00057	0.00077	0.253	0.037	0.029	0.637
Flex. hall. long	0.00069	0.00059	0.00028	0.145	0.029	0.024	0.475
Flex. dig. long.	0.00050	0.00025	0.00030	0.117	0.034	0.024	0.427
Peron. brev.	0.00058	0.00038	0.00018	0.130	0.024	0.013	0.446
Peron. long.	0.00102	0.00051	0.00040	0.189	0.030	0.026	0.539
Ant. tib.	0.00098	0.00038	0.00041	0.206	0.040	0.018	0.476
Ext. hall. long.	0.00025	0.00009	0.00013	0.091	0.016	0.017	0.275
Ext. dig. long.	0.00045	0.00025	0.00015	0.134	0.026	0.021	0.336

A1.6 Summary Table of Muscle Physiological and Tendon Mean Cross-section for Five Cadavers, together with the Ratio (100Ap/At)

Ligamentous Structure		Mean coordinates (m.) X_T	Y_T	Z_T	Range of values either side of the mean (m.) + X_T	−	+ Y_T	−	+ Z_T	−
Deltoid Anterior Band	*0	0.0192	0.0035	-0.0262	0.0020	0.0019	0.0053	0.0038	0.0054	0.0039
	*1	0.0205	-0.0115	-0.0250	0.0046	0.0048	0.0048	0.0051	0.0033	0.0016
Deltoid Mid Band	0	0.0150	0.0012	-0.0296	0.0059	0.0048	0.0052	0.0034	0.0079	0.0030
	1	0.0116	-0.0202	-0.0221	0.0073	0.0078	0.0026	0.0025	0.0053	0.0025
Deltoid Posterior Band	0	0.0057	-0.0001	-0.0276	0.0087	0.0038	0.0041	0.0051	0.0075	0.0058
	1	0.0021	-0.0075	-0.0210	0.0057	0.0040	0.0026	0.0022	0.0040	0.0024
Anterior Fibulotalar	0	0.0043	-0.0119	0.0244	0.0042	0.0059	0.0020	0.0024	0.0030	0.0043
	1	0.0143	-0.0106	0.0179	0.0023	0.0030	0.0008	0.0029	0.0016	0.0034
Fibulocalcaneal	0	-0.0019	-0.0156	0.0272	0.0025	0.0038	0.0037	0.0052	0.0033	0.0037
	1	-0.0160	-0.0288	0.0167	0.0029	0.0033	0.0038	0.0054	0.0018	0.0039
Posterior Fibulotalar	0	-0.0066	-0.0105	0.0201	0.0037	0.0043	0.0034	0.0022	0.0052	0.0053
	1	-0.0145	-0.0092	0.0014	0.0042	0.0050	0.0029	0.0041	0.0027	0.0016
Inferior Extensor Retinaculum	*P	0.0352	0.0029	0.0136	0.0060	0.0043	0.0031	0.0029	0.0028	0.0043
	0	0.0153	-0.0269	0.0226	0.0024	0.0051	0.0021	0.0020	0.0031	0.0027

*Note 0 = Origin; 1 = Insertion; P = Proximal Point

A1.7 Summary Table of Mean Ligament and Retinaculum Line of Action Data for Five Cadavers, referred to the Mid-Malleolar Origin

Point	Mean coordinates (m.)			Range of values either side of the mean (m.)					
	X_T	Y_T	Z_T	+ X_T	-	+ Y_T	-	+ Z_T	-
Tc. lateral exit	0.0015	-0.0163	0.0258	0.0015	0.0017	0.0024	0.0053	0.0083	0.0063
Tc. medial exit	0.0147	-0.0050	-0.0278	0.0036	0.0026	0.0042	0.0031	0.0112	0.0044
Tc. origin	0.0081	-0.0104	-0.0022	0.0033	0.0013	0.0012	0.0011	0.0012	0.0025
Tcn. lateral exit	-0.0224	-0.0581	0.0151	0.0060	0.0077	0.0093	0.0074	0.0107	0.0056
Tcn. medial exit	0.0389	-0.0055	-0.0106	0.0029	0.0056	0.0076	0.0095	0.0059	0.0073
Tcn. origin	0.0171	-0.0222	-0.0017	0.0029	0.0014	0.0035	0.0071	0.0047	0.0030

A1.8 Origin and Exit Data for the Tc. and Tcn. Axes: Mean Data for Five Cadavers referred to the Mid-Malleolar Origin

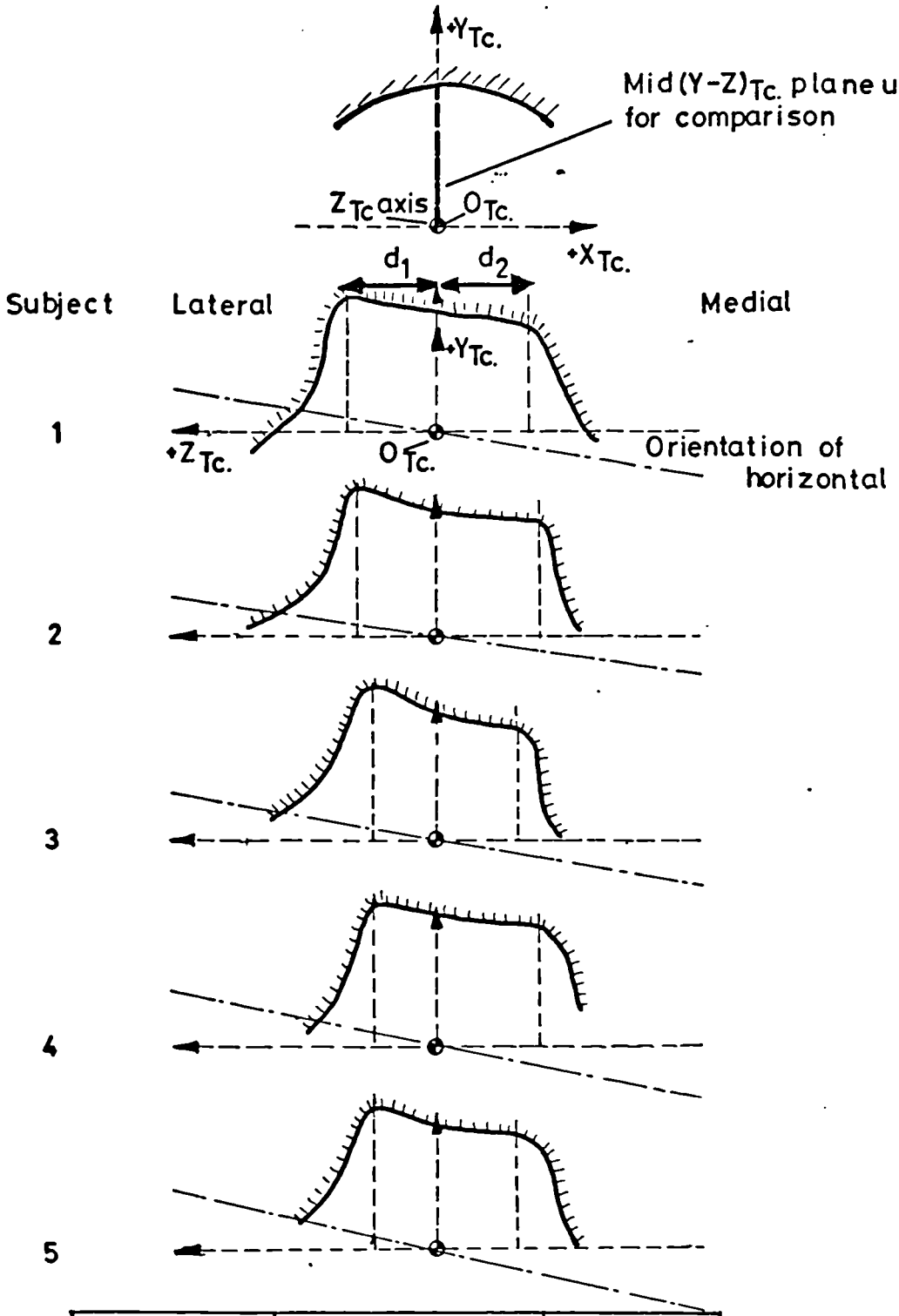

Subject	d_1 (mm.)	d_2 (mm.)
1	13.2	13.8
2	11.6	15.1
3	9.2	11.9
4	9.4	15.0
5	9.1	12.7
MEAN	10.5	13.7

A1.9(a) Mediolateral Tc. Joint Sections and Parameters

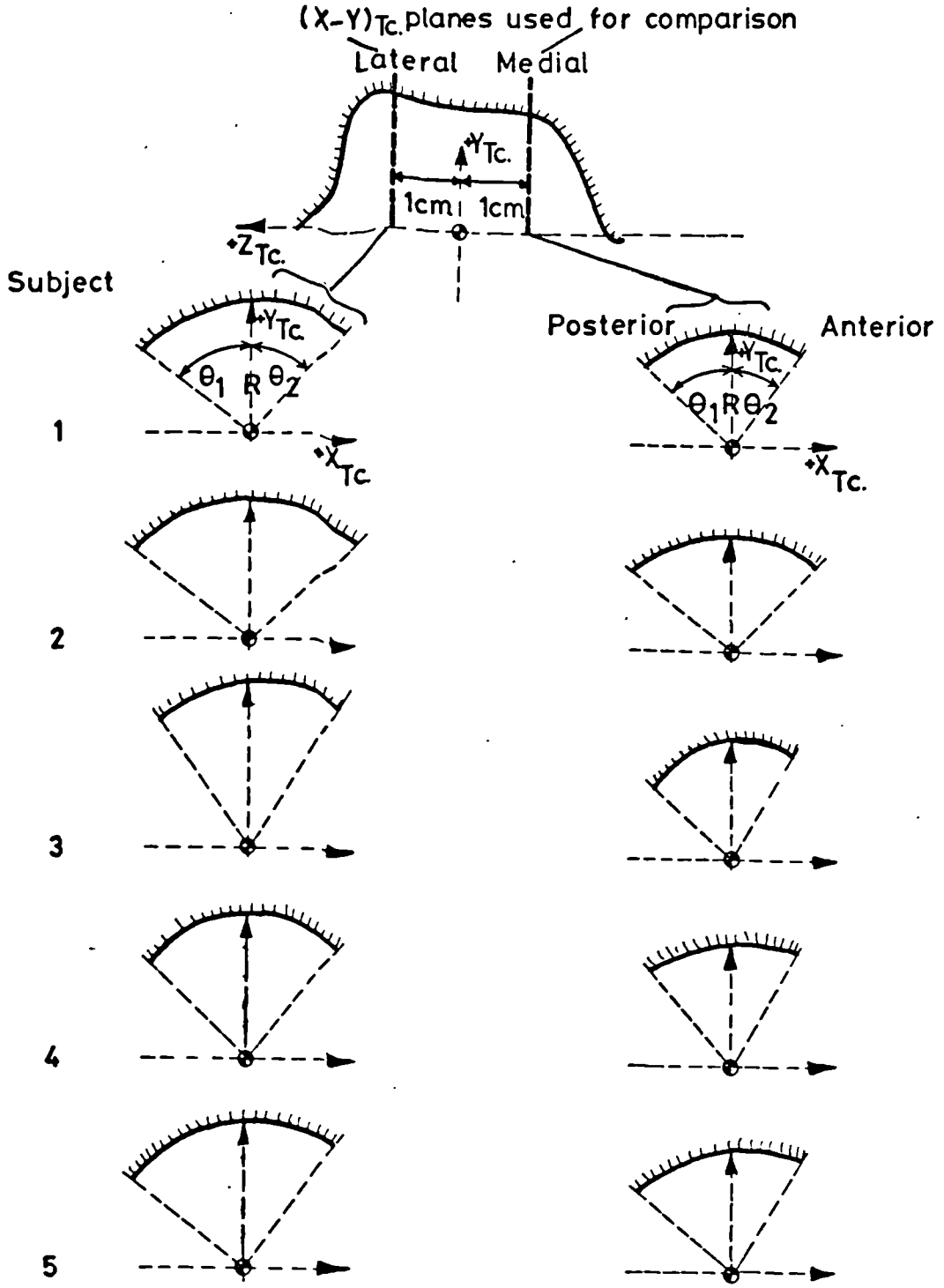

Subject	Lateral Section θ_1°	θ_2°	R_1 (mm.)	Medial Section θ_1°	θ_2°	R_2 (mm.)
1	53	42	19.5	48	31	16.5
2	53	46	20.1	52	30	16.6
3	46	32	23.7	49	30	17.6
4	47	39	30.8	41	44	17.9
5	53	37	30.9	49	36	17.9
MEAN	50.4	39.2	21.0	47.8	34.2	17.3

A1.9(b) Anteroposterior Tc. Joint Sections and Parameters

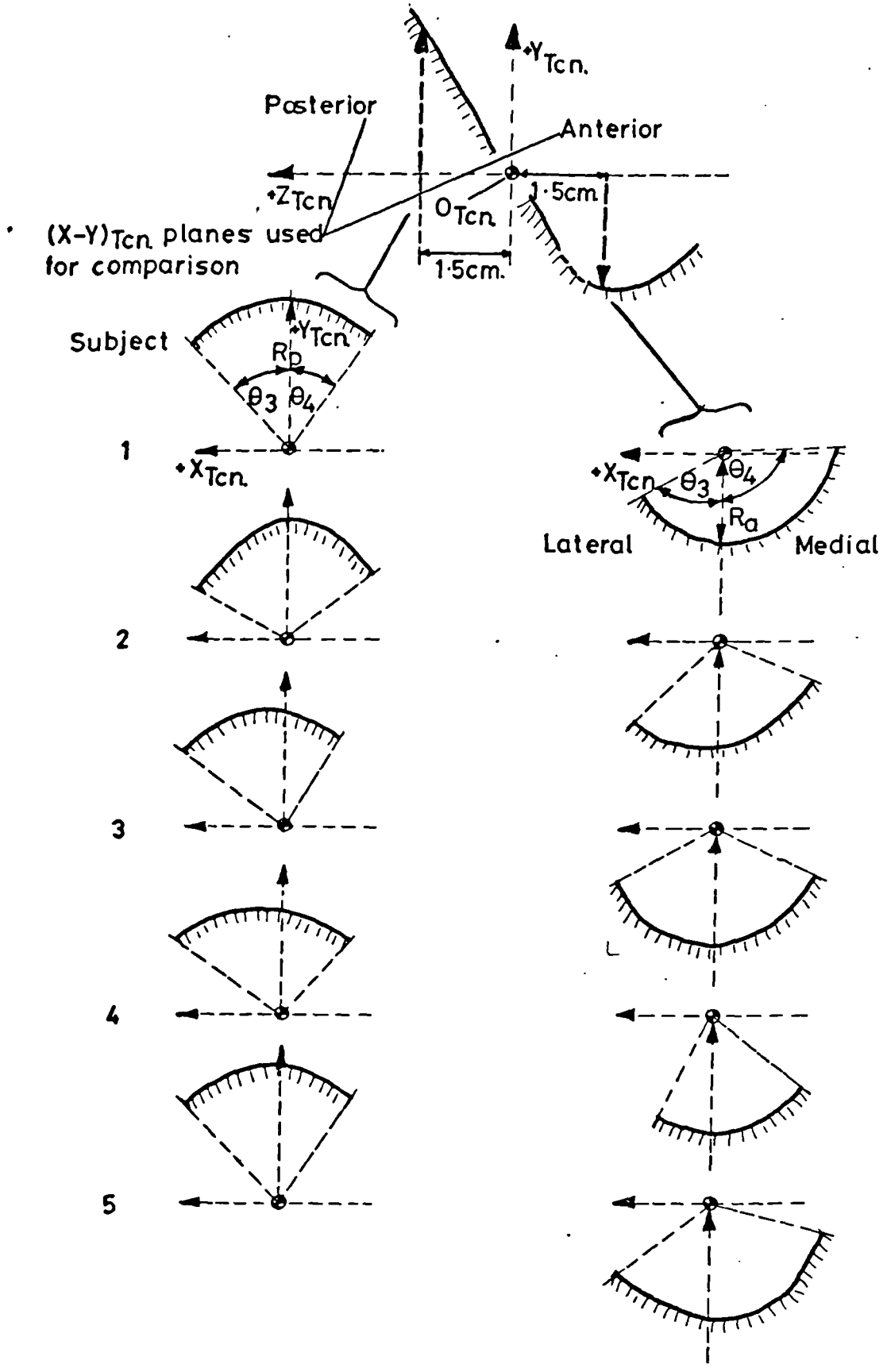

See A1.10(b) for tabulation of parameters θ_3° θ_4° R_a and R_p

A1.10(a) Mediolateral Tcn. Joint Sections and Parameters

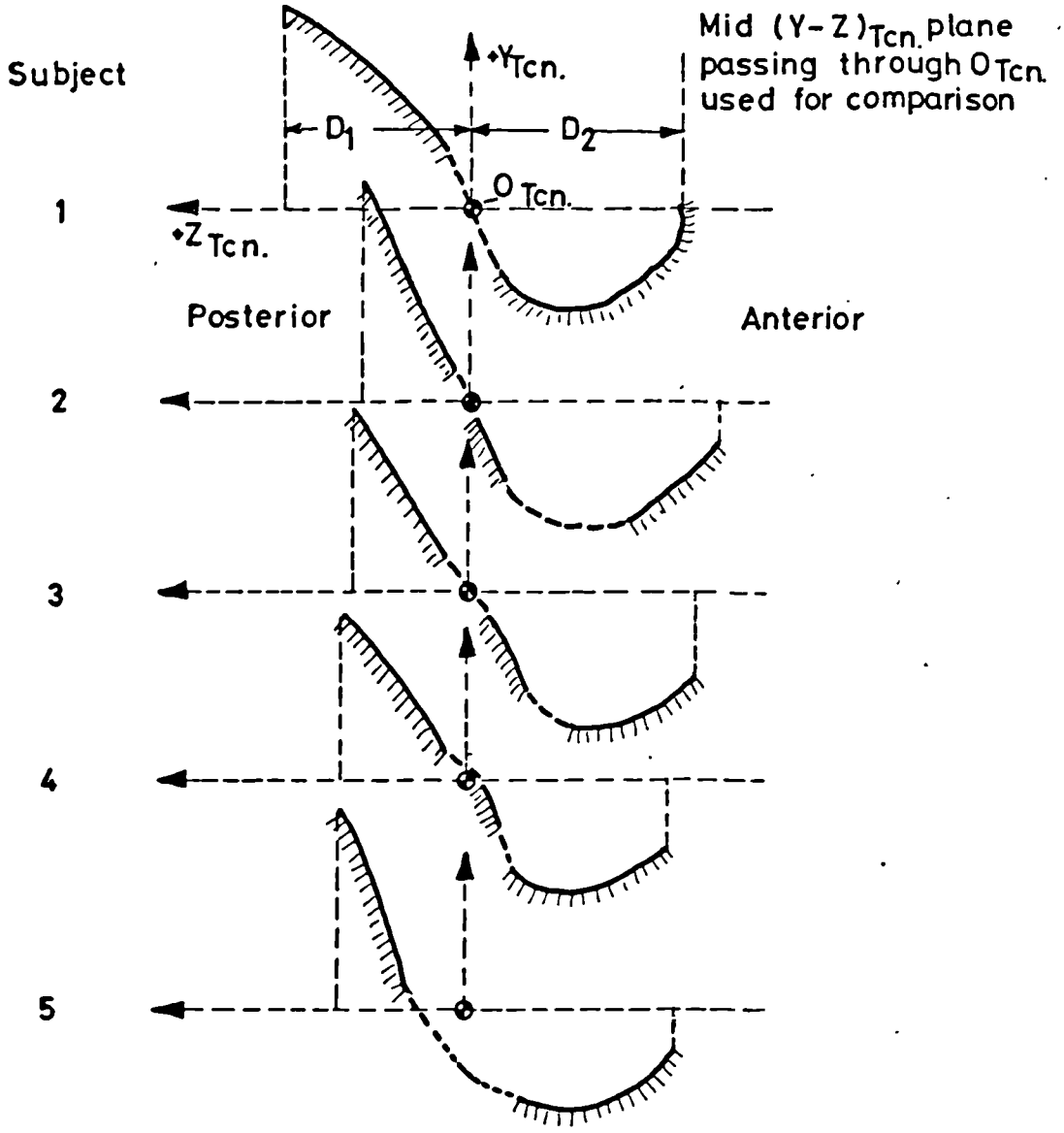

Subject	Posterior facets				Anterior facets			
	θ_3°	θ_4°	R_p(mm.)	D_1(mm.)	θ_3°	θ_4°	R_a(mm.)	D_2(mm.)
1	43	34	24.5	22.5	62	93	14.5	28.5
2	61	53	19.0	15.0	47	67	17.0	33.6
3	54	31	18.5	15.0	62	65	18.8	30.5
4	55	42	17.0	17.0	27	51	18.5	27.0
5	40	34	22.2	17.0	53	75	18.2	28.0
MEAN	52.4	38.8	20.2	17.3	50.2	70.2	17.4	29.5

A1.10(b) Anteroposterior Tcn. Joint Sections and Parameters

APPENDIX 2

EXPERIMENTAL CALCULATIONS

A2.1 The Muscle Group Participation Factors

Muscle	Tendon Cross-Section At $(cm.)^2$	Participation Factor (At/ΣAt group)
Peron. brev.	0.130	0.42
Peron. long.	0.189	0.58
(ΣAt Peron.)	0.319	Σ1.00
Post tib.	0.253	0.49
Flex. hall. long.	0.145	0.28
Flex. dig. long.	0.117	0.23
(ΣAt Post. tib.)	0.515	Σ1.00
Ant. tib	0.206	0.48
Ext. hall. long.	0.091	0.21
Ext. dig. long.	0.134	0.31
(ΣAt Ant. tib.)	0.431	Σ1.00

A2.2 The Potential Moments of the Ligaments

The first stage of the calculations is to set up the axes systems described in 3.4.8 using the anthropometric data in Appendix 1.8.

A2.2.1 The Tc. Axis System

Referring to figure 3.11(a)

(Tc. origin-Tc. lateral exit) = $Z_{Tc.}$ axis in the table system

giving,

$$\{Z\}_{Tc.} = \{-0.0066 \quad -0.0059 \quad 0.0280\} \quad (m.)$$

and arbitrarily defining the magnitude of $O_{Tc.}(y)$ as 0.1 metre,

$$\{0\}_{Tc.} = \{0.0000 \quad 0.1000 \quad 0.0000\} \quad (m.)$$

The vector cross-product of $\{0\}_{Tc.}$ and $\{Z\}_{Tc.}$ gives $\{X\}_{Tc.}$

$$\{X\}_{Tc.} = \{0\}_{Tc.} \text{ cross } \{Z\}_{Tc.}$$

$$= \det. \begin{vmatrix} 0.0000 & 0.1000 & 0.0000 \\ -0.0066 & -0.0059 & 0.0280 \end{vmatrix}$$

which in direction cosine form is

$$X\{l,m,n\}_{Tc.} = \{0.973 \quad 0.000 \quad 0.229\}$$

and $\{Z\}_{Tc.}$ in direction cosines

$$Z\{l,m,n\}_{Tc.} = \{-0.225 \quad -0.201 \quad -0.973\}$$

and

$$Y\{l,m,n\}_{Tc.} = Z\{l,m,n\}_{Tc.} \text{ cross } X\{l,m,n\}_{Tc.}$$

$$= \det. \begin{vmatrix} -0.225 & -0.201 & 0.953 \\ 0.973 & 0.000 & 0.229 \end{vmatrix}$$

$$= \{-0.046 \quad 0.980 \quad 0.195\}$$

we now have the components for $[R]_{T\rightarrow Tc.}$ which in its assembled form is,

$$[R]_{T\rightarrow Tc.} = \begin{matrix} X \\ Y \\ Z \end{matrix} \begin{bmatrix} \\ \{l,m,n\}_{Tc.} \\ \\ \end{bmatrix} = \begin{bmatrix} 0.973 & 0.000 & 0.229 \\ -0.046 & 0.980 & 0.195 \\ -0.225 & -0.201 & 0.953 \end{bmatrix}$$

and the translation vector $\{T\}_{OM\rightarrow OTc.}$ from the Table to the Tc. origin is,

$$\{T\}_{OM\rightarrow OTc.} = \{-0.0081 \quad -0.0104 \quad -0.0022\} \text{ (m.)}$$

A2.2.2 The Tcn. Axis System

Referring to figure 3.11(b) and following an essentially similar method to that outlined in A2.2.1,

(Tcn. origin-Tcn. lateral exit) = $Z_{Tcn.}$ axis in the table system

giving

$$\{Z\}_{Tcn.} = \{-0.0395 \quad -0.0359 \quad 0.0168\} \text{ (m.)}$$

and arbitrarily defining the magnitude of $O_{Tcn}(y)_{T.}$ as 0.1 metre,

$$\{0\}_{Tcn.} = \{0.0000 \quad 0.1000 \quad 0.0000\} \text{ (m.)}$$

$\{X\}_{Tcn.}$ is given by,

$$\{X\}_{Tcn.} = \{0\}_{Tcn.} \text{cross } \{Z\}_{Tcn.}$$

$$= \det. \begin{vmatrix} 0.0000 & 0.1000 & 0.0000 \\ -0.0395 & -0.0359 & 0.0168 \end{vmatrix}$$

which gives, in direction cosine form,

$$X\{l,m,n\}_{Tc.} = \{0.391 \quad 0.000 \quad 0.920\}$$

and $\{Z\}_{Tcn.}$ in direction cosines,

$$Z\{l,m,n\}_{Tcn.} = \{-0.706 \quad -0.641 \quad 0.300\}$$

and

$$Y\{l,m,n\}_{Tcn.} = Z\{l,m,n\}_{Tcn.} \text{cross } X\{l,m,n\}_{Tcn.}$$

$$= \det. \begin{vmatrix} -0.706 & -0.641 & 0.300 \\ 0.391 & 0.000 & 0.920 \end{vmatrix}$$

$$= \{-0.590 \quad 0.767 \quad 0.251\}$$

and $[R]_{T \to Tcn.}$,

$$[R]_{T \to Tcn.} = \begin{matrix} X \\ Y \\ Z \end{matrix} \begin{bmatrix} \\ \\ \{l,m,n\}_{Tcn.} \end{bmatrix} = \begin{bmatrix} 0.391 & 0.000 & 0.920 \\ -0.591 & 0.767 & 0.251 \\ -0.706 & -0.641 & 0.300 \end{bmatrix}$$

and the translation vector from the table to the Tcn.

origin,

$$\{T\}_{OM\ Tcn.} = \{0.0171 \quad -0.0222 \quad -0.0017\}\ (m.)$$

A2.2.3 Specimen Calculation of Potential Moments

An example of the potential moment calculation is given using the Anterior-fibulotalar ligament data in Appendix 1.7. Using the algebraic expressions in 4.2.2 and referring to figure 4.1,

$$\{RoL\}_T = \{0.0043 \quad -0.0119 \quad 0.0244\}\ (m.)$$
$$\{RiL\}_T = \{0.0143 \quad -0.0106 \quad 0.0179\}\ (m.)$$
$$\{RoL\}_T - \{RiL\}_T = \{-0.0100 \quad -0.0013 \quad 0.0065\}\ (m.)$$

evaluating equations 4.1, 4.2 and 4.3,

$$L\{l,m,n\}_T = \{-0.833 \quad -0.108 \quad 0.541\}$$

evaluating equations 4.4 and 4.5 gives the direction cosines in the Tc. and Tcn. systems,

$$L\{l,m,n\}_{Tc.} = \{-0.687 \quad 0.380 \quad 0.726\}$$
$$L\{l,m,n\}_{Tcn.} = \{0.172 \quad 0.545 \quad 0.820\}$$

equations 4.6 and 4.7 give the ligament insertion in the Tc. and Tcn. systems,

$$\{RiL\}_{Tc.} = \{0.0106 \quad 0.0034 \quad 0.0178\}\ (m.)$$
$$\{RiL\}_{Tcn.} = \{0.0169 \quad 0.0155 \quad 0.0004\}\ (m.)$$

finally the potential moments, equations 4.8 and 4.9 are,

$$\{M_L\}_{Tc.} = \{0.0018 \quad -0.0200 \quad 0.0028\}\left(\frac{\text{Newton metres}}{\text{Newton ligt. force}}\right)$$

$$\{M_L\}_{Tcn.} = \{0.0125 \quad -0.0138 \quad 0.0066\}\left(\frac{\text{Newton metres}}{\text{Newton ligt. force}}\right)$$

The values calculated for the remaining ligaments and the Retinaculum are tabulated in Table A2.1.1 and plotted in figures 4.2 and 4.3.

Ligament	Potential Moments: Newton metres/unit ligament force					
	Tc. Components			Tcn. Components		
	X	Y	Z	X	Y	Z
Deltoid post.	0.0099	* -0.0115	-0.0005	-0.0126	** -0.0187	0.0025
Deltoid mid.	* 0.0223	-0.0018	-0.0088	0.0022	** -0.0159	-0.0115
Deltoid ant.	* 0.0244	0.0042	0.0059	0.0127	-0.0103	** -0.0159
Aft.	0.0018	* -0.0200	0.0028	0.0125	** -0.0138	0.0066
Pft.	-0.0011	* 0.0219	-0.0040	0.0020	0.0153	** -0.0289
Fc.	-0.0202	* 0.0235	-0.0028	-0.0199	** 0.0256	-0.0124
Retinaculum	-0.0122	* 0.0184	0.0146	-0.0062	** 0.0209	0.0052

* identifies the greatest Tc. components
**identifies the greatest Tcn. components

Table A2.2.1 Potential moments due to the ankle collateral ligaments for 0° Tc. and Tcn. angles

A2.3 Estimate of the Approximate Inertial and Gravitational Moments of the Foot

The calculations were based upon the test results obtained for a single subject, in normal locomotion. They were intended to give some feel for the order of magnitude of the inertial and gravitational forces acting on the foot rather than be an accurate and precise guide. Cine film (at 50 Hz.) of the lateral aspect of the foot was used to estimate the angular displacement of the foot (θ) relative to the ground during the heel strike period - where the angular acceleration of the foot is thought to be greatest. The derivatives - angular velocity ($\dot{\theta}$) and angular acceleration ($\ddot{\theta}$) - were calculated using the method of differences.

The rotational moment of inertia and typical dimensions were obtained from Chandler et al (1975). The moment of inertia was estimated as 0.003kgm.^{2} - acting about the centre of gravity. The rotary moment of inertia, about the heel point of contact, was estimated from (referring to figure A2.3.1),

$$I_h = I_g + mr^2 \qquad \ldots \text{A2.3.1}$$

where I_h = rotary moment of inertia of the foot about the heel (kgm.^{2})

I_g = rotary moment of inertia of the foot about the centre of gravity (kgm.^{2})

m = mass of the foot

r = radius of centre of gravity with respect to the heel (m.)

taking $I_g \simeq 0.003$kgm.^{2}, m=0.840kg. and r as $(0.0133^2+0.1062^2)^{\frac{1}{2}}$m.

$$I_h \simeq 0.013 \text{kgm.}^2 \quad \text{(Note this is for a bare foot)}$$

referring to table A2.3.1 the peak angular acceleration $\hat{\ddot{\theta}}$ is given as,

$$-0.9 \times \frac{2\pi}{360} \times \frac{1}{1/50}\, s^{-1} \times \frac{1}{1/50}\, s^{-1}$$

$$\hat{\ddot{\theta}} \simeq -40 \text{ rad/s}^2$$

Thus the peak moment $(\hat{M})_i$ due to the angular acceleration about the heel, $(\hat{M})_i = -I_h \hat{\ddot{\theta}}$ is

$$= -(0.013.-40)$$

$$(M)_i = 0.5 \text{ Nm.}$$

The moments due to gravity about the heel $(M)_g$ were calculated as the product of the weight of the foot times the projection of radius r on the X axis in figure A2.3.1, thus,

$$(M)_g = m.g.r_p \qquad \ldots \text{ A2.3.2}$$

where

g = gravitational constant (m/s^2)

r_p = projection of r on the X axis (m.)

taking $r_p^* \simeq 0.096$m., $g \simeq -9.81$ m/s^2 and $m = 0.840$ kg. (r_p^* corresponding to the peak acceleration of -39.3 rad/s^2),

$$(M)_g = -((0.840).(9.81).(0.096)) \text{ Nm.}$$

$$(M)_g = -0.80 \text{ Nm.}$$

The net moment due to the inertial and gravitational component

$$(M)_g+(\hat{M})_i = (-0.80+0.50) = -0.30 \text{ Nm.}$$

The values obtained for the heel strike period for test subject seven are tabulated in table A2.3.1

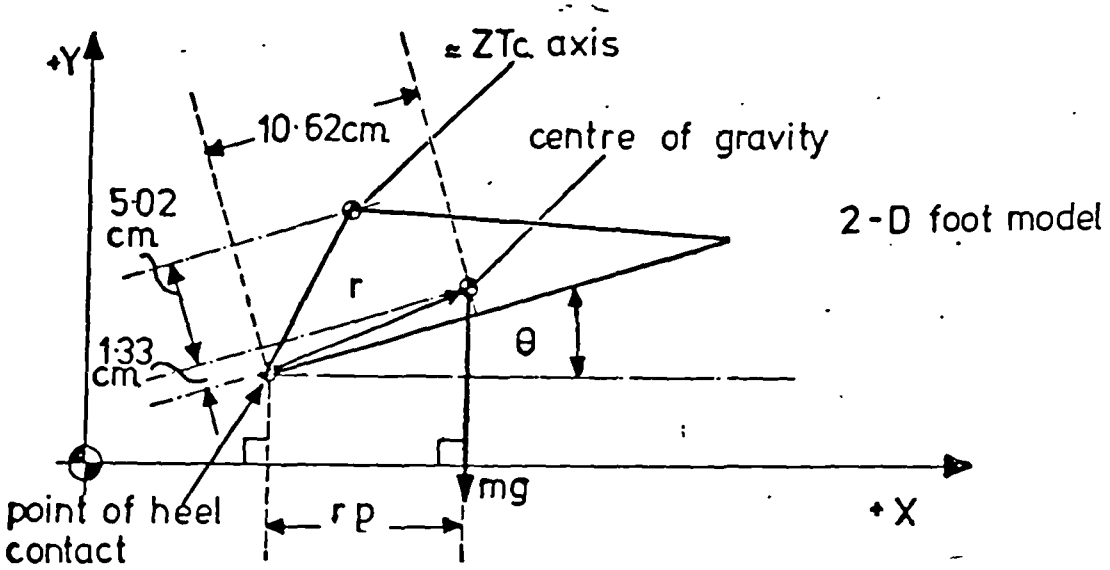

A2.3.1 Two-Dimensional Representation of the Foot used in the Estimation of Inertial and Gravitational Moments Acting about the Heel at Heel Strike

θ° *	$\Delta(\theta^\circ)$**	$\Delta(\Delta(\theta^\circ))$***	Moment due to inertia of foot $(M)_i$ Nm.	Moment due to gravity $(M)_g$ Nm.	Net Moment Nm.
hs 34.9					
	5.9				
29.0		0.3	0.16	-0.66	-0.50
	5.6				
23.0		0.4	0.22	-0.71	-0.49
	5.2				
18.2		0.7	0.39	-0.75	-0.36
	4.5				
13.7		0.9	0.50	-0.79	-0.29
	3.6				
10.1		0.8	0.44	-0.82	-0.38
	2.8				
7.3		0.7	0.39	-0.84	-0.45
	2.1				
5.2		0.6	0.33	-0.85	-0.52
	1.5				
3.7		0.6	0.33	-0.86	-0.53
	0.9				
2.8		0.3	0.16	-0.86	-0.70
	0.6				
2.2		0.1	-0.05	-0.86	-0.91
	0.7				
1.5		0.1	0.05	-0.86	-0.81
	0.6				
0.9		0.1	0.05	-0.86	-0.81
	0.5				
0.4					

* angular displacement - degrees
** angular velocity - degrees per 1/50th second
*** angular acceleration - degrees per $(1/50 \times 1/50)s^2$
hs heel strike

Table A2.3.1 Estimated Gravitational and Inertial Moments

APPENDIX 3

THE CALCULATIONS AND COMPUTER PROGRAMS

A3.1 Equations of Parallax

The equations of parallax were written and incorporated into the KINESB and KINEDB programs. The parallax corrections were small, less than 5mm. maximum, and generally were much less than this. The correction of the apparent coordinates of a point P,(X_a,Y_a,Z_a) to obtain the true coordinates $P(X_t,Y_t,Z_t)$ are given by the following: referring to figure A3.1.1(a) from similar triangles the front camera gives (where subscript a = apparent, t = true),

$$(Z_a/Z_t) = (FD/(FD-X_t)) \qquad \text{A3.1.1}$$

and for the left camera,

$$(X_{al}/X_t) = (LD/(LD+Z_t)) \qquad \text{A3.1.2}$$

and for the right camera,

$$(X_{ar}/X_t) = (RD/(RD-Z_t)) \qquad \text{A3.1.3}$$

from equations A3.1.1, A3.1.2,

$$X_t = X_{al}.FD(LD+Z_a)/(LD.FD+Z_a.X_{al}) \qquad \text{A3.1.4}$$

and from equations A3.1.1, A3.1.3,

$$X_t = X_{ar}.FD.(RD-Z_a)/(RD.FD-Z_a.X_{ar}) \qquad \text{A3.1.5}$$

Once X_t has been calculated (from A3.1.4 or A3.1.5) substitution into A3.1.1 gives,

$$Z_t = Z_a(1-X_t/FD) \qquad \text{A3.1.6}$$

The true Y coordinate, Y_t, is calculated from additional equations, consider figure A3.1.1(b) where similar triangles give,

$$(Y_a-h)/(Y_t-h) = FD/\ FD-X_t) \qquad A3.1.7$$

hence,

$$Y_t = Y_a-X_t.(Y_a-h)/FD \qquad A3.1.8$$

The camera distances involved were estimated as:

FD = 5.760 (m.)

RD = 3.300 (m.)

LD = 2.150 (m.)

h = 0.495 (m.)

An example of how the above equations were used in the KINESB program:

KINESB LINE

```
132  FFS(I,1)=RFS(I,1)*(1-FFS(I,3)/RD)/(1-FFS(I,3)*RFS(I,1)/
                                                    (RD*FD)
133  FFS(I,2)=FFS(I,2)*FFS(I,1)*FFS(I,2)-0.495)/FD
134  FFS(I,3)=FFS(I,3)*(1-FFS(I,1)/FD)
```

where

I is the number of marker points

and array dimension code,

1 = X coordinate (equation A3.1.5)

2 = Y coordinate (equation A3.1.8)

2 = Z coordinate (equation A3.1.6)

FFS (on left hand side) = array of true coordinates

FFS (on right hand side) = array of apparent coordinates from front camera

RFS = array of apparent coordinates from right camera.

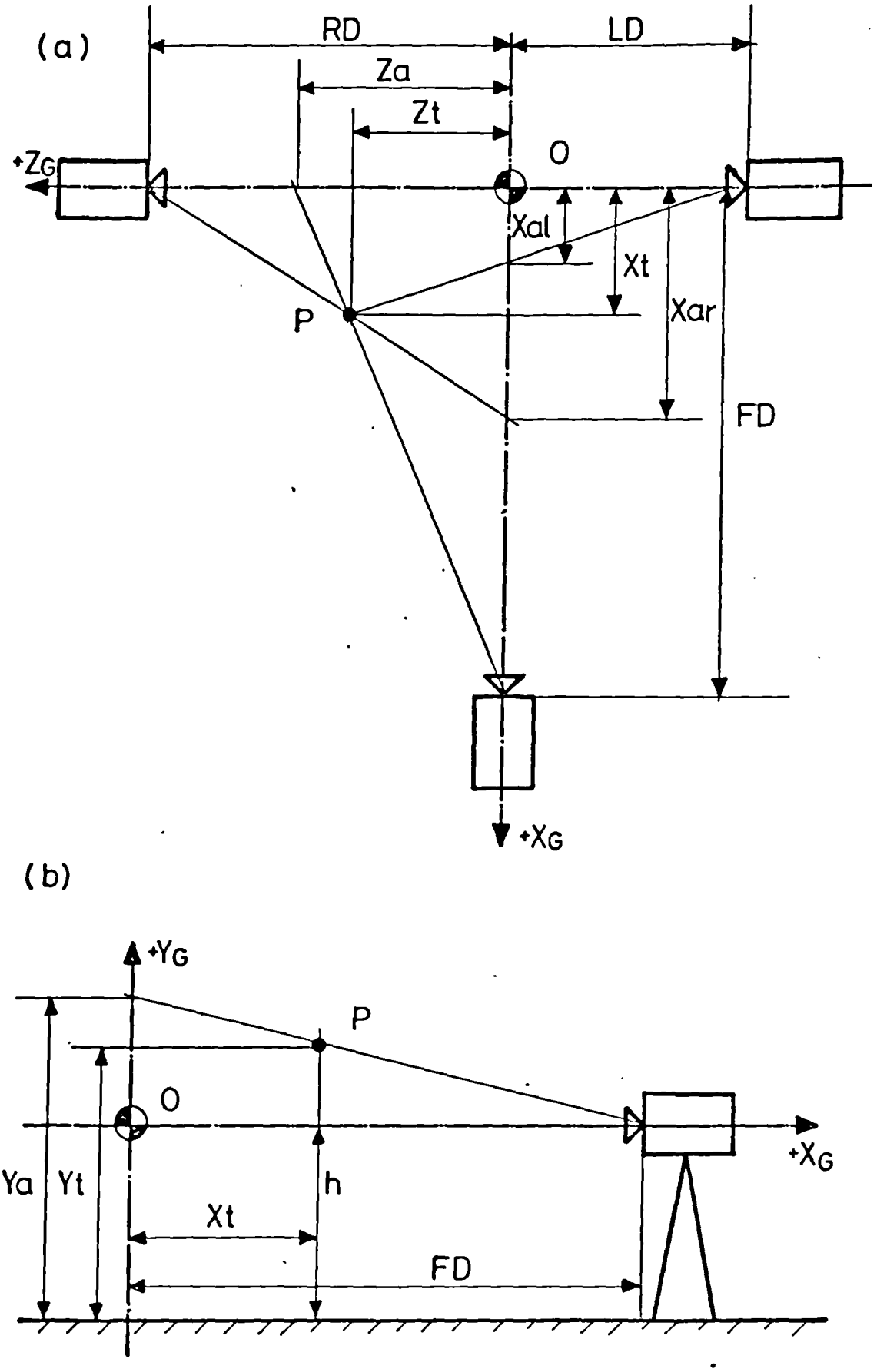

Figure A3.1.1 Plan (a) and Side Elevation (b) of the Camera System Orientation Relative to the Laboratory Ground System

A3.2 The Calculation of Bony Points

A3.2.1 The Equations

Referring to figure A3.2.1 the coordinates of the bony prominence P are given in vector notation as,

$$\{P\} = \{B\} + \frac{\gamma}{\alpha}\{B\} - \frac{\gamma}{\alpha}\{A\} \qquad \text{A3.2.1}$$

or

$$\{P\} = -\{A\}C + \{B\}(C + 1) \quad (\text{where } C = \tfrac{\gamma}{\alpha}) \qquad \text{A3.2.2}$$

This equation, written as a FORTRAN statement (line 190 KINESB program) is,

```
MAR(I,J) = -FFS((I*2),J)*COEF(I)+FFS((I*2+1),J)*(COEF(I)+1.0)
```

A3.2.3

for (I) markers with (J) coordinates where

MAR(I,J) = $\{P\}$

FFS((I*2),J) = $\{A\}$

FFS((I*2+1),J) = $\{B\}$

COEF(I) = C

A3.2.2 Calculation of the Coefficient C

The magnitude of C depends upon whether the marker is long or short, the skin thickness t, α and β. The following table, A3.2.1, lists the markers and calculated values of C The t values are tabulated in A1.2.

A trial was undertaken with a long marker affixed to different bony landmarks on the shank and foot segment of a test subject. When deflected and released the dynamic motion of the marker appeared to be heavily damped; when the test subject stamped the displacement of the outer marker bead was observed to be less than +3mm. With regard to the analysis, the marker performance indicated that the displacement due to dynamic loading was largely angular

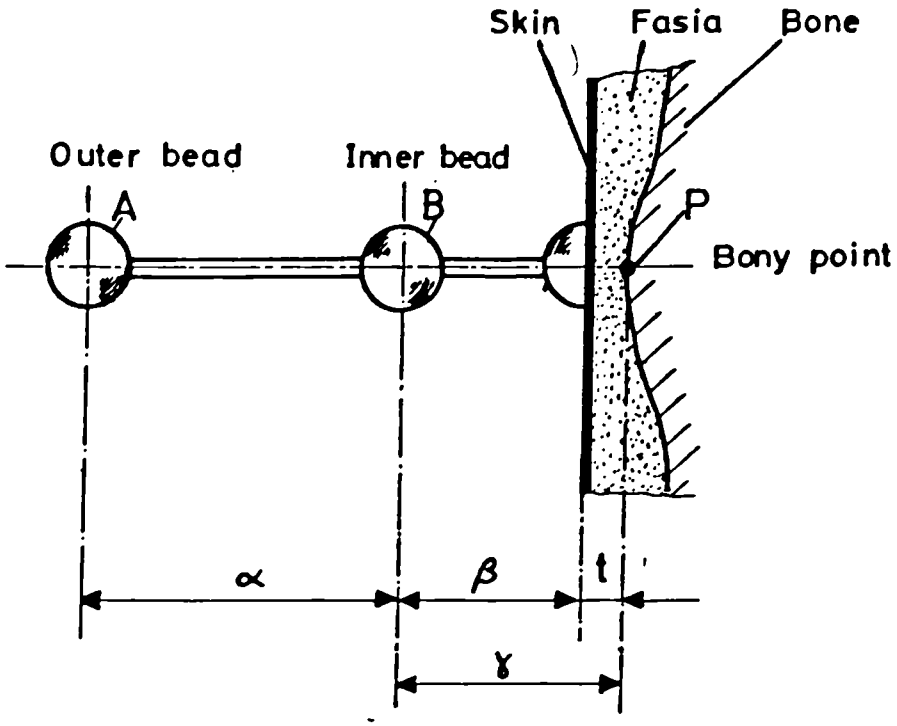

Figure A3.2.1 Surface Marker in Relation to a Bony Prominence

and that therefore the predicted position of a bony landmark which it represented would vary less than ⁺1mm. for ⁺5mm. displacement of the outer marker bead.

Location	Markers A	Markers B	Short(S)/ Long(L)	t (m.)	α (m.)	β (m.)	γ (β+t) (m.)	C
Medial Condyle	14	15	L	0.0075	0.035	0.020	0.0275	0.7869
Lateral Condyle	6	7	L	0.0074	0.035	0.020	0.0274	0.7817
Tibial Tubercle	8	9	S	0.0030	0.025	0.015	0.0180	0.7212
Most Medial Point Medial Malleolus	12	13	L	0.0024	0.035	0.020	0.0224	0.6403
Most Lateral Point Lateral Malleolus	4	5	S	0.0030	0.025	0.015	0.0180	0.7814
Calcaneal Insertion of Achilles Tendon	16	17	L	0.0056	0.035	0.020	0.0256	0.7303
Navicular Tuberosity	10	11	S	0.0026	0.025	0.015	0.0176	0.7028
Metatarsal Five Base	2	3	L	0.0045	0.035	0.020	0.0245	0.7006

Table A3.2.1 Calculation of Skin Thickness Coefficient C

A3.3 The Calculation of Missing Marker Coordinates

As noted in 6.3.1, only side camera views of the heel markers were obtained during the actual tests. The method used by Morrison (1968) was employed for predicting the three true coordinates of the heel marker. The two apparent coordinates of each heel marker point were obtained from the right camera view. The additional information required to use the method is the distance between the markers whose coordinates are to be estimated, and a marker whose three coordinates in space are already known. This is why, at the beginning of each test (Phases one and two, 5.3.4), the subject was filmed whilst facing away from the front camera; the heel markers could be seen by all three cameras as well as the metatarsal five marker, point 2. The distances between heel marker point 16 and 17 and marker point 2, d16-2 and d17-2 respectively, were then calculated by Pythagorean geometry. In the static film test, the subject faced the front camera and the apparent coordinates X_{a16}, X_{a17}, Y_{a16} and Y_{a17} were measured. The following calculation illustrates how the true coordinates (subscript t) were obtained for markers 16 and 17.

from equation A3.1.3 $X_{ar}/X_t = RD/(RD-Z_t)$ A3.3.1

and A3.1.8 $Y_t = (Y_a - X_t(Y_a-h)/FD)$ A3.3.2

referring to figure A3.3.1, from Pythagoras,

$$(d17\text{-}2)^2 = (X_{t17}-X_{a2})^2+(Y_{t17}-Y_2)^2+(Z_{t17}-Z_{t2})^2 \quad \text{A3.3.3}$$

substituting for Y_{t2} and X_{t2} using A3.3.1 and A3.3.2 above,

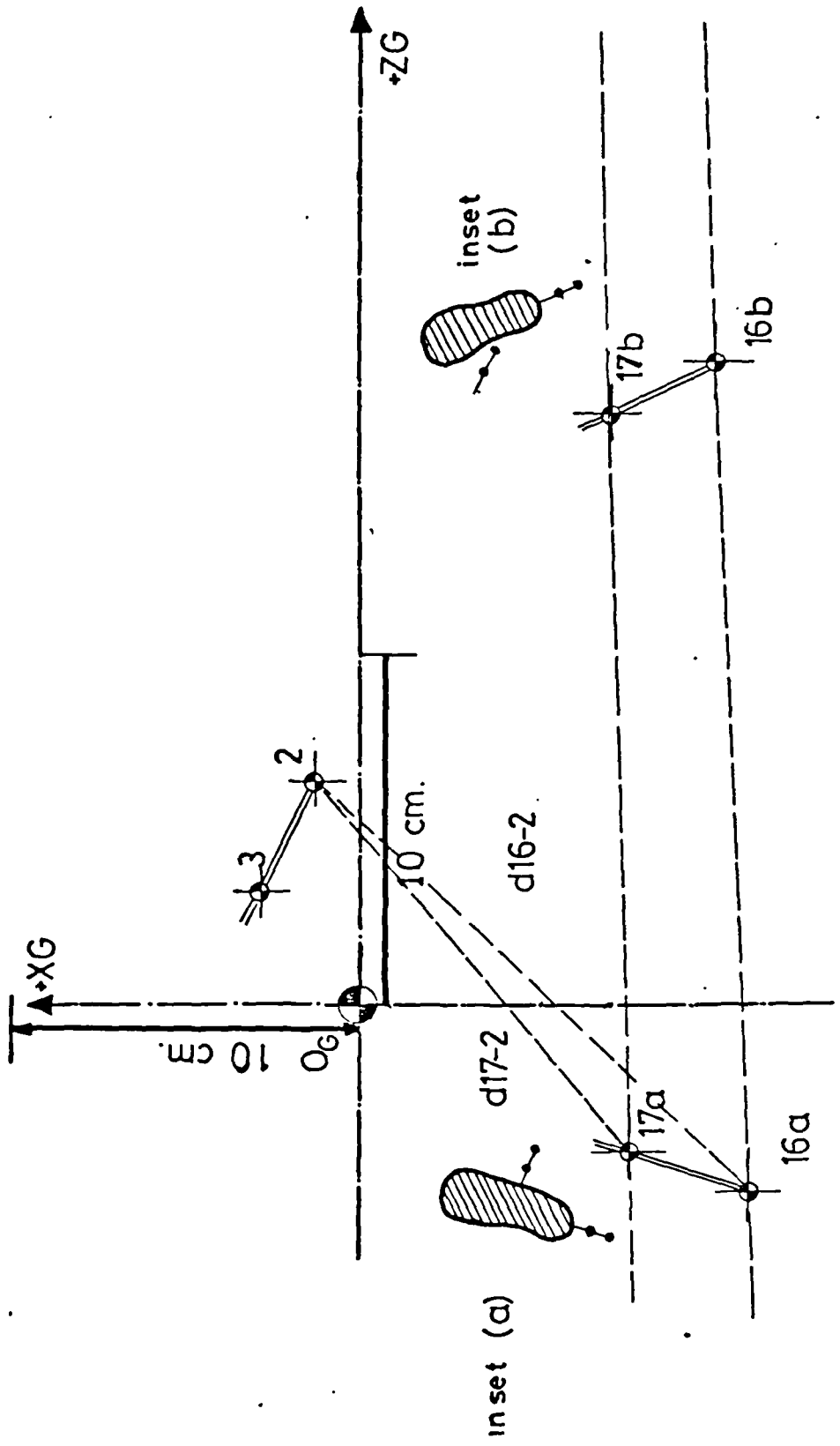

Figure A3.3.1 Illustration of the Two Solutions to the Quadratic Equation Formulated in A3.3, (a) is the Required Solution (b) is Rejected

$$(d_{17-2})^2 = (X_{t17}-X_{a2}(1-\frac{Z_{t2}}{RD}))^2+(Y_{t17}-Y_{a2}+(Y_{a2}-h).\frac{Z_{t2}}{RD})^2+(Z_{t17}-Z_{t2})^2$$

A3.3.4

which can be simplified to,

$$A.Z_{t17}^2+B.Z_{t17}+C = 0 \qquad \text{A3.3.5}$$

a quadratic equation in Z_{t17} where,

$$A = b^2+d^2+1$$
$$B = a.b+c.d-e$$
$$C = a^2+c^2+e^2-(d_{17-2})^2$$

and further

$$a = X_{t2}-X_{a17}$$
$$b = X_{a17}/RD$$
$$c = Y_{t2}-Y_{a17}+Y_{a17}/RD$$
$$d = -h/RD$$
$$e = Z_{t2}$$

Thus from the true coordinates of marker 2 and the apparent coordinates of marker 17, together with the distance d17-2, the true coordinates of marker 17 may be calculated. By an exactly similar method the true coordinates of marker 16 may be calculated.

The quadratic equation gives two roots and the correct choice of root will be shown by a numerical sample. The three static camera views of the subject's leg with the heel facing the front camera gave the following data;

coordinates in metres	Marker 2 True coordinates	Marker 3 True coordinates	Marker 16 Apparent coordinates	Marker 17 Apparent coordinates
X	0.0133	0.0271	-0.0112	-0.0795
Y	0.0338	0.0239	0.0613	0.0496
Z	0.0639	0.0323	———	———

taking RD = 3.3m., FD = 7.6m., h = 0.495m., d17-2 = 0.1736m., and d16-2 = 0.1414m., the following values for Z_{t17} and Z_{t16} obtained,

Marker			Corresponding value of X_t
* 17	Root 1	Z_{t17} = -0.0540m.	-0.1140m.
	Root 2	Z_{t17} = +0.1850m.	-0.1060m.
* 16	Root 1	Z_{t16} = -0.0420m.	-0.0810m.
	Root 2	Z_{t16} = +0.1710m.	-0.0750m.

The X_t values were obtained by substituting for Z_t and X_{ar} in equation A3.3.1. These values are plotted on figure A3.3.1 together with the X-Z coordinates of markers 2 and 3. The inset profile (a) of the right foot in figure A3.3.1 shows that the algebraically smaller Z_t roots are the required values (annotated * in the above table). The larger roots correspond to a physiologically impossible solution where the metatarsal five marker has moved to the medial side of the right foot, illustrated by inset profile (b) in figure A3.3.1.

An example of the application of this is given in lines 153 to 179 KINESB program in Appendix 3.5.

A3.4 Computer Programs and their Organisation

A3.4.1 Introduction

The computer programs were arranged so that they could be run in sequence using simple one line commands, see figure A3.4.1. To identify each subject and the test type uniquely masking parameters were used in each command. The subjects were identified by their initial, PP for example, which corresponds to masking parameter %A in figures 6.9 and A3.4.1. The test type was identified by a number, 1, 2 or 3 (1 = normal locomotion, 2 = -10° side slope and 3 = +10° side slope) which corresponds to masking parameter %B in figures 6.9 and A3.4.1. To run all the programs in sequence the commands in figure A3.4.1 were input into the computer in the order shown, allowing for each stage to be completed before the next was initiated. Each command refers to a runfile sequence of commands which actually runs a computer job assigning input and output files and the program to be used. In order to run one complete set of programs for one subject and one test, seven computer files were required. These will be described in order below, with the format of data within the file and the stage of analysis to which they apply. Note that the KINES program only requires to be run once for one subject since the relation between the subject anthropometry and external marker systems remains constant throughout all the tests. Refer to figure 6.1 which shows the Analysis stages and main computer programs.

A3.4.2 Stage One Analysis

This was performed by KINESB and takes the static film data views from three cameras together with the anthropometric data to calculate subject anthropometry

in relation to the external reference axes systems.

The input files are,

CADAVER: this contains two blocks of data, the skin thickness coefficients (table A3.2.1), the cadaver anthropometry (tabulated in A1.4, A1.7 and A1.8).

Line	Skin thickness coefficients from A3.2.1
1	Metatarsal five base
2	Lateral malleolus
3	Lateral condyle
4	Tibial tubercle
5	Navicular tuberosity
6	Medial malleolus
7	Medial condyle
8	Achilles tendon

Coordinates of Cadaver Anthropometry from Appendices 1.4, 1.7 and 1.8

	x(m.)	y(m.)	z(m.)		
9	.	.	.	Origin	Deltoid Mid Band
10	.	.	.	Insertion	
11	.	.	.	Prox.	Calf muscle
12	.	.	.	Dist.	
13	.	.	.	Prox.	Ant. tib.
14	.	.	.	Dist.	
15	.	.	.	Prox.	Ext. dig. long.
16	.	.	.	Dist.	
17	.	.	.	Prox.	Ext. hall. long.
18	.	.	.	Dist.	
19	.	.	.	Prox.	Post. tib.
20	.	.	.	Dist.	

21	Prox.	Flex. dig. long.
22	Dist.	
23	Prox.	Flex. hall. long.
24	Dist.	
25	Prox.	Peron. long.
26	Dist.	
27	Prox.	Peron. brev.
28	Dist.	
29	Origin	Anterior fibulotalar ligament
30	Insertion	
31	Origin	Posterior fibulotalar ligament
32	Insertion	
33		Tc. origin
34		Tc. lateral exit
35		Tcn. origin
36		Tcn. lateral exit

Note that ligament components listed in the above file were included at an early stage in the program development and were not subsequently included into the analysis.

KINES%A: This contains four blocks of data, from the front, left and right camera static data obtained for test phases one and two (see 5.3.4), then the camera distance parameters from A3.1.

Front camera data, for each point Y_G and Z_G apparent

Line		coordinates were obtained
1	Field marker	calibration board reference points 1 and 2
2	Field marker	(subject facing front camera)
3	Marker bead 2	"

4	Marker bead 3	(subject facing front camera)
5	Marker bead 4	"
6	Marker bead 5	"
7	Marker bead 6	"
8	Marker bead 7	"
9	Marker bead 8	"
10	Marker bead 9	"
11	Marker bead 10	"
12	Marker bead 11	"
13	Marker bead 12	"
14	Marker bead 13	"
15	Marker bead 14	"
16	Marker bead 15	"
17	Field marker	(subject facing away from front camera)
18	Marker bead 16	"
19	Marker bead 17	"
20	Marker bead 2	"
21	Marker bead 3	"

Left camera data, for each point X_G and Y_G apparent coordinates were obtained

22	Field marker	calibration board reference point 1 then 2
23	Field marker	(subject facing front camera)
24	Marker bead 10	"
25	Marker bead 11	"
26	Marker bead 12	"
27	Marker bead 13	"
28	Marker bead 14	"
29	Marker bead 15	"
30	Field marker	(subject facing away from front camera)
31	Marker bead 16	"
32	Marker bead 17	"

33	Marker bead 2	(Subject facing away from front camera)
34	Marker bead 3	"

Right camera data, for each point X_G and Y_G apparent coordinates were obtained

35	Field marker	calibration board reference point 1 then 2
36	Field marker	(Subject facing front camera)
37	Marker bead 2	"
38	Marker bead 3	"
39	Marker bead 4	"
40	Marker bead 5	"
41	Marker bead 6	"
42	Marker bead 7	"
43	Marker bead 8	"
44	Marker bead 9	"
45	Marker bead 16	"
46	Marker bead 17	"
47	FD LD RD	Camera distance parameters

A3.4.3 Stage Two Analysis

This takes the dynamic test data from three cameras and computes for each frame the relationship between the Tc. and Tcn. axes and the ground system origin. The input files are,

%ARESULTS1: this contains the rotation and translation data computed by KINESB relating the External shank and hindfoot systems to the Internal Tc. and Tcn. systems respectively in the form,

Line		
1	$\{X_{OEs.} \quad Y_{OEs.} \quad Z_{OEs.}\}$	$(\{T\}_{OEs.\rightarrow OTc.})$
2	$\begin{bmatrix} . & . & . \end{bmatrix}$	$([R]_{Es.\rightarrow Tc.})$
3	$\begin{bmatrix} . & . & . \end{bmatrix}$	
4	$\begin{bmatrix} . & . & . \end{bmatrix}$	
5	$\{X_{OEh.} \quad Y_{OEh.} \quad Z_{OEh.}\}$	$(\{T\}_{OEh.\rightarrow OTcn.})$
6	$\begin{bmatrix} . & . & . \end{bmatrix}$	$([R]_{Eh.\rightarrow Tcn.})$
7	$\begin{bmatrix} . & . & . \end{bmatrix}$	
8	$\begin{bmatrix} . & . & . \end{bmatrix}$	

%AFK%B: containing the number of frames and front camera static calibration data followed by the dynamic test marker points as,

Line		
1	Number of frames of test data = N	
2	Field marker, calibration board reference point 1 then 2	
	Then dynamic points, apparent Y_G and Z_G coordinates were obtained for each point	
3	Field marker; marker beads 2, 5,	repeated for N frames
4	7, 9 and 11	
.		
.		
N+3		

%ALK%B: containing the number of frames, and the left camera static calibration data followed by the dynamic test marker points as follows,

1	Number of frames of test data = N
2	Field marker, calibration board reference point 1 then 2

Then dynamic points, apparent X_G and Y_G coordinates were obtained for each point

3	Field marker; marker beads 2 and 3	repeated for N frames
4		
.		
.		
N+3		

%ARK%B: containing the number of frames, the right camera phase one static calibration data followed by the dynamic test marker points as the following,

Line	
1	Number of frames of test data = N
2	Field marker, calibration board reference point 1 then 2

Then dynamic points, apparent X_G and Y_G coordinates were obtained for each point

3	Field marker; marker beads 2, 5, 7, 9 and 17	repeated for N frames
4		
.		
.		
N+3		

A3.4.4 Stage Three Analysis

This takes for each frame, the translations and rotations between Tc. and Tcn. system and the ground system origin, the force platform data and the subject data. It calculates external forces and moments in the Tc. and Tcn. system, the orientation of the muscle groups and the Mark I model solution in the FORCED1B version and the Mark II model solution in the FORCED2B version.

The input files are,

SUBJECT%A: containing the force platform gain factors, muscle participation factors (in A2.1) and the subject weight in Newtons, as follows,

Line	
1	Top amplifier gain factor, Bottom amplifier gain factor
2	Participation factors - Ant. tib., Ext. dig. long. and Ext. hall. long.
3	Participation factors - Post. tib., Flex. dig. long. and Flex. hall. long.
4	Participation factors - Peron. long. and Peron. brev.
5	Subject weight - in Newtons

%AOF%B: this contains the number of points, the digitised force data output from the PDP12 computer in six blocks and the slope parameter,

Line		
1	Number of points = N	
2	Force channel DC shift correction factor	
3	Force channel sampled point	} repeated N times
.		
.		
6N+2	Slope parameter (0 = Normal locomotion, +1 = +10° slope, -1 = -10° slope)	(There are six blocks of data, follow the above format for Fx, Fy, Fz, Mx, My and Mz)

%A%BRESULTK1: this contains the translation and rotation data computed by KINEDB relating the Tc. and Tcn. systems to the ground system for each frame, as follows,

Line		
1	$\{X_{OTc.} \quad Y_{OTc.} \quad Z_{OTc.}\}$	$(\{T\}_{OG.\rightarrow OTc.})$
2	$\begin{bmatrix} . & . & . \end{bmatrix}$	$([R]_{G.\rightarrow Tc.})$
3	$\begin{bmatrix} . & . & . \end{bmatrix}$	
4	$\begin{bmatrix} . & . & . \end{bmatrix}$	
5	$\{X_{OTcn.} \quad Y_{OTcn.} \quad Z_{OTcn}\}$	$(\{T\}_{OG.\rightarrow OTcn.})$
6	$\begin{bmatrix} . & . & . \end{bmatrix}$	$([R]_{G.\rightarrow Tcn.})$
7	$\begin{bmatrix} . & . & . \end{bmatrix}$	
8	$\begin{bmatrix} . & . & . \end{bmatrix}$	
	repeated for N frames	
8N		

%ARESULTS2: this contains the subject anthropometry calculated by KINESB and has the same data sequence as CADAVER from line 9 to line 33.

The final output files are %A%BRESULTF1 and %A%BRESULTF2, corresponding to FORCED1B and FORCED2B respectively. From these are obtained centre of pressure, external forces and moments, Tc. and Tcn. joint forces and the muscle forces.

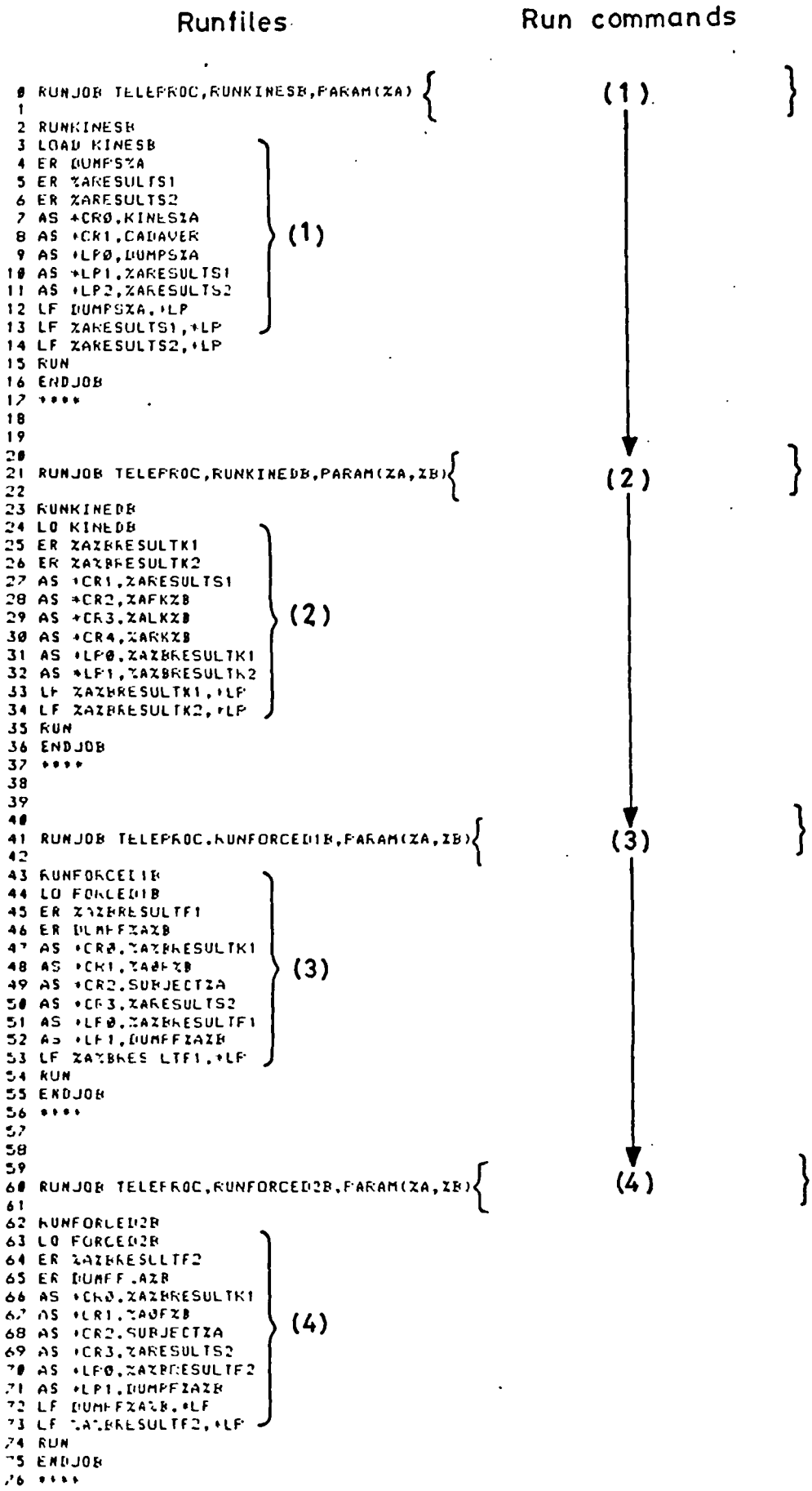

Figure A3.4.1 Program Run Commands and their Associated Runfiles

A3.5 KINESB Program Listing

```
      0       LIST
      1       PROGRAM(KINES)
      2       INPUT 1=CR0
      3       INPUT 2=CR1
      4       OUTPUT 6=LP0
      5       OUTPUT 7=LP1
      6       OUTPUT 8=LP2
      7       TRACE 2
      8       END
      9       MASTER PROG
     10       REAL LD,LFM,LFS,LRS,MAR,LXMG,N
     11       DIMENSION W(3),ANTH(28,3),V(3),RTCG(3,3),DD(2),FFM(6),LFM(
6),RFM(6
     12      *),FFS(17,3),FRS(5,3),LFS(7,2),LRS(5,2),RFS(11,2),Z(4,3),SC
ALE(3),T
     13      *ETTC(3),X(3),Y(3),MAR(8,3),YY(3),P(3,3),Q(3,3),R(3,3),S(3,
3),AAA(3
     14      *),TTC(3),TEHTCN(3),TTCN(3),RTC(3,3),RTCN(3,3),RETG(3,3),RT
CMG(3,3)
     15      *,RENG(3,3),ZZ(3),COEF(8)
     16 C
     17 C     IN THIS PROGRAM 3 SETA OF DATA ARE READ IN FROM STATIC
FILES
     18 C     THE DATA IS SCALED, CORRECTED FOR DC SHIFT AND PARALLAX.
THE
     19 C     THE UNKNOWN MARKERS ARE CALCULATED. THE INTERNAL AXES ARE
     20 C     RELATED TO THE EXTERNAL AXES. THE ANTHROPOMETRIC DATA IS
     21 C     ALSO CALCULATED.
     22 C     READ IN RAW CAMERA DATA
     23 C
     24 C     FRONT CAMERA FORWARD
     25       READ(1,1000)(FFM(I),I=1,6)
     26       READ(1,2000)(FFS(I,3),FFS(I,2),I=1,15)
     27 C
     28 C     FRONT CAMERA REVERSE
     29 C
     30       READ(1,3000)(FRS(I,3),FRS(I,2),I=1,5)
     31 C
     32 C     LEFT CAMERA FORWARD
     33       READ(1,1000)(LFM(I),I=1,6)
     34 C
     35       READ(1,4000)((LFS(I,J),J=1,2),I=1,7)
     36 C
     37 C     LEFT CAMERA REVERSE
     38 C
     39       READ(1,3000)((LRS(I,J),J=1,2),I=1,5)
     40 C
     41 C     RIGHT CAMERA FORWARDS
     42 C
     43       READ(1,1000)(RFM(I),I=1,6)
     44       READ(1,5000)((RFS(I,J),J=1,2),I=1,11)
     45 C
     46 C     WRITE OUT ALL THE INPUT QUANTITIES
     47 C
     48       WRITE(6,792)
     49   792 FORMAT(1H0,12HINPUT VALUES)
     50       WRITE(6,793)(FFM(I),I=1,6)
     51       WRITE(6,794)(FFS(I,3),FFS(I,2),I=1,15)
     52       WRITE(6,794)(FRS(I,3),FRS(I,2),I=1,5)
     53       WRITE(6,793)(LFM(I),I=1,6)
     54       WRITE(6,794)((LFS(I,J),J=1,2),I=1,7)
     55       WRITE(6,794)((LRS(I,J),J=1,2),I=1,5)
     56       WRITE(6,793)(RFM(I),I=1,6)
     57       WRITE(6,794)((RFS(I,J),J=1,2),I=1,11)
     58   793 FORMAT((1X,6(F7.2,3X)))
     59   794 FORMAT((1X,2(F7.2,3X)))
     60 C
     61 C     INPUT CAMERA DISTANCES
     62 C
     63       READ(1,180)FD,LD,RD
     64 C
     65 C     CALCULATE MAGNIFICATION FACTORS
     66 C
     67       FZMG=0.3/(FFM(5)-FFM(3))
     68       FYMG=0.25/(FFM(6)-FFM(4))
```

```
      LXMG=0.3/(LFM(5)-LFM(3))
      RXMG=0.3/(RFM(5)-RFM(3))
      RYMG=0.25/(RFM(6)-RFM(4))
C
C     CALCULATE DC SHIFT OF MARKERS
C
      DPFZ=FFM(3)-FFM(1)
      DPFY=FFM(4)-FFM(2)
      DPLX=LFM(3)-LFM(1)
      DPRX=RFM(3)-RFM(1)
      DPRY=RFM(4)-RFM(2)
C
C     CORRECT FOR DC SHIFT AND MAGNIFY DATA
C
C     FRONT CAMERA FORWARD
C
      DO 10 I=2,15
      FFS(I,2)=(FFS(I,2)-FFS(1,2)-DPFY)*FYMG
      FFS(I,3)=-(FFS(I,3)-FFS(1,3)-DPFZ)*FZMG
   10 CONTINUE
C
C     FRONT CAMERA REVERSE
C
      DO 20 I=2,5
      FRS(I,2)=(FRS(I,2)-FRS(1,2)-DPFY)*FYMG
      FRS(I,3)=-(FRS(I,3)-FRS(1,3)-DPFZ)*FZMG
   20 CONTINUE
C
C    LEFT CAMERA FORWARD
C
      DO 30 I=2,7
      LFS(I,1)=-(LFS(I,1)-LFS(1,1)-DPLX)*LXMG
   30 CONTINUE
C
C     LEFT CAMERA REVERSE
C
      DO 40 I=2,5
      LRS(I,1)=-(LRS(I,1)-LRS(1,1)-DPLX)*LXMG
   40 CONTINUE
C
C     RIGHT CAMERA FORWARD
C
      DO 50 I=2,11
      RFS(I,1)=(RFS(I,1)-RFS(1,1)-DPRX)*RXMG
   50 CONTINUE
      DO 55 I=10,11
      RFS(I,2)=(RFS(I,2)-RFS(1,2)-DPRY)*RYMG
   55 CONTINUE
C
C      CALCULATE TRUE STATIC POINTS 10-15 USING PARALLAX
EQUATIONS
C     OBTAINING 10-15 X APPT FROM LS DATA, 10-15 Y&Z APPT FROM
FS DATA
C
      DO 60 I=10,15
      FFS(I,1)=LFS((I-8),1)*(1+FFS(I,3)/LD)/(1+FFS(I,3)*LFS((I-8
),1)/(LD
     **FD))
      FFS(I,2)=FFS(I,2)-FFS(I,1)*(FFS(I,2)-0.495)/FD
      FFS(I,3)=FFS(I,3)*(1-FFS(I,1)/FD)
   60 CONTINUE
C
C     CALCULATE TRUE STATIC POINTS 2-9 USING PARALLAX EQUATIONS
C      OBTAINING 2-9 X APPT FROM RS DATA AND 2-9 Y&Z APPT FROM
FS DATA
C
      DO 70 I=2,9
      FFS(I,1)=RFS(I,1)*(1-FFS(I,3)/RD)/(1-FFS(I,3)*RFS(I,1)/(RD
*FD))
      FFS(I,2)=FFS(I,2)-FFS(I,1)*(FFS(I,2)-0.495)/FD
      FFS(I,3)=FFS(I,3)*(1-FFS(I,1)/FD)
   70 CONTINUE
C
C     CALCULATE TRUE 2,3,16 & 17 FROM FRONT AND LEFT REVERSE
STATIC RUNS
```

```
C
      DO 80 I=2,5
      J=I-1
      Z(J,1)=LRS(I,1)*(1+FRS(I,3)/LD)/(1+FRS(I,3)*LRS(I,1)/(LD*F
D))
      Z(J,2)=FRS(I,2)-Z(J,1)*(FRS(I,2)-0.495)/FD
      Z(J,3)=FRS(I,3)*(1-Z(J,1)/FD)
   80 CONTINUE
C
C      CALCULATE D162...(DD(1)) & D172...(DD(2))
C
      DO 90 I=1,2
      DD(I)=SQRT((Z(I,1)-Z(3,1))**2+(Z(I,2)-Z(3,2))**2+(Z(I,3)-Z
(3,3))**
     *2)
   90 CONTINUE
C
C     CALCULATE TRUE 16 & 17 COORDINATES USING FFFS TRUE Z & FRS
 APPT
C     16 & 17
C
      DO 100 I=10,11
      A=FFS(2,1)-RFS(I,1)
      B=RFS(I,1)/RD
      C=FFS(2,2)-RFS(I,2)*(1.0-1.0/RD)
      D=-0.495/RD
      E=FFS(2,3)
      AA=(B**2+D**2+1.0)
      BB=2*(A*B+C*D-E)
      CC=A**2+C**2+E**2-DD(I-9)**2
      IF(BB**2.GT.4*A*C)GO TO 125
      WRITE(6,700)
  700 FORMAT(10X,39HNO SOLUTION BSQ LT 4AC,VARIABLES FOLLOW)
      K=I+6
      WRITE(6,800)K,(FFS(2,J),J=1,3),RFS(I,1),RFS(I,2)
  800 FORMAT(1H ,10X,I3,10X,3(F10.5,5X),2(F10.5,5X))
      GO TO 9999
  125 EE=SQRT(BB**2-4*AA*CC)
      FF=(-BB+EE)/(2*AA)
      GG=(-BB-EE)/(2*AA)
      IF(FF.LT.GG)GG=FF
      FFS((I+6),3)=GG
      FFS((I+6),1)=RFS(I,1)*(1-GG/RD)
      FFS((I+6),2)=RFS(I,2)-(RFS(I,2)-0.495)*GG/RD
  100 CONTINUE
C
C     READ IN COEF ARRAY
C
      READ(2,8000)(COEF(I),I=1,8)
C
C     CALCULATE TRUE BONY POINTS USING COEF ARRAY
C      ALL 8 MARKER POINTS GO INTO AN ARRAY CALLED MAR
C
      DO 130 I=1,8
      DO 130 J=1,3
      MAR(I,J)=-FFS((I*2),J)*COEF(I)+FFS((I*2+1),J)*(COEF(I)+1.0
)
  130 CONTINUE
C
C     CALCULATE THE BONY POINTS REL TO MALL ORIGIN
C
      DO 160 J=1,3
      W(J)=(MAR(2,J)+MAR(6,J))/2.0
      DO 160 I=1,8
      MAR(I,J)=MAR(I,J)-W(J)
  160 CONTINUE
      WRITE(6,168)
  168 FORMAT(1H0,17HTRUE MARKER ARRAY)
      WRITE(6,170)((FFS(I,J),J=1,3),I=1,17)
C
C     CALCULATE MARKER DISTANCES
C
      WRITE(6,166)
  166 FORMAT(1H0,16HMARKER DISTANCES)
      DO 167 I=1,8
```

```
      SUM=0.0
      DO 165 J=1,3
      SQ=(FFS(I*2,J)-FFS((I*2+1),J))**2
      SUM=SUM+SQ
  165 CONTINUE
      SUM=SQRT(SUM)
      WRITE(6,7500)SUM
  167 CONTINUE
      WRITE(6,169)
  169 FORMAT(1H0,16HBONY POINT ARRAY)
      WRITE(6,170)((MAR(I,J),J=1,3),I=1,8)
  170 FORMAT((1H0,3(F6.4,5X)))
C
C     CALCULATE SCALE FACTORS FOR ANTHROPOMETRIC DATA
C
      WRITE(6,185)
  185 FORMAT(1H0,13HSCALE FACTORS)
      SCALE(1)=((MAR(1,1)+MAR(5,1))/2.0-MAR(8,1))/0.0842
      SCALE(2)=((MAR(2,2)+MAR(6,2))/2.0-MAR(1,2))/0.0616
      SCALE(3)=(MAR(2,3)-MAR(6,3))/0.0656
      WRITE(6,795)(SCALE(I),I=1,3)
C      READ IN ANTHROPOMETRIC DATA AND SCALE
C
      READ(2,180)((ANTH(I,J),J=1,3),I=1,28)
  180 FORMAT(3F0.0)
      DO 190 I=1,28
      DO 190 J=1,3
      ANTH(I,J)=ANTH(I,J)*SCALE(J)
  190 CONTINUE
      WRITE(6,795)((ANTH(I,J),J=1,3),I=1,28)
  795 FORMAT(3F8.4)
C
C     EXTERNAL TIBIAL SYSTEM RELATED TO GROUND
      DO 200 J=1,3
      X(J)=FFS(9,J)-FFS(5,J)
      Y(J)=FFS(7,J)-FFS(5,J)
      TETTC(J)=-FFS(5,J)+W(J)*ANTH(25,J)
  200 CONTINUE
      WRITE(6,795)(X(I),I=1,3)
      WRITE(6,795)(Y(I),I=1,3)
      WRITE(6,215)
  215 FORMAT(1H0,22HTETTC,RETG,RTCG FOLLOW)
      WRITE(6,7000)(TETTC(J),J=1,3)
      CALL AXIS(X,Y,RETG,2)
      WRITE(6,7000)((RETG(I,J),J=1,3),I=1,3)
C
C     INPUT YY VALUES
C
      YY(1)=0.0
      YY(2)=0.1
      YY(3)=0.0
C
C
C     TC SYSTEM RELATED TO THE GROUND SYSTEM
C
      DO 210 J=1,3
      Y(J)=YY(J)-ANTH(25,J)
      ZZ(J)=ANTH(26,J)-ANTH(25,J)
  210 CONTINUE
      CALL AXIS(Y,ZZ,RTCG,3)
      WRITE(6,7000)((RTCG(I,J),J=1,3),I=1,3)
C
C     CALCULATE TTC
C
      CALL RVECT(TETTC,RETG)
C
C     CALCULATE RTC AND TTC
C
      DO 220 I=1,3
      DO 220 J=1,3
      Q(J,I)=RETG(I,J)
      R(I,J)=RTCG(I,J)
  220 CONTINUE
      CALL MATMUL(RTCG,Q)
C
```

```
C      RENAME RTCG AND TETTC
C
       DO 230 I=1,3
       TTC(I)=TETTC(I)
       DO 230 J=1,3
       RTC(I,J)=RTCG(I,J)
  230 CONTINUE
C
C      EXTERNAL HEEL SYSTEM RELATED TO THE GROUND SYSTEM
C
       DO 240 J=1,3
       ZZ(J)=FFS(2,J)-(FFS(2,J)+FFS(11,J))/2.0
       X(J)=-FFS(17,J)+(FFS(2,J)+FFS(11,J))/2.0
       TEHTCN(J)=-(FFS(2,J)+FFS(11,J))/2.0+W(J)+ANTH(27,J)
  240 CONTINUE
       WRITE(6,245)
  245 FORMAT(1H0,24HTEHTCN,REHG,RTCNG FOLLOW)
       WRITE(6,7000)(TEHTCN(J),J=1,3)
       CALL AXIS(ZZ,X,REHG,1)
       WRITE(6,7000)((REHG(I,J),J=1,3),I=1,3)
C
C      TCN SYSTEM RELATED TO THE GROUND SYSTEM
C
       DO 250 J=1,3
       Y(J)=YY(J)-ANTH(27,J)
       ZZ(J) ANTH(28,J)-ANTH(27,J)
  250 CONTINUE
       CALL AXIS(Y,ZZ,RTCNG,3)
       WRITE(6,7000)((RTCNG(I,J),J=1,3),I=1,3)
C
C      CALCULATE TTCN
C
       CALL RVECT(TEHTCN,REHG)
C
C      CALCULATE RTCN AND TTCN
C
C
       DO 260 I=1,3
       DO 260 J=1,3
       P(J,I)=REHG(I,J)
       S(I,J)=RTCNG(I,J)
  260 CONTINUE
       CALL MATMUL(RTCNG,P)
C
C      RENAME RTCNG AND TEHTCN
C
       DO 270 I=1,3
       TTCN(I)=TEHTCN(I)
       DO 270 J=1,3
       RTCN(I,J)=RTCNG(I,J)
  270 CONTINUE
C
C
C      CALCULATION OF THE ORIGIN AND INSERTION OF THE CALF GROUP
C
       DO 280 J=1,3
       AAA(J)=ANTH(3,J)-ANTH(4,J)
  280 CONTINUE
       BBB=SQRT(AAA(1)**2+AAA(2)**2+AAA(3)**2)
       DY=(MAR(3,2)+MAR(7,2))/2.0-MAR(8,2)
       DO 290 J=1,3
       AAA(J)=(AAA(J)*DY)/BBB
       ANTH(3,J)=AAA(J)+MAR(8,J)
       ANTH(4,J)=MAR(8,J)
  290 CONTINUE
C
C      CALCULATE TC ANTHROPOMETRY
C
C
       DO 300 I=1,3
       DO 305 J=1,3
       ANTH(I,J)=ANTH(I,J)-ANTH(25,J)
       W(J)=ANTH(I,J)
  305 CONTINUE
       CALL RVECT(W,R)
       DO 310 K=1,3
```

```
      ANTH(I,K)=W(K)
  310 CONTINUE
  300 CONTINUE
C
C     CALCULATE TCN ANTHROPOMETRY
C
      DO 320 I=4,24
      DO 325 J=1,3
      ANTH(I,J)=ANTH(I,J)-ANTH(27,J)
      W(J)=ANTH(I,J)
  325 CONTINUE
      CALL RVECT(W,S)
      DO 330 K=1,3
      ANTH(I,K)=W(K)
  330 CONTINUE
  320 CONTINUE
C*************************************************************
C
C     OUTPUT QUANTITIES
C
C*************************************************************
      WRITE(7,7000)(TTC(I),I=1,3)
      WRITE(7,7000)((RTC(I,J),J=1,3),I=1,3)
      WRITE(7,7000)(TTCN(I),I=1,3)
      WRITE(7,7000)((RTCN(I,J),J=1,3),I=1,3)
      WRITE(7,7500)DD(2)

      WRITE(7,7000)FD,LD,RD
      WRITE(8,7000)((ANTH(I,J),J=1,3),I=1,24)
 7000 FORMAT((1H0,3(F9.4,5X)))
C
 1000 FORMAT(6F0.0)
 2000 FORMAT(30F0.0)
 3000 FORMAT(10F0.0)
 4000 FORMAT(14F0.0)
 5000 FORMAT(22F0.0)
 7500 FORMAT(1H0,F7.4)
 8000 FORMAT(16F0.0)
 9999 CONTINUE
      STOP
      END
      SUBROUTINE MATMUL(X,Y)
C     MATMUL COMPUTES MATRIX PRODUCT "X*Y"
      DIMENSION X(3,3),Y(3,3),Z(3,3)
      DO 5 I=1,3
      DO 5 J=1,3
      SUM=0.0
      DO 6 K=1,3
    6 SUM=SUM+X(I,K)*Y(K,J)
    5 Z(I,J)=SUM
      DO 7 I=1,3
      DO 7 J=1,3
      X(I,J)=Z(I,J)
    7 CONTINUE
      RETURN
      END
      SUBROUTINE AXIS(A,B,DMAT,T)
C
C     THIS SUBROUTINE CALCULATES THE X PRODUCT OF FALSE VECTOR A
&TRUE
C     VECTOR B TO GIVE TRUE VECTOR C ORTHOGONAL TO A &B.........
.......
C     THEN THE X PRODUCT OF B TRUE AND C TRUE GIVES A TRUE
```

```
.......
    432 C     THE DIRECTION COSINES ARE THEN CALCULATED AND THEN PUT IN
DMAT ..
    433 C     THE EXACT SEQUENCE DEPENDS UPON THE ORIENTATION
    434 C     PARAMETER ..."T" USED IN THE CALL STATEMENT, SEE BELOW.
    435 C
    436       INTEGER T
    437       DIMENSION A(3),B(3),C(3),DMAT(3,3)
    438 C     CALCULATE X-PRODUCT OF A AND B TO GIVE C
    439       C(1)=A(2)*B(3)-A(3)*B(2)
    440       C(2)=A(3)*B(1)-A(1)*B(3)
    441       C(3)=A(1)*B(2)-A(2)*B(1)
    442 C     CALCULATE X PRODUCT OF B & C TO GIVE A
    443       A(1)= B(2)*C(3)-B(3)*C(2)
    444       A(2)= B(3)*C(1)-B(1)*C(3)
    445       A(3)= B(1)*C(2)-B(2)*C(1)
    446 C     CALCULATE DIRECTION COSINES
    447       AMOD=SQRT(A(1)**2+A(2)**2+A(3)**2)
    448       BMOD=SQRT(B(1)**2+B(2)**2+B(3)**2)
    449       CMOD=SQRT(C(1)**2+C(2)**2+C(3)**2)
    450       DO 10 I=1,3
    451       A(I)=A(I)/AMOD
    452       B(I)=B(I)/BMOD
    453       C(I)=C(I)/CMOD
    454    10 CONTINUE
    455 C     CALCULATE HEEL SYSTEM ORIENTATION   T=1  (A=Z, B=X, C=Y)
    456       IF(T.EQ.2) GO TO 40
    457       IF(T.EQ.3)GO TO 60
    458       DO 20 I=1,3
    459       DMAT(1,I)=B(I)
    460       DMAT(2,I)=C(I)
    461       DMAT(3,I)=A(I)
    462    20 CONTINUE
    463       WRITE(6,77)
    464    77 FORMAT(1H0,9HI AM AT 1)
    465       GO TO 30
    466    40 CONTINUE
    467 C     CALCULATE TIBIAL SYSTEM ORIENTATION  T=2  (A=X, B=Y, C=Z)
    468       DO 50 I=1,3
    469       DMAT(1,I)=A(I)
    470       DMAT(2,I)=B(I)
    471       DMAT(3,I)=C(I)
    472    50 CONTINUE
    473       WRITE(6,78)
    474    78 FORMAT(1H0,9HI AM AT 2)
    475       GO TO 30
    476    60 CONTINUE
    477 C
    478 C     ALTERNATIVE ORIENTATION            T=3  (A=Y, B=Z, C=X)
    479 C
    480       WRITE(6,79)
    481    79 FORMAT(1H0,9HI AM AT 3)
    482       DO 31 J=1,3
    483       DMAT(1,J)=C(J)
    484       DMAT(2,J)=A(J)
    485       DMAT(3,J)=B(J)
    486    31 CONTINUE
    487    30 CONTINUE
    488    81 FORMAT(3F8.4)
    489       RETURN
    490       END
    491       SUBROUTINE RVECT(R,S)
    492 C     RVECT ROTATES VECTOR "R" FROM SYSTEM 1 INTO SYSTEM 2
    493 C     USING THE "S" TRANSFORMATION 1-2
    494       DIMENSION R(3),S(3,3),Q(3)
    495       DO 113 K=1,3
    496       Q(K)=R(K)
    497   113 CONTINUE
    498       DO 111 I=1,3
    499       SUM=0.0
    500       DO 112 J=1,3
    501       SUM=SUM+S(I,J)*Q(J)
    502   112 CONTINUE
    503       R(I)=SUM
    504   111 CONTINUE
```

```
505         RETURN
506         END
507         FINISH
```

A3.6 KINEDB Program Listing

```
        0       LIST
        1       PROGRAM(KINED)
        2       INPUT 1=CR1
        3       INPUT 2=CR2
        4       INPUT 3=CR3
        5       INPUT 4=CR4
        6       OUTPUT 6=LP0
        7       OUTPUT 7=LP1
        8       TRACE 2
        9       END
       10       MASTER PROG
       11       REAL LFM,LS,LXMG,LD,N
       12       DIMENSION P(3),Q(3),R(3),S(3),TTC(3),TTCN(3),FFM(6),RFM(6)
     .LFM(6),RTC(383
       13      *RTC(3,3),RTCN(3,3),HMAT(3,3),TMAT(3,3),AA(100),F(8,3,50),R
     S(6,2,50),
       14      *),LS(2,2,50),DTTC(50),DTTCN(50)
       15 C
       16 C     THIS PROGRAM READS IN 3 SETS OF FILM DATA, MAGNIFIES,CORRE
     CTS
       17 C     FOR DC SHIFT, CORRECTS FOR PARALLAX, FILTERS THE DATA
     USING A
       18 C     4TH ORDER BUTTERWORTH FILTER, CALCULATES THE ORIENTATION
     OFTHE TC
       19 C     AND TCN SYSTEMS RELATIVE TO THE GRID SYSTEM FOR EACH FRAME
       20 C
       21 C     READ IN BASIC PARAMETERS,TTC,RTC,TTCN,RTCN,D172
       22 C                          FD,LD,RD
       23 C
       24       READ(1,1000)(TTC(I),I=1,3)
       25       READ(1,2000)((RTC(I,J),J=1,3),I=1,3)
       26       READ(1,1000)(TTCN(I),I=1,3)
       27       READ(1,2000)((RTCN(I,J),J=1,3),I=1,3)
       28       READ(1,1500) D172
       29
       30       READ(1,1000)FD,LD,RD
       31 C
       32 C     READ IN FRONT CAMERA DATA
       33 C
       34       READ(2,3000) IFF
       35       READ(2,4000)(FFM(I),I=1,6)
       36       DO 10 K=1,IFF
       37       READ(2,5000)DY,F(7,3,K),F(7,2,K),((F(I,3,K),F(I,2,K)),I=1,
     5)
       38    10 CONTINUE
       39 C
       40 C     READ IN LEFT CAMERA DATA
       41 C
       42       READ(3,3000) ILF
       43       READ(3,4000)(LFM(I),I=1,6)
       44       DO 20 K=1,ILF
       45       READ (3,6000)DY,LS(2,1,K),LS(2,2,K),LS(1,1,K),LS(1,2,K)
       46    20 CONTINUE
       47 C
       48 C     READ IN RIGHT CAMERA DATA
       49 C
       50       READ(4,3000) IRF
       51       READ(4,4000)(RFM(I),I=1,6)
       52       DO 30 K=1,IRF
       53       READ(4,5000)DY,RS(6,1,K),RS(6,2,K),((RS(I,1,K),RS(I,2,K)),
     I=1,5)
       54    30 CONTINUE
       55 C
       56 C     MAGNIFICATION FACTORS
       57 C
       58       FZMG=0.3/(FFM(5)-FFM(3))
       59       FYMG=0.25/(FFM(6)-FFM(4))
       60       LXMG=0.3/(LFM(5)-LFM(3))
       61       RXMG=0.3/(RFM(5)-RFM(3))
       62       RYMG=0.25/(RFM(6)-RFM(4))
       63 C
       64 C     CALCULATE STATIC DC SHIFT OF FIELD MARKERS
       65 C
       66       DFFZ =FFM(3)-FFM(1)
       67       DFFY =FFM(4)-FFM(2)
```

```
      DPLX =LFM(3)-LFM(1)
      DPRX=RFM(3)-RFM(1)
      DPRY =RFM(4)-RFM(2)
C
C     FRONT CAMERA
C
C     DC SHIFT CORRECTION FOR D-MAC
C
      DO 40 K=1,IFF
      DO 40 I=1,5
      F(I,2,K)=F(I,2,K)-F(7,2,K)-DPFY
      F(I,3,K)=-(F(I,3,K)-F(7,3,K)-DPFZ)
   40 CONTINUE
C
C     FILTER POINTS 2-5 Y&Z FRONT
C
      DO 50 I=1,5
      DO 50 J=2,3
      DO 60 K=1,IFF
   60 AA(K)=F(I,J,K)
      CALL FILTER(AA,IFF,10.0,0.02)
      DO 70 K=1,IFF
   70 F(I,J,K)=AA(K)
   50 CONTINUE
C
C     MAGNIFY DATA
C
      DO 80 K=1,IFF
      DO 80 I=1,5
      F(I,2,K)=F(I,2,K)*FYMG
      F(I,3,K)=F(I,3,K)*FZMG
   80 CONTINUE
C
C     LEFT CAMERA
C
C     DC SHIFT CORRECTION FOR D-MAC
C
      DO 90 K=1,ILF
      LS(1,1,K)=-(LS(1,1,K)-LS(2,1,K)-DPLX)
   90 CONTINUE
C
C     FILTER POINT 6 X LEFT
C
      DO 100 K=1,ILF
  100 AA(K)=LS(1,1,K)
      CALL FILTER(AA,ILF,10.0,0.02)
      DO 110 K=1,ILF
      LS(1,1,K)=AA(K)
  110 CONTINUE
C
C     MAGNIFY DATA
C
      DO 120 K=1,ILF
      LS(1,1,K)=LS(1,1,K)*LXMG
  120 CONTINUE
C
C     RIGHT CAMERA
C
C     DC SHIFT CORRECTION FOR D-MAC
C
      DO 130 K=1,IRF
      RS(5,2,K)=RS(5,2,K)-RS(6,2,K)-DPRY
      DO 130 I=1,5
      RS(I,1,K)=RS(I,1,K)-RS(6,1,K)-DPRX
  130 CONTINUE
C
C     FILTER POINTS 2-5,7: X RIGHT & 7: Y RIGHT
C
      DO 140 K=1,IRF
  140 AA(K)=RS(5,2,K)
      CALL FILTER(AA,IRF,10.0,0.02)
      DO 150 K=1,IRF
      RS(5,2,K)=AA(K)
  150 CONTINUE
      DO 160 I=1,5
```

```
      DO 170 K=1,IRF
  170 AA(K)=RS(I,1,K)
      CALL FILTER(AA,IRF,10.0,0.02)
      DO 180 K=1,IRF
  180 RS(I,1,K)=AA(K)
  160 CONTINUE
C
C     MAGNIFY DATA
C
      DO 183 K=1,IRF
      RS(5,2,K)=RS(5,2,K)*RYMG
  183 CONTINUE
      DO 187 K=1,IRF
      DO 187 I=1,5
      RS(I,1,K)=RS(I,1,K)*RXMG
  187 CONTINUE
C
C     ALL THE DATA HAS BEEN SHIFTED ,MAGNIFIED ,AND FILTERED NOW
 IT REQUIRES
C     PARALLAX CORRECTION ,SHIFTING INTO MARKER SETS AND
PREDICTION OF THE
C     MISSING MARKER
C
C     PARALLAX CORRECTION FOR POINTS 2,3,4,5 USING ELEMENTS 1-4
RS-ARRAY
C     AND 1-4 F-ARRAY
C
      DO 190 I=1,4
      DO 190 K=1,IRF
      F(I,1,K)=RS(I,1,K)*(1-F(I,3,K)/RD)/(1-RS(I,1,K)*F(I,3,K)/(
RD*FD))
      F(I,2,K)=F(I,2,K)-F(I,1,K)*(F(I,2,K)-0.495)/FD
      F(I,3,K)=F(I,3,K)*(1-F(I,1,K)/FD)
  190 CONTINUE
C
C     PARALLAX CORRECTION FOR POINT 6 USING ELEMENT 1 LS-ARRAY
AND 5
C     IN F-ARRAY
C
      DO 200 K=1,IRF
      F(5,1,K)=LS(1,1,K)*(1+F(5,3,K)/LD)/(1+LS(1,1,K)*F(5,3,K)/(
LD*FD))
      F(5,2,K)=F(5,2,K)-F(5,1,K)*(F(5,2,K)-0.495)/FD
      F(5,3,K)=F(5,3,K)*(1-F(5,1,K)/FD)
  200 CONTINUE
C
C     NOW MARKERS 2-6 ARE IN F-ARRAY ELEMENTS 1-5
C
C     CALCULATE 7. (X7 & Y7 APPT. IN ROW 5 RS-ARRAY )
C
      DO 210 K=1,IRF
      A=F(1,1,K)-RS(5,1,K)
      B=RS(5,1,K)/RD
      C=F(1,2,K)-RS(5,2,K)*(1.0-1.0/RD)
      D=-0.495/RD
      E=F(1,3,K)
C
C     CALCULATE QUADRATIC EQUATION COEFFICIENTS AA, BB, & CC
C
      AAA=B**2+D**2+1.0
      BB=2*(A*B+C*D-E)
      CC=A**2+C**2+E**2-D172**2
C
C     B-SQ < 4AC : FAILS
C
      IF(BB**2.GT.4*AAA*CC) GO TO 220
      WRITE(6,700)
  700 FORMAT(10X,39HNO SOLUTION BSQ LT 4AC,VARIABLES FOLLOW)
      WRITE(6,800)K,(F(1,I,K),I=1,3),RS(5,1,K),RS(5,2,K)
  800 FORMAT(1H ,10X,I3,10X,3(F10.5,5X),2(F10.5,5X))
      GO TO 210
  220 CONTINUE
      DD=SQRT(BB**2-4*AAA*CC)
      LE=-(BB+DD)/(2.0*AAA)
      FF=(DD-BB)/(2.0*AAA)
```

```
C
C     ALGEBRAICALLY SMALLER ROOT SELECTED
C
      F(6,3,K)=FF
      IF(FF.GT.EE) F(6,3,K)=EE
      F(6,1,K)=RS(5,1,K)+(1-F(6,3,K)/RD)
      F(6,2,K)=RS(5,2,K)-((RS(5,2,K)-0.495)*F(6,3,K)/RD)
  210 CONTINUE
C
C     THIS SECTION WRITES OUT MARKER ARRAYS FOR FRAMES
C     1,K/3 AND K FOR EACH TEST. WITH THE STATIC DATA
C     IT ENABLES APPROX. POSITION OF BONY STRUCTURES
C     OF THE HINDFOOT TO BE PROJECTED ON THE CENTRE OF
C     PRESSURE PATH.
C
      INT=IRF/3
      WRITE(7,211)
  211 FORMAT(1H0,30HMARKER DATA FOR FRAMES 1,K/3,K)
      WRITE(7,212)
  212 FORMAT(1H0,8HFRAME(1))
      WRITE(7,7000)((F(I,J,1),J=1,3),I=1,6)
      WRITE(7,213)
  213 FORMAT(1H0,10HFRAME(K/3))
      WRITE(7,7000)((F(I,J,INT),J=1,3),I=1,6)
      WRITE(7,214)
  214 FORMAT(1H0,8HFRAME(K))
      WRITE(7,7000)((F(I,J,IRF),J=1,3),I=1,6)
C
C     F-ARRAY HOLDS TRUE EXT MARKERS 2-7 REL TO GRID IN ELEMENTS
1-6
C
C     CALCULATE TCN SYSTEM
C
      DO 230 K=1,IRF
      DO 240 I=1,3
      Q(I)=(F(5,I,K)+F(1,I,K))/2.0
      R(I)=F(1,I,K)-Q(I)
      S(I)=-F(6,I,K)+Q(I)
  240 CONTINUE
      CALL AXIS(R,S,HMAT,1)
C
C     HMAT HOLDS HEEL SYSTEM RELATIVE TO GRID
C
      DO 265 I=1,3
      SUM=0.0
      DO 260 J=1,3
      SUM=SUM +HMAT(J,I)*TTCN(J)
  260 CONTINUE
      F(5,I,K)=SUM+Q(I)
  265 CONTINUE
C
C     ROW 5 F-ARRAY HOLDS TCN ORIGIN REL TO GRID
C
      CALL MATMUL(HMAT,RTCN)
C
C     HMAT ON RETURN HOLDS RTCN*HMAT
C
      DO 266 I=6,8
      DO 266 J=1,3
      F(I,J,K)=HMAT((I-5),J)
  266 CONTINUE
  230 CONTINUE
C
C     ROWS 6-8 F-ARRAY NOW HOLD [R] GRID-TCN
C
C     CALCULATE TC SYSTEM
C
      DO 270 K=1,IRF
      DO 280 I=1,3
      R(I)=F(4,I,K)-F(2,I,K)
      S(I)=F(3,I,K)-F(2,I,K)
  280 CONTINUE
      CALL AXIS(R,S,TMAT,2)
C
C     TMAT HOLDS TIBIAL SYSTEM RELATIVE TO GRID
```

```
C
      DO 305 I=1,3
      SUM=0.0
      DO 300J=1,3
      SUM=SUM+TMAT(J,I)*TTC(J)
  300 CONTINUE
      F(1,I,K)=SUM+F(2,I,K)
  305 CONTINUE
C
C     ROW 1 F-ARRAY HOLDS TC ORIGIN RELATIVE TO GRID
C
      CALL MATMUL(TMAT,RTC)
C
C     TMAT ON RETURN HOLDS RTC*TMAT
C
      DO 306 I=2,4
      DO 306 J=1,3
      F(I,J,K)=TMAT((I-1),J)
  306 CONTINUE
  270 CONTINUE
C
C     ROWS 2-5 F-ARRAY NOW HOLD [R] GRID-TC
C
      DO 310 K=1,IRF
      WRITE(6,7000)((F(I,J,K),J=1,3),I=1,8)
  310 CONTINUE
 1000 FORMAT(3F0.0)
 1500 FORMAT(F0.0)
 2000 FORMAT(9F0.0)
 3000 FORMAT(I2)
 4000 FORMAT(6F0.0)
 5000 FORMAT(13F0.0)
 6000 FORMAT(5F0.0)
 7000 FORMAT((1H0,3(F6.4,5X)))
```

```
  350 CONTINUE
      STOP
      END
```

```
      SUBROUTINE FILTER(Q,N,FCUT,T)
C
C     THIS FILTER ROUTINE IS BASED ON THE 4 TH ORDER BUTTERWORTH
C     FILTER ADAPTED BY BJ ANDREWS
C     Q= INPUT DATA
C     N= NO OF POINTS
C     FCUT= CUT OFF FREQUENCY IN HZ
C     W1= RESULTS
C     T= TIME INTERVAL IN SECS
C
      DIMENSION C(10),Q(N),AD(130),W1(130),W(130)
      NR=N+20
      TR=Q(N)-Q(1)
      IF (FCUT.GE.1.0/(2.0*T)) GO TO 17
      XPI=3.141592654
      T1=SIN(XPI*FCUT*T)
      T2=COS(XPI*FCUT*T)
      TT=T1/T2
      A=COS(XPI/8.0)*TT
      B=SIN(XPI/8.0)*TT
      C(1)=2*(A+B)
      C(2)=2*(A+B)**2
      C(3)=2*((A**2+B**2)*(B+A))
      C(4)=(A**2+B**2)**2
      C(5)=1+C(1)+C(2)+C(3)+C(4)
      C(6)=-4+4*C(4)-2*C(1)+2*C(3)
      C(7)=6+6*C(4)-2*C(2)
      C(8)=-4+2*C(1)-2*C(3)+4*C(4)
      C(9)=1-C(1)+C(2)+C(4)-C(3)
      DO 30 K44= N,130
      AD(K44)=0.0
   30 CONTINUE
      DO 2 L= 1,N
      AD(L+4)= Q(L)-(L-1)*TR/(N-1)-Q(1)
    2 CONTINUE
      DO 9 L=1,4
      AD(L)=0.0
      W(L)=0.0
    9 CONTINUE
      N1= N+24
      DO 18 K= 1,NR
      W(K+4)=(C(4)*(AD(K+4)+4*AD(K+3)+6*AD(K+2)+4*AD(K+1)+AD(K))
     -(W(K+3)
     **C(6)+W(K+2)*C(7)+W(K+1)*C(8)+W(K)*C(9)))/C(5)
   18 CONTINUE
      DO 37 JKJ= 1,NR
      W(JKJ)=W(JKJ+4)
   37 CONTINUE
      DO 15 K= 1,4
      K4= N1-K
      W1(K4+1)=0.0
      W(K4+1)=0.0
   15 CONTINUE
      DO 16 K=1,NR
      K5= N1-K
      W1(K5-3)=(C(4)*(W(K5-3)+4*W(K5-2)+6*W(K5-1)+4*W(K5)+W(K5+1
     ))-(W1(K
     +5-2)*C(6)+W1(K5-1)*C(7)+W1(K5)*C(8)+W1(K5+1)*C(9)))/C(5)
   16 CONTINUE
      DO 21 K= 1,N
   21 W1(K)= W1(K)+(K-1)*TR/(N-1)+Q(1)
      DO 17 K= 1,N
      Q(K)= W1(K)
   17 CONTINUE
      RETURN
      END
      SUBROUTINE MATMUL(Y,X)
      DIMENSION X(3,3),Y(3,3),Z(3,3)
      DO 5 I=1,3
      DO 5 J=1,3
      SUM=0.0
      DO 6 K=1,3
    6 SUM=SUM+X(I,K)*Y(K,J)
    5 Z(I,J)=SUM
      DO 7 I=1,3
```

```
      DO 7 J=1,3
      Y(I,J)=Z(I,J)
    7 CONTINUE
      RETURN
      END
      SUBROUTINE AXIS(A,B,DMAT,T)
C
C     THIS SUBROUTINE CALCULATES THE X PRODUCT OF FALSE VECTOR A
 &TRUE
C     VECTOR B TO GIVE TRUE VECTOR C ORTHOGONAL TO A &B.....
.....
C     THEN THE X PRODUCT OF B TRUE AND C TRUE GIVES A TRUE
...........
C     THE DIRECTION COSINES ARE THEN CALCULATED AND THEN PUT IN
DMAT .
C     THE EXACT SEQUENCE DEPENDS UPON WHETHER HEEL OR TIBIA IS
USED ..
C
      INTEGER T
      DIMENSION A(3),B(3),C(3),DMAT(3,3)
C     CALCULATE X-PRODUCT OF A AND B TO GIVE C
      C(1)=A(2)*B(3)-A(3)*B(2)
      C(2)=A(3)*B(1)-A(1)*B(3)
      C(3)=A(1)*B(2)-A(2)*B(1)
C     CALCULATE X PRODUCT OF B & C TO GIVE A
      A(1)= B(2)*C(3)-B(3)*C(2)
      A(2)= B(3)*C(1)-B(1)*C(3)
      A(3)= B(1)*C(2)-B(2)*C(1)
C     CALCULATE DIRECTION COSINES
      AMOD=SQRT(A(1)**2+A(2)**2+A(3)**2)
      BMOD=SQRT(B(1)**2+B(2)**2+B(3)**2)
      CMOD=SQRT(C(1)**2+C(2)**2+C(3)**2)
      DO 10 I=1,3
      A(I)=A(I)/AMOD
      B(I)=B(I)/BMOD
      C(I)=C(I)/CMOD
   10 CONTINUE
C     CALCULATE HEEL SYSTEM ORIENTATION
      IF(T.EQ.2) GO TO 40
      DO 20 I=1,3
      DMAT(1,I)=B(I)
      DMAT(2,I)=C(I)
      DMAT(3,I)=A(I)
   20 CONTINUE
      GO TO 30
   40 CONTINUE
C     CALCULATE TIBIAL SYSTEM ORIENTATION
      DO 30 I=1,3
      DMAT(1,I)=A(I)
      DMAT(2,I)=B(I)
      DMAT(3,I)=C(I)
   30 CONTINUE
      RETURN
      END
      FINISH
 **** 
```

A3.7 FORCED1B Program Listing

```
      0        LIST
      1        PROGRAM(FORCED1)
      2        INPUT 1=CR0
      3        INPUT 2=CR1
      4        INPUT 3=CR2
      5        INPUT 4=CR3
      6        OUTPUT 7=LP1
      7        OUTPUT 6=LP0
      8        TRACE 2
      9        END
     10        MASTER PROG2
     11        REAL MTC,MTCN,M,MCOMP
     12        INTEGER A,SLOPE
     13        DIMENSION SCALE(6),FE(6,99),MTCN(3,50),CPZ(50),CPX(50),TTC
(3,50),R
     14       *TC(3,3,50),TTCN(3,50),RTCN(3,3,50),MTC(3,50),FTC(3,50),FTC
N(3,50),
     15       *P1(3),P2(3),P3(3),Q1(3),R1(3,3),R2(3,3),R3(3,3),SM1(3),SM2
(3),SF1(
     16       *3),SF2(3),ANTH(24,3),MCOMP(10,3,50),FCOMP(10,3,50),T(8),ST
C(7,50),
     17       *STCN(6,50)
     18 C
     19 C     THIS PROGRAM CALCULATES THE TC AND TCN SYSTEM MOMENTS
USING
     20 C     FORCE DATA IN FILE, AND KINEMATIC DATA IN FILE. IT OUTPUTS
     21 C     FORCES AND MOMENTS IN A) EXTERNAL, B) TC AND C) TCN
SYSTEMS
     22 C     THEN IT FORMULATES THE TC SYSTEM FORCE AND MOMENT EQUATION
S
     23 C
     24 C     READ IN FORCE DATA
     25 C                          A= NUMBER OF POINTS
     26 C                          B- DC LEVEL
     27 C     ALSO CORRECTING FOR DC SHIFT
     28 C
     29 C     THIS SEGMENT READS IN FORCE DATA
     30 C
     31        READ(2,1100)A
     32        L=2*A
     33        DO 10 I=1,6
     34        READ(2,1000)B
     35        WRITE(7,1750)L,B
     36        READ(2,1500)(FE(I,J),J=1,L)
     37        DO 10 J=1,A
     38        FE(I,J)=FE(I,(2*J-1))-B
     39    10 CONTINUE
     40  1750 FORMAT(3X,I2,3X,F6.3)
     41 C
     42 C     READ IN TOP AMP(TA) AND BOTTOM AMP(BA) FACTORS
     43 C
     44        READ(3,1001)TA,BA
     45  1001 FORMAT(2F0.0)
     46 C
     47 C     SET FORCE AND MOMENT FACTORS
     48 C
     49        F=0.0195313
     50        M=0.0051563
     51 C
     52 C     CALCULATE SCALE FACTORS
     53 C
     54        SCALE(1)=TA*F/1.0
     55        SCALE(2)=BA*F/1.0
     56        SCALE(3)=TA*F/(-2.0)
     57        SCALE(4)=BA*M/1.25
     58        SCALE(5)=TA*M/2.0
     59        SCALE(6)=BA*M/(-1.25)
     60 C
     61 C     SCALE FORCES AND MOMENTS
     62 C
     63        DO 20 J=1,A
     64        DO 20 I=1,6
     65        FE(I,J)=FE(I,J)*SCALE(I)
     66    20 CONTINUE
     67 C
```

```
C     WRITE EXTERNAL FORCES AND MOMENTS ON LP0
C
      WRITE(6,5000)
      WRITE(6,25)
   25 FORMAT(1H0,27HEXTERNAL FORCES AND MOMENTS)
      WRITE(6,5200)
      WRITE(6,30)((FE(I,J),I=1,6),J=1,A)
   30 FORMAT((1H ,1X,6(F6.1,5X)))
      WRITE(6,5000)
      READ(2,1100)SLOPE
 1100 FORMAT(I2)
C
C     THIS SECTION COMPUTES THE CENTRE OF PRESSURE PATH
C     ACCORDING TO THE SIGN OF THE TEST SLOPE
C
C          -1 = TEST FOOT DOWNHILL
C
C           0 = ON THE LEVEL
C
C          +1 = TEST FOOT UPHILL
C
      IF(SLOPE)110,100,110
  100 CONTINUE
      DO 105 J=1,A
      CPX(J)=(FE(6,J)+0.04*FE(1,J))/FE(2,J)
      CPZ(J)=(0.04*FE(6,J)-FE(4,J))/FE(2,J)
  105 CONTINUE
      GO TO 120
  110 CONTINUE
      DO 115 J=1,A
      YCOORD=0.0
      CPX(J)=(FE(6,J)+0.1935*FE(1,J))/(FE(2,J)-SLOPE*0.1763*FE(1
,J))
      YCOORD=(SLOPE*0.1763+CPX(J)+0.1935)
      CPZ(J)=(YCOORD*FE(3,J)-FE(4,J))/FE(2,J)
  115 CONTINUE
  120 CONTINUE
      WRITE(6,5000)
      WRITE(6,130)SLOPE
  130 FORMAT(1H0,8HSLOPE = ,I2,5X,18HCENTRE OF PRESSURE)
      WRITE(6,135)
  135 FORMAT(1H0,5X,12HX-COORDINATE,5X,12HZ-COORDINATE)
      DO 140 J=1,A
      WRITE(6,145)CPX(J),CPZ(J)
  145 FORMAT(1H ,8X,F6.4,11X,F6.4)
  140 CONTINUE
C
C     READ IN RESULTS OF KINEDB AND CORRECT Y COORDINATE FOR DC
SHIFT
C
      DO 40 K=1,A
      READ(1,2000)(TTC(I,K),I=1,3)
      READ(1,3000)((RTC(I,J,K),J=1,3),I=1,3)
      READ(1,2000)(TTCN(I,K),I=1,3)
      READ(1,3000)((RTCN(I,J,K),J=1,3),I=1,3)
      TTC(2,K)=TTC(2,K)+0.049
      TTCN(2,K)=TTCN(2,K)+0.049
   40 CONTINUE
C
C     CALCULATE MOMENTS ABOUT TC AND TCN ORIGIN .... MTC AND
MTCN
C     RESPECTIVELY, DUE TO THE EXTERNAL FORCES AND MOMENTS
C
      DO 50 K=1,A
      MTC(1,K)=FE(4,K)-TTC(2,K)*FE(3,K)+TTC(3,K)*FE(2,K)
      MTC(2,K)=FE(5,K)-TTC(3,K)*FE(1,K)+TTC(1,K)*FE(3,K)
      MTC(3,K)=FE(6,K)-TTC(1,K)*FE(2,K)+TTC(2,K)*FE(1,K)
      MTCN(1,K)=FE(4,K)-TTCN(2,K)*FE(3,K)+TTCN(3,K)*FE(2,K)
      MTCN(2,K)=FE(5,K)-TTCN(3,K)*FE(1,K)+TTCN(1,K)*FE(3,K)
      MTCN(3,K)=FE(6,K)-TTCN(1,K)*FE(2,K)+TTCN(2,K)*FE(1,K)
   50 CONTINUE
      DO 60 K=1,A
      DO 70 I=1,3
      F1(I)=MTC(I,K)
      F2(I)=MTCN(I,K)
```

```
      Q1(I)=FE(I,K)
      DO 70 J=1,3
      R1(I,J)=RTC(I,J,K)
      R2(I,J)=RTCN(I,J,K)
   70 CONTINUE
      CALL RCROSSV(R1,P1,SM1)
      CALL RCROSSV(R1,Q1,SF1)
      CALL RCROSSV(R2,P2,SM2)
      CALL RCROSSV(R2,Q1,SF2)
      DO 60 I=1,3
      MTC(I,K)=SM1(I)
      FTC(I,K)=SF1(I)
      MTCN(I,K)=SM2(I)
      FTCN(I,K)=SF2(I)
   60 CONTINUE
C
C     WRITE MTC, FTC, MTCN AND FTCN AS RESULTS ON LP0
C
      WRITE(6,5000)
      WRITE(6,5100)
 5100 FORMAT(1H0,33HEXT FORCES + MOMENTS IN TC SYSTEM)
      WRITE(6,5200)
 5200 FORMAT(1H0,3X,2HFX,9X,2HFY,9X,2HFZ,9X,2HMX,9X,2HMY,9X,2HMZ
)
      DO 80 K=1,A
      WRITE(6,6000)((FTC(I,K),I=1,3),(MTC(I,K),I=1,3))
 6000 FORMAT((1X,6(F6.1,5X)))
   80 CONTINUE
      WRITE(6,5000)
      WRITE(6,6100)
 6100 FORMAT(1H0,34HEXT FORCES + MOMENTS IN TCN SYSTEM)
      WRITE(6,5200)
      DO 90 K=1,A
      WRITE(6,6000)((FTCN(I,K),I=1,3),(MTCN(I,K),I=1,3))
   90 CONTINUE
      WRITE(6,5000)
C
C     THIS SECTION CALCULATES FRAME BY FRAME:
C
C  1..TRANS. TC TO TCN ORIGIN IN TC SYSTEM IN TTC
C  2..TRANS. TCN TO TC ORIGIN IN TCN SYSTEM IN TTCN
C  3..ROT.   TCN TO TC SYSTEM IN RTC
C  4..ROT    TC TO TCN SYSTEM IN RTCN
C
      DO 160 K=1,A
      DO 150 I=1,3
      P1(I)=TTCN(I,K)-TTC(I,K)
      DO 150 J=1,3
      R1(I,J)=RTC(I,J,K)
      R2(I,J)=RTCN(I,J,K)
      R3(J,I)=R1(I,J)
  150 CONTINUE
      CALL RCROSSV(R1,P1,P2)
      CALL RCROSSV(R2,P1,P3)
      CALL MATMUL(R2,R3)
      DO 160 I=1,3
      TTC(I,K)=P2(I)
      TTCN(I,K)=-P3(I)
      DO 160 J=1,3
      RTC(I,J,K)=R2(J,I)
      RTCN(I,J,K)=R2(I,J)
  160 CONTINUE
      WRITE(7,121)
  121 FORMAT(1H0,40HTTC TTCN RTC RTCN FOR ELEMENT 1 FOLLOW  )
      WRITE(7,2010)(TTC(I,1),I=1,3)
      WRITE(7,2010)(TTCN(I,1),I=1,3)
      WRITE(7,3010)((RTC(I,J,1),J=1,3),I=1,3)
      WRITE(7,3010)((RTCN(I,J,1),J=1,3),I=1,3)
C
C
C     READ IN ANTHROPOMETRIC DATA FROM RESULTS2
C
      READ(4,2000)((ANTH(I,J),J=1,3),I=1,24)
C
C     CALCULATE THE ORIGIN OF THE CALF GROUP IN THE TC SYSTEM
```

```
C      AND ROTATE AND TRANSLATE INTO THE TC SYSTEM
C
       DO 170 I=1,3
       P1(I)=ANTH(4,I)
  170 CONTINUE
       DO 180 K=1,A
       DO 190 I=1,3
       P2(I)=P1(I)-TTCN(I,K)
       DO 190 J=1,3
       R2(I,J)=RTC(I,J,K)
  190 CONTINUE
       CALL RCROSSV(R2,P2,P3)
       DO 180 I=1,3
       FCOMP(1,I,K)=P3(I)
  180 CONTINUE
       WRITE(7,118)
  118 FORMAT(1H0,20HFCOMP(1,I,1) FOLLOWS)
       WRITE(7,2010)((FCOMP(1,I,1),I=1,3))
C
C      COMPUTE THE LINE OF ACTION FOR THE DELTOID AND CALF ALSO
C      THE POTENTIAL MOMENT, PUTTING CALF IN LINE 1 AND DELTOID
C     IIN LINE 7 OF FCOMP AND MCOMP
C
       DO 200 I=1,3
       P1(I)=ANTH(1,I)
       P2(I)=ANTH(2,I)
  200 CONTINUE
       CALL DCM(P1,P2)
       DO 210 K=1,A
       DO 220 J=1,3
       FCOMP(7,J,K)=P2(J)
       MCOMP(7,J,K)=P1(J)
       Q1(J)=FCOM (1,J,K)
       P3(J)=ANTH(3,J)
  220 CONTINUE
       CALL DCM(P3,Q1)
       DO 210 J=1,3
       FCOMP(1,J,K)=Q1(J)
       MCOMP(1,J,K)=P3(J)
  210 CONTINUE
       WRITE(7,119)
  119 FORMAT(1H0,30HFCOMP AND MCOMP ROW 1+7 FOLLOW)
       WRITE(7,3010)((FCOMP(1,J,1),J=1,3),(MCOMP(1,J,1),J=1,3))
       WRITE(7,3010)((FCOMP(7,J,1),J=1,3),(MCOMP(7,J,1),J=1,3))
C
C      CALCULATE THE FORCE AND MOMENT VECTORS FOR THE REMAINING
C      ANTHROPOMETRY
C
       DO 230 I=5,23,2
       DO 240 J=1,3
       P1(J)=ANTH(I,J)
       P2(J)=ANTH((I+1),J)
  240 CONTINUE
       CALL DCM(P1,P2)
       DO 230 J=1,3
       ANTH(I,J)=P1(J)
       ANTH((I+1),J)=P2(J)
  230 CONTINUE
       WRITE(7,122)
  122 FORMAT(1H0,17HANTH(I,J) FOLLOWS)
       WRITE(7,2010)(((ANTH(I,J),J=1,3),I=1,24))
C
C      READ MUSCLE PARTICIPATION FACTORS FROM SUBJECT FILE
C
       READ(3,1500)(T(I),I=1,8)
C
C      CALCULATE MUSCLE RESULTANTS PUTTING:
C
C      ATM=L15 ANTH
C      ATF=L16
C      PTM=L17
C      PTF=L18
C       PM=L19
C       PF=L20
C
```

```
      DO 250 J=1,2
      DO 250 I=1,3
C
C      PERONEAL  GROUP
C
      ANTH(18+J,I)=T(7)*ANTH(16+J,I)+T(8)*ANTH(18+J,I)
C
C     POSTERIOR TIBIAL GROUP
C
      ANTH(16+J,I)=T(4)*ANTH(10+J,I)+T(5)*ANTH(12+J,I)+T(6)*ANTH
(14+J,I)
C
C
C     ANTERIOR TIBIAL GROUP
C
      ANTH(14+J,I)=T(1)*ANTH(4+J,I)+T(2)*ANTH(6+J,I)+T(3)+ANTH(8
+J,I)
C
  250 CONTINUE
      WRITE(7,251)
  251 FORMAT(1H0,36HROWS 15-20 ANTH HOLD MUSCLE RESULTS )
      WRITE(7,2010)(((ANTH(I,J),J=1,3),I=15,20))
C
C     ROTATE FORCES INTO THE TC SYSTEM( AT,PT,P,AFT,PFT )
C
      DO 260 L=1,5
      DO 260 K=1,A
      DO 270 I=1,3
      P1(I)=ANTH((14+2*L),I)
      DO 270 J=1,3
      R1(I,J)=RTC(I,J,K)
  270 CONTINUE
      CALL RCROSSV(R1,P1,P2)
      DO 260 I=1,3
      FCOMP((L+1),I,K)=P2(I)
  260 CONTINUE
C
C     CALCULATE MOMENTS IN THE TC SYSTEM( AT,PT,P,AFT,PFT )
C
      DO 280 L=1,5
      N=2*L+14
      DO 280 K=1,A
      P1(1)=-TTCN(2,K)*ANTH(N,3)+TTCN(3,K)*ANTH(N,2)+ANTH((N-1).
1)
      P1(2)=TTCN(1,K)*ANTH(N,3)-TTCN(3,K)*ANTH(N,1)+ANTH((N-1),2
)
      P1(3)=-TTCN(1,K)*ANTH(N,2)+TTCN(2,K)*ANTH(N,1)+ANTH((N-1),
3)
      DO 285 I=1,3
      DO 285 J=1,3
      R1(I,J)=RTC(I,J,K)
  285 CONTINUE
      CALL RCROSSV(R1,P1,P2)
      DO 280 I=1,3
      MCOMP((L+1),I,K)=P2(I)
  280 CONTINUE
C
C     WRITE OUT THE FORCE AND MOMENT EQUATIONS
C
      WRITE(6,290)
  290 FORMAT(1H0,10X,100H**********************************************
********
     *********************************************)
      WRITE(6,295)
  295 FORMAT(1H0,36HTC SYSTEM FORCE AND MOMENT EQUATIONS)
      WRITE(6,290)
      DO 320 J=1,3
      IF(J-2)311,312,313
  311 WRITE(6,300)
      GO TO 314
  312 WRITE(6,301)
      GO TO 314
  313 WRITE(6,302)
  314 CONTINUE
      WRITE(6,299)
```

```
      DO 330 K=1,A
      WRITE(6,310)((FCOMP(I,J,K),I=1,10),FTC(J,K))
  330 CONTINUE
      WRITE(6,290)
  320 CONTINUE
      DO 340 J=1,3
      IF(J-2)341,342,343
  341 WRITE(6,303)
      GO TO 344
  342 WRITE(6,304)
      GO TO 344
  343 WRITE(6,305)
  344 CONTINUE
      WRITE(6,299)
      DO 350 K=1,A
      WRITE(6,310)((MCOMP(I,J,K),I=1,10),MTC(J,K))
  350 CONTINUE
      WRITE(6,290)
  340 CONTINUE
  299 FORMAT(1H0,4X,8H  CALF  ,2X,8HANT TIB ,2X,8HPOST TIB,2X,8H
PERONEAL
     *,2X,8H ANT FT ,2X,8HPOST FT ,2X,8HDELTOID ,2X,8H********,2
X,8H****
     *****,2X,8H********,2X,8HEXTERNAL)
  300 FORMAT(1H ,10X,11HX-FORCES(N))
  301 FORMAT(1H ,10X,11HY-FORCES(N))
  302 FORMAT(1H ,10X,11HZ-FORCES N))
  303 FORMAT(1H ,10X,13HX-MOMENTS(NM))
  304 FORMAT(1H ,10X,13HY-MOMENTS(NM))
  305 FORMAT(1H ,10X,13HZ-MOMENTS(NM))
  310 FORMAT(1H ,3X,10(F8.4,2X),1H=,F7.1)
C
C     SOLUTION OF THE EQUATIONS MK1
C     THE CALF GROUP AND ANTERIOR TIBIAL GROUP ARE USED TO
C     CALCULATE THE TC JOINT FORCES
C
C     SET L=1      CALF GROUP
C     SET L=2      ANTERIOR TIBIAL GROUP
C
      DO 400 K=1,A
      L=2
      STC(1,K)=0.0
      IF(MTC(3,K).LT.0.0)GO TO 410
      L=1
      STC(2,K)=0.0
  410 CONTINUE
C
C     SOLVE FOR CALF OR ANT TIB FORCE
C
      STC(L,K)=MTC(3,K)/MCOMP(L,3,K)
      STC(5,K)=-FTC(3,K)-FCOMP(L,3,K)*STC(L,K)
      DO 420 I=1,2
      FTC(I,K)=-FTC(I,K)-FCOMP(L,I,K)*STC(L,K)
      MTC(I,K)=(MTC(I,K)-MCOMP(L,I,K)*STC(L,K))*100.0
  420 CONTINUE
      STC(3,K)=(FTC(1,K)-MTC(2,K))/2.0
      STC(6,K)=(FTC(1,K)+MTC(2,K))/2.0
      STC(4,K)=(FTC(2,K)+MTC(1,K))/2.0
      STC(7,K)=(FTC(2,K)-MTC(1,K))/2.0
C
C     THE TC SOLUTIONS ARE OBTAINED
C
C        CALF=STC(1,K)
C     ANT TIB=STC(2,K)
C      FX-LAT=STC(3,K)
C      FY-LAT=STC(4,K)
C      FZ-LAT=STC(5,K)
C      FX-MED=STC(6,K)
C      FY-MED=STC(7,K)
C
C
C     THE RESULTANT TC JOINT FORCE AND MOMENT IS CALCULATED
C
C     F1 RESULTANT MOMENT
C     Q1 RESULTANT FORCE
```

```
C
      P1(1)=MTC(1,K)/100.0
      P1(2)=MTC(2,K)/100.0
      P1(3)=0.0
      Q1(1)=STC(3,K)+STC(6,K)
      Q1(2)=STC(4,K)+STC(7,K)
      Q1(3)=STC(5,K)
C
C     CALCULATE MOMENTS ABOUT THE TCN ORIGIN
C
      P1(1)=-TTC(2,K)*Q1(3)+TTC(3,K)*Q1(2)+P1(1)
      P1(2)=TTC(1,K)*Q1(3)-TTC(3,K)*Q1(1)+P1(2)
      P1(3)=-TTC(1,K)*Q1(2)+TTC(2,K)*Q1(1)+P1(3)
      DO 430 I=1,3
      DO 430 J=1,3
      R1(I,J)=RTCN(I,J,K)
  430 CONTINUE
      CALL RCROSSV(R1,P1,P2)
      CALL RCROSSV(R1,Q1,P3)
      STCN(3,K)=-P3(3)
      STCN(6,K)=-P2(3)
      STCN(2,K)=-(P3(2)+50*P2(1))/2.0
      STCN(5,K)=-(P3(2)-50*P2(1))/2.0
      STCN(1,K)=-(P3(1)-50*P2(2))/2.0
      STCN(4,K)=-(P3(1)+50*P2(2))/2.0
C
C     THE TCN SOLUTIONS ARE OBTAINED
C
C     FX POST=STCN(1,K)
C     FY POST=STCN(2,K)
C     FZ POST=STCN(3,K)
C      FX ANT=STCN(4,K)
C      FY ANT=STCN(5,K)
C     MZ RESU=STCN(6,K)
C
  400 CONTINUE
C
C     WRITE TC SOLUTIONS
C
      WRITE(6,290)
      WRITE(6,450)
  450 FORMAT(1H0,10X,19HTC SYSTEM SOLUTIONS)
      WRITE(6,460)
  460 FORMAT(1H0,4X,8H  CALF  ,2X,8HANT-TIB ,2X,8H FX-LAT ,2X,8H
FY-LAT
     *,2X,8H FZ-LAT ,2X,8H FX-MED ,2X,8H FY-MED )
      DO 463 K=1,A
      WRITE(6,465)(STC(I,K),I=1,7)
  463 CONTINUE
  465 FORMAT(1H ,3X,7(F8.1,2X))
C
C     WRITE TCN SOLUTIONS
C
      WRITE(6,290)
      WRITE(6,470)
  470 FORMAT(1H0,10X,20HTCN SYSTEM SOLUTIONS)
      WRITE(6,480)
  480 FORMAT(1H0,4X,8HFX-POST ,2X,8HFY-POST ,2X,8HFZ-POST ,2X,8H
FX-ANT
     *,2X,8H FY-ANT ,2X,9HMZ(RES)NM)
      DO 483 K=1,A
      WRITE(6,490)(STCN(I,K),I=1,6)
  483 CONTINUE
  490 FORMAT(1H ,3X,6(F8.1,2X))
      WRITE(6,290)
      READ(3,1000)AGE
      DO 500 K=1,A
C
C     CALCULATE THE RESULTANT FORCES NORMALISING FOR BODY WEIGHT
C
      STC(3,K)=STC(3,K)+STC(6,K)
      STC(4,K)=STC(4,K)+STC(7,K)
      STC(3,K)=SQRT(STC(3,K)**2+STC(4,K)**2+STC(5,K)**2)
      STC(4,K)=SQRT(STCN(1,K)**2+STCN(2,K)**2+STCN(3,K)**2)
      STC(5,K)=SQRT(STCN(4,K)**2+STCN(5,K)**2)
```

```
      DO 510 I=1,5
      STC(I,K)=STC(I,K)/AGE
  510 CONTINUE
  500 CONTINUE
      WRITE(6,520)
  520 FORMAT(1H0,10X,17HNORMALISED FORCES)
      WRITE(6,530)
  530 FORMAT(1H0,4X,8H  CALF  ,2X,8HANT-TIB ,2X,8H TC-RES
.2X,8HPOST-TCN
     *,2X,8H ANT-TCN )
      DO 540 K=1,A
      WRITE(6,550)(STC(I,K),I=1,5)
  540 CONTINUE
  550 FORMAT(1H .3X,5(F8.2,2X))
      WRITE(6,290)
      WRITE(6,290)
 5000 FORMAT(1H0,50H**********************************************
******)
 1000 FORMAT(F0.0)
 1500 FORMAT(9F0.0)
 2000 FORMAT(3F0.0)
 2010 FORMAT(1X,3(F6.4,5X))
 3000 FORMAT(9F0.0)
 3010 FORMAT(1X,9(F6.4,5X))
      STOP
      END
      SUBROUTINE MATMUL(X,Y)
C
C     MATMUL COMPUTES MATRIX PRODUCT "X*Y"
C
      DIMENSION X(3,3),Y(3,3),Z(3,3)
      DO 5 I=1,3
      DO 5 J=1,3
      SUM=0.0
      DO 6 K=1,3
    6 SUM=SUM+X(I,K)*Y(K,J)
    5 Z(I,J)=SUM
      DO 7 I=1,3
      DO 7 J=1,3
      X(I,J)=Z(I,J)
    7 CONTINUE
      RETURN
      END
      SUBROUTINE RCROSSV(R,V1,V2)
C
C     THIS SUBROUTINE ROTATES VECTOR 1 FROM SYSTEM 1 INTO SYSTEM
2 TO
C     GIVE VECTOR 2 USING THE R1-2 ROTATION MATRIX
C
      DIMENSION R(3,3),V1(3),V2(3)
      DO 10 I=1,3
      SUM=0.0
      DO 20 J=1,3
      SUM=SUM+R(I,J)*V1(J)
   20 CONTINUE
      V2(I)=SUM
   10 CONTINUE
      RETURN
      END
      SUBROUTINE DCM(X,Y)
C
C     THIS SUBROUTINE TAKES X=ORIGIN
C                           Y=INSERTION
C
C     IT CALCULATES DIRECTION COSINES AND POTENTIAL MOMENTS
C
C     DIRECTION COSINES AS ORIGIN-INSERTION=POTENTIAL FORCE
C     AND ORIGIN CROSS POTENTIAL FORCE     =POTENTIAL MOMENTS
C
C                          X=POTENTIAL MOMENT
C                           Y=POTENTIAL FORCE
C
      DIMENSION X(3),Y(3),Z(3)
      SUM=0.0
      DO 10 I=1,3
```

```
576         Z(I)=X(I)-Y(I)
577         SUM=SUM+Z(I)**2
578      10 CONTINUE
579         SUM=SQRT(SUM)
580         DO 20 I=1,3
581         Z(I)=Z(I)/SUM
582      20 CONTINUE
583         X(1)=-Y(2)*Z(3)+Y(3)*Z(2)
584         X(2)=-Y(3)*Z(1)+Y(1)*Z(3)
585         X(3)=-Y(1)*Z(2)+Y(2)*Z(1)
586         DO 30 I=1,3
587         Y(I)=Z(I)
588      30 CONTINUE
589         RETURN
590         END
591         FINISH
592
```

A3.8 FORCED2B Program Listing

```
      0       LIST
      1       PROGRAM(FORCE02)
      2       INPUT 1=CR0
      3       INPUT 2=CR1
      4       INPUT 3=CR2
      5       INPUT 4=CR3
      6       OUTPUT 7=LP1
      7       OUTPUT 6=LP0
      8       TRACE 2
      9       END
     10       MASTER PROG2
     11       REAL MTC,MTCN,M,MCOMP,MMTCN
     12       INTEGER A,SLOPE
     13       DIMENSION SCALE(6),FE(6,99),MTCN(3,50),CPZ(50),CPX(50),TTC
(3,50),R
     14      *TC(3,3,50),TTCN(3,50),RTCN(3,3,50),MTC(3,50),FTC(3,50),FTC
N 3,50),
     15      *P1(3),P2(3),P3(3),Q1(3),R1(3,3),R2(3,3),R3(3,3),SM1(3),SM2
(3),SF1(
     16      *3),SF2(3),ANTH(24,3),MCOMP(10,3,50),FCOMP(10,3,50),T(8),ST
C(9,50),
     17      *STCN(6,50),FFTC(2,50),MMTC(2,50),P4(3),P5(3),P6(3)
     18 C
     19 C     THIS PROGRAM CALCULATES THE TC AND TCN SYSTEM MOMENTS
USING
     20 C     FORCE DATA IN FILE, AND KINEMATIC DATA IN FILE. IT OUTPUTS
     21 C     FORCES AND MOMENTS IN A) EXTERNAL, B) TC AND C) TCN
SYSTEMS
     22 C     THEN IT FORMULATES THE TC SYSTEM FORCE AND MOMENT EQUATION
S
     23 C
     24 C     SOLUTION MK1 CALCULATES CALF/ANT TIB GROUP ACTIVITY AND
THE
     25 C     TCN SYSTEM MZ RESIDUAL
     26 C
     27 C     SOLUTION MK2 CALCULATES THE LEVEL OF POST TIB/PERONEAL
GROUP
     28 C     ACTIVITY NECESSARY TO EQUILIBRATE THE RESIDUAL
     29 C
     30 C
     31 C     READ IN FORCE DATA
     32 C                          A= NUMBER OF POINTS
     33 C                          B= DC LEVEL
     34 C     ALSO CORRECTING FOR DC SHIFT
     35 C
     36 C     THIS SEGMENT READS IN FORCE DATA
     37 C
     38       READ(2,1100)A
     39       L=2*A
     40       DO 10 I=1,6
     41       READ(2,1000)B
     42       WRITE(7,1750)L,B
     43       READ(2,1500)(FE(I,J),J=1,L)
     44       DO 10 J=1,A
     45       FE(I,J)=FE(I,(2*J-1))-B
     46    10 CONTINUE
     47  1750 FORMAT(3X,I2,3X,F6.3)
     48 C
     49 C     READ IN TOP AMP(TA) AND BOTTOM AMP(BA) FACTORS
     50 C
     51       READ(3,1001)TA,BA
     52  1001 FORMAT(2F8.0)
     53 C
     54 C     SET FORCE AND MOMENT FACTORS
     55 C
     56       F=0.0195313
     57       M=0.0051563
     58 C
     59 C     CALCULATE SCALE FACTORS
     60 C
     61       SCALE(1)=TA*F/1.0
     62       SCALE(2)=BA*F/1.0
     63       SCALE(3)=TA*F/(-2.0)
     64       SCALE(4)=BA*M/1.25
     65       SCALE(5)=TA*M/2.0
```

```
      SCALE(6)=BA*M/(-1.25)
C
C     SCALE FORCES AND MOMENTS
C
      DO 20 J=1,A
      DO 20 I=1,6
      FE(I,J)=FE(I,J)*SCALE(I)
   20 CONTINUE
C
C     WRITE EXTERNAL FORCES AND MOMENTS ON LP0
C
      WRITE(6,5000)
      WRITE(6,25)
   25 FORMAT(1H0,2/HEXTERNAL FORCES AND MOMENTS)
      WRITE(6,5200)
      WRITE(6,30)((FE(I,J),I=1,6),J=1,A)
   30 FORMAT((1H ,1X,6(F6.1,5X)))
      WRITE(6,5000)
      READ(2,1100)SLOPE
 1100 FORMAT(I2)
C
C     THIS SECTION COMPUTES THE CENTRE OF PRESSURE PATH
C     ACCORDING TO THE SIGN OF THE TEST SLOPE
C
C          -1 = TEST FOOT DOWNHILL
C
C           0 = ON THE LEVEL
C
C          +1 = TEST FOOT UPHILL
C
      IF(SLOPE)110,100,110
  100 CONTINUE
      DO 105 J=1,A
      CPX(J)=(FE(6,J)+0.04*FE(1,J))/FE(2,J)
      CPZ(J)=(0.04*FE(6,J)-FE(4,J))/FE(2,J)
  105 CONTINUE
      GO TO 120
  110 CONTINUE
      DO 115 J=1,A
      YCOORD=0.0
      CPX(J)=(FE(6,J)+0.1935*FE(1,J))/(FE(2,J)-SLOPE*0.1763*FE(1
,J))
      YCOORD=(SLOPE*0.1763+CPX(J)+0.1935)
      CPZ(J)=(YCOORD*FE(3,J)-FE(4,J))/FE(2,J)
  115 CONTINUE
  120 CONTINUE
      WRITE(6,5000)
      WRITE(6,130)SLOPE
  130 FORMAT(1H0,8HSLOPE = ,I2,5X,18HCENTRE OF PRESSURE)
      WRITE(6,135)
  135 FORMAT(1H0,5X,12HX-COORDINATE,5X,12HZ-COORDINATE)
      DO 140 J=1,A
      WRITE(6,145)CPX(J),CPZ(J)
  145 FORMAT(1H ,8X,F6.4,11X,F6.4)
  140 CONTINUE
C
C     READ IN RESULTS OF KINEDR AND CORRECT Y COORDINATE FOR DC
SHIFT
C
      DO 40 K=1,A
      READ(1,2000)(TTC(I,K),I=1,3)
      READ(1,3000)((RTC(I,J,K),J=1,3),I=1,3)
      READ(1,2000)(TTCN(I,K),I=1,3)
      READ(1,3000)((RTCN(I,J,K),J=1,3),I=1,3)
      TTC(2,K)=TTC(2,K)+0.049
      TTCN(2,K)=TTCN(2,K)+0.049
   40 CONTINUE
C
C     CALCULATE MOMENTS ABOUT TC AND TCN ORIGIN .... MTC AND
MTCN
C     RESPECTIVELY, DUE TO THE EXTERNAL FORCES AND MOMENTS
C
      DO 50 K=1,A
      MTC(1,K)=FE(4,K)-TTC(2,K)*FE(3,K)+TTC(3,K)*FE(2,K)
      MTC(2,K)=FE(5,K)-TTC(3,K)*FE(1,K)+TTC(1,K)*FE(3,K)
```

```
      MTC(3,K)=FE(6,K)-TTC(1,K)*FE(2,K)+TTC(2,K)*FE(1,K)
      MTCN(1,K)=FE(4,K)-TTCN(2,K)*FE(3,K)+TTCN(3,K)*FE(2,K)
      MTCN(2,K)=FE(5,K)-TTCN(3,K)*FE(1,K)+TTCN(1,K)*FE(3,K)
      MTCN(3,K)=FE(6,K)-TTCN(1,K)*FE(2,K)+TTCN(2,K)*FE(1,K)
   50 CONTINUE
      DO 60 K=1,A
      DO 70 I=1,3
      P1(I)=MTC(I,K)
      P2(I)=MTCN(I,K)
      Q1(I)=FE(I,K)
      DO 70 J=1,3
      R1(I,J)=RTC(I,J,K)
      R2(I,J)=RTCN(I,J,K)
   70 CONTINUE
      CALL RTIMESV(R1,P1,SM1)
      CALL RTIMESV(R1,Q1,SF1)
      CALL RTIMESV(R2,P2,SM2)
      CALL RTIMESV(R2,Q1,SF2)
      DO 60 I=1,3
      MTC(I,K)=SM1(I)
      FTC(I,K)=SF1(I)
      MTCN(I,K)=SM2(I)
      FTCN(I,K)=SF2(I)
   60 CONTINUE
C
C     WRITE MTC, FTC, MTCN AND FTCN AS RESULTS ON LP0
C
      WRITE(6,5000)
      WRITE(6,5100)
 5100 FORMAT(1H0,33HEXT FORCES + MOMENTS IN TC SYSTEM)
      WRITE(6,5200)
 5200 FORMAT(1H0,3X,2HFX,9X,2HFY,9X,2HFZ,9X,2HMX,9X,2HMY,9X,2HMZ
)
      DO 80 K=1,A
      WRITE(6,6000)((FTC(I,K),I=1,3),(MTC(I,K),I=1,3))
 6000 FORMAT(1X,6(F6.1,5X)))
   80 CONTINUE
      WRITE(6,5000)
      WRITE(6,6100)
 6100 FORMAT(1H0,34HEXT FORCES + MOMENTS IN TCN SYSTEM)
      WRITE(6,5200)
      DO 90 K=1,A
      WRITE(6,6000)((FTCN(I,K),I=1,3),(MTCN(I,K),I=1,3))
   90 CONTINUE
      WRITE(6,5000)
C
C     THIS SECTION CALCULATES FRAME BY FRAME:
C
C  1..TRANS. TC TO TCN ORIGIN IN TC SYSTEM IN TTC
C  2..TRANS. TCN TO TC ORIGIN IN TCN SYSTEM IN TTCN
C  3..ROT.  TCN TO TC SYSTEM IN RTC
C  4..ROT    TC TO TCN SYSTEM IN RTCN
C
      DO 160 K=1,A
      DO 150 I=1,3
      P1(I)=TTCN(I,K)-TTC(I,K)
      DO 150 J=1,3
      R1(I,J)=RTC(I,J,K)
      R2(I,J)=RTCN(I,J,K)
      R3(J,I)=R1(I,J)
  150 CONTINUE
      CALL RTIMESV(R1,P1,P2)
      CALL RTIMESV(R2,P1,P3)
      CALL MATMUL(R2,R3)
      DO 160 I=1,3
      TTC(I,K)=P2(I)
      TTCN(I,K)=-P3(I)
      DO 160 J=1,3
      RTC(I,J,K)=R2(J,I)
      RTCN(I,J,K)=R2(I,J)
  160 CONTINUE
      WRITE(7,121)
  121 FORMAT(1H0,40HTTC TTCN RTC RTCN FOR ELEMENT 1 FOLLOW  )
      WRITE(7,2010)(TTC(I,1),I=1,3)
      WRITE(7,2010)(TTCN(I,1),I=1,3)
```

```
      WRITE(7,3010)((RTC(I,J,1),J=1,3),I=1,3)
      WRITE(7,3010)((RTCN(I,J,1),J=1,3),I=1,3)
C
C
C     READ IN ANTHROPOMETRIC DATA FROM RESULTS2
C
      READ(4,2000)((ANTH(I,J),J=1,3),I=1,24)
C
C     CALCULATE THE ORIGIN OF THE CALF GROUP IN THE TC SYSTEM
C     AND ROTATE AND TRANSLATE INTO THE TC SYSTEM
C
      DO 170 I=1,3
      P1(I)=ANTH(4,I)
  170 CONTINUE
      DO 180 K=1,A
      DO 190 I=1,3
      P2(I)=P1(I)-TTCN(I,K)
      DO 190 J=1,3
      R2(I,J)=RTC(I,J,K)
  190 CONTINUE
      CALL RTIMESV(R2,P2,P3)
      DO 180 I=1,3
      FCOMP(1,I,K)=P3(I)
  180 CONTINUE
      WRITE(7,118)
  118 FORMAT(1H0,20HFCOMP(1,I,1) FOLLOWS)
      WRITE(7,2010)((FCOMP(1,I,1),I=1,3))
C
C     COMPUTE THE LINE OF ACTION FOR THE DELTOID AND CALF ALSO
C     THE POTENTIAL MOMENT, PUTTING CALF IN LINE 1 AND DELTOID
C    IIN LINE 7 OF FCOMP AND MCOMP
C
      DO 200 I=1,3
      P1(I)=ANTH(1,I)
      P2(I)=ANTH(2,I)
  200 CONTINUE
      CALL DCM(P1,P2)
      DO 210 K=1,A
      DO 220 J=1,3
      FCOMP(7,J,K)=P2(J)
      MCOMP(7,J,K)=P1(J)
      Q1(J)=FCOMP(1,J,K)
      P3(J)=ANTH(3,J)
  220 CONTINUE
      CALL DCM(P3,Q1)
      DO 210 J=1,3
      FCOMP(1,J,K)=Q1(J)
      MCOMP(1,J,K)=P3(J)
  210 CONTINUE
      WRITE(7,119)
  119 FORMAT(1H0,30HFCOMP AND MCOMP ROW 1+7 FOLLOW)
      WRITE(7,3010)((FCOMP(1,J,1),J=1,3),(MCOMP(1,J,1),J=1,3))
      WRITE(7,3010)((FCOMP(7,J,1),J=1,3),(MCOMP(7,J,1),J=1,3))
C
C     CALCULATE THE FORCE AND MOMENT VECTORS FOR THE REMAINING
C     ANTHROPOMETRY
C
      DO 230 I=5,23,2
      DO 240 J=1,3
      P1(J)=ANTH(I,J)
      P2(J)=ANTH((I+1),J)
  240 CONTINUE
      CALL DCM(P1,P2)
      DO 230 J=1,3
      ANTH(I,J)=P1(J)
      ANTH((I+1),J)=P2(J)
  230 CONTINUE
      WRITE(7,122)
  122 FORMAT(1H0,17HANTH(I,J) FOLLOWS)
      WRITE(7,2010)(((ANTH(I,J),J=1,3),I=1,24))
C
C     READ MUSCLE PARTICIPATION FACTORS FROM SUBJECT FILE
C
      READ(3,1500)(T(I),I=1,8)
C
```

```
C     CALCULATE MUSCLE RESULTANTS PUTTING:
C
C     ATM=L15 ANTH
C     ATF=L16
C     PTM=L17
C     PTF=L18
C      PM=L19
C      PF=L20
C
      DO 250 J=1,2
      DO 250 I=1,3
C
C      PERONEAL GROUP
C
      ANTH(18+J,I)=T(7)*ANTH(16+J,I)+T(8)*ANTH(18+J,I)
C
C     POSTERIOR TIBIAL GROUP
C
      ANTH(16+J,I)=T(4)*ANTH(10+J,I)+T(5)*ANTH(12+J,I)+T(6)*ANTH
(14+J,I)
C
C
C     ANTERIOR TIBIAL GROUP
C
      ANTH(14+J,I)=T(1)*ANTH(4+J,I)+T(2)*ANTH(6+J,I)+T(3)*ANTH(8
+J,I)
C
  250 CONTINUE
      WRITE(7,251)
  251 FORMAT(1H0,36HROWS 15-20 ANTH HOLD MUSCLE RESULTS )
      WRITE(7,2010)(((ANTH(I,J),J=1,3),I=15,20))
C
C     ROTATE FORCES INTO THE TC SYSTEM( AT,PT,P,AFT,PFT )
C
      DO 260 L=1,5
      DO 260 K=1,4
      DO 270 I=1,3
      P1(I)=ANTH((14+2*L),I)
      DO 270 J=1,3
      R1(I,J)=RTC(I,J,K)
  270 CONTINUE
      CALL RTIMESV(R1,P1,P2)
      DO 260 I=1,3
      FCOMP((L+1),I,K)=P2(I)
  260 CONTINUE
C
C     CALCULATE MOMENTS IN THE TC SYSTEM( AT,PT,P,AFT,PFT )
C
      DO 280 L=1,5
      N=2*L+14
      DO 280 K=1,4
      P1(1)=-TTCN(2,K)*ANTH(N,3)+TTCN(3,K)*ANTH(N,2)+ANTH((N-1),
1)
      P1(2)=TTCN(1,K)*ANTH(N,3)-TTCN(3,K)*ANTH(N,1)+ANTH((N-1),2
)
      P1(3)=-TTCN(1,K)*ANTH(N,2)+TTCN(2,K)*ANTH(N,1)+ANTH((N-1),
3)
      DO 285 I=1,3
      DO 285 J=1,3
      R1(I,J)=RTC(I,J,K)
  285 CONTINUE
      CALL RTIMESV(R1,P1,P2)
      DO 280 I=1,3
      MCOMP((L+1),I,K)=P2(I)
  280 CONTINUE
C
C     WRITE OUT THE FORCE AND MOMENT EQUATIONS
C
      WRITE(6,290)
  290 FORMAT(1H0,10X,100H**********************************************
********
     *********************************************)
      WRITE(6,295)
  295 FORMAT(1H0,36HTC SYSTEM FORCE AND MOMENT EQUATIONS)
      WRITE(6,290)
```

```
      DO 320 J=1,3
      IF(J-2)311,312,313
  311 WRITE(6,300)
      GO TO 314
  312 WRITE(6,301)
      GO TO 314
  313 WRITE(6,302)
  314 CONTINUE
      WRITE(6,299)
      DO 330 K=1,A
      WRITE(6,310)((FCOMP(I,J,K),I=1,10),FTC(J,K))
  330 CONTINUE
      WRITE(6,290)
  320 CONTINUE
      DO 340 J=1,3
      IF(J-2)341,342,343
  341 WRITE(6,303)
      GO TO 344
  342 WRITE(6,304)
      GO TO 344
  343 WRITE(6,305)
  344 CONTINUE
      WRITE(6,299)
      DO 350 K=1,A
      WRITE(6,310)((MCOMP(I,J,K),I=1,10),MTC(J,K))
  350 CONTINUE
      WRITE(6,290)
  340 CONTINUE
  299 FORMAT(1H0,4X,8H  CALF  ,2X,8HANT TIB ,2X,8HPOST TIB,2X,8H
PERONEAL
     *,2X,8H ANT FT ,2X,8HPOST FT ,2X,8HDELTOID ,2X,8H********,2
X,8H****
     *****,2X,8H********,2X,8HEXTERNAL)
  300 FORMAT(1H ,10X,11HX-FORCES(N))
  301 FORMAT(1H ,10X,11HY-FORCES(N))
  302 FORMAT(1H ,10X,11HZ-FORCES(N))
  303 FORMAT(1H ,10X,13HX-MOMENTS(NM))
  304 FORMAT(1H ,10X,13HY-MOMENTS(NM))
  305 FORMAT(1H ,10X,13HZ-MOMENTS(NM))
  310 FORMAT(1H ,3X,10(F8.4,2X),1H=,F7.1)
C
C     SOLUTION OF THE EQUATIONS MK1
C     THE CALF GROUP AND ANTERIOR TIBIAL GROUP ARE USED TO
C     CALCULATE THE TC JOINT FORCES
C
C     SET L=1      CALF GROUP
C     SET L=2      ANTERIOR TIBIAL GROUP
C
      DO 400 K=1,A
      L=2
      STC(1,K)=0.0
      IF(MTC(3,K).LT.0.0)GO TO 410
      L=1
      STC(2,K)=0.0
  410 CONTINUE
C
C     SOLVE FOR CALF OR ANT TIB FORCE
C
      STC(L,K)=MTC(3,K)/MCOMP(L,3,K)
      STC(5,K)=-FTC(3,K)-FCOMP(L,3,K)*STC(L,K)
      DO 420 I=1,2
      FFTC(I,K)=-FTC(I,K)-FCOMP(L,I,K)*STC(L,K)
      MMTC(I,K)=(MTC(I,K)-MCOMP(L,I,K)*STC(L,K))*100.0
  420 CONTINUE
      STC(3,K)=(FFTC(1,K)-MMTC(2,K))/2.0
      STC(6,K)=(FFTC(1,K)+MMTC(2,K))/2.0
      STC(4,K)=(FFTC(2,K)+MMTC(1,K))/2.0
      STC(7,K)=(FFTC(2,K)-MMTC(1,K))/2.0
C
C     THE TC SOLUTIONS ARE OBTAINED
C
C        CALF=STC(1,K)
C     ANT TIB=STC(2,K)
C      FX-LAT=STC(3,K)
C      FY-LAT=STC(4,K)
```

```
C       FZ=LAT*STC(5,K)
C       FX=MED*STC(6,K)
C       FY=MED*STC(7,K)
C
C
C     THE RESULTANT TC JOINT FORCE AND MOMENT IS CALCULATED
C
C     P1=RESULTANT MOMENT
C     Q1=RESULTANT FORCE
C
      P1(1)=MMTC(1,K)/100.0
      P1(2)=MMTC(2,K)/100.0
      P1(3)=0.0
      Q1(1)=STC(3,K)+STC(6,K)
      Q1(2)=STC(4,K)+STC(7,K)
      Q1(3)=STC(5,K)
C
C     CALCULATE MOMENTS ABOUT THE TCN ORIGIN
C
      P1(1)=-TTC(2,K)*Q1(3)+TTC(3,K)*Q1(2)+P1(1)
      P1(2)=TTC(1,K)*Q1(3)-TTC(3,K)*Q1(1)+P1(2)
      P1(3)=-TTC(1,K)*Q1(2)+TTC(2,K)*Q1(1)+P1(3)
      DO 430 I=1,3
      DO 430 J=1,3
      R1(I,J)=RTCN(I,J,K)
  430 CONTINUE
      CALL RTIMESV(R1,P1,P2)
      STCN(6,K)=-P2(3)
      WRITE(7,432)K
  432 FORMAT(2X,I2)
      WRITE(7,432)L
      WRITE(7,431)STCN(6,K)
  431 FORMAT(2X,F8.2)
C
C     THE SOLUTION OF THE EQUATIONS MK2
C
C     THE PERONEAL/POST TIB GROUP ARE USED TO EQUILIBRATE THE
C     RESIDUAL Z MOMENT IN THE TCN SYSTEM (IN STCN(6,K))
C
C     IF STCN(6,K) -VE THEN N=3  POSTERIOR TIBIAL GROUP
C     IF STCN(6,K) +VE THEN N=4 PERONEAL GROUP
C
C     STCN(8,K) HOLDS POST TIB VALUES
C      STCN(9,K) HOLDS PERONEAL VALUES
C
C
C     MOMENT EQUATIONS DUE TO THE JOINT FORCES
C
C     P1-EXT COMPONENTS
C     P2-PERONEAL
C     P3-ANT TIB/CALF COMPONENTS
C
      N=3
      STC(9,K)=0.0
      IF(STCN(6,K).LT.0.0)GO TO 440
      N=4
      STC(8,K)=0.0
  440 CONTINUE
      WRITE(7,432)N
      DO 445 I=1,3
      P1(I)=-FTC(I,K)
      P2(I)=-FCOMP(N,I,K)
      P3(I)=-FCOMP(L,I,K)
      Q1(I)=-TTC(I,K)
  445 CONTINUE
      CALL RCROSSF(Q1,P1)
      CALL RCROSSF(Q1,P2)
      CALL RCROSSF(Q1,P3)
C
C     NOW THE JOINT FORCE COMPONENTS ARE IN MOMENT FORM ABOUT
C     THE TCN ORIGIN AND ARE ADDED TO  THE MOMENTS DUE TO
C      THESE FORCES ABOUT THE TC ORIGIN
C
      DO 450 I=1,2
      P1(I)=P1(I)+MTC(I,K)
```

```
      P2(I)=P2(I)-MCOMP(N,I,K)
      P3(I)=P3(I)-MCOMP(L,I,K)
  450 CONTINUE
C
C     NOW WE HAVE TO ROTATE THE MOMENTS DUE TO THE TC JOINT
C      FORCES INTO THE TCN SYSTEM FOR  Z COMPONENT ONLY
C
      CALL RTIMESV(R1,P1,P4)
      CALL RTIMESV(R1,P2,P5)
      CALL RTIMESV(R1,P3,P6)
      Q1(1)=P4(3)
      Q1(2)=P5(3)
      Q1(3)=P6(3)
      WRITE(7,2010)(Q1(I),I=1,3)
C
C     WE NOW FORM THE FINAL EQN IN P1 AND Q1
C
      P1(1)=MTC(3,K)
      P1(2)=-MCOMP(N,3,K)
      P1(3)=-MCOMP(L,3,K)
      WRITE(7,2010)(P1(I),I=1,3)
      Q1(1)=-Q1(1)/Q1(2)
      Q1(3)=-Q1(3)/Q1(2)
      P1(1)=P1(1)/P1(2)
      P1(3)=P1(3)/P1(2)
      STC(L,K)=-(Q1(1)+P1(1))/(Q1(3)+P1(3))
      STC((N+5),K)=-(P1(3)+STC(L,K)+P1(1))
C
C      THUS PUTTING CALF/ANT TIB IN STC(1/2,K)
C             POST TIB/PERONEAL   IN STC(8/9,K)
C
C
C     SOLVE FOR FZ-LAT
C
      STC(5,K)=-FTC(3,K)-FCOMP(L,3,K)*STC(L,K)-FCOMP(N,3,K)*STC(
(N+5),K)
C
C     CALCULATE THE REMAINING FORCE AND MOMENT EQUATIONS
C
      DO 455 I=1,2
      FTC(I,K)=-FTC(I,K)-FCOMP(L,I,K)*STC(L,K)-FCOMP(N,I,K)*STC(
(N+5),K)
      MTC(I,K)=MTC(I,K)-MCOMP(L,I,K)*STC(L,K)-MCOMP(N,I,K)*STC((
N+5),K)
      MTC(I,K)=100.0*MTC(I,K)
  455 CONTINUE
      STC(3,K)=(FTC(1,K)-MTC(2,K))/2.0
      STC(6,K)=(FTC(1,K)+MTC(2,K))/2.0
      STC(4,K)=(FTC(2,K)+MTC(1,K))/2.0
      STC(7,K)=(FTC(2,K)-MTC(1,K))/2.0
C
C     THE TC SOLUTIONS ARE OBTAINED
C
C        CALF=STC(1,K)
C     ANT TIB=STC(2,K)
C      FX-LAT=STC(3,K)
C      FY-LAT=STC(4,K)
C      FZ-LAT=STC(5,K)
C      FX-MED=STC(6,K)
C      FY-MED=STC(7,K)
C
C
C     THE RESULTANT TC JOINT FORCE AND MOMENT IS CALCULATED
C
C     P1-RESULTANT MOMENT
C     Q1 RESULTANT FORCE
C
      P1(1)=MTC(1,K)/100.0
      P1(2)=MTC(2,K)/100.0
      P1(3)=0.0
      Q1(1)=STC(3,K)+STC(6,K)
      Q1(2)=STC(4,K)+STC(7,K)
      Q1(3)=STC(5,K)
C
C     CALCULATE MOMENTS ABOUT THE TCN ORIGIN
```

```
C
      P1(1)=-TTC(2,K)*Q1(3)+TTC(3,K)*Q1(2)+P1(1)
      P1(2)=TTC(1,K)*Q1(3)-TTC(3,K)*Q1(1)+P1(2)
      P1(3)=-TTC(1,K)*Q1(2)+TTC(2,K)*Q1(1)+P1(3)
      DO 460 I=1,3
      DO 460 J=1,3
      R1(I,J)=RTCN(I,J,K)
  460 CONTINUE
      CALL RTIMESV(R1,P1,P2)
      CALL RTIMESV(R1,Q1,P3)
      STCN(3,K)=-P3(3)
      STCN(6,K)=-P2(3)
      STCN(2,K)=-(P3(2)+50*P2(1))/2.0
      STCN(5,K)=-(P3(2)-50*P2(1))/2.0
      STCN(1,K)=-(P3(1)-50*P2(2))/2.0
      STCN(4,K)=-(P3(1)+50*P2(2))/2.0
C
C     THE TCN SOLUTIONS ARE OBTAINED
C
C     FX POST=STCN(1,K)
C     FY POST=STCN(2,K)
C     FZ POST=STCN(3,K)
C      FX ANT=STCN(4,K)
C      FY ANT=STCN(5,K)
C     MZ RESD=STCN(6,K)
C
  400 CONTINUE
C
C     WRITE TC SOLUTIONS
C
      WRITE(6,290)
      WRITE(6,461)
  461 FORMAT(1H0,10X,19HTC SYSTEM SOLUTIONS)
      WRITE(6,462)
  462 FORMAT(1H0,4X,8H  CALF  ,2X,8HANT-TIB ,2X,8H FX-LAT ,2X,8H
 FY-LAT
     *,2X,8H FZ-LAT ,2X,8H FX-MED ,2X,8H FY-MED ,2X,8HPOST-TIB,2
X,8HPERO
     *NEAL)
      DO 463 K=1,A
      WRITE(6,465)(STC(I,K),I=1,9)
  463 CONTINUE
  465 FORMAT(1H ,3X,9(F8.1,2X))
C
C     WRITE TCN SOLUTIONS
C
      WRITE(6,290)
      WRITE(6,470)
  470 FORMAT(1H0,10X,20HTCN SYSTEM SOLUTIONS)
      WRITE(6,480)
  480 FORMAT(1H0,4X,8HFX-POST ,2X,8HFY-POST ,2X,8HFZ-POST ,2X,8H
 FX-ANT
     *,2X,8H FY-ANT ,2X,9HMZ(RES)NM)
      DO 483 K=1,A
      WRITE(6,490)(STCN(I,K),I=1,6)
  483 CONTINUE
  490 FORMAT(1H ,3X,6(F8.1,2X))
      WRITE(6,290)
      READ(3,1000)AGE
      DO 500 K=1,A
C
C     CALCULATE THE RESULTANT FORCES NORMALISING FOR BODY WEIGHT
C
      STC(3,K)=STC(3,K)+STC(6,K)
      STC(4,K)=STC(4,K)+STC(7,K)
      STC(3,K)=SQRT(STC(3,K)**2+STC(4,K)**2+STC(5,K)**2)
      STC(4,K)=SQRT((STCN(1,K)**2+STCN(2,K)**2+STCN(3,K)**2)
      STC(5,K)=SQRT(STCN(4,K)**2+STCN(5,K)**2)
      STC(6,K)=STC(8,K)
      STC(7,K)=STC(9,K)
      DO 510 I=1,7
      STC(I,K)=STC(I,K)/AGE
  510 CONTINUE
  500 CONTINUE
      WRITE(6,520)
```

```
  518   520 FORMAT(1H0,10X,17HNORMALISED FORCES)
  549       WRITE(6,530)
  550   530 FORMAT(1H0,4X,8H  CALF  ,2X,8HANT-TIB ,2X,8H TC-RES
.2X,8HPOST-TCN
  551      *,2X,8H ANT-TCN ,2X,8HPOST-TIB,2X,8HPERONEAL)
  552       DO 540 K=1,6
  553       WRITE(6,550)(STC(I,K),I=1,7)
  554   540 CONTINUE
  555   550 FORMAT(1H ,3X,7(F8.2,2X))
  556       WRITE(6,290)
  557  5000 FORMAT(1H0,50H**********************************************
**********)
  558  1000 FORMAT(F0.0)
  559  1500 FORMAT(99F0.0)
  560  2000 FORMAT(3F0.0)
  561  2010 FORMAT(1X,3(F6.4,5X))
  562  3000 FORMAT(9F0.0)
  563  3010 FORMAT(1X,9(F6.4,5X))
  564       STOP
  565       END
  566       SUBROUTINE MATMUL(X,Y)
  567 C
  568 C     MATMUL COMPUTES MATRIX PRODUCT "X*Y"
  569 C
  570       DIMENSION X(3,3),Y(3,3),Z(3,3)
  571       DO 5 I=1,3
  572       DO 5 J=1,3
  573       SUM=0.0
  574       DO 6 K=1,3
  575     6 SUM=SUM+X(I,K)*Y(K,J)
  576     5 Z(I,J)=SUM
  577       DO 7 I=1,3
  578       DO 7 J=1,3
  579       X(I,J)=Z(I,J)
  580     7 CONTINUE
  581       RETURN
  582       END
  583       SUBROUTINE RTIMESV(R,V1,V2)
  584 C
  585 C     THIS SUBROUTINE ROTATES VECTOR 1 FROM SYSTEM 1 INTO SYSTEM
2 TO
  586 C     GIVE VECTOR 2 USING THE R1-2 ROTATION MATRIX
  587 C
  588       DIMENSION R(3,3),V1(3),V2(3)
  589       DO 10 I=1,3
  590       SUM=0.0
  591       DO 20 J=1,3
  592       SUM=SUM+R(I,J)*V1(J)
  593    20 CONTINUE
  594       V2(I)=SUM
  595    10 CONTINUE
  596       RETURN
  597       END
  598       SUBROUTINE DCM(X,Y)
  599 C
  600 C     THIS SUBROUTINE TAKES X=ORIGIN
  601 C                           Y=INSERTION
  602 C
  603 C     IT CALCULATES DIRECTION COSINES AND POTENTIAL MOMENTS
  604 C
  605 C     DIRECTION COSINES AS ORIGIN-INSERTION=POTENTIAL FORCE
  606 C     AND ORIGIN TIMES POTENTIAL FORCE     =POTENTIAL MOMENTS
  607 C
  608 C                           X=POTENTIAL MOMENT
  609 C                            Y=POTENTIAL FORCE
  610 C
  611       DIMENSION X(3),Y(3),Z(3)
  612       SUM=0.0
  613       DO 10 I=1,3
  614       Z(I)=X(I)-Y(I)
  615       SUM=SUM+Z(I)**2
  616    10 CONTINUE
  617       SUM=SQRT(SUM)
  618       DO 20 I=1,3
  619       Z(I)=Z(I)/SUM
```

```
      20 CONTINUE
         X(1)=-Y(2)*Z(3)+Y(3)*Z(2)
         X(2)=-Y(3)*Z(1)+Y(1)*Z(3)
         X(3)=-Y(1)*Z(2)+Y(2)*Z(1)
         DO 30 I=1,3
         Y(I)=Z(I)
      30 CONTINUE
         RETURN
         END
         SUBROUTINE RCROSSF(R,F)
C
C        THIS SUBROUTINE CALCULATES THE CROSS PRODUCT R*F
C
         DIMENSION R(3),F(3),Z(3)
         Z(1)=R(2)*F(3)-R(3)*F(2)
         Z(2)=R(3)*F(1)-R(1)*F(3)
         Z(3)=R(1)*F(2)-R(2)*F(1)
         DO 10 I=1,3
         F(I)=Z(I)
      10 CONTINUE
         RETURN
         END
         FINISH
```

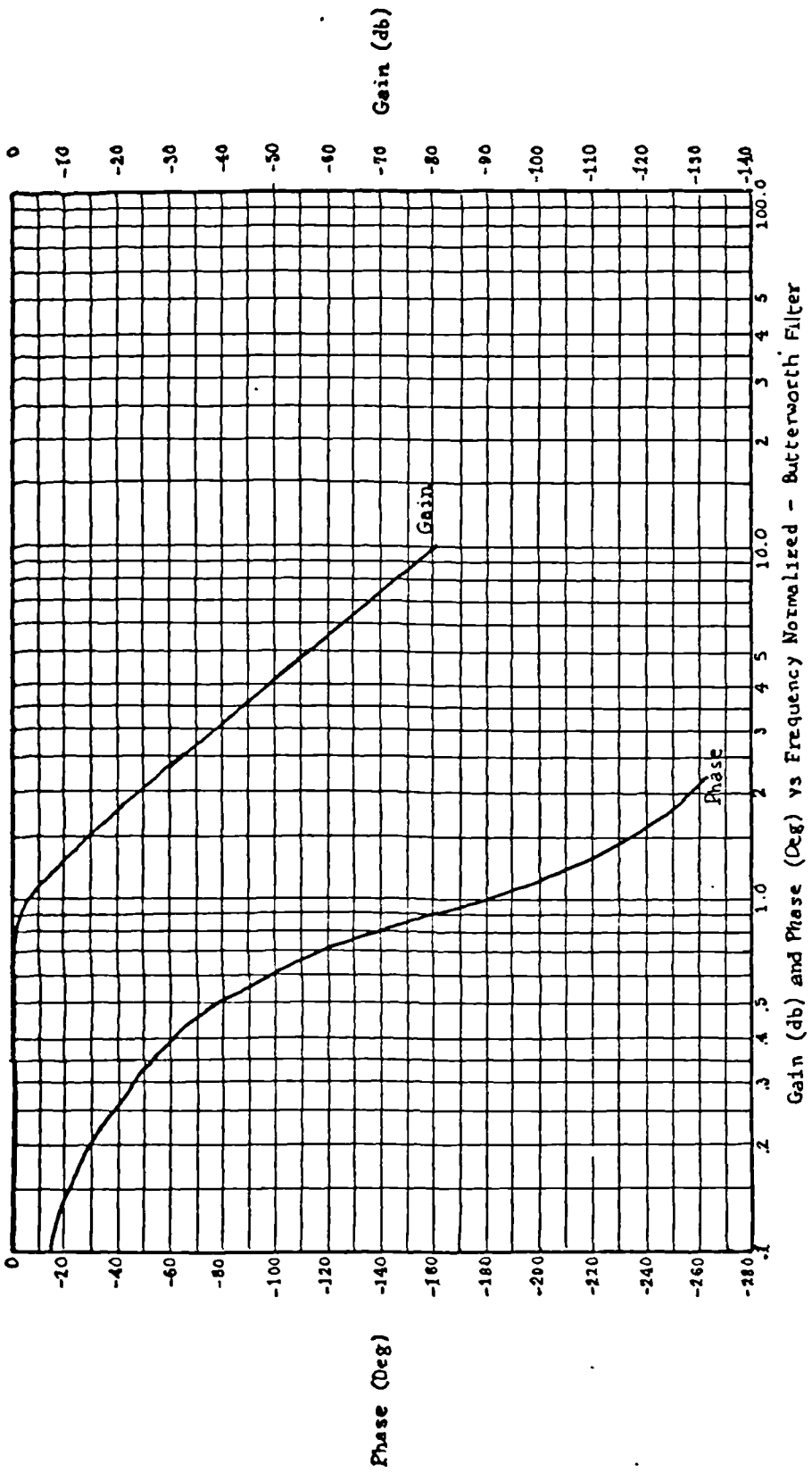

A3.9 Gain and Phase Characteristics of a Fourth Order Butterworth Filter (Adapted from Andrews, 1975)

A3.10 Experimental Test Subject Details

Subject No	Height(m.)	Weight(N.)	Age(years)
1	1.83	736	24.2
2	1.80	649	23.7
3	1.90	806	23.2
4	1.77	675	22.7
5	1.78	768	26.9
6	1.78	752	25.8
7	1.76	688	23.1
Mean Values	1.80	725	24.2